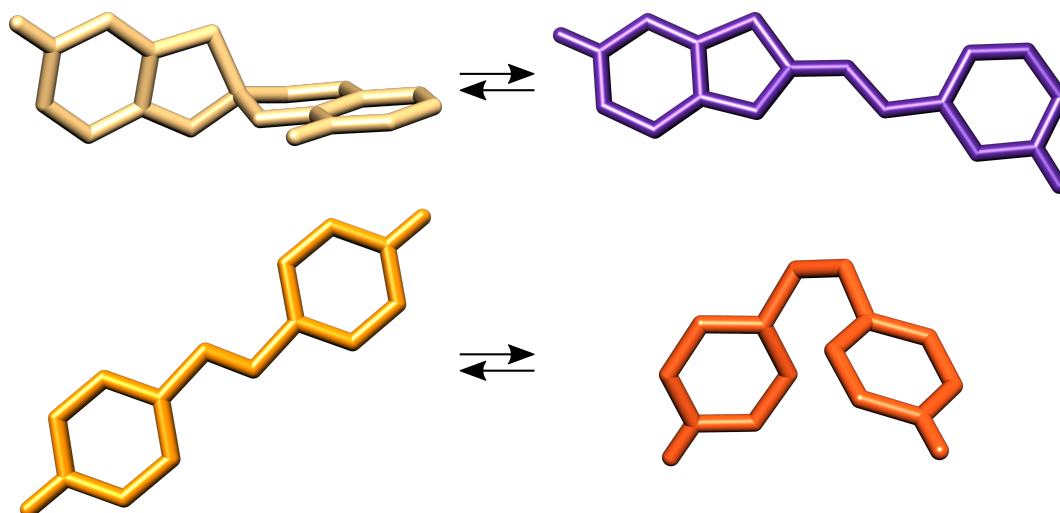


Photo- and Mechanoresponsive Polymeric Systems



Dissertation

Zur Erlangung des Doktorgrades
der Mathematisch-Naturwissenschaftlichen Fakultät
der Christian-Albrechts-Universität zu Kiel

Vorgelegt von

Mathias Dowds (geb. Schulz)

Kiel, 2019

Erste Gutachterin: Prof. Dr. Anne Staubitz
Zweite Gutachterin: Prof. Dr. Anna McConnell
Tag der mündlichen Prüfung: 13. Dezember 2019
Zum Druck genehmigt: 13. Dezember 2019

gez. Prof. Dr. Frank Kempken
Dekan der Mathematisch-Naturwissenschaftlichen Fakultät
der Christian-Albrechts-Universität zu Kiel

A scientist must also be absolutely like a child.
If he sees a thing, he must say that he sees it,
whether it was what he thought he was going to see or not.

See first, think later, then test.

But always see first. Otherwise you will only see what you were expecting.
Most scientists forget that.

Douglas Adams (1952 – 2001), *So Long, and Thanks for All the Fish* **1984**.

Für Jacob.

Preamble

Die vorliegende Arbeit wurde unter Anleitung von
Prof. Dr. Anne Staubitz
in der Zeit von Februar 2013 bis September 2019
am Otto Diels-Institut für Organische Chemie
der Christian-Albrechts-Universität zu Kiel angefertigt.
Teile der Ergebnisse wurden in Kooperationen im Rahmen des
SFB 677 „Funktion durch Schalten“ erzielt.

Diese Arbeit wurden in Teilen in Peer-Review-Zeitschriften publiziert oder zur Veröffentlichung eingereicht und in Form des Manuskripts des Originalartikels in die Arbeit aufgenommen. Die als „Supporting Information“ veröffentlichten experimentellen Daten wurden ebenfalls in diese Arbeit integriert. Die Anteile der verschiedenen Autoren an den Veröffentlichungen werden im jeweiligen Kapitel spezifiziert. Die Vervielfältigungsberechtigungen wurden eingeholt und sind im Appendix eingegliedert.

Bereits veröffentlicht (geordnet nach Kapitelreihenfolge in dieser Arbeit):

- (1) M. Schulz-Senft, M. Lipfert, A. Staubitz, Mechanopolymerchemie: Molekulare Wirkung durch Kraft, *Chem. Unserer Zeit* **2014**, *48*, 200-214. DOI: 10.1002/ciuz.201400640
- (2) S. Shree, M. Schulz-Senft, N. H. Alsleben, Y. K. Mishra, A. Staubitz, R. Adelung, Light, Force, and Heat: A Multi-Stimuli Composite that Reveals its Violent Past, *ACS Appl. Mater. Interfaces* **2017**, *9*, 38000-38007. DOI: 10.1021/acsami.7b09598
- (3) S. Shree, M. Dowds, A. Kuntze, S. Li, Y. K. Mishra, A. Staubitz, R. Adelung, Self-reporting mechanochromic coating: a glassfiber reinforced polymer composite that predicts impact induced damage, *Mater. Horiz.* **2019**. DOI: 10.1039/C9MH01400D
- (4) M. Schulz-Senft, P. J. Gates, F. D. Sönnichsen, A. Staubitz, Diversely halogenated spiropyran - Useful synthetic building blocks for a versatile class of molecular switches, *Dyes Pigm.* **2017**, *136*, 292-301. DOI: 10.1016/j.dyepig.2016.08.039
- (5) M. Dowds, D. Bank, J. Strüben, D. Presa Soto, F. D. Sönnichsen, F. Renth, F. Temps, A. Staubitz, Efficient reversible photoisomerisation with large solvodynamic size-switching of a main chain poly(azobenzene-*alt*-trisiloxane), *J. Mater. Chem. C* **2020**. DOI: 10.1039/C9TC05193G
- (6) L.-Y. He, M. Schulz-Senft, B. Thiedemann, J. Linshoef, P. J. Gates, A. Staubitz, Nucleophile-Selective Cross-Coupling Reactions with Vinyl and Alkynyl Bromides on a Dinucleophilic Aromatic Substrate *Eur. J. Org. Chem.* **2015**, 2498-2502. DOI: 10.1002/ejoc.201500138

Zur Veröffentlichung eingereicht:

- (7) M. Dowds, S. Shree, J. Strüben, X. Jin, D. Presa Soto, R. Adelung, A. Staubitz, Reversible Volume Switching of a Poly(silazobenzyl-siloxane), *eingereicht bei Chem. Mater.* **2019**.



Eigenständigkeitserklärung

Hiermit erkläre ich, Mathias Dowds, an Eides statt, die vorliegende Dissertation selbstständig und ausschließlich unter Zuhilfenahme der angegebenen Quellen und Hilfsmittel angefertigt zu haben. Inhalt und Form der Arbeit habe ich, abgesehen von Beratung durch meine Betreuerin, Prof. Dr. Anne Staubitz, eigenständig erarbeitet und verfasst. Bei der Entstehung der Arbeit wurden die Regeln guter wissenschaftlicher Praxis der Deutschen Forschungsgemeinschaft eingehalten. Teile der Ergebnisse aus Veröffentlichung (3) entstanden während meiner Diplomarbeit. In Teil II, Kapitel 3.1 wird dieser Anteil spezifiziert. Diese Dissertation ist mein erster Promotionsversuch, mir wurde kein akademischer Grad aberkannt.

Kiel, im Januar 2020.

Mathias Dowds (geb. Schulz)





Kurzzusammenfassung

Polymere und Polymermaterialien haben seit der Entdeckung von Makromolekülen vor fast einhundert Jahren vielfältige Anwendungen gefunden. Diese Arbeit trägt zur Weiterentwicklung zweier Hauptforschungsgebiete im Bereich Chemie und Materialwissenschaften von Polymeren bei: verstärkte Polymerkomposite und photoschaltbare Systeme aus Polymeren oder Makrozyklen.

Keramik- oder faserverstärkte Kompositmaterialien werden insbesondere in großen, stark belasteten Strukturen wie Windrädern oder Flugzeugen eingesetzt. In dieser Arbeit wird die Entwicklung eines Kompositsystems vorgestellt, das die Exposition des Materials gegen die Stimuli Temperaturänderung, UV-Strahlung und mechanische Belastung anzeigt. Das keramisch verstärkte Kompositmaterial zeigte reversible Thermo- und Photochromie. Gleichzeitig stellt dieses Komposit das erste Material dar, in dem Spiropyran in einer Polymermatrix mechanisch induziert schalten, ohne kovalent an das Polymer gebunden zu sein. Das Konzept wurde in glasfaserverstärkten Kompositen fortgeführt, wobei ein sichtbarer Farbumschlag vor dem Materialversagen demonstriert werden konnte. Im Rahmen von Variationen des Matrixpolymers wurde eine bisher unbeschriebene Zersetzungsreaktion von Spiropyranen entdeckt.

Die außergewöhnlich unterschiedliche Färbung der zwei Schaltzustände in Spiropyranen – Spiropyran und Merocyanin – zeugt von großen geometrischen Änderungen begleitete einschneidende Veränderungen der beteiligten π -Systeme. Während der Farbumschlag und der Größenunterschied im Konzept der mechanisch schaltbaren Komposite angewandt wurden, lässt sich die Ausdehnungsänderung der π -Konjugation nutzen, um die Leitfähigkeit konjugierter Polymere zu schalten. Als Machbarkeitsnachweis wurde ein Spiropyran mit Hexylthiophensubstituenten – ein häufiges Strukturelement in Polymeren für organische Elektronik – funktionalisiert. Das synthetisierte Molekül zeigte schaltbare Konjugation, wie mittels schaltbarer Fluoreszenz nachgewiesen wurde. Dichtefunktionaltheoretische Berechnungen stützen diesen Befund.

Im Forschungszweig photomechanischer Polymere werden Materialien verwandt, die mit makroskopischen Änderungen auf Stimuli reagieren. Wir konnten den Einbau von Azobenzol-schaltern in lineare Polymer zeigen. Hierbei stellen Siloxan-Brücken genügend geometrische Flexibilität bereit, um effiziente Photoschaltung zu ermöglichen. Die Schalteigenschaften der Polymere wurden in Hinblick auf die Schaltdynamik und Größenänderung sowohl in Lösung als auch im Film analysiert. Zusätzlich wurde ein makrozyklisches Azobenzoldimer mit Siloxanbrücken synthetisiert, das effiziente Photoschaltbarkeit bei langsamer thermischer Rückisomerisierung zeigte.





Abstract

Polymers and materials made thereof have found manifold applications since the discovery of macromolecules almost a century ago. This thesis contributes to the development of two main research areas in the field of chemistry and materials science of polymers: reinforced polymer composites and photoswitchable systems of polymers or macrocycles.

Polymer composites with reinforcements such as ceramics or fibers are particularly applied in large, highly stressed structures such as wind turbines. Within this thesis, the development of a composite system that indicates exposure of the material to the stimuli temperature change, UV irradiation and mechanical stress is demonstrated. The ceramic reinforced composite showed reversible thermo- and photochromism. This composite represents the first example to show mechanically induced switching of spiropyran molecules in a polymer matrix without being covalently bound to the matrix. The concept was advanced in glass fiber reinforced composites, demonstrating visible color changes before failure of the material. In the context of variation of the polymer matrix, a formerly undescribed degradation reaction of spiropyrans was discovered.

The exceptional color difference of the two switching states of spiropyran – spiropyran and merocyanine – indicates drastic changes of the involved π systems, that are accompanied by large geometrical changes. While the changes in color and size were utilized in the concept of mechanoswitchable composites, the change in the expanse of the conjugation can be used to switch the conductivity of conjugated polymers. In a proof of concept, hexylthiophene substituents – a common structural motif in polymers for organic electronics – were attached to a spiropyran. The synthesized molecule showed switchable conjugation, as was demonstrated by switchable fluorescence and supported by density functional theory calculations.

The field of photomechanical polymers covers polymer based materials that respond to stimuli with macroscopical changes. We demonstrated the incorporation of azobenzene switches in linear polymers. Siloxane linkers provided sufficient geometrical flexibility to allow efficient photoswitching. The switching properties of the polymers were analyzed with respect to the switching dynamics and size changes in solution and film. Additionally, a macrocyclic azobenzene dimer with siloxane linkers was synthesized, that showed efficient photoswitching and slow thermal backisomerization.



Foreword

This thesis presents the synthesis of spiropyran and azobenzene photoswitches and the application of these switches in polymers. The research that led to this thesis was conducted in the context of the Collaborative Research Center 677 "Function by Switching" in collaboration with the Institute of Physical Chemistry and the Institute for Materials Science, University of Kiel. The collaborations required a broad approach covering several aspects of the main topic photo- and mechanoresponsive polymeric systems.

The thesis is divided in five parts, excluding preamble and appendix. The results and their discussions are separated into two parts, according to the utilized molecular switch: **Part II** (spiropyrans) and **Part III** (azobenzenes). The results that were published or submitted to publication are also included in these parts. As every publication has its individual introduction, the Parts II and III begin with detailed introductions of the applied switches.

Part I, "Introduction & Objectives" provides a general overview of the topics and concepts that are employed in this thesis: molecular switches and polymers (composites, semiconducting polymers, and silicones). Parts of the section on polymers were published as a review article "Mechanically Induced Chemistry of Polymers".

Part IV contains the summary of the results of this thesis and possible future directions based on this research.

Part V includes all experimental methods and data, including those that were published as "Supporting Information" accompanying the publications. Results of DFT calculations are also presented here.

The **Appendix** contains a publication I contributed to during the work on this thesis. The reprinting permissions for all publications are collected here, next to bibliography and lists of figures, tables, and schemes.

The references are numbered consecutively through this thesis. Each part is followed by a corresponding bibliography, a complete bibliography is provided in the appendix. The published or submitted manuscripts contain their individual bibliographies.



Contents

Preamble	I
Eigenständigkeitserklärung	V
Kurzzusammenfassung	VII
Abstract	IX
Foreword	XI
I. Introduction & Objectives	1
1. Introduction	3
1.1. Switching on the Molecular Scale	3
1.2. Polymers	5
1.2.1. Mechanically Induced Chemistry of Polymers	9
1.2.2. Polymer Composites	25
1.2.3. Semiconducting Polymers	26
1.2.4. Poly(siloxanes)	30
2. Objectives	35
2.1. Spiroyrans in Polymer Materials	35
2.2. Azobenzene-siloxanes in Polymers and Macrocycles	37
Bibliography of Part I	39
II. Spiroyrans and their Implementation into Polymer Materials	45
1. Spiroyrans Dyes	47
1.1. Photochromism of Spiroyrans	47
1.2. Mechanochromism of Spiroyrans	49
2. Spiroyrans Dyes as Additive in Composites	51
2.1. Multi-Stimuli Response of a Spiroyrans / Zinc Oxide / PTU Composite	51
2.2. Failure Indication in Spiroyrans / Glassfiber Composites	61

3. Spiropyran Dyes for the Covalent Incorporation into Conducting Polymers	71
3.1. Halide Functionalized Spiropyrans	73
3.2. Stille Coupling Reactions of Spiropyrans	85
3.3. Preparation of a Spiropyran Connected to 3-Hexylthiophenes	89
3.3.1. Synthetic Route	89
3.3.2. Exploration of the Unexpected Methoxy Cleavage by DFT	90
3.3.3. Characterization of Photochemical Properties	94
3.3.4. DFT Modelling of the Electronic Properties	97
3.3.5. Conclusion	99
Bibliography of Part II	101
III. Azobenzenes and Siloxanes	105
1. Azobenzene Dyes	107
2. Covalent Incorporation Azobenzene Units into the Backbones of Poly(siloxanes)	111
2.1. A Linear Poly(Azobenzene-siloxane)	113
2.2. A Potentially Cross-Linkable Linear Poly(Azobenzene-siloxane)	126
3. A Macrocyclic Azobenzene-Siloxane Dimer	137
3.1. Background	137
3.2. Synthesis & Properties	138
Bibliography of Part III	143
IV. Summary & Future Directions	149
Spiropyrans in Polymer Materials	151
Azobenzene and Siloxanes	156
Bibliography of Part IV	159
V. Experimental Part	161
1. General Methods & Materials for Unpublished Synthesis	163
1.1. Equipment Used for Synthesis & Analysis of Unpublished Substances	163
1.2. Chemicals & Solvents Used in the Synthesis and Analysis of Unpublished Substances	164

2. Spiropyran in Composites	167
2.1. Supporting Information for <i>ACS Mat. Interfaces</i> 2017 , <i>9</i> , 38000-38007.	167
2.2. Supporting Information for <i>Mater. Horiz.</i> 2019 submitted	176
3. Spiropyran Dyes with Halide and Pseudohalide Groups	191
3.1. Supporting Information for <i>Dyes and Pigments</i> 2017 , <i>136</i> , 292-301.	191
3.2. Unpublished Syntheses	264
3.2.1. Synthesis of 5-Iodo-1,3,3-trimethyl-2-methylene-3 <i>H</i> -indolene (13)	264
3.2.2. Synthesis of 5',8-Diiodo-1',3',3'-trimethyl-6-nitrospiro[chromene-2,2'-indoline] (9b)	264
3.3. NMR Spectra of Unpublished Substances	265
3.3.1. ¹ H and ¹³ C{ ¹ H} Spectra of 5-Iodo-1,3,3-trimethyl-2-methylene-3 <i>H</i> -indolene (13) in CDCl ₃	265
4. Stille Coupling Reactions of Spiroyrans 9a–c	267
4.1. Standardized Synthetic Procedure	267
4.1.1. Reaction of 5',8-Dibromo-1',3',3'-trimethyl-6-nitrospiro-[chromene-2,2'-indoline] (9a)	268
4.1.2. Reaction of 5',8-Diiodo-1',3',3'-trimethyl-6-nitrospiro- [chromene-2,2'-indoline] (9b)	269
4.1.3. Reaction of Bis-5',8-(trifluoromethylsulfonyl)-1',3',3'-trimethyl-6-nitrospiro-[chromene-2,2'-indoline] (9c)	270
4.2. Aromatic Regions of the ¹ H NMR Spectra of the Stille Coupling Reactions of 9a–c in CDCl ₃	271
4.2.1. Reaction of 9a	271
4.2.2. Reactions of 9b	272
4.2.3. Reactions of 9c	273
5. Spiropyran Dyes for the Incorporation into Poly(thiophenes)	275
5.1. Syntheses	275
5.1.1. Synthesis of 5-(3-Hexylthien-2-yl)-2,3,3-trimethyl-3 <i>H</i> -indole (27)	275
5.1.2. Synthesis of 5-(3-Hexylthien-2-yl)-1,2,3,3-tetramethyl- 3 <i>H</i> -indolium Iodide (28)	276
5.1.3. Synthesis of 2-Hydroxy-3-iodobenzaldehyde (22)	276
5.1.4. Synthesis of 3-Iodo-2-methoxybenzaldehyde (24)	277
5.1.5. Synthesis of 3-Iodo-2-methoxy-5-nitrobenzaldehyde (25)	278
5.1.6. Synthesis of 3-(3-Hexylthien-2-yl)-2-hydroxy-5-nitro- benzaldehyde (26)	278
5.1.7. Synthesis of 5',8-Di(3-hexylthien-2-yl)-1',3',3'-trimethyl-6-nitrospiro-chromene-2,2'-indoline (19)	279
5.2. DFT Calculations of 5',8-Di(3-methylthiophen-2-yl)-1',3',3'-trimethyl-6-nitrospiro-[chromene-2,2'-indoline] (40)	281
5.2.1. Closed Form 40a	282

5.2.2.	Open Form, TTC-Geometry 40b	285
5.2.3.	Open Form, TTT-Geometry 40c	288
5.3.	DFT Calculations of Phenol and Anisole Derivatives and the Corresponding Phenolates for the Estimation of Intramolecular Hydrogen Bonds	291
5.3.1.	Phosphate (33a)	293
5.3.2.	Hydrogen Phosphate (33b)	293
5.3.3.	Methyl Phosphate (33c)	294
5.3.4.	Phenol (29a)	295
5.3.5.	Anisole (29b)	295
5.3.6.	Phenolate (29c)	296
5.3.7.	2-Hydroxybenzaldehyde (30a)	297
5.3.8.	2-Methoxybenzaldehyde (30b)	298
5.3.9.	2-Formylphenolate (30c)	299
5.3.10.	2-Hydroxy-5-nitrobenzaldehyde (3a)	300
5.3.11.	2-Methoxy-5-nitrobenzaldehyde (3b)	301
5.3.12.	2-Formyl-4-nitrophenolate (3c)	302
5.3.13.	2-Hydroxy-5-nitro-3-thien-2-ylbenzaldehyde (31a)	303
5.3.14.	2-Methoxy-5-nitro-3-thien-2-ylbenzaldehyde (31b)	304
5.3.15.	2-Formyl-4-nitro-6-(thien-2-yl)phenolate (31c)	305
5.3.16.	2-Hydroxy-5-nitro-3-(3-methylthien-2-yl)benzaldehyde (32a)	306
5.3.17.	2-Methoxy-5-nitro-3-(3-methylthien-2-yl)benzaldehyde (32b)	308
5.3.18.	2-Formyl-4-nitro-6-(3-methylthien-2-yl)phenolate (32c)	309
5.4.	NMR Spectra	311
5.4.1.	5-(3-Hexylthien-2-yl)-2,3,3-trimethyl-3 <i>H</i> -indole (27)	311
5.4.2.	5-(3-Hexylthienyl)-1,2,3,3-tetramethyl-3 <i>H</i> -indolium Iodide (28)	312
5.4.3.	3-Iodo-2-methoxy-benzaldehyde (24)	313
5.4.4.	3-Iodo-2-methoxy-5-nitro-benzaldehyde (25)	314
5.4.5.	3-(3'-Hexylthien-2-yl)-2-hydroxy-5-nitro-benzaldehyde (26)	315
5.4.6.	5',8-Di(3-hexylthiophen-2-yl)-1',3',3'-trimethyl-6-nitrospiro-(chromene-2,2'-indoline) (19)	316
5.4.7.	Photodegradation of 19	317
6.	Azobenzene as Repeating Unit in a Polymer	319
6.1.	Synthesis of an Alternating Poly-(Azobenzene-Trisiloxane) and its Characterization in Solution	319
6.2.	Synthesis of a Cross-Linkable Alternating Poly-(Azobenzene-Trisiloxane) and its Characterization in a Freestanding Film	352
7.	A Macrocyclic Azobenzene	381
7.1.	Syntheses	381
7.1.1.	Synthesis of 3,3'-Diiodoazobenzene (65)	381

7.1.2. Synthesis of 3,3'-Bis(trimethylstannyl)azobenzene (63)	381
7.1.3. Synthesis of (1(<i>E</i>),5(<i>E</i>))-2,2,4,4,6,6,8,8-Octamethyl-1,5-(3,3')-diazobenzene-3,7-dioxa-2,4,6,8-tetrasilacyclooctaphane (64)	382
7.2. X-ray Diffraction Crystal Structure of the (1(<i>E</i>),5(<i>E</i>)) -Isomer 64a	384
7.3. DFT Calculations of all Switching States	391
7.3.1. (<i>E</i>),(<i>E</i>)-Isomer 64a	391
7.3.2. (<i>E</i>),(<i>Z</i>)-Isomer 64b	395
7.3.3. (<i>Z</i>),(<i>Z</i>)-Isomer 64c	398
7.4. NMR Spectra	401
7.4.1. 3,3'-Diiodoazobenzene (65)	401
7.4.2. 3,3'-Bis(trimethylstannyl)azobenzene (63)	402
7.4.3. Macrocyclic Azobenzene Dimer 64	404
Bibliography of Part V	409
Appendix	411
Miscellaneous Publication: Nucleophile-Selective Cross-Coupling Reactions	413
Permissions to Reprint	423
T. P. Kaloni, et al., <i>The Journal of Physical Chemistry C</i> 2015 , <i>119</i> , 3979-3989.	425
M. Schulz-Senft et al., <i>Chemie in Unserer Zeit</i> 2014 , <i>48</i> , 200-214.	427
S. Shree et al., <i>ACS Applied Materials & Interfaces</i> 2017 , <i>9</i> , 38000-38007.	431
M. Schulz-Senft et al., <i>Dyes and Pigments</i> 2017 , <i>136</i> , 292-301.	433
S. Shree et al., <i>Materials Horizons</i> 2019 , DOI: 10.1039/c9mh01400d and M. Dowds et al., <i>Journal of Materials Chemistry C</i> 2020 , DOI: 10.1039/C9TC05193G	435
M. Schulz-Senft et al., <i>Dyes and Pigments</i> 2017 , <i>136</i> , 292-301.	443
L.-Y. He et al., <i>European Journal of Organic Chemistry</i> 2015 , 2498-2502.	445
Bibliography	449
List of Figures	463
List of Tables	464
List of Schemes	465
Abbreviations	469
Danksagung	471

Part I.

Introduction & Objectives

1. Introduction

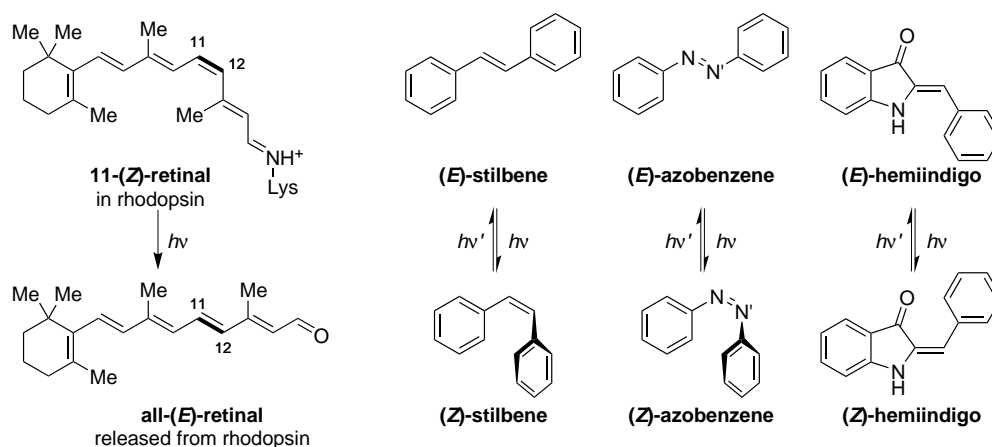
Light, more specifically sunlight, is one of the reasons why life on Earth exists. It is the major cause for relatively moderate temperatures, allowing for liquid water to remain on the surface for long periods of time. As electromagnetic radiation, it interacts with matter. Besides the mentioned heating effect on the planet itself, living organisms evolved several ways that allowed them to utilize the energy of sunlight. Poikilothermal (cold-blooded) animals such as lizards seek the early sunlight to increase their body temperature after cold nights. Phototrophic organisms harvest the energy of sunlight to induce photosynthetic reactions, which are the main source for organic molecules on Earth.^[1] While the warming effect is unselective and the photosynthesis is irreversible,^[1] an additional, selective and reversible process of light-matter interaction has evolved:^[2] the detection of light by visual systems, such as the eye.



Figure I.1. Effects of sunlight in nature. Sunlight warms the Earth, allowing for large amounts of liquid water as habitat for aquatic life. It helps poikilothermal animals such as turtles to warm their bodies. Plants utilize sunlight as a source of energy in photosynthesis. Visual receptors in eyes rely on reversible photoisomerization. © M. Dowds, 2019.

1.1. Switching on the Molecular Scale

Generally, a switching process requires two (or more) stable or at least metastable states.^[3,4] For any useful application, interconversion between those states should happen in high yields, while the stimuli for the individual reactions should be separated.^[5] Besides several other stimuli, such as variation of pH or electrochemical stimulation, inducing reversible



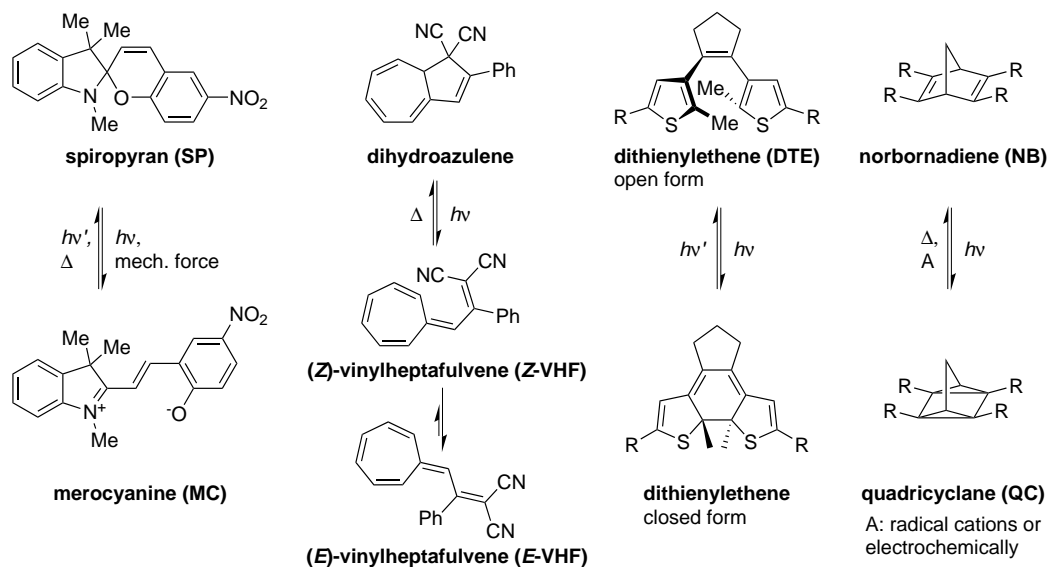
Scheme I.1 Examples of photoswitchable molecules with (*E*),(*Z*)-isomerization. Retinal is shown in its natural occurrence. It is bound to rhodopsin by a Schiff-base linkage with a lysin residue. All-*trans* retinal is released from the protein and is switched back separately. In stilbenes, azobenzenes and hemiindigo, the (*E*) \rightarrow (*Z*) and (*E*) \rightarrow (*Z*) isomerization are induced by irradiation with light.

switching reactions by light has been widely applied. The irradiation with light provides several advantages: it can be applied non-invasively to gaseous, liquid and solid substrates with spatial control. While the variation of the light intensity mostly effects ensemble phenomena such as heating or photostationary equilibria, molecular phenomena are mostly controlled by the light's frequency (and thereby wavelength).

In the retina of the human eye, the reception of light occurs within rhodopsin, a membrane protein.^[2] It is bound to the chromophoric molecule 11-(*Z*)-retinal, which isomerizes to all-(*E*)-retinal upon irradiation with light.^[2,6,7] This isomerization triggers a series of structural changes in rhodopsin, culminating in the release of all-(*E*)-retinal from the protein.^[6,7] While human rhodopsin and similar photoreceptor proteins in microbial and animal life use the protein environment as amplifier, the underlying principle of light-induced (*E*) \rightleftharpoons (*Z*) isomerization of double bonds is a versatile trigger.

This working principle was adapted in synthetic photoswitches. The most relevant classes of photoswitches that use (*E*) \rightleftharpoons (*Z*) isomerization of double bonds are stilbenes, azobenzenes and hemiindigos (see Scheme I.1).^[8] Typically, the (*E*)-configuration of the double bond is thermodynamically favored. Thus, the (*E*) \rightarrow (*Z*) isomerization can be induced with light of higher wavelengths (lower energies) than the (*Z*) \rightarrow (*E*) backswitching, which also occurs thermally.^[8] Of those mentioned examples, azobenzene derivatives emerged as widely used family of photoswitches (see Part III).^[3,9] The formation of the central azo group is possible via various synthetic routes, leading to a variety of chemical modifications.^[10] In addition, the photoswitching of azobenzenes occurs without any side reaction or degradation, making virtually infinite switching cycles possible.^[11]

Aside from the isomerization of double bonds, light can induce opening and closing of rings (see Scheme I.2).^[3,8] The photoinduced electrocyclic ring opening is used in the switching of spiropyran (SP) dyes to their merocyanine (MC) counterparts and in the isomerization of dihydroazulene (DHA) to vinylheptafulvene (VHF). Contrary to these two examples,



Scheme I.2 Examples of photoswitchable molecules showing ring-opening or cyclization reactions. The switching of $SP \rightleftharpoons MC$ can also be induced by mechanical force or thermally. Quadricyclanes and vinylheptafulvenes cannot be switched back photochemically.

systems based on dithienylethene (DTE) and norbornadiene (NB) undergo photoinduced electrocyclization.^[8] In addition to the photochemical control of these reactions, other stimuli are also relevant.^[8] Since VHF and quadricyclane (QC) are photochemically stable, the re-isomerization towards DHA and NB is induced thermally or via radical pathways ($QC \rightarrow NB$).^[8] Spirogyrans have drawn much interest, as the switching is extraordinarily versatile. Besides light, pH, electrochemical stimulation, the $SP \rightarrow MC$ isomerization can be induced mechanically (see subsection 1.2.1 and Part II).^[12] This variety of potential stimuli led to the implementation of spirogyrans in a vast range of applications, ranging from switchable surface properties to detection of mechanical stress.^[12–14]

1.2. Polymers

Since their first description by Hermann Staudinger,^[15] natural and synthetic polymers have developed into materials that influence basically every aspect of life. Polymers are used as sealants and adhesives, the structural backbone of airplanes is constructed using polymeric materials; while most polymer classes are insulators, some show semiconductivity and are applied in (organic) electronics.^[16] In general, the synthesis of polymers follows two principle kinetic mechanisms: step growth and chain growth polymerization (see Figure I.2). Synthetically, three main polymer formation reactions are described: the elimination of molecular fragments in condensation reactions, the addition reaction to a multiple bond, and the opening reaction of a ring. Typically, polycondensations show step growth mechanisms, whereas polyaddition and ring opening polymerizations show chain growth mechanisms.^[16]

In step growth polymerizations, many oligomers are formed initially that combine to polymers at high conversions (see Figure I.2 c). Thus, the molecular weight is a function

of the conversion and the stoichiometric ratio r (Equation I.1), being the fraction of the amount of monomers (or functional groups). For an arbitrary condensation reaction that involves two functional groups, n_X represents the amount of the first functional group and n_Y the amount of the second functional group. Whatever group is in excess is placed as numerator, so that r can be less than or equal to unity.

$$r = \frac{n_X}{n_Y} \leq 1 \quad (1.1)$$

Carothers' equation (Equation I.2) describes the growing of polymer chains as function of conversion of monomers p .^[17] Apparently, a mismatch of the involved functional group limits the possibility to obtain high molecular weights. Here, \bar{X}_n is the degree of polymerization (the number average of chain lengths) that shows inverse proportionality to p . In the easiest case, polymerization of one monomer type that bears the two reactive functional groups, the Carothers' equation for the so-called A-B systems follows Equation I.3. This behavior dictates the necessity of high purities and exact stoichiometries of all involved reagents to reach high conversion and thereby obtain high molecular weights by step growth polymerization reactions.

$$r < 1 : \quad \bar{X}_n = \frac{r + 1}{r - 2rp + 1} \quad (1.2)$$

$$r = 1 : \quad \bar{X}_n = \frac{1}{1 - p} \quad (1.3)$$

In contrast, chain growth polymerizations show continuous growth of the initiated chains, allowing high molecular weights even at low conversions (see Figure I.2 d)). Kinetically, the picture is more complex than for step growth polymerizations.^[16,17] Five general elementary reactions must be considered: the initiation of reactive species, the initial reaction of that species with the first monomer, the propagation of the chain formation by addition of new monomers, termination reactions that end the growing of the chain by quenching the reactive species, and chain transfer reactions that initiate the growing of a new chain while stopping the growth of the initial chain. The \bar{X} of each chain grows linearly with increasing conversion (Equation I.4).

$$\bar{X} \propto p \quad (1.4)$$

With continuing lifetime of the chain, termination becomes statistically more likely. As a result, an equilibrium between initiation, propagation and termination forms. In this equilibrium, the rates of initiation and termination are equal and each chain grows to the so-called kinetic chain length ν , before the growth is terminated. The kinetic chain length is proportional to the concentration of monomers $[M]$ and square root of the concentration of initiator $[I]$. It also depends on the rate constants for the initiation, k_i , propagation, k_p , and termination, k_t (Equation I.5). Depending on the type of termination,

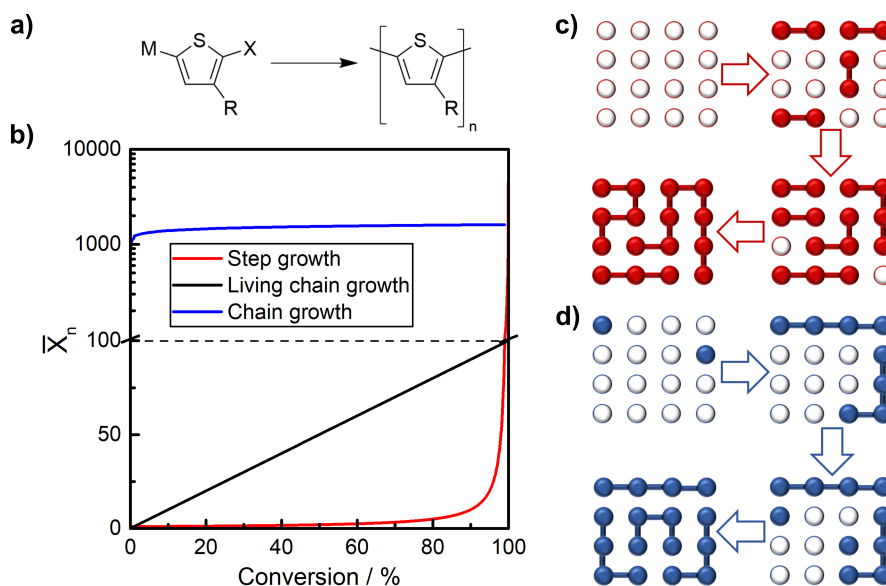


Figure I.2. Step growth and chain growth polymerization mechanisms. **a)** Hypothetically, the polymerization of bifunctional thiophenes with metal (M) and halide (X) substituents can follow a step growth or a chain growth mechanism. **b)** Degree of polymerization (\bar{X}_n) vs. conversion of step growth (red), chain growth (blue), and living chain growth (black) polymerization reactions. The graphs correspond to Equation I.3 (step growth) and Equation I.6 (living chain growth), with $[M]_0/[I]_0 = 100$. Note the change of the scale from linear to logarithmic at $\bar{X}_n = 100$. The graph of chain growth was sketched to illustrate v (Equation I.5) **c)** Visualization of the step growth mechanism. Initially, many oligomers are formed that combine to longer chains at high conversions. **d)** Visualization of the chain growth mechanism. Initially, few reactive centers are formed that continuously add monomers to the growing chains, before the growth is terminated and new chains are initiated.

$\bar{X}_n = v$ for disproportionation or recombination, $\bar{X}_n = 2v$ for chain-chain combination, or $v < \bar{X}_n < 2v$ for combinations of different termination reactions. The initiation reactions that generate the growing chains are typically much slower than the chain propagation and termination reactions (typical ratio for free radical polymerizations: $k_i/k_p/k_t = 10^{-5}/10^3/10^8$ L mol⁻¹ s⁻¹).^[18] Therefore the chains grow fast until they reach v , even before significant amounts of monomer are consumed.^[16,17]

$$v = \frac{k_p[M]}{\sqrt{k_t 2k_d[I]}} \quad (I.5)$$

The case of a fast initiation of propagating chains and the absence of termination or chain transfer reaction is described as living chain growth. Here, the chains grow linearly with increasing conversion. The ratio of the starting concentrations of monomer $[M]_0$ and initiator $[I]_0$ determine the final chain length at full conversion (Equation I.6).

$$\bar{X}_n = \frac{[M]_0 \cdot p}{[I]_0} \quad (I.6)$$

For the incorporation of photochromes into polymeric materials, various possibilities have been applied. The classification of these combined systems starts at the basic question, whether the photochromes are bound to the polymer chains or embedded into a polymer matrix without bonding (Figure I.3, green and red box, respectively).^[19] If the photochromes are bound to the polymer chains, the type of bonding (Figure I.3, blue branch) or the geometry of the incorporation (yellow branch) can be used as criteria for distinguishing these systems. While some examples of photochromes bound to polymers by coordinative bonds have been reported, covalent bonding has been applied more often.^[14,19,20] With both types of bonding, the photochrome can be implemented into the main chains of polymers, attached as side chains to polymers or used as cross-linking unit.^[14,19,20] When placed into the main chain, it was possible to incorporate either one or multiple photochromic units per chain.^[14,19,20]

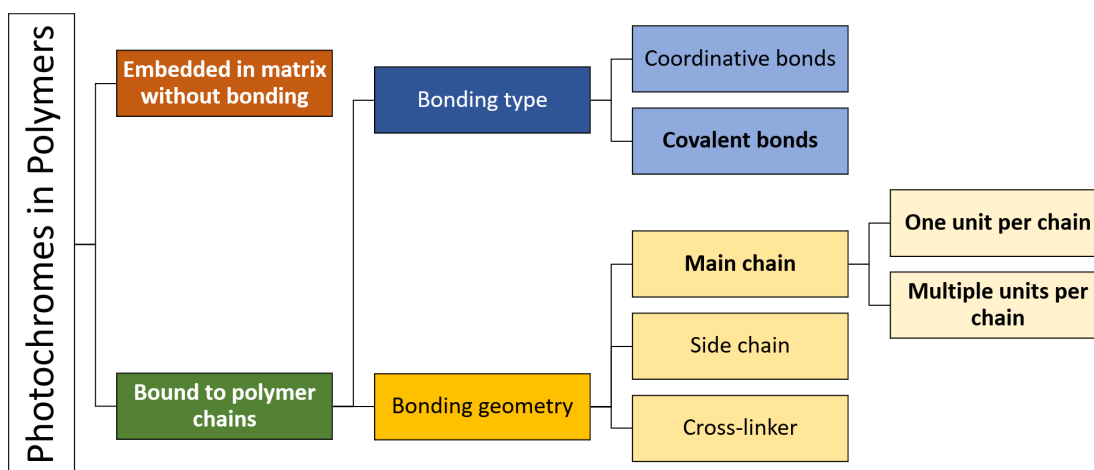


Figure I.3. Possibilities to classify photochromic polymer systems. The concepts that were applied in this thesis are highlighted in bold.

Besides the choice of the applied chromophore and its way of implementation, the polymer itself must match the requirements of the application. Proper tuning of the mentioned aspects enabled the development of various systems with impressive functions. Polymers can mediate between molecular and macroscopical phenomena, leading to two general effects: amplification of the photochrome switching to bulk phenomena and transferring external macroscopical forces to the molecular switches.^[14,19–23]

Spiroyrans in a poly(3-hexylthiophene) (P3HT) matrix can be used to photoswitch the channel conductance of an organic field effect transistor (OFET).^[24] Switching of ensembles of azobenzenes can induce bending of films.^[25] Photoinduced liquefaction of was used in the synthesis of self-healing materials.^[26,27] Polymers transfer the mechanical force to switch spiroyrans in solution,^[28] by stretching or compression of polymer samples,^[29] and by swelling of hydrogels.^[30]

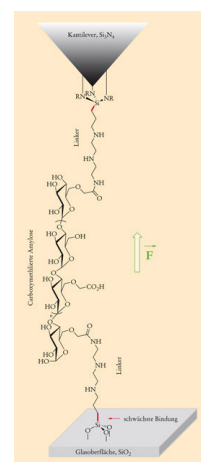
1.2.1. Mechanically Induced Chemistry of Polymers

Various aspects of mechanochemistry in biological and synthetic polymers were presented and described in a review.^[31] This includes discussions of pericyclic reactions (which can yield different products in mechanically induced reactions as opposed to light- or thermally induced reactions), mechanochemistry in single molecules, switching states of spiropyran and force transfer in elastomeric or glassy polymers. The review article was published in "Chemie in Unserer Zeit" in 2014.^[31] Reprinted with permission (See page 427) from Mathias Schulz-Senft, Matthias Lipfert, Anne Staubitz, Mechanopolymerchemie - Molekulare Wirkung durch Kraft, *Chem. Unserer Zeit* **2014**, 48, 200-214. © 2014 Wiley-VCH Verlag GmbH & Co. KGaA, Weinheim.

DOI: 10.1002/ciuz.201400640

Abstract

Published Version (German) Um eine chemische Reaktion herbeizuführen, muss im Allgemeinen Energie zugeführt werden, zumindest, um die Aktivierungsbarriere zu überwinden. Im einfachsten Fall wird die Reaktionsmischung erhitzt oder bestrahlt; bei der Elektrochemie wird elektrische Energie über Elektroden eingebracht und auch die freiwerdende Energie anderer Reaktionen, chemische Energie, kann genutzt werden. Doch wie steht es mit der mechanischen Energie? Kann man einfach an einem Molekül „ziehen“, um Bindungen zu brechen? Und ist die Art der zugeführten Energie relevant für den mechanistischen Reaktionsverlauf? Können gar andere, mit Wärme oder Licht nicht zugängliche Reaktionen möglich werden? Die Mechanopolymerchemie untersucht diese Zusammenhänge und ihre Grundlagen und hat in den letzten fünf Jahren erstaunliche neue Erkenntnisse zu Tage gefördert.



Translated Version (English) Starting a chemical reaction typically requires the addition of energy, at least to overcome the activation energy. The simplest approach is heating or irradiating the reaction mixture. In electrochemistry, electrical energy is transferred *via* electrodes into the mixture. Besides, other chemical reactions can release energy. But what about mechanical energy? Is it possible to simply "pull" a molecule to break bonds? Does the kind of supplied energy influence the mechanochemical reaction path? Are even reactions becoming possible that are not accessible by heating or light? Mechanochemistry of polymers investigates these relations and their foundations and has revealed surprising new insights in the last five years.

Scientific Contribution to this Publication

For this short review, I conducted the literature research and wrote the article with support of Anne Staubitz. I drew the schemes and Matthias Lipfert edited the images.



Molekulare Wirkung durch Kraft

Mechanopolymerchemie

MATHIAS SCHULZ-SENF | MATTHIAS LIPFERT | ANNE STAUBITZ

Um eine chemische Reaktion herbeizuführen, muss im Allgemeinen Energie zugeführt werden, zumindest, um die Aktivierungsbarriere zu überwinden. Im einfachsten Fall wird die Reaktionsmischung erhitzt oder bestrahlt; bei der Elektrochemie wird elektrische Energie über Elektroden eingebracht und auch die freiwerdende Energie anderer Reaktionen, chemische Energie, kann genutzt werden. Doch wie steht es mit der mechanischen Energie? Kann man einfach an einem Molekül „ziehen“, um Bindungen zu brechen? Und ist die Art der zugeführten Energie relevant für den mechanistischen Reaktionsverlauf? Können gar andere, mit Wärme oder Licht nicht zugängliche Reaktionen möglich werden? Die Mechanopolymerchemie untersucht diese Zusammenhänge und ihre Grundlagen und hat in den letzten fünf Jahren erstaunliche neue Erkenntnisse zu Tage gefördert [1].

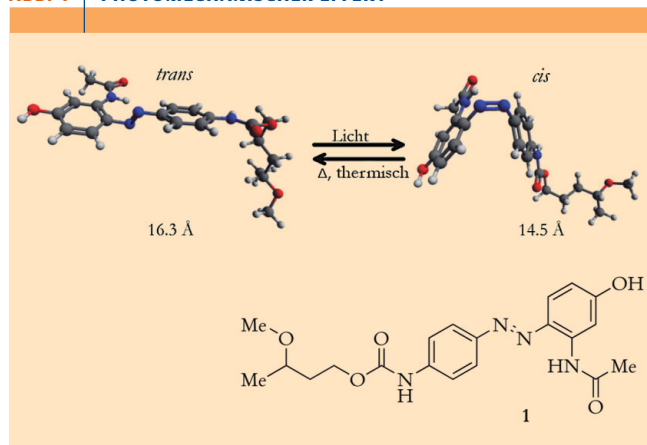
Mechanochemie bei Polymeren

Dass Polymere überhaupt existieren, war in den Anfängen der makromolekularen Chemie keine Selbstverständlichkeit. Hermann Staudingers Hypothese über die Existenz von Makromolekülen – lange Ketten sich wiederholender Einheiten – wurde weithin nicht akzeptiert und verspottet. So schrieb Heinrich Wieland (Nobelpreis 1927 für die Aufklärung der Zusammensetzung der Gallensäure) in einem Brief an Staudinger: „Lieber Herr Kollege, lassen Sie doch die Vorstellung mit den großen Molekülen, organische Moleküle mit einem Molekulargewicht über 5000 gibt es nicht. Reinigen Sie Ihre Produkte, wie z. B. den Kautschuk, dann werden diese kristallisieren und sich als niedermolekulare Stoffe erweisen.“

Staudinger ließ sich jedoch nicht beirren und verfolgte weiterhin seinen Weg, um die Existenz von Polymeren zu beweisen. So verwundert es nicht, dass er einen großen Teil seiner Aufmerksamkeit der Analyse dieser Molekülgruppe widmete. Staudingers wegweisende Entdeckungen wurden 1953 mit dem Nobelpreis für Chemie gewürdigt.

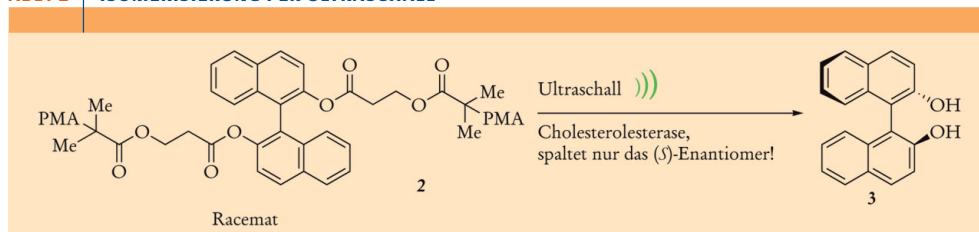
Anfang der 1930er Jahre beobachtete Staudinger beim Walzen von Kautschuk und Polystyrol eine Abnahme der Viskosität, die er als Molekulargewichtsabnahme interpretierte [2]. Damit stellte er als erster die Hypothese auf, dass mechanisch induzierte chemische Reaktionen in Polymeren ablaufen können. Aus dieser Entdeckung entwickelte sich in der kautschukverarbeitenden Industrie das Mastikationsverfahren: Dabei wird Kautschuk bei 70–80 °C gewalzt und die Polymerketten werden auseinandergerissen.

In der gleichen Dekade konnte mittels Ultraschall eine Zersetzung natürlicher Polymere wie Agar bewirkt werden [3]. Im Rahmen ihrer Untersuchungen zur Viskosität verschiedener langer Paraffinketten, $H(CH_2)_nH$, machten Kauzmann und Eyring eine bemerkenswerte Beobachtung [4]: Bei kurzen Kohlenwasserstoffketten ($n < 12$) zeigte sich ein linearer Anstieg der Viskosität mit der Kettenlänge. Der bei längeren Ketten beobachtete Anstieg folgte jedoch nicht mehr einer linearen Kurve. Vielmehr zeigten Kohlenwasserstoffe mit Kettenlängen $n > 30$ eine Viskosität, die eher für kürzere Oligomere mit $20 < n < 30$ typisch war. Dieses Ergebnis wurde so interpretiert, dass eine lange Polymerkette nicht als Gesamtheit, sondern in Kettensegmenten fließt. „Sehr lange Ketten“ hingegen (deren Länge nicht näher genannt wurde), zeigten eine deutlich niedrigere Viskosität als erwartet, was durch das Modell des segmentartigen Flusses nicht mehr erklärt werden konnte. So kamen Kauzmann und

ABB. 1 | PHOTOMECHANISCHER EFFEKT


Erstmalige Beschreibung des photomechanischen Effekts [7]. Ein Diazobenzolfarbstoff 1 wurde in Polymere wie Nylon oder Celluloseacetat nichtkovalent eingelagert. Durch Bestrahlung mit Licht erfolgt eine trans-cis-Isomerisierung des Farbstoffes, die mit einer Verkürzung des Moleküls einhergeht. Die Folge war eine makroskopisch sichtbare Verkürzung der Faser.

ABB. 2 | ISOMERISIERUNG PER ULTRASCHALL



Die enantiomeren Formen eines racemischen BINOL-haltigen Polymers **2** können unter Ultraschall reversibel isomerisieren. Nur das (S)-Enantiomer wird durch das Enzym hydrolysiert [11].

Eyring bereits 1940 zu der bemerkenswerten Hypothese, dass unter den angewandten rheologischen Bedingungen so hohe Zugkräfte entlang der Kette auftraten, dass diese reißen konnten, was zu kürzeren Segmenten führte.

Schon seit den 1930er Jahren war bekannt, dass Ultraschall in einer Polymerlösung zu einer Kettenverkürzung führt. Jedoch erst in den 1970er Jahren wurden die zugehörigen Mechanismen der Kraftübertragung genauer untersucht [5]. Die Ergebnisse schlugen sich aber nicht in einem breiteren Interesse an dem Phänomen nieder. Erst in den 1990er Jahren wurde von Smith das Verhalten von Polymeren in Lösung unter Ultraschall detailliert untersucht. Hierbei zeigte sich, dass die beobachtete Kettenverkürzung von Parametern wie Lösungsmittel, Konzentration der Polymere oder Intensität des Ultraschalls abhängt [6].

Der nächste große Schritt in der Untersuchung von mechanischen Effekten in Polymeren erfolgte mit der Beobachtung des photomechanischen Effekts in Nylon 1966 [7]. Hierbei zeigte ein aus Nylonfäden gewebtes Band mit einem nicht kovalent eingelagerten, dispergierten Diazoniumfarbstoff **1** bei Belichtung eine Längenänderung (Abbildung 1). Der Effekt war zwar relativ klein; es kam zu einer Verkürzung eines 30 cm langen Bandes um 0,33 mm. Bei einer Beladung von eininhalb Gewichtsprozent Farbstoff im Polymer ist der Effekt dennoch beachtlich. Noch erstaunlicher ist, dass diese Längenänderung reversibel war und in der Dunkelheit wieder rückgängig gemacht wurde. Dies war der erste Bericht, bei dem eine Längenänderung auf molekularer Ebene direkt in ein makroskopisches Bauteil übertragen wurde. Dieser Effekt konnte an verschiedenen Kunststoffen (Celluloseacetat [7], Polyethylacrylat [8], Polystyrol (PS) und Polymethylacrylat (PMA) [9]) mit Diazonium- und Spiropyranfarbstoffen gezeigt werden [10].

Der photomechanische Effekt und auch die zuvor beschriebenen mechanisch induzierten Kettenverkürzungen von Polymeren blieben aber ein Randphänomen der Forschung.

Neuere Entwicklungen

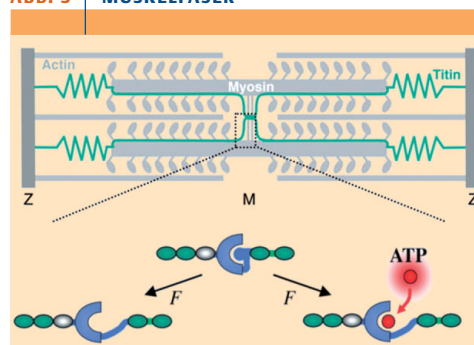
Erst in den 2000er Jahren wurden die Mechanochemie und die Mechanopolymerchemie wieder aufgegriffen. Hierbei wurden die historischen Wege umgekehrt beschritten. Zu-

nächst wurde Ultraschall als Kraftübertragungsquelle bei gelösten Polymeren angewandt und die gewonnenen Ergebnisse auf Festkörper übertragen. So sind bis heute homolytische Bindungsspaltungen mit oder ohne Abspaltung eines Molekülfragments, Cycloreversionen und Isomerisierungen durch rein mechanische Kräfte beschrieben worden.

Isomerisierungen

Die Isomerisierung eines zentral eingebauten Molekülbestandteils durch Zugkräfte ist rein intuitiv wenig verwunderlich und konnte beispielsweise an einem von PMA flankiertem BINOL-System **2** gezeigt werden. Durch Ultraschall können die Isomere des BINOL-Fragments hin und her isomerisieren. Da jedoch nur das (S)-Enantiomer in der anschließenden Hydrolyse durch das Enzym Cholesterolesterase umgesetzt wird, wird dieses Enantiomer dem Gleichgewicht beständig entzogen. So gelang eine dynamische

ABB. 3 | MUSKELFASER



Aufbau eines Sarkomers, der Basiseinheit einer Muskelfaser. Die eigentliche Muskelkontraktion kommt zustande, indem das Myosin am Aktin in Richtung der sogenannten Z-Scheiben vorbei gleitet. Titin verbindet die M- und die Z-Zone. Durch mechanische Dehnung wird eine ATP-Bindedomäne frei und ein dort liegender Tyrosinrest kann phosphoryliert werden. Dieses wiederum setzt eine Signalkaskade in Gang. Adaptiert von Ref. [13] und reproduziert mit Genehmigung der National Academy of Sciences of the USA, Copyright National Academy of Sciences of the USA 2008.

ABB. 4 SPALTUNG THERMISCH – ULTRASCHALL

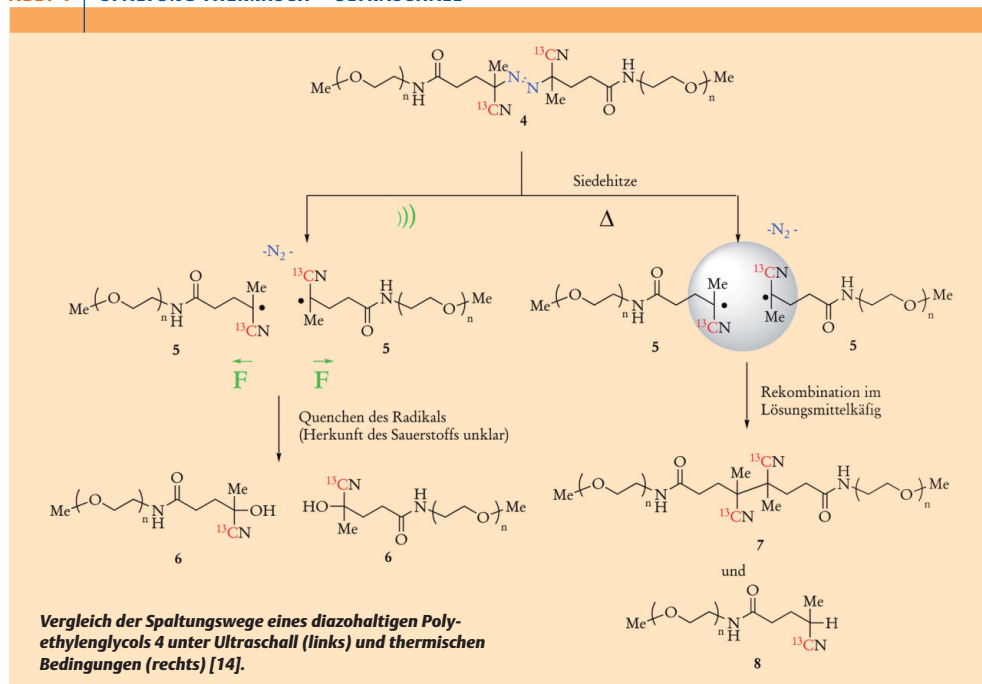
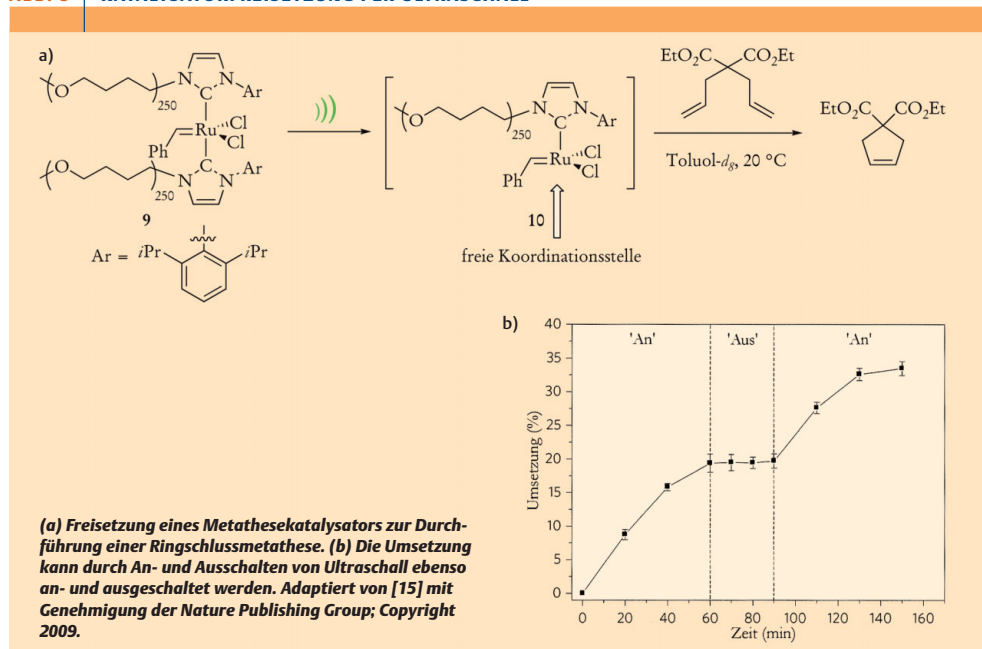


ABB. 5 KATALYSATORFREISETZUNG PER ULTRASCHALL



kinetische Racematspaltung, bei der letztendlich nahezu das gesamte Racemat in das (*S*)-BINOL **3** überführt wird (Abbildung 2) [11].

Besonders interessant aber ist die Bedeutung der Mechanopolymerchemie in biologischen Systemen. So häufen sich in letzter Zeit Berichte, dass Proteine nicht nur durch chemische Stimuli reguliert werden, sondern auch durch mechanische Reize [12]. Titin (auch Connectin) ist das größte bekannte Protein, das in quergestreiften Muskeln eine wichtige Rolle bei der Wahrnehmung von Kräften spielt. An seinem C-Terminus, wo es mit der sogenannten M-Bande des Sarkomers, der Basiseinheit der Muskelfaser, in Verbindung steht, konnte eine Kinase-Domäne nachgewiesen werden, die auf mechanischen Zug reagiert (Abbildung 3). Im entspannten Zustand sind eine entscheidende ATP-Bindungsstelle und ein autoinhibitorischer Tyrosinrest im gefalteten Protein verborgen und dadurch inhibiert. Um die ATP-Bindestelle zugänglich zu machen, und den autoinhibitorischen Tyrosinrest zu phosphorylieren, muss das Protein durch Kräfte partiell entfaltet werden. So kann eine Signalkaskade in Gang gebracht werden, die dem Körper die Belastung des Muskels mitteilt [13].

Homolytische Bindungsspaltungen

Der einfachste Fall einer Bindungsspaltung ist die Homolyse. Um zu demonstrieren, dass dies durch mechanische Kräfte im Ultraschallbad gelingen kann, wurde ein diazo-verbundenes Polyethylenglycol **4**, das strukturell eng mit dem klassischen Radikalstarter AIBN (*Azo-bis-isobutyronitril*) verwandt ist, als Modellsystem benutzt (Abbildung 4) [14]. Durch Ultraschalleinwirkung verringerte sich das Molekulargewicht von 40 kDa auf 20 kDa, während die Polydispersität der Probe klein blieb. Die Ketten wurden also offensichtlich mittig gespalten.

Eine thermische Kettenspaltung wurde durch Kühlung der Lösung auf 6–9 °C ausgeschlossen. In einem Kontroll-experiment wurde die Polymerprobe auf 82 °C erwärmt. Hierbei verringerte sich ebenfalls die Kettenlänge, aber in geringerem Maße als bei der Ultraschallbehandlung und bei Vergrößerung der Polydispersität. Die Autoren erklären diese Beobachtung mit einer Rekombination der radikalischen

Kettenenden von **5** im Lösungsmittelkäfig. Bei der Ultraschallbehandlung wurden die Kettenenden von **5** durch die Reißbewegung zu schnell aus dem Lösungsmittelkäfig entfernt, bevor die Rekombination stattfinden konnte. Die so postulierten Erklärungen konnten durch ¹³C-Isotopenmarkierung der Cyanogruppen (geminal zur Diazogruppe) bestätigt werden. Nach der Ultraschallbehandlung wurden die ¹³C-Atome am Kettenende von **6** nachgewiesen, hingegen befanden sie sich nach thermischer Behandlung vorwiegend in der Mitte von **7** als auch in kleineren Anteilen am Ende des Polymers **8**.

Spaltung koordinativer Bindungen

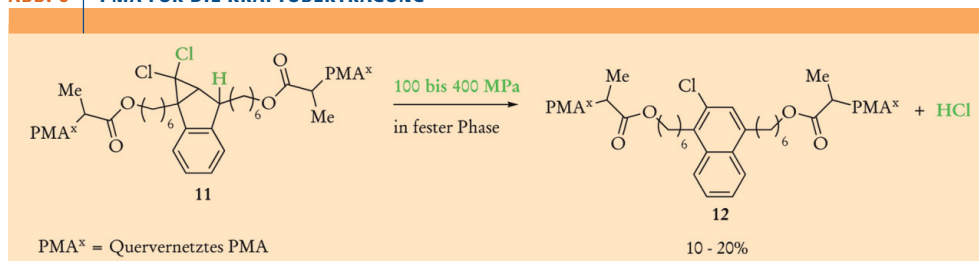
Nicht nur kovalente Bindungen lassen sich durch Ultraschalleinwirkung spalten, auch für koordinative Bindungen wurde die Bindungsspaltung berichtet.

Das Knüpfen von C-C-Bindungen erfolgt häufig über Übergangsmetallvermittelte Reaktionen. Hierbei werden Komplexe von Übergangsmetallen als Katalysatoren eingesetzt. Katalysatorkomplexe benötigen freie Koordinationsstellen, um beispielsweise Olefine und Aromaten zu komplexieren und in räumliche Nähe zu bringen und zu aktivieren.

Für den Metathesekatalysator **9** wurde die mechanische Aktivierung eindrucksvoll gezeigt (Abbildung 5 a) [15]. Durch Ultraschall kann einer der Carbenliganden zur Dissoziation angeregt werden, so dass im Komplex **10** eine freie Koordinationsstelle entsteht. An diese kann ein Olefin koordinieren und so eine Olefinmetathese initiiert werden. Ohne Ultraschall oder mit einem vergleichbaren, aber nicht polymergebundenen Metathesekatalysator konnte keine Umsetzung beobachtet werden. Es wurde auch gezeigt, dass die Reaktion bei Abschalten des Ultraschalls zum Erliegen kommt (Abbildung 5 b), aber danach wieder „angeschaltet“ werden kann. Es ist noch nicht gelungen, das An- und Ausschalten reversibel zu vollziehen, d. h. ohne Ultraschall regeneriert sich der Katalysator **9** nicht. Dies wäre ein bedeutender Meilenstein in der Entwicklung schaltbarer Katalysatoren.

Eine mögliche Anwendung solcher mechanosensitiven Katalysatoren wäre beispielsweise eine durch mechanische

ABB. 6 | PMA FÜR DIE KRAFTÜBERTRAGUNG



Unter Druck wird aus dem gem-Dichlorocyclopropan-System Salzsäure freigesetzt. Um die Kraftübertragung zu gewährleisten, ist die funktionelle Einheit in quervernetztes PMA eingebunden [16].

1: PERICYCLISCHE REAKTIONEN UND DIE WOODWARD-HOFFMANN-FUKUI-REGELN

Pericyclische Reaktionen verlaufen nicht über reaktive Zwischenstufen. Sämtliche Bindungsbrüche und -Bildungen der Reaktion laufen gleichzeitig, d. h. konzertiert ab.

Viele pericyclische Reaktionen weisen eine hohe Stereoselektivität auf. Die Grenzorbitaltheorie (engl. FMO-Theory, „frontier molecule orbital“) kann die entstehenden stereoselektiven Produkte erklären.

In Molekülen werden die Orbitale der einzelnen Atome (AO) durch Linearkombination zu Molekülorbitalen (MO) kombiniert. Hierbei entstehen „bindende“ und „antibindende“ MO. Bindende MO sind durch einen Energiegewinn verglichen zu den AO gekennzeichnet, antibindende MO durch einen Energieverlust. Der Energiegewinn für das bindende MO ist umso größer, je energetisch ähnlicher die kombinierten AO einander sind. Nach Kombination der Orbitale werden die Bindungselektronen gemäß der Hundschen Regeln in die entstandenen MO „verteilt“.

Die besetzten Orbitale niedriger Energien (d. h. unterhalb der Grenzorbitale) spielen im Allgemeinen bei Reaktionen keine Rolle. Daher werden in der Grenzorbitaltheorie lediglich die Orbitale an der Grenze zwischen besetzten und unbesetzten Orbitalen betrachtet. Dies sind das höchste besetzte MO („highest occupied molecule orbital“, HOMO) und das niedrigste unbesetzte MO („highest unoccupied molecule orbital“, LUMO). Radikale besitzen noch das einfach besetzte MO („single occupied molecule orbital“, SOMO).

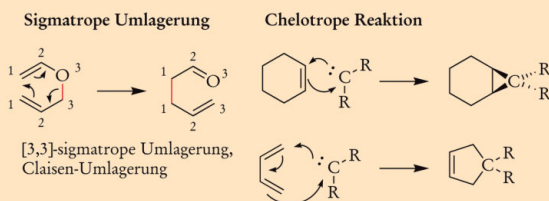


Abb. 14 Schematische Darstellung von sigmatropen Umlagerungen und chelotropen Reaktionen. Die wandernde Bindung in der Claisen-Umlagerung ist rot hervorgehoben. Chelotrope Reaktionen sind Ringchlussreaktionen z. B. zu einem 3- oder 5-Ring.

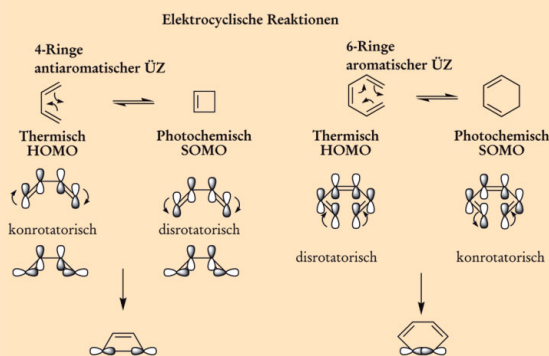


Abb. 15 Beispiele elektrocyclischer Reaktionen an 4- und 6-Ringen. Der Ringschluss geht jeweils mit dem Verlust einer π -Bindung einher. Im Beispiel der Isomerisierung von Merocyanin zum Spiropyran sind das beteiligte π -System sowie der resultierende Ring rot hervorgehoben (Abb. 11 und 12).



Abb. 16 Der Diels-Alder-Platz am Otto-Diels-Institut für Organische Chemie der Universität Kiel. Otto Diels und sein Schüler Kurt Alder entdeckten die nach ihnen benannte Reaktion 1929 in Kiel und wurden im Jahr 1950 mit dem Nobelpreis geehrt.

Damit eine pericyclische Reaktion abläuft, müssen die Energien des HOMO des einen und des LUMO des anderen Reaktanden einander ausreichend ähnlich sein und überlappen.

Pericyclische Reaktionen werden in vier Gruppen eingeteilt: Sigmatrope Umlagerungen (Abbildung 14), chelotrope Reaktionen (Abbildung 14), elektrocyclische Reaktionen (Abbildung 15) und Cycloadditionen (Abbildung 17).

Bei sigmatropen Umlagerungen wandern σ -Bindungen entlang eines π -Systems durch Verschieben der Doppelbindungen. Im gesamten Molekül bleibt die Anzahl an σ - und π -Bindungen gleich.

Chelotrope Reaktionen sind Ringbildungsreaktionen, bei denen eine isolierte π -Bindung oder ein lineares konjugiertes π -System mit einem einzelnen Atom mit einem voll besetzten p-Orbital einen Ring bildet. Damit muss das Atom entweder eine reaktive Spezies wie ein Singulettcarbon sein, oder anderweitig freie Elektronenpaare besitzen. Die ringöffnende Rückreaktion wird als Fragmentierung bezeichnet.

Als elektrocyclische Reaktion wird die Cyclisierung von linearen konjugierten π -Systemen unter Verlust einer π -Bindung und Ausprägung einer neuen σ -Bindung bezeichnet. Die Rückreaktion ist ebenfalls eine elektrocyclische Reaktion. Wichtige Beispiele sind die Isomerisierungen von Spiropyranen zu Merocyaninen (vgl. Kasten 2).

Cycloadditionen sind die Ringschlussreaktionen zweier linearer π -Systeme. Zwei π -Bindungen der Reaktanden werden zu zwei σ -Bindungen im Produkt. Die Rückreaktion wird als Cycloreversion bezeichnet. Eine allgemein bedeutende Cycloaddition ist die in den 1920ern in Kiel entdeckte Diels-Alder-Reaktion, bei der ein Dien und ein Alken zu einem Cyclohexen reagieren (Abbildung 16).

Die Regeln an zwei Beispielen erklärt:

Da die beschriebenen Reaktionen grenzorbitalkontrolliert ablaufen, spielt die Orbitalsymmetrie eine entscheidende Rolle. Diese symmetriekontrollierten Reaktionen verlaufen gemäß den Woodward-Hoffmann-Fukui-Regeln, benannt nach ihren Entdeckern.

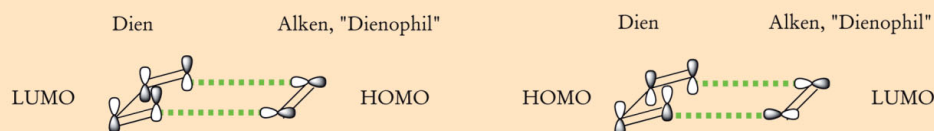
Die Regeln beschreiben den Zusammenhang zwischen der Anzahl der beteiligten Atome und den Reaktionsbedingungen. Cycloadditionen können prinzipiell auf zwei Arten initiiert werden: **thermisch oder photochemisch**.

Die bei der Bindungsbildung beteiligten Orbitale müssen jeweils konstruktiv interferieren. Bei der thermischen Aktivierung reagieren die Grenzorbitale der Startmaterialien direkt miteinander. Wie in Abbildung 17 gezeigt ist, lassen sich die Grenzorbitale eines Diens (z.B. HOMO) mit denen eines Alkens (z.B. LUMO) im Fall einer [4+2]-Cycloaddition aufgrund gleicher Vorzeichen linear kombinieren. Eine photochemische Aktivierung besetzt eines der beiden vorherigen LUMOs einfach mit einem Elektron und führt zu einem SOMO. Ein SOMO eines Diens kann mit einem LUMO eines Dienophils nicht auf beiden

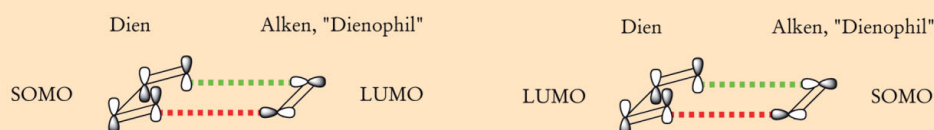
Seiten konstruktiv interferieren, genauso wenig wie ein LUMO eines Diens mit einem SOMO eines Dienophils. Damit sind [4+2]-Cycloaddition thermisch erlaubt und photochemisch verboten. [2+2]-Cycloadditionen zeigen ein gegensätzliches Verhalten. Hierbei ist die Symmetrie der Grenzorbitale der beteiligten Spezies gleich, sodass HOMO und LUMO aufgrund unterschiedlicher Symmetrie nicht kombiniert werden können. Erst nach photochemischer Anregung ist die Geometrie des entstandenen SOMOs kompatibel mit einem HOMO und eine Cycloaddition kann stattfinden.

[4+2]-Cycloaddition Diels-Alder-Reaktion

Thermisch

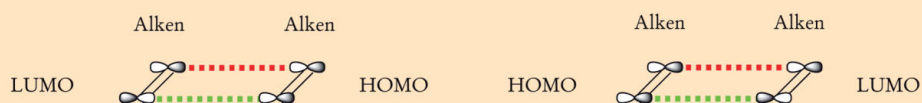


Photochemisch



[2+2]-Cycloaddition

Thermisch



Photochemisch

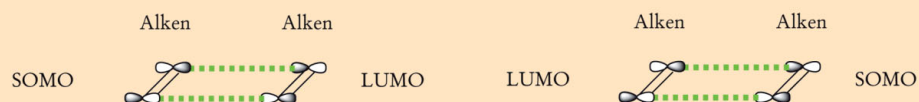


Abb. 17 Die Woodward-Hoffmann-Fukui-Regeln für den Fall der Diels-Alder-Reaktion und der [2+2]-Cycloaddition. Molekülorbitale gleicher Vorzeichen können konstruktiv kombiniert werden (grün gepunktete Linien), bei unterschiedlichen Vorzeichen geht die Kombination nicht mit einem Energiegewinn einher (rot gepunktete Linien). Die Darstellung veranschaulicht die Symmetrie der beteiligten Orbitale und vernachlässigt deren relative Energie.

ABB. 7 RINGÖFFNUNG

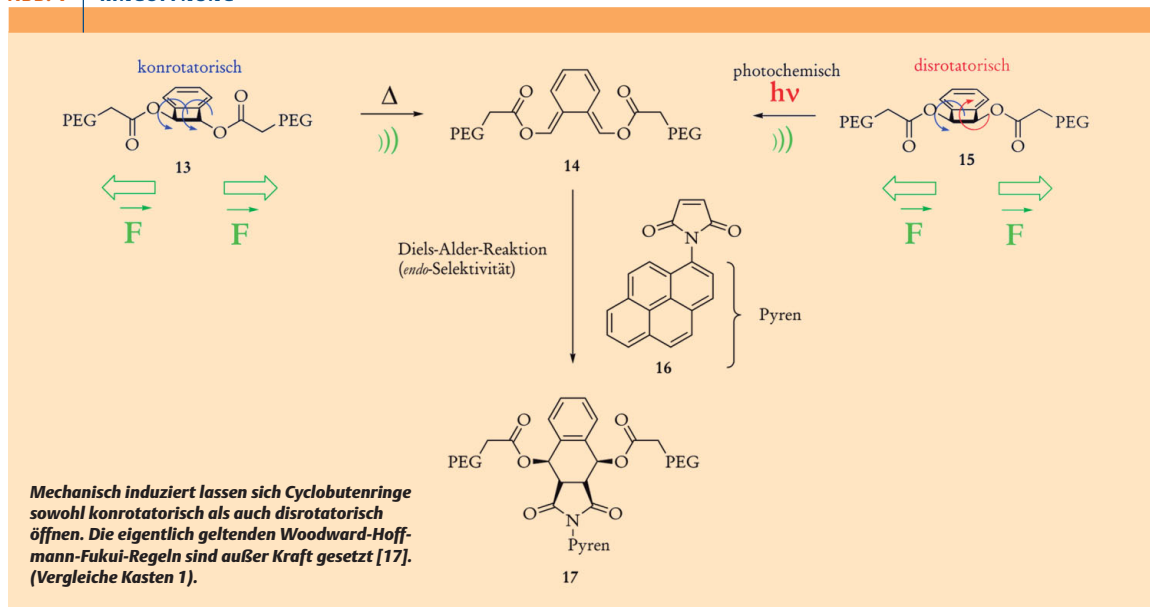
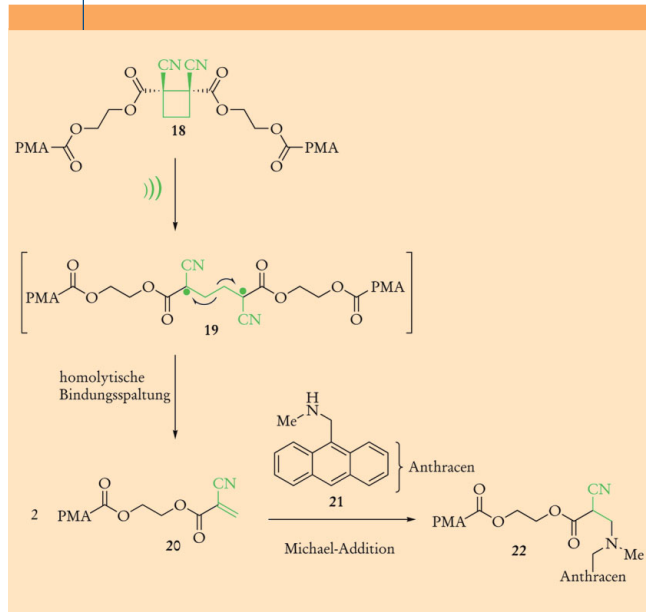


ABB. 8 KETTENSPLTUNG



Wird ein 1,2-Dicyanocyclobutan 18, eingebaut in PMA, durch Ultraschall aktiviert, entsteht über ein Diradikal 19 als Zwischenstufe ein Cyanoacrylat 20, dessen Existenz durch Abfangen mit einem Nukleophil 21 in einer Michael-Addition nachgewiesen werden konnte [18].

Energie induzierte Selbstheilung von Materialien. Die Möglichkeit, mechanophore Metathesekatalysatoren auch für die ringöffnende Metathesereaktion einzusetzen, wurde bereits demonstriert [15]. Inwiefern sich diese Erkenntnisse auf feste Materialien übertragen lassen, ist aber noch ungewiss.

Freisetzung kleiner Moleküle

Die Spaltung von Bindungen kann mit der Freisetzung kleiner Moleküle einhergehen. Im oben beschriebenen Fall der homolytischen Bindungsspaltung wurde Stickstoff aus diazohaltigen Polymeren freigesetzt.

Ein weiteres Beispiel für die mechanophore Freisetzung eines reaktiven Moleküls ist die Freisetzung von Salzsäure, HCl (Abbildung 6) [16]. Die labile, in PMA eingebaute mechanophore Einheit war ein modifiziertes Indensystem 11. Die *gem*-Dichlorcyclopropaneinheit steht dabei unter Ringspannung, während Produkt 12 nach Umlagerung und Eliminierung zusätzlich durch den entstandenen aromatischen Ring stabilisiert wird. Obwohl die für diese Reaktion notwendigen Drücke mit 100 bis 400 MPa recht hoch waren, ist die Umsetzung von bis zu 20 % der mechanophoren Einheiten in fester Phase beachtlich.

Cycloreversionen

Da offensichtlich selektiv schwache Bindungen gebrochen werden können, lässt sich Ultraschall für eine Reihe anderer Reaktionen als Energiequelle nutzen. Beispielsweise wurden mittlerweile verschiedene Ringöffnungsreaktionen

und Katalysatoraktivierungen durch Ultraschall induziert. Ein besonders ungewöhnlicher Fall sind die elektrozyklischen Ringöffnungsreaktionen, die Cycloreversionen. Dieser Typ der pericyclischen Reaktion folgt normalerweise den Woodward-Hoffmann-Fukui-Regeln (Infokasten 1).

Ein benzenelliertes Cyclobuten **13** in der Mitte eines **Polyethylenglycol**-Polymers konnte durch Ultraschall zur Ringöffnung gebracht werden (Abbildung 7) [17]. Dabei entstand das reaktive cyclohexadienanelierte Butadien **14**, welches mit einem ^{13}C -markierten Maleimid **16** abgefangen und analysiert werden konnte. Ungewöhnlich waren allerdings die Beobachtungen, die beim Einsatz der *cis*- und *trans*-Stereoisomere der Cyclobutene gemacht wurden: Das Butadien **14**, in dem die beiden exocyclischen Doppelbindungen *trans*-konfiguriert sind, kann *thermisch* nur aus dem *trans*-Cyclobuten **13** entstehen (da die Woodward-Hoffmann-Fukui-Regeln eine konrotatorische Ringöffnung bedingen), während es *photochemisch* nur aus dem *cis*-Cyclobuten **15** durch disrotatorische Ringöffnung entstehen kann.

Mechanochemisch jedoch wird das 5,6-Bismethylencyclohexa-1,3-dien **14** aus beiden, *cis*- und *trans*-Butadien erzeugt, so dass die Woodward-Hoffmann-Fukui-Regeln hier außer Kraft gesetzt sind und ein radikalischer Verlauf angenommen werden kann. Streng genommen handelt es sich also bei diesen ultraschallinduzierten Reaktionen nicht um pericyclische Reaktionen, sondern sie können auch bei den homolytischen Bindungsspaltungen (siehe vorheriger Abschnitt) eingeordnet werden.

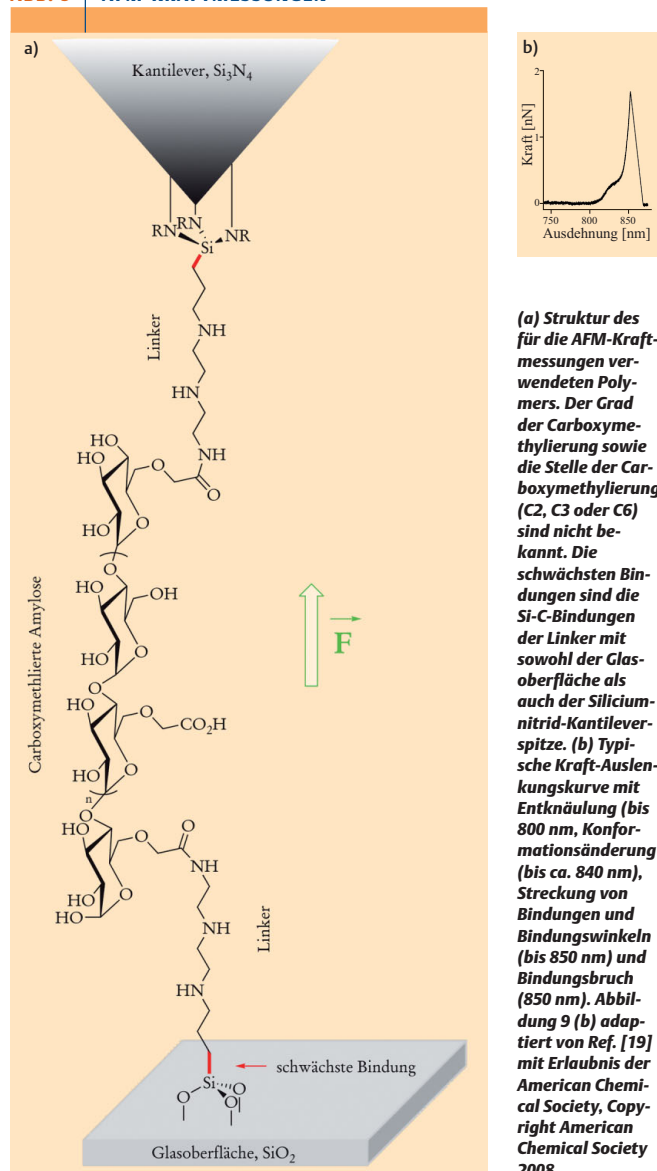
Nach dieser erfolgreichen Demonstration der elektrozyklischen Ringöffnung begann die Entwicklung von Systemen, die nicht nur von theoretischem Interesse sind, sondern auch erste Anwendungen versprechen. Ein Ansatz war die Untersuchung einer Cycloreversion, die unter Zug zum Reißen einer Polymerkette führt, wobei aber die entstehenden Kettenenden hochreaktiv sind [18]. Dadurch soll eine anschließende Quervernetzungsreaktion möglich sein, die so nach einer Kurzzeitbelastung des Materials zur Selbstheilung des Werkstückes führt. Diese Idee wurde durch den Einbau eines 1,2-Dicyanocyclobutans in PMA **18** erprobt (Abbildung 8). Durch Ultraschall konnten Zugkräfte aufgebaut werden, die durch homolytische Bindungsspaltung wahrscheinlich zum Diradikal **19** führten, das dann unter Rekombination zu zwei Molekülen **20** reagierte. Der Nachweis dieses Cyanoacrylates gelang eindeutig durch Abfangen der relativ reaktiven Endgruppe durch ein sekundäres Amin **21** in einer Michael-Reaktion zum Produkt **22**.

Kraftübertragung auf Moleküle Analyse der Kraftübertragung

Mögen die oben genannten Beispiele auf den ersten Blick eher speziell wirken, die Bedeutung der Mechanochemie der Polymere ist jedem intuitiv bekannt: Seile können reißen, Plastikschüsseln zerbrechen oder Beschichtungen zerkratzt werden.

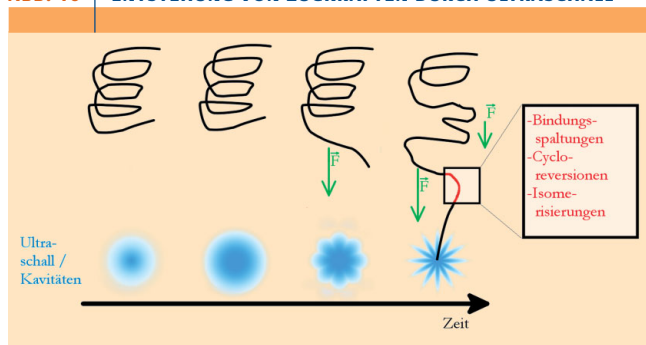
Um dieses Materialversagen auf der Molekülebene besser verstehen zu können, kann die dynamische Einzelmo-

ABB. 9 AFM-KRAFTMESSUNGEN



(a) Struktur des für die AFM-Kraftmessungen verwendeten Polymeres. Der Grad der Carboxymethylierung sowie die Stelle der Carboxymethylierung (C2, C3 oder C6) sind nicht bekannt. Die schwächsten Bindungen sind die Si-C-Bindungen der Linker mit sowohl der Glasoberfläche als auch der Siliciumnitrid-Kantileverspitze. (b) Typische Kraft-Auslenkungskurve mit Entknäulung (bis 800 nm), Konformationsänderung (bis ca. 840 nm), Streckung von Bindungen und Bindungswinkeln (bis 850 nm) und Bindungsbruch (850 nm). Abbildung 9 (b) adaptiert von Ref. [19] mit Erlaubnis der American Chemical Society, Copyright American Chemical Society 2008.

kül-Kraftmikroskopie („Atomic Force Microscopy“, AFM) mittels eines Rasterkraftmikroskops angewandt werden. Hierbei wird ein Polymermolekül zwischen einer Oberfläche und einem Kantilever fixiert und das Molekül gedehnt, wobei die aufgewendete Kraft gemessen wird. Im dargestellten Beispiel handelt es sich um ein carboxymethyliertes Amylosemolekül, das mit einem Aminosilylan-Anker auf einer Glasoberfläche fixiert wurde (Abbildung 9 a). Die

ABB. 10 | ENTSTEHUNG VON ZUGKRÄFTEN DURCH ULTRASCHALL


Die Ausbreitung von Ultraschallwellen in einer Flüssigkeit bedeutet, dass sich eine regelmäßige Abfolge von Überdruck- durch Kompression, und Unterdruckphasen (Rarefaktion) von der Ultraschallquelle aus ausbreitet. Infolge des Unterdrucks können im Ultraschallfeld kleine Vakuumbasen (Hohlräume) entstehen. Wenn diese kollabieren, werden die Polymerketten in der Nähe mitgerissen, so dass entlang der Polymerketten Kräfte auftreten, die zu chemischen Reaktionen führen können. Adaptiert von [1c] und reproduziert mit Erlaubnis von Wiley VCH, Copyright Wiley VCH 2013.

schwächste Bindung ist hierbei die Si-C-Bindung, die zuerst reißt. Trägt man nun die Ausdehnung gegen die aufgewendete Kraft auf, so ergeben sich typische Kraft-Ausdehnungskurven (Abbildung 9 b) [19].

Bei einer Distanz von weniger als 800 nm wird lediglich die Verknäuelung des Polymers aufgehoben, doch ab einem gewissen Wert steigt die aufgewendete Kraft an: Es kommt zu einer Änderung der Sesselkonformation der Glycosylbausteine zur Wannenkonformation. Danach wird ein schlagartiger Anstieg der Kraft beobachtet, da nun Bindungen gedehnt und Bindungswinkel aufgeweitet werden und so aus dem potentiellen Energieminimum gebracht werden. Dann erfolgt ein schlagartiges Reißen der Polymerkette. Das Einwirken der Kraft erniedrigt somit die Aktivierungsenergie der Bindungsspaltung. Die Bindungsspaltung ist jedoch trotz Aufwendung von Kraft ein thermischer Prozess. Außerdem konnte gezeigt werden, dass eine höhere Zuggeschwindigkeit die für einen Bindungsbruch nötigen Kräfte erhöht. Eine langsame, kontinuierliche Krafteinwirkung kann also ein Polymer über längere Zeit erheblich schwächen.

Ein homolytischer Bindungsbruch ist allerdings nur unter bestimmten Bedingungen das Resultat des Ziehens an den Amylosemolekülen. Sind die Proben Feuchtigkeit ausgesetzt, so wird beim Anlegen von Zugkräften im AFM nicht der beschriebene Bindungsbruch beobachtet. Stattdessen tritt eine kraftinduzierte Hydrolyse der Glykosidbindung zwischen der Amylose und dem Linker auf [20].

Übertragung der Kraft auf Mechanophore in flüssiger Phase

Eine wichtige Fragestellung ist jedoch, wie Kraft auf Moleküle in einer Lösung übertragen werden kann. Gängige

Möglichkeiten sind Ultraschall, aber auch das Pressen der Reaktionsmischung durch Düsen.

Ultraschallwellen haben eine Frequenz von über 20 kHz. Sie erzeugen in Flüssigkeiten und Lösungen mikroskopisch kleine Bläschen, Kavitäten. Das Kollabieren dieser Blasen führt zu einem schlagartigen Zurückströmen der umgebenden Flüssigkeit. Hierbei können enorme Druckschwankungen und -spitzen in der Größenordnung von mehreren 100 MPa erreicht werden. In der Nähe kollabierender Kavitäten befindliche Polymerketten werden mit dem Lösungsmittel in das freie Volumen gezogen. Hierbei werden die Kettenenden nahe den Kavitäten deutlich schneller beschleunigt als die weiter entfernten Kettenenden. Die auftretenden Geschwindigkeitsgradienten innerhalb der Kette erzeugen eine potentielle Energie, die genügt, um Bindungen zu brechen (Abbildung 10) [1c].

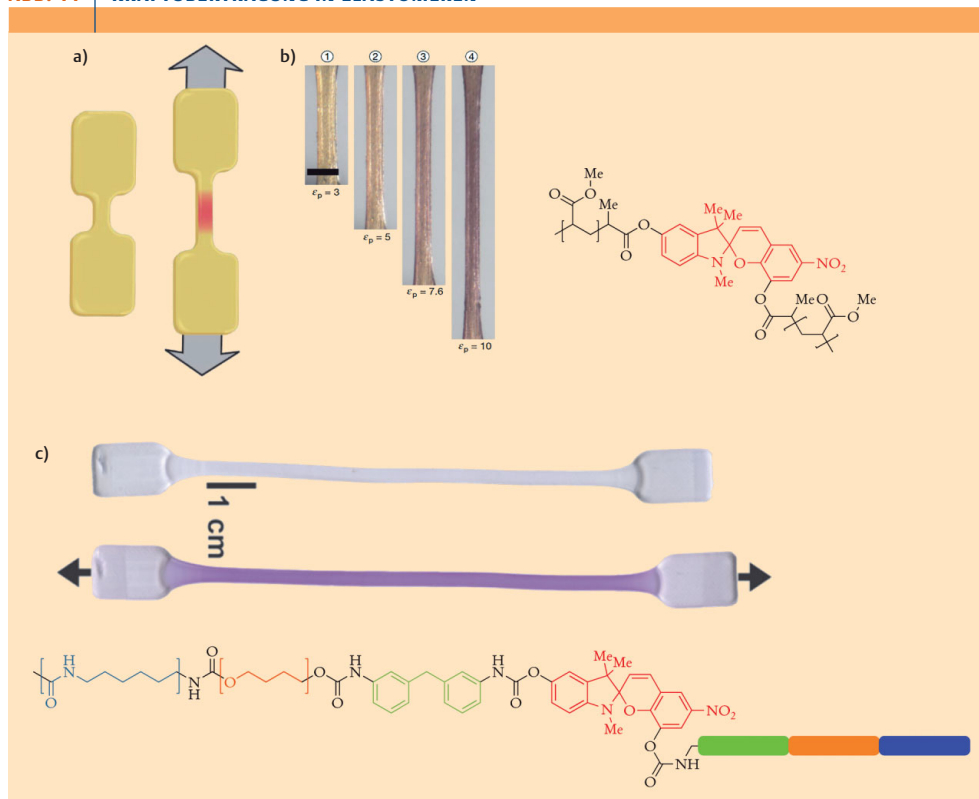
Kraftübertragung in festen Mechanophoren

Um die Möglichkeiten der Kraftübertragung in fester Phase zu diskutieren, muss man sich über das Verhalten der Polymerketten im festen Zustand Gedanken machen: Da die Ketten in Polymeren sehr lang sind, kommt es zu starken Kettenverwicklungen. Dadurch wird verhindert, dass sich das Ensemble aus Polymerketten vollständig regelmäßig anordnet. So bilden Polymere keine klassischen Kristalle wie niedermolekulare Stoffe, sondern weisen allenfalls kristalline Teilbereiche auf, die von amorphen Bereichen umgeben sind. Wenn sich einzelne kristalline Bereiche im Feststoff ausprägen, spricht man von Semikristalliten. In amorphen Polymeren sind die Polymerketten so stark verknäuel, dass sich keine kristallinen Bereiche ausprägen.

Während klassische, molekulare Substanzen die Aggregatzustände fest, flüssig und gasförmig aufweisen, gibt es bei den meisten Polymeren noch zusätzlich den viskoelastischen Zustand. Dieser tritt im Temperaturbereich zwischen der Glasübergangstemperatur, T_g , und der Schmelztemperatur auf. Unterhalb von T_g liegen Polymere in einem festen glasähnlichen Zustand vor. Aufgrund der kovalenten Bindungen der Monomere in der Polymerkette ist jede Translationsbewegung eines Segments ein Prozess, der sich auf den Rest der Kette auswirkt. Dadurch bildet sich ein fließendes System nur schwer aus. In vereinfachter Weise kann man die Bewegung einzelner Kettensegmente betrachten. Oberhalb von T_g werden die vorher zu einem Glas erstarrten Polymerkettensegmente beweglicher und durch temperaturbedingte Ausdehnung erhöht sich das freie Volumen. Die Kettensegmente können sich durch Belegung dieses zusätzlichen Volumens stärker bewegen, was makroskopisch zu einer gummiähnlichen Konsistenz führt. Abhängig von der vorliegenden Phase ergeben sich zwei Möglichkeiten, Kräfte an Polymerketten anzulegen.

Polymere wie PMA oder PU besitzen eine T_g unterhalb von 25 °C und liegen in dem elastischen, gummiähnlichen Zustand vor. Proben dieser Polymere lassen sich einfach dehnen. Hierbei werden die zuvor verknäuelten Ketten zunächst gestreckt, aneinander vorbeigezogen und brechen ir-

ABB. 11 | KRAFTÜBERTRAGUNG IN ELASTOMEREN



(a) Schematische Darstellung von Hundeknochenwerkstücken, welche gedehnt werden und eine Sollbruchstelle aufweisen [24]. (b) Dehnen eines PMA-Hundeknochens mit Spiropyranen in der Hauptkette. Das Polymer verfärbt sich deutlich, was die Schaltung vom Spiropyran ins Merocyanin zeigt. (c) Spiropyran in PU. Das zunächst weiße Polymer wird durch Dehnung violett (Übergang Spiropyran zum Merocyanin). Nach Absetzen der Kraft erfolgt zunächst kein spontanes Rückschalten. Dies ist jedoch mittels Belichtung möglich. Damit ist dies das erste Elastomer, das reversibel geschaltet werden konnte [22]. (a) und (b): adaptiert von [24] und reproduziert mit Genehmigung der Nature Publishing Group, Copyright Nature Publishing Group 2009. (c): adaptiert von [22] mit Genehmigung der American Chemical Society, Copyright American Chemical Society 2010.

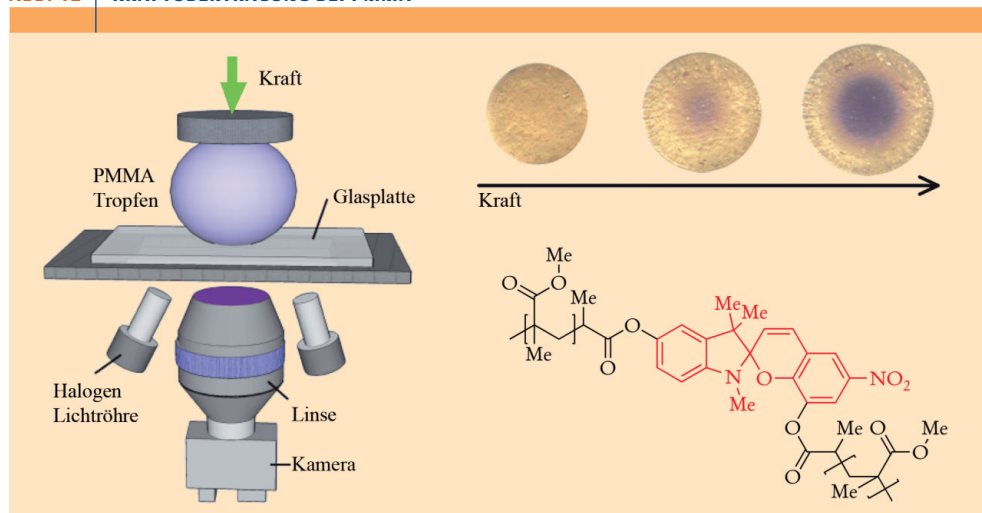
gendwann am schwächsten Glied. Um die Wirkung von Kraft auf einen Festkörper aus einem solchen Material zu testen, stellt man ein hundeknochenförmiges Werkstück her, das eine dünne Sollbruchstelle in der Mitte aufweist (Abbildung 11 a). Dann wird an beiden Enden eine definierte Kraft ausgeübt und die Veränderung des Feststoffes analysiert (Abbildung 11 b und c).

Bei PMMA ist die Glasübergangstemperatur durch die zusätzliche Methylgruppe im Vergleich zu PMA höher als Raumtemperatur (T_g von PMMA: 105 °C; T_g von PMA: 10 °C) [21]. Da sie somit im glasähnlichen Zustand vorliegen, lassen sich Werkstücke aus PMMA nicht bei Raumtemperatur dehnen. Der experimentelle Aufbau zur Analyse der Auswirkung mechanischer Kraft muss daher anders gestaltet werden. Die Probe wird in einen schraubstockähnlichen

Aufbau gespannt und zusammengepresst (Abbildung 12). Die hierbei auftretenden Kräfte innerhalb des Polymers sind groß genug, um die mechanophoren Gruppen zu aktivieren.

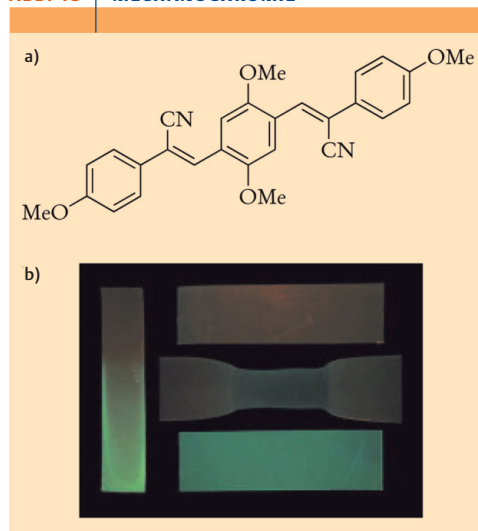
Basierend auf den zuvor diskutierten mittels Ultraschall erzeugten Effekten an gelösten Polymeren wurde nun das Verhalten ähnlicher Systeme in Polymerfeststoffen untersucht. Die Arbeitsgruppe um Moore zeigte, dass sich Spiropyranfarbstoffe in sowohl elastischen (PMA, PU, Abbildung 11) als auch thermoplastischen (PMMA, PS, Abbildung 12) Polymerwerkstücken durch Anlegen von Druck- oder Zugkräften z. T. reversibel schalten lassen, was erstmals auch an praktische Anwendungen der Mechanochemie denken lässt. Das spiropyranhaltige PU stellt eine Neuheit dar: es war erstmals möglich, nach Beenden der Dehnung

ABB. 12 | KRAFTÜBERTRAGUNG BEI PMMA



Das Spiropyran-PMMA Copolymer wird auf einer Glasplatte zusammengedrückt und währenddessen beobachtet. Mit zunehmender Stauchung wird ebenfalls die C-O-Bindung im Spiropyran gebrochen und eine Farbänderung beobachtet [24]. Adaptiert von [24] mit Genehmigung der Nature Publishing Group, Copyright Nature Publishing Group 2009.

ABB. 13 | MECHANOCROMIE



(a) Struktur des verwendeten OPV Farbstoff. (b) In LLDPE (Lineares Low Density Polyethylen) eingelagert zeigen die Farbstoffaggregate eine rote Färbung, während isolierte Moleküle eine grüne Färbung aufweisen. Das Aufbrechen der Aggregate kann sowohl prozesstechnisch hervorgerufen werden (links und unten rechts), als auch durch Dehnen des Werkstücks (mitte rechts). Adaptiert von [23] und reproduziert mit Erlaubnis von Wiley VCH, Copyright Wiley VCH 2013.

den verfarbten Feststoff mittels Belichtung mit sichtbarem Licht wieder zurückzuschalten [22].

Um eine Farbänderung mechanochromer Systeme hervorzurufen, muss der Farbstoff jedoch nicht zwingend kovalent in die Polymerumgebung eingebunden werden. Oligo(*p*-phenylvinylene) (OPV) sind eine Farbstoffklasse, die in Lösungen Aggregate bildet. Diese Aggregate bilden sich auch bei der Verarbeitung in Polymeren. In der Polymer-schmelze entstehen regelmäßig angeordnete Bereiche der Farbstoffe. Nach Erstarren der Schmelze sind diese fixiert. Wird nun ein wie oben beschriebenes Hundeknochenwerkstück gedehnt, werden die Farbstoffaggregate auseinandergerissen und die Farbe verändert sich (Abbildung 13). Diese Farbänderung lässt sich nicht wieder rückgängig machen [1b, 23].

Bedeutung und mögliche Einsatzgebiete der Mechanochemie

Insbesondere die Verknüpfung von Phänomenen der makroskopischen Welt wie Streckung oder Stauchung mit molekularen Effekten – Brechen von Bindungen – prädestiniert mechanophore Polymere für entsprechende Sensoren. Ruft die mechanische Belastung eine Farbänderung hervor, spricht man von Chromophoren.

Ein besonders interessanter Chromophor ist das Spiropyranraster, welches in eine Merocyaninform isomerisieren kann. Diese Umwandlung kann durch mehrere Stimuli hervorgerufen werden, z. B. Bestrahlung mit UV-Licht, Absenkung des pH-Wertes oder Zugabe von Lewis-Säuren (Infokasten 2). Die gezeigten kraftinduzierten Isomerisierungen

2: DIE SCHALTZUSTÄNDE VON SPIROPYRANEN

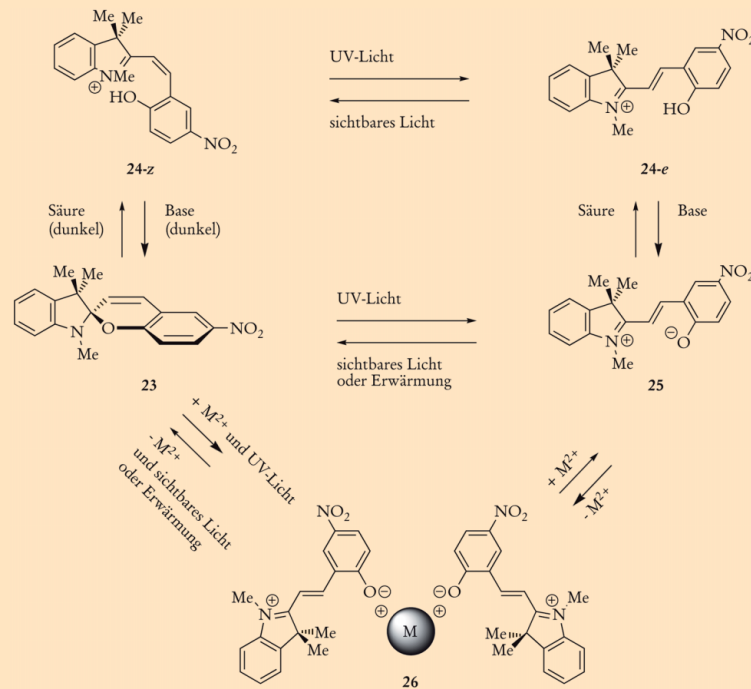


Abb. 18 Strukturelle Änderungen von Spiropyranverbindungen 23 unter Einfluss der Stimuli Licht, pH-Wert und Metallionen. Bestrahlung von 23 mit UV-Licht führt über eine electrocyclische Ringöffnung zur offenen Merocyaninform 25. Das Merocyanin 25 wird durch Zugabe von Säure ebenso protoniert wie das Spiropyran 23, welches auch ohne zusätzliche Beleuchtung zum protonierten Merocyanin 24-z reagiert. Die Spezies 23 und 25 bilden bei Zugabe zweiwertiger Metallionen einen $M(MC)_2$ Komplex 26.



Abb. 19 Einfluss verschiedener Metallionen auf die Farbe von Spiropyran 23 und gebildetem Komplex 26. In den Kolben befinden sich gesättigte Lösungen folgender Salze in Aceton: $MgCl_2$ (links), $NiCl_2$ (mitte), $CuSO_4$ (rechts). Beleuchtet wurde mit einer UV-LED ($\lambda = 366 \text{ nm}$, $P = 500 \text{ mW}$) über zweimal 1 min.

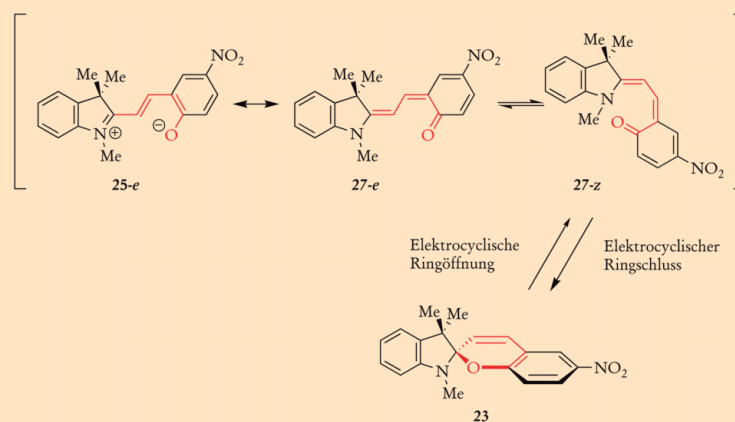


Abb. 20 Electrocyclische Ringöffnung und -schluss zwischen Spiropyran und Merocyaninform. Die offene Spezies liegt als Gleichgewicht zwischen zwitterionischer und chinoider Form vor. Das z-Chinoid 27-z ist aufgrund der räumlichen Nähe zwischen den Sauerstoff- und Stickstoffatomen in der Lage, einen electrocyclischen Ringschluss zu vollziehen.

(Abbildungen 11 und 12) lassen spiropyranbasierte Mechanophore als Indikatoren für Dehnungen in Bauteilen wie beispielsweise Brücken denkbar werden. Ein als Lack aufgetragenes Mechanophor könnte durch Farbänderung das Ausdehnen von Bauteilen anzeigen. Hierbei müssen allerdings Aspekte wie die Photo- und pH-Sensitivität von Spiropyranen beachtet werden. Spiropyrane können sich nach etlichen Schaltzyklen zersetzen, wenn die offene Form von

Sauerstoff angegriffen wird und dann nicht mehr zurückschalten kann.

Die OPV-basierten Systeme bieten aufgrund ihrer Funktionsweise etliche Vorteile: das für Spiropyrane bekannte Problem des Photobleachings durch UV-Licht entfällt hier und da die Farbstoffe nicht kovalent in Polymere eingebaut werden, ist die Synthese und Verarbeitung deutlich einfacher als für spiropyranbasierte Systeme. Die mechanisch

GLOSSAR

BINOL (1,1'-Binaphthol): Chiraler Ligand. In Kreuzkupplungsreaktionen genutzt, um am Katalysator eine chirale Umgebung zu erzeugen und stereoselektiv Produkte zu erzeugen.

C-Terminus (N-Terminus): Enden eines (Poly-)Peptidstrangs. Bezeichnet die Carbonsäure- (C-Terminus) und die Aminfunktionalität (N-Terminus).

Carben: Reaktive Kohlenstoffspezies mit freiem Elektronenpaar am Kohlenstoff (Singlet-Carben), oder zwei ungepaarten Elektronen am Kohlenstoff (Triplet-Carben).

Chromophor (gr. „Farbträger“): Für die Farbigkeit verantwortlicher Teil in Farbstoffen und Materialien.

Elastomer: Verformbares, festes Polymer. Nach Beendigung der Belastung kehrt es in die ursprüngliche Form zurück.

Mechanophor: Farbstoff, der auf mechanische Einflüsse durch Änderung der Farbigkeit reagiert.

Metathese: Rutheniumkatalysierte Kreuzkupplung. Kupplung zweier Alkene unter Verlust einer Ethyleneinheit.

Polydispersität (Polydispersitätsindex, PDI): Maß für die Einheitlichkeit der Kettenlängen in Polymeren. Definiert als Quotient aus durchschnittlicher und massengewichteter Kettenlänge. Sind alle Ketten gleich lang, ist der PDI gleich 1.

Rasterkraftmikroskopie (AFM): Methode zur Oberflächenanalyse. Eine Nadel („Kantilever“) wird in Reichweite atomarer Kräfte (Van-der-Waals, Coulomb) an einer Oberfläche entlanggeführt. Kann auch zur Analyse einzelner Moleküle verwendet werden.

Thermoplast: In bestimmtem Temperaturbereich verformbares und flüssiges Polymer. Unterhalb dieser Temperatur (T_g) liegt es in einem glasähnlichen Zustand vor.

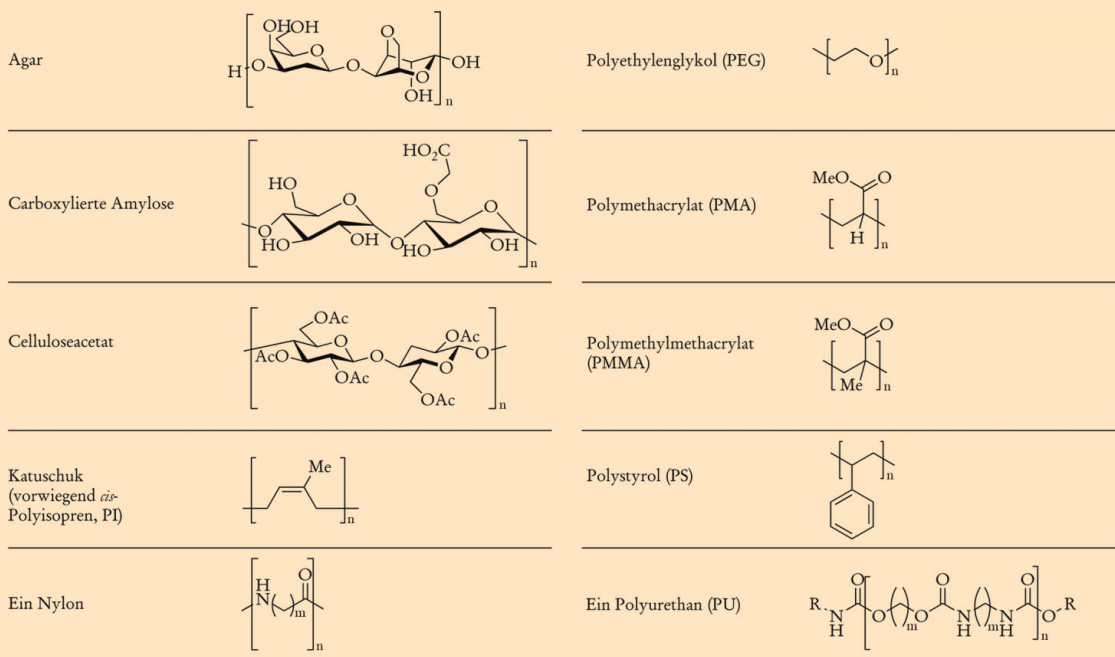


Abb. 21 Strukturen der im Text diskutierten Polymere.

gestörten Farbstoffaggregate lassen sich jedoch nicht wieder in ihre ursprüngliche Form bringen (Abbildung 13). Dies macht OPVs als dauerhaft abzulesende Indikatoren mechanischer Belastung denkbar.

Sowohl die mechanisch induzierte Freisetzung kleiner Moleküle als auch die Katalysatoraktivierung versprechen Anwendungen im Bereich selbstheilender Werkstoffe. Die gebildeten reaktiven Spezies können das Material durch die geeigneten Reaktionen (Abbildungen 5,6 und 8) regenerieren.

In der Polymertechnik sind Kraftübertragungen wie Molecular Milling, Mastikation oder Spritzguss üblich; hier handelt es sich um Polymere in fester, viskoelastischer oder geschmolzener Phase. Bei der Verarbeitung mittels Spritzguss- und Extrusionsverfahren treten große Scherkräfte im Material auf. Daher eignen sich diese Verfahren nicht zur Herstellung von Polymeren, welche sich durch mechanophore Aktivierung selbst heilen können. Dagegen lässt sich die Behandlung von Polymeren in Lösungen mit Ultraschall besonders leicht durchführen und wird deshalb in der Grundlagenforschung eingesetzt, um molekulare Vorgänge unter Kraftereinwirkung besser erfassen zu können.

Die mechanische Aktivierung von Polymeren in Lösung ist nicht nur von akademischem Interesse. Gerade das erwähnte An- und Ausschalten des Metathesekatalysators zeigt das Potential mechanophorer Systeme. Ultraschall als Initiator für chemische Reaktionen stellt eine interessante Alternative zu den herkömmlichen Initiatoren Licht und Wärme dar und lässt sich unabhängig von ihnen einsetzen.

Zusammenfassung

Chemischen Reaktionen kann auf verschiedenen Wegen Energie zugeführt werden, doch mechanische Energie blieb bisher ein Randphänomen. Ein selektiver Bindungsbruch in kleinen Molekülen benötigt große mechanische Kräfte, die sich nicht einfach auf einzelne Bindungen übertragen lassen. Da mechanische Arbeit das Produkt aus Kraft und Weg ist, ergeben sich für kurze Wege (im Bereich von Bindungslängen) große Kräfte für eine Bindungsspaltung. Makromoleküle sind jedoch länger und durch den größeren Weg sind die benötigten Kräfte für eine Bindungsspaltung geringer. Es wurden Bindungsspaltungen, Cycloreversionen und Isomerisierungen unter Einfluss mechanischer Energie beobachtet. Weiterhin kann mechanische Energie auch andere Reaktionsmechanismen hervorrufen als thermische oder Photoenergie. Praktische Anwendungen in diesem jungen Forschungsfeld entstehen noch und reichen derzeit von besserem Verständnis der Polymerzersetzung durch mechanische Kräfte zur Entwicklung von Dehnungssensoren mit mechanochromen Polymeren.

Summary

Although many methods can be employed to transfer energy to a chemical reaction, mechanical energy has not been widely used: It is difficult to apply mechanical forces high enough to lead to breaking bonds to small molecules. Work is the

product of force and displacement but when the distances are small, very high forces are needed to obtain sufficient energy to break a bond. The situation is different in polymers, where the path length can be high. Here, bond cleavage, cycloreversions and isomerisations can be observed when mechanical energy is supplied, both in solution and solid systems. Mechanical energy can lead to different mechanistic pathways than those observed under thermal conditions or irradiation. Practical applications of the mechanochemistry of polymers are only just emerging and range from a better understanding of polymer decomposition under force to the development of strain sensors using mechanochromic polymers.

Schlagwörter

Polymerchemie, Schaltbare Moleküle, Mechanochemie, Mechanophore, Spiropyrane, Mechanochromie

Literatur

- [1] (a) M. K. Beyer und H. Clausen-Schaumann *Chem. Rev.* **2005**, *105*, 2921; (b) M. M. Caruso, D. A. Davis, Q. Shen, S. A. Odom, N. R. Sottos, S. R. White und J. S. Moore *Chem. Rev.* **2009**, *109*, 5755; (c) J. N. Brantley, K. M. Wiggins und C. W. Bielawski *Polym. Int.* **2013**, *62*, 2.
- [2] (a) H. Staudinger *Ber. Dtsch. Chem. Ges.* **1930**, *63*, 921; (b) H. Staudinger und W. Heuer *Ber. Dtsch. Chem. Ges.* **1934**, *67*, 1159.
- [3] E. W. Flösdorf und L. A. Chambers *J. Am. Chem. Soc.* **1933**, *55*, 3051.
- [4] W. Kauzmann und H. Eyring *J. Am. Chem. Soc.* **1940**, *62*, 3113.
- [5] A. M. Basedow und K. H. Ebert *Makromol. Chem.* **1975**, *176*, 745.
- [6] (a) G. J. Price und P. F. Smith *Polym. Int.* **1991**, *24*, 159; (b) G. J. Price und P. F. Smith *Polymer* **1993**, *34*, 4111; (c) G. J. Price und P. F. Smith *Eur. Polym. J.* **1993**, *29*, 419.
- [7] E. Merian *Text. Res. J.* **1966**, *36*, 612.
- [8] G. Smets und F. De Blauwe *Pure Appl. Chem.* **1974**, *39*, 225.
- [9] H. S. Blair und H. I. Pogue *Polymer* **1982**, *23*, 779.
- [10] M. Camacho-Lopez, H. Finkelmann, P. Palfy-Muhoray und M. Shelley *Nat. Mater.* **2004**, *3*, 307.
- [11] K. M. Wiggins und C. W. Bielawski *Angew. Chem.* **2012**, *124*, 1672.
- [12] C. Seifert und F. Gräter *Biochim. Biophys. Acta* **2013**, *1830*, 4762.
- [13] E. M. Puchner, A. Alexandrovich, A. L. Kho, U. Hensen, L. V. Schäfer, B. Brandmeier, F. Gräter, H. Grubmüller, H. E. Gaub und M. Gautel *Proc. Natl. Acad. Sci. U. S. A.* **2008**, *105*, 13385.
- [14] K. L. Berkowski, S. L. Potisek, C. R. Hickenboth und J. S. Moore *Macromolecules* **2005**, *38*, 8975.
- [15] A. Piermattei, S. Karthikeyan und R. P. Sijbesma *Nat. Chem.* **2009**, *1*, 133.
- [16] C. E. Diesendruck, B. D. Steinberg, N. Sugai, M. N. Silberstein, N. R. Sottos, S. R. White, P. V. Braun und J. S. Moore *J. Am. Chem. Soc.* **2012**, *134*, 12446.
- [17] C. R. Hickenboth, J. S. Moore, S. R. White, N. R. Sottos, J. Baudry und S. R. Wilson *Nature* **2007**, *446*, 423.
- [18] M. J. Kryger, M. T. Ong, S. A. Odom, N. R. Sottos, S. R. White, T. J. Martinez und J. S. Moore *J. Am. Chem. Soc.* **2010**, *132*, 4558.
- [19] S. W. Schmidt, M. K. Beyer und H. Clausen-Schaumann *J. Am. Chem. Soc.* **2008**, *130*, 3664.
- [20] S. W. Schmidt, A. Kersch, M. K. Beyer und H. Clausen-Schaumann *Phys. Chem. Chem. Phys.* **2011**, *13*, 5994.
- [21] *Polymer Handbook*; 4. Aufl.; J. Brandrup, E. H. Immergut und E. A. Grulke, Hrsg.; John Wiley & Sons, Inc.: New York, **1999**.
- [22] C. K. Lee, D. A. Davis, S. R. White, J. S. Moore, N. R. Sottos und P. V. Braun *J. Am. Chem. Soc.* **2010**, *132*, 16107.
- [23] C. Löwe und C. Weder *Adv. Mater.* **2002**, *14*, 1625.
- [24] D. A. Davis, A. Hamilton, J. Yang, L. D. Cremer, D. V. Gough, S. L. Potisek, M. T. Ong, P. V. Braun, T. J. Martinez, S. R. White, J. S. Moore und N. R. Sottos *Nature* **2009**, *459*, 68.

Dank

M. S.-S., M. L. und A. S. danken dem Sonderforschungsbereich SFB 677 „Funktion durch Schalten“ für finanzielle Unterstützung.

Die Autoren



Matthias Schulz-Senft beendete das Chemiestudium an der Universität Kiel mit einer Diplomarbeit in der Arbeitsgruppe von Prof. Dr. Anne Staubitz. Seine Forschung zu schaltbaren Polymeren führt er als Doktorand in dieser Arbeitsgruppe weiter. Die Anfangszeit seiner Promotion wird durch das Graduiertenkolleg des SFB 677 (Funktion durch Schalten) mit einem Stipendium gefördert.



Matthias Lipfert hat sein Chemiestudium an der Universität Kiel mit einer Masterarbeit in der Arbeitsgruppe von Prof. Dr. Frank D. Sönnichsen im Jahr 2013 abgeschlossen. Als Doktorand führt er die begonnene Forschung an den Elastin-ähnlichen Biopolymeren mit Schwerpunkt NMR in dieser Arbeitsgruppe fort.



Anne Staubitz studierte Biochemie in Tübingen und fertigte ihre Diplomarbeit bei Prof. Dr. Paul Knochel an der LMU München an. Danach promovierte sie auf dem Gebiet der Naturstoffsynthese bei Prof. Dr. Varinder Aggarwal an der University of Bristol. Es folgte ein Postdoc-Aufenthalt bei Prof. Dr. Ian Manners, ebenfalls University of Bristol, bei dem sie auf dem Gebiet der Amino-Borane arbeitete und das erste lösliche Polyaminoboran herstellen konnte. 2010 kehrte sie nach Deutschland zurück und ist derzeit Juniorprofessorin für Organische Chemie an der Universität Kiel. Ihre Arbeitsschwerpunkte sind schaltbare Polymere (SFB 677, „Funktion durch Schalten“), chemoselektive Kreuzkupplungen und halbleitende Polymere (Emmy-Noether-Programm der DFG).

Korrespondenzadresse

Prof. Dr. Anne Staubitz
Otto-Diels-Institut für Organische Chemie
Christian-Albrechts-Universität zu Kiel
Otto-Hahn-Platz 3/4
24098 Kiel
astaubitz@oc.uni-kiel.de

1.2.2. Polymer Composites

The term "composites" describes materials that are a combination of two or more components. The individual components contribute different physical or chemical properties (flexibility, tensile strength, ductility, surface tension, resistance against pH, moisture, or UV irradiation, etc.) to the composite material, making the new material superior compared to the component materials.^[32,33] Reinforced concrete is probably the most relevant industrial composite with enormous influence on the world since its development. Technically speaking, the human body could also be seen as a composite. The skeleton provides the internal stability, while muscles make movements possible.

In case of polymer-based materials, the polymer matrix is combined with filler particles or fiber reinforcements.^[32] The matrix material can consist of thermoplastic polymers or cross-linked thermosets. Almost all thermoplastic polymers (E.g. polyamides, polyethylene, polypropylene, polystyrene, and others) can be reinforced with particles or fibers (see Figure I.4).^[16,34] Various thermosets were used as matrix components in composites, epoxide, phenol, formaldehyde or urethane resins represent a few examples.^[33,35]

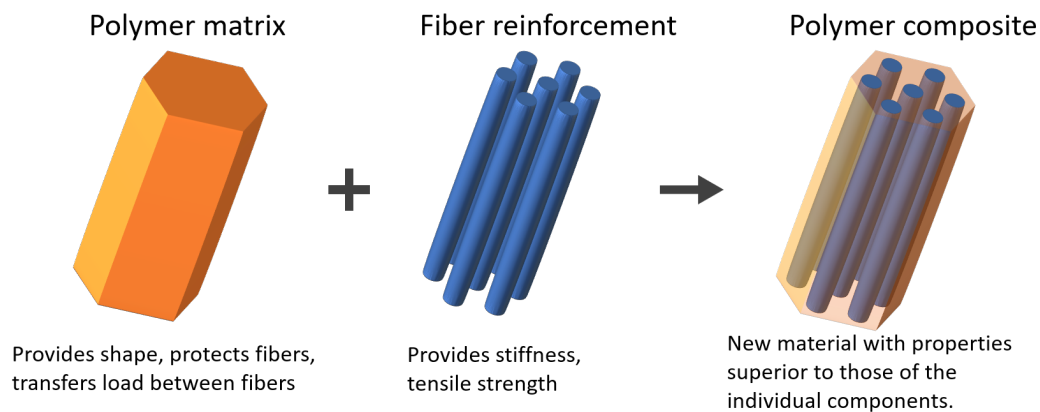


Figure I.4. Schematic structure of fiber reinforced polymer composites.

Metal oxides, ceramics, silicon and carbon nanotubes, as well as fullerenes are commonly used filling materials in particle reinforced polymers.^[36,37] They can be used as macroparticles or with a diameter in the nanometer scale.^[37–39] In fiber reinforced materials, various fiber materials are applied, ranging from steel and carbon fibers to aramid and glass fibers.^[32,33] It is also possible to incorporate fibers of polymers, such as nylon or natural fibers obtained from cotton, hemp, bamboo, or others.^[32,40–42]

The vast variety of possible matrices, filler sizes, materials and types lead to applications of polymer composite materials in virtually every aspect of life. Reinforced polymer composites are applied wherever high durability and/or low weights of the material is required. Huge wind turbine blades for off-shore wind power plants are constructed with polymer composites,^[35] as well as are dental fillings.^[37] Other applications include automotive and aerospace components, orthopedic implants, sport rackets and fuel cell materials.^[38–40,43]

1.2.3. Semiconducting Polymers

In 1977, the first semiconducting organic polymer was discovered by Heeger, MacDiarmid and Shirakawa.^[44] Their synthesis of doped polyacetylene paved the road to the broad variety of conducting organic oligomers and polymers and started the field of organic electronics. This pioneering work was honored with the Nobel Prize for chemistry 33 years later.^[45–47]

Semiconducting organic polymers rely on the conjugation of π electrons to generate an environment that supports the mobility of charge carriers. The repeat units consist of aryl, alkenyl or alkynyl units, whose π systems are connected in the polymer's main chain, delocalizing the π electrons.^[48] By linear combination of the frontier orbitals of the backbone, the highest occupied molecular orbitals (HOMOs) form a continuous, fully occupied π band. Equivalently, the lowest unoccupied molecular orbitals (LUMOs) combine to a continuous, unoccupied π^* band. The bands are energetically separated by the so-called band gap E_G , which is described by the energetically upper limit of the π band and the lower limit of the π^* band (see Figure I.5).^[49] Distortions and interruptions of the delocalization lead to increased band gaps, while improved delocalization and doping reduce the band gap. The band gaps of organic electronic materials can be tailored by the variation of the repeating units, introduction of dopants or influencing the crystallization behavior of the polymers among others.^[50,51] The Peierl's distortion prevents a perfectly delocalized π system. This effect distorts the hypothetically entirely equal π bonds towards a partially alternating sequence of σ and π bonds, partially localizing the electrons.^[52]

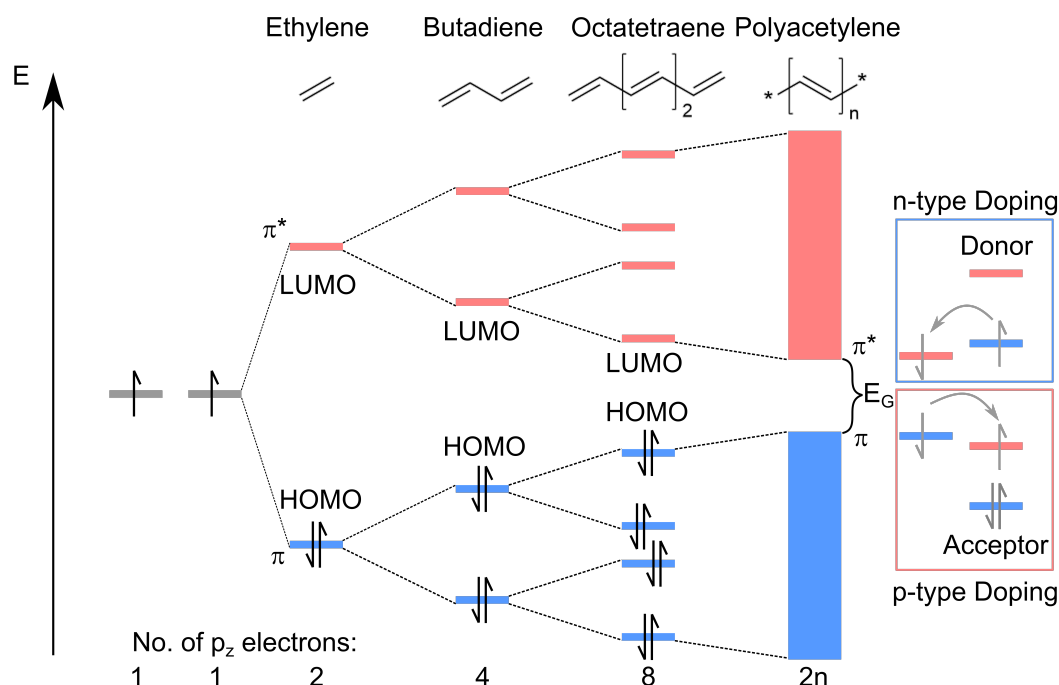


Figure I.5. Transformation of orbitals from individual sp^2 hybridized carbon to isolated π and π^* orbitals in ethylene and successive further transformation into the band structure of polyacetylene. **Right:** Electron donors transfer unpaired electrons as charge carriers into the LUMO level of the polymer (n-type doping). Electron acceptors abstract unpaired electrons from the polymer's HOMO, creating holes as charge carriers (p-type doping).

However, the conductivity of conjugated polymers can be drastically increased by the use of dopants. Hereby, strong electron donors or acceptors are introduced into the vicinity of the polymer. Electron donors possess a HOMO energy slightly above the LUMO level of the polymer, enabling electron transfer into the LUMO level (n-type doping) and creating unpaired electrons as charge carriers. In contrast, the LUMO energy of acceptors is slightly below the HOMO energy of the polymer, leading to the abstraction of electrons from the polymer's HOMO (p-type doping) and creating holes as charge carriers (see Figure I.5).

The band gap of semiconducting organic polymers often lies in the range of the visible light (ca. 380 nm to 780 nm, 3 eV to 1.5 eV).^[53] The absorption of photons with visible wavelengths leads to excitation of electrons into the π^* band, leaving an unoccupied, positively charged hole in the π band and thus an increased conductivity.^[48] This photovoltaic effect can be used in the construction of organic photovoltaic (OPV) devices, in which the electron hole pairs are separated to collect a photocurrent.^[48,49]

In contrast to silicon-based solar cells, OPV units can be semitransparent, opening new applications, such as photovoltaic windows.^[54] The impressive potential of this application was demonstrated at the Expo 2015 in Milan. Large so-called "solar trees" with semitransparent OPV leaves provided shade for the German pavilion (see Figure I.6).^[55] Another important advantage of organic semiconductors compared to the inorganic equivalents is the potentially cost and energy efficient fabrication by printing techniques.^[56] The mentioned large-scale OPV leaves were produced using solely printing methods.^[55] Several further advantages result from the possible use of printing techniques: devices using organic electronics can be thin, flexible and light weight.^[57] Besides OPVs, semiconducting organic polymers were applied in numerous devices, such as organic light emitting diodes (OLEDs), OFETs and even microelectromechanical systems (MEMSs).^[57,58]



Figure I.6. Solar trees constructed with OPV modules at the Expo 2015, Milan. Adapted from reference.^[55] © 2015 S. Berny et al., licensed under Creative Commons CC BY 4.0.

Polythiophenes

While various building blocks were used in the design and synthesis of conjugated polymers, polythiophene derivatives emerged to be among the most popular materials in OPVs, OFETs and other transistors (compare Figure I.7).^[59–62] Typically, the thiophene repeating units are linked at their 2- and 5-positions, while the 3- and 4-positions can be functionalized with solubilizing groups or other substituents^[59]

The conducting properties of polythiophenes are drastically influenced by the geometry of the thiophene backbone. The thiophene rings of unsubstituted oligothiophenes are arranged in perfect planarities in crystal structures.^[63] With increasing length of the oligomers, the band gap decreases from dimers over tetramers and hexamers to octamers from 2.94 eV to 1.87 eV, 1.54 eV and 1.39 eV, respectively.^[59,64] The structure of oligothiophenes and the delocalization of the frontier orbitals is shown in Figure I.7.^[64] This behavior confirms the delocalization principle that was described in the previous section and Figure I.5. In-depth density functional theory (DFT) studies revealed that a twist of neighboring thiophene rings by 36° increases the HOMO-LUMO gap of unsubstituted sexithiophene by 0.68 eV. Simultaneously, the average interring bond lengths increased by 0.07 Å.^[65] Typically, the thiophene rings in sexithiophene show a distance of 1.44 Å.^[66] Since oligothiophenes are highly crystalline, solubilizing groups were introduced at the 3- and/or 4-positions of the thiophenes to enhance the processability of polythiophenes.^[67] Commonly used solubilizing groups are hexyl chains at the 3-position of the monomer to give P3HT. Hexyl chains also guarantee a good chain separation and efficient crystallization.^[68] The separation of the polythiophene chains prevents inter-molecular hopping of charge carriers and thereby increases the band gap to 1.84 eV.^[69]

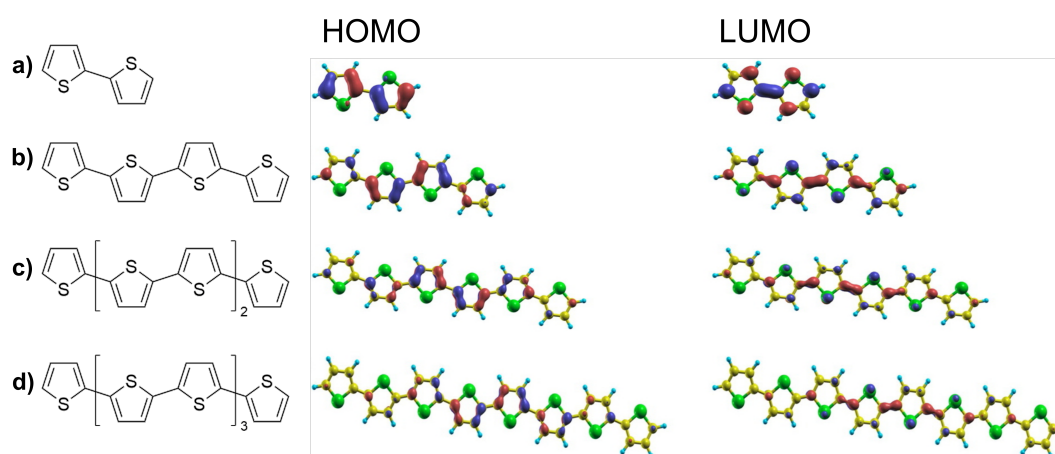
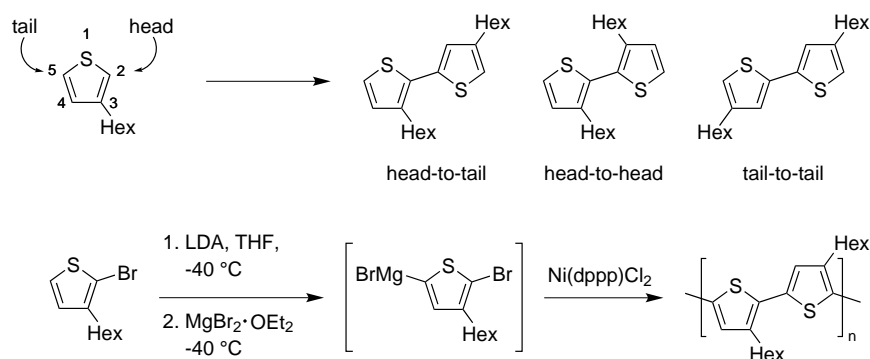


Figure I.7. Structure (left) and frontier orbitals of oligothiophenes. DFT calculated structure of thiophene a) dimer, b) tetramer, b) hexamer and d) octamer and depiction of the HOMO (middle) and LUMO (right). The yellow, cyan and green spheres represent C, H, and S atoms, respectively. Adapted with permission from T. P. Kaloni, G. Schreckenbach, M. S. Freund, *J. Phys. Chem. C* **2015**, *119*, 3979–3989.^[64] © 2015 American Chemical Society.

Bearing a substituent at the 3-, but not at the 4-position, the monomers for P3HT are intrinsically unsymmetrical, which can result in three different regioisomers after coupling two thiophene units (see Scheme I.3, top). Statistical distribution of the substituents' orientation in P3HT leads to significant twisting of the polythiophene chains due to sterical hindrance of the alkyl side chains, thus decreasing the conjugation.^[70] Depending on the functionalization of the 2- and 5- positions of the thiophene monomers, the polymerization of P3HT can be achieved by electropolymerization,^[71] nickel or palladium mediated cross-coupling reactions,^[67] or oxidative coupling.^[67]



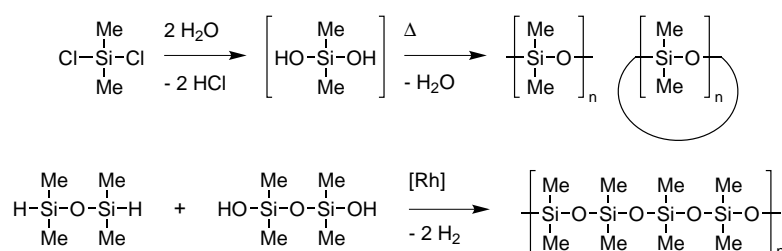
Scheme I.3 Regioselective synthesis of P3HT. **Top:** Depiction of the three different possibilities of linking thiophene rings in 3-hexylthiophene dyads. **Bottom:** Living polymerization of regioregular P3HT. Selective lithiation of the 5-position, followed by transmetalation gives 2-bromo-5-bromomagnesio-3-hexylthiophene, that can undergo Kumada cross-coupling.

In order to overcome the random orientation of the hexyl chains and thus increase the planarity of P3HT, synthetic routes using metal catalyzed cross-coupling reactions of difunctional thiophenes were successful.^[72–75] The key step of those synthetic routes is the selective metalation on the 5-position, which is considered the "tail". The "head", the 2-position, bears an halogen atom, commonly bromine (see Scheme I.3) The selective metalation of thiophenes was demonstrated with Grignard, organozinc, stannyl, and boron groups.^[76] Potentially, the polymerization by cross-coupling of such substances can follow either chain growth or step growth mechanism, as discussed above (see Figure I.2). For the synthesis of P3HT chains with controllable and adjustable lengths, chain growth polymerizations would be desirable. Chain growth cross-coupling polymerizations the association of the metal catalyst and the forming chain for the complete reaction time, instead of dissociation of the catalyst after each cross-coupling cycle. It was shown that nickel(0) catalysts stay associated to the growing chain during Kumada coupling of 2-bromo-5-chloromagnesio-3-hexylthiophene (see Scheme I.3.^[77] Thus, it is possible to synthesize P3HT in a quasi-living polymerization (see Scheme I.3).^[67] Proper choice of the quenching agent in the polymerization by Kumada coupling enables full control of the end groups.^[78,79]

1.2.4. Poly(siloxanes)

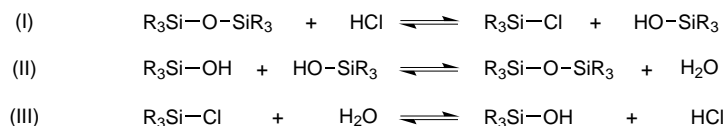
The backbone of poly(siloxanes) consists of Si-O repeating units with two side chains attached to the silicon. In the most common example, poly(dimethylsiloxane) (PDMS), the side chains are methyl groups. Poly(siloxanes) find broad applications in household and industrial environments. They are used as coatings,^[80–82] sealings,^[82,83] insulators,^[82] and defoamers.^[82] The growing field of soft robotics also relies on silicones as flexible substrates.^[84] These applications made poly(siloxanes) the most widely used inorganic or semi-inorganic polymers. The silicon-oxygen bond introduces some remarkable features into the polymers, rendering the materials' properties very different to organic polymers with only elements of period 2 in the backbone. In comparison to poly(oxymethylene) (POM), which consists of C-O repeating units in its backbone, the glass-transition temperature (T_g) is lowered by approximately 40 °C (POM: $T_g = -82$ °C, PDMS: $T_g = -123$ °C).^[85] This can mainly be attributed to the highly flexible Si-O bond. The ether bond in POM is 1.43 Å long and the C-O-C and O-C-O angles show typical values of tetrahedral bonding.^[86] In contrast, the siloxane bond in PDMS is significantly longer (1.64 Å) and only the O-Si-O angle shows tetrahedral bonding (110°), whereas the Si-O-Si bond angle is opened to 143°.^[86] Additionally, the rotation around the Si-O bond appears without a significant energy barrier, compared to a rotational energy for C-O bonds in ethers of 19.1 kJ mol⁻¹.^[87,88] Torsional rotations around the silicon atom also occur without a significant increase of energy.^[86,88]

Siloxane polymers can be synthesized following both, step growth and chain growth mechanisms. Chlorosilanes hydrolyze to silanols that form linear and cyclic oligomers and polymers in polycondensation reactions (see Scheme I.4, top).^[89–91] In this reaction sequence, the chain length is highly dependent on the pH value of the reaction medium, since the released hydrogen chloride can induce protolysis of the formed siloxane bond as well. It is thus necessary to remove the emerging hydrogen chloride from the reaction mixture to obtain high molecular weights.



Scheme I.4 Synthesis of PDMS by step growth polymerizations. **Top:** The hydrolysis of chlorosilanes with water yields hydroxysilanes, that directly undergo polycondensation to form linear or cyclic oligomers and polymers.^[91] **Bottom:** Silanes and hydroxysilanes can react to PDMS by rhodium catalyzed dehydrogenation polymerization.^[92]

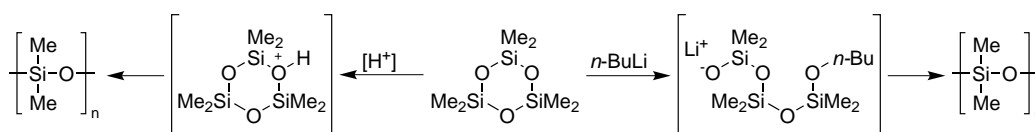
The condensation of silanols and the acid catalyzed hydrolysis of siloxanes can be described by a set of three elementary equilibrium reactions (see Scheme I.5).^[93] These reactions represent the hydrolysis of siloxane bonds by acids such as hydrochloric acid (Scheme I.5, (I)), the condensation of two silanols (II) and the hydrolysis of the chlorosilanes (III).



Scheme I.5 Siloxane degradation catalyzed by hydrochloric acid. The formation and cleavage of siloxane bonds in acidic conditions is described by these three elementary equilibrium reactions.^[93]

An alternative to this sensitive polycondensation can be provided by dehydrogenation reactions that are catalyzed by rhodium complexes (see Scheme I.4, bottom).^[92,94] Here, silanes are coupled to silanols while hydrogen is released from the reaction mixture. Due to the step-growth mechanism, the optimal dispersity of polycondensations reactions is $\bar{D} = M_w/M_n = 2$.^[16]

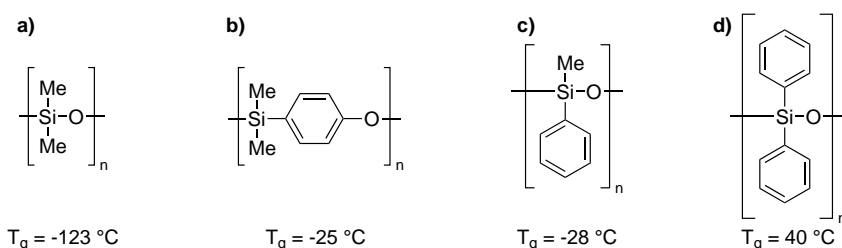
While the discussed polycondensations use single repeating units and linear precursors, the ring-opening polymerization (ROP) starts from cyclic siloxane oligomers. The siloxane bonds of these cycles can be broken by acids such as hydrochloric acid or bases such as butyllithium (see Scheme I.6).^[95,96] Depending on the charge of the intermediate, ROPs are distinguished into cationic and anionic polymerizations. Compared to the polycondensation methods, ROPs give access to linear poly(siloxanes) with high molecular weights, low dispersities and better control of the end groups.



Scheme I.6 Ring-opening polymerization of cyclic siloxanes. Hexamethylcyclotrisiloxane can undergo cationic (**Left**) and anionic (**Right**) ring-opening and subsequent polymerization to linear PDMS.

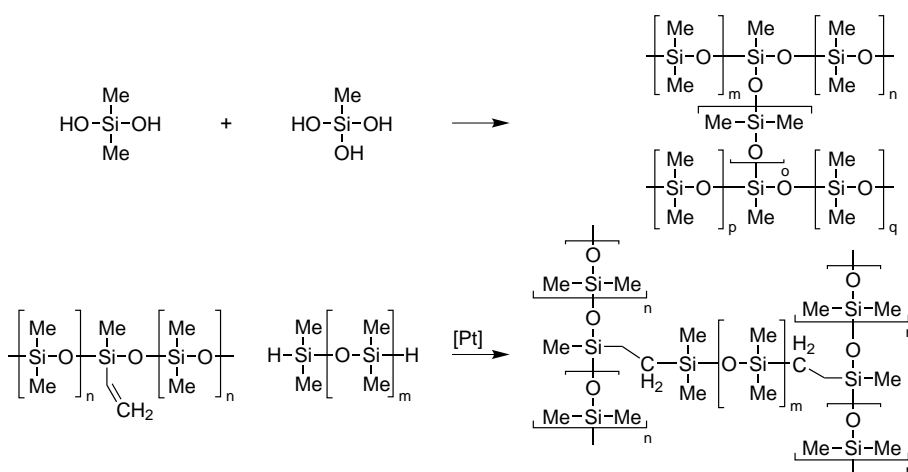
The physical properties of poly(siloxanes) can be adjusted to match the requirements of the desired application. While linear PDMS shows one of the lowest glass transitions of any common polymer ($T_g = -123^\circ\text{C}$),^[85,97] variation of the backbone and side chains increases the T_g drastically (see Scheme I.7, a)). The T_g of poly(siloxanes) increases with increasing size of the substituents in the side chains.^[97] This is contrary to the behavior of polymers with carbon-based backbones and was attributed to the high flexibility of the siloxane bonds.^[97] Introducing one phenyl group per siloxane group increases the glass transition by approximately 100°C (Scheme I.7, b) and c)). Insertion of phenylene into the main chain results in a T_g of -25°C ; substitution of a methyl group by a phenyl group leads to a T_g of -28°C .^[97-99] Poly(diphenylsiloxane) shows a glass transition above room temperature ($T_g = 40^\circ\text{C}$).^[97] Such modifications also result in changes of other properties such as liquid crystallinity, thermal stability, thermo-oxidative stability, gas permeativity and solvent resistance.^[89,100]

Besides the modification of linear poly(siloxanes), the glass transition can also be influenced by modifying the architecture of the polymers. Increasing the degree of cross-linking results in increased viscosity and glass transition.^[89] For PDMS, the ratio between CH_3 and Si can be



Scheme I.7 Variation of backbone and side chains of poly(siloxanes). **a)** Poly(dimethylsiloxane),^[85,97] **b)** Poly(dimethyloxyphenylenesilane),^[98,99] **c)** Poly(methylphenylsiloxane),^[97] **d)** Poly(diphenylsiloxane).^[97]

used to quantify the degree of cross-linking. The CH_3/Si ratio is 2 for linear PDMS. With decreasing CH_3/Si ratio, the polymers remain fluid until $\text{CH}_3/\text{Si} = 1.7$ before appearing as highly viscous resins. Further decrease of $\text{CH}_3/\text{Si} \leq 1$ leads to glassy and brittle materials that show gel-like character.^[89]



Scheme I.8 Top: Incorporation of trivalent silanols during the polycondensation leads to PDMS with cross-links. The length of the cross-linking chains is distributed statistically. **Bottom:** Cross-linking of PDMS by hydrosilylation. Subsequent to the polymerization, vinyl side chains can undergo hydrosilylation with silanes. The length of the cross-linker can be varied.

In polycondensations of silanols, trivalent or tetravalent silanols can be incorporated to act as branching site in the polymeric backbone (see Scheme I.8, top). Thus, the cross-linking siloxane chains are connected to the main chain via siloxane bonds. Since the formation of cross-linking chains occurs simultaneously to the formation of the polymers' main chains, the length of the cross-links cannot be controlled directly, they show the same statistical distribution of chain length as the backbone. However, the degree of cross-linking can be adjusted by variation of the ratio between divalent and multivalent silanols.

For a better control of the cross-linking units, a functionalization of the linear chains subsequent to the polymerization is required. When vinyl groups are introduced into the side chains of PDMS, they can be linked to silanes by platinum-catalyzed hydrosilylation (see Scheme I.8, bottom). Vinyl side chains can also undergo cross-coupling,^[101] thiol-ene^[101,102] and other radical reactions^[103] or cycloaddition reactions,^[104] providing access to various classes of side chains and cross-linkers.

2. Objectives

The work presented in this thesis covers the functionalization of polymeric materials with photoswitchable units. Merging these two classes of compounds provides the possibility to obtain materials with properties that exceed the properties of the individual materials. Photoswitchable molecules introduce a response to external stimuli such as light, electrical energy etc. into polymers. On the other hand, polymers can amplify those molecular responses to macroscopical effects and transfer macroscopical stress such as mechanical force to the switchable sites. Two general ways of incorporating the photoswitches into the materials were pursued: as additive in composite materials and as part of the polymers' main chains. In this thesis, spiropyrans (Part II) and azobenzenes (Part III) were applied as switchable moieties.

Researching the properties of such photoswitchable polymers covers interdisciplinary aspects. Especially the analysis of the mechanical properties of polymer samples and the analysis of photochemical switching mechanisms require external expertise. Thus, these aspects should be investigated in collaboration with the groups of Rainer Adelung, Institute for Materials Science and Friedrich Temps, Institute of Physical Chemistry, University of Kiel.

2.1. Spiropyrans in Polymer Materials

Reinforced polymer composite materials represent one of the most widely applied classes of polymer materials. Failure of these materials cannot be properly predicted, since the underlying mechanisms are not yet fully understood. Up to now, the detection of small defects

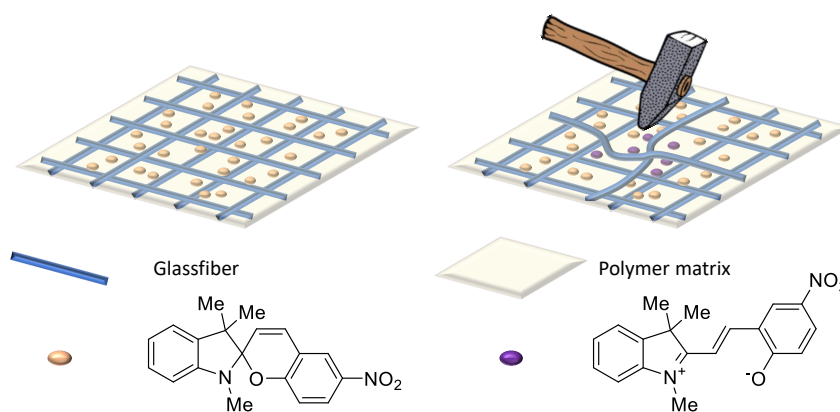
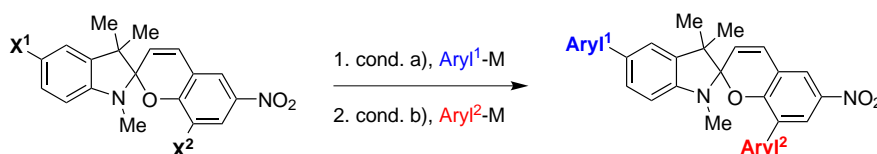


Figure I.8. Will the incorporation of spiropyrans as additives in composites (here: glassfiber-reinforced) result in detection of mechanical forces?

in large parts such as airplane parts relies on cost-intensive methods such as radiography, ultrasound inspection and acoustic methods.^[105,106] Since spiropyrans can be switched by mechanical forces (see section 1.2), their use in reinforced composites could be a potential detector for materials failure. In cooperation with the group of Rainer Adelung, a composite that reacts with a change in color to mechanical force should be developed (Figure I.8, see Part II, section 1.2). To broaden the applicability of this system, the reinforcement and matrix should be optimized.

The differences in the conjugated π systems of spiropyran (SP) and merocyanine (MC) that lead to the intense color of MC may be utilized to switch the conductivity of conjugated polymers (Figure I.9). The largest effects would be expected for a covalent incorporation of spiropyrans into the main chain of conjugated polymers. For this purpose, the reactivity of spiropyrans in cross-coupling reactions was to be investigated.



Scheme I.9 The development of electrophile and site selective cross-coupling reactions should provide the possibility to selectively functionalize the indole and the chromene site of spiropyran.

Variation of halide (and pseudohalide) substituents at the indole and chromene site of the spiropyran scaffold should provide a library of spiropyrans (see Part II, section 3.1). The obtained dyes should be used as starting materials in electrophile-selective cross-coupling reactions (Scheme I.9, see Part II, section 3.2). If possible, a synthetic route to selective functionalization of the indole- and chromene sites should be established. Thus, the synthetic possibilities of connecting spiropyrans to various conjugated polymers was to be evaluated. To prove the principle, spiropyran was to be incorporated into P3HT main chains (Figure I.9). P3HT is accessible via a living polymerization that provides control of chain length and end groups (see Scheme I.3 and subsection 1.2.3).^[79]

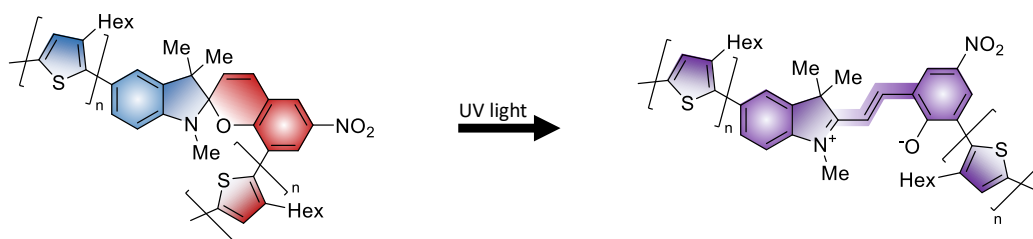


Figure I.9. If conducting polymers such as P3HT are linked to spiropyran, two separated π -systems (blue and red) should form. After switching to the merocyanine form, the conjugation should spread throughout the complete molecule (purple).

2.2. Azobenzene-siloxanes in Polymers and Macrocycles

Azobenzenes are another widely applied class of photochromic molecules. In contrast to spiroyrans, they do not undergo photoinduced ring opening/cyclization, but *cis/trans* isomerization of the central N=N double bond. This (*E*)/(*Z*) isomerization induces smaller changes of the azobenzenes' π system compared to the large differences that occur in the SP/MC system. In the metastable (*Z*)-isomer of azobenzenes, the phenyl groups are located in a closer distance than in the stable (*E*)-isomer.^[107,108] Therefore, it is not possible to enrich the metastable isomer by the application of mechanical force, as it is known for spiroyrans. Instead, the formation of the stable (*E*)-isomer is being promoted by applying mechanical forces to azobenzenes.^[109–111] Nevertheless, the switching process of azobenzenes occurs without side reactions and can be repeated for virtually an infinite amount of cycles.^[112]

When combined with flexible polymers such as PDMS, azobenzenes can be used to switch the shape of the material.^[113] The flexibility of siloxanes was used by Jan Strüben to design and synthesize a linear polymer with strictly alternating azobenzene and trisiloxane units in its backbone.^[114] The aim of this thesis was the optimization of the established syntheses of azobenzene monomer^[115] and the polymer (see Part III, section 2.1).^[114] In addition, the switching behavior of the polymer was to be investigated thoroughly (Figure I.10) in solution (see Part III, section 2.1) and film (see Part III, section 2.2). In order to gain access to post-synthetic functionalization and curing of the material, reactive side groups were to be introduced into the polymer (see Part III, section 2.2).

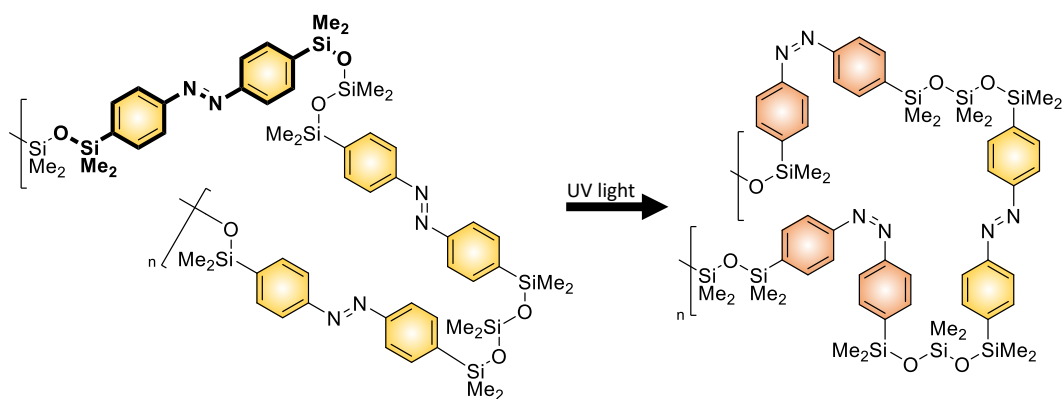


Figure I.10. In polymers, trisiloxane linkers between azobenzene units provide enough flexibility to switch (*E*)-azobenzenes (yellow) to (*Z*)-azobenzenes (orange). The atoms that were introduced by one azobenzene monomer are highlighted as bold.

The alternation of azobenzene and siloxane units in the main chain of polymers is a relatively seldom architecture. Yet, it proved to allow the azobenzenes' photoisomerization, even in constraint environments such as films. In order to explore the capabilities and limitations of this building motif, other examples of azobenzene-siloxanes were to be synthesized. For this purpose, the tendency of siloxanes to form macrocycles (as discussed in the previous chapter) was planned to be utilized. A macrocyclic azobenzene-siloxane

(oligomer) would represent a model system to evaluate the flexibility of the siloxane linkers (see Part III, chapter 3). Typically, the switching properties of azobenzenes are drastically altered when being incorporated in macrocycles.^[116] Thus, the switching of azobenzene units in azobenzene-siloxane macrocycles was to be expected to indicate the rigidity of such a system.

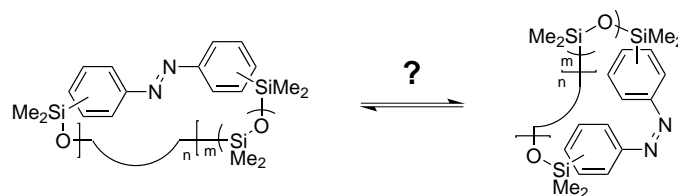


Figure I.11. Azobenzophanes were to be synthesized to test the flexibility of siloxane linkers in the constrained environment of macrocycles. Rigid cycles were expected to drastically influence the azobenzene's switching properties.

Bibliography of Part I

- [1] M. P. Johnson, *Essays Biochem.* **2016**, *60*, 255–273.
- [2] K.-W. Yau, R. C. Hardie, *Cell* **2009**, *139*, 246–264.
- [3] *Molecular Switches*, 2nd, (Eds.: B. L. Feringa, W. R. Browne), Wiley-VCH, Weinheim, Germany, **2011**.
- [4] J.-P. Launay, C. Coudret, C. Joachim in *Dekker Encyclopedia of Nanoscience and Nanotechnology, Third Edition*, CRC Press, **2014**, pp. 2723–2735.
- [5] B. L. Feringa, *Angew. Chem. Int. Ed.* **2018**, *56*, 11060–11078.
- [6] O. P. Ernst, D. T. Lodowski, M. Elstner, P. Hegemann, L. S. Brown, H. Kandori, *Chem. Rev.* **2014**, *114*, 126–163.
- [7] P. S.-H. Park in *Advances in Pharmacology, Vol. 70*, Elsevier, Oxford, **2014**, pp. 1–36.
- [8] Z. L. Pianowski, *Chem. - Eur. J.* **2019**, *25*, 5128–5144.
- [9] L. Dong, Y. Feng, L. Wang, W. Feng, *Chem. Soc. Rev.* **2018**, *47*, 7339–7368.
- [10] E. Merino, *Chem. Soc. Rev.* **2011**, *40*, 3835–3853.
- [11] H. M. D. Bandara, S. C. Burdette, *Chem. Soc. Rev.* **2012**, *41*, 1809–1825.
- [12] R. Klajn, *Chem. Soc. Rev.* **2014**, *43*, 148–184.
- [13] *Photomechanical Materials, Composites, and Systems*, (Ed.: T. J. White), John Wiley & Sons, Inc., Hoboken, **2017**.
- [14] M. Li, Q. Zhang, Y.-N. Zhou, S. Zhu, *Prog. Polym. Sci.* **2018**, *79*, 26–39.
- [15] H. Staudinger, *Ber. Dtsch. Chem. Ges. B* **1926**, *59*, 3019–3043.
- [16] S. Koltzenburg, M. Maskos, O. Nuyken, *Polymer Chemistry*, Springer-Verlag, Berlin Heidelberg, **2017**.
- [17] G. Odian, *Principles of Polymerization*, 4th ed., John Wiley & Sons, Inc., Hoboken, **2004**.
- [18] K. Matyjaszewski, T. P. Davis, *Handbook of Radical Polymerization*, John Wiley & Sons, Inc., Hoboken, **2002**.
- [19] F. Ciardelli, G. Ruggeri, A. Pucci, *Chem. Soc. Rev.* **2013**, *42*, 857.
- [20] P. Weis, W. Tian, S. Wu, *Chem. - Eur. J.* **2018**, *24*, 6494–6505.
- [21] M. M. Caruso, D. A. Davis, Q. Shen, S. A. Odom, N. R. Sottos, S. R. White, J. S. Moore, *Chem. Rev.* **2009**, *109*, 5755–5798.

- [22] P. Dopieralski, P. Anjukandi, M. Rückert, M. Shiga, J. Ribas–Arino, D. Marx, *J. Mater. Chem.* **2011**, *21*, 8309.
- [23] J. N. Brantley, K. M. Wiggins, C. W. Bielawski, *Polym. Int.* **2013**, *62*, 2–12.
- [24] Y. Li, H. Zhang, C. Qi, X. Guo, *J. Mater. Chem.* **2012**, *22*, 4261.
- [25] Y. Yu, M. Nakano, T. Ikeda, *Nature* **2003**, *425*, 145–145.
- [26] P. Karageorgiev, D. Neher, B. Schulz, B. Stiller, U. Pietsch, M. Giersig, L. Brehmer, *Nat Mater* **2005**, *4*, 699–703.
- [27] D. Habault, H. Zhang, Y. Zhao, *Chem. Soc. Rev.* **2013**, *42*, 7244–7256.
- [28] S. L. Potisek, D. A. Davis, N. R. Sottos, S. R. White, J. S. Moore, *J. Am. Chem. Soc.* **2007**, *129*, 13808–13809.
- [29] D. A. Davis, A. Hamilton, J. Yang, L. D. Cremer, D. Van Gough, S. L. Potisek, M. T. Ong, P. V. Braun, T. J. Martínez, S. R. White, J. S. Moore, N. R. Sottos, *Nature* **2009**, *459*, 68–72.
- [30] W. Qiu, P. A. Gurr, G. G. Qiao, *ACS Appl. Mater. Interfaces* **2019**, *11*, 29268–29275.
- [31] M. Schulz-Senft, M. Lipfert, A. Staubitz, *Chem. Unserer Zeit* **2014**, *48*, 200–214.
- [32] V. Vasiliev, E. Morozov, *Mechanics and Analysis of Composite Materials*, Elsevier, Oxford, **2001**.
- [33] T. Sathishkumar, S. Satheeshkumar, J. Naveen, *J. Reinf. Plast. Compos.* **2014**, *33*, 1258–1275.
- [34] L. Tong, A. P. Mouritz, M. K. Bannister, *3D Fibre Reinforced Polymer Composites*, Elsevier, Oxford, **2002**.
- [35] R. P. L. Nijssen, *Composite Materials*, VKCN, Marknesse, **2015**.
- [36] J. N. Coleman, U. Khan, W. J. Blau, Y. K. Gun'ko, *Carbon* **2006**, *44*, 1624–1652.
- [37] *Dental Composite Materials for Direct Restorations*, (Ed.: V. Miletic), Springer Nature, Cham, Switzerland, **2018**.
- [38] *Polymer Composites: Macro- and Microcomposites, Vol. 1*, (Eds.: S. Thomas, J. Kuruvilla, S. K. Malhotra, K. Goda, M. S. Sreekala), Wiley-VCH, Weinheim, **2012**.
- [39] *Polymer Composites: Nanocomposites, Vol. 2*, (Eds.: S. Thomas, J. Kuruvilla, S. K. Malhotra, K. Goda, M. S. Sreekala), Wiley-VCH, Weinheim, **2012**.
- [40] *Polymer Composites: Biocomposites, Vol. 3*, (Eds.: S. Thomas, J. Kuruvilla, S. K. Malhotra, K. Goda, M. S. Sreekala), Wiley-VCH, Weinheim, **2014**.
- [41] F. Ahmad, H. S. Choi, M. K. Park, *Macromol. Mater. Eng.* **2015**, *300*, 10–24.
- [42] K.-t. Lau, P.-y. Hung, M.-H. Zhu, D. Hui, *Composites Part B* **2018**, *136*, 222–233.
- [43] *Sustainable Polymer Composites and Nanocomposites*, (Eds.: Inamuddin, S. Thomas, R. Kumar Mishra, A. M. Asiri), Springer Nature, Cham, Switzerland, **2019**.

- [44] H. Shirakawa, E. J. Louis, A. G. MacDiarmid, A. J. Heeger, *J. Chem. Soc. Chem. Commun.* **1977**, 578–580.
- [45] H. Shirakawa, *Angew. Chem. Int. Ed.* **2001**, *40*, 2574–2580.
- [46] A. G. MacDiarmid, *Angew. Chem. Int. Ed.* **2001**, *40*, 2581–2590.
- [47] A. J. Heeger, *Angew. Chem. Int. Ed.* **2001**, *40*, 2591–2611.
- [48] A. Köhler, H. Bässler, *Electronic Processes in Organic Semiconductors: An Introduction*, Wiley-VCH, Weinheim, **2015**.
- [49] H. Bässler, A. Köhler in *Unimolecular and Supramolecular Electronics I, Vol. 312*, (Ed.: R. M. Metzger), Springer Berlin Heidelberg, Berlin, Heidelberg, **2011**, pp. 1–65.
- [50] S. Holliday, J. E. Donaghey, I. McCulloch, *Chem. Mater.* **2014**, *26*, 647–663.
- [51] *Conjugated Polymers*, (Eds.: K. Müllen, J. R. Reynolds, T. Masuda), Royal Society of Chemistry, Cambridge, **2014**.
- [52] C. Castiglioni, G. Zerbi, M. Gussoni, *Solid State Commun.* **1985**, *56*, 863–866.
- [53] J. C. S. Costa, R. J. S. Taveira, C. F. R. A. C. Lima, A. Mendes, L. M. N. B. F. Santos, *Opt. Mater.* **2016**, *58*, 51–60.
- [54] F. Yang, Y. Zhang, Y. Hao, Y. Cui, W. Wang, T. Ji, F. Shi, B. Wei, *Appl. Opt.* **2015**, *54*, 10232.
- [55] S. Berny, N. Blouin, A. Distler, H.-J. Egelhaaf, M. Krompiec, A. Lohr, O. R. Lozman, G. E. Morse, L. Nanson, A. Pron, T. Sauermann, N. Seidler, S. Tierney, P. Tiwana, M. Wagner, H. Wilson, *Adv. Sci.* **2016**, *3*, 1500342.
- [56] D. Li, W.-Y. Lai, Y.-Z. Zhang, W. Huang, *Adv. Mater.* **2018**, *30*, 1704738.
- [57] L. Torsi, M. Magliulo, K. Manoli, G. Palazzo, *Chem. Soc. Rev.* **2013**, *42*, 8612.
- [58] *Organic Electronics: Structural and Electronic Properties of OFETs*, (Ed.: C. Wöll), Wiley-VCH, Weinheim, **2009**.
- [59] T. P. Kaloni, P. K. Giesbrecht, G. Schreckenbach, M. S. Freund, *Chem. Mater.* **2017**, *29*, 10248–10283.
- [60] E. Zeglio, O. Inganäs, *Adv. Mater.* **2018**, *30*, 1800941.
- [61] H. Li, W. Shi, J. Song, H.-J. Jang, J. Dailey, J. Yu, H. E. Katz, *Chem. Rev.* **2019**, *119*, 3–35.
- [62] C. Zhao, Y. Guo, Y. Zhang, N. Yan, S. You, W. Li, *J. Mater. Chem. A* **2019**, *7*, 10174–10199.
- [63] L. Zhang, N. S. Colella, B. P. Cherniawski, S. C. B. Mannsfeld, A. L. Briseno, *ACS Appl. Mater. Interfaces* **2014**, *6*, 5327–5343.
- [64] T. P. Kaloni, G. Schreckenbach, M. S. Freund, *J. Phys. Chem. C* **2015**, *119*, 3979–3989.

- [65] S. S. Zade, M. Bendikov, *Chem. - Eur. J.* **2007**, *13*, 3688–3700.
- [66] G. Horowitz, B. Bachet, A. Yassar, P. Lang, F. Demanze, J.-L. Fave, F. Garnier, *Chem. Mater.* **1995**, *7*, 1337–1341.
- [67] A. Marrocchi, D. Lanari, A. Facchetti, L. Vaccaro, *Energy Environ. Sci.* **2012**, *5*, 8457–8474.
- [68] K. Tremel, S. Ludwigs, *Adv. Polym. Sci.* **2014**, *265*, 39–82.
- [69] T. V. Richter, C. H. Braun, S. Link, M. Scheuble, E. J. W. Crossland, F. Stelzl, U. Würfel, S. Ludwigs, *Macromolecules* **2012**, *45*, 5782–5788.
- [70] *P3HT Revisited - from Molecular Scale to Solar Cell Devices*, (Ed.: S. Ludwigs), Springer-Verlag, Berlin Heidelberg, **2014**.
- [71] K. Wagner, M. Zanoni, A. B. S. Elliott, P. Wagner, R. Byrne, L. E. Florea, D. Diamond, K. C. Gordon, G. G. Wallace, D. L. Officer, *J. Mater. Chem. C* **2013**, *1*, 3913.
- [72] A. Yokoyama, R. Miyakoshi, T. Yokozawa, *Macromolecules* **2004**, *37*, 1169–1171.
- [73] E. E. Sheina, J. Liu, M. C. Iovu, D. W. Laird, R. D. McCullough, *Macromolecules* **2004**, *37*, 3526–3528.
- [74] A. Iraqi, G. W. Barker, *J. Mater. Chem.* **1998**, *8*, 25–29.
- [75] I. A. Liversedge, S. J. Higgins, M. Giles, M. Heaney, I. McCulloch, *Tetrahedron Letters* **2006**, *47*, 5143–5146.
- [76] D. Haynes, R. McCulloch in *Conjugated Polymers*, (Eds.: K. Müllen, J. R. Reynolds, T. Masuda), RSC Polymer Chemistry 9, Royal Society of Chemistry, Cambridge, **2014**, pp. 180–200.
- [77] R. Miyakoshi, A. Yokoyama, T. Yokozawa, *J. Am. Chem. Soc.* **2005**, *127*, 17542–17547.
- [78] R. H. Lohwasser, M. Thelakkat, *Macromolecules* **2010**, *43*, 7611–7616.
- [79] R. H. Lohwasser, M. Thelakkat, *Macromolecules* **2011**, *44*, 3388–3397.
- [80] K.-. H. Kaesler in *High-Performance Organic Coatings*, (Ed.: A. S. Khanna), Woodhead Publishing Series in Metals and Surface Engineering, Woodhead Publishing, **2008**, pp. 225–246.
- [81] G. Barroso, Q. Li, R. K. Bordia, G. Motz, *J. Mater. Chem. A* **2019**, *7*, 1936–1963.
- [82] J. K. Fink, *Liquid Silicone Rubber*, John Wiley & Sons, Inc., Hoboken, **2019**.
- [83] R. M. Minas'yan, *Polym. Sci. Ser. D* **2011**, *4*, 206–208.
- [84] C. Appiah, C. Arndt, K. Siemsen, A. Heitmann, A. Staubitz, C. Selhuber-Unkel, *Adv. Mater.* **2019**, *0*, 1807747.
- [85] J. Brandrup, E. H. Immergut, E. A. Grulke, *Polymer Handbook*, 4., John Wiley & Sons, New York, **1999**.

- [86] M. Rehahn, W. L. Mattice, U. W. Suter, *Rotational Isomeric State Models in Macromolecular Systems*, Springer Berlin Heidelberg, **1997**.
- [87] L. Goodman, V. Pophristic, *Chem. Phys. Lett.* **1996**, *259*, 287–295.
- [88] B. C. Cope, D. E. Packham, G. Leggett, J. C. Beech, G. B. Lowe, D. Briggs, D. M. Brewis, A. D. Crocombe, D. G. Dixon, W. J. Van Ooij, B. Parbhoo, C. M. Warwick, J. Pritchard, S. Millington, C. Chatfield, J. Comyn, D. A. Dillard, B. Kneafsey, M. E. R. Shanahan, A. V. Pocius in *Handbook of Adhesion*, (Ed.: D. E. Packham), John Wiley & Sons, Ltd, Chichester, **2005**, pp. 439–525.
- [89] W. Noll, *Chemistry and Technology of Silicones*, Academic Press, New York, **1968**.
- [90] R. Schliebs, J. Ackermann, *Chem. Unserer Zeit* **1987**, *21*, 121–127.
- [91] J. Ackermann, V. Damrath, *Chem. Unserer Zeit* **1989**, *23*, 86–99.
- [92] R. Zhang, J. E. Mark, A. R. Pinhas, *Macromolecules* **2000**, *33*, 3508–3510.
- [93] M. Cypryk, Y. Apeloig, *Organometallics* **2002**, *21*, 2165–2175.
- [94] M. Jeon, J. Han, J. Park, *ACS Catal.* **2012**, *2*, 1539–1549.
- [95] Q. Wang, H. Zhang, G. K. S. Prakash, T. E. Hogen-Esch, G. A. Olah, *Macromolecules* **1996**, *29*, 6691–6694.
- [96] B. Yactine, A. Ratsimihety, F. Ganachaud, *Polym. Adv. Technol.* **2010**, *21*, 139–149.
- [97] P. R. Dvornic in *Silicon-Containing Polymers: The Science and Technology of Their Synthesis and Applications*, (Eds.: R. G. Jones, W. Ando, J. Chojnowski), Springer Netherlands, Dordrecht, **2000**, pp. 185–212.
- [98] C. U. Pittman, W. J. Patterson, S. P. McManus, *J. Polym. Sci. Polym. Chem. Ed.* **1976**, *14*, 1715–1734.
- [99] M. J. Owen, P. R. Dvornic in *Polymer Data Handbook*, (Ed.: J. E. Mark), Oxford University Press, Oxford, **1999**, pp. 821–825.
- [100] *Polymer Data Handbook*, (Ed.: J. E. Mark), Oxford University Press, Oxford, **1999**.
- [101] M. A. Gauthier, M. I. Gibson, H.-A. Klok, *Angew. Chem. Int. Ed.* **2009**, *48*, 48–58.
- [102] S. J. Dünki, E. Cuervo-Reyes, D. M. Opris, *Polym. Chem.* **2017**, *8*, 715–724.
- [103] G. Agrawal, J. Wang, B. Brüster, X. Zhu, M. Möller, A. Pich, *Soft Matter* **2013**, *9*, 5380.
- [104] L. Yang, K. Cao, Y. Huang, G. Chang, F. Zhu, J. Yang, *High Perform. Polym.* **2014**, *26*, 463–469.
- [105] M. Bowkett, K. Thanapalan, *Syst. Sci. Control Eng.* **2017**, *5*, 168–177.
- [106] M. Bowkett, K. Thanapalan in *Failure Analysis and Prevention*, (Ed.: A. Ali), InTech, **2017**.
- [107] C. J. Brown, *Acta Crystallogr.* **1966**, *21*, 146–152.

- [108] A. Mostad, C. Rømming, *Acta Chem. Scand.* **1971**, *25*, 3561–3568.
- [109] R. Turanský, M. Konôpka, N. L. Doltsinis, I. Štich, D. Marx, *ChemPhysChem* **2010**, *11*, 345–348.
- [110] R. Turanský, M. Konôpka, N. L. Doltsinis, I. Štich, D. Marx, *Phys. Chem. Chem. Phys.* **2010**, *12*, 13922.
- [111] S. K. Surampudi, H. R. Patel, G. Nagarjuna, D. Venkataraman, *Chem. Commun.* **2013**, *49*, 7519–7521.
- [112] S. Venkataramani, U. Jana, M. Dommaschk, F. D. Sönnichsen, F. Tuczek, R. Herges, *Science* **2011**, *331*, 445–448.
- [113] E. Kizilkan, J. Strueben, A. Staubitz, S. N. Gorb, *Sci. Robot.* **2017**, *2*, eaak9454.
- [114] J. Strueben, PhD thesis, Christian-Albrechts-Universität, Kiel, **2015**.
- [115] J. Strüben, J. Hoffmann, D. Presa-Soto, C. Näther, A. Staubitz, *Acta Crystallogr. Sect. E: Crystallogr. Commun.* **2016**, *72*, 1590–1594.
- [116] R. Reuter, H. A. Wegner, *Chem. Commun.* **2011**, *47*, 12267–12276.

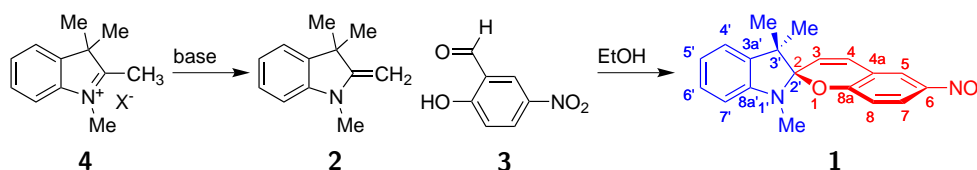
Part II.

Spiropyrans and their Implementation into Polymer Materials

1. Spiropyran Dyes

SPs **1** can be synthesized by a condensation reaction of Fischer bases **2** (1,3,3-trimethyl-2-methylene-3*H*-indolenes) with salicylic aldehyde derivatives **3** in protic organic solvents, typically ethanol.^[117–119] Since methylene bases **2** tend to dimerize, they are typically generated in situ from quaternary indolium salts **4**.^[117] While this synthesis route provides spiropyrans in high purities and high yields, an excess of the methylene base **2** can result in the condensation of two indole units and one salicylic aldehyde.^[117,120,121]

In this thesis, the nomenclature and numbering of spiropyran molecules follow the recommendations made by the International Union of Pure and Applied Chemistry (IUPAC).^[122] While all compounds were synthesized without control of the stereochemistry as racemic mixtures, they are depicted in their 2,2'-(*R*) configuration for clarity.

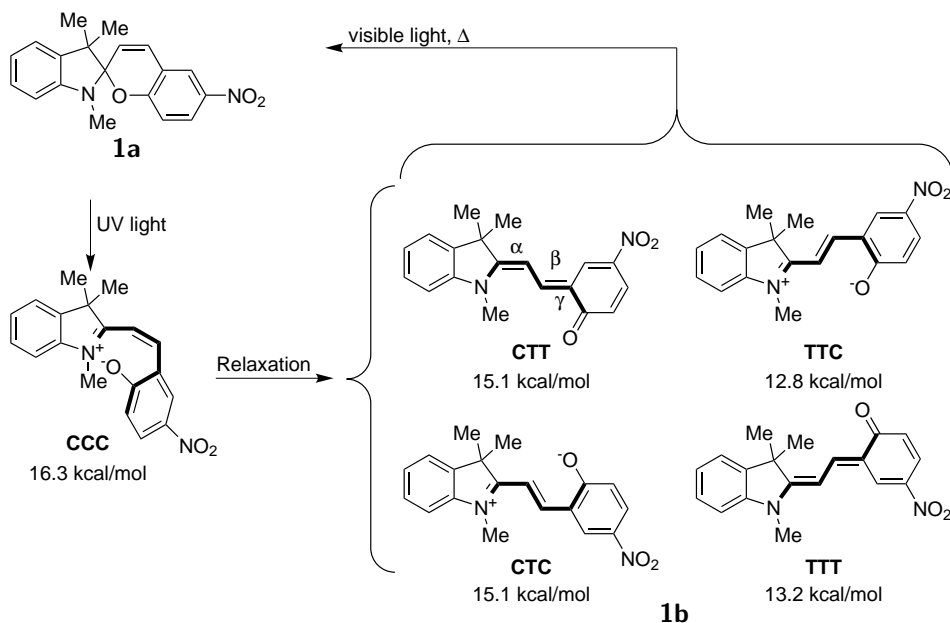


Scheme II.1 Typical synthesis of the spiropyran **1**. The indole side is highlighted in blue and the chromene side in red.

Spiropyrans can undergo a reversible ring-opening reaction yielding merocyanines. This reaction can be triggered by light, heat, electrochemical oxidation and reduction, protonation, metal ions and the polarity of the solvent.^[119] This isomerization is accompanied by drastic changes of several properties,^[12,119] such as the dipole moment,^[123,124] the dielectric constants,^[125] the geometrical dimensions,^[126] the absorption and emission behavior.^[127,128] Various applications^[12,119] of SPs were based upon these properties, most notably as sensor for gases^[129] or mechanical stress.^[14,23,29] Additionally, the SP→MC isomerization can be utilized in photoswitchable OFETs.^[24]

1.1. Photochromism of Spiropyrans

The mechanism of the photochemical ring-opening strongly depends on the substituents. The photoisomerization of a spiropyran with a proton at the 6-position of the chromene site involves only singlet states.^[130] Introduction of a nitro group at the 6-position – as in the spiropyran **1** in Scheme II.1 – leads to triplet states during the isomerization process that slow down the photoisomerization.^[131] Since the singlet pathway is not excluded, this additional triplet path increases the quantum yields of nitro spiropyrans **1a** compared to



Scheme II.2 Switching of the spiropyran **1**. Upon UV irradiation, the spiro C2–O bond of the closed isomer **1a** is broken and the open merocyanine isomer **1b** is formed. The initially formed cisoid merocyanine **CCC** relaxes to the transoid isomers in picoseconds. By rotation around the dihedral angles α , β and γ (highlighted as bold bonds in structure **CTT**), four isomers were found in solution: **CTT**, **CTC**, **TTC** and **TTT**.^[136] The gas phase free energy of each conformer is shown in relation to the closed spiropyran **1a**.^[137] Depending on the dipole moments of the conformers, either the zwitterionic (**CTC** and **TTC**) or the quinoidal (**CTT** and **TTT**) resonance forms are favored.^[137] The ring closure appears thermally and upon irradiation with visible light.

unsubstituted spiropyrans.^[132–135] The different MC isomers can be labeled according to the dihedral angles (α , β and γ) of the three central double bonds (Scheme II.2).

Initial irradiation with UV light or heating breaks the C–O bond of the central spiro moiety while the surrounding geometry is maintained.^[138] (Structure **CCC**, Scheme II.2) The resulting cis MC relaxes by isomerization of the former ethylene bridge to a *transoid* species in short time scales.^[130,135,139] Depending on the energy source, the bond scission can be described as electrocyclic ring opening (thermal isomerization) or heterolytic bond cleavage (photoisomerization).^[12] Accordingly, the quinoidal (thermal isomerization) or the zwitterionic (photoisomerization) resonance structures predominant the character of the ephemeral **CCC** isomer.^[12] While electron withdrawing groups (EWGs) at the 6-position facilitate the polar zwitterionic pathway, substitution with electron rich electron donating groups (EDGs) increase the nonpolar quinoidal characteristics of the cis intermediate.^[140]

After (*Z*)→(*E*) relaxation of the central double bond, the resulting *trans* merocyanines absorb in the visible range ($\lambda_{max} \approx 550$ nm). The time constant of the rise of this absorption was found to be approximately 1 ps.^[131] Due to the mentioned sterical repulsions, only merocyanine isomers with (*E*)-geometries of the central double bond (**CTC**, **CTC**, **TTC** and **TTT**) are found in solution (See Scheme II.2).^[136] Of these four isomers, the **TTT** and **TTC** isomers are the most stable ones.^[137,141,142] While the **TTC** isomer is stabilized by attractive forces between the indolium and phenolate charges in the zwitterion, this stabilization is not

possible in the **TTT** isomer.^[143,144] Concomitantly, the calculated dipole moment of **TTC** was found to be approximately 1 D higher than the dipole moment of **TTT**.^[137] These two conformers can be distinguished by single molecule fluorescence spectroscopy: **TTC** emits at ca. 590 nm and **TTT** at ca. 635 nm.^[145] In most organic solvents, the polar species **TTC** of the merocyanine **1b** is dominant.^[146] However, due to its lower polarity, the **TTT** isomer is enriched in unpolar solvents as *n*-hexane.^[145] The isomerization from **TTC** to **TTT** can be induced photochemically, but the competing fluorescence and ring closure limit the quantum yields.^[147,148] The ring closure occurs thermally, following first order kinetics.^[149] The contribution of the two conformers **TTC** and **TTT** as starting point of the thermal ring closure was not investigated yet. Photochemically, the ring closure can be initialized from both, **TTC** and **TTT** forms, following a singlet state pathway.^[135,147]

The thermal ring closure reaction is predominant in the solid state, resulting in the absence of detectable photochromism. Suppressing the thermal back reaction makes the photochromism of SP detectable at low temperatures (90 K).^[150] A different attempt of increasing the photochromism of spiropyrans in solid materials is the incorporation of spiropyran dyes in polyoxometalates, which stabilize the MC forms by creating a highly polar environment.^[151] Incorporation into metal organic frameworks provides a comparable effect, leading to stabilization of the MC form.^[152] This design can be transferred to solution, where coordination cages can bind spiropyrans and merocyanines in their cavities.^[128,153]

While the closed SP form is thermodynamically stable for most systems, the open MC forms can be stabilized, leading to a so-called reversed photochromism.^[12] The phenolate moiety of the MC structures can bind to cations, either in complexes^[154,155] or surfaces, as in silica gel.^[156,157] Similarly, protonation of the SP form induces ring opening and results in protonation of the phenolate group in the zwitterion.^[12,119] This effect was used to preserve the open MC forms after electrochemically induced switching of multi-spiropyran polymers.^[158] Being fixed in the protonated merocyanine forms MCH^+ , photochemical control of the $(E) \rightarrow (Z)$ isomerization from the **TTT** to the **TTC** isomer becomes possible.^[158]

1.2. Mechanochromism of Spiropyrans

Since the switching of spiropyran results in changes of various properties, several energy sources can be used to trigger the ring opening.^[12,119] Besides the mentioned photo-, acido- and electrochromism, the ring opening can be induced by the application of mechanical forces. Upon switching, the change of distance is largest between the 8- and 5'-position.^[29] The carbon atoms at these positions are separated by 4.5 Å in the closed SP form **1a**, which increases to 10.6 Å in the open MC forms **1b TTC** and **TTT**.^[12]

Mechanical forces can be applied to molecules in the solid state by grinding or milling.^[159–161] In solution, the forces can be applied by ultrasonic irradiation or shear forces, which can both be seen as local variations in flow rates.^[21,23,162] In sonicated solutions, the SP \rightarrow MC isomerization rate depends on the degree of polymerization of the mechanophoric polymers.^[163,164] The attachment of polymers to the named 8- and 5'-positions of spiropyran facilitates the

transfer of the mechanical force to the central mechanochrome.^[14,165] This effect leads to mechanoswitching upon elongation of samples made of these polymers.^[14,29]

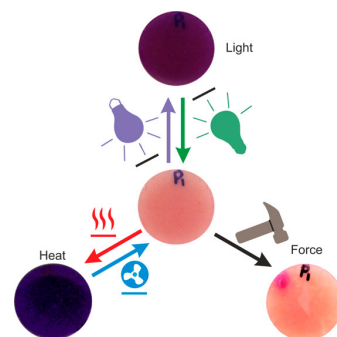
2. Spiropyran Dyes as Additive in Composites

The covalent incorporation of spiropyrans into the backbone of polymers results in impressive stress responses.^[14,29] However, the synthesis of the reported mechanochromic polymeric materials typically requires several sophisticated steps. For the application as photo- or mechanochromic coating, the non-covalent incorporation of spiropyran in polymeric matrices is a promising strategy.^[166] The reported examples of photoswitchable spiropyrans in spatially confined environments such as polyoxometalates, metal organic frameworks or molecular cages suggest that SPs may also be able to switch in several other polymer matrices.^[128,151–153] By using SP as an additive, the amount of spiropyran as expensive component can be easily varied and several matrix materials can be tested.

2.1. Multi-Stimuli Response of a Spiropyran / Zinc Oxide / PTU Composite

In cooperation with the Functional Nanomaterials group of Rainer Adelung, we found and reported a poly(thiourethane) (PTU)/SP composite that responded to heat, light and mechanical force.^[167] Reprinted from: Sindu Shree, Mathias Schulz-Senft, Nils H. Alsleben, Yogendra Kumar Mishra, Anne Staubitz, Rainer Adelung, Light, Force, and Heat: A Multi-Stimuli Composite that Reveals its Violent Past, *ACS Appl. Mater. Interfaces* **2017**, *9*, 38000–38007. Copyright 2017 American Chemical Society; reprinted with permission (See page 431).

DOI: 10.1021/acsami.7b09598



Abstract

A self-reporting polythiourethane/tetrapodal-ZnO (PTU/T-ZnO) composite is produced using spiropyran as an additive at a concentration as low as 0.5 wt %. Exposure to heat, UV light and mechanical force caused the spiropyran to undergo reversible isomerization indicated by a reversible color change. The studies have been conducted with a constant spiropyran concentration at 0.5 wt %, meanwhile varying the T-ZnO concentration from 0 to 7.5 wt %. The tetrapodal ZnO served as a prism: the light scattering effect of T-ZnO created a visual impression of uniform color distribution. The interconnected network of the tetrapodals of ZnO embedded in the PTU matrix enhanced the mechanical stability of the polymer leading to high impact resistance up to ca. 232 kPa. PTU/spiropyran also

emerged as a possible thermal sensing coating, due to its temperature sensitivity. Due to the broad green luminescence band (ca. 535 nm) in T-ZnO, the colored merocyanine form which absorbs in this region of the spectrum switches back to spiropyran at this wavelength. High concentrations of T-ZnO were shown to reduce the effect one of the switching triggers i.e., ultraviolet light. Using this property of T-ZnO it was possible to achieve a switchable system with the possibility of separating the stimuli.

Scientific Contribution to this Publication

For this article, I synthesized and provided the spiropyran switch **1** and supported Sindu Shree in writing the manuscript.

Light, Force, and Heat: A Multi-Stimuli Composite that Reveals its Violent Past

Sindu Shree,^{*,†} Mathias Schulz-Senft,[‡] Nils H. Alsleben,[†] Yogendra Kumar Mishra,^{*,†} Anne Staubitz,^{*,‡,§,||} and Rainer Adelung^{*,†}

[†]Institute for Materials Science, Functional Nanomaterials, Kiel University, Kaiserstr. 2, D-24143 Kiel, Germany

[‡]Otto-Diels-Institute for Organic Chemistry, Kiel University, Otto-Hahn-Platz 4, D-24118 Kiel, Germany

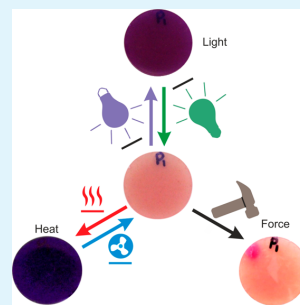
[§]Institute for Organic and Analytical Chemistry, University of Bremen, Leobener Str. 7, NW2 C, 28359 Bremen, Germany

^{||}MAPEX Center for Materials and Processes, University of Bremen, Bibliothekstraße 1, Bremen 28359, Germany

Supporting Information

ABSTRACT: A self-reporting polythiourethane/tetrapodal-ZnO (PTU/T-ZnO) composite is produced using spiropyran as an additive at a concentration as low as 0.5 wt %. Exposure to heat, UV light and mechanical force caused the spiropyran to undergo reversible isomerization indicated by a reversible color change. The studies have been conducted with a constant spiropyran concentration at 0.5 wt %, meanwhile varying the T-ZnO concentration from 0 to 7.5 wt %. The tetrapodal ZnO served as a prism: the light scattering effect of T-ZnO created a visual impression of uniform color distribution. The interconnected network of the tetrapodal of ZnO embedded in the PTU matrix enhanced the mechanical stability of the polymer leading to high impact resistance up to ~232 kPa. PTU/spiropyran also emerged as a possible thermal sensing coating, due to its temperature sensitivity. Due to the broad green luminescence band (~535 nm) in T-ZnO, the colored merocyanine form which absorbs in this region of the spectrum switches back to spiropyran at this wavelength. High concentrations of T-ZnO were shown to reduce the effect one of the switching triggers i.e., ultraviolet light. Using this property of T-ZnO it was possible to achieve a switchable system with the possibility of separating the stimuli.

KEYWORDS: Self-reporting spiropyran switch, merocyanine (MC), polythiourethane (PTU), tetrapodal-zinc oxide (T-ZnO), photochromic, thermochromic and mechanochromic properties



1. INTRODUCTION

Self-reporting materials are capable of showing a measurable, often visible indication of the conditions they have been subjected to. Spiroyrans are molecular switches that undergo a reversible molecular transformation to a merocyanine (MC) form in response to different stimuli such as mechanical stress,^{1–4} light,⁵ and heat⁶ and thereby showing a color change.^{7,8} As the intensity of the color is linked to the amount of active molecules present, spiropyran should be an ideal self-reporting material.^{9,10} Several self-assembly, self-reporting materials and optical sensors based on spiropyran have been successfully produced.^{11–15} In most of such systems, the spiropyran is either covalently linked to a polymer chain,^{16–18} or grafted on metallic surfaces.^{19–22} Most known systems of spiropyran as a mechanical stress indicator require its covalent incorporation into the main chain or as cross-links of the polymer.^{23–27} This results in long synthesis routes from commercially available starting materials to the final product, thus complicating the scale-up process.^{1,5} There have been examples of studies on the mechanical sensitivity of spiropyran derivatives in crystal form, illustrating mechanochromic switching under high hydro static pressure.^{28–32} This implies that spiropyran can be used as an additive in the polymer composite

system and would provide a more cost-effective solution.^{33–35} Photoinduced mechanical switching of spiropyran in a composite system has been demonstrated in poly(ethyl methacrylate-co-methyl acrylate) (PEMMA) films.³⁶ These films were produced by blending 3 wt % of spiropyran, and the stiffness of the material was altered by the photoinduced switching. However, mechanoswitching has not yet been demonstrated.³⁶ In order to use spiropyran as sensor for mechanical stress, it is crucial to reduce the weight fraction of spiropyran to an absolute minimum such that the physical and chemical properties of the polymer matrix remain uninfluenced. Applications involving stress indicators used as coatings, must withstand exposure to sunlight.^{36,37} As several stimuli induce switching in spiropyran, for outdoor applications it is substantial to separate the stimuli. Such stress sensitive coatings should not switch due to UV irradiation. To a create stimuli separation, the presented research uses tetrapodal zinc oxide (T-ZnO) as an additional filler. ZnO is an n-type inorganic semiconductor with a direct wide band gap of ~3.3 eV at 300 K

Received: July 3, 2017

Accepted: October 2, 2017

Published: October 2, 2017

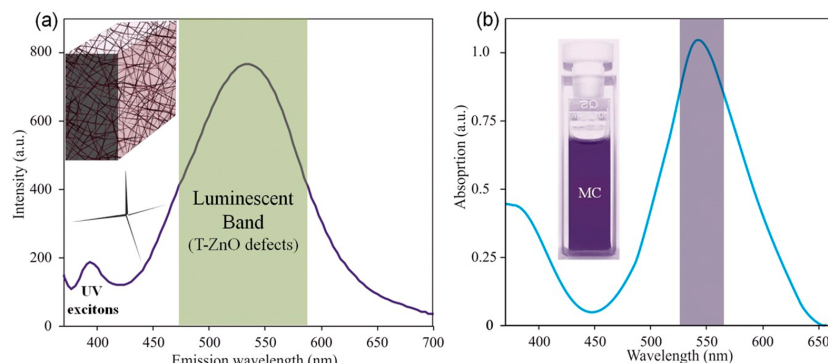


Figure 1. Sketch of (a) a PL spectrum of PDMS/T-ZnO composite and (b) an absorption spectrum of MC, which shows the ring opening reaction of spiroyrans upon UV light irradiation (365 nm) to the open MC form.

and exhibits a blue-green luminescence at room temperature and can be efficiently used for engineering different properties of the polymer based composites, e.g., optical, mechanical, electrical, wettability, etc.^{38–45} For example, in the PDMS/T-ZnO composite system, where the polymer matrix is highly cross-linked, T-ZnO exhibits a strong defect mediated green emission (520–570 nm) under UV irradiation.^{40,46} The representative images for the T-ZnO based PDMS composite and corresponding photoluminescence (PL) spectrum are schematically shown in Figure 1a.^{40,47} The PL emission around 380 nm corresponds to bandgap exciton emission from T-ZnO, however the broad green emission band is mainly the contribution from different types of defects such as zinc interstitials, oxygen vacancies, etc. present in the T-ZnO.⁴⁰ At high filling fractions of T-ZnO, the intensity of green PL emission with respect to exciton increases. Therefore, a defined amount of T-ZnO could be used for required luminescence features in a polymer composite. In the present work composites with merely 3.5–7.5 wt % T-ZnO have been fabricated for the accessibility of the broad green PL band. The open form that is merocyanine (Figure 1b) which has a strong absorption peak in the visible region (550–570 nm) closes to the spiroyrans form under green light illumination.^{8,9,16} The defects present in ZnO induce green emissions under UV irradiation^{45,48,49} and this should accelerate the switching of the merocyanine form back to the spiroyrans, thus shifting the photostationary equilibrium toward the spiroyrans form. In addition, the tetrapodal structure of T-ZnO forms an interconnected 3D network thus increasing the overall mechanical stability of the polymer matrix.^{47,50–53} The composite samples presented here were prepared with a commercially bought polythiourethane (PTU) kit. This kit contains pentaerythritol tetrakis(3-mercaptopropionate) (PETMP) and hexamethylene diisocyanate (HDI) monomers.^{50,52} The monomers were mixed and polymerized in a solvent-free polyaddition reaction with negligible shrinking.⁵² Because of the highly cross-linking PETMP component and the linear HDI component, the PTU uniquely possesses both, thermo-set and thermoplastic properties. PTU is an ideal matrix for coatings, because it is stable up to 250 °C and it is relatively chemically inert.⁵⁰ In a two component composite, T-ZnO was used to enhance the mechanical stability of the PTU matrix which led to a high impact resistance.^{50–52}

Here we present the first example of a polymer/ceramic composite, which acts as a sensor to impact pressure, temperature and UV irradiation by a visible color change. The photoinduced switching of spiroyrans was altered successfully by the addition of T-ZnO, while the mechanically induced switching was maintained. In addition, this is the first report on the mechanically induced switching of spiroyrans in a polymer composite. In the chosen three-component system PTU/T-ZnO/spiroyrans, the mechanochromic sensor is the most expensive component. Reducing the weight fraction of spiroyrans to 0.5 wt % offers the production feasibility of these composites at a larger scale. In previous reports, spiroyrans has been used as an initiation center from which polymerization in two directions has been performed. Well known examples include PMA,⁵⁴ PMMA⁵⁵ (which were polymerized using ATRP) or PLA¹⁴ (which has been performed with ring opening polymerization). In these examples, the spiroyrans content by weight was ca. 0.2 wt %, ca. 0.1 wt %, or 0.04–0.43 wt %, respectively.¹⁴ However, it must not be overlooked that the covalent linking of the spiroyrans in the main chain of the polymer adds reaction steps and thus involves additional costs. In context to industry level productions, the presented strategy will save the fabrication costs which is the main motivation of the study here.

2. EXPERIMENTAL SECTION

1,3,3-Trimethyl-2-methyleneindoline was purchased from Sigma-Aldrich Co. (Aldrich, 97%), 2-hydroxy-5-nitrobenzaldehyde was purchased from TCI Co. (>97%) and ethanol was purchased from Acros (anhydrous, ≥ 99.5%, stored over molecular sieves). All reagents were used without further purification. The spiroyrans dye (SP) was synthesized as follows. 1,3,3-Trimethyl-2-methyleneindoline (5.20 g, 30.0 mmol) and 2-hydroxy-5-nitrobenzaldehyde (5.01 g, 30.0 mmol) were dissolved in EtOH (350 mL) and heated to 78 °C for 6 h. Then the reaction mixture was cooled to –25 °C and the crystallized product was obtained after filtration as a green powder (7.69 g, 23.8 mmol, 79%). The highly cross-linked polythiourathane (PTU) was produced by combining two components, pentaerythritol tetrakis(3-mercaptopropionate) (PETMP) and hexamethylene diisocyanate (HDI). These were procured from FPT Fluid- & Prozesstechnik GmbH. The NMR studies of the as purchased components revealed that the PETMP and HDI were >95% pure. The used abbreviations and analytical equipment have listed at text page in Supporting Information. The molecular structures of 1,3,3-Trimethyl-2-methyleneindoline compound and PTU polymer are given at the materials page in Supporting Information. The plotted NMR spectra

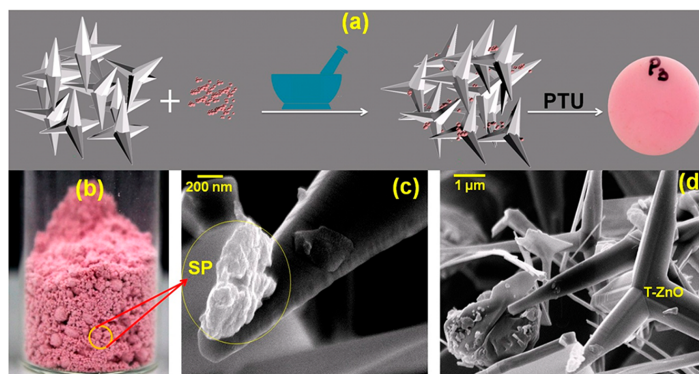


Figure 2. Schematic in (a) is a pictorial representation of the sample preparation method. Digital camera image (right panel in a) of a representative polymer composite after dispersion and polymerization. (b) Digital camera image of the mixture of T-ZnO and spirocyanine before dispersing into the PTU matrix. (c) and (d) SEM micrographs at high and low magnifications corresponding to the powdered T-ZnO and spirocyanine mixture.

corresponding to materials under different conditions are shown in Supporting Information (SI) Figures S1–S4.

The tetrapodal zinc oxide (T-ZnO) powder was produced by the flame transport synthesis method (FTS).^{18,20} T-ZnO and the spirocyanine were ground together with a mortar and pestle (Figure 2a). This powdered mixture was then dispersed by hand into the first component of PTU, the PETMP (4.17 g, 8.50 mmol). The prepared mixture was degassed in a desiccator to remove all the remaining air bubbles for 10 min. To this PETMP blend, the second component, HDI (5.83 g, 34.6 mmol) was added, mixed well and degassed. The Spirocyranine did not dissolve in the mixture, behaving like a typical additive in the polymer composite system. Finally, this mixture of components was poured into silicone molds to fabricate pellet shaped samples with a diameter of 15 mm (the panel on the far right in Figure 2a). The molds were placed in an oven at 80 °C for 3 h. The PTU formed due to the polyaddition reaction between PETMP and HDI.

In all the samples, the concentration of spirocyanine was kept constant at 0.5 wt % with respect to weight of PTU and the concentration of T-ZnO in PTU was varied from 0 wt % to 7.5 wt %. The details of all the fabricated samples are given in Table 1. All

measured area of impact was $1.53 \times 10^{-4} \text{ m}^2$, hence pressure per impact was 24 kPa.

3. RESULTS AND DISCUSSION

The ZnO (including the tetrapods used) is known to be very stable and is a nonreactive semiconductor in solid state under atmospheric conditions. The spirocyanine that was used in the experiments presented here is also chemically stable. Therefore, no chemical interaction is expected between the additives. However, to further reduce the interaction possibility, solvent free grinding procedure was followed for sample preparation. Since these tetrapods are solid in nature, the spirocyanine is mainly coated on their surface as it is almost impossible for spirocyanine to penetrate inside bulk T-ZnO. The photograph in Figure 2b shows the powdered mixture of spirocyanine and T-ZnO before adding it to the PTU matrix. To understand the morphology of the hand ground additive mixture, it was studied using scanning electron microscopy (SEM). The SEM micrographs in Figure 2(c-d) corresponding to mixed powder (Figure 2b) reveal intact T-ZnO crystals with clusters of spirocyanine molecules and amorphous particles around the arms of the tetrapods. In the final state of the sample (digital camera image on the right panel, Figure 2a), the color appears to be quite uniform. Due to the light scattering effect caused by the hexagonal wurtzite-type ZnO crystals, the spirocyanine visually appeared to be homogeneously distributed throughout the powdered mixture.³⁹

The photochromic activity of spirocyanine in the polymer composite was studied in a sample sequence, i.e., SP, P₁, P₂, P₃, and P₄ were subjected to UV irradiation for 30 s (central wavelength = 360–370 nm), (Figure 3a), and were switched back with green light (central wavelength = 520–530 nm) irradiation for 30 s, (Figure 3b). The sample series with T-ZnO, P₁, P₂, P₃, and P₄ showed negligible agglomeration of the ZnO or spirocyanine in the PTU matrix. Within the sample series, the addition of increased amounts of T-ZnO seemed to deepen the coloring before and after illumination. The variation in the color of the polymer composites suggested that in this case it might not be a straightforward isomerization from spirocyanine to merocyanine. Referring to the works of Uchida et al., such color variation is observed when there is molecular stacking of the merocyanine form.⁵⁶ The observed switching in some of the samples might be between merocyanine in the form of H

Table 1. Abbreviations and the Details on the Varying Concentration of T-ZnO and Spirocyranine in PTU

sample name	total additives in PTU (wt %)	T-ZnO in PTU (wt %)	spirocyanine in PTU (wt %)
SP	0.5	0	0.5
P ₁	1	0.5	0.5
P ₂	2	1.5	0.5
P ₃	4	3.5	0.5
P ₄	8	7.5	0.5

samples were prepared in a chemical fume hood with a UV shielding door under identical experimental conditions. Photochromic, thermochromic and mechanophoric tests were performed in a dark room to avoid accidental switching.

The “Hammer test” test (schematic is given in Supporting Information, SI Figure S5) involved a hammer weighing 2.141 kg with a hinge at its base falling freely on the samples. The test was repeated until a color change was observed. The force required to damage the system was determined by the number of hits needed to cause a color change from orange to purple. The impact force was calculated using the following equation $F = m \cdot g \cdot \sin \theta = m \cdot g \cdot h / l$ where F is Force, m is weight of the hammer head, g is acceleration due to gravity, h is height of fall, and l is length of the hammer. The force per impact was calculated to be 3.63 N. Pressure per impact was calculated using $P = F/a$ where a is the area of impact or point of contact. The

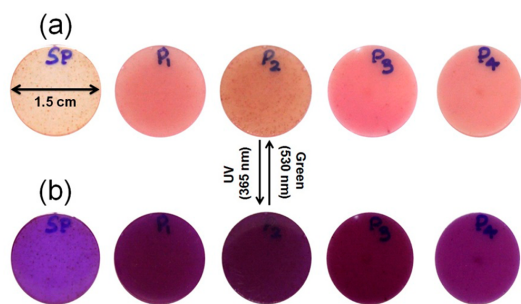


Figure 3. (a) The polymer composites, SP, P₁, P₂, P₃, and P₄ before UV irradiation, the composites appear yellow-orange in color. (b) The photochromic response of polymer composites was analyzed by irradiating the samples with UV light (365 nm) for 30 s. The reversibility of the isomerization was verified by switching the samples back to their original form with a green light (520–530 nm) irradiation for 30 s. All the images were taken using a white standard for white balancing the camera.

stacking to merocyanine in the form of J stacking.⁵⁶ Further reports underline this hypothesis, which requires more detailed analyses in this particular case.^{57,58}

Compared to the SP sample (Figure 3a, b, first on the left), the samples P₁ with 0.5 wt % and P₂ with 1.5 wt % of T-ZnO (2nd and third samples from left) showed a darker color. A further increase of the fraction of T-ZnO appeared to reduce the color intensity (P₃ and P₄, 3.5 and 7.5 wt % T-ZnO). UV/Visible spectroscopy supports this observation. Absorption spectra in the range 700–500 nm were recorded for the switched samples (Figure 4a). The samples P₁ and P₂ showed higher absorptions than the SP sample. The sample P₄ with the highest fraction of T-ZnO exhibited the smallest absorption. The observed higher absorption in samples P₁ and P₂ is most likely due to the multiple reflections caused by the prism like tetrapodal ZnO structures as compared to the pure sample SP. As there is no green emission in the pure sample SP, the absorption is higher than that of samples P₃ and P₄. These findings validated the theory that the T-ZnO may function as a light guide for UV irradiation and that it thereby can serve to improve the photochromic switching of spiropyran. The photochromicity of spiropyran was restrained in the samples P₃ and P₄, this was probably due to a combination of the UV absorption of T-ZnO and its green emission. These combined effects appeared to reduce the effective photoswitching of spiropyran under UV irradiation. Despite their different photoswitching efficiencies, all samples showed a clear reversible switching with no signs of photo bleaching up to

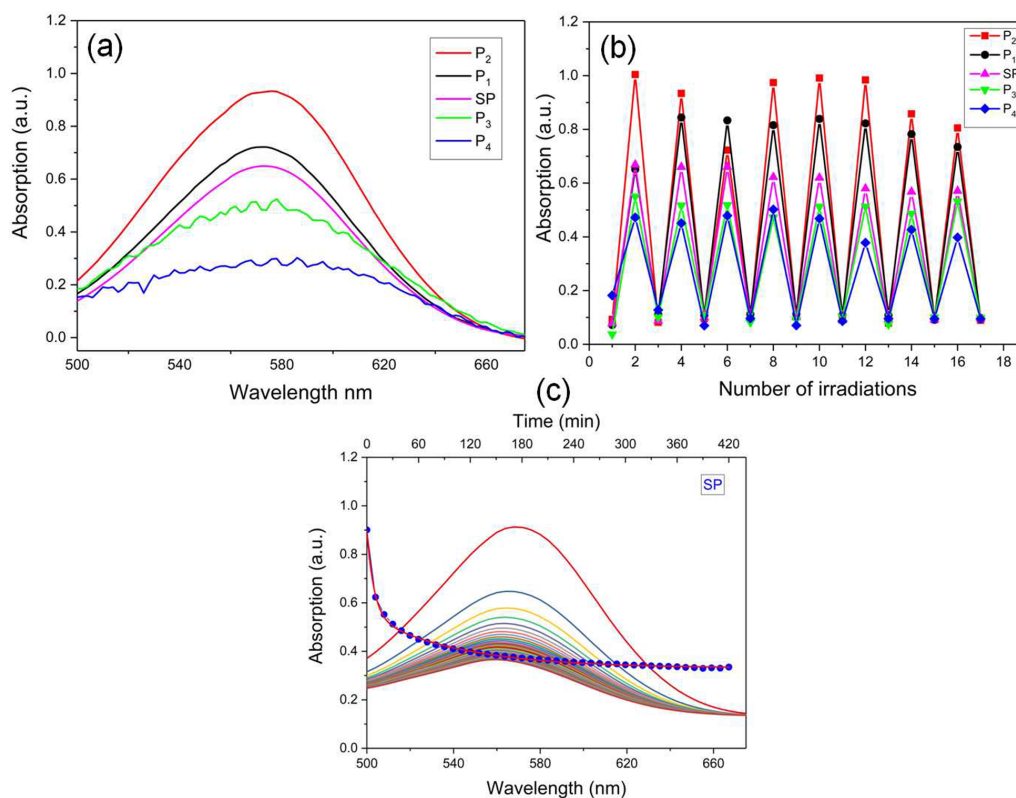


Figure 4. (a) Absorption spectra of the polymer composites SP, P₁, P₂, P₃, and P₄ after UV irradiation for 30 s. (b) Cyclic absorbance measurements of SP, P₁, P₂, P₃, and P₄ at 560–570 nm before and after UV illumination followed by green illumination for 17 irradiation series. (c) Back switching or thermal relaxation of merocyanine in the sample SP.

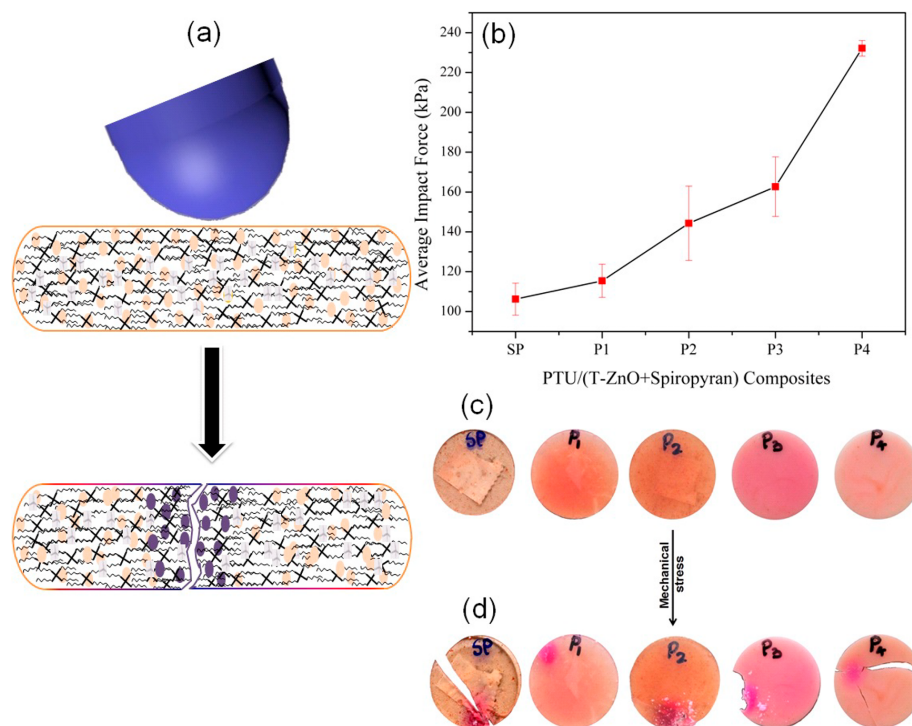


Figure 5. (a) Pictorial representation of the crack formation and the color switching in the polymer composites subjected to the “Hammer test”. (b) Plot showing the average impact force required to damage the polymer matrix causing a color change (c) Polymer composites before being subjected to the mechanical stress. (d) Polymer composites after being subjected to the “Hammer test”. The bruises caused by the high impact force of the hammer in the samples are visible as the polymer composites at the point of impact, which turned purple.

17 irradiations (Figure 4b). The ripples observed in the spectra of the samples P_3 and P_4 might be an effect caused by the whispering gallery mode resonances from the hexagonal arms of ZnO tetrapods.^{59,60} For a qualitative study on the “Turn Off” mechanism of merocyanine to spiropyran, the sample SP was irradiated with UV light for 30 s and was allowed to thermally relax to a photostationary equilibrium. Meanwhile, an absorption spectrum was recorded every 10 min, cf. Figure 4c. To follow the decay of merocyanine, the absorbance between the range 562–568 nm has been recorded and is plotted in Figure 4c. The thermal decay of merocyanine at this range follows a biexponential curve with the individual half lifetimes of $\tau_1 = 7$ min 15 s and $\tau_2 = 83$ min 23 s. This system with the second order kinetics is similar to the solid suspension of spiropyran nanocrystals studied by Breslin et al.^{61,62} However, the total relaxation of merocyanine was not observed even after 6 h of thermal decay time, the broad peak of merocyanine can still be observed in the absorption spectra shown in Figure 4c. This is an ideal system for an indication of damage by a color change which is easily detectable even for the naked eye hours after the damage has occurred.

The response of the composites with respect to mechanical force was analyzed by exposing the samples to a “Hammer test” (for more details see SI Figure S5). In this test, a hammer with a spherical shaft (tip) was allowed to fall from a defined height onto the sample (each hit generating pressure up to 24 kPa), while observing the color and other changes occurring in the

sample during repeated hammering. Over several hits, a color change from yellow-orange to purple occurred, while at the same time cracks appeared. To help visualization the hammering test, a schematic representation in the polymer composites is shown in Figure 5a. The average impact force required to change the color of the polymer composites SP, P_1 , P_2 , P_3 , and P_4 governed by the conservation of momentum was calculated (Supporting Information, SI Table S1) and plotted (with error bars) as shown in Figure 5b. From the plot (Figure 5b) it is clear that the force needed to cause switching of spiropyran in the sample P_4 was much higher in comparison to the other samples with lower weight fraction of T-ZnO. This might be the effect of the interconnected nature of T-ZnO, higher concentration of the network of tetrapodal structure embedded in the polymer matrix enhanced the mechanical stability allowing the system to endure higher impact force.^{38,40,47} The digital camera pictures in Figure 5c and d demonstrate the samples before and after they were subjected to the “Hammer test”. In Figure 5d, the color change after the mechanical stress is clearly visible. In all the samples, the color change only appeared at the point of impact (POI) evidently indicating the area which underwent the high mechanical stress. The sample P_1 showed a color change at the POI before the cracks appeared. The force required to cause a switch in P_1 is slightly (~ 115 kPa) higher than for the sample SP (~ 106 kPa). With merely 0.5 wt % of T-ZnO in the polymer composite, P_1

showed higher impact resistance and effective fatigue indication. Monitoring the samples after hammering is a challenging task. It is difficult to measure the absorption spectra of these samples after the "Hammer Test" as the samples either have cracks or they fall apart.

In addition to the composite's response to light and force, heat was also investigated. The effect of T-ZnO on the thermochromic activity of spiropyran was examined in detail. The samples SP, P₁, P₂, P₃, and P₄ were positioned as represented in the enclosed black frame of Figure 6 and heated

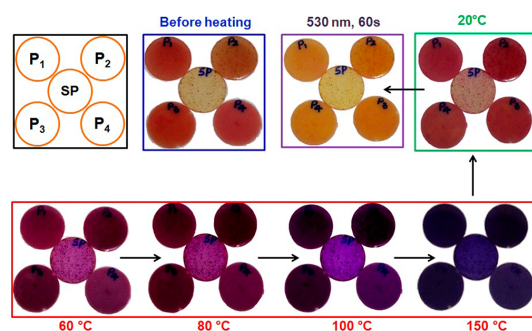


Figure 6. Schematic representation of the sample positions during the thermochromic tests for clarity. The polymer composites shown in the blue frame are the SP, P₁, P₂, P₃, and P₄ before heat treatment. The red frame shows the samples heated up to 60, 80, 100, and 150 °C and held for 30 s. The green frame presents the composites cooled to room temperature, 20 °C. The purple frame shows the cooled composites after green light irradiation (560 nm) 60 s.

on a heating plate. The red frame encloses all the samples, which were heated together and held for a period of 30 s at 60, 80, 100, and 150 °C. With the exception of sample SP, which turned opaque, no polymer composites with T-ZnO showed any changes. All the samples seemed to attain a similarly colored state at each temperature. The polymer composites at 150 °C displayed an intense color change. At such high temperature, the unordered polymer chains in PTU gain higher mobility increasing the free volume in the polymer matrix. With higher free volume, there is lower spatial hindrance to form merocyanine. Hence, in the red frame of Figure 6, the image captured at 150 °C illustrates that every sample reached similar dark purple colored state independent of the concentration of T-ZnO. In some cases reported in the literature, heat is used to switch the mechanically opened merocyanine back to spiropyran²⁵ and examples of inverse thermal switching of the spiropyran derivative that was used here in aqueous media have also been published before.⁶³ However, the thermodynamic equilibrium between spiropyran and the merocyanine depends mainly on two effects, the first effect comes from the functional groups of the spiropyran dye which changes the electron density in the molecule and second effect comes from the polarity of the surrounding (typically the solvent). Mostly studied mechanochromic systems consist of spiropyran in the polymer backbones whereas the system presented here can be visualized as a "frozen colloidal solution".²⁴ The PTU matrix can be seen as solvent and due to its high polarity, merocyanine is stabilized. The effect of inverse thermal switching of the same spiropyran dye dissolved in an aqueous media has been reported. However, the addition of T-ZnO seemed to have no

particular effect on the thermochromic activity of spiropyran. To avoid decomposition of PTU, the samples were cooled together from 150 °C to room temperature (20 °C). As seen in the image enclosed by the green frame in Figure 6, all the polymer composites switched back to almost their preheated state. Whereas heating caused no damage to the switches, the samples did not completely recover their original state after cooling. The cooled samples were irradiated with green light (530 nm) for 60 s to prove that the remaining merocyanine present can be switched back to spiropyran.

4. CONCLUSIONS

In summary, our research findings demonstrate a simple dispersion based method to produce multistimuli composite materials with potential real life applications such as stress reporting sensor, photochromic and thermochromic coating etc. It consists of a polymer matrix, polythiourethane (PTU), in which tetrapodal ZnO particles are dispersed as a solid support. The most important component of the system studied here, responsible for the multistimuli activity, is spiropyran. Spiropyran was successfully utilized as a thermo-, photo-, and mechanochromic switch as a composite at a low concentration of 0.5 wt % with respect to the polymer matrix. This is the first example of mechanochromism of spiropyran in a polymer composite system, without covalently binding to the polymer matrix. Additionally, it was possible to tune the response of spiropyran to UV light with the assistance of T-ZnO. Both enhancing and suppressing the photochromism was achieved by merely varying the concentration of T-ZnO, while keeping the thermo- and mechanical switching behavior of spiropyran unaffected. At low concentrations, T-ZnO works as a light guide for the UV light, because of its crystalline facets. High concentrations of T-ZnO lead to a decrease in the photo-switching of spiropyran, which is a result of the combination of its UV absorption and the broad green emission. Additionally, the T-ZnO increased the impact resistivity of the PTU/SP composites. The switching under stress and heat of spiropyran were proven independent from the fraction of T-ZnO. This successful stimuli separation by a nonstandard integration of self-reporting ability in polymer composites opens the door for numerous outdoor applications.

■ ASSOCIATED CONTENT

Supporting Information

The Supporting Information is available free of charge on the ACS Publications website at DOI: 10.1021/acsami.7b09598.

Used abbreviations and analytical equipment (Text); Material structural formula and details (Materials); Plotted NMR spectra of different materials analytical plotted NMR spectra under different conditions (Figures S1–S4); Hammer test setup (Figure S5); Average impact forces required to damage the samples (Table S1) (PDF)

■ AUTHOR INFORMATION

Corresponding Authors

- *(S.S.) E-mail: sisi@tf.uni-kiel.de.
- *(Y.K.M.) E-mail: ykm@tf.uni-kiel.de.
- *(A.S.) E-mail: staubitz@uni-bremen.de.
- *(R.A.) E-mail: ra@uni-kiel.de.

ORCID

Yogendra Kumar Mishra: 0000-0002-8786-9379

Author Contributions

The manuscript was written through contributions of all authors. All authors have given approval to the final version of the manuscript.

Notes

The authors declare no competing financial interest.

ACKNOWLEDGMENTS

This project was supported by the Special Research Area 677 "Function by Switching" project C14 of the Deutsche Forschungsgemeinschaft (DFG). The Institutional Strategy of the University of Bremen, funded by the German Excellence Initiative, has supported this research. The authors thank Dr. Viktor Hrkac for the fruitful feedback and discussions.

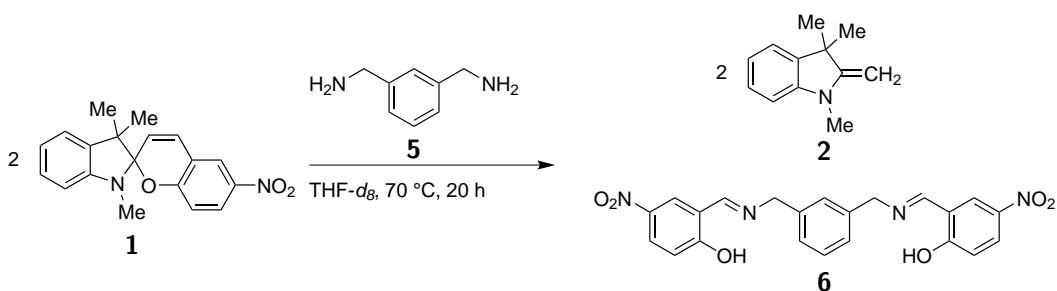
REFERENCES

- (1) Caruso, M. M.; Davis, D. A.; Shen, Q.; Odom, S. A.; Sottos, N. R.; White, S. R.; Moore, J. S. Mechanically-Induced Chemical Changes in Polymeric Materials. *Chem. Rev.* **2009**, *109* (11), 5755–5798.
- (2) Schulz-Senft, M.; Lipfert, M.; Staubit, A. Mechanopolymers. *Chem. Unserer Zeit* **2014**, *48* (3), 200–214.
- (3) Mo, S.; Meng, Q.; Wan, S.; Su, Z.; Yan, H.; Tang, B. Z.; Yin, M. Tunable Mechanoresponsive Self-Assembly of an Amide-Linked Dyad with Dual Sensitivity of Photochromism and Mechanochromism. *Adv. Funct. Mater.* **2017**, *27* (28), 1701210.
- (4) Gossweiler, G. R.; Brown, C. L.; Hewage, G. B.; Sapiro-Gheiler, E.; Trautman, W. J.; Welshofer, G. W.; Craig, S. L. Mechanochemically Active Soft Robots. *ACS Appl. Mater. Interfaces* **2015**, *7* (40), 22431–22435.
- (5) Zhang, J.; Zou, Q.; Tian, H. Photochromic Materials: More Than Meets The Eye. *Adv. Mater.* **2013**, *25* (3), 378–399.
- (6) Funasako, Y.; Takaki, A.; Inokuchi, M. Photo-, Thermo-, and Piezochromic Nafion Film Incorporating Cationic Spiropyran. *Chem. Lett.* **2016**, *45* (12), 1397–1399.
- (7) Seefeldt, B.; Kasper, R.; Beining, M.; Mattay, J.; Arden-Jacob, J.; Kemnitzer, N.; Drexhage, K. H.; Heilemann, M.; Sauer, M. Spiroprans as Molecular Optical Switches. *Photochem. Photobiol. Sci.* **2010**, *9* (2), 213–220.
- (8) Schulz-Senft, M.; Gates, P. J.; Sönnichsen, F. D.; Staubit, A. Diversely Halogenated Spiroprans - Useful Synthetic Building Blocks for a Versatile Class of Molecular Switches. *Dyes Pigm.* **2017**, *136*, 292–301.
- (9) Klajn, R. Spiropyran-Based Dynamic Materials. *Chem. Soc. Rev.* **2014**, *43* (1), 148–184.
- (10) Radu, A.; Byrne, R.; Alhashimy, N.; Fusaro, M.; Scarmagnani, S.; Diamond, D. Spiropyran-Based Reversible, Light-Modulated Sensing with Reduced Photofatigue. *J. Photochem. Photobiol., A* **2009**, *206* (2–3), 109–115.
- (11) Malic, E.; Weber, C.; Richter, M.; Atalla, V.; Klamroth, T.; Saalfrank, P.; Reich, S.; Knorr, A. Microscopic Model of the Optical Absorption of Carbon Nanotubes Functionalized with Molecular Spiropyran Photoswitches. *Phys. Rev. Lett.* **2011**, *106* (9), 97401.
- (12) Kinashi, K.; Nakamura, S.; Imamura, M.; Ishida, K.; Ueda, Y. The Mechanism for Negative Photochromism of Spiropyran in Silica. *J. Phys. Org. Chem.* **2012**, *25* (6), 462–466.
- (13) Araujo, J. V.; Rifaie-Graham, O.; Apebende, E. A.; Bruns, N. Chapter 11. Self-Reporting Polymeric Materials with Mechanochromic Properties. In *Bio-inspired Polymers*; Royal Society of Chemistry: Cambridge, 2016; pp 354–401.
- (14) Peterson, G. L.; Larsen, M. B.; Ganter, M. A.; Storti, D. W.; Boydston, A. J. 3D-Printed Mechanochromic Materials. *ACS Appl. Mater. Interfaces* **2015**, *7* (1), 577–583.
- (15) Nam, Y.-S.; Yoo, I.; Yarimaga, O.; Park, I. S.; Park, D.-H.; Song, S.; Kim, J.-M.; Lee, C. W.; Sun, L.-D.; Zhang, Y.-W.; Yan, C.-H. Photochromic Spiropyran-Embedded PDMS for Highly Sensitive and Tunable Optochemical Gas Sensing. *Chem. Commun.* **2014**, *50* (32), 4251–4254.
- (16) Bonafacino, J.; Tse, M.-L. V.; Pun, C.-F. J.; Cheng, X.; Chan, W. K. E.; Boersma, A.; Tam, H.-Y. Characterization of Spirooxazine and Spiropyran Hosted in Poly (Methyl Methacrylate) for Germicidal UV Source Indicator Application. *Opt. Photonics J.* **2013**, *3* (7A), 11–16.
- (17) Lee, C. K.; Davis, D. A.; White, S. R.; Moore, J. S.; Sottos, N. R.; Braun, P. V. Force-Induced Redistribution of a Chemical Equilibrium. *J. Am. Chem. Soc.* **2010**, *132* (45), 16107–16111.
- (18) Huang, C.-Q.; Wang, Y.; Hong, C.-Y.; Pan, C.-Y. Spiropyran-Based Polymeric Vesicles: Preparation and Photochromic Properties. *Macromol. Rapid Commun.* **2011**, *32* (15), 1174–1179.
- (19) Xie, X.; Mistlberger, G.; Bakker, E. Reversible Photodynamic Chloride-Selective Sensor Based on Photochromic Spiropyran. *J. Am. Chem. Soc.* **2012**, *134* (41), 16929–16932.
- (20) Gelebart, A. H.; Jan, M. D.; Varga, M.; Konya, A.; Vantomme, G.; Meijer, E. W.; Selinger, R. L. B.; Broer, D. J. Making Waves in a Photoactive Polymer Film. *Nature* **2017**, *546* (7660), 632–636.
- (21) Wan, S.; Zheng, Y.; Shen, J.; Yang, W.; Yin, M. On-off-on" Switchable Sensor: A Fluorescent Spiropyran Responds to Extreme pH Conditions and Its Bioimaging Applications. *ACS Appl. Mater. Interfaces* **2014**, *6* (22), 19515–19519.
- (22) Binil, I. I.; Mahima, S.; Thomas, K. G. Light-Induced Modulation of Self-Assembly on Spiropyran-Capped Gold Nanoparticles: A Potential System for the Controlled Release of Amino Acid Derivatives. *J. Am. Chem. Soc.* **2003**, *125* (24), 7174–7175.
- (23) Belhoub, A.; Boucher, F.; Jacquemin, D. Grafting Spiropyran Molecular Switches on TiO₂: A First-Principles Study. *J. Phys. Chem. C* **2016**, *120* (32), 18281–18288.
- (24) Davis, D. A.; Hamilton, A.; Yang, J.; Cremer, L. D.; Van Gough, D.; Potisek, S. L.; Ong, M. T.; Braun, P. V.; Martínez, T. J.; White, S. R. Force-Induced Activation of Covalent Bonds in Mechanoresponsive Polymeric Materials. *Nature* **2009**, *459* (7243), 68–72.
- (25) Wan, S.; Ma, Z.; Chen, C.; Li, F.; Wang, F.; Jia, X.; Yang, W.; Yin, M. A Supramolecule-Triggered Mechanochromic Switch of Cyclodextrin-Jacketed Rhodamine and Spiropyran Derivatives. *Adv. Funct. Mater.* **2016**, *26* (3), 353–364.
- (26) Florea, L.; Diamond, D.; Benito-Lopez, F. Photo-Responsive Polymeric Structures Based on Spiropyran. *Macromol. Mater. Eng.* **2012**, *297* (12), 1148–1159.
- (27) Li, M.; Liu, W.; Zhang, Q.; Zhu, S. Mechanical Force Sensitive Acrylic Latex Coating. *ACS Appl. Mater. Interfaces* **2017**, *9* (17), 15156–15163.
- (28) Wang, Y.; Tan, X.; Zhang, Y.-M.; Zhu, S.; Zhang, L.; Yu, B.; Wang, K.; Yang, B.; Li, M.; Zou, B. Dynamic Behavior of Molecular Switches in Crystal Under Pressure and Its Reflection on Tactile Sensing. *J. Am. Chem. Soc.* **2015**, *137* (2), 931–939.
- (29) Rosario, R.; Gust, D.; Hayes, M.; Jahnke, F.; Springer, J.; Garcia, A. A. Photon-Modulated Wettability Changes on Spiropyran-Coated Surfaces. *Langmuir* **2002**, *18* (21), 8062–8069.
- (30) Choi, C. L.; Koski, K. J.; Olson, A. C. K.; Alivisatos, A. P. Luminescent Nanocrystal Stress Gauge. *Proc. Natl. Acad. Sci. U. S. A.* **2010**, *107* (50), 21306–21310.
- (31) Choi, C. L.; Li, H.; Olson, A. C. K.; Jain, P. K.; Sivasankar, S.; Alivisatos, A. P. Spatially Indirect Emission in a Luminescent Nanocrystal Molecule. *Nano Lett.* **2011**, *11* (6), 2358–2362.
- (32) Choi, C. L.; Koski, K. J.; Sivasankar, S.; Alivisatos, A. P. Strain-Dependent Photoluminescence Behavior of CdSe/CdS Nanocrystals with Spherical, Linear, and Branched Topologies. *Nano Lett.* **2009**, *9* (10), 3544–3549.
- (33) Larkowska, M.; Wuebbenhorst, M.; Kucharski, S. Spirooxazine Photoisomerization and Relaxation in Polymer Matrices. *Int. J. Polym. Sci.* **2011**, *2011*, 627195.
- (34) Hemmer, J. R.; Smith, P. D.; Horn, M.; Alnemrat, S.; Mason, B. P.; Alaniz, J. R.; Osswald, S.; Hooper, J. P. High Strain-rate Response of Spiropyran Mechanophores in PMMA. *J. Polym. Sci., Part B: Polym. Phys.* **2014**, *52* (20), 1347–1356.
- (35) Wu, Z.; Pan, K.; Lü, B.; Ma, L.; Yang, W.; Yin, M. Tunable Morphology of Spiropyran Assemblies: From Nanospheres to Nanorods. *Chem. - Asian J.* **2016**, *11* (21), 3102–3106.

- (36) Samoylova, E.; Ceseracciu, L.; Allione, M.; Diaspro, A.; Barone, A. C.; Athanassiou, A. Photoinduced Variable Stiffness of Spiropyran-Based Composites. *Appl. Phys. Lett.* **2011**, *99* (20), 201905.
- (37) Pardo, R.; Zayat, M.; Levy, D. Reaching Bistability in a Photochromic Spirooxazine Embedded Sol-gel Hybrid Coatings. *J. Mater. Chem.* **2009**, *19* (37), 6756–6760.
- (38) Mishra, Y. K.; Kaps, S.; Schuchardt, A.; Paulowicz, I.; Jin, X.; Gedamu, D.; Freitag, S.; Claus, M.; Wille, S.; Kovalev, A.; Gorb, S. N.; Adelung, R. Fabrication of Macroscopically Flexible and Highly Porous 3D Semiconductor Networks from Interpenetrating Nanostructures by a Simple Flame Transport Approach. *Part. Part. Syst. Charact.* **2013**, *30* (9), 775–783.
- (39) Rodnyi, P. A.; Khodyuk, I. V. Optical and Luminescence Properties of Zinc Oxide (Review). *Opt. Spectrosc.* **2011**, *111* (5), 776–785.
- (40) Jin, X.; Götz, M.; Wille, S.; Mishra, Y. K.; Adelung, R.; Zollfrank, C. A Novel Concept for Self-Reporting Materials: Stress Sensitive Photoluminescence in ZnO Tetrapod Filled Elastomers. *Adv. Mater.* **2013**, *25* (9), 1342–1347.
- (41) Wang, C. H.; Liao, W. S.; Lin, Z. H.; Ku, N. J.; Li, Y. C.; Chen, Y. C.; Wang, Z. L.; Liu, C. P. Optimization of the Output Efficiency of GaN Nanowire Piezoelectric Nanogenerators by Tuning the Free Carrier Concentration. *Adv. Energy Mater.* **2014**, *4* (16), 1400392.
- (42) Chang, M.; Cao, X.; Zeng, H. Electrodeposition Growth of Vertical ZnO Nanorod/Polyaniline Heterostructured Films and Their Optical Properties. *J. Phys. Chem. C* **2009**, *113* (35), 15544–15547.
- (43) Song, J.; Li, J.; Li, X.; Xu, L.; Dong, Y.; Zeng, H. Quantum Dot Light-Emitting Diodes Based on Inorganic Perovskite Cesium Lead Halides (CsPbX₃). *Adv. Mater.* **2015**, *27* (44), 7162–7167.
- (44) Faraji, N.; Ulrich, C.; Wolff, N.; Kienle, L.; Adelung, R.; Mishra, Y. K.; Seidel, J. Visible-Light Driven Nanoscale Photoconductivity of Grain Boundaries in Self-Supported ZnO Nano- and Microstructured Platelets. *Adv. Electron. Mater.* **2016**, *2* (9), 1600138.
- (45) Janotti, A.; Van de Walle, C. G. Fundamentals of Zinc Oxide as a Semiconductor. *Rep. Prog. Phys.* **2009**, *72* (12), 126501.
- (46) Diep, V. M.; Armani, A. M. Flexible Light-Emitting Nanocomposite Based on ZnO Nanotetrapods. *Nano Lett.* **2016**, *16* (12), 7389–7393.
- (47) Jin, X.; Deng, M.; Kaps, S.; Zhu, X.; Holken, I.; Mess, K.; Adelung, R.; Mishra, Y. K. Study of Tetrapodal ZnO-PDMS Composites: A Comparison of Fillers Shapes in Stiffness and Hydrophobicity Improvements. *PLoS One* **2014**, *9* (9), e106991.
- (48) Zeng, H.; Duan, G.; Li, Y.; Yang, S.; Xu, X.; Cai, W. Blue Luminescence of ZnO Nanoparticles Based on Non-equilibrium Processes: Defect Origins and Emission Controls. *Adv. Funct. Mater.* **2010**, *20* (4), 561–572.
- (49) Kaps, S.; Bhowmick, S.; Gröttrup, J.; Hrkac, V.; Stauffer, D.; Guo, H.; Warren, O. L.; Adam, J.; Kienle, L.; Minor, A. M.; Adelung, R.; Mishra, Y. K. Piezoresistive Response of Quasi-One-Dimensional ZnO Nanowires Using an in Situ Electromechanical Device. *ACS Omega* **2017**, *2* (6), 2985–2993.
- (50) Strzelec, K.; Bączek, N.; Ostrowska, S.; Wąsikowska, K.; Szykowska, M. I.; Grams, J. Synthesis and Characterization of Novel Polythiourethane Hardeners for Epoxy Resins. *C. R. Chim.* **2012**, *15* (11), 1065–1071.
- (51) Raja, S. N.; Olson, A. C. K.; Thorkelsson, K.; Luong, A. J.; Hsueh, L.; Chang, G.; Gludovatz, B.; Lin, L.; Xu, T.; Ritchie, R. O.; Alivisatos, A. P. Tetrapod Nanocrystals as Fluorescent Stress Probes of Electrospun Nanocomposites. *Nano Lett.* **2013**, *13* (8), 3915–3922.
- (52) Hölken, I.; Hoppe, M.; Mishra, Y. K.; Gorb, S. N.; Adelung, R.; Baum, M. Complex Shaped ZnO Nano- and Microstructure Based Polymer Composites: Mechanically Stable and Environmentally Friendly Coatings for Potential Antifouling Applications. *Phys. Chem. Chem. Phys.* **2016**, *18* (10), 7114–7123.
- (53) Nasajpour, A.; Mandla, S.; Shree, S.; Mostafavi, E.; Sharifi, S.; Khalilpour, A.; Saghazadeh, S.; Hassan, S.; Mitchell, M. J.; Leijten, J.; Hou, X.; Moshaverinia, A.; Annabi, N.; Adelung, R.; Mishra, Y. K.; Shin, S. R.; Tamayol, A.; Khademhosseini, A. Nanostructured Fibrous Membranes with Rose Spike-like Architecture. *Nano Lett.* **2017**, *17*, 6235–6240.
- (54) Potisek, S. L.; Davis, D. A.; Sottos, N. R.; White, S. R.; Moore, J. S. Mechano-phore-Linked Addition Polymers. *J. Am. Chem. Soc.* **2007**, *129* (45), 13808–13809.
- (55) Beiermann, B. A.; Davis, D. A.; Kramer, S. L. B.; Moore, J. S.; Sottos, N. R.; White, S. R. Environmental Effects on Mechanochemical Activation of Spiropyran in Linear PMMA. *J. Mater. Chem.* **2011**, *21* (23), 8443–8447.
- (56) Emi, U.; Reiko, A.; Yasuo, N. Switching between Solid and Liquid Phases of Spiropyran by Photochromic Reaction. *Chem. Lett.* **2014**, *43* (10), 1619–1621.
- (57) Kajikawa, K.; Anzai, T.; Takezoe, H.; Fukuda, A. Non-centrosymmetric and Centrosymmetric J-Aggregation in Photo-merocyanine Monolayer Studied by Second-Harmonic Generation and Absorption Spectroscopy. *Thin Solid Films* **1994**, *243* (1–2), 587–591.
- (58) Kajikawa, K.; Hara, M.; Sasabe, H.; Knoll, W. J. Aggregates in a Langmuir-Blodgett Monolayer Probed by Scanning Near-Field Optical Microscopy. *Colloids Surf., A* **1997**, *126* (2–3), 97–101.
- (59) Zhang, Y.; Zhou, H.; Liu, S. W.; Tian, Z. R.; Xiao, M. Second-Harmonic Whispering-Gallery Modes in ZnO Nanotetrapod. *Nano Lett.* **2009**, *9* (5), 2109–2112.
- (60) Reimer, T.; Paulowicz, I.; Röder, R.; Kaps, S.; Lupan, O.; Chemnitz, S.; Benecke, W.; Ronning, C.; Adelung, R.; Mishra, Y. K. Single Step Integration of ZnO Nano- and Microneedles in Si Trenches by Novel Flame Transport Approach: Whispering Gallery Modes and Photocatalytic Properties. *ACS Appl. Mater. Interfaces* **2014**, *6* (10), 7806–7815.
- (61) Godsi, O.; Peskin, U.; Kapon, M.; Natan, E.; Eichen, Y. Site Effects in Controlling the Chemical Reactivity in Crystals: Solid-State Photochromism of N-(N-Propyl)nitrospiropyran. *Chem. Commun.* **2001**, *0* (20), 2132–2133.
- (62) Breslin, V. M.; Garcia-Garibay, M. A. Transmission Spectroscopy and Kinetics in Crystalline Solids Using Aqueous Nanocrystalline Suspensions: The Spiropyran-Merocyanine Photochromic System. *Cryst. Growth Des.* **2017**, *17* (2), 637–642.
- (63) Shiraishi, Y.; Itoh, M.; Hirai, T. Thermal Isomerization of Spiropyran to Merocyanine in Aqueous Media and Its Application to Colorimetric Temperature Indication. *Phys. Chem. Chem. Phys.* **2010**, *12* (41), 13737–13745.

2.2. Failure Indication in Spiropyran / Glassfiber Composites

In cooperation with the Functional Nanomaterials group of Rainer Adelung, the composite system from the previous section was improved. By introducing glassfibers, it was possible to initialize and visualize the mechanophoric switching of spiropyrans in a PTU matrix, *before* failure of the material. Alteration of the composite design by using an epoxy matrix extinguished the visible response. It was possible to assign this behavior to an unexpected and formerly unreported degradation of the spiropyran dye **1** by xylylenediamine (**5**) that is contained in the epoxy resin. The degradation products could be assigned to be the imine **6** and the indolene **2** (see Scheme II.3).



Scheme II.3 Degradation reaction of the spiropyran **1** with the epoxy-additive **5**.

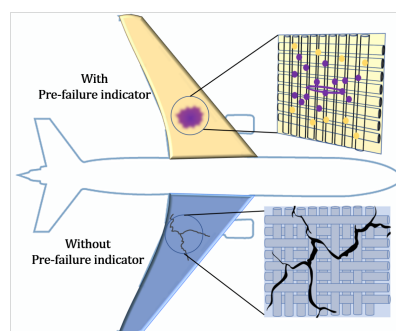
The manuscript was published in *Materials Horizons*: Sindu Shree, Mathias Dowds, Alina Kuntze, Yogendra Kumar Mishra, Anne Staubitz, Rainer Adelung, Self-Reporting Mechanochromic Coating: Glassfiber Reinforced Polymer Composites Predicting Impact Induced Damage, *Mater. Horiz.* **2019**.

DOI: 10.1039/C9MH01400D

Reproduced from ref.^[168] with permission from the Royal Society of Chemistry (See page 435).

Abstract

A major conflict faced in the largescale machineries is real-time damage identification. High mechanical stability offered by the glassfiber reinforced polymer composites (GFRPCs) also poses issues with unpredictable material failure. This creates a requirement for cost-effective stress sensors to indicate material damage before a malfunction occurs and to precisely identify the initial site and the extent of a damage. The challenge in GFRPCs is that the failure may originate at arbitrary positions, minute differences in the fiber/matrix coupling eventually develop into the



primary point of a failure. This work presents a molecular stress-sensitive sensor embedded in polymer matrices such as polythiourethane (PTU) and Epoxy, reinforced by glassfibers. Spiropyran (SP) is used as a self-reporting particle filler. Polymer matrix covering the woven glassfibers contains as little as 0.5 wt% SP. In the given study, the PTU/SP composite with and without glassfiber reinforcement are studied for their self-reporting property. However, only the samples with reinforcement behave like ideal self-reporter by exposing a damage via color change well before any visible cracks appeared. Comparison tests of SP with different matrices show that the amine-based hardener used to cross-link epoxy resin reacts with the SP molecules. Underlying mechanisms involved in the mechanochromic responses of the PTU/SP composites are investigated and discussed.

Scientific Contribution to this Publication

For this article, I synthesized and provided the spiropyran switch **1** and supported Sindu Shree in writing the manuscript. I designed the experimental setup to investigate why the composite with an epoxy matrix did not show the same predicted color effects as the PTU based sample. I performed the corresponding experiments, analyses and interpretations, which lead to the discovery of a new degradation pathway of the spiropyran dye in an industrially extremely relevant thermoset polymer. I wrote the respective paragraphs of the manuscript and supporting information.



COMMUNICATION

View Article Online
View Journal

Cite this: DOI: 10.1039/c9mh01400d

Received 4th September 2019,
Accepted 15th October 2019

DOI: 10.1039/c9mh01400d

rsc.li/materials-horizons

Self-reporting mechanochromic coating:
a glassfiber reinforced polymer composite
that predicts impact induced damage†Sindu Shree,*^a Mathias Dowds,^{ib} Alina Kuntze,^a Yogendra Kumar Mishra,^{ib} ‡*^a
Anne Staubitz^{ib} ^{bcd} and Rainer Adelung*^a

A major problem of glassfiber reinforced polymer composite (GFRPCs)-based large-scale machinery is its proper damage assessment. Often employed GFRPCs have high endurance; however, their failure is highly unpredictable. This leads to a requirement for cost-effective stress sensors to precisely indicate initial stages of damage and its extent before a malfunction occurs. A failure may originate at arbitrary positions in GFRPCs, and minute differences in the fiber/matrix coupling may eventually develop into the primary point of a failure. In this work 0.5 wt% of a molecular stress-sensitive sensor is embedded in polythiourethane (PTU), reinforced with glassfibers, and unreinforced samples are used as controls. Spiropyran (SP) is used as a self-reporting functional additive. Only the samples with reinforcement behaved like a desirable self-reporter by exposing damage *via* color change well before any visible cracks appeared. In unreinforced samples, color change and crack formation occurred simultaneously, with descriptive, however not predictive, function. Comparison tests of SP with a different matrix show that the amine-based hardener used to cross-link epoxy resins reacts with the SP molecules, destroying them and thus deactivating their mechanochromic properties. The mechanisms that are responsible for the responses of the PTU/SP composites with and without glassfibers are investigated and discussed.

Introduction

A prognostic tool to predict internal damage in a polymer composite well before it leads to material failure has been an

New concepts

Pre-damage indications in airplane wings, wind turbine blades or other composite based technologies can be life-saving. Damage analysis can be cost effective when it is identified in time for restoration. With very little effort, stress sensing smart polymer composite-based coatings can be efficiently produced. Unlike the existing methods of post-damage analysis, identifying damage before it causes severe impairment is the motivation of the present work. Here we offer a strategy for glassfiber reinforced polymer composite fabrication in combination with a mechanochromic molecular switch, spiropyran. The mechanochrome shows a colour change from yellow to purple in response to force by undergoing reversible isomerization. The presented production strategy does not involve any complicated synthesis or functionalization. Instead, a molecular stress sensor, spiropyran, is employed as an additive. The polythiourethane based reinforced polymer composite with only 0.5 wt% mechanochrome demonstrated a strong colour change under periodic impact. This *in situ* damage recognition technique requires no complex instrumentation. The colour gradient can be directly correlated with the integrated impact force experienced by the composite. The samples reinforced with a woven glassfiber mat show a clear indication of impact with an evident colour change at 456 kPa well before the failure of the material at 1.2 MPa.

objective of several studies.^{1–3} In addition to damage indication, a reliable material requires high mechanical strength and flexibility.^{4–6} Lightweight glass and carbon fiber reinforced polymer composites (GFRPCs or CFRPCs) are high-performance materials due to their superior mechanical stability. They have been commercialized in numerous fields such as the automotive and aviation industries, wind energy power generators and construction engineering.^{4,7} Despite these advantages, environmental conditions, such as exposure to UV irradiation, temperature changes, high winds, humidity, *etc.*, lead to accumulative and irreparable damage.^{8–10} To reveal the sites of the origin of the damage, industries employ non-destructive techniques,¹¹ namely, visual inspection,¹² acoustic emission,¹³ shearography,¹⁴ pulsed thermography,¹¹ X-ray/gamma-ray analysis,¹¹ *etc.*

Despite the effectivity of these methods, they are mostly applicable for post-damage analysis and are time consuming as

^a Functional Nanomaterials, Institute for Materials Science, Kiel University, Kaiserstr. 2, D-24143, Kiel, Germany. E-mail: sisi@tf.uni-kiel.de, ra@tf.uni-kiel.de

^b Otto-Diels-Institute for Organic Chemistry, Kiel University, Otto-Hahn-Platz 4, 24118 Kiel, Germany

^c Institute for Organic and Analytical Chemistry, University of Bremen, Leobener Str. 7, 28359 Bremen, Germany

^d MAPEX Center for Materials and Processes, University of Bremen, Bibliothekstr. 1, 28359 Bremen, Germany

† Electronic supplementary information (ESI) available. See DOI: 10.1039/c9mh01400d

‡ Present address: Mads Clausen Institute, NanoSYD, University of Southern Denmark, Alsion 2, 6400 Sønderborg, Denmark. E-mail: mishra@mci.sdu.dk

the entire length and width of the material need to be scanned to discover and evaluate the depth of damage. To reduce the inspection time and to receive live information on the state of a material, more recently self-reporting coatings have been developed. For example, glassfibers embedded in epoxy resins that were functionalized with fluorescent proteins were used as delamination indicators.¹⁵ Another stress-sensitive material was photoluminescent tetrapodal-zinc oxide (ZnO-T) filled polydimethylsiloxane (PDMS) composites that indicated stress induced damage.^{16–18} However, such components must be dismantled for damage assessment and they require additional complicated equipment for analysis, making these *ex situ* techniques complex. The key disadvantage of an *ex situ* analysis is that the damaged parts need to be removed and often transported for testing. Furthermore, these processes can be inconclusive in finding the point of impact. With a built-in sensor, this intricate step of handling damaged parts may largely be avoided. The current study therefore focuses on fabricating a polymer composite with an *in situ* stress sensor with pre-failure indication.

Spiropyran (SP) is a widely employed stimuli responsive molecular switch that has been used in composite systems as a functional additive.^{19–22} It is an organic molecule that isomerizes in response to heat, light and, most importantly, to mechanical stress.^{21,23–26} By undergoing a transformation from the closed (spiropyran) into the open (merocyanine) form the dye changes its color in immediate response to the aforementioned stimuli from almost colorless to an intense purple colour,^{20,22} making SP a molecular sensor, which indicates the changes in its surroundings. Such molecular force sensors if embedded in a polymer composite then can provide a possibility of indicating damage at an early stage. To study the compatibility of SP as a functional additive with different polymer matrices, highly cross-linked polythiourethane (PTU) and epoxy resins were used. The thermally and chemically inert PTU is highly transparent, colorless and stable to UV exposure, and it has emerged as an ideal matrix for antifouling and anticorrosion coatings.^{27,28} Monomers involved in the fabrication of PTU²⁹ are comparatively less toxic than a bisphenol-A containing epoxy resin.^{30–32}

The fabrication process shown in the presented work of polymer composites with an *in situ* indicator involves only an additional step to the standardised the hand lay-up³³ method of lamination. However, here the overall cost of this process is comparatively much lower than the cumulative cost of a conventional post-damage analysis approach. This damage identifying strategy based on a molecular switch is minimalistic and efficient: merely ~0.5 wt% of SP in a composite can be sufficient for direct damage detection, which was demonstrated in recent work on PTU/SP composites. There an interconnected network of ZnO-T was used as an additional filler to enhance the photochromic response and to provide mechanical reinforcement.¹⁹ However, this stress responsive composite only showed a color change concurrent with material failure. The current work is a major advancement on this idea, because it demonstrates a straightforward production of a mechanochrome combined with a glassfiber reinforced PTU composite

with the possibility of predicting macroscopic stress induced damage. Detailed investigations on the composite samples revealed the *in situ* mechanochromic sensing capability of the polymer composite which provided a pre-indication of an imminent and propagating material failure. Direct relevance of the gradual color change in the mechanochromic polymer composite to the accumulated impact force is presented and discussed in detail.

Periodic impact testing of the mechanochromic polymer composite

Before discussing the utilization of the mechanochromic SP based polymer composite for outdoor applications, the effects of ambient conditions on its switching abilities have to be considered. Due to multiple triggers, SP embedded in PTU isomerizes in response to UV irradiation and heat.¹⁹ In outdoor applications, these two triggers might cause hindrance or misperception when only a mechanochromic response is expected. Typically, the exterior surfaces of GFRPCs are coated with a protecting layer to prevent material degradation under constant UV exposure.^{34,35} Such a coating in turn might help in stimuli separation in the presented multi-stimuli system. To verify this, a PTU/SP sample was partially coated with a UV blocking layer and irradiated with UV light for 30 s (see Fig. SI-1, ESI†). The thin UV protective layer appeared to be sufficient to prevent accidental switching of SP. Hence such existing UV blocking strategies would preserve the molecular switches intended to be mechanochromes from imparting an unprecedented outcome. Effects of ambient temperature changes can be eliminated as the recorded range of ambient temperatures for exterior surfaces is –40 °C to 50 °C. This range is below the observed activation temperature required to cause isomerisation of SP embedded in PTU,¹⁹ making the given SP based polymer composite appropriate for mechanochromic stress indicators even for outdoor machines.

The PTU and spiropyran polymer composite without reinforcement is labelled PTU/SP, the PTU and spiropyran sample with glassfiber reinforcement is called GFPS and the epoxy and spiropyran composite with reinforcement is named GFES. All the samples comprised 0.5 wt% of SP (for detailed description of sample preparation see Fig. 1a). These samples were subjected to a periodic impact force using a self-made “Hammer test” (see Fig. SI-2, ESI†) generating one strike per second, each strike yielding up to ~24 kPa impact pressure.¹⁹ For an ideal damage detection, it is essential that a color change appears before the material fails. The reinforced polymer composites were examined under a scanning electron microscope (SEM) directly after sample preparation. The cross-sectional SEM micrographs of the samples GFPS and GFES (Fig. 1b–g) showed no sign of any delamination between the molecular switches and the polymer matrix.

During the periodic impact test, two stages were identified: average number of hits required to induce a color change and the average number of hits leading to material failure. To track

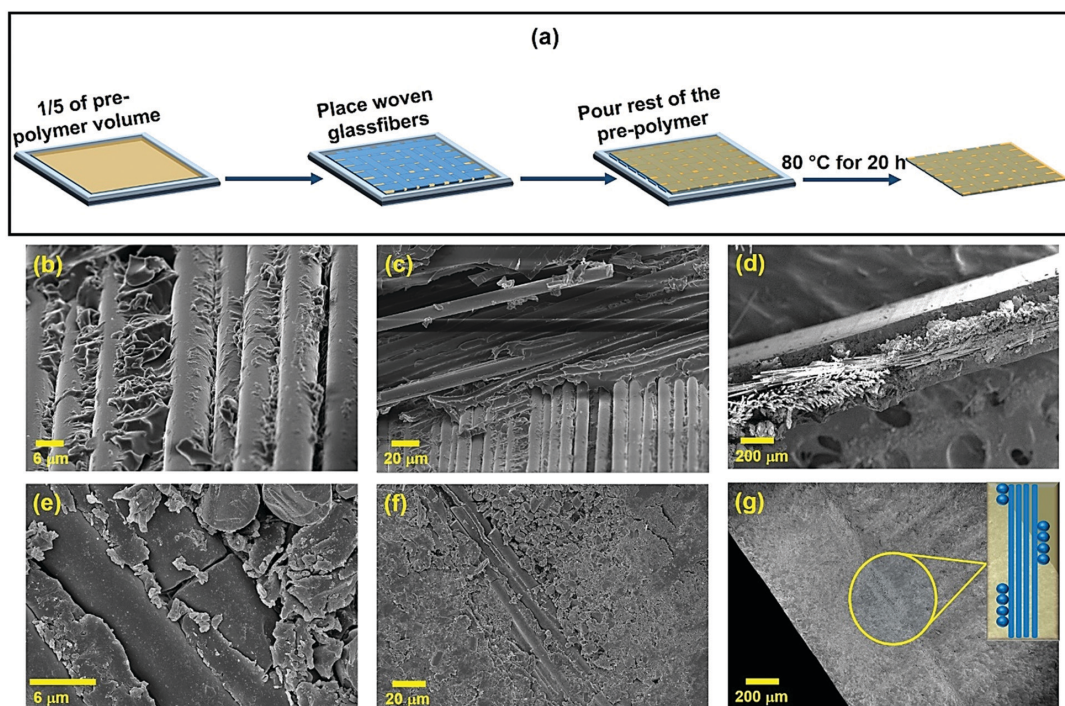


Fig. 1 (a) A sketch of the sample with the glassfiber reinforcement preparation method. First step: the pre-polymer mixture (1/5 of the total volume of prepolymer) was poured into a silicone mold. Second step: a woven glassfiber mat was sliced to fit the mold exactly and placed on the pre-polymer. Third step: the rest of the pre-polymer (4/5) was poured onto the glassfiber mat. Fourth step: this arrangement was placed in a furnace for 20 h at 80 °C to complete the polymerization. Final step: the cured reinforced polymer composite was sliced into smaller pieces for the “Hammer test”. SEM micrographs of the cross-section of the GFPS and GFES samples at consecutively decreasing magnifications. (b)–(d) Micrographs with decreasing magnification of the woven glassfiber mat covered by PTU/spiropyran on either side of the mat. (e)–(g) Micrographs with decreasing magnification of the woven glassfiber matrix embedded in the epoxy/spiropyran matrix. The sketch in image (g) represents the alignment of the fiber mat uniformly infiltrated by the SP containing matrix.

these features, an image was taken after each impact; the photomontage of the tests on the polymer composite PTU/SP and GFPS is shown in Fig. 2 and 3 (related image stacks of the impact tests are given in the ESI†). The corresponding forces were calculated with the equation presented in the ESI† and the results are summarized in Table 1.¹⁹ In order to verify that the periodic impact did not induce a large temperature change and to confirm that the color change observed in this study was a mechanochromic effect and not a thermochromic effect, the samples (GFPS) were subjected to a “Hammer test” under the surveillance of an infrared (IR) camera. Temperatures at and around the point of impact were measured at the end of the periodic impact test (the results are presented in the ESI† as Fig. SI-3). This measurement showed a ~6–8 °C temperature rise from the room temperature (~25 °C). To activate thermochromism in the polymer composite PTU/SP, the temperature has to be ≥60 °C.¹⁹ As such high temperatures were not reached it is safe to assume that the effect observed during the impact test in this study was a mechanochromic effect.

In the sample PTU/SP, switching of SP to merocyanine and the material failure occurred almost simultaneously (see Fig. 2 and Table 1). At the impact pressure of ~432 kPa, the sample

PTU/SP failed while a strong color developed only a strike earlier (408 kPa). Although a discoloration (in Fig. 2) could already be observed at 264 kPa (image 12, strike 11), it was insufficient evidence for the upcoming damage. The SP additive in the sample GFPS (Fig. 3) self-reported damage with a strong color change at the point of impact at ~432 kPa (image 19), well before the cracks appeared (image 45 Fig. 2). Even in GFPS a slight color change emerged at 264 kPa (image 12 in Fig. 2), but such changes could only be tracked by a camera with a high resolution, whereas the color change arising at ~456 kPa was visible to the naked eye.

For more precise quantification in tracking the color change, the average brightness of the green color channel contribution in these images was tracked at the point of impact using ImageJ (Fig. 4). As these samples were not colorless to begin with, rather yellow-orange, the red and blue channels were less sensitive than the green channel to the color change (separated RGB image stacks are given in the ESI†). The accumulated impact pressure corresponding to the number of strikes was plotted against the green color contribution (see Fig. 4); a standardised green color scale bar is provided for reference. The average green color intensity was observed to be in direct relation to the

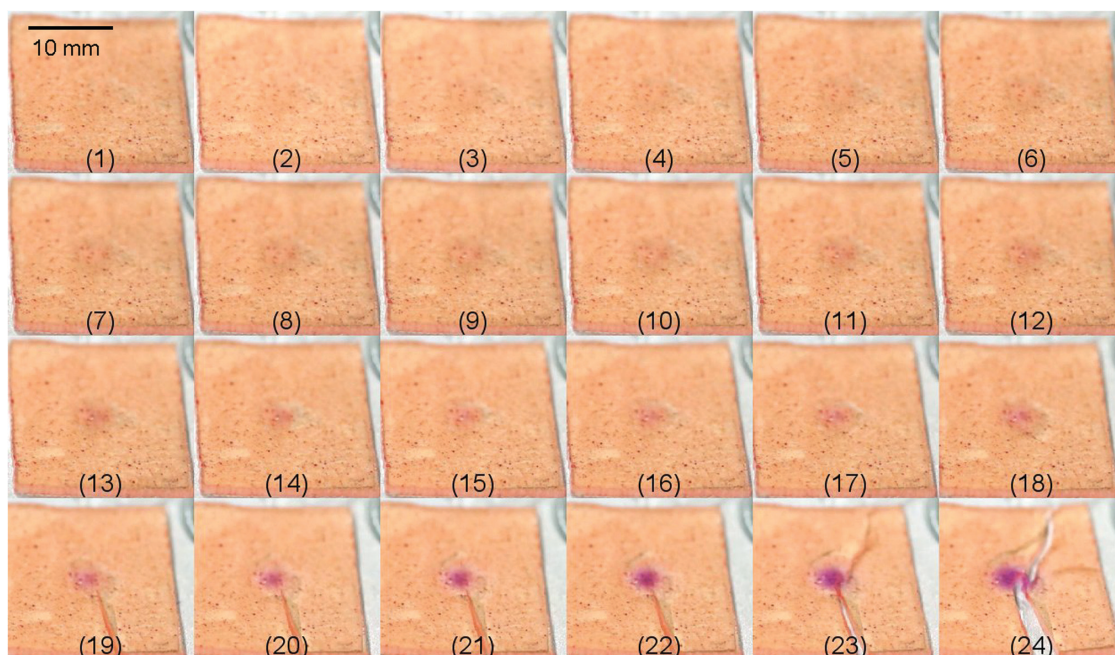


Fig. 2 Periodic impact test of the polymer composites without glassfiber reinforcement. (1) The first image of the series was of the sample before the test started. An image was taken after every strike and combined in this photomontage of the test until material failure occurred (at (19)). A slight discoloration appeared already in the fourth image at the point of impact. The purple color of the open form of the mechanochrome (merocyanine) developed in the 12th image. A crack emerged at the 19th strike with a further color change. The color change due to mechanical stress intensified gradually while the cracks in the sample propagated further.

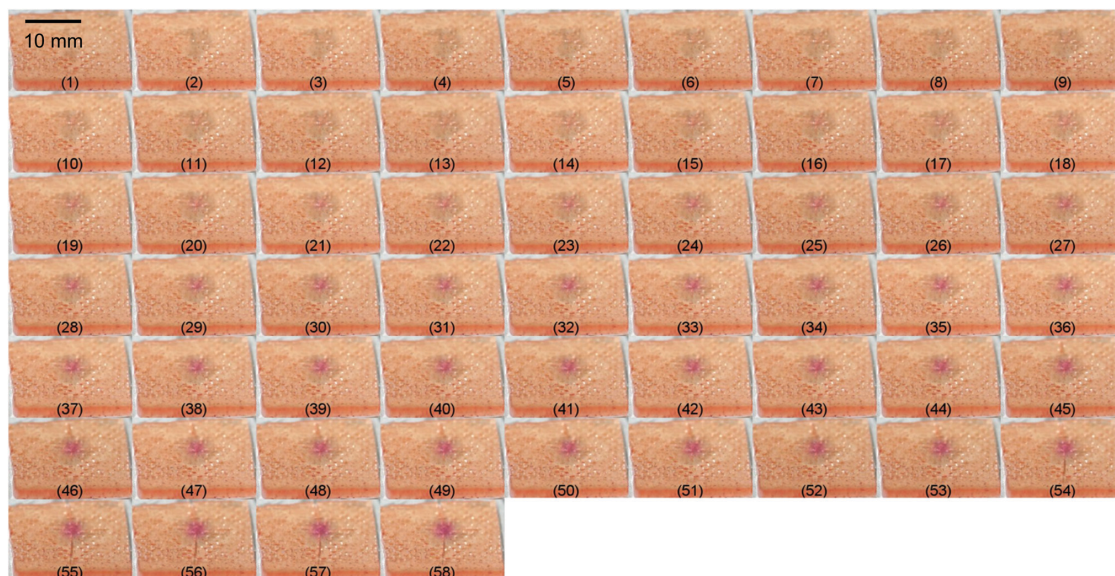


Fig. 3 Periodic impact test of the polymer composites with glassfiber reinforcement (GFPS). (1) The first image of the series shows the sample before the test started. An image was taken after every strike to track the material damage and the color change of the mechanochrome. This photomontage contains images of every strike until material failure occurred. A discoloration appeared in the second image at the point of impact. A visibly perceivable color change due to mechanical stress (isomerization of spiropran to merocyanine) developed in the 19th image. After 54 strikes, a crack emerged with a further color change. The color change intensified gradually until the sample cracked further.

Materials Horizons

Table 1 The calculated average number of hits under the "Hammer test" required to cause damage in the polymer composites with and without the woven glassfibers

Sample	Force required to show a visible color change (kPa)	Force required to cause material failure (kPa)
PTU/SP	408	432
GFPS	648	1248
GFES	No color change	720

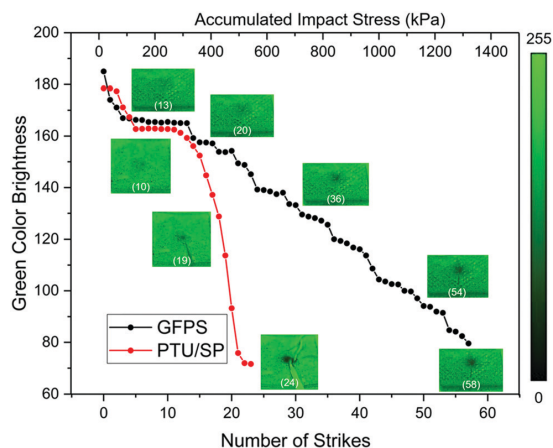


Fig. 4 Quantitative analysis of the color development during the periodic impact test. This plot visualized the changes in the brightness of the green color channel after each impact. Images of samples PTU/SP and GFPS showing color change corresponding to the subjected impact are presented. On the right side of the plot is the green color scale bar that was used as a reference for quantification.

development of the molecular switch isomerisation. The plot (Fig. 4) contains the response of PTU/SP and GFPS to mechanical

stress. For the initial three strikes on the sample PTU/SP, there was a very slight color development, and four to six strikes induced a continuous and substantial color change that finally showed as a significant drop in the green color intensity immediately after the material failed. The strikes six to twelve caused no further color development. After the 13th strike (288 kPa), a prompt decrease in green channel could be observed until the 18th strike (408 kPa); strikes 19 to 22 induced cracks and a drastic color change at the same time. A maximum color change was visible after the material failed at ~ 528 – 552 kPa. Contrary to the un-reinforced sample, the sample GFPS showed a notable color development before severe material damage. Similar to the sample PTU/SP, the color development stopped after 288 kPa. As the periodic impact test continued, the color change progressed steadily, and the green channel darkened around the 35th strike. This visible indication grew stronger episodically until the material failed at the 52nd strike (Fig. 4). This might be an indication of the stress distribution in this particular polymer composite.

The glassfiber reinforced samples GFPS and GFES demonstrated much higher impact resistance compared to the sample PTU/SP. The samples GFPS and GFES developed cracks only after 54 hits (corresponding to ~ 1.2 MPa) and 30 hits (~ 720 kPa) respectively (Fig. 5). Although the polymer composite with the epoxy matrix (GFES) exhibited a good impact resistivity with only minor fractures after 30 hits (~ 720 kPa); no color change occurred at the point of impact.

Interaction of the mechanochrome with the epoxy resin and amine-based hardener

The mechanochrome in GFES samples (Fig. 5) clearly did not respond to the applied impact force with a color change. As the

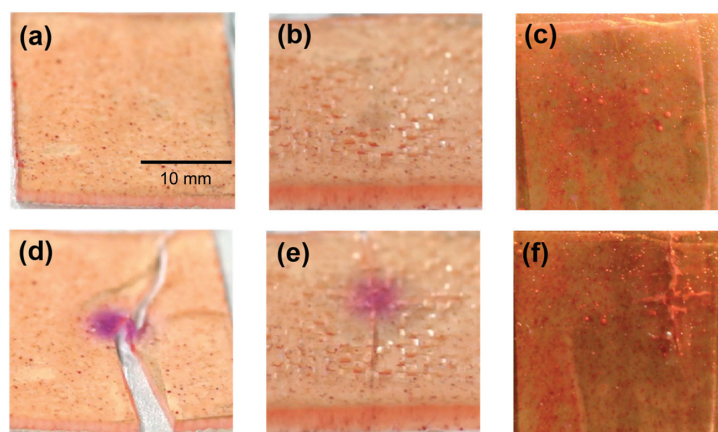


Fig. 5 (a), (b) and (c) are the samples PTU/SP, GFPS and GFES before the "Hammer test". (d), (e) and (f) are the respective images after the impact test. In (a) and (b) polymer composites PTU/SP and GFPS before the mechanochromic test showed a similar color as they had the same PTU matrix. (c) GFES showed a different and darker color before the mechanochromic test. (d) and (e) are the images of the completely damaged PTU/SP and slightly cracked GFPS after the mechanochromic test showing an evident color change. (f) is the fractured GFES that does not exhibit a color change.

curing mixture of the commercial epoxy resin was a complex system to analyze, reactivity of SP with each component of the polymer was investigated separately. The physical curing conditions were adapted in a way that the reactions could be analyzed by nuclear magnetic resonance (NMR) spectroscopy. For these experiments (see Fig. SI-3 and SI-4, ESI[†]), SP samples with individual and representative components of both the hardener and the epoxy resin were dissolved in tetrahydrofuran (THF). During these tests (results are presented in the ESI[†]), evidence of an amine induced cleavage of SP to form its precursor indoline and imines was observed. In an equimolar mixture with xylylenediamine, 90% of the SP molecules reacted to form indoline. This was an unexpected observation, as the spirocyanine was synthesized under basic conditions using secondary amines as catalysts.²² However, in the NMR experiments with the other components such as salicylic acid and two epoxy compounds, SP remained inert. The exact experimental procedure and evaluation of the obtained data are provided in the ESI[†]. Despite the differences compared to the normal curing procedure, it is possible that this or a similar reaction occurs between the epoxy resin, hardener and SP while curing. Excess amines present in the hardener while producing the polymer composites with only 0.5 wt% of SP facilitate such a reaction. The fragmentation product, 1,3,3-trimethyl-2-methyleneindoline, is commercially available as a dark red liquid, explaining the red coloration of the sample GFES.

Conclusions

Compatibility tests of a mechanochrome, with PTU and a commercially relevant epoxy matrix, were performed. The molecular switch, SP, proved to be compatible with PTU and showed excellent mechanochromic properties. However it was incompatible with the curing conditions of the epoxy matrix. The curing conditions were simulated in solution with the representative compounds of the hardener and the epoxy prepolymers and the results were monitored by NMR spectroscopy. It was possible to observe a degradation of up to 90% of SP in the presence of one equivalent of xylylenediamine. Consequently, there is a need to find other, less reactive mechanochromes which would be compatible with the epoxy curing process. The PTU/spirocyanine polymer composite was reinforced with woven glassfiber mats, to improve its impact strength. The presented system with the PTU matrix displayed a color switch at the point of impact to approx. 25% of the impact force that corresponded to eventual material failure. In the range between the first notable color change and the point of failure, the sample's episodic color change responded almost linearly to the applied impact force. An alarming and evident indication was provided by the built-in stress sensor SP. The color change due to mechanical stress in the sample GFPS occurred at the initial stage of the surface damage before the integrity of the composite's internal structure was compromised. Thus the reinforced PTU composite, GFPS, was produced and tested for its mechanosensitivity. It emerged as a desirable

material for impact sensing. To observe the change of SP to merocyanine (color change from yellow to purple), the histogram of the green color channel in the image series was used as an efficient tool to track the stress applied to a lamina to realize the extent of damage.

Materials and methods

A detailed synthetic procedure for the molecular switch, SP, and its analytical data are provided in the ESI[†]. The "epoxy resin L", the "hardener S" and the plain woven glassfiber mat with an areal density of 163 gm⁻² used for the reinforcement were purchased from R&G Faserverbundwerkstoffe GmbH. The PTU matrix, a two-component polymer, was bought from FPT Fluid- & Prozesstechnik GmbH. Both matrices were used and processed without any further treatment, following the suppliers' instructions.

The samples contained SP as a stress indicator to compare the mechanochromicity and the impact resistance of the composite system. In all the samples, SP was used at a concentration of 0.5 wt% and the glassfiber concentration was ~8 wt%. Polymer composites with and without glassfibers were prepared as follows. The PTU composite containing solely spirocyanine (PTU/SP) as an additive without the glassfibers was produced analogously to a previous work.¹⁹ This composite system was further reinforced with woven glassfibers (GFPS). Initially, the monomers, pentaerythritol tetrakis(3-mercaptopropionate) (PETMP) and hexamethylene diisocyanate (HDI), were mixed at a weight ratio of 1:1.4 respectively with SP (0.5 wt% of the whole polymer composite). Part of this mixture (1/5 of the total volume of prepolymer) was cast into a mold so that a uniform layer was obtained (Fig. 1a). A rectangular woven glassfiber mat (70 × 70 mm²) was placed over the mixture and the remaining (4/5) uncured monomers/SP mixture was poured over the glassfiber mat. Subsequently, the sample was placed for 20 h in a furnace at 80 °C (Fig. 1a). To compare the GFPS composite system to a commercially available epoxy polymer, epoxy/spirocyanine coated glassfiber (GFES) samples were prepared similarly. The first step was to disperse SP into the hardener and epoxy resin (45 : 100 parts by volume of hardener : resin) was later added to the dispersion; the unpolymerized mixture was coated onto the glassfiber mat as shown in Fig. 1a. The coated glassfiber mats (thickness, 5 mm) were later cut into smaller samples (20 × 20 mm²) for further investigations.

Conflicts of interest

There are no conflicts to declare.

Acknowledgements

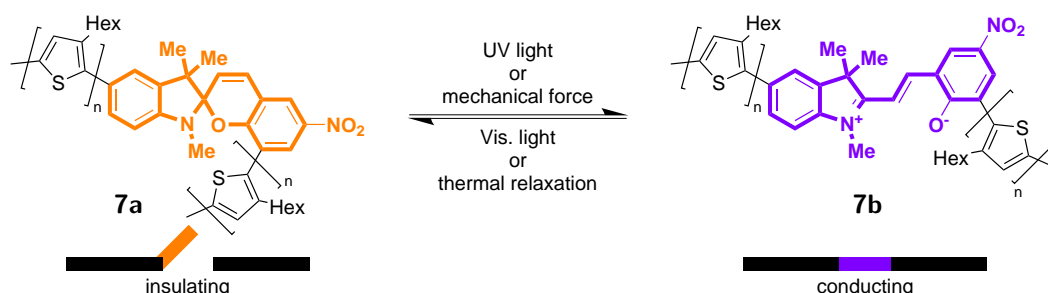
This project was funded by the German Research Foundation (DFG) as a project within the Collaborative Research Center 677 "Function by Switching", Project C-14, Mechanochromic Composites.

References

- 1 B. J. Blaiszik, S. L. B. Kramer, S. C. Olugebefola, J. S. Moore, N. R. Sottos and S. R. White, *Annu. Rev. Mater. Res.*, 2010, **40**, 179.
- 2 N. Bruns and D. S. Clark, *Chimia*, 2011, **65**, 245.
- 3 S. N. Raja, A. C. K. Olson, K. Thorkelsson, A. J. Luong, L. Hsueh, G. Chang, B. Gludovatz, L. Lin, T. Xu, R. O. Ritchie and A. P. Alivisatos, *Nano Lett.*, 2013, **13**, 3915.
- 4 K. J. Narayana and R. Gupta Burela, *Mater. Today: Proc.*, 2018, **5**, 5580.
- 5 S. S. Yao, F. L. Jin, K. Y. Rhee, D. Hui and S. J. Park, *Composites, Part B*, 2018, **142**, 241.
- 6 S. Y. Fu, X. Q. Feng, B. Lauke and Y. W. Mai, *Composites, Part B*, 2008, **39**, 933.
- 7 T. Ozbakkaloglu, J. C. Lim and T. Vincent, *Eng. Struct.*, 2013, **49**, 1068.
- 8 K. K. Singh, R. K. Singh and P. Kumar, *J. Reinf. Plast. Compos.*, 2009, **28**, 601.
- 9 V. Tamužs, J. Andersons, K. Aniskevich, J. Jansons and J. Korsgaard, *Mech. Compos. Mater.*, 1998, **34**, 321.
- 10 V. Giurgiutiu, *Structural Health Monitoring of Aerospace Composites*, Academic Press, Oxford, 2016.
- 11 R. Yang, Y. He and H. Zhang, *Renewable Sustainable Energy Rev.*, 2016, **60**, 1225.
- 12 S. Ataya and M. M. Z. Ahmed, *Eng. Failure Anal.*, 2013, **35**, 480.
- 13 A. Jüngert, in 7th Fib PhD Symp. Stuttgart, Ger., 2008, p. 1.
- 14 Y. Y. Hung, Y. S. Chen, S. P. Ng, L. Liu, Y. H. Huang, B. L. Luk, R. W. L. Ip, C. M. L. Wu and P. S. Chung, *Mater. Sci. Eng., R*, 2009, **64**, 73.
- 15 O. Rifaie-Graham, E. A. Apebende, L. K. Bast and N. Bruns, *Adv. Mater.*, 2018, **30**, 1.
- 16 X. Jin, M. Götz, S. Wille, Y. K. Mishra, R. Adelung and C. Zollfrank, *Adv. Mater.*, 2013, **25**, 1342.
- 17 T. Reimer, I. Paulowicz, R. Röder, S. Kaps, O. Lupan, S. Chemnitz, W. Benecke, C. Ronning, R. Adelung and Y. K. Mishra, *ACS Appl. Mater. Interfaces*, 2014, **6**, 7806.
- 18 V. M. Diep and A. M. Armani, *Nano Lett.*, 2016, **16**, 7389.
- 19 S. Shree, M. Schulz-Senft, N. H. Alsleben, Y. K. Mishra, A. Staubitz and R. Adelung, *ACS Appl. Mater. Interfaces*, 2017, **9**, 38000.
- 20 S. Shree, M. Schulz-Senft, X. Jin, Y. K. Mishra, A. Staubitz and R. Adelung, 3rd Int. Conf. Nanotechnologies Biomed. Eng. IFMBE Proc., Springer, Singapore, 2016, p. 146.
- 21 R. Klajn, *Chem. Soc. Rev.*, 2014, **43**, 148.
- 22 E. Samoylova, L. Ceseracciu, M. Allione, A. Diaspro, A. C. Barone and A. Athanassiou, *Appl. Phys. Lett.*, 2011, **99**, 1.
- 23 M. Schulz-Senft, P. J. Gates, F. D. Sönnichsen and A. Staubitz, *Dye. Pigm.*, 2017, **136**, 292.
- 24 M. Schulz-Senft, M. Lipfert and A. Staubitz, *Chem. Unserer Zeit*, 2014, **48**, 200.
- 25 B. Seefeldt, R. Kasper, M. Beining, J. Mattay, J. Arden-jacob, N. Kemnitzer, K. Heinz, M. Heilemann and M. Sauer, *Photochem. Photobiol. Sci.*, 2016, **9**, 213.
- 26 J. Zhang, J. Wang and H. Tian, *Mater. Horiz.*, 2014, **1**, 169.
- 27 I. Hölken, M. Hoppe, Y. K. Mishra, S. N. Gorb, R. Adelung and M. J. Baum, *Phys. Chem. Chem. Phys.*, 2016, **18**, 7114.
- 28 K. Strzelec, N. Baczek, S. Ostrowska, K. Wąsikowska, M. I. Szykowska and J. Grams, *C. R. Chim.*, 2012, **15**, 1065.
- 29 M. D. Campiñez, C. Ferris, M. V. De Paz, A. Aguilar-De-Leyva, J. Galbis and I. Caraballo, *Int. J. Pharm.*, 2015, **480**, 63.
- 30 J. Michałowicz, *Environ. Toxicol. Pharmacol.*, 2014, **37**, 738.
- 31 J. I. Eid, S. M. Eissa and A. A. El-Ghor, *J. Basic. Appl. Zool.*, 2015, **71**, 10.
- 32 L. B. Bourne, F. J. M. Milner and K. B. Alberman, *Br. J. Ind. Med.*, 1959, **16**, 81.
- 33 T. P. Sathishkumar, S. Satheeshkumar and J. Naveen, *J. Reinf. Plast. Compos.*, 2014, **33**, 1258.
- 34 B. Zhang, in 6th Annual GRASP Symposium, 2010, p. 4.
- 35 E. Cortés, F. Sánchez, A. O'Carroll, B. Madramany, M. Hardiman and T. M. Young, *Materials*, 2017, **10**, 1146.

3. Spiropyran Dyes for the Covalent Incorporation into Conducting Polymers

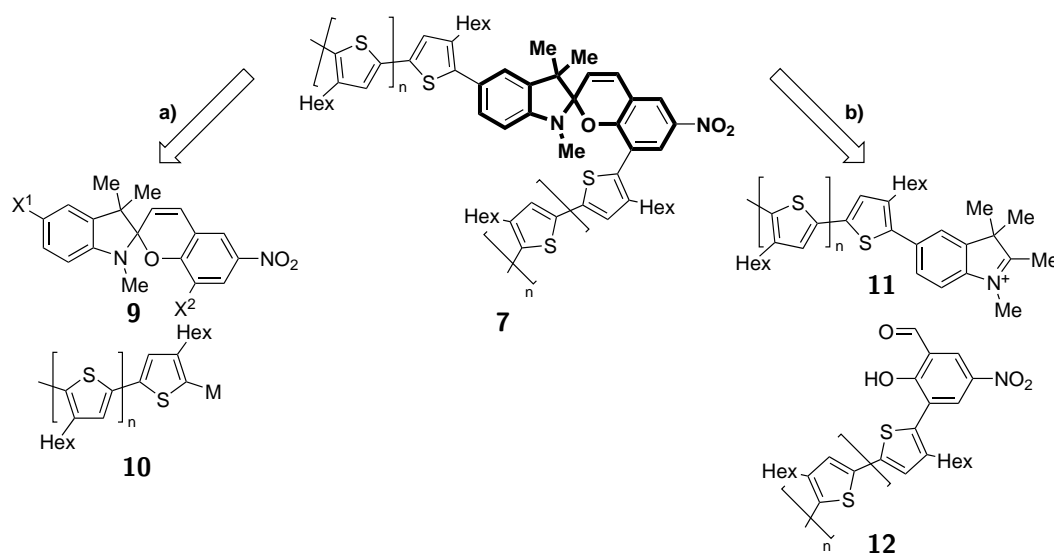
Organic polymers that are used in electronic devices mostly consist of aromatic units in their backbones. The immense change of size and polarity that occurs when spiropyran is switched to merocyanine was used to influence the channel conductance in a P3HT based OFET.^[24] In this example, the spiropyran was used as additive in a P3HT layer. We hypothesize that a larger effect can be expected if the spiropyran dye and the conducting polymer are bound covalently. If the polymer chains are attached to opposed sides of the molecule, it is conceivable that a P3HT functionalized spiropyran **7** reduces its bandgap upon switching from the closed form **7a** to the open form **7b**. In the closed form **7a**, the central spiro-carbon atom will prevent the conjugation in the closed SP. Using the chain growth polymerization by Kumada coupling as described in Part I subsection 1.2.3, the degree of polymerization of the P3HT chains can be varied. Thus, the ratio of SP and P3HT can be varied to investigate a potential mechanically induced switching of the conductivity.



Scheme II.4 Schematic of the use of spiropyran as conductivity switch in P3HT. While the central spiro carbon atom in the closed form **7a** breaks the electron conjugation (top), the push-pull system in the open form **7b** should be conjugated throughout the complete molecule.

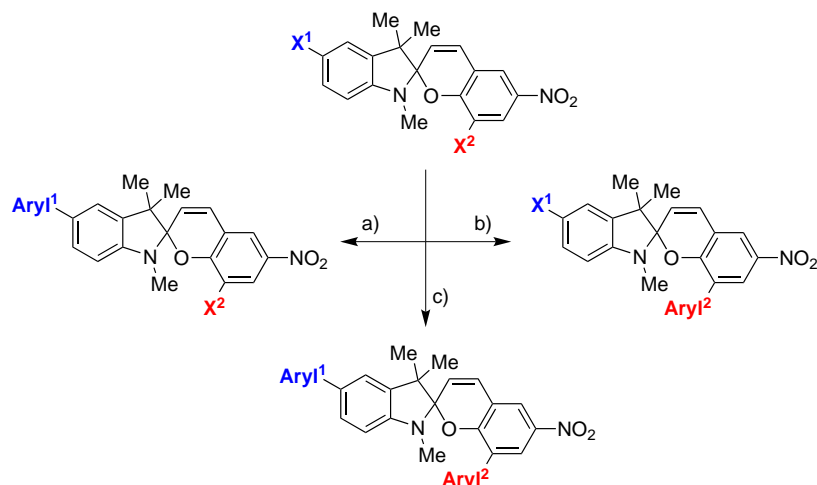
For the synthesis of a P3HT-SP-P3HT triad, two basic synthetic strategies are feasible: either synthesizing the polymer before the connection with the spiropyran or using spiropyran as starting point for the chain growth polymerization. The controlled polymerization of P3HT can be accomplished by Kumada coupling.^[79] The initial reaction in this polymerization is the formation of an aromatic Grignard compound. Since the nitro and amino groups in spiropyrans are often incompatible with Grignard reagents, this strategy is not promising. Sommer and coworkers circumvented the disturbance of the nitro group by placing a bromide substituent at that position. The obtained spiropyran was then used as electrophilic component in Suzuki cross-coupling reactions.^[169–172] As described above, such a substitution drastically changes the isomerization characteristics of spiropyrans. This leaves a functionalized P3HT polymer as precursor for **7**. Since the nitro and amino

groups of spiropyran also prevent a lithiation to synthesize spiropyran with organometallic functionalities, the P3HT should bear metal functional groups. As discussed in Part I, subsection 1.2.3, synthesizing P3HT with bromide end groups has been established.^[79] This provides the possibility for further functionalization of **8** via cross-coupling reactions. The key step in the synthetic strategy towards a poly(thiophene) with switchable conductivity is the connection of the photoswitching unit with the conducting polymer. Here, two possibilities can be investigated: cross-coupling of P3HT with the dye as final step in a convergent synthetic strategy (Scheme II.5, pathway **a**) or the connection of P3HT with precursors of spiropyran, which are subsequently condensed to the dye moiety (Scheme II.5, pathway **b**). Thelakkat and coworkers pursued the first strategy when they used the polythiophene **8** with Br/H end groups in a Suzuki cross-coupling reaction with a dithienylethene instead of a SP bearing boronic esters in their synthesis of a photoswitchable P3HT.^[173]



Scheme II.5 Retrosynthetic disconnection of spiropyran connected with P3HT. **a)** Convergent synthetic route with cross-coupling of **10** and **9** as final step. **b)** synthetic route with cross-coupling of **10** previous to the spiropyran formation from the precursors bearing P3HT, **11** and **12** as final step.

The convergent synthetic strategy was chosen as the first approach to be adapted for the implementation of spiropyran into P3HT. By making use of the different electron densities at the two sides of SP, it should be possible to selectively couple P3HT chains to either the indole or chromene, or both sides of spiropyran. Variation of the halide and pseudohalide functional groups was estimated to increase the synthetic versatility. The resulting library of spiropyran dyes should give access to a selective functionalization of spiropyran with aromatic systems and thereby conducting polymers (Scheme II.6).



Scheme II.6 Schematic of the selective functionalization of spiropyrans with aryl groups. Spiropyrans bearing various halide or pseudohalide substituents should be used as electrophile in cross-coupling reactions to selectively react **a)** either the indole ($X^1 \rightarrow \text{Aryl}^1$, blue), **b)** the chromene ($X^2 \rightarrow \text{Aryl}^2$, red) or **c)** both sites with organometal aryl groups.

3.1. Halide Functionalized Spiropyrans

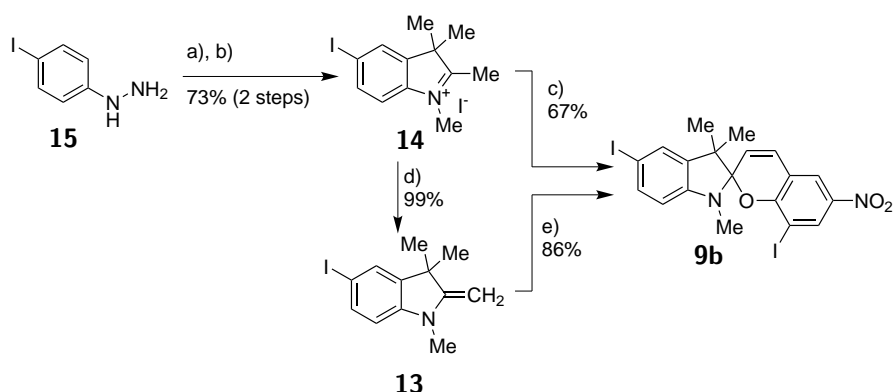
I was able to synthesize 13 novel SPs (The spiropyrans **9d** ($X^1 = \text{Br}$, $X^2 = \text{I}$) and **9c** ($X^1 = \text{OTf}$, $X^2 = \text{OTf}$), compounds **9b** and **9n** in Ref.^[174] were first synthesized in the context of my diploma thesis, but in lower yields) and analyze these dyes in terms of their switching and absorption properties. The results were published in *Dyes and Pigments* in 2017.^[174] Reprinted from Mathias Schulz-Senft, Paul J. Gates, Frank D. Sönnichsen, Anne Staubitz, Diversely Halogenated Spiropyrans – Useful Synthetic Building Blocks for a Versatile Class of Molecular Switches, *Dyes Pigm.* **2017**, *136*, 292-301. Copyright 2016 Elsevier Ltd; reprinted with permission (See page 443).

DOI: 10.1016/j.dyepig.2016.08.039



In further studies, I established the synthesis of the iodo-indolene **13** by deprotonation of the indolium iodide **14** (Compound **3b** in Ref.^[174]) (Scheme II.7). The indolene **13** was then used in the synthesis of the diiodo-spiropyran **9b** (Compound **9e** in Ref.^[174]) without the requirement of a base catalyst. This increased the yield in the spiropyran condensation **9b** from 67% to 86%. While this prolongs the synthetic route from 4-iodophenylhydrazine

(**15**, Compound **7b** in Ref.^[174]) to the final spiropyran **9b** from three to four steps, the overall yield was increased from 49% to 62% (Compare Part V, section 3.2).



Scheme II.7 Optimized synthetic route of **9b**. By synthesizing the intermediate **13**, it was possible to increase the overall yield of **9b** starting from **15** from 49% to 62%. a) 3-methyl-2-butanone, acetic acid, 130 °C, 3 h; b) iodomethane, 45 °C, 15 h; c) 3-iodo-2-hydroxy-5-nitrobenzaldehyde, piperidine, ethanol, 78 °C, 3 h; d) sodium hydroxide, water, toluene, 50 °C, 3 h, e) 3-iodo-2-hydroxy-5-nitrobenzaldehyde, ethanol, 78 °C, 3 h. a), b), c) are taken from Ref.^[174]

Abstract

Spiropyrans are dyes that can be reversibly switched to a highly colored merocyanine form by a number of stimuli such as light, mechanical force or temperature. To make use of these molecules, there is a requirement to functionalize them appropriately. Herein we report a library of spiropyrans bearing two (pseudo) halide functional groups on either half of the molecule. Such halide substituents are valuable, because they themselves may be used as reactive sites in cross-coupling reactions, for example. Different combinations of halides, for which different reactivities in cross-coupling reactions may be expected, will facilitate selective consecutive cross-coupling reactions and condensations. Data concerning the UV-vis characteristics, the photostationary equilibria of the materials as well as the half-life of the merocyanine forms in solution are presented.

Scientific Contribution to this Publication

For this publication, I synthesized all molecules. In the context of my Diploma Thesis, I had already successfully synthesized the following molecules in lower yields: the precursor molecules **2b**, **3a**, **3c**, **5b**, **8a**, **8c**, **8d** and the SPs **9b**, **9n**, **9i**.^[175] The precursor molecule **2c** was synthesized earlier following a different route in the context of my Diploma Thesis.^[175] The photoswitching behavior of SPs **9b**, **9n**, **9i** was not analyzed by UV-vis or NMR spectroscopy in my Diploma Thesis.^[175] I designed the UV-vis experiments and analyzed the results. The nuclear magnetic resonance (spectroscopy) (NMR) experiments were projected by me and Frank Sönnichsen; Frank Sönnichsen designed and conducted the experiments; I analyzed the results. Paul J. Gates measured high-resolution mass spectrometry (HRMS) data. I wrote the manuscript with support of Anne Staubitz.



Contents lists available at ScienceDirect

Dyes and Pigments

journal homepage: www.elsevier.com/locate/dyepig

Diversely halogenated spiropyran - Useful synthetic building blocks for a versatile class of molecular switches

Mathias Schulz-Senft ^a, Paul J. Gates ^b, Frank D. Sönnichsen ^a, Anne Staubitz ^{a, c, d, *}^a Otto-Diels-Institute for Organic Chemistry, University of Kiel, Otto-Hahn-Platz 4, 24098, Kiel, Germany^b School of Chemistry, University of Bristol, Cantock's Close, Bristol, BS8 1TS, UK^c Institute for Organic and Analytical Chemistry, University of Bremen, Leobener Str. NW2 C, 28359, Bremen, Germany^d MAPEX Center for Materials and Processes, University of Bremen, Bibliothekstraße 1, 28359, Bremen, Germany

ARTICLE INFO

Article history:

Received 18 July 2016
 Received in revised form
 14 August 2016
 Accepted 16 August 2016
 Available online 21 August 2016

Keywords:

Molecular switch
 Spiropyran
 Organic synthesis
 3*H*-indole
 Photochromism

ABSTRACT

Spiropyran is a dye that can be reversibly switched to a highly colored merocyanine form by a number of stimuli such as light, mechanical force or temperature. To make use of these molecules, there is a requirement to functionalize them appropriately. Herein we report a library of spiropyran bearing two (pseudo) halide functional groups on either half of the molecule. Such halide substituents are valuable, because they themselves may be used as reactive sites in cross-coupling reactions, for example. Different combinations of halides, for which different reactivities in cross-coupling reactions may be expected, will facilitate selective consecutive cross-coupling reactions and condensations. Data concerning the UV/vis characteristics, the photostationary equilibria of the materials as well as the half-life of the merocyanine forms in solution are presented.

© 2016 Elsevier Ltd. All rights reserved.

1. Introduction

Molecular switches are molecules that can exist in two or more metastable states. They can be transformed from one state into the other by applying external stimuli such as changes in pH, irradiation with light or by mechanical force [1–3]. Molecular switches are therefore instrumental for the development of new “intelligent” materials, [4] or molecular machines [5]. Spiropyran belongs to the most important molecular switches, because of the exceptionally large variety of diverse stimuli that can be used for switching: Their isomerization between a closed spiropyran form and an open merocyanine form can be induced by light, [6] pH, [7–10] the presence of ions, [11–13] pressure, [14] mechanical force [1,2,14–21] as well as electric fields [19,22]. Of those stimuli, the light induced switching provides to be easily accessible and nondestructive. In addition, the absorption coefficient for the merocyanine forms is extremely high (ca. 45,000 L mol⁻¹ cm⁻¹ at 550 nm) [23] so that only very low concentrations of switches have

to be present to detect switching events visually (Fig. 1).

The photochemical properties of the open merocyanine form, with its closed ring systems connected by an sp³ carbon centre, are in striking contrast to the properties of the spiropyran.

Whereas spiropyran consists of two separated π-electron systems and therefore absorb only in the UV region of the spectrum, merocyanines possess one planar π-system. In this π-system, the electrons are delocalized across the entire molecule, which causes a broad absorption maximum at ca. 550 nm. Irradiation with light of wavelengths that correspond to the absorption maxima leads to a decrease in the concentration of the irradiated species. Therefore, UV irradiation induces the ring opening, whereas visible light facilitates the ring closure (Fig. 1).

Since 2007, spiropyran has been used as mechanophore [6]. Therefore, they represent a relatively rare class of molecules in which a mechanical force induces a chemical transformation. Because spiropyran is also a chromophore, it is possible to visualize the switching event. The mechanical rupture of the bond between the spiro carbon atom and the oxygen atom can be induced by grinding of the solid spiropyran [2]. The use of spiropyran as mechano active sensors in materials (such as polymers) requires a covalent connection of the mechanophore to polymeric chains [1]. This construction principle enables the material to

* Corresponding author. Institute for Organic and Analytical Chemistry, University of Bremen, Leobener Str. NW2 C, 28359, Bremen, Germany.

E-mail addresses: astaubitz@oc.uni-kiel.de, staubitz@uni-bremen.de (A. Staubitz).

<http://dx.doi.org/10.1016/j.dyepig.2016.08.039>

0143-7208/© 2016 Elsevier Ltd. All rights reserved.

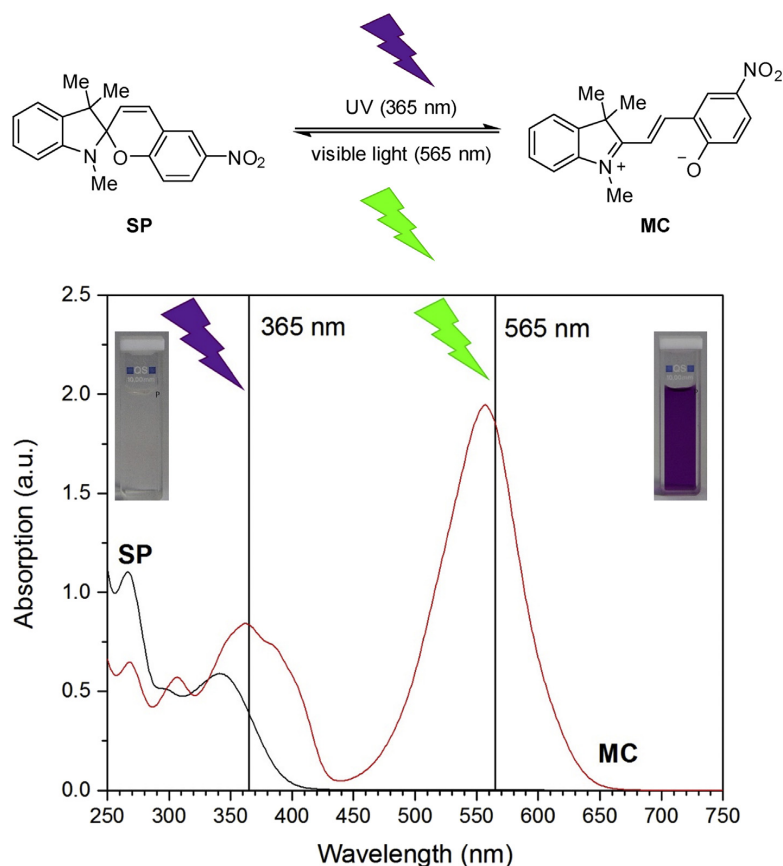


Fig. 1. top: Switching states of spiropyrans. The closed spiropyran form (SP) undergoes a ring opening upon irradiation with UV light (365 nm, purple flash) to the open merocyanine form (MC). Irradiation with visible light (565 nm, green flash) induces a ring closure and drives the equilibrium towards the SP side. Bottom: Absorption spectra and photographs of the two states. The absorption spectrum of the SP is plotted in black, the spectrum of the MC in red. Flashes and vertical lines represent the wavelengths used for switching. Whereas the colorless SP form does not absorb at wavelengths higher than 400 nm, the solution of MC shows a dark purple color which results from a broad absorption with a maximum wavelength of approx. 550 nm. The solution in acetonitrile had a concentration of 65 $\mu\text{mol/L}$ and irradiation times of 30 s were used. (For interpretation of the references to color in this figure legend, the reader is referred to the web version of this article.)

respond to stretching or compression by a color change [6].

Thus, mechanical forces applied to the periphery of the molecule are being transferred to the central bond. DFT calculations suggest a functionalization of the spiropyran at both, the chromene and the indole side, which was confirmed experimentally [14]. However, the possibilities to access these two positions are very limited. To date, a covalent incorporation of spiropyran to the backbones of polymers was achieved by six methods: electropolymerization, [24] introduction of an ATRP initiator by ester condensation to a phenolic spiropyran, followed by radical polymerization, [18] polyurethane (PU) formation, [17] hydrosilation, [19] ring-opening polymerization (ROP) with ϵ -caprolactone, [15] ring-opening metathesis polymerization (ROMP), [21] and polycondensation by Suzuki coupling [25–27]. The incorporation into polysiloxanes by hydrosilation as well as the usage of ATRP, ROP or ROMP methods or polycondensations to form PU use hydroxyl groups at the spiropyran. In contrast, due to a limited availability of spiropyran with halide functions, very few examples of functionalization of spiropyran by cross coupling have been reported [25–27]. Especially the differentiating functionalization of the two

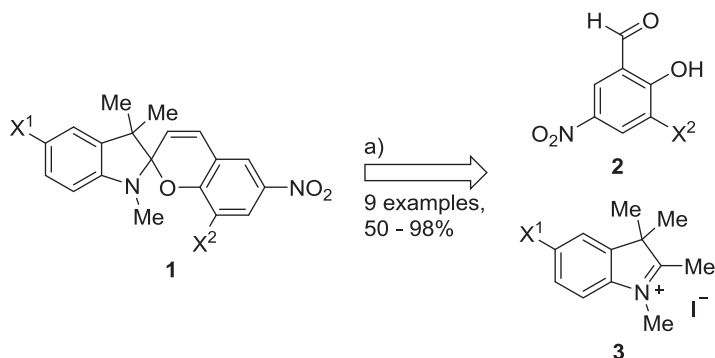
halves of the molecule (indoline and chromene) with groups of different reactivity promises a broader variety of options for further functionalizations and thus a wider applicability of spiropyran.

Therefore, to make spiropyran amenable as electrophiles in cross coupling reactions, a library of spiropyran was synthesized that contained several substitution patterns of bromide, iodide and trifluoromethanesulfonyl as leaving groups.

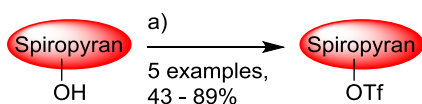
2. Experimental part¹

Spiropyran **1** are typically synthesized by a condensation reaction of a Fischer's base and a salicylaldehyde **2** (Scheme 1, section 2.2.1) [28]. The Fischer's base is released *in situ* from an indolium salt **3** under basic conditions. To establish a general procedure (9 examples) for the versatile functionalization of spiropyran, it was

¹ Further information concerning the used chemicals (supplier, purity, and purification procedures), equipment and experimental data (detailed procedures, purification, characterization, NMR spectra) are provided in the supporting material.



Scheme 1. Synthetic overview of the syntheses of spiropyrans with X^1 and $X^2 = \text{Br, I, OH}$. a) ethanol, piperidine (2 eq.), reflux, yields varying from 50 to 98%.



Scheme 2. Introduction of trifluoromethylsulfonates. a) TF_2O , pyridine, DCM, 0–40 °C.

crucial to synthesize these precursors **2** (section 2.1.1) and **3** (section 2.1.2) bearing the desired functional groups, halides and hydroxides.

The hydroxy groups were to be converted into trifluoromethylsulfonates after the spiropyran formation (Scheme 2). Therefore, we established a versatile synthesis (5 examples) using trifluoromethylsulfonic anhydride as electrophile in DCM/pyridine as solvent/base system under a nitrogen atmosphere (section 2.2.2).

2.1. Syntheses of the precursor molecules

2.1.1. Salicylaldehyde derivatives

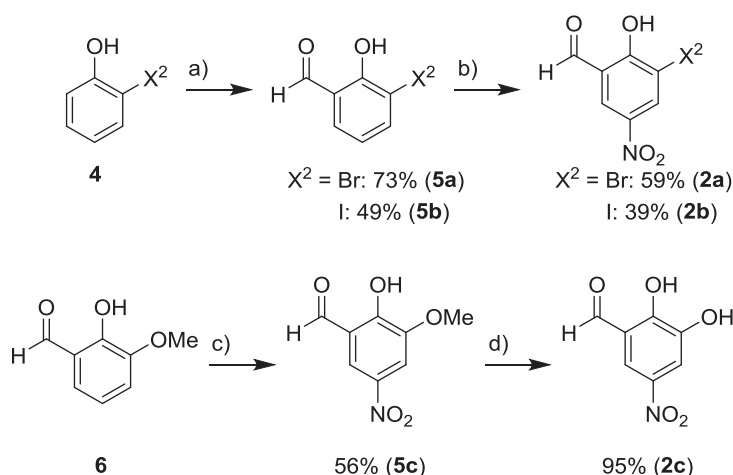
The 3-halide-5-nitrosalicylaldehydes (**2a** and **2b**) were synthesized in a two-step reaction sequence, starting from 2-halide

phenol **4** (Scheme 3). By a magnesium (II) directed *ortho*-formylation with paraformaldehyde, the aldehyde functions were selectively introduced in moderate to good yields of 73% ($X^2 = \text{Br}$) or 49% ($X^2 = \text{I}$, Lit. 84% [29]) to obtain the salicylaldehydes **5a** and **5b**. The procedure for the synthesis of the 2-hydroxy-3-iodobenzaldehyde was reported before [29] and could be adapted for the synthesis of the bromo functionalized species. A *meta*-selective nitration was performed to prepare the nitrosalicylaldehydes **2a** and **2b** in moderate yields of 59% ($X^2 = \text{Br}$) or 39% ($X^2 = \text{I}$). An equimolar amount of fuming nitric acid in acetic acid was used as nitrating agent.

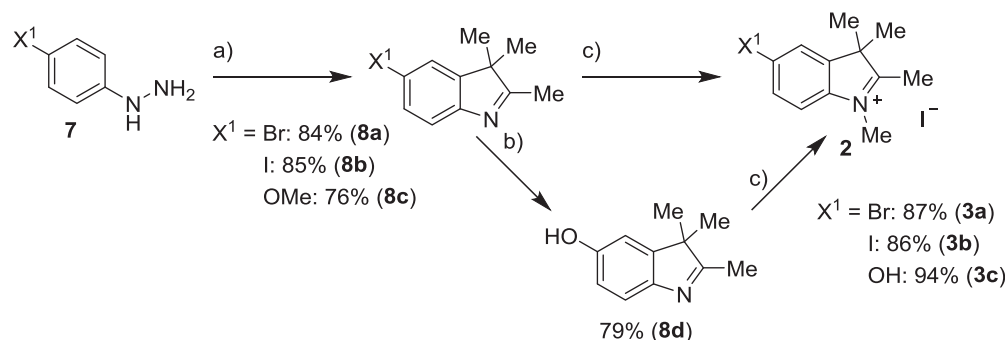
The synthesis of 3-hydroxysalicylaldehyde (**2c**) started from *ortho*-vanillin (**6**) [14]. First, the nitro group was introduced using fuming nitric acid in acetic acid as nitrating agent in a yield of 56% (Lit. 50% [14]). Afterwards, the methoxy group was transferred into a hydroxy group using hydrobromic acid in an excellent yield of 95% (Lit. 86% [14]).

2.1.2. Indolium salts

The indole species were prepared as indolium iodide salts **3a–c** in a linear synthetic route, starting from 1,4-substituted phenyl hydrazines **7** (Scheme 4). It was possible to prepare the trimethyl-



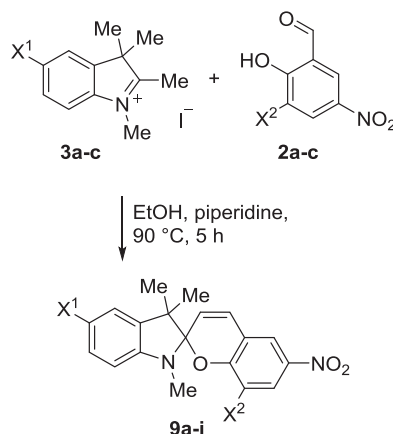
Scheme 3. Synthetic routes to obtain the salicylaldehyde precursors. a) paraformaldehyde, magnesium chloride, trimethylamine, THF, reflux. b) nitric acid/acetic acid, 15–40 °C. c) nitric acid in acetic acid, 15 °C. d) hydrobromic acid, reflux. Overall yields: $X^2 = \text{Br}$: 43%, $X^2 = \text{I}$: 19%, $X^2 = \text{OH}$: 53%.



Scheme 4. Synthetic route to obtain indolium salts, a) 3-methyl-2-butanone; for $X^1 = \text{OMe}$: ethanol, reflux; for $X^2 = \text{Br, I}$: acetic acid, reflux. b) for $X^1 = \text{OMe}$: hydrobromic acid, reflux. c) iodomethane, reflux. Overall yields: $X^1 = \text{Br}$: 73%, $X^2 = \text{I}$: 73%, $X^1 = \text{OH}$: 56%.

Table 1

Synthesized spiropyrans. The starting materials **2a–c** and **3a–c** were used as equimolar solution in EtOH (17 mol/L), 2 eq. of piperidine were added and the solution was heated to reflux for 3–5 h.



Entry	Compound	X^1	X^2	Yield ^a
1	9a	Br	Br	78%
2	9b	Br	I	50%
3	9c	Br	OH	88%
4	9d	I	Br	79%
5	9e	I	I	62%
6	9f	I	OH	75%
7	9g	OH	Br	90%
8	9h	OH	I	83%
9	9i	OH	OH	98% ^b

^a The spiropyrans were obtained as solids and are likely mixtures of open and closed form.

^b Reported yield: 99% [14].

3*H*-indoles bearing bromide (**8a**), iodide (**8b**) and methoxy (**8c**) substituents at the 5-position via a Fischer indole synthesis in good yields ranging from 76% to 84%. The methoxy group in the 5-position was cleaved with a yield of 79% using hydrobromic acid to give the 5-hydroxy indole **8d**. Three trimethyl-3*H*-indoles (**8a, b, d**) were successfully transferred into tetramethyl-3*H*-indolium iodide salts (**3a–c**) in excellent yields >86% using iodomethane as both, solvent and reagent.

A method which had already been reported for the synthesis of 5-bromo indole was used to synthesize both, the 5-bromo (**8a**, 84%, Lit. 97% [30]) and 5-iodo (**8b**) precursor. The synthesis of the 5-iodo indolium salt **3b** has been reported earlier using different conditions which gave lower yields compared to our route (70% [31] and

74% [32]). The 5-hydroxy indolium salt **3c** was synthesized using a method previously reported [14,18].

Further details (exact procedures, yields and analytical data) are provided in the [supplementary material](#).

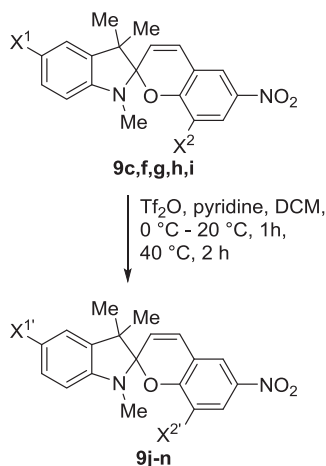
2.2. Syntheses of spiropyrans

2.2.1. Spiropyran condensations

Spiropyrans were synthesized from indolium salts **3a–c** and salicylaldehydes **2a–c** using a versatile piperidine promoted procedure in ethanol as solvent (Table 1). The base was required to induce the *in situ* formation of 2-methyleneindolines (Fischer's bases) as reactive species from indolium salts **3**. For the synthesis of

Table 2

Introducing trifluoromethanesulfonyl groups into spiropyrans. Trifluoromethanesulfonyl anhydride (1.2 eq. per OH group) was used as electrophile, pyridine (4 eq. per OH group) as base and DCM (0.25 mol/L) as solvent.



Entry	Compound	X ^{1'}	X ^{2'}	Yield ^a
1	9j	Br	OTf	74%
2	9k	I	OTf	56%
3	9l	OTf	Br	43%
4	9m	OTf	I	43%
5	9n	OTf	OTf	89%

^a The spiropyrans were obtained as solids and are likely to predominantly consist of the open merocyanine form.

spiropyran, the use of indolium salts is advantageous compared to directly using the corresponding Fischer's bases as starting materials, because indolium salts are stable against air and moisture and as solids easy to handle. All spiropyran products were obtained after crystallization from the reaction mixture. If necessary, they were further purified by recrystallization. The spiropyran bearing either bromide, iodide or hydroxy functions showed a negative photochromism on silica gel. This means that they have ring opened to give the zwitterionic merocyanine isomer whose hydroxy groups can interact with the silica surface by hydrogen bonding leading to severe yield losses for the purification *via* column chromatography [11].

The colors of the reaction mixtures and the corresponding isolated products were mostly dark brown, violet or blue. This suggested the presence of merocyanine species in the solid. We characterized the products using solution based techniques like NMR- or UV/vis-spectroscopy and therefore could not determine the exact composition of the solids as synthesized. The spiropyran's solvatochromism [6,33] was used to optimize the solvents for the NMR-characterization in order to obtain pure spectra of the closed or the corresponding open species, respectively.

2.2.2. Transformation of hydroxy groups into trifluoromethanesulfonyl groups

The functionalization of the hydroxy groups to give the corresponding trifluoromethanesulfonyl groups was accomplished using trifluorosulfonyl anhydride as trifluorosulfonylating agent and pyridine as base in DCM as a solvent (Table 2). Under strict exclusion of oxygen and water, it was possible to obtain the five desired spiropyran in good yields varying from 43% to 89%. The transformation of hydroxy groups into trifluoromethane-sulfonyl groups suppressed the inverse photochromism on silica gel. Therefore, it was possible to purify the spiropyran with trifluoromethanesulfonyl

groups using column chromatography or filtration through silica gel. Nevertheless, in the case of **9k** – **m** (Table 2, Entry 2 to 4), the binding of the merocyanine isomer to silica gel was noticeable resulting in somewhat lower yields of 43 to 56%. Especially the trifluoromethanesulfonyl groups at the indole side of the molecule (**9l** and **9m**, entries 3 and 4) showed significant binding to silica gel, so that **9l** could not be purified by chromatography. Therefore, several washing and precipitation steps were needed to remove pyridine and trifluoromethanesulfonyl anhydride from the product. This also resulted in loss of yield.

2.3. Sample preparation for UV/vis and PSS characterizations

A stock solution of each new spiropyran (100 mL, ca. 0.1 mmol/L) in acetonitrile was prepared. A defined volume (1–5 mL) was taken out of this solution and diluted to 10 mL to obtain the various desired sample concentrations (ca. 10–50 μmol/L).

The exact concentrations of the stock solutions are provided in the [supplementary material](#).

For the determination of the ratio between spiropyran and merocyanine species in dark environment by ¹H NMR spectroscopy, 500 μL of the most concentrated solution (ca. 50 μmol/L) and 50 μL of deuterated acetonitrile were combined.

2.4. Photochromic properties

All the synthesized spiropyran were examined with respect to their photochromic properties. UV/vis spectra of all spiropyran were measured while ensuring that measurements were taken in a concentration range in which the Beer-Lambert law is valid: Solutions of each spiropyran in acetonitrile were prepared in five different concentrations to obtain the absorption coefficients. This was done for the photostationary states after irradiation with

Table 3

Absorption maxima and half-life times from the photostationary states. In some cases, a half-life time could not be determined, as explained in the footnotes.

Entry	Compound	X ¹	X ²	Absorption maximum ^a		Half-life time $t_{1/2}$ (min:sec) ^a	
				$\pi-\pi^*$ transition of chromene	Merocyanine transition	After PSS ⁵⁶⁵	After PSS ³⁶⁵
1	9a	Br	Br	315 nm	556 nm	23:07	15:21
2	9b	Br	I	306 nm	559 nm	22:16	11:28
3	9c	Br	OH	355 nm	568 nm	n.n. ^b	00:55
4	9d	I	Br	308 nm	559 nm	25:07	14:23
5	9e	I	I	314 nm	561 nm	08:51	13:21
6	9f	I	OH	355 nm	570 nm	n.n. ^b	01:12
7	9g	OH	Br	320 nm	547 nm	285:32	n.n. ^c
8	9h^d	OH	I	320 nm	549 nm	271:45	n.n. ^c
9	9j	Br	OTf	308 nm	536 nm	253:17	n.n. ^c
10	9k	I	OTf	311 nm	538 nm	208:11	n.n. ^c
11	9l	OTf	Br	331 nm	561 nm	n.n. ^b	02:43
12	9m	OTf	I	335 nm	557 nm	n.n. ^b	02:41
13	9n	OTf	OTf	304 nm	537 nm	121:20	56:30

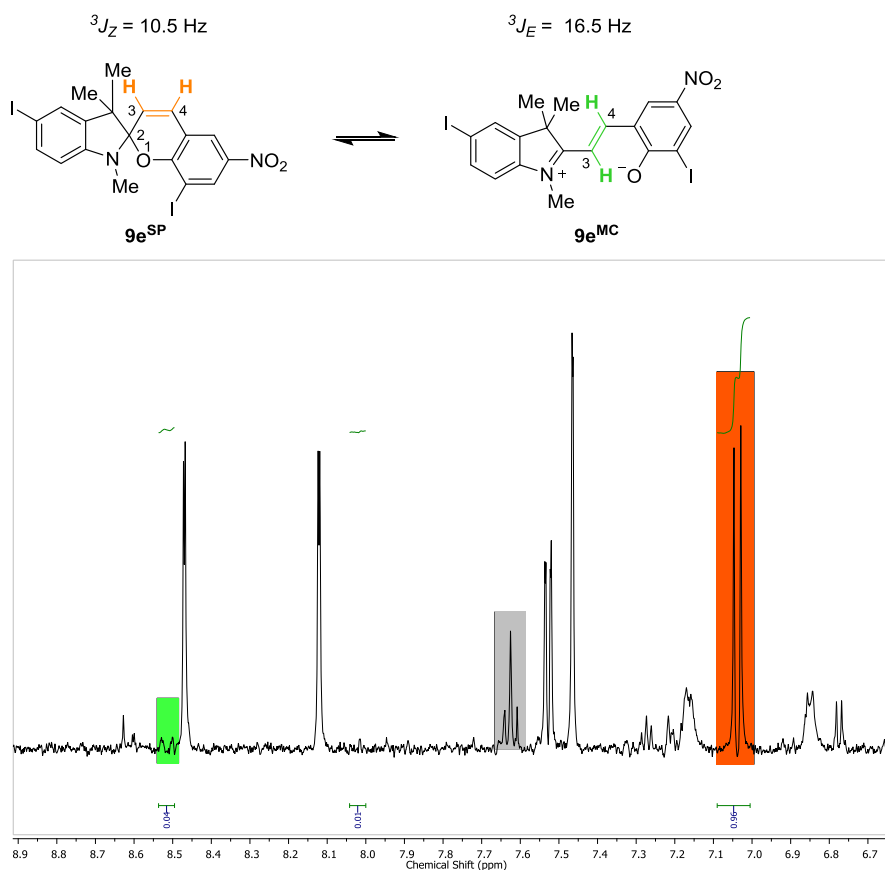
^a In acetonitrile, concentrations ranged between 10 and 50 $\mu\text{mol/L}$.^b The absorption spectra of the PSS (565 nm) and of the equilibrium in the dark showed no differences.^c The concentration of merocyanine at the PSS (365 nm) was lower than the concentration of merocyanine in dark environment.^d Because the UV/vis spectrum of the highest concentration showed a strong deviation from the expected linear increase, only the four other concentrations were used for the calculation of molar absorbances.

Fig. 2. ¹H NMR spectroscopic determination of the ratio between **9e^{MC}** and **9e^{SP}** form in dark equilibrium. **a)** Structures of the species present in solution. The investigated protons are highlighted. **b)** Excerpt of the aromatic region of the ¹H NMR spectrum of the solution in acetonitrile after relaxation in dark environment for 24 h (sample concentration: 34 $\mu\text{mol/L}$). The specific protons are highlighted in orange (**9e^{SP}**) and green (**9e^{MC}**). Integration gives a ratio of 96/4. Grey boxes are used to mark residual impurities of deuterated acetonitrile. The third integral is used to determine the error of the integration. In this example, the integral of the baseline is 0.01. (For interpretation of the references to colour in this figure legend, the reader is referred to the web version of this article.)

visible and UV light (565 nm and 365 nm) as well as for the equilibria in the dark. The exact ratio (and thus, with the information of the total sample amount the concentration) of open and closed form in the dark was determined by ^1H NMR-measurements and used to calculate both, the molar absorption coefficient of the merocyanine form and its amount in the PSS³⁶⁵.

The spectra and calculations for the diiodo functionalized dye **9e** will be described in greater detail as an example. All other spectra are provided in the [supplementary material](#). Detailed information on the used UV-light and visible light irradiation sources are also provided there.

2.4.1. Photostationary state: visible light ($\lambda = 565$ nm)

Before the sample solutions were measured, the photochemical equilibrium between closed spiropyran and open merocyanine form was shifted towards the closed form by irradiation with visible light ($\lambda = 565$ nm) until the UV/vis spectra did not change anymore, which typically took about 30 s. For the determination of the absorption coefficient, solutions with five different concentrations in the range of 5–50 $\mu\text{mol/L}$ of spiropyran in acetonitrile were used. The spectra showed two major absorption bands, representing $\pi-\pi^*$ transitions in the indolene (~250–290 nm) and the chromene moiety (~300–350 nm) [33,34]. In the photostationary equilibrium under these conditions no merocyanine form was present² (which had a typical broad absorption band at ca. 500–600 nm) [6]. Since only the chromene moiety contributes to a light yellow color of the solution, this absorption wavelength (in the case of **9e**: 314 nm, see [Table 3](#) for all maxima values) could be used for the calculation of the molar extinction coefficient. Because these absorption spectra do not contain any significant absorption at wavelengths higher than 500 nm, no merocyanine form is present. An overview of the determined properties of all spiropyran dyes **9a–n** is provided in [Table 3](#). A detailed description of the used analysis procedure and the plotted UV/vis spectra of the PSS⁵⁶⁵ and their concentration dependence are provided in the [supplementary material](#).

2.4.2. Photostationary state: UV light ($\lambda = 365$ nm)

The solutions used in section 2.4.1 were irradiated with UV light ($\lambda = 365$ nm) until an equilibrium was reached, which typically took approx. 30 s. Plots of the obtained absorption spectra contain an absorption maximum at ca. 550 nm (For **9e**: 561 nm). Since the spiropyran form **9a–n^{SP}** does not absorb at wavelengths higher than 500 nm, the observed absorption maximum depends completely on the amount of merocyanine **9a–n^{MC}** present in the solution. A detailed description of the used analysis procedure and the plotted UV/vis spectra of the PSS³⁶⁵ and their concentration dependence are provided in the [supplementary material](#).

2.4.3. Equilibrium in a dark environment

For all synthesized dyes **9a–n**, the PSS³⁶⁵ decayed with a half-life time for the decay of less than 30 min³. Therefore, it was not possible to directly determine the amount of merocyanine in the PSS³⁶⁵ via ^1H NMR spectroscopy. Due to the known formation of J- and H-aggregates by merocyanines, [6] increasing the concentration for faster NMR measurements was not an option.

It was possible to measure the equilibrium between closed and

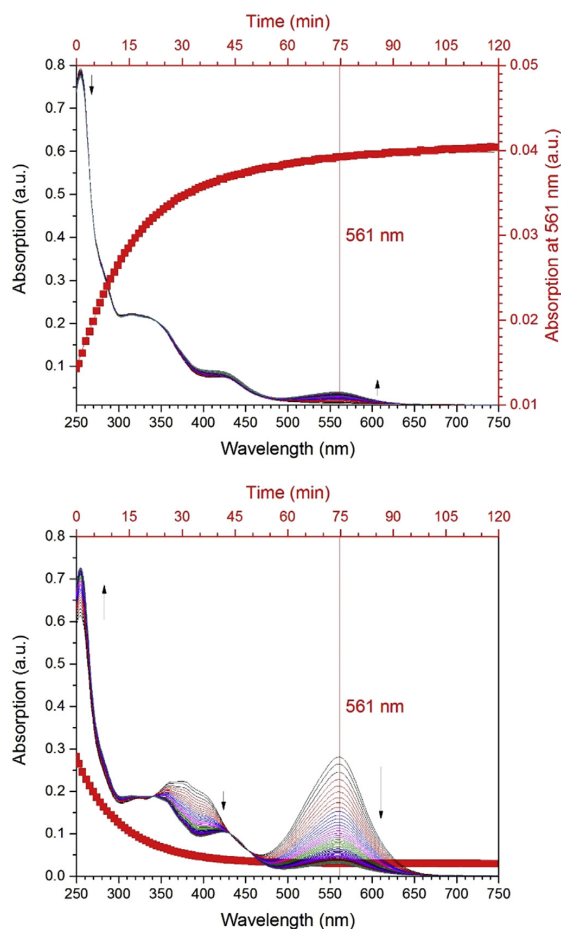


Fig. 3. Relaxation of the **9e** system to an equilibrium (Sample concentration: 38 μmol in acetonitrile). Top: After stopping irradiation with green light (565 nm, until the photostationary state was reached), the merocyanine absorption at 561 nm increased with a half-life time of 8 min 51 s bottom: Irradiation of the sample with UV light (365 nm, until the photostationary state was reached) enriched the merocyanine species. After removal of the illumination source, this was found to decay with a half-life time of 13 min 21 s. (For interpretation of the references to colour in this figure legend, the reader is referred to the web version of this article.)

open form which formed under dark conditions by both, UV/vis and ^1H NMR spectroscopy. The UV/vis solution or the NMR sample,⁴ respectively, were kept dark for at least 24 h prior to the measurement. Following the earlier described procedure, it was possible to calculate the concentration dependence of the absorption maximum corresponding to the merocyanine transition (typically circa 550 nm). In the case of **9e**, it is 828 L (mol cm)⁻¹. By ^1H NMR spectroscopy, the ratio **9e^{MC}**/**9e^{SP}** was determined to be 4/96. For a comparison of the two species, the signals corresponding to protons of the ethylene bridge (*H*-3 and *H*-4) in the chromene moiety were used ([Fig. 2](#)). These protons form doublets, with coupling constants of circa $^3J_Z = 10.5$ Hz for **9e^{SP}** and $^3J_E = 16.5$ Hz

² In the case of **9c** and **9f**, after irradiation with visible light, the solution contained a significant amount of the merocyanine species in the PSS.

³ For the dyes **9g–k**, a decay measurement was not performed, because the concentration of merocyanine was lower at the PSS³⁶⁵ compared to dark conditions. This is because the merocyanine form also absorbs at this wavelength, leading to the formation of the spiropyran form, an effect that is not present in the dark equilibrium.

⁴ A detailed procedure of sample preparation is provided in the [supplementary material](#).

for **9e^{MC}**.

Thereby, the molar extinction coefficient of **9e^{MC}** was calculated as follows:

$$\epsilon^{MC,561} = \frac{828}{4\%} \frac{L}{\text{mol cm}} = 20700 \frac{L}{\text{mol cm}}$$

2.4.4. Relaxation of the photostationary states

Eventually, we also examined the relaxation of the photostationary states (Fig. 3). To analyze the relaxation from the spiropran form, the sample was irradiated at 565 nm to reach the photostationary state with enhancement of the spiropran; then the light was switched off and the UV/vis spectra measured in dependence of the time. The absorbance at 561 nm, which corresponds to the absorption maximum increased with a half-life time of 8 min 51 s. The same procedure was used for analyzing the relaxation from the merocyanine form: irradiation at 365 nm to enhance the merocyanine concentration to equilibrium, switching off the light and recording the absorbance at 561 nm. The half-life time in this case was 13 min 21 s.

3. Results and discussion

The absorption spectra and photochromic properties of 13 formerly unknown spiroprans were investigated. Table 3 contains the wavelengths of the absorption maxima of the $\pi-\pi^*$ transitions of the chromene and merocyanine moieties as well as the observed half-life times of the systems' relaxation from the photostationary states towards the equilibrium in dark. The $\pi-\pi^*$ transitions of the chromene moieties in the closed forms **9a–n^{SP}** vary between 304 nm (**9n^{SP}**; Table 3, entry 13) and 355 nm (**9c,f**; entries 3,6). As expected, a change of the substitution at this side of the molecule results in a large change of these absorption maxima. While bromide (**9a,d,g,i**; entries 1,4,7,11), iodide (**9b,e,h,m**; entries 2,5,8,12) and trifluoromethylsulfonyl groups (**9j,k,n**; entries 9,10,13) at the chromene side show similar wavelengths between 304 and 320 nm, hydroxyl functions (**9c,f**; entries 3,6) result in a bathochromic shift with absorption maxima at wavelengths of 355 nm.

A similar trend can be found for the merocyanine transition with

observed maximum wavelengths between 536 nm (**9j**; entry 9) and 570 nm (**9f**; entry 6). Again, a change in the substitution of the chromene side results in large changes of the absorption maxima's wavelengths. Trifluoromethylsulfonyl groups induce a hypsochromic shift of about 20 nm compared to bromide and iodide functionalities, whereas hydroxy groups induce a bathochromic shift of about 10 nm compared to the halide functionalities. Varying the substitution of the indole side (X^1) does not result in a larger change of the absorption wavelength. For example, compounds **9a,d,g,i** (entries 1,4,7,11) all bear a bromide as functional group at the chromene side, while the functional groups at the indole side vary: bromide (**9a**; entry 1), iodide (**9d**; entry 4), hydroxy (**9g**; entry 7), Trifluoromethylsulfonyl (**9i**; entry 11). The observed absorption wavelengths vary only between 547 (**9g**; entry 7) and 561 nm (**9i**; entry 7). For this absorption, hydroxy groups induce a hypsochromic shift, compared to the dyes with bromide or iodide at this position. Trifluoromethylsulfonyl groups at the indole side do not significantly influence the absorption maximum of the merocyanine transition significantly.

Relaxation of the systems after the PSS⁵⁶⁵ takes place with longer half-life times (08:51–285:32 min) than the relaxation after PSS³⁶⁵ (0:55–56:30 min). For 3 compounds (**9c,f,m**; entries 3,6,12), it was not possible to determine the half-life time, because the absorption spectra at the PSS⁵⁶⁵ and the equilibrium in dark are the same. The shortest half-life time was observed for compound **9e** (entry 5), which bears two iodide functionalities. Compounds with either hydroxy groups at the indole side (**9g,h**; entries 7,8) or trifluoromethylsulfonyl groups at the chromene side (**9j,k**; entries 9,10) show the slowest relaxation with half-life times ranging from 208 to 285 min. Two compounds with trifluoromethylsulfonyl groups at the chromene side (**9j,k**; entries 9,10) and two compounds with hydroxy groups at the indole side (**9g,h**; entries 8,9) could not be analyzed concerning their decay after PSS³⁶⁵, because the amount of merocyanine was higher in the dark equilibrium. The other compounds with trifluoromethylsulfonyl or hydroxy groups show the fastest decay, with half-life times ranging from 55 s (**9c**; entry 3) to 2:41 min (**9m**, entry 12). Most other relaxations show half-life times in the range of approx. 10–15 min, only the dye with two trifluoromethylsulfonyl groups (**9n**, entry 13) shows a significantly slower decay ($t_{1/2} = 56:30$ min).

Table 4

Determination of the molar extinction coefficient of merocyanine and the merocyanine: spiropran ratio at the PSS (365 nm). A table showing errors of the ¹H NMR integration and resulting errors of the other properties is provided in the [supplementary material](#).

Entry	Compound	Equilibrium in dark environment			PSS (365 nm)	
		Molar absorption (L (mol cm) ⁻¹)	Ratio [MC]:[SP]	ϵ^{MC} (L (mol cm) ⁻¹)	Molar absorption (L (mol cm) ⁻¹)	Ratio [MC]:[SP]
1	9a	1858	08:92	23,225	30,591	100:0 ^a
2	9b	1082	12:88	9327	11,500	100:0 ^{a,b}
3	9c	2424	07:93	34,628	27,520	79:31
4	9d	1576	07:93	22,514	19,770	88:12
5	9e	828	04:96	20,700	8320	40:60
6	9f	2209	06:94	36,817	24,215	66:34
7	9g	31,621	58:42	54,519	1747	03:97
8	9h	15,851	56:44	28,305	1972	07:93
9	9j	21,876	59:41	37,078	6885	19:81
10	9k	23,936	52:48	43,031	5274	11:89
11	9l^f	336	02:98	16,800	24,402	100:0 ^d
12	9m	289	16:84	1806	6292	100:00 ^d
13	9n	6879	27:73	25,477	11,532	45:55

^a The calculated ϵ^{MC} led to an apparent amount of more than one equivalent of merocyanine in the PSS³⁶⁵, which is due to an integration error in this ¹H NMR spectroscopic measurement of ± 0.01 . However, the observed extinction coefficient in the PSS is included in the error ranges. Plots of all NMR spectra including integrals and a detailed table with errors are provided in the [supplementary material](#).

^b A different proton signal was used for integration, due to an overlap of the ethylene protons of the merocyanine species.

^c Due to very low total absorptions of the merocyanine transition, it was necessary to use concentrations from 60 to 100 $\mu\text{mol/L}$ for UV/vis and ¹H NMR spectroscopy.

^d The calculated ϵ^{MC} led to an apparent amount of more than one equivalent of merocyanine in the PSS³⁶⁵. The measured absorptions in the dark were close to the device's detection limits.

For 13 spiropyran dyes **9a–n** we were able to determine the molar extinction coefficients of the merocyanine transitions (see Table 4). Therefore, the absorption at the equilibrium state in dark was plotted against the overall concentration. The obtained values range from 289 L (mol cm)⁻¹ (**9m**; entry 12) to 31,621 L (mol cm)⁻¹ (**9g**; entry 7). While compounds with only halide functionalities (**9a,b,d,e**; entries 1,2,4,5) or trifluoromethylsulfonyl functional groups at the indole side (**9l,m**; entries 11,13) show low absorptions coefficients at approx. 1000 L (mol cm)⁻¹, hydroxy groups at the chromene side rise the absorption coefficients to approx. 2500 L (mol cm)⁻¹ (**9c,f**; entries 3,6). The introduction of hydroxy groups at the indole side increases the measured absorptions further to values of 15 or 30 kL (mol cm)⁻¹ (**9g,h**; entries 7,8). Transformation of hydroxy to trifluoromethylsulfonyl groups at the chromene side increases the absorption to approx. 20 kL (mol cm)⁻¹ (**9j,k**; entries 9,10). These absorptions originate solely from absorptions of the merocyanine species **9a–n**^{MC}. Thereby, the ratios **9**^{MC}:**9**^{SP} were determined by ¹H NMR spectroscopy under exclusion of light and could be used to calculate the molar extinction coefficients ϵ^{MC} of the merocyanine forms. These values range from 9327 L (mol cm)⁻¹ (**9b**; entry 2) to 54,519 L (mol cm)⁻¹ (**9g**; entry 7).

The measured absorptions at the PSS³⁶⁵ were divided by the calculated molar extinction coefficients to obtain the ratio [MC]:[SP]. Three compounds (**9a,b,m**; entries 1,2,12) show a complete switch. For the other compounds, the amount of **9**^{MC} is between 3 and 88%. The four compounds which had the highest molar absorption in the dark show significantly lower absorptions at the PSS³⁶⁵ and thereby a smaller proportion of **9**^{MC} is present (3–19%; **9f–k**; entries 6–10).

4. Conclusion

Thirteen novel spiropyran dyes were synthesized and characterized in terms of their UV/vis spectra and their switching properties. Eight of these dyes were synthesized in good to excellent yields (50–90%) by condensation reactions. In addition, a versatile method (five examples) was established that gives access to trifluoromethane sulfonyl groups as functionalization of spiropyran in good yields (43–89%). Importantly, the functional groups that were introduced (I, Br, OTf) are all highly suitable for cross-coupling reactions, enabling access to spiropyran functionalized with unsaturated groups which was not possible before. Owing to the combination of halide with/and hydroxyl functionalities on the molecules, condensation reactions with the hydroxyl groups can be performed on one end of the molecule, whereas the halide gives access to cross-coupling based extensions of the spiropyran scaffold. The decay times of the photostationary states at the absorption maxima merocyanine (365 and 565 nm) were determined and vary between 55 s and 56 min for 365 nm and between 9 min and 285 min for 565 nm. It was possible to determine the amount of merocyanine in the photostationary states (365 nm) (3–100%) by applying a combined UV/vis and ¹H NMR spectroscopic analysis. This method also allowed us to calculate the molar extinction coefficients of the merocyanine species (9.3–25 k (L (mol cm)⁻¹)). Work is ongoing to establish selective cross-coupling procedures for this new library of spiropyran.

Acknowledgements

This project was supported by the Special Research Area 677 “Function by Switching” of the Deutsche Forschungsgemeinschaft (DFG). Initial funding was provided by the DECHEMA (Gesellschaft für Chemische Technik und Biotechnologie) by a Max-Buchner-fellowship for A. S.. We are grateful to Prof. Dr. Thisbe K.

Lindhorst for the donation of a 6 month Ph. D. position for M. S.-S.. This research has been supported by the Institutional Strategy of the University of Bremen, funded by the German Excellence Initiative.

Appendix A. Supplementary data

Supplementary data related to this article can be found at <http://dx.doi.org/10.1016/j.dyepig.2016.08.039>.

References

- Caruso MM, Davis DA, Shen Q, Odom SA, Sottos NR, White SR, et al. Mechanically-induced chemical changes in polymeric materials. *Chem Rev* 2009;109:5755–98. <http://dx.doi.org/10.1021/cr9001353>.
- Beyer MK, Clausen-Schaumann H. Mechanochemistry: the mechanical activation of covalent bonds. *Chem Rev* 2005;105:2921–48. <http://dx.doi.org/10.1021/cr030697h>.
- Schulz-Senft M, Lipfert M, Staubitz A. Mechanochemie: Molekulare Wirkung durch Kraft. *Chem Unserer Zeit* 2014;48:200–14. <http://dx.doi.org/10.1002/ciuz.201400640>.
- Natali M, Giordani S. Molecular switches as photocontrollable “smart” receptors. *Chem Soc Rev* 2012;41:4010–29. <http://dx.doi.org/10.1039/C2CS35015G>.
- Wiley: Molecular Switches, 2nd, Completely Revised and Enlarged Edition, 2 Volume Set - Ben L. Feringa, Wesley R. Browne n.d. <http://eu.wiley.com/WileyCDA/WileyTitle/productCd-3527313656.html> (accessed May 13, 2015).
- Klajn R. Spiropyran-based dynamic materials. *Chem Soc Rev* 2014;43:148–84. <http://dx.doi.org/10.1039/c3cs60181a>.
- Florea L, Diamond D, Benito-Lopez F. Photo-responsive polymeric structures based on spiropyran. *Macromol Mater Eng* 2012;297:1148–59. <http://dx.doi.org/10.1002/mame.201200306>.
- Raymo FM, Giordani S. Signal processing at the molecular level. *J Am Chem Soc* 2001;123:4651–2. <http://dx.doi.org/10.1021/ja005699n>.
- Wojtyk JTC, Wasey A, Xiao N-N, Kazmaier PM, Hoz S, Yu C, et al. Elucidating the mechanisms of acidochromic spiropyran-merocyanine interconversion. *J Phys Chem A* 2007;111:2511–6. <http://dx.doi.org/10.1021/jp068575r>.
- Keum S-R, Lee K-B, Kazmaier PM, Buncel E. A novel method for measurement of the merocyanine-spiropyran interconversion in non-activated 1, 3, 3-trimethylspiro-(2H-1-benzopyran-2, 2'-indoline) derivatives. *Tetrahedron Lett* 1994;35:1015–8. [http://dx.doi.org/10.1016/S0040-4039\(00\)79953-9](http://dx.doi.org/10.1016/S0040-4039(00)79953-9).
- Kinashi K, Nakamura S, Imamura M, Ishida K, Ueda Y. The mechanism for negative photochromism of spiropyran in silica: negative photochromism of spiropyran. *J Phys Org Chem* 2012;25:462–6. <http://dx.doi.org/10.1002/poc.1926>.
- Kinashi K, Harada Y, Ueda Y. Thermal stability of merocyanine form in spiropyran/silica composite film. *Thin Solid Films* 2008;516:2532–6. <http://dx.doi.org/10.1016/j.tsf.2007.04.120>.
- Wojtyk JTC, Kazmaier PM, Buncel E. Modulation of the spiropyran-merocyanine reversion via metal-ion selective complexation: trapping of the “transient” cis-merocyanine. *Chem Mater* 2001;13:2547–51. <http://dx.doi.org/10.1021/cm010038q>.
- Davis DA, Hamilton A, Yang J, Cremer LD, Van Gough D, Potisek SL, et al. Force-induced activation of covalent bonds in mechanoresponsive polymeric materials. *Nature* 2009;459:68–72. <http://dx.doi.org/10.1038/nature07970>.
- O'Bryan G, Wong BM, McElhanon JR. Stress sensing in polycaprolactone films via an embedded photochromic compound. *ACS Appl Mater Interfaces* 2010;2:1594–600. <http://dx.doi.org/10.1021/am100050v>.
- Kingsbury CM, May PA, Davis DA, White SR, Moore JS, Sottos NR. Shear activation of mechanophore-crosslinked polymers. *J Mater Chem* 2011;21:8381. <http://dx.doi.org/10.1039/c0jm04015k>.
- Lee CK, Davis DA, White SR, Moore JS, Sottos NR, Braun PV. Force-induced redistribution of a chemical equilibrium. *J Am Chem Soc* 2010;132:16107–11. <http://dx.doi.org/10.1021/ja106332g>.
- Potisek SL, Davis DA, Sottos NR, White SR, Moore JS. Mechanochemically-linked addition polymers. *J Am Chem Soc* 2007;129:13808–9. <http://dx.doi.org/10.1021/ja076189x>.
- Wang Q, Gossweiler GR, Craig SL, Zhao X. Cephalopod-inspired design of electro-mechano-chemically responsive elastomers for on-demand fluorescent patterning. *Nat Commun* 2014;5:4899. <http://dx.doi.org/10.1038/ncomms5899>.
- Gossweiler GR, Brown CL, Hewage GB, Sapiro-Gheiler E, Trautman WJ, Welschofer GW, et al. Mechanochemically active soft robots. *ACS Appl Mater Interfaces* 2015;7:22431–5. <http://dx.doi.org/10.1021/acsami.5b06440>.
- Gossweiler GR, Kouznetsova TB, Craig SL. Force-rate characterization of two spiropyran-based molecular force probes. *J Am Chem Soc* 2015;137:6148–51. <http://dx.doi.org/10.1021/jacs.5b02492>.
- Wagner K, Byrne R, Zanoni M, Gambhir S, Dennany L, Breukers R, et al. A multiswitchable poly(terthiophene) bearing a spiropyran functionality: understanding photo- and electrochemical control. *J Am Chem Soc* 2011;133:5453–62. <http://dx.doi.org/10.1021/ja114634a>.

- [23] Buback J, Kullmann M, Langhojer F, Nuernberger P, Schmidt R, Würthner F, et al. Ultrafast bidirectional photoswitching of a spiropran. *J Am Chem Soc* 2010;132:16510–9. <http://dx.doi.org/10.1021/ja1062746>.
- [24] Wagner K, Zanonì M, Elliott ABS, Wagner P, Byrne R, Florea LE, et al. A merocyanine-based conductive polymer. *J Mater Chem C* 2013;1:3913. <http://dx.doi.org/10.1039/c3tc30479e>.
- [25] Sommer M, Komber H. Spiropran main-chain conjugated polymers. *Macromol Rapid Commun* 2013;34:57–62. <http://dx.doi.org/10.1002/marc.201200688>.
- [26] Komber H, Müllers S, Lombeck F, Held A, Walter M, Sommer M. Soluble and stable alternating main-chain merocyanine copolymers through quantitative spiropran–merocyanine conversion. *Polym Chem* 2014;5:443. <http://dx.doi.org/10.1039/c3py00853c>.
- [27] Metzler L, Reichenbach T, Brügger O, Komber H, Lombeck F, Müllers S, et al. High molecular weight mechanochromic spiropran main chain copolymers via reproducible microwave-assisted Suzuki polycondensation. *Polym Chem* 2015;6:3694–707. <http://dx.doi.org/10.1039/C5PY00141B>.
- [28] Minkin VI. Photo-, Thermo-, Solvato-, and Electrochromic Spiroheterocyclic Compounds. *Chem Rev* 2004;104:2751–76. <http://dx.doi.org/10.1021/cr020088u>.
- [29] Brady RM, Hatzis E, Connor T, Street IP, Baell JB, Lessene G. Synthesis of conformationally constrained benzoylureas as BH3-mimetics. *Org Biomol Chem* 2012;10:5230–7. <http://dx.doi.org/10.1039/c2ob25618e>.
- [30] Völker SF, Renz M, Kaupp M, Lambert C. Squaraine dyes as efficient coupling bridges between triarylamine redox centres. *Chem Eur J* 2011;17:14147–63. <http://dx.doi.org/10.1002/chem.201102227>.
- [31] Fegan A, Shirude PS, Balasubramanian S. Rigid cyanine dyenucleic acid labels. *Chem Commun* 2008:2004–6. <http://dx.doi.org/10.1039/B801629A>.
- [32] Gerowska M, Hall L, Richardson J, Shelbourne M, Brown T. Efficient reverse click labeling of azide oligonucleotides with multiple alkynyl Cy-Dyes applied to the synthesis of HyBeacon probes for genetic analysis. *Tetrahedron* 2012;68:857–64. <http://dx.doi.org/10.1016/j.tet.2011.11.041>.
- [33] Keum S-R, Roh S-J, Ahn S-M, Lim S-S, Kim S-H, Koh K. Solvatochromic behavior of non-activated indolinobenzospiropran 6-carboxylates in aqueous binary solvent mixtures. Part II¹. *Dyes Pigments* 2007;74:343–7. <http://dx.doi.org/10.1016/j.dyepig.2006.02.013>.
- [34] Tyler NW, Becker RS. Photochromic spiroprans. I. Absorption spectra and evaluation of the π -electron orthogonality of the constituent halves. *J Am Chem Soc* 1970;92:1289–94. <http://dx.doi.org/10.1021/ja00708a031>.

3.2. Stille Coupling Reactions of Spiropyrans

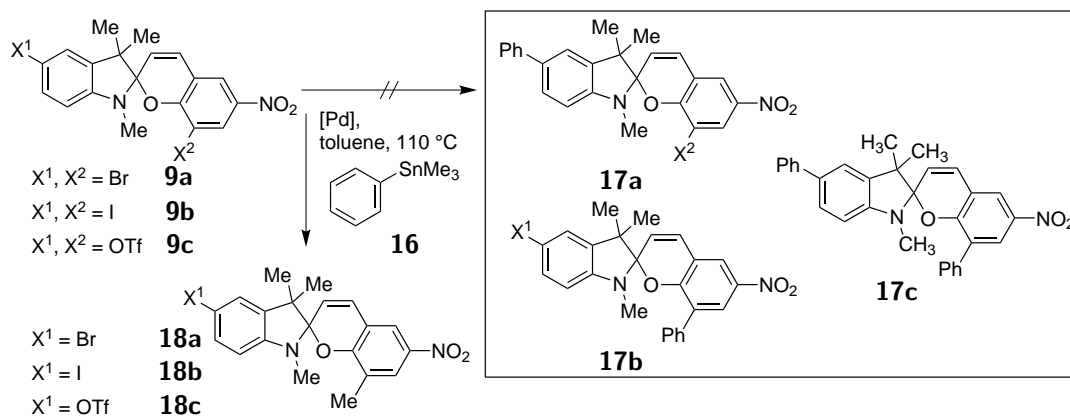
Since hydroxy groups cannot be used as electrophilic cross-coupling partners, the compounds **9c,f-i** in Ref.^[174] were not considered for the use in test reactions. Thus, out of the library of spiropyrans **9** (compounds **9a-n** in Ref.^[174]), it was planned to test the di-halide compounds **9a,b,d,e** (Compounds **9a,b,d,e** in Ref.^[174]) and the spiropyrans with triflate substituents **9c,f-i** (Compounds **9j-n** in Ref.^[174]) in selective Stille cross-coupling reactions. To gain an overview of the reactivity of the different substituents, the initial experiments were carried out using the symmetrically functionalized spiropyrans **9a-c**. Thereby, it was possible to scope the reactivity of each substituent (iodide, bromide and triflate) on both, the indole and chromene site. Three different products were to be expected in the reactions with trimethylphenylstannane (**16**): selective coupling at the 5'-position at the indole side, replacing X¹ yields compound **17a**; selective coupling at the chromene's 8-position yields compound **17b**; whereas coupling at both positions yields compound **17c**.

Typically, the expected reactivity of these substituents in Stille reactions is I > OTf > Br.^[176] The reactivity of aromatic halides in cross-coupling reactions strongly depends on the electron density at the C-X substituted carbon atoms. Electrophilic cross-coupling partners R-Xds with substitution patterns that result in high electron densities at the carbon atoms are less likely to react than compounds with low electron densities at the involved carbon atoms.^[177] In nitro spiropyrans **9**, the electron density at the 5'-position (X¹) of the indole site is higher than the electron density at the 8 position (X²) of the chromene site.^[178] This should result in a higher reactivity of the chromene site. Therefore, the use of the symmetrically substituted spiropyrans **9a-c** should result in either selective coupling at the 8-position (yielding **17b**) or symmetrical coupling on both positions (yielding **17c**).

Trimethylphenylstannane (**16**) was used as nucleophile in the scoping reactions. The syntheses were carried out in toluene under nitrogen atmosphere at 110 °C. It was possible to run parallel reactions while monitoring the progress of the reaction by ¹H NMR spectroscopy. For this purpose, small samples were obtained from the reaction mixture and analyzed by NMR spectroscopy after removal of the catalyst and solvent. After the reaction time indicated in Table II.1, the reaction mixture was passed through a silica column (eluent: toluene) and the obtained product mixture was analyzed by 2D NMR spectroscopy (See Figure II.1 for example).

With Pd(PPh₃)₄ as a catalyst (Table II.1, Entries 1–3), the bromo substituted compound **9a** showed a conversion of the starting material of 23% after a reaction time of 5 d. The conversion of the iodo spiropyran **9b** was significantly higher, being 36%. In contrast, the triflate groups of **9c** did not undergo any reaction after 24 h. The bromide substituents in compound **9a** and the iodide substituents in compound **9b** exhibited the same selectivity: only the substituent at the chromene side (X²) was replaced with a methyl group (**18**). Since the substitution with bromide or iodide had no apparent effect on the selectivity, the following variations (Table II.1, Entries 4–13) were carried out using only **9b** and **9c** as starting material.

Table II.1. Investigation of the reactivity of the spiroyrans **9a–c** in Stille reactions with trimethylphenylstannane (**16**). The expected products **17a–c** (inside the black box) were not observed. Instead, **18a–c** were obtained.



Entry No.	Starting Material X^1 X^2	Catalyst System	Additive	Reaction Time	Conversion	Product
1	Br Br 9a	$\text{Pd}(\text{PPh}_3)_4$	–	5 d	29%	18a
2	I I 9b	$\text{Pd}(\text{PPh}_3)_4$	–	5 d	36%	18b
3	OTf OTf 9c	$\text{Pd}(\text{PPh}_3)_4$	–	24 h	0%	18c
4	I I 9b	$\text{Pd}(\text{PPh}_3)_4$	LiCl	15 h	17%	18b
5	OTf OTf 9c	$\text{Pd}(\text{PPh}_3)_4$	LiCl	15 h	18%	18c
6	I I 9b	$\text{Pd}(\text{PPh}_3)_4$	CuI	48 h	15%	18b
7	OTf OTf 9c	$\text{Pd}(\text{PPh}_3)_4$	CuI	48 h	0%	18c
8	I I 9b	$\text{Pd}(\text{P}t\text{-Bu}_3)_2$	LiCl	5 d	36%	18b
9	OTf OTf 9c	$\text{Pd}(\text{P}t\text{-Bu}_3)_2$	LiCl	5 d	0%	18c
10	I I 9b	$\text{Pd}_2\text{dba}_3/\text{SPhos}$	LiCl	5 d	86%	18b
11	OTf OTf 9c	$\text{Pd}_2\text{dba}_3/\text{SPhos}$	LiCl	5 d	11%	18c
12	I I 9b	$\text{Pd}(\text{dppf})\text{Cl}_2$	LiCl	5 d	32%	18b
13	OTf OTf 9c	$\text{Pd}(\text{dppf})\text{Cl}_2$	LiCl	5 d	7%	18c

However, no traces of the formation of any of the expected products **17a–c** were detected in the ^1H NMR or $^{13}\text{C}\{^1\text{H}\}$ 1D and 2D spectra of the reaction mixtures. In Figure II.1, the aromatic region of the ^1H NMR of product mixture of the reaction of dibromo spiropyran **9a** and **16** with $\text{Pd}(\text{PPh}_3)_4$ as a catalyst (Table II.1, Entry 1) is shown as an example. Two sets of signals corresponding to the starting material **9a** and the product **18a** could be identified. The transfer of the methyl group occurred unexpectedly, as alkyl groups are being transferred typically 20 times slower than aryl groups.^[179] A possible explanation could be the steric hindrance of the neighboring indolene side of the spiropyran. It was reported that sterically demanding stannanes react significantly more slowly.^[179] Figure II.2 displays the crystal structure of 8-bromo-1',3',3'-trimethyl-6-nitrospiro-[chromene-2,2'-indoline].^[180] The axis of the C–Br bond is roughly parallel ($\alpha=24^\circ$) to the phenyl plane in the indolene side, while the protons of the adjacent methyl groups are 3.7 Å (C–CH₃) and 4.1 Å (N–CH₃)

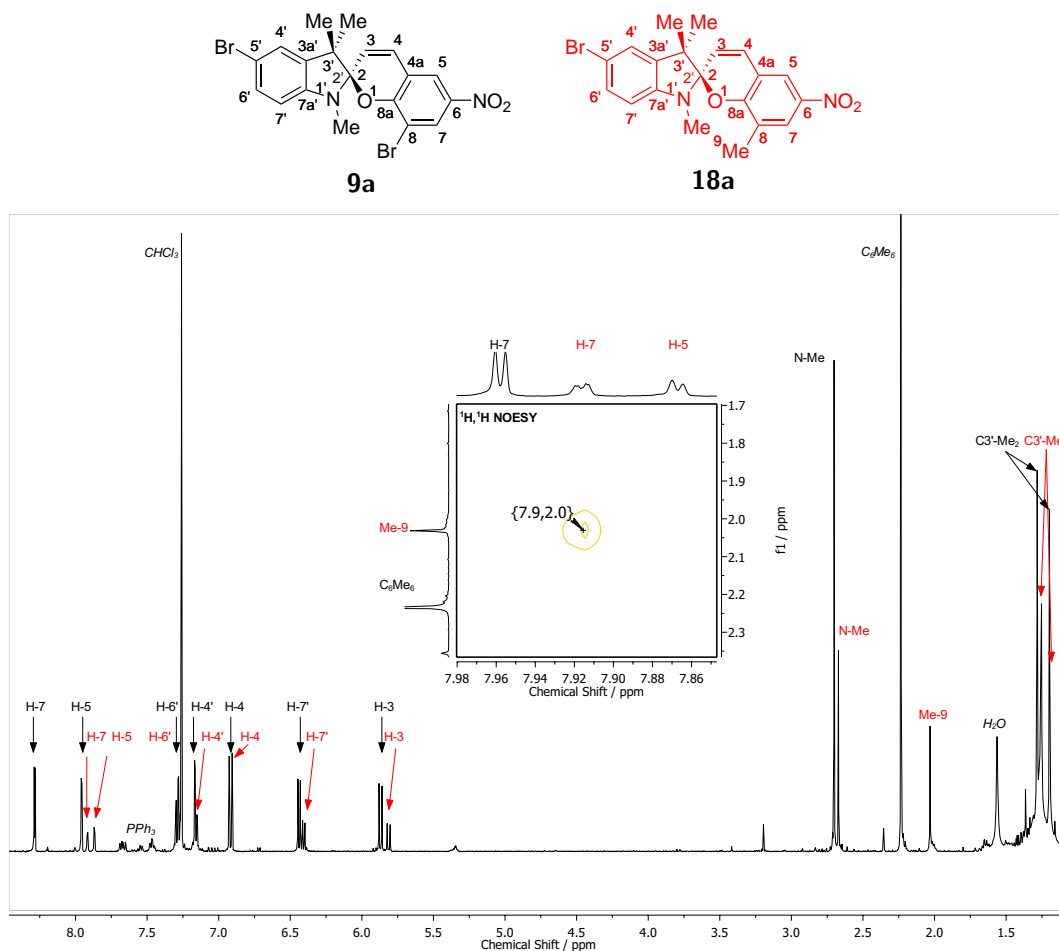


Figure II.1. Fully assigned ^1H NMR spectrum of the Stille reaction of **9a** (black) to the product **18a** (red). Signals corresponding to PPh_3 ligands, the internal standard hexamethylbenzene (C_6Me_6), water and the solvent CDCl_3 are labeled in italic. **Inset:** enlarged sector of the $^1\text{H}, ^1\text{H}$ NOESY spectrum, displaying the methyl group Me-9 and the neighboring proton H-7.

away (see Figure II.2, page 88).^[180] Therefore, the available space was apparently too small for transfer of the phenyl residue.

To circumvent this unexpected reaction, lithium chloride and copper(I) iodide were tested as additives (Table II.1, Entries 4–7) in order to increase the rate of the reaction. The addition of lithium chloride resulted in a 17% conversion of **9b** after only 15 h. Under these conditions, the spiropyran **9c** with triflate groups showed a similar conversion of 18%. However, the reaction products were identified to be (**18b,c**). The reaction of **9b** with copper(I) iodide was significantly slower with a conversion of 15% after 48 h. Again, only **18b** was found as product. Using copper(I) iodide as additive did not increase the reactivity of **9c**, which remained inert. Lithium chloride improved the reactivity of both, **9b** and **9c** and was used as additive for the subsequent investigation of the catalyst's influence.

A change of the ligands in the palladium(0) complex $\text{Pd}(\text{P}t\text{-Bu}_3)_2$ together with lithium chloride (Table II.1, Entries 8 and 9) did not improve the conversion compared to $\text{Pd}(\text{PPh}_3)_4$. The 8-iodo substituent of **9b** reacted with a conversion of 36%, whereas **9c** remained inert.

Using 2-dicyclohexylphosphino-2',6'-dimethoxybiphenyl (SPhos) as reactive ligand and dibenzylideneacetone (dba) as ligand in the precursor Pd₂dba₃ (Table II.1, Entries 10 and 11) increased the conversion of the iodo substituent of **9b** to 86% after 5 d. The chromene site of **9c** reacted with a conversion of 11%. This catalyst system also only yielded the protonated products **18b** and **18c**.

To change the oxidation state of palladium from 0 to II, 1,1'-bis(diphenylphosphino)ferrocene (dppf) was used as ligand in Pd(dppf)Cl₂ and lithium chloride as additive (Table II.1, Entries 12 and 13). After a reaction time of 5 d, 32% of **18b** and 7% of **18c** were formed.

Conclusion In all reactions, no conversion of the substituent X¹ at the 5'-position was found. While it was possible to react up to 86% of the iodo substituent at the 8-position, no formation of the corresponding cross-coupling product **17b** could be detected. Instead, the reaction conditions that lead to consumption of starting the materials **9a–c** yielded the coupling of the methyl group. These results indicate low reactivities in the spiropyrans **9a,b,d,e** with halide and **9c,f–i** with triflate functions in cross-coupling reactions.

The transfer of the methyl group occurred unexpected, as alkyl groups are being transferred typically 20 times slower than aryl groups.^[179] A possible explanation could be the steric hinderance of the neighboring indolene side of the spiropyran. It was reported that sterically demanding stannanes react significantly slower.^[179] Figure II.2 displays the crystal structure of 8-bromo-1',3',3'-trimethyl-6-nitrospiro-[chromene-2,2'-indoline].^[180] The axis of the C–Br bond is roughly parallel ($\alpha = 24^\circ$) to the phenyl plane in the indolene side, while the protons of the adjacent methyl groups are 3.7 Å (C–CH₃) and 4.1 Å (N–CH₃) away.^[180] Therefore, the available space was apparently too small for transfer of the relatively bulky phenyl residue.

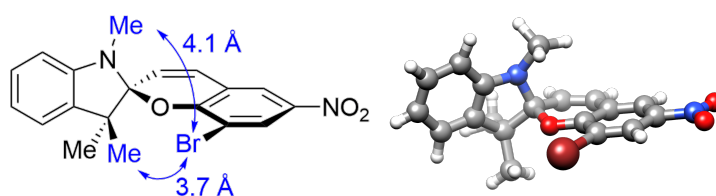


Figure II.2. Crystal structure of 8-bromo-spiropyran.^[180] The distances between the bromine atom and the neighboring protons are highlighted in the structure drawing in blue. Note that the stereochemistry is 2,2'-(*S*) in this example.

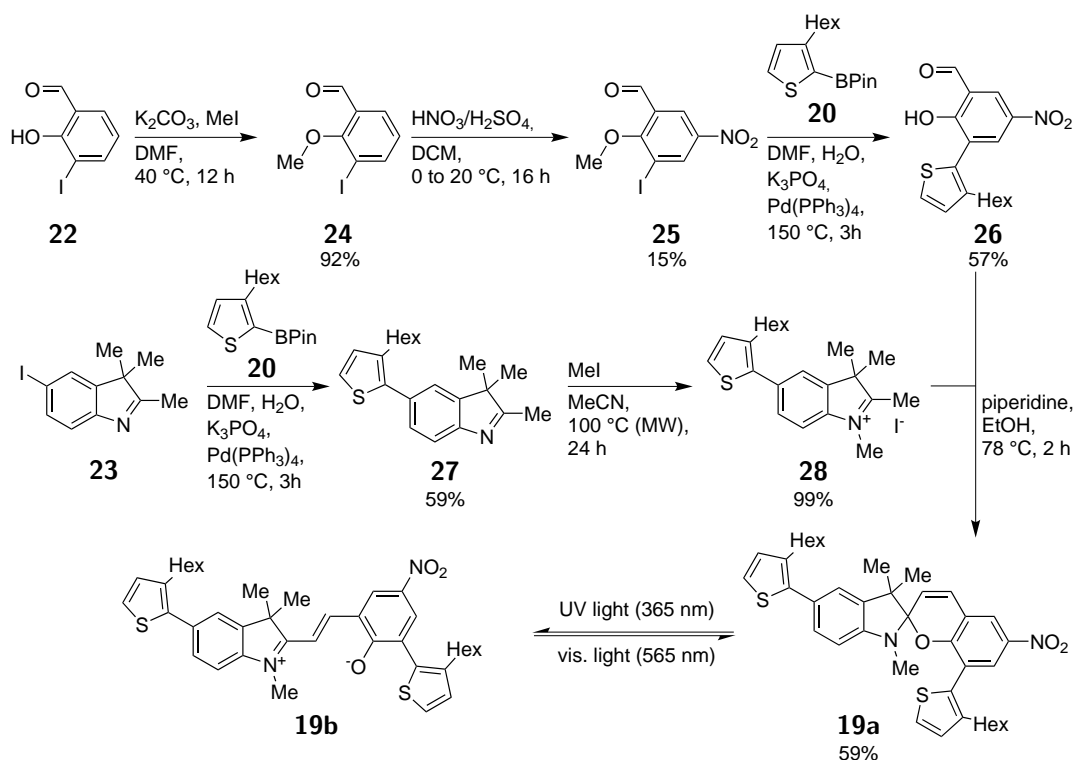
The unexpected results revealed two aspects of the reactivity in the spiropyrans **9a–c** first, the reactivity of the indolene site as electrophile in Stille reactions was too low under the scoped reaction conditions; second, the chromene site proved higher reactivity, however, the steric constrains prevented a transfer of the aryl group. These synthetic obstacles might be resolved by an extensive screening of catalysts, solvents and other parameters. Such an optimization was beyond the scope of this thesis and thus the synthetic strategy of using spiropyrans with halide and pseudohalide functional groups in cross-coupling reactions to obtain the P3HT functionalized spiropyran **7** was not pursued any further.

3.3. Preparation of a Spiropyran Connected to 3-Hexylthiophenes

Since the direct use of spiropyrans in cross-coupling did not lead to promising results, the left retrosynthetic path that was presented in Scheme II.5, page 72, was ruled out. As alternative, the functionalization of spiropyran precursors with aryl groups remained. Thereby, the spiropyran formation would be the final step in the synthesis of **7** according to the right path in Scheme II.5.

3.3.1. Synthetic Route

To explore the possibility to link poly(thiophenes) with boronic esters as end groups to spiropyrans, the first attempt was to connect one thiophene ring to each side of the spiropyran core, resulting in the dithiophenyl-spiropyran **19** (see Scheme II.8). The commercially available 2-boronpinacol-3-hexylthiophene **20** was chosen as representative for polythiophenes since it provides an electron density at the relevant 2-position comparable to the electron density in its polymer equivalent **21**. In the synthetic route of **19**, 3-iodo-2-hydroxybenzaldehyde (**22**) and the 5-iodoindole **23** were used as starting materials.



Scheme II.8 Synthesis of the thiophene-functionalized spiropyran **19**.

The synthesis of the chromene site of **19** started with methylating the hydroxy group in a nucleophilic substitution. Potassium carbonate and iodomethane were used as reagents to obtain 2-iodo-3-methoxybenzaldehyde (**24**) in a yield of 92%. Subsequently, a nitro group was introduced in the 5-position to give 2-iodo-3-methoxy-5-nitrobenzaldehyde (**25**) in 15%,

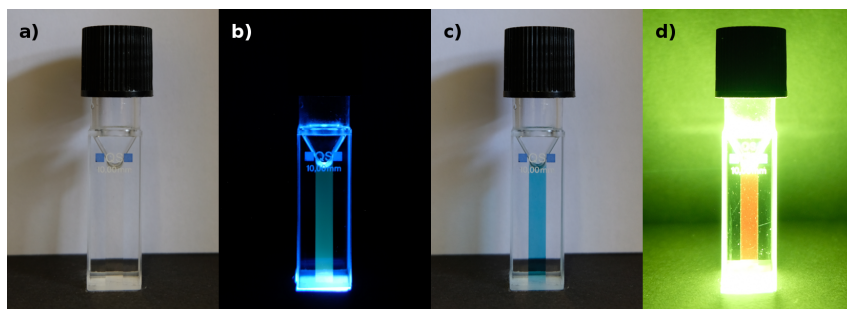


Figure II.3. Photographs of the switching states and fluorescence of the dithiophene-spiropyran **19** in THF (ca. 0.1 mmol/L). **a)** Closed state **19a** without irradiation. **b)** Blue fluorescence during irradiation with UV light (365 nm). **c)** Open state **19b** after UV irradiation. **d)** Orange fluorescence during irradiation with green light (565 nm). © M. Dowds, 2019.

which was then used as electrophile in a Suzuki cross-coupling reaction with the boron functionalized thiophene **20**. The desired spiropyran precursor **26** was obtained in a yield of 57%. Remarkably, no further deprotection reaction was required to transfer the methoxy to a hydroxy group, which is being discussed below.

The indole site of **19** was synthesized via a Suzuki coupling of **23** and **20** to form the 5-thienylindole **27** in a yield of 59%. Subsequently, **27** was methylated with iodomethane in acetonitrile to give the indolium salt **28** in quantitative yield. The two precursors **26** and **28** were then used to synthesize the spiropyran **19** in a piperidine-catalyzed condensation in 59% yield. In initial experiments, the photoswitching of **19** was tested. By irradiation with UV light, the colorless closed spiropyran **19a** was switched to the blue open merocyanine form **19b**. During the irradiation, an intense turquoise fluorescence appeared (See Figure II.3).

3.3.2. Exploration of the Unexpected Methoxy Cleavage by DFT

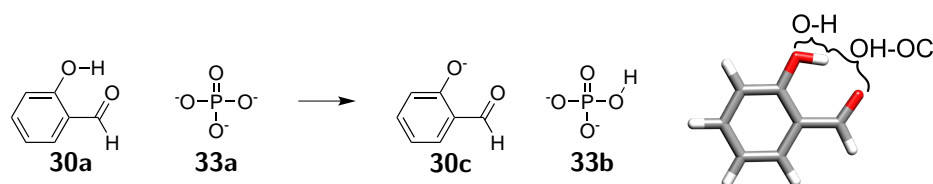
The unexpected cleavage of the methoxy group during the synthesis of **26** was evaluated by DFT calculations. For this purpose, the geometries of five different phenol derivatives **3a**, **29a**, **30a**, **31a**, and **32a** (for structures and results, see Table II.2) and the corresponding anisole derivatives **3b**, **29b**, **30b**, **31b**, and **32b** (for structures and results, see Table II.3) were optimized at the B3LYP/6-311+G* level of theory. Detailed results of the optimizations are presented in Part V, section 5.3.

To estimate the acidity of the phenol groups of **3a**, **29a**, **30a**, **31a**, and **32a**, two geometrical values were chosen for comparison (see Table II.2). The length of the O–H bond was 0.96 Å in phenol (**29a**) and shortened by 0.02 Å, when a formyl substituent was introduced in the *ortho*-position, as in salicylic aldehyde (**30a**). Introducing other substituents in **3a**, **31a**, and **32a** did not decrease the O–H bond any further. In addition, the strength of the potential hydrogen bond between the neighboring hydroxy and formyl groups was estimated by comparing the OH–OC distance (for a visualization, see Table II.2). Compared to salicylic aldehyde (**30a**, 1.82 Å), this distance decreased slightly when a nitro group is introduced *para* to the hydroxy group (1.81 Å in **3a**). Electron donating 2-thienyl substituents *ortho* to the hydroxy group shortened the distance by 0.05 Å in **31a** and 0.04 Å

in **32a**. These findings are in agreement to a literature study, revealing a stabilizing effect of electron withdrawing groups in the 5-position and electron donating groups in the 3-position of 2-hydroxybenzaldehyde derivatives.^[181] It is well-established that thiophene rings act as electron donating groups in respect to benzene rings.^[182] The slight increase of the OH–OC distance in **32a** compared to **31a** result from the methyl substituent at the thiophene’s 3-position in **32a**. The optimized structure **32a** shows a larger twist between the thiophene and benzene planes (46.1°) than the structure of **31a** (27.1°). Thus, the electron conjugation in **32a** is compromised compared to **31a**.

Table II.2. Geometrical properties of phenol derivatives and reaction energy of the deprotonation with phosphate as base.

The starting materials **3a**, **29a**, **30a**, **31a**, and **32a** and phosphate (**33a**), as well as the products **3c**, **29c**, **30c**, **31c**, and **32c** and hydrogen phosphate (**33b**) were optimized by DFT (B3LYP/6-311+G* level of theory). The reaction energies ΔE_{rct} of the proton transfer from the phenols **3a**, **29a**, **30a**, **31a**, and **32a** to phosphate (**33a**) were derived. **Top:** Exemplary reaction of 2-hydroxybenzaldehyde (**30a**) and phosphate (**33a**) to give 2-formylphenolate (**30c**) and hydrogen phosphate (**33b**). The calculated O–H bond length and OH–OC distance are visualized in the optimized structure of **30a**. **Bottom:** Listed results.

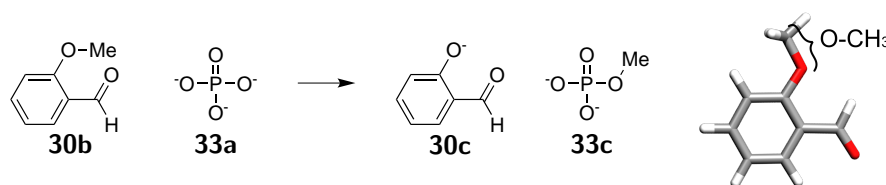


Entry No.	Starting Material	Distance		ΔE_{rct} / kcal mol ⁻¹
		O–H / Å	OH–OC / Å	
1		29a 0.96	–	-230.5
2		30a 0.98	1.82	-232.8
3		3a 0.98	1.81	-254.1
4		31a 0.98	1.77	-259.1
5		32a 0.98	1.78	-257.2

Analysis of the structures of the anisoles **3b**, **29b**, **30b**, **31b**, and **32b** showed a similar trend (see Table II.3). In the reference anisole (**29b**), the O–C bond of the methoxy group had a length of 1.42 Å. While introducing the formyl group of **30b** did not alter this distance, the electron withdrawing nitro group at the 4-position in **3b** elongated the O–C bond by 0.01 Å. The electron donating thieryl substituents of **31b** and **32b** stretched the O–C bond by another 0.01 Å. Here, no influence of the methyl substituent in the thiophene's 3-position of **32b** was observed.

Table II.3. Geometrical properties of anisole derivatives and reaction energy of the cleavage of the methoxy group with phosphate as base.

The starting materials **3b**, **29b**, **30b**, **31b**, and **32b** and phosphate (**33a**), as well as the products **3c**, **29c**, **30c**, **31c**, and **32c** and methyl phosphate (**33c**) were optimized by DFT (B3LYP/6-311+G* level of theory). The reaction energies ΔE_{rct} of the methylum transfer from the anisoles **3b**, **29b**, **30b**, **31b**, and **32b** to phosphate (**33a**) were derived. **Top:** Exemplary reaction of 2-methoxybenzaldehyde (**30b**) and phosphate (**33a**) to give 2-formylphenolate (**30c**) and methyl phosphate (**33c**). The calculated O–C bond length is visualized in the optimized structure of **30b**. **Bottom:** Listed results.



Entry No.	Starting Material	Distance O–CH ₃ / Å	ΔE_{rct} / kcal mol ⁻¹
1		29b 1.42	-232.4
2		30b 1.42	-242.1
3		3b 1.43	-263.5
4		31b 1.44	-270.7
5		32b 1.44	-268.2

Although the analysis of the geometrical properties of the optimized structures indicated a weakening of the O–C bond in the methoxy group of 2-methoxy-5-nitro-3-(thien-2-yl)-benzaldehyde (**31b**) compared to anisole (**29b**), the observed differences were too small to draw definite conclusions. Therefore, the energetical aspects of the deprotonation and demethylation reactions were calculated. In addition to the phenol **3a**, **29a**, **30a**, **31a**, and **32a** and anisole **3b**, **29b**, **30b**, **31b**, and **32b** derivatives, the corresponding phenolate ions **3c**, **29c**, **30c**, **31c**, and **32c** were optimized by DFT. Since the reaction mixture contained potassium phosphate as base, the phosphate anion (**33a**) was chosen to act as proton or methyl group acceptor. Phosphate and the resulting products hydrogen phosphate (**33b**) and methyl phosphate (**33c**) were also optimized by DFT.

To calculate the energy of the reactions, the sums of the zero-point energy corrected electron energies (E_{ZPE}) of the starting materials (E_{start}) and the products (E_{prod}) were formed. For the deprotonation reaction, E_{ZPE} of the phenols **3a**, **29a**, **30a**, **31a**, and **32a**, and E_{ZPE} of the phosphate anion (**33a**) were taken into account to calculate E_{start} (Equation II.1, left). The energy of the products E_{prod} was calculated using E_{ZPE} of the phenolate ions **3c**, **29c**, **30c**, **31c**, and **32c** and hydrogen phosphate (**33b**, see Equation II.2). Simultaneously, the E_{ZPE} of the anisoles **3b**, **29b**, **30b**, **31b**, and **32b** and methyl phosphate (**33c**) were used to calculate E_{start} (Equation II.3) and E_{prod} for the transfer of the methyl group (Equation II.4).

Phenols :

$$E_{start} = E_{ZPE} (ROH) + E_{ZPE} (PO_4^{3-}) \quad (II.1)$$

$$E_{prod} = E_{ZPE} (RO^-) + E_{ZPE} (HPO_4^{2-}) \quad (II.2)$$

Anisoles :

$$E_{start} = E_{ZPE} (ROMe) + E_{ZPE} (PO_4^{3-}) \quad (II.3)$$

$$E_{prod} = E_{ZPE} (RO^-) + E_{ZPE} (MePO_4^{2-}) \quad (II.4)$$

With the energies E_{start} and E_{prod} , it was possible to calculate the energy ΔE_{rct} of the reactions by subtracting E_{start} from E_{prod} (see Equation II.5). Negative values of ΔE_{rct} express an energy benefit of the products compared to the starting materials. Therefore, increased labilities of the O–H or O–Me bonds and stabilization of the phenolate ions would result in decreased values of ΔE_{rct} . Detailed values for E_{ZPE} of the starting materials and the products are shown in Table V.10, Part V, section 5.3 (Page 292).

$$\Delta E_{rct} = E_{prod} - E_{start} \quad (II.5)$$

Comparison of the obtained reaction energies ΔE_{rct} confirmed the assumptions made from the geometrical analysis. Since phenol (**29a**) is a stronger acid ($pK_a = 9.98$) than hydrogen phosphate (**33b**, $pK_a = 12.26$), the products phenolate (**29c**) and **33b** should be energetically favored compared to the starting materials **29a** and phosphate (**33a**).

Indeed, a ΔE_{rct} of $-230.5 \text{ kcal mol}^{-1}$ was found for the deprotonation of **29a** (Table II.2, Entry 1). When comparing the different phenol derivatives, changes of ΔE_{rct} should only result from the substituents of the phenol/phenolate pair. As expected from the structural analysis, the *ortho*-formyl substituent of salicylic aldehyde (**30a**) stabilized the product slightly by $2.3 \text{ kcal mol}^{-1}$ (Table II.2, Entry 2). The nitro group *para* to the hydroxy group drastically stabilized the phenolate **3c** by additional $21.3 \text{ kcal mol}^{-1}$ (Table II.2, Entry 3). This large effect was not expected after the structural analysis. However, the thiophene substituent of **31** lead to further stabilization of the products by $5.0 \text{ kcal mol}^{-1}$ to $\Delta E_{\text{rct}} = -259.1 \text{ kcal mol}^{-1}$ (Table II.2, Entry 4). The sterical hindrance caused by the methyl group at the thiophene's 3-position in **32** also effected ΔE_{rct} , which was raised by $1.9 \text{ kcal mol}^{-1}$ (Table II.2, Entry 5). The calculated ΔE_{rct} for the anisole/phenolate pairs **34**, **35**, **36**, **37**, and **38** with phosphate (**33a**) and methyl phosphate (**33c**) as counterpart showed the same trend. Remarkably, the formation of 2-formylphenolate (**30c**) from 2-methoxybenzaldehyde (**30b**) is stabilized by $9.7 \text{ kcal mol}^{-1}$ compared to the anisole/phenolate pair **29b,c** (Table II.3, Entry 2). The other variations of the substituents induced the same stability effects as described for the deprotonation. The largest stabilization was found for the thienyl-substituted anisole/phenolate pair **31b** and **39** with $\Delta E_{\text{rct}} = -270.7 \text{ kcal mol}^{-1}$.

In conclusion, the hydroxy group is stabilized intramolecular hydrogen bonding to the neighboring oxygen of the aldehyde. This effect accounts for the difference of approximately 10 kcal mol^{-1} between the 2-hydroxybenzaldehyde/phenolate pairs **3a,c**, **30a,c**, **31a,c**, and **32a,c** and the methoxy counterparts **3b,c**, **30b,c**, **31b,c**, and **32b,c**. The introduction of an electron withdrawing nitro group *para* to the hydroxy or methoxy groups and electron donating thiophene groups, however, wielded larger influence on the acidity of the hydroxy groups and lability of the methoxy groups. Variation of the thienyl substituent revealed a sterical effect, sterically demanding substituents at the thiophene's 3-position lead to a twist and reduced the described electronic effect. Since the results were obtained in gas-phase calculations, the obtained values cannot be transferred directly to the solution. Nevertheless, the results show a clear trend and suggest that the methoxy group of **26** was destabilized due to the described effects. In the synthesis of **26**, an aqueous solution of potassium phosphate (1 mol/L) was mixed with *N,N*-dimethylformamide (DMF) (70/30, v/v) and used as solvent system. The highly polar environment should stabilize the phenolates to a larger extend than unpolar solvents.

3.3.3. Characterization of Photochemical Properties

The photoswitching properties of **19** were investigated by UV-vis and fluorescence spectroscopy. Initially, a stock solution of **19** in THF with a concentration of $100 \mu\text{mol/L}$ was prepared and diluted to prepare sample solutions with concentrations ranging from $10 \mu\text{mol/L}$ to $100 \mu\text{mol/L}$. With these solutions, the validity of the Beer-Lambert-law was tested and a mid-level concentration of $50 \mu\text{mol/L}$ was used to determine the thermal relaxation. The freshly dissolved solution of **19** showed no significant absorption band of the MC species **19b**.

Irradiation with UV light (365 nm) gave rise to a broad absorption with a peak wavelength of 610 nm in the photostationary state (PSS)-365. Upon irradiation with green light (565 nm), the majority of **19b** was switched back to the SP form **19a**. However, ca. 10% of the absorption remained.

Initial experiments suggested a relatively fast thermal decay of the merocyanine **19b**; thus, the spectral range was narrowed to the merocyanine absorption from 500 nm to 750 nm to ensure quick and reliable measurements. Applying a first-order exponential fit derived the half-life time to be 28.0 ± 0.1 s. For testing the stability during cyclic switching, the MC absorption at 610 nm of a solution of **19** was recorded after alternating irradiation with UV or green light for 30 s each. The absorption of **19b** remained almost constant for three UV irradiation cycles before decreasing linearly. After merely eight full irradiation cycles, no significant amount of MC absorption was detectable. The photodegradation was also investigated by ^1H NMR spectroscopy. After 50 min of irradiation with UV light (365 nm), no signals corresponding to the ethylene bridge in either the (*Z*) or (*E*)-configuration were found. Instead, a broadening of the signals in the aromatic region suggested the formation of various photoproducts or polymers (see Part V, subsection 5.4.7, page 317).

Since merocyanines are known to exhibit a red fluorescence upon excitation with green light, the influence of the thiophene groups to this fluorescence was investigated. The expected fluorescence band was detected with a maximum at 615 nm upon excitation of **19b** with 565 nm. In addition, a light blue fluorescence with two maxima at 433 nm and 461 nm was found upon excitation of **19a** with 365 nm.

The combination of these effects, short half-life time, strong photodegradation and additional fluorescence bands suggests a strong electronic influence of the thiophene units on the SP/MC core. Typically, an electron deficient chromene site stabilizes the MC form, leading to slower thermal relaxation to the SP form and an equilibrium between SP and MC (compare section 3.1 and Part V, section 3.1).

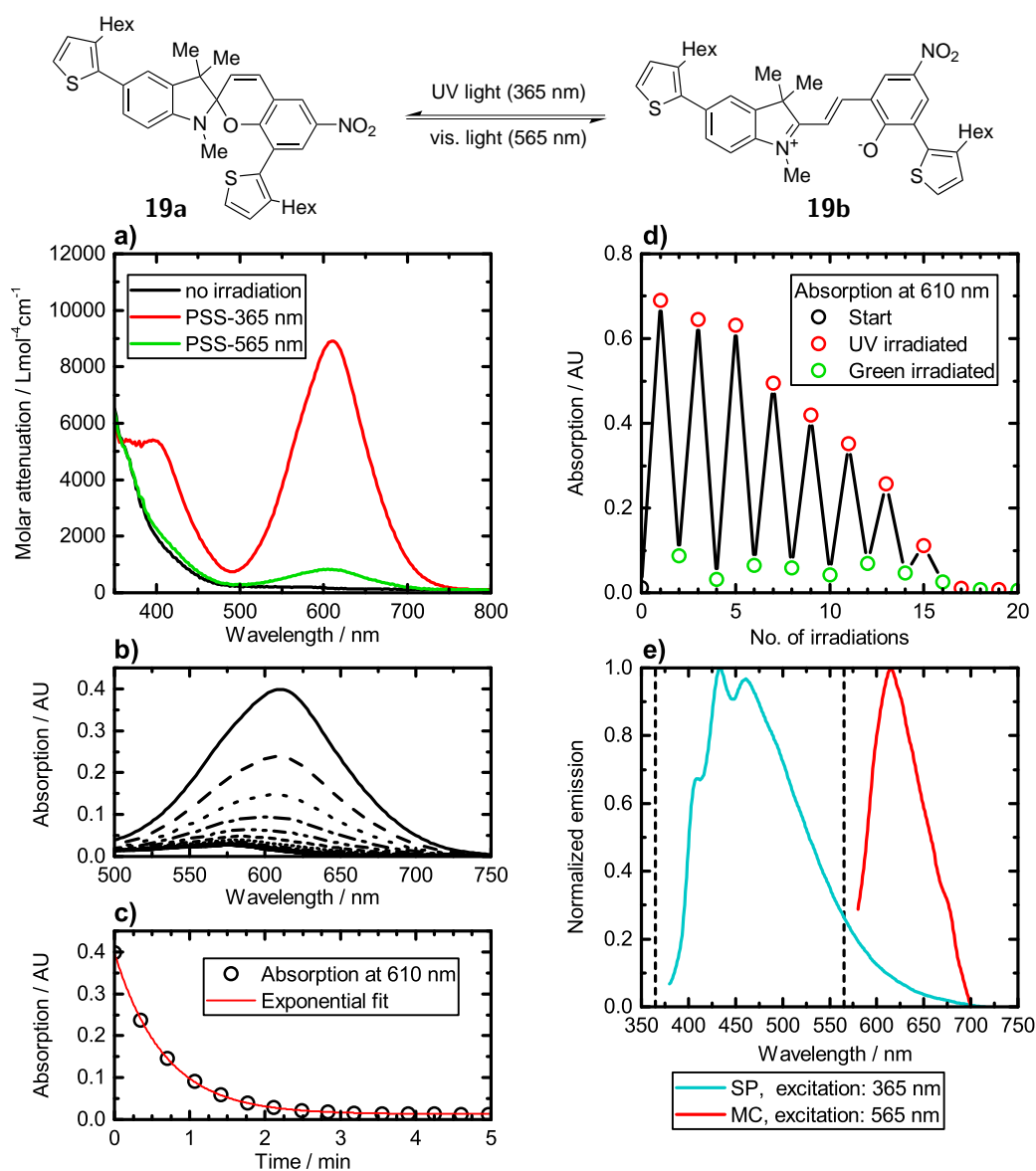


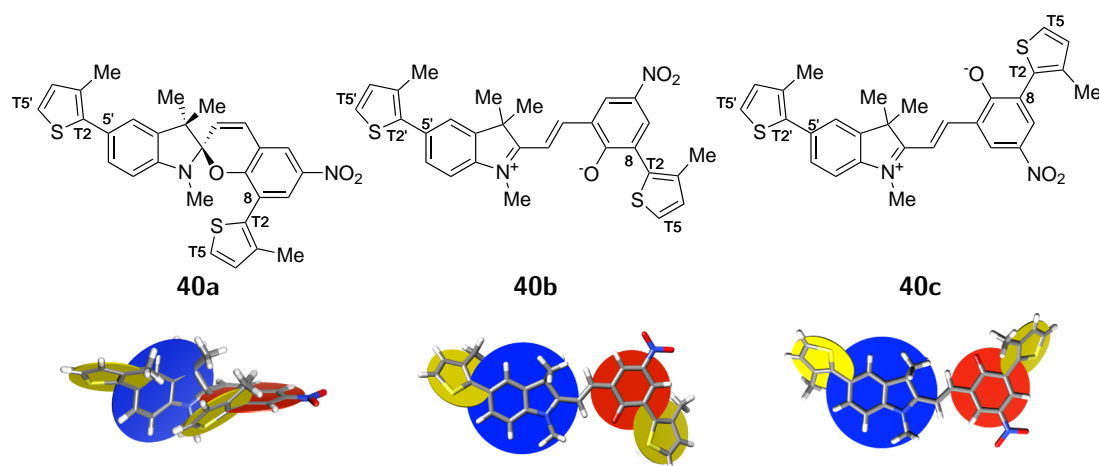
Figure II.4. Absorption and emission characteristics of the dithiophene substituted spiropyran **19a** and the corresponding merocyanine **19b**. **a)** Absorption spectrum of a solution of **19** in THF (ca. 30 $\mu\text{mol/L}$) directly after dissolving (black curve), after irradiation with UV light (365 nm, red curve) and after irradiation with green light (565 nm, green curve). **b)** Spectral changes in the merocyanine region during thermal relaxation (50 $\mu\text{mol/L}$). The spectra were recorded with an interval of 20 s. **c)** Decay of the merocyanine absorption (610 nm, black circles). An exponential fit (red line) determined the half-life time to be 28.0 ± 0.1 s. **d)** Repetitive switching of **19** (100 $\mu\text{mol/L}$) with UV (red circles) and green light (green circles) for 30 s. **e)** Emission spectrum of **19**. The normalized emission of **19a** after excitation with 365 nm is shown in turquoise and the normalized emission of **19b** is shown in red. The excitation wavelengths are depicted as dash lines.

3.3.4. DFT Modelling of the Electronic Properties

For a thorough evaluation of the observed behavior of **19**, the model compound **40** was chosen for optimization by DFT modeling at the B3LYP/6-311G* level of theory. Herein, the alkyl groups at the thiophenes were shortened from hexyl to methyl. Thereby, the calculation time is reduced while the electronic effect of the substituents remains comparable. The structures of the SP form **40a** and the two MC forms **40b** and **40c** were optimized. For evaluating the conjugation between the thiophenes and adjacent aromatic rings, four geometrical parameters were determined: the two C–C bond lengths between the thiophene and neighboring aromatic rings and the angles between the corresponding planes. The angle between the planes of the indole and chromene site of the molecule was determined to evaluate the planarity and thus the conjugation throughout the whole molecule.

Table II.4. DFT optimized structures of **40a**, **40b**, and **40c** and selected geometrical parameters and physical properties of the three isomers of **40** obtained by DFT optimization.

Top: chemical structures of the SP isomer **40a**, the (*Z*)-MC isomer **40b** and the (*E*)-MC isomer **40c**. The carbon atoms that were used for the distance measurement (results in Table II.4) are labeled. **Middle:** the corresponding optimized structures. Highlighted are the planes of the thiophene rings (yellow), the indole unit (blue) and the chromene unit (red). **Bottom:** Comprised geometrical parameters. With ϕ_{I-T} , the angle between the indole (blue) and neighboring thiophene (yellow) planes; ϕ_{C-T} , the angle between chromene (red) and neighboring thiophene (yellow) planes; ϕ_{I-C} , the angle between indole (blue) and chromene (red) planes; and ΔE_{H-L} , the energy gap between HOMO and LUMO levels.



Compound	$d_{5'-T2'}$	ϕ_{I-T}	d_{8-T2}	ϕ_{C-T}	ϕ_{I-C}	$d_{8-5'}$	$d_{T5-T5'}$	ΔE_{H-L}
SP 40a	1.41 Å	47.4°	1.47 Å	43.2°	73.8°	6.35 Å	6.85 Å	3.77 eV
(<i>Z</i>)-MC 40b	1.47 Å	44.6°	1.46 Å	32.6°	3.6°	10.61 Å	16.95 Å	2.40 eV
(<i>E</i>)-MC 40c	1.47 Å	44.6°	1.47 Å	49.7°	0.6°	10.63 Å	16.31 Å	2.31 eV

The C–C bond length $d_{5'-T2'}$ between thiophene and the indole unit in the spiropyran form **40a** is the shortest with 1.41 Å. This is significantly shorter compared to the typical inter-ring distance in sexithiophene of 1.44 Å.^[66] All other C–C bonds between thiophene and the adjacent aromatic rings range from 1.46 Å to 1.47 Å. The twist angles ϕ_{I-T} between the indole and neighboring thiophene rings is similar for all three isomers in the range of

44.6° to 47.4°. For the spiropyran form **40a** and the merocyanine isomer **40c**, the twist angles ϕ_{C-T} between the chromene and thiophene planes show comparable values of 43.2° and 49.7°. In contrast, the chromene and thiophene planes in **40b** are twisted only by 32.6°. While the indole and chromene planes in the closed form **40a** are twisted by 73.8°, they are almost parallel in the open isomers **40b** and **40c** (3.6° and 0.6°, respectively).

These parameters indicate a relatively low conjugation of electrons throughout thiophenes and the adjacent indole and chromene rings compared to oligo- and polythiophenes.^[65] During the excitation and photoinduced switching of spiropyran, two electron transitions are dominant, the transition from the HOMO to the LUMO and the transition from the HOMO-1 to the LUMO.^[183] In the system **40a**, the HOMO is located solely on the indole site, whereas the three other frontier orbitals (HOMO-1, LUMO, LUMO+1) are located solely on the chromene site of the molecule (for visualization of frontier orbitals and energy values, see Part V, subsection 5.2.1). The derived HOMO-LUMO gap of 3.77 eV is larger than the value of 3.03 eV, which was calculated for a nitro-spiropyran without thiophene substituents **1**.^[24] An efficient electron transition from occupied to unoccupied orbitals requires a sufficient geometrical overlap of the involved orbitals.^[184] Therefore, the HOMO-1 and the LUMO orbitals were taken into account. However, despite the localization on opposed sites of the spiro center, both highest occupied molecular orbitals spread throughout the spiropyran scaffold and the adjacent thiophene rings.

The HOMO-LUMO gap in the merocyanine isomers **40b** and **40c** is 0.74 eV and 0.83 eV smaller than the gap in the closed form **40a**. For the basic spiropyran **1**, a decrease of the energy gap of only 0.37 eV was found.^[24] In both merocyanine isomers, the LUMO orbitals are localized on the merocyanine scaffold, whereas the HOMO orbitals were localized mostly on the chromene site and the neighboring thiophene ring. The indole ring and the neighboring thiophene ring bore smaller electron densities in the HOMO level. Interestingly, the HOMO-1 level spreaded throughout the complete structure in both geometries **40b** and **40c**.

For a potential mechanoinduced switching of the polymer **7**, the geometrical changes must be taken into account. To evaluate the geometrical change, two distances were determined for the optimized structures of **40a-c**. The carbon atoms that bear the substituents at the 8- and 5'-position are 6.85 Å apart in the closed form **40a** ($d_{8-5'}$, Table II.4). This distance is almost exactly the same in both open geometries **40b** and **40c** with 10.61 Å and 10.63 Å, respectively. In **40a**, the two thiophene rings point towards a similar direction – namely roughly along the C-C bond between position 5' and the neighboring thiophene. Thus, the distance between the outermost carbon atoms at the 5-positions of both thiophenes ($d_{T5-T5'}$, Table II.4) is only 0.5 Å longer. In contrast, the thiophene rings of the open isomers **40b** and **40c** point towards opposite sites of the molecule. The thiophene units in the (*Z*)-isomer **40b** are oriented in almost antiparallel directions, maximizing the distance $d_{T5-T5'}$ to be 16.95 Å. This distance is shortened to 16.31 Å in the (*E*)-isomer **40c**. Here, both thiophene rings are located on one half of the molecule, directing away from the indole nitrogen.

3.3.5. Conclusion

The synthesis of the mono-hexylthiophene spiropyran **19** proved to be reliable and versatile. The crucial Suzuki cross-coupling reactions to form the precursors **26** and **27** should be transferable to the coupling of iodo indoles and benzaldehydes (**23** and **25**) with boron functionalized P3HT **21**. A large influence of the thiophenes on the spiropyran's switching properties was indicated by UV-vis spectroscopy. This influence resulted in blue fluorescence, which is atypical for spiropyrans, indicating one or more conjugated π systems that cover the thiophenes and adjacent phenyl rings. DFT optimizations confirmed an electron conjugation between thiophenes and the adjacent aromatic systems in the SP form **40a**. In the open forms **40b** and **40c**, the conjugation was found to be distributed throughout the complete molecule, opposed to the closed form, where the sp^3 hybridization of the central carbon atom prevents this conjugation. Thus, the HOMO–LUMO gap decreased upon ring opening. Upon ring opening, the molecule elongates significantly. The distance between the 8- and 5'-positions increased by approximately 4.3 Å from the closed form **40a** to both open forms **40b** and **40c**. For the distance between the outer carbon atoms at the thiophenes' 5-positions, a significant difference between **40b** and **40c**. In the (*Z*)-isomer **40b**, these positions are almost 0.65 Å further apart than in the (*E*)-isomer **40c**. This corresponds to an elongation by 10.6 Å in respect to the closed isomer **40a**.

Recapitulating, the described findings make the polymer-functionalized spiropyran **7** a promising candidate for the further development of photoswitchable organic conductors. The large geometrical changes suggest a potential mechanoactivation of the switching. While the calculated band gap is slightly smaller in the (*E*)-merocyanine **40c**, mechanical actuation will probably yield the (*Z*)-merocyanine **40b** as predominant product. When attaching poly(thiophene), the resulting polymer will probably have an increased conductivity after switching the spiropyran to merocyanine.

Bibliography of Part II

- [12] R. Klajn, *Chem. Soc. Rev.* **2014**, *43*, 148–184.
- [14] M. Li, Q. Zhang, Y.-N. Zhou, S. Zhu, *Prog. Polym. Sci.* **2018**, *79*, 26–39.
- [21] M. M. Caruso, D. A. Davis, Q. Shen, S. A. Odom, N. R. Sottos, S. R. White, J. S. Moore, *Chem. Rev.* **2009**, *109*, 5755–5798.
- [23] J. N. Brantley, K. M. Wiggins, C. W. Bielawski, *Polym. Int.* **2013**, *62*, 2–12.
- [24] Y. Li, H. Zhang, C. Qi, X. Guo, *J. Mater. Chem.* **2012**, *22*, 4261.
- [29] D. A. Davis, A. Hamilton, J. Yang, L. D. Cremar, D. Van Gough, S. L. Potisek, M. T. Ong, P. V. Braun, T. J. Martínez, S. R. White, J. S. Moore, N. R. Sottos, *Nature* **2009**, *459*, 68–72.
- [65] S. S. Zade, M. Bendikov, *Chem. - Eur. J.* **2007**, *13*, 3688–3700.
- [66] G. Horowitz, B. Bachet, A. Yassar, P. Lang, F. Demanze, J.-L. Fave, F. Garnier, *Chem. Mater.* **1995**, *7*, 1337–1341.
- [79] R. H. Lohwasser, M. Thelakkat, *Macromolecules* **2011**, *44*, 3388–3397.
- [117] V. I. Minkin, *Chem. Rev.* **2004**, *104*, 2751–2776.
- [118] B. S. Lukyanov, M. B. Lukyanova, *Chem. Heterocycl. Compd.* **2005**, 281–311.
- [119] L. Kortekaas, W. R. Browne, *Chem. Soc. Rev.* **2019**, *48*, 3406–3424.
- [120] S.-R. Keum, S.-M. Ahn, S.-J. Roh, S.-J. Park, S.-H. Kim, K. Koh, *Magn. Reson. Chem.* **2006**, *44*, 90–94.
- [121] S.-R. Keum, B.-S. Ku, M.-H. Lee, G.-Y. Chi, S.-S. Lim, *Dyes Pigment.* **2009**, *80*, 26–29.
- [122] G. P. Moss, *Pure Appl. Chem.* **1998**, *70*, 143–216.
- [123] M. Levitus, G. Glasser, D. Neher, P. F. Aramendía, *Chem. Phys. Lett.* **1997**, *277*, 118–124.
- [124] M. Bletz, U. Pfeifer-Fukumura, U. Kolb, W. Baumann, *J. Phys. Chem. A* **2002**, *106*, 2232–2236.
- [125] Q. Shen, L. Wang, S. Liu, Y. Cao, L. Gan, X. Guo, M. L. Steigerwald, Z. Shuai, Z. Liu, C. Nuckolls, *Adv. Mater.* **2010**, *22*, 3282–3287.
- [126] I. Panaiotov, S. Taneva, A. Bois, F. Rondelez, *Macromolecules* **1991**, *24*, 4250–4254.
- [127] J. Chen, F. Zeng, S. Wu, *ChemPhysChem* **2010**, *11*, 1036–1043.
- [128] P. Howlader, B. Mondal, P. C. Purba, E. Zangrando, P. S. Mukherjee, *J. Am. Chem. Soc.* **2018**, *140*, 7952–7960.

- [129] M. E. Genovese, E. Colusso, M. Colombo, A. Martucci, A. Athanassiou, D. Fragouli, *J. Mater. Chem. A* **2017**, *5*, 339–348.
- [130] C. Lenoble, R. S. Becker, *J. Phys. Chem.* **1986**, *90*, 62–65.
- [131] N. P. Ernsting, T. Arthen-Engeland, *J. Phys. Chem.* **1991**, *95*, 5502–5509.
- [132] H. Görner, *Phys. Chem. Chem. Phys.* **2001**, *3*, 416–423.
- [133] A. K. Chibisov, H. Görner, *Phys. Chem. Chem. Phys.* **2001**, *3*, 424–431.
- [134] J. Hoble, M. J. Lear, H. Fukumura in *Photochemistry of Organic Molecules in Isotropic and Anisotropic Media*, (Eds.: V. Ramamurthy, K. S. Schanze), Molecular and Supramolecular Photochemistry, Marcel Dekker, Basel, **2003**, pp. 353–367.
- [135] J. Buback, M. Kullmann, F. Langhojer, P. Nuernberger, R. Schmidt, F. Würthner, T. Brixner, *J. Am. Chem. Soc.* **2010**, *132*, 16510–16519.
- [136] J. Hoble, V. Malatesta, R. Millini, L. Montanari, W. O Neil Parker, Jr, *Phys. Chem. Chem. Phys.* **1999**, *1*, 3259–3267.
- [137] R. D. Amos, R. Kobayashi, *Mol. Phys.* **2015**, *113*, 1674–1681.
- [138] N. P. Ernsting, *Chem. Phys. Lett.* **1989**, *159*, 526–531.
- [139] S. A. Krysanov, M. V. Alfimov, **1982**, *91*, 4.
- [140] S. Swansburg, E. Buncel, R. P. Lemieux, *J. Am. Chem. Soc.* **2000**, *122*, 6594–6600.
- [141] C. J. Wohl, D. Kuciauskas, *J. Phys. Chem. B* **2005**, *109*, 22186–22191.
- [142] G. Balasubramanian, J. Schulte, F. Müller-Plathe, M. C. Böhm, *Chem. Phys. Lett.* **2012**, *554*, 60–66.
- [143] J. Hoble, V. Malatesta, *Phys. Chem. Chem. Phys.* **2000**, *2*, 57–59.
- [144] J. Hoble, U. Pfeifer-Fukumura, M. Bletz, T. Asahi, H. Masuhara, H. Fukumura, *J. Phys. Chem. A* **2002**, *106*, 2265–2270.
- [145] D. Kim, Z. Zhang, K. Xu, *J. Am. Chem. Soc.* **2017**, *139*, 9447–9450.
- [146] N. A. Murugan, S. Chakrabarti, H. Ågren, *J. Phys. Chem. B* **2011**, *115*, 4025–4032.
- [147] J. Buback, P. Nuernberger, M. Kullmann, F. Langhojer, R. Schmidt, F. Würthner, T. Brixner, *J. Phys. Chem. A* **2011**, *115*, 3924–3935.
- [148] S. Ruetzel, M. Diekmann, P. Nuernberger, C. Walter, B. Engels, T. Brixner, *J. Chem. Phys.* **2014**, *140*, 224310.
- [149] J. Whelan, D. Abdallah, J. Wojtyk, E. Buncel, *J. Mater. Chem.* **2010**, *20*, 5727–5735.
- [150] J. Harada, Y. Kawazoe, K. Ogawa, *Chem. Commun.* **2010**, *46*, 2593.
- [151] C. Menet, H. Serier-Braut, O. Oms, A. Dolbecq, J. Marrot, A. Saad, P. Mialane, S. Jobic, P. Deniard, R. Dessapt, *RSC Adv.* **2015**, *5*, 79635–79643.
- [152] D. E. Williams, C. R. Martin, E. A. Dolgoplova, A. Swifton, D. C. Godfrey, O. A. Ejegbavwo, P. J. Pellechia, M. D. Smith, N. B. Shustova, *J. Am. Chem. Soc.* **2018**, *140*, 7611–7622.

- [153] D. Samanta, D. Galaktionova, J. Gemen, L. J. W. Shimon, Y. Diskin-Posner, L. Avram, P. Král, R. Klajn, *Nat. Commun.* **2018**, *9*, 641.
- [154] J. T. C. Wojtyk, P. M. Kazmaier, E. Buncel, *Chem. Mater.* **2001**, *13*, 2547–2551.
- [155] S. V. Paramonov, V. Lokshin, O. A. Fedorova, *J. Photochem. Photobiol. C* **2011**, *12*, 209–236.
- [156] K. Kinashi, Y. Harada, Y. Ueda, *Thin Solid Films* **2008**, *516*, 2532–2536.
- [157] K. Kinashi, S. Nakamura, M. Imamura, K. Ishida, Y. Ueda, *J. Phys. Org. Chem.* **2012**, *25*, 462–466.
- [158] L. Kortekaas, J. Chen, D. Jacquemin, W. R. Browne, *J. Phys. Chem. B* **2018**, *122*, 6423–6430.
- [159] T. El-Sayed, A. Aboelnaga, M. A. El-Atawy, M. Hagar, *Molecules* **2018**, *23*, 1348.
- [160] J. L. Howard, Q. Cao, D. L. Browne, *Chem. Sci.* **2018**, *9*, 3080–3094.
- [161] C. Bolm, J. G. Hernández, *Angew. Chem. Int. Ed.* **2019**, *58*, 3285–3299.
- [162] T. G. McKenzie, F. Karimi, M. Ashokkumar, G. G. Qiao, *Chem. - Eur. J.* **2019**, *25*, 5372–5388.
- [163] P. A. May, N. F. Munaretto, M. B. Hamoy, M. J. Robb, J. S. Moore, *ACS Macro Lett.* **2016**, *5*, 177–180.
- [164] M. Schaefer, B. Icli, C. Weder, M. Lattuada, A. F. M. Kilbinger, Y. C. Simon, *Macromolecules* **2016**, *49*, 1630–1636.
- [165] L. Florea, D. Diamond, F. Benito-Lopez, *Macromol. Mater. Eng.* **2012**, *297*, 1148–1159.
- [166] M. Larkowska, M. Wuebbenhorst, S. Kucharski, *Int. J. Polym. Sci.* **2011**, *2011*, 1–6.
- [167] S. Shree, M. Schulz-Senft, N. H. Alsleben, Y. K. Mishra, A. Staubitz, R. Adelung, *ACS Appl. Mater. Interfaces* **2017**, *9*, 38000–38007.
- [168] S. Shree, M. Dowds, A. Kuntze, Y. K. Mishra, A. Staubitz, R. Adelung, *Mater. Horiz.* **2020**, *10*.1039.C9MH01400D.
- [169] M. Sommer, H. Komber, *Macromol. Rapid Commun.* **2013**, *34*, 57–62.
- [170] H. Komber, S. Müllers, F. Lombeck, A. Held, M. Walter, M. Sommer, *Polym. Chem.* **2014**, *5*, 443.
- [171] L. Metzler, T. Reichenbach, O. Brügger, H. Komber, F. Lombeck, S. Müllers, R. Hanselmann, H. Hillebrecht, M. Walter, M. Sommer, *Polym. Chem.* **2015**, *6*, 3694–3707.
- [172] S. B. Schmidt, F. Kempe, O. Brügger, M. Walter, M. Sommer, *Polymer Chemistry* **2017**, *8*, 5407–5414.
- [173] P. Bauer, M. Sommer, J. Thurn, M. Pärs, J. Köhler, M. Thelakkat, *Chem. Commun.* **2013**, *49*, 4637–4639.

- [174] M. Schulz-Senft, P. J. Gates, F. D. Sönnichsen, A. Staubitz, *Dyes Pigm.* **2017**, *136*, 292–301.
- [175] M. Schulz, Diploma Thesis, Christian-Albrechts-Universität, Kiel, **2012**.
- [176] G. Espino, A. Kurbangalieva, J. M. Brown, *Chem. Commun.* **2007**, 1742.
- [177] C. Cordovilla, C. Bartolomé, J. M. Martínez-Ilarduya, P. Espinet, *ACS Catal.* **2015**, *5*, 3040–3053.
- [178] M. Yurtsever, B. Ustamehmetoglu, A. S. Sarac, A. Mannschreck, *Int. J. Quantum Chem.* **1999**, *75*, 111–117.
- [179] V. Farina, V. Krishnamurthy, W. J. Scott in *Organic Reactions, Vol. 50*, John Wiley & Sons, Inc., **2004**, pp. 1–93.
- [180] S. M. Aldoshin, L. O. Atovmyan, O. A. D'yachenko, M. A. Gal'bershtam, *Izv. Akad. Nauk SSSR Ser. Khim.* **1981**, 2720–2729.
- [181] G. Pareras, M. Palusiak, M. Duran, M. Solà, S. Simon, *J. Phys. Chem. A* **2018**, *122*, 2279–2287.
- [182] T. Yamamoto, Z.-h. Zhou, T. Kanbara, M. Shimura, K. Kizu, T. Maruyama, Y. Nakamura, T. Fukuda, B.-L. Lee, N. Ooba, S. Tomaru, T. Kurihara, T. Kaino, K. Kubota, S. Sasaki, *J. Am. Chem. Soc.* **1996**, *118*, 10389–10399.
- [183] S. Prager, I. Burghardt, A. Dreuw, *J. Phys. Chem. A* **2014**, *118*, 1339–1349.
- [184] T. Chen, L. Zheng, J. Yuan, Z. An, R. Chen, Y. Tao, H. Li, X. Xie, W. Huang, *Sci. Rep.* **2015**, *5*, 10923.

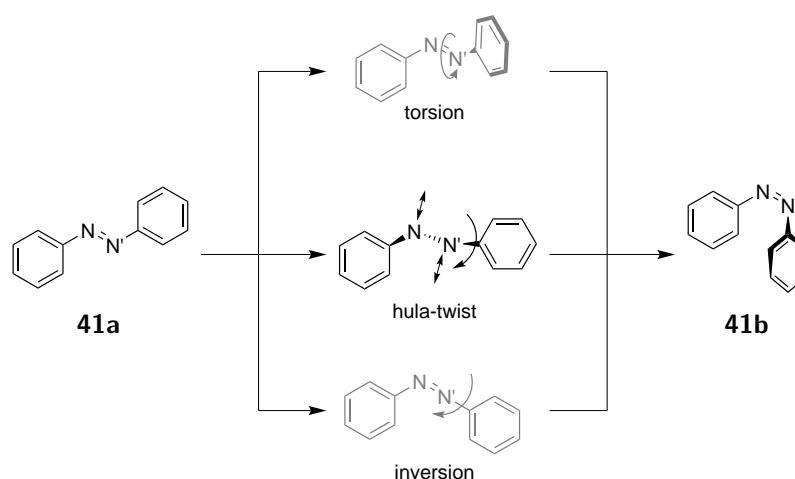
Part III.

Azobenzenes and Siloxanes

1. Azobenzene Dyes

Azobenzenes form the world's most relevant class of dyes with a tremendous variability: over 50% of the commercial dyes are azobenzene derivatives.^[185] The thermal and chemical stability of the azo group and its resistance against photo bleaching contributed to the broad use. Besides their vast use as colorants, azobenzenes are among the earliest known photoswitchable compounds in organic chemistry. The photoinduced isomerization of the central N=N double bond from *trans* (*E*) to *cis* (*Z*) was first reported in 1937.^[186]

The N=N double bond in the azo group is typically thermodynamically stable in its (*E*)-conformation.^[11] The isomerization towards the (*Z*)-isomer can be induced by irradiation with ultraviolet (UV) light (365 nm)^[186] or by electrostatic stimulation,^[187,188] while the (*Z*)→(*E*) isomerization occurs thermally and can be induced by irradiation with blue light (440 nm).^[11] This reversible isomerization takes place without any side products or photodegradation.^[189] Thus, thousands of switching cycles can be achieved.^[112] The isomers differ immensely in geometry: the planar (*E*)-isomer **41a** is significantly smaller than the bent (*Z*)-isomer **41b**.^[107,108,190] This geometry change induces a dipole moment of 3.1 D in the (*Z*)-isomer (0 D in (*E*)-azobenzene).^[191]



Scheme III.1 Possible isomerization mechanisms of azobenzene (**41**).^[192] **Top:** Torsion around the central double bond. **Middle:** Hula-twist, a pedal-like concerted motion of the nitrogen atoms and phenyl rings which is the predominant path in solution and confined environments. **Bottom:** Inversion, the phenyl rings approach each other in the molecular plane.

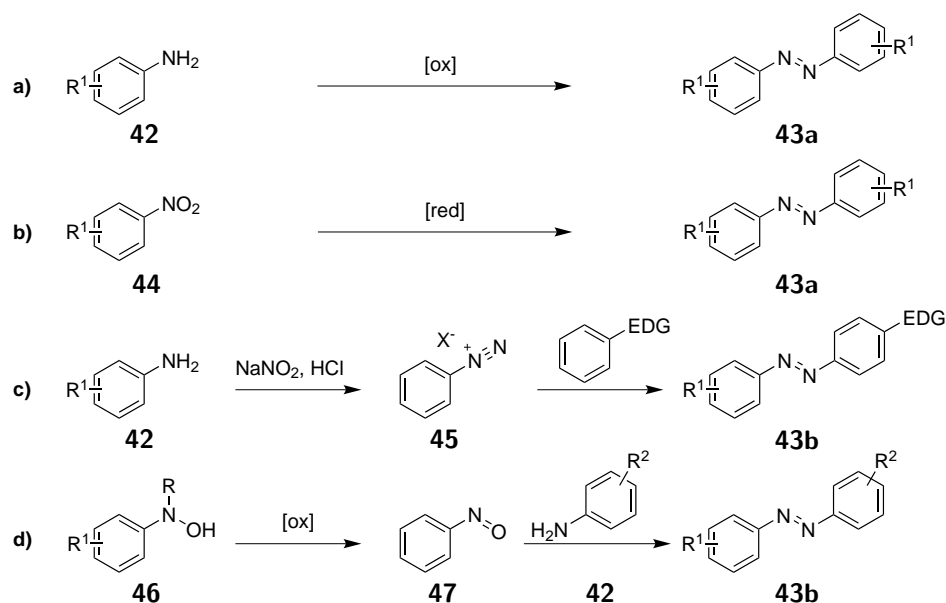
Mechanistic studies of the photoinduced switching process proved a fast isomerization on a pico second time scale.^[11,189] First, the switching mechanism of azobenzene (**41**) was regarded as either a torsional rotation around the N=N double bond or an inversion of the

double bond by movement of the phenyl rings in the molecular plane (Scheme III.1, top and bottom).^[11] In both mechanisms, one phenyl ring executes a large amplitude motion. Because azobenzenes showed photoswitchability even in confined environments,^[193–198] these reaction pathways were insufficient to describe the switching. Instead, a concerted twist (or "hula-twist", Scheme III.1, middle) mechanism was found.^[192,199–201]

Here, the nitrogen atoms and the phenyl rings execute a concerted pedal-like movement. Thus, the phenyl rings remain mostly in place during the switching process, making it the predominant pathway in constrained surroundings.^[189] Since the isomerization dynamics were found to be independent from solvent viscosity, the hula-twist mechanism was assigned to be the main switching pathway in solution as well.^[189,192]

Azobenzenes can be synthesized via several routes, according to desired substitution and available precursors (Scheme III.2).^[10]

Symmetrically substituted azobenzenes are often synthesized from anilines in an oxidative coupling or from nitrobenzenes in a reductive coupling (Scheme III.2 a) and b), respectively).^[10] The oxidizing reagents used in the coupling of anilines cover a broad range of metallic and non-metallic oxidants.^[10] For example, AgO,^[202] permanganates,^[203,204] MnO₂,^[205,206] Pb(OAc)₄,^[207,208] hypervalent iodines like PhI(OAc)₂,^[209,210] oxigen with copper(I) catalysts^[211–213] and others^[214] were reported in the synthesis of azobenzenes. Similarly, various reducing reagents such as LiAlH₄,^[215,216] NaBH₄,^[217,218] KOH,^[219,220] Zn/NaOH^[221–223] and others^[224] were used in the reductive coupling of nitrobenzenes.^[10]

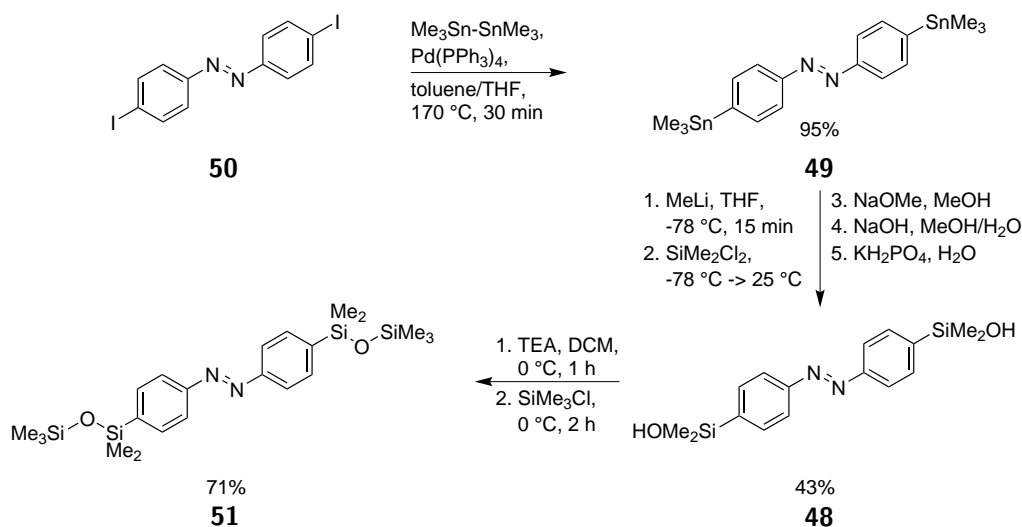


Scheme III.2 Common synthetic routes towards azobenzenes **43**.^[10] **a)** Oxidative coupling of anilines **42**. **b)** Reductive coupling of nitrobenzenes **44**. **c)** Azo coupling. After diazotation of anilines **42**, diazonium salts **45** undergo electrophilic aromatic substitution with electron rich aromatic systems, *para* to an EDG. **d)** Mills reaction. Hydroxyanilines **46** are first oxidized to nitrosobenzenes **47**, followed by a condensation with anilines **42**. The routes **a)** and **b)** are limited to the synthesis of symmetrical azobenzenes **43a**, whereas the routes **c)** and **d)** can yield unsymmetrical azobenzenes **43b**.

The most common syntheses to yield unsymmetrically substituted azobenzenes are the azo coupling reaction and the Mills reaction (Scheme III.2 c) and d), respectively).^[10] The initial step of an azo coupling is the diazotation of a primary amine to a diazonium salt, which can further react with aromatic nucleophiles.^[10] The electrophilic aromatic substitution of the weak electrophilic diazonium salts with electron rich aromatic nucleophiles is pH sensitive.^[225] By azo coupling reactions, cyclophanes,^[226] calixarenes^[227] and porphyrins^[228] could be functionalized with azobenzene moieties. Heterocyclic azo compounds, such as azoimidazoles can also be synthesized using this method.^[229,230] The Mills reaction comprises the formation of nitrosobenzenes and their condensation with anilines to yield azobenzenes.^[231] Herein, the synthesis of the nitrosoarenes by oxidation of aromatic hydroxyamines is the crucial step. Various oxidizing reagents such as *t*-butyl hypochlorite,^[231] FeCl₃,^[232–234] H₂SO₅,^[235] acetic acid/hydrogen peroxide,^[236] KMnO₄,^[237] hypervalent iodines like PhI(OAc)₂^[238] and others^[10,237] were used. This reaction sequence was used in the synthesis of azopyridines.^[234]

2. Covalent Incorporation Azobenzene Units into the Backbones of Poly(siloxanes)

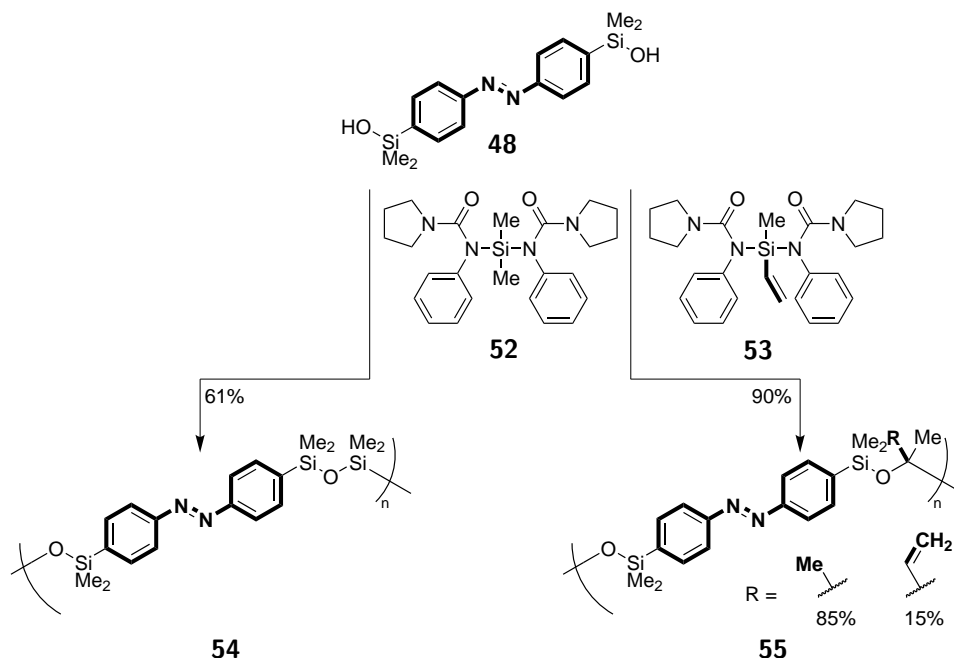
For the preparation of linear azobenzene-trisiloxane copolymers, the method developed by Strüben was optimized (see Scheme III.3).^[114,115] An azobenzene with two hydroxydimethylsilyl substituents **48** is used as monomer. The siloxane substituents are introduced via a tin-lithium exchange of 4,4'-bis(trimethylstannyl)-azobenzene (**49**) and subsequent quenching with dimethyldichlorosilane. By adjusting the concentration of the potassium dihydrogenphosphate buffer in the hydrolysis of the chlorosilane intermediate (step 5 in Scheme III.3), it was possible to increase the yield of this crucial synthesis to 43% compared to the published yield of 35%.^[115] The yields in the syntheses of the bis-stannyl **49** and diiodo **50** precursors were increased moderately from 49% to 62% over two steps compared to the reported synthesis.^[212]



Scheme III.3 Synthesis of the siloxane functionalized azobenzene **48** and the disiloxane functionalized azobenzene **51**.

The synthesized 4,4'-bis(hydroxydimethylsilyl)azobenzene (**48**) was used as monomer in the polycondensation of **48** and the silanes **52** and **53** as co-monomers, yielding two linear azobenzene-trisiloxane copolymers **54** and **55** (see Scheme III.4). The polymerization procedures were optimized compared to the procedure reported for the synthesis of the polymer **54** by maintaining the addition speed and temperature electronically, increasing the yield of **54** from 55% to 61%.^[114] The polymer **54** consists of strictly alternating azobenzene and hexamethyltrisiloxane units, whereas 15% of the trisiloxane units in **55** bear a vinyl

group for future cross-linking of the polymer. Additionally, an azobenzene **51** with disiloxane substituents in the *para*-positions was synthesized starting from **48**. This compound served as reference in the ^1H diffusion-ordered spectroscopy (DOSY) NMR^[239] and femtosecond transient absorption spectroscopy (FTAS) analysis of the polymer **54**.



Scheme III.4 Polymerization of the polymers **54** and **55** by polycondensation. The azobenzene unit and the variable substituent in **53** and **55** are highlighted in bold. Reaction conditions: addition of **52** and **53** in chlorobenzene at $-40\text{ }^\circ\text{C}$ over 8 h, followed by monitored progression at $25\text{ }^\circ\text{C}$ for 5 d (**54**) or 8 d (**55**).

The syntheses towards **54** and **51**, as well as the analysis of their switching behavior in terms of size switching (by DOSY NMR and gel permeation chromatography (GPC)) and ultrafast switching dynamics (by FTAS) have been prepared for publication in cooperation with the Molecular Physical Chemistry and Laser Chemistry group of Friedrich Temps of the Institute of Physical Chemistry, University Kiel. The results are comprised in the submitted manuscript in section 2.1. The experimental details are contained in the supporting information in Part V, section 6.1.

In cooperation with the Functional Nanomaterials group of Rainer Adelung of the Institute for Materials Science University Kiel, a film of **55** was produced. The synthesis of **55** and the analysis of the film's switching were prepared for publication and the manuscript is provided in section 2.2. The experimental details are contained in the supporting information in Part V, section 6.2.

2.1. A Linear Poly(Azobenzene-siloxane)

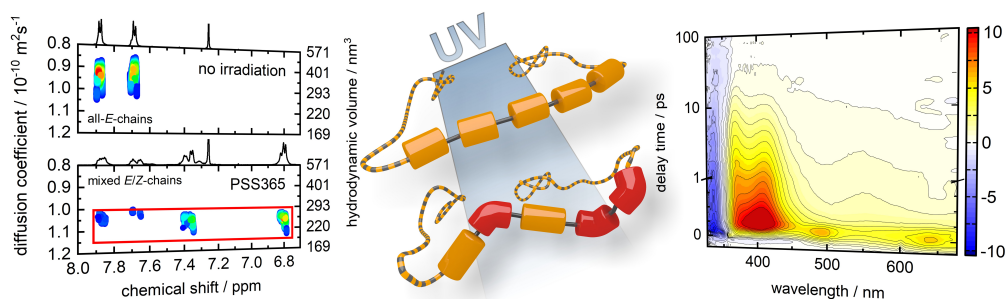
The manuscript was published in the *Journal of Materials Chemistry C*.^[240] Mathias Dowds, Dennis Bank, Jan Strueben, David Presa Soto, Frank D. Sönnichsen, Falk Renth, Friedrich Temps, Anne Staubitz, Efficient reversible photoisomerisation with large solvodynamic size-switching of a main chain poly(azobenzene-*alt*-trisiloxane), *J. Mater. Chem. C* **2020**. DOI: 10.1039/C9TC05193G

Reproduced from ref.^[240] with permission of the Royal Society of Chemistry (see 435)

Abstract

A photo-responsive linear poly(azobenzene) with an alternating sequence of azobenzene switching units directly connected by trisiloxane linkers was synthesised via a step-growth polycondensation. Due to its specific design and high molecular weight, the polymer features a very high chromophore load of 45 wt-% and a large number (≈ 130) of photoswitching units. Its photoswitching upon UV irradiation at 365 nm was studied in several solvents and compared to the corresponding free azobenzene siloxane congener. Efficient $E \rightarrow Z$ isomerisation with high conversion yields was observed for the polymeric and isolated azobenzene alike. In the slightly polar solvents chloroform and THF, this resulted in a photo-induced decrease in hydrodynamic volume of 22% (THF) and 32% (chloroform). In *n*-hexane, however, a light-triggered collapse of the solvated polymer coil lead to a globular non-solvated form with a 70% decrease in volume. Ultrafast transient electronic absorption measurements showed that the underlying excited-state reaction pathways for the azobenzene units in the polymer main chain are essentially similar to those for the analogous single azobenzene in solution. The data suggest a sequential deactivation via ultrafast internal conversion from the initially excited S₂ state to the S₁ state, followed by intramolecular vibrational redistribution in the S₁ state and subsequent electronic deactivation and isomerisation to the electronic ground state. The processes are only moderately slowed down for the main-chain azobenzene units compared to the free azobenzene in solution and conform to the accepted scenario of unsubstituted azobenzene.

main-chain azobenzene polymer - high-loaded - ultrafast dynamics



The results explain the efficient and nearly unimpeded isomerisation of the embedded azobenzene molecular switches that is highly unusual for a main-chain azobenzene polymer.

Due to the unique combination of a high chromophore load and large number of photo-switchable units in the main chain in a regular alternating architecture, coupled with large conversion yields, the poly(azobenzene-trisiloxane) should find applications as photo-responsive material, in particular when large switching amplitudes are essential.

Scientific Contribution to this Manuscript

I synthesized all used compounds. Jan Strueben and David Presa Soto established the syntheses of the molecules **48**, **49**, **50**, **52**, and **54**, I optimized the yields. I established the synthesis of molecule **51**. I performed the analyses of the size switching behavior and the UV-vis measurements of the molecules **49** and **48** (shown in the ESI, Part V, section 6.1). Dennis Bank and Friedrich Temps designed the FTAS experiment and Dennis Bank conducted the measurement and analyzed the data. UV-vis spectroscopy of the molecules **51** and **54** was performed by Dennis Bank. I wrote the manuscript with the support of Dennis Bank, Falk Renth, Friedrich Temps and Anne Staubitz.



Cite this: DOI: 10.1039/c9tc05193g

Efficient reversible photoisomerisation with large solvodynamic size-switching of a main chain poly(azobenzene-*alt*-trisiloxane)^{†‡}

 Mathias Dowds,[‡] Dennis Bank,[‡] Jan Strueben,[‡] David Presa Soto,[‡] Frank D. Sönnichsen,[‡] Falk Renth,[‡] Friedrich Temps[‡] and Anne Staubitz[‡]

A photo-responsive linear poly(azobenzene) with an alternating sequence of azobenzene switching units connected by trisiloxane linkers was synthesised via step-growth polycondensation. By its design, the polymer features a high chromophore load (45 wt%) and a large number (≈ 130) of photoswitching units per chain. The ensuing photoisomerisation upon UV irradiation with 365 nm light was studied in several solvents and compared to the corresponding free azobenzene siloxane congener. Efficient $E \rightarrow Z$ isomerisation with high conversion yields was observed for the polymeric and isolated azobenzenes alike. In the slightly polar solvents tetrahydrofuran (THF) and chloroform, this resulted in a photo-induced decrease in solvodynamic volume of 22% (THF) and 32% (chloroform). In *n*-hexane, however, a light-triggered collapse of the solvated polymer coil lead to a globular non-solvated form with a 70% decrease in volume. Ultrafast transient electronic absorption measurements showed that the underlying excited-state reaction pathways for the azobenzene units in the polymer main chain are essentially similar to those of the analogous single azobenzene in solution. The data suggest a sequential deactivation via ultrafast internal conversion from the initially excited S_2 state to the S_1 state, followed by intramolecular vibrational redistribution in the S_1 state, and subsequent $E \rightarrow Z$ isomerisation and deactivation to the electronic ground state. These processes are slowed down only moderately for the main chain azobenzene units compared to the free azobenzene in solution and conform to the accepted scenario for unsubstituted azobenzene. The results explain the efficient, nearly unconstrained isomerisation of the embedded molecular switching units that is highly unusual for a main chain azobenzene polymer. Due to the unique combination of a high chromophore load and large number of photo-switchable units in the main chain in a regular alternating architecture, coupled with a high conversion yield, the poly(azobenzene-*alt*-trisiloxane) should find applications as photo-responsive material, in particular when large switching amplitudes are essential.

Received 20th September 2019,
Accepted 9th December 2019

DOI: 10.1039/c9tc05193g

rsc.li/materials-c

Introduction

Photochromic molecules that are capable of reversible light-driven transformations receive considerable interest as nanoscopic

building blocks in photo-responsive materials and functional molecular systems and machines.^{1–5} In particular, different light-triggered polymeric materials have been applied successfully for high-density optical data storage, photo-control of phase transitions and surface properties, or in the context of solar energy conversion.^{6–12} In order to translate the molecular response into a desired macroscopic function, the embedding of the functional unit into complex environments such as polymers or liquid crystals is often required.^{13–15} In those environments, however, the molecular switching may be impeded by the restricted free volume in the surrounding matrix.^{16,17} In such cases, an increase of the available free volume, *e.g.*, by addition of plasticisers, functionalisation of the chromophores with additional long alkyl or oligomer chains, or the use of long, flexible spacer units has been suggested to improve the photoswitching behaviour.^{18–22}

Azobenzenes (ABs) are popular photochromic molecular switches due to the large-amplitude changes in length, volume,

^a Otto-Diels-Institute of Organic Chemistry, Christian-Albrechts-University Kiel, Otto-Hahn-Platz 4, D-24098 Kiel, Germany

^b Institute of Organic and Analytical Chemistry, University of Bremen, Leobener Str. 7, D-28359 Bremen, Germany. E-mail: staubitz@uni-bremen.de

^c MAPEX Center for Materials and Processes, University of Bremen, Bibliothekstraße 1, D-28359 Bremen, Germany

^d Institute of Physical Chemistry, Christian-Albrechts-University Kiel, Olshausenstr. 40, D-24098 Kiel, Germany. E-mail: temps@phc.uni-kiel.de, renth@phc.uni-kiel.de

^e Universidad de Oviedo, Facultad de Química, Departamento de Química Orgánica e Inorgánica, Julián Clavería s/n, 33006, Oviedo, Spain

[†] Electronic supplementary information (ESI) available: Detailed synthetic procedures and analytical data of all compounds including plots of UV-vis spectra, femto-second time-resolved spectroscopy analysis, ¹H, ¹³C{¹H}, and ²⁹Si{¹H} NMR spectra. Specifications of the LED equipment. See DOI: 10.1039/c9tc05193g

[‡] Equally contributing authors.

dipole moment, and the non-linear optical properties associated with the photo-reversible $E \rightarrow Z$ isomerisation of the N=N double bond. The relative ease of chemical modifications, and their remarkable photostability that allows repeated photoswitching for thousands of times are further attractive features.^{14,15,23,24}

The UV-vis absorption spectra of both AB isomers feature a weak band in the visible spectral range due to the forbidden $S_1(n\pi^*)$ transition, and a much stronger band in the UV due to the allowed $S_2(\pi\pi^*)$ transition. Irradiation into the latter is usually done to affect $E \rightarrow Z$ conversion. The Z -isomer on the other hand is switched back to the E -isomer in the visible spectral range, where its absorption is comparatively higher than that of the E -isomer.^{14,23}

Extensive studies using ultrafast spectroscopies and quantum chemical calculations have shown that the favourable photoswitching properties of AB are closely related to the mechanism of the underlying excited-state processes on the femto- to picosecond time scales.^{14,23,25–27} Recent results indicate that the isomerisation proceeds from the S_1 state irrespective of the excitation wavelength and involves a torsional motion of the central CNNC moiety, possibly assisted by a certain degree of simultaneous CNN bending. Upon S_2 excitation in the UV, extremely fast internal conversion (IC) populates the S_1 state quantitatively, however, in a different region on the S_1 potential energy hypersurface (PEHS) than by direct S_1 photoexcitation in the visible spectral range. This opens up an additional non-reactive pathway that explains the reduced quantum yields for UV compared to visible excitation. The torsional mechanism resembles the hula-twist mechanism initially suggested for the volume-conserving $E \rightarrow Z$ isomerisation of polyenes, explaining the successful photo-isomerisation of rotation-restricted bridged derivatives and the ability of ABs to isomerise even in strongly confined environments and under external forces.^{28–33} This makes ABs ideal candidates for the use as photoswitchable molecular actuators in polymeric environments,^{13,34–36} where embedding of the chromophores could be performed by doping, as covalently bound side chains, or integrated into the polymer main chains. However, in particular for main chain incorporation, additional derivatisation of the AB units by flexible side chains, or the use of extremely long flexible linkers, has often proved necessary to improve the switching behaviour, at the expense of, *e.g.*, synthetic accessibility, dye load or overall switching amplitude.^{13,22,37–40}

In the present paper, we aim to exploit the full potential of AB as photoresponsive molecular unit by the design of a linear poly(azobenzene) that maintains the favourable photoswitching properties of AB in solution despite carrying the photoreactive units in the main chain with a high chromophore load (see Fig. 1). This is achieved by an exactly alternating sequence of ABs and hexamethyltrisiloxanes as short linker units that provide high chain flexibility and should lead to a low glass transition temperature in the solid state (T_g of poly(dimethyl siloxane): -120 °C).⁴¹ The need for additional derivatisations to preserve photoswitchability is thus alleviated.^{17,37,39} To our knowledge, there is only one previous example of a main chain AB-siloxane polymer, which has been reported by Irie and Suzuki.¹⁹ By comparison, the

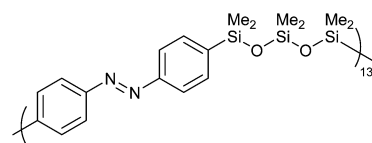


Fig. 1 Chemical structure of the azobenzene-trisiloxane polymer with the photochromic units in the main chain synthesized in this work.

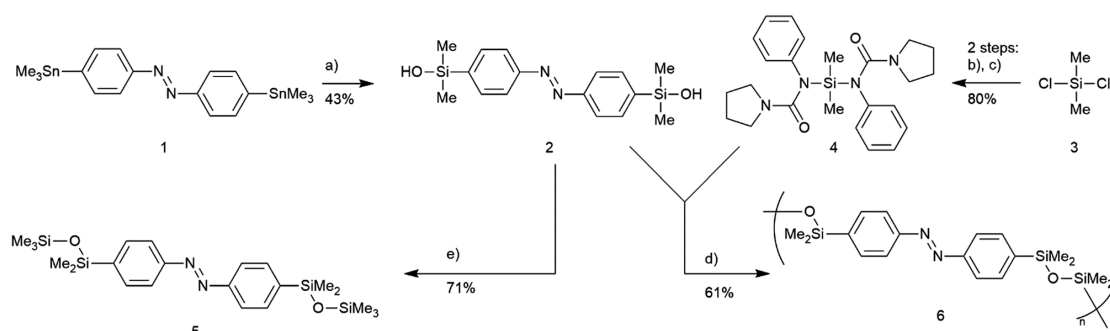
number of azobenzene units in our polymer is larger by a factor of 7 and the chromophore load could be substantially increased to 45 wt%. On these premises, we report on the synthesis, static photoswitching properties and photo-induced ultrafast dynamics of the alternating linear poly(azobenzene-*alt*-trisiloxane) **6** and the congener 4,4'-bis(disiloxane)-azobenzene **5**, which forms a suitable reference with the same chemical structure as the repetition unit in the polymer. The photoswitching behaviour was monitored by UV-vis absorption and ^1H NMR spectroscopies in thermal equilibrium and in the photostationary states upon irradiation with 365 nm light in several solvents. ^1H DOSY NMR spectroscopy and gel permeation chromatography (GPC) were applied to determine the photo-induced change in solvodynamic volume. In addition, femtosecond time-resolved transient absorption spectroscopy was employed to study the photo-induced processes of the AB chromophores in solution for the polymer **6** and the reference compound **5**. The mechanistic information provided by the ultrafast measurements^{32,33,42,43} allowed us to rationalise the nearly unconstrained switching of the AB chromophores in the main chain of the polymer.

Results

Synthesis

The strategy for the synthesis of the regular alternating polymer **6** was based on a step-growth polycondensation of the hydroxy-silane azobenzene derivative **2** with the activated ureasilane **4** (Scheme 1). Starting from 4-iodoaniline, the monomer precursor bis(trimethyltin)-azobenzene **1** was synthesised in two steps as described recently.⁴⁴ In a third step, **1** was subjected to a tin-lithium exchange.⁴⁵ Subsequent quenching with dichlorodimethylsilane (**3**) followed by hydrolysis then gave the azobenzene **2** derivatised with hydroxyl dimethyl silane substituents with an isolated yield of 43%.⁴⁶ The overall yield of monomer **2** including all three synthetic steps was increased from 17% to 27% compared to reported syntheses.^{44,46} The derivative **2** also served as the starting point for the synthesis of the reference compound 4,4'-bis(disiloxane)-azobenzene **5**. Deprotonation with triethylamine, and subsequent reaction with trimethylsilyl chloride afforded the target molecule **5** in a yield of 71%.

The activated bis-ureasilane co-monomer **4** was synthesised starting from dichlorodimethylsilane (**3**) by condensation with pyrrolidine, followed by an insertion reaction of phenyl isocyanate. The co-monomer **4** was obtained in a yield of 80% over the two steps, which is comparable to previously reported syntheses.^{47,48} Finally, step-growth polycondensation of azobenzene **2** with ureasilane **4** as co-monomers gave the desired



Scheme 1 Overview showing the syntheses of the 4,4'-bis(dimethyl siloxane)-azobenzene **5** and the azobenzene trisiloxane copolymer **6** via 4,4'-bis(hydroxydimethyl silyl)-azobenzene **2** as intermediate. The urea derivative **4** that acted as co-monomer was synthesised in two steps from dichlorodimethylsilane (**3**) as starting material. Details of steps (a–e) and the synthesis of 4,4'-bis(trimethylstannyl)-azobenzene (**1**) via 4,4'-diiodoazobenzene can be found in the ESI.†

strictly alternating linear polymer **6** in a yield of 61%. Polymer analytics performed by gel permeation chromatography (GPC) showed a molecular weight (M_w) of 50.6 ± 0.8 kDa, corresponding to a degree of polymerisation of 130. The measured polydispersity index (PDI) of 1.95 is close to the theoretical maximum PDI of 2.00 for step growth polycondensations expected for quantitative monomer conversion.⁴⁹ During the polymerisation in chlorobenzene, the protonated urea precipitated. As this is a very stable product, it presumably provides the driving force in the reaction and shifts the equilibrium to the product side, thus increasing the yield.⁵⁰ There was no evidence of side products such as macrocyclic oligomers or hydrolysis of the siloxane bonds. The synthetic route *via* the highly reactive co-monomer **4** therefore allowed us to obtain the poly(azobenzene-*alt*-trisiloxane) **6** with a high degree of polymerisation, and without side reactions that typically accompany the polycondensation of siloxanes.^{41,51}

Photoswitching properties

The thermal equilibrium states and photostationary states obtained by UV irradiation with 365 nm light for the reference azobenzene derivative **5** and the AB-siloxane polymer **6** were characterized by ¹H NMR spectroscopy in *n*-hexane-*d*₁₄, THF-*d*₆ and CDCl₃ as solvents, and by static UV-vis absorption spectroscopy in *n*-hexane (see Fig. 2).

UV-vis spectroscopy. The static UV-vis spectra of the *E*-isomers of the reference compound **5** and the AB-siloxane polymer **6** in chloroform, THF and *n*-hexane as solvent are given in the top panels of Fig. 2 as solid lines. The spectra were normalised to a maximum intensity of unity, since absolute extinctions per AB chromophore could not be determined for the polymer solution. The dotted lines show the spectra of the photostationary states obtained by irradiation with 365 nm light using the same scaling factors. As can be seen, the spectra of the *E*-isomers are virtually identical for the reference compound **5** and the polymer **6** and showed no significant solvatochromic effect. The spectra feature a strong absorption band in the UV due to the $S_2(\pi\pi^*)$ transition and a much weaker $S_1(n\pi^*)$ band in the visible spectral range. The $S_2(\pi\pi^*)$ bands exhibit

absorption maxima around $\lambda = 325$ nm and show two additional shoulders at the red edge around $\lambda = 350$ – 370 nm; the $S_1(n\pi^*)$ bands had maxima of around $\lambda = 450$ nm. The band positions are thus shifted only slightly compared to unsubstituted AB, indicating that the siloxane substituents and likewise the embedding of the AB chromophores into the main chain of the siloxane polymer had little effect on its absorption properties.

The normalised spectra of the reference compound **5** in the photostationary states PSS₃₆₅ (dashed lines in Fig. 2) show a similar decrease of the $S_2(\pi\pi^*)$ band intensity by $\approx 70\%$ in all three solvents accompanied by an approximate doubling of the $S_1(n\pi^*)$ absorption. The S_2 band of the PSS₃₆₅ apparently undergoes an hypsochromic shift with increasing polarity of the solvent from $\lambda_{\max} = 305$ nm in *n*-hexane to 298 nm in THF and 296 nm in chloroform. The solvatochromic red-shift is small for the S_1 band, where the maxima are located between 444 nm (*n*-hexane) and 438 nm (chloroform). The spectra of the polymer **6** (Fig. 2, top right panel) without irradiation showed the same solvatochromic behaviour. For the PSS₃₆₅ in chloroform and THF, the intensity changes of the S_2 and S_1 bands are comparable to those of the monomer **5**, whereas in *n*-hexane, the intensity of the $S_2(\pi\pi^*)$ band is decreased comparatively less by $\approx 55\%$, indicating a slightly lower extent of photoswitching for the polymer in this unpolar solvent.

Overall, these changes indicate that a significant conversion to the *Z*-isomer photoproduct took place in both cases. To investigate the photostability of the polymer **6**, it was subjected to repeated alternating irradiations into the photostationary states with UV light (PSS₃₆₅) and with blue light ($\lambda_{\max} = 450$ nm, PSS₄₅₀). The absorption of the $S_2(\pi\pi^*)$ band and the $S_1(n\pi^*)$ band was traced for five complete cycles and showed no sign of photodegradation in chloroform and *n*-hexane. In THF, the absorption continuously decreased after every irradiation cycle, indicating a slow overall degradation presumably by reaction with peroxide species caused by the UV irradiation of the solvent (see ESI,† Fig. S2).⁵²

Finally, the spectral changes induced by the thermal *Z* → *E* back-isomerisation were recorded at a series of time delays, starting from the PSS₃₆₅ in *n*-hexane solution for both compounds.

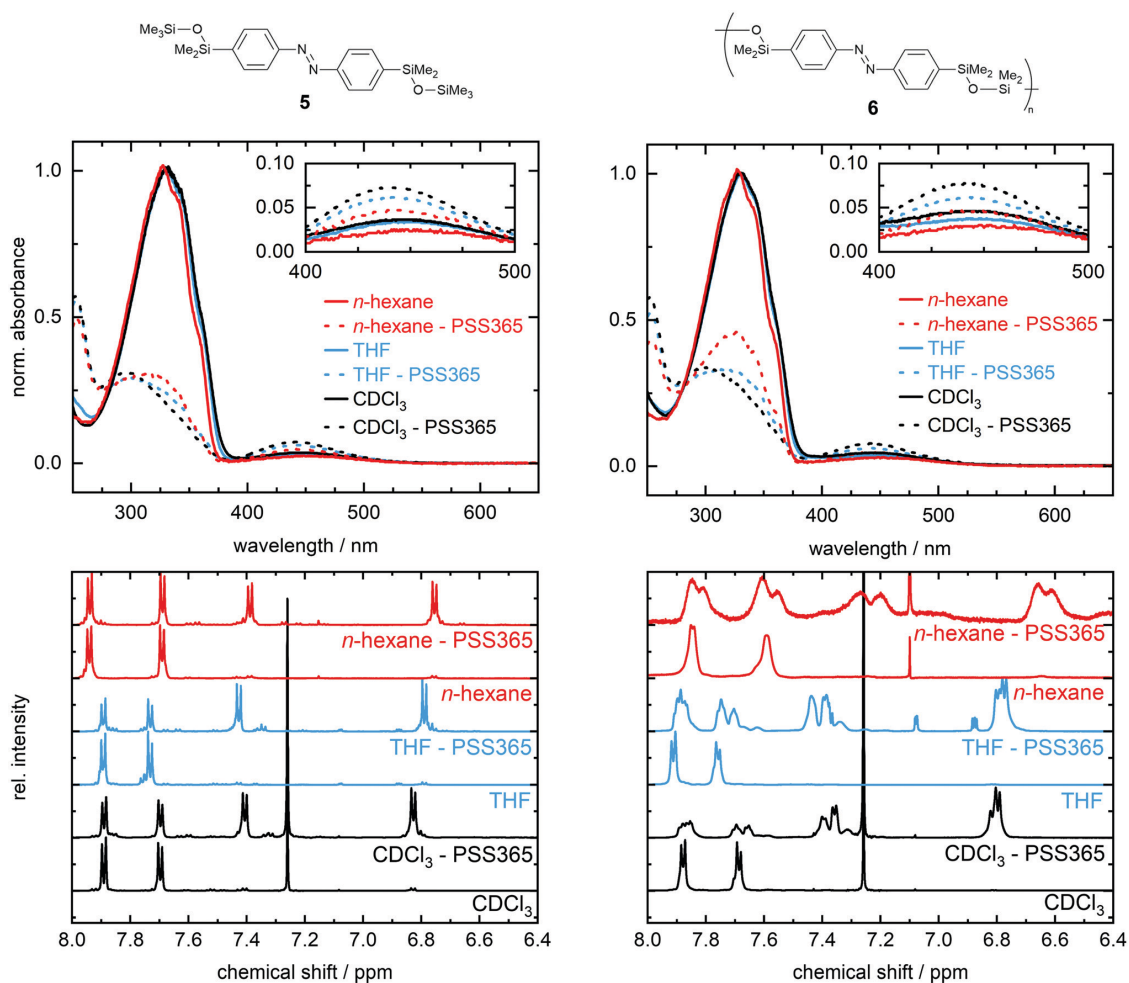


Fig. 2 Top: Normalised UV-vis spectra for the AB-siloxane reference compound **5** (left) and the AB-siloxane polymer **6** (right) in chloroform, THF, and *n*-hexane as solvents. The spectra for the *E*-isomers are given by solid black, blue and red lines, respectively, the spectra of the photostationary states PSS-365 are displayed as corresponding dashed lines. Bottom: ¹H NMR spectra of the aromatic regions for compound **5** in solutions of CDCl₃ (black), THF (blue) and *n*-hexane (red). The intensities were rescaled for clarity.

This gave a thermal half-life of $t_{1/2} = 15 \pm 2$ h for the *Z*-isomer of the reference AB **5**, and of $t_{1/2} = 25 \pm 2$ h for the embedded *Z*-isomer units in the polymer **6** (see ESI,† Fig. S10 and S11).

¹H NMR spectroscopy. Before irradiation, the ¹H NMR spectra in Fig. 2 (bottom panels) showed only signals for the *E*-isomer. This indicated that this is the thermally stable AB isomer in all solvents and irrespective of the environment (free in solution vs. covalently linked into the main chain). The equilibrium spectra for the polymer **6** in THF and CDCl₃ were virtually identical to those for the “free” reference compound **5**. In particular, the signals related to the aromatic protons of the azobenzene units in the polymer **6** showed the same chemical shifts and coupling constants (see ESI,† synthetic procedures), and were only negligibly broadened compared to the reference compound **5**. In CDCl₃, for example, the signals showed an

average line width of 3.91 Hz for the polymer **6**, compared to 2.80 Hz for the single azobenzene **5**. This indicates a uniform local environment for the AB units,⁵³ proving the regular, alternating structure of the main chain functionalised polymer. Furthermore, the absence of any significant line broadening effects suggests a fairly high chain mobility within the polymer backbone.⁵³

Except for some changes in chemical shifts, the spectra of **5** in *n*-hexane possessed the same characteristics as in the other two solvents. The lines in the thermal equilibrium spectrum of polymer **6** in *n*-hexane appeared slightly broadened by comparison with the equilibrium spectra in THF or chloroform and also compared to the corresponding spectrum of **5** in *n*-hexane in thermal equilibrium. As all other possible influencing factors are equal, we therefore attribute the broadening to

differences in the solvation of the polymer coil (see also ^1H DOSY spectra below).

The ^1H spectra for the photostationary states (PSS₃₆₅) all show additional signals due to the formation of the *Z*-isomer that appear high-field shifted compared to the *E*-isomer and indicate successful isomerisation. Integration of the signals of the aromatic protons of both isomers for the solutions in chloroform, THF and *n*-hexane gave respective *E* → *Z* conversion yields of 67%, 64%, and 46% for azobenzene **5**, and very similar values of 67% and 58% for the polymer **6** in chloroform and THF. The PSS₃₆₅ of polymer **6** in *n*-hexane consisted of signals corresponding to collapsed coils and a broad signal background attributed to larger polymer aggregates. For the collapsed coils, an *E* → *Z* conversion of 50% was found (see Table S3 in the ESI†).§

Furthermore, the PSS₃₆₅ spectra for all three polymer solutions show a doubling of the signals (*i.e.*, the signals appear as pairs). This would be expected for a partial isomerisation of the *E*-isomer units within the polymer chain. The line widths of the individual signals stayed approximately constant in THF and CDCl₃, but were significantly larger in *n*-hexane, indicating a heterogeneous local environment and/or a lower mobility of the polymer chain compared to the other two solvents.

The photostability of the reference molecule **5** and the polymer **6** was also studied by ^1H NMR spectroscopy in CDCl₃ by subjecting the samples to cyclic alternating irradiation into the PSS₃₆₅ and PSS₄₅₀ photostationary states for five times. The integrals of the aromatic protons were used to calculate the resulting molar fractions of *E*- and *Z*-isomers. To ensure that the PSS was reached, the ^1H spectra for a series of different irradiation times were recorded and the molar fractions of *E*- and *Z*-isomers were traced (see ESI†, Fig. S3–S6). For both substances, no further changes in the molar fractions were observed after approximately one minute of irradiation, confirming that the corresponding PSS had been reached. No sign of photodegradation was found.

Photo-induced size switching

^1H DOSY NMR. In order to obtain information on the photo-induced size switching, the diffusion coefficients of the monomer azobenzene **5** and the polymer **6** were determined in chloroform-*d*, THF-*d*₆ and *n*-hexane-*d*₁₄ by diffusion-ordered ^1H NMR spectroscopy (^1H DOSY NMR). These measurements were performed in the thermal equilibrium and in the photostationary states after irradiation with 365 nm light (PSS₃₆₅). Fig. 3 displays the corresponding DOSY spectra in chloroform. Additional spectra at shorter irradiation times and in the photostationary state after irradiation with blue light (PSS₄₅₀) were recorded in chloroform as solvent, but are not shown here for the sake of clarity. The diffusion coefficients *D* were obtained from the DOSY experiments by T_1/T_2 fitting using

§ In the ^1H DOSY, we did not take the broad background signals into account, which are presumably caused by polymer aggregates: their overall amplitude is small and their analysis carries a large error. The collapsed coils that were used for the volume determination consisted of a 50/50 mixture of *E* and *Z* isomers (see ESI†, Table S3).

the Topspin 4 software (Bruker), and subsequently used to calculate the solvodynamic radii and corresponding solvodynamic volumes V_h via the Stokes–Einstein equation. The most relevant results are summarised in Table 1 (the full set of values and details including the determination of the solvent viscosities are provided in the ESI†).

The aromatic region of the ^1H DOSY spectrum for the azobenzene **5** in the thermal equilibrium depicted in Fig. 3 (top left panel) features only signals related to the aromatic protons of the *E*-isomer. The corresponding spectrum in the PSS₃₆₅ on the other hand shows additional signals: these are due to the photo-induced formation of the *Z*-isomer. These signals appear shifted to higher field than for the *E*-isomer, as was already observed in the standard ^1H spectra (*cf.* previous Subsection). In both spectra, the signal positions for the *E*-isomer along the ordinate correspond to the same diffusion coefficient *D* of $7.8 \times 10^{-10} \text{ m}^2 \text{ s}^{-1}$ and a solvodynamic volume of $V_h = 0.63 \text{ nm}^3$. The diffusion coefficients in THF and *n*-hexane, $D = 8.5$ and $13.4 \times 10^{-10} \text{ m}^2 \text{ s}^{-1}$, are higher due to the lower viscosities of those solvents, but correspond to virtually identical solvodynamic volumes (*cf.* Table 1). On average, V_h equals 0.65 nm^3 .

As can be seen clearly in the PSS₃₆₅ spectrum, the signals for the *Z*-isomer appeared at a higher diffusion coefficient and a smaller solvodynamic volume V_h of 0.45 nm^3 in chloroform. In THF and *n*-hexane, similar values of $V_h = 0.51$, and 0.48 nm^3 were found. The observed changes correspond to an average reduction of 20% in solvodynamic volume compared to the *E*-isomer.

The ^1H DOSY NMR spectra for the azobenzene polymer **6** in chloroform solution in Fig. 3 (right panels) lacked any signals related to the *Z*-isomer prior to irradiation. However, these signals are clearly present in the PSS₃₆₅, which is evidence for a successful photoisomerisation. The signal positions along the ordinate correspond to diffusion coefficients and solvodynamic volumes of individual polymer coils each containing on average >100 chromophore units. Unlike for the two isomers of the individual AB molecules **5** in Fig. 3 (top left panel) the signals for the *E*- and *Z*-isomers occur at the same ordinate position in the PSS spectrum of the polymer, as both isomers occur in each single polymer chain. For the all-*E* coils present in thermal equilibrium, the signals correspond to solvodynamic volumes of 370 and 360 nm^3 in chloroform and THF, respectively, and to a significantly lower value of 130 nm^3 in *n*-hexane. These differences likely reflect that chloroform and THF are better solvents than *n*-hexane for the unswitched polymer.

Upon irradiation, the solvodynamic radii and thus the solvodynamic volumes decrease considerably, to respective values of 250 and 280 nm^3 in chloroform and THF, and to 40 nm^3 in *n*-hexane (*cf.* Table 1 for the corresponding diffusion constants). For the latter, the small resulting volume and the extent of the volume decrease indicate a complete collapse of the solvated polymer coil to a globular, non-solvated form.

Gel permeation chromatography (GPC). In addition to the ^1H DOSY NMR experiments, the azobenzene-trisiloxane polymer **6** was analysed by conventional GPC in THF with

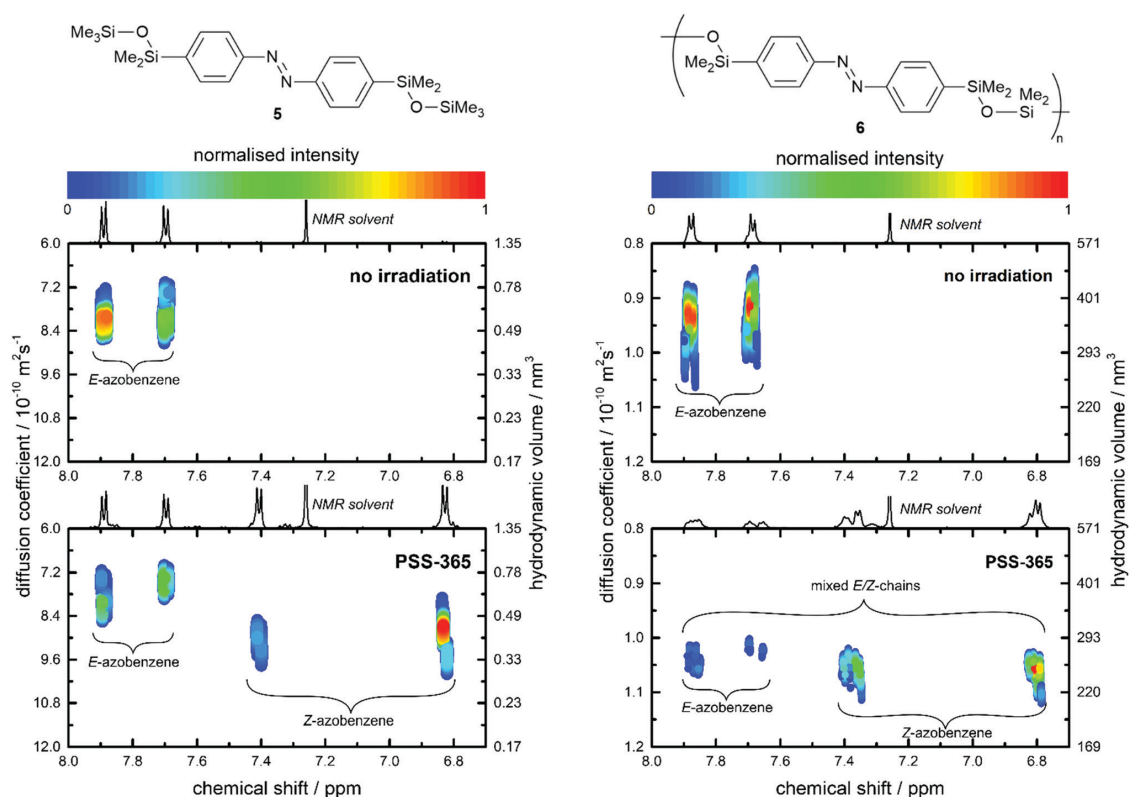


Fig. 3 Aromatic regions of the ^1H DOSY NMR spectra of the reference azobenzene derivative **5** (left) and the functionalised polymer **6** (right) in solutions of CDCl_3 showing the effect of photoswitching on the diffusion coefficients and solvodynamic volumes. The left axes refer to the measured diffusion constants, the right axes correspond to the calculated solvodynamic volumes. Note that the diffusion rate decreases while the particle size increases. The corresponding 1D ^1H spectra are displayed above the top axes. The intensities of the DOSY spectra were normalised for each spectrum individually for clarity and are colour-coded as indicated by the colour bars. For the sake of clarity, the assignments of the signals are indicated by coloured rectangles.

calibration against polystyrene as standard under thermal equilibrium conditions and in the PSS_{365} . A detailed description of sample preparation, execution of the measurements, and graphs of the elution traces are included in the ESI.† Under ambient conditions, the apparent number-averaged molecular weight (M_n) was determined as 25.9 ± 0.5 kDa and the weight averaged molecular weight (M_w) to be 50.6 ± 0.8 kDa,

corresponding to a polydispersity index (PDI) of 1.95. The measurement was repeated after irradiating the quartz cuvettes with UV light at 365 nm into the PSS_{365} , yielding lower apparent molecular weights of 19.4 ± 0.8 kDa (M_n) and 37.2 ± 1.9 kDa (M_w), respectively (see Fig. S1 in the ESI†). The decrease in apparent molecular weight was thus approx. 25%.

Photo-induced ultrafast dynamics and isomerisation mechanism

The recorded two-dimensional transient absorption maps showing the change in optical density ΔOD upon S_2 ($\pi\pi^*$) photo-excitation at $\lambda_{\text{exc}} = 320$ nm for the reference AB-siloxane **5** and the polymer **6** as a function of probe wavelength and pump-probe delay time are depicted in Fig. 4(a) and (b) for probe wavelengths in the range $\lambda_{\text{probe}} = 325\text{--}675$ nm. The data were acquired up to delay times of 1 ns, but are displayed here only for delay times from -0.2 to 100 ps for the sake of clarity, using a linear scale up to delay times of 1 ps, and a logarithmic scale thereafter.

The spectro-temporal transient absorption maps are very similar in both cases. Both show negative signals at the shortest probe wavelengths ($\lambda_{\text{probe}} < 360$ nm) due to the photo-bleaching

Table 1 Diffusion coefficients D and solvodynamic volumes V_h determined by ^1H DOSY NMR in thermal equilibrium at 25 °C and in the photostationary states upon irradiation with 365 nm light for solutions of the azobenzene derivative **5** and the polymer **6** in chloroform- d , THF- d_8 and n -hexane- d_{14}

Solvent	Conditions	$D/10^{-10} \text{ m}^2 \text{ s}^{-1}$		V_h/nm^3	
		5	6	5	6
CDCl_3	Thermal	7.8	0.93	0.63	370
THF	Thermal	8.5	1.0	0.62	360
n -Hexane	Thermal	13.4	2.3	0.67	130
CDCl_3	PSS_{365}	7.5 (E) 8.7 (Z)	1.1	0.70 (E) 0.45 (Z)	250
THF	PSS_{365}	8.7 (E) 9.1 (Z)	1.1	0.59 (E) 0.51 (Z)	280
n -Hexane	PSS_{365}	13.6 (E) 14.9 (Z)	3.5	0.63 (E) 0.48 (Z)	40

of the *E*-isomer ground-state absorbance (GSB). A refilling of the GSB within a few picoseconds is evident, but remains incomplete even at the maximal monitored delay time of 1 ns. The positive signals at $\lambda_{\text{probe}} > 360$ nm are related to excited-state absorption (ESA). In the probe wavelength range from 475 to 675 nm, the ESA features two maxima at $\lambda_{\text{probe}} = 500$ and 615 nm and rises immediately after excitation. Its maximum occurs at $\Delta t \approx 150$ fs and is followed by a dominant decay within < 0.3 ps. Between 375 and 450 nm, a slightly delayed rise of an intense ESA band peaking around $\lambda_{\text{probe}} = 400$ nm can be discerned. The subsequent decay of this band and the remaining transient absorption signals at larger wavelengths happen on a time scale of several picoseconds. After ≈ 35 ps, spectro-temporal changes are negligible. The permanent absorption changes feature the remaining negative GSB in the UV due to the *E*-isomer bleach. Corresponding positive absorptions in the visible due to the formation of the *Z*-isomer cannot be observed, however, presumably due to the much lower absorption coefficients of the related $S_1(n\pi^*)$ band.

A quantitative global analysis of the data was performed based on the singular value decomposition (SVD) of the time-zero corrected data matrices,⁵⁴ which yielded four relevant SVD components in both cases (see ESI,† for further details on the global fit procedure). A global fit was then achieved by a simultaneous non-linear least-squares fit to the SVD time traces by a sum of three exponential decay functions convoluted with the instrument response function (IRF) and a step function also convoluted with the IRF to account for the permanent absorption changes. The time constants resulting from the global fits are collected in Table 2.

In order to elucidate the molecular processes following the initial $S_2(\pi\pi^*)$ photo-excitation of the azobenzene *E*-isomers, the wavelength-dependent amplitudes of the global decay constants were transformed into so-called evolution-associated absorption difference spectra (EADS) according to a strictly sequential kinetic scheme. This allows one to describe the observed spectro-temporal absorption changes by an inter-conversion between successive EADS with lifetimes given by

the globally fitted time constants and facilitates the interpretation of the results. The EADS are labelled according to the time constants and depicted in Fig. 4(c). As can be seen, the EADS for the photo-excited azobenzene **5** and the polymer **6** resemble each other closely, in line with the observed similar transient absorption changes in both cases, cf. Fig. 4(a) and (b). The first spectra $EADS_1$ (solid and dashed dark blue lines in Fig. 4(c)) by definition correspond to the time-zero transient absorption changes and should be related to molecules in the Franck-Condon (FC) region of the photo-excited S_2 state. They show positive signals in the visible region due to ESA bands associated with electronic transitions to several higher lying states. Negative signals occur for probe wavelengths below ~ 360 nm due to strong GSB and possibly also a minor contribution by stimulated emission from the S_2 state, presumably superimposed by ESA. The evolution towards $EADS_2$ happens with virtually identical time constants, $\tau_1 = 0.14$ ps and 0.15 ps, for the azobenzene monomer and in the polymer, respectively. The $EADS_2$ spectra are clearly different in shape compared to $EADS_1$ and show an intense ESA band peaking at ~ 400 nm, as well as a further positive band with low amplitude at longer probe wavelengths. Negative signals related to GSB appear only at probe wavelengths ≤ 350 nm, blue-shifted and with lower amplitude compared to $EADS_1$. In line with previous studies on UV-excited *E*-azobenzene, the significant changes are attributed to ultrafast $S_2 \rightarrow S_1$ internal conversion (IC), and the $EADS_2$ spectra can be related to vibrationally hot molecules immediately after entering the $S_1(n\pi^*)$ state. The subsequent evolution to the $EADS_3$ spectra occurs with $\tau_2 = 0.6$ ps in the model compound **5** and only slightly slower ($\tau_2 = 1.0$ ps) in the azobenzene polymer **6**. The resulting $EADS_3$ spectra share the spectral signatures of ESA and GSB, *i.e.*, positive bands centered around 400 and 550 nm and negative signals below 350 nm, with their precursors. Both contributions are observed with comparatively lower amplitude. In line with recent studies, we assign the underlying process to intramolecular vibrational relaxation (IVR) of the initial vibrationally hot molecules in the S_1 state with time constant τ_2 . The spectral

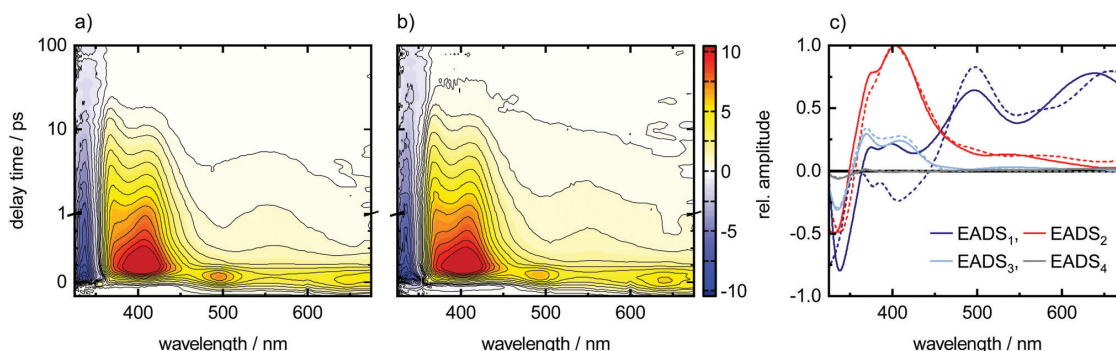
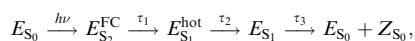


Fig. 4 Two-dimensional spectro-temporal transient absorption maps after $S_2(\pi\pi^*)$ excitation at $\lambda_{\text{exc}} = 320$ nm of (a) the *E*-AB-siloxane monomer **5** and (b) the *E*-AB-siloxane polymer **6**. (c) Evolution-associated difference spectra (EADS) obtained by the global SVD-based data analysis of the transient absorption changes upon $S_2(\pi\pi^*)$ excitation at 320 nm of the *E*-AB-siloxane polymer **6** (solid lines) and the *E*-AB-siloxane monomer **5** (dotted lines).

Table 2 Time constants from global fits to the spectro-temporal absorption data of monomer **5** and polymer **6** in *n*-hexane following $S_2(\pi\pi^*)$ photo-excitation. The error limits correspond to the 2σ confidence intervals of the fits

	Monomer 5	Polymer 6
τ_1 /ps	0.14 ± 0.01	0.15 ± 0.01
τ_2 /ps	0.60 ± 0.10	1.00 ± 0.20
τ_3 /ps	5.30 ± 0.03	8.30 ± 0.80
τ_4 /ps	∞	∞

evolution ends with the final EADS₄ spectra, which are formed with $\tau_3 = 5.3$ and 8.3 ps for the azobenzene **5** and the azobenzene polymer **6**, respectively, and correspond to the absorption difference spectra of the *E*- and *Z*-isomers. This time scale is thus clearly related to the isomerization and electronic deactivation of the remaining molecules in the S_1 excited state leading to the electronic ground states of the *E*- and *Z*-isomers. The resulting kinetic scheme taking into account the assignments based on the description of the spectro-temporal evolution of the recorded transient absorption data by the EADS is given by



where the different species have been labelled by their electronic states as subscripts. The Franck–Condon states and vibrationally hot species are indicated by corresponding additional superscripts. The time constants above the arrows are those given in Table 2.

Discussion

We have synthesised a poly(azobenzene-*alt*-trisiloxane) with azobenzenes as functional photoswitchable units in the main chain connected by trisiloxane linkers in an alternating sequence. The specific design of the polymer was chosen in order to achieve a high chromophore load and a large number of photo switchable units without compromising the favourable photoswitching properties of the azobenzene chromophore. In order to assess the prospects of the new polyazobenzene as a photo-responsive material, this discussion deals first with the characterisation of the photoswitching properties by static UV-vis absorption and ^1H NMR experiments in several solvents and then addresses the photo-induced change in solvodynamic volume of the polymer in solution as seen by ^1H DOSY NMR spectroscopy and gel permeation chromatography (GPC). Finally, the mechanistic insight into the underlying ultrafast photo-induced processes obtained from femtosecond time-resolved transient absorption spectroscopy is discussed.

Photoswitching properties

The static UV-vis spectra of the *E*-isomers of the reference compound **5** and the AB-siloxane polymer **6** in *n*-hexane, THF, and chloroform (*cf.* Fig. 2) were virtually identical in both environments and resembled that of unsubstituted azobenzene closely. This hints at an essentially undisturbed conformation

of the central N=N moiety and a similar local environment for the chromophores in the solvated polymer, compared to the free molecules in solution. The spectral changes upon irradiation into the photostationary states PSS₃₆₅ indicate that a significant conversion to the *Z*-isomer photoproduct took place in both cases. In particular, the observed decreases of the $S_2(\pi\pi^*)$ band by $\approx 70\%$ for compound **5** in all studied solvents, and likewise for polymer **6** in chloroform and THF (by 70%) and by $\approx 55\%$ in *n*-hexane, should represent lower limits to the overall *E* → *Z* conversion yields in the PSS₃₆₅, considering that the *Z*-isomers very likely contribute to the absorptions in the relevant wavelength range. A direct comparison with the data obtained by ^1H NMR spectroscopy, which would be desirable in order to determine photoisomerisation quantum yields, was not feasible at the time: The irradiation conditions (and concentrations) in both experiments were different.

Nevertheless, it is evident from the UV-vis spectra that the conversion yield for the main chain AB units in the polymer compared to the azobenzene in free solution is essentially unaffected. This confirms that the isomerisation of the azobenzene functional units is not severely altered by their embedding into the polymer main chain. Accordingly, polymer **6** showed stable isomerisation yields for five cycles. Further quantitative evidence for a successful photoisomerisation in both environments is provided by the ^1H NMR spectra in *n*-hexane-*d*₁₄, THF-*d*₈ and CDCl₃ as solvents. These gave high *E* → *Z* conversion yields of 67%, 64%, and 46% for the model compound **5** in chloroform, THF and *n*-hexane, respectively. Matching values of 67% and 58% were also found for the polymer **6** in the relatively polar solvents chloroform and THF. In the non-polar *n*-hexane, irradiation with 365 nm light resulted in a conversion yield of 50% despite evidence for a photo-induced collapse of the polymer coil by the observed substantial line broadening (see below for a detailed discussion). Judged by the large number of chromophores in each polymer chain in combination with high conversion yields, polymer **6** is expected to show significant changes of its macroscopic properties in response to irradiation. The photostability of the reference compound **5** and the polymer **6** was proven by ^1H NMR measurements of five irradiation cycles in CDCl₃ (see ESI,† Fig. S3–S6).

Photo-induced size switching

The ^1H DOSY NMR data for the model azobenzene **5** show a smaller diffusion coefficient for the *Z*-isomer corresponding to a decrease in solvodynamic volume by $\approx 25\%$ on average. The decrease can be related qualitatively to the more globular shape of the *Z*-isomer that is evidenced by its smaller end-to-end distance of ≈ 0.6 nm compared to ≈ 0.9 nm for the more elongated *E*-isomer. Hence, according to the Perrin formulas⁵⁵ for the translational diffusion coefficients of prolate and oblate ellipsoids, a smaller solvodynamic volume for the *Z*-isomer is reasonable. An apparently contrasting behaviour has been observed for embedded azobenzenes in bulk polymers or on densely packed surfaces, where the more spherical shape of the *Z*-isomers caused a higher spatial demand.^{56–58} However, these findings rather reflect the free volume and efficient packing,

which depend on the details of the chromophore-matrix interactions, including chemical structure,⁵⁹ and are thus not directly related to the friction in solution.

The corresponding data for the polymer **6** indicates a photo-induced decrease in solvodynamic volume of 22% and 32% in THF and chloroform, respectively. In *n*-hexane, however, the solvodynamic volume shrinks to only $\approx 30\%$ of its initial size. The resulting small value of 40 nm³ and the extent of the collapse are consistent with a photo-induced transition from a solvated polymer coil to a globular non-solvated form. Indeed, a decrease in solubility, especially in non-polar solvents is reasonable if one considers the increased overall polarity of the polymer coils with higher *Z*-isomer content. This increased polarity arises from the significantly higher dipole moment of the *Z*-isomers (typically 3.1–4.0 D compared to 0–1.2 D for *E*-azobenzenes),^{57,58} and leads to a less favourable interaction between the polymer, which is now more polar, and the unpolar solvent. Taking the solvodynamic volume for the reference compound in *n*-hexane (see Table 1) and the degree of polymerisation of ≈ 130 as a basis, it can be concluded that in the PSS₃₆₅, the polymer coil is hardly solvated at all in *n*-hexane. These findings are in line with the strong broadening of the signals in the corresponding 1D ¹H NMR spectra observed in the PSS₃₆₅ with *n*-hexane as solvent (see Fig. 3). It cannot be excluded that the much smaller photo-induced decreases in solvodynamic volume in THF and chloroform stem from a lesser extent of solvation. However, considering that the dipole moment for the *Z*-isomers is higher than for the *E*-isomers, a decrease of solvation in the polar solvents THF and chloroform is unlikely. It is much more likely that the decrease in solvodynamic volume reflects the different coil topologies due to isomerisation. These observations are corroborated by the GPC data, where the decrease in apparent molecular weight was approximately 25%, which was consistent with the reduction of the solvodynamic volume by $\approx 22\%$ in THF in the PSS₃₆₅ observed in the ¹H DOSY NMR experiments.

Photo-induced ultrafast dynamics

The observed time-resolved transient absorption data summarised by the kinetic scheme (1) in the previous section provide detailed insight into the photo-induced dynamics of the AB reference molecule **5** and AB in the main chain of polymer **6** after S₂($\pi\pi^*$) excitation at $\lambda_{\text{exc}} = 320$ nm. In both cases, the observed dynamics conforms well to the case of unsubstituted azobenzene.^{14,23,25–27,42} The scheme suggests that the first step after excitation to the FC region of the S₂($\pi\pi^*$) state is an extremely fast internal conversion (IC) to the S₁($n\pi^*$) state with a time constant of $\tau_1 = 0.15$ ps. This is in excellent agreement with previously reported experimental S₂ lifetimes of 0.05–0.2 ps for free AB in solution.^{25–27,60,61} The subsequent bi-exponential decay of the population of vibrationally hot molecules formed in the S₁ state is characterised by a sub-picosecond time constant of $\tau_2 = 0.6$ ps (monomer) and $\tau_2 = 1.0$ ps (polymer), and a slower component of $\tau_3 = 5.3$ ps and 8.3 ps, respectively. This is only slightly slower than for the parent azobenzene, for which corresponding time constants of

$\tau_2 \approx 0.3$ – 0.5 ps and $\tau_3 \approx 2.3$ – 3.5 ps have been found.^{25,26,42,60,62} According to the currently accepted mechanistic interpretation, the vibrationally excited molecules in the S₁ state undergo either intramolecular vibrational relaxation (IVR) or electronic deactivation to the S₀ state *via* a competing non-reactive pathway, which both happen on the sub-picosecond time-scale in azobenzene.^{25,26} As the non-reactive pathway is not accessible *via* direct optical excitation, the scenario explains the observed lower quantum yields upon UV excitation compared to visible excitation.^{14,23,25,26} Indeed, the observed decrease in amplitude for the ESA and the apparent partial GSB recovery on that time scale might be interpreted in favour of the suggested competing non-reactive electronic deactivation pathway. As depicted in the kinetic scheme, time constant τ_3 corresponds to the time scale of the *E* → *Z* isomerisation that proceeds analogously to the reaction pathway found after direct S₁($n\pi^*$) excitation at visible wavelengths. Compared to unsubstituted free AB,^{14,23,25,60} slightly slower dynamics in the S₁ state are observed for the monomer **5**, possibly due to the fairly large siloxane substituents. It is remarkable that incorporation of the AB chromophore into the polymer chain in **6** then only leads to an increase by $\approx 60\%$ for both time constants compared to the monomer. This behaviour may be contrasted with results for S₁($n\pi^*$) excitation of an azobenzene covalently linked into the main chain of cross-linked polybutylmethacrylate particles in colloidal solution, where a more than 20-fold increase of the mean excited-state lifetime from $\tau = 3$ ps to $\tau = 65$ ps was observed for the most tightly (1:10) cross-linked particles.³² Likewise, a 10-fold increase of the excited-state lifetime for the *E*-isomer of an azobenzene encapsulated into a supramolecular host-guest complex compared to free chromophore in solution was observed upon excitation at 320 nm.⁴² In both cases, sterical hindrance and effective forces acting on the azobenzene moiety have been discussed to rationalize the observed significant changes in the photo-induced dynamics. Evidently, the *E* → *Z* isomerisation is barely hindered in the siloxane polymer **6** despite of the covalent linkage of the azobenzene into the main chain. It proceeds more or less undisturbed *via* unchanged excited-state pathways as for the monomer **5** and unsubstituted azobenzene in solution. Overall, the recorded transient absorption data thus provide a clear rationale for the observed high conversion yields by nearly unconstrained isomerisation reactions as for azobenzenes in solution.

Conclusions

A photo-responsive linear polymer with an exactly alternating sequence of azobenzenes as photochromic molecular switching units in the main chain linked by trisiloxanes was synthesised *via* a new synthetic route in very good yield and with high molecular weight ($M_n = 50.6$ kDa). The resulting poly(azobenzene-*alt*-trisiloxane) has an effective chromophore load of ≈ 45 wt% by design and contains on average ≈ 130 azobenzene units per polymer chain. Its photochemical properties and the photo-induced size switching in solution, which demonstrates the

potentially high intrinsic switching amplitudes, were studied by static UV-vis absorption spectroscopy, GPC, as well as 1D and 2D DOSY ^1H NMR experiments in several solvents. In addition, detailed insights into the underlying ultrafast photo-induced processes were obtained by femtosecond time-resolved transient absorption spectroscopy. In order to put these quantitative results into context, they were compared to a monomeric azobenzene siloxane derivative with analogous chemical structure as the repetition unit of the polymer. The spectroscopic characterisation shows efficient $E \rightarrow Z$ photoisomerisation reactions in both cases, leading to comparable high conversion yields of >50% in the photostationary states reached upon irradiation with 365 nm light. As a consequence, the solvodynamic volumes of the polymer decreased substantially already in the better solvents chloroform (32%) and THF (22%). In *n*-hexane however, a light-triggered reversible collapse of the solvated polymer coil lead to a globular non-solvated form with a 70% decrease in volume. These findings suggest that the isomerisation of the main chain azobenzene switches occurs essentially unhindered as in monomer analogue **5** in solution. Indeed, the ultrafast transient electronic absorption measurements showed that the incorporation of the azobenzene moiety into the highly flexible polymer backbone led only to a moderate slowdown ($\approx 60\%$) of the excited-state dynamics after excitation to the S_2 state in the UV compared to the monomer analogue, and proceeds on virtually identical reaction pathways conforming to the accepted scenario for azobenzene.^{14,23,25,26} In both cases, a sequential deactivation *via* ultrafast internal conversion to the S_1 state and subsequent electronic deactivation and isomerisation to the electronic ground state takes place. These results explain why high conversion yields comparable to the monomeric azobenzene reference molecule can be achieved also for the azobenzene-functionalised polymer. In addition, extended experiments were performed over several cycles of alternating irradiation in the UV and in the visible and proved the good photostability of the polymer. Due to its high chromophore load, perfectly regular structure and achievable high conversion yield, the new poly(azobenzene-*alt*-trisiloxane) should be an ideal candidate for various kinds of applications as photo-responsive functional material, in particular when large switching amplitudes are desired.

Conflicts of interest

There are no conflicts to declare.

Acknowledgements

This work was funded by the German Research Foundation (DFG) in the context of the Collaborative Research Centre 677 "Function by Switching", Projects A01 and C14. This research has been supported by the Institutional Strategy of the University of Bremen, funded by the German Excellence Initiative. D.P.S. thanks the EU COST Action CM 1302: Smart Inorganic Polymers.

Notes and references

- H. Bouas-Laurent and H. Dürr, *Pure Appl. Chem.*, 2001, 639–665.
- V. Balzani, A. Credi and M. Venturi, *Chem. Soc. Rev.*, 2009, 38, 1542–1550.
- M.-M. Russew and S. Hecht, *Adv. Mater.*, 2010, 22, 3348–3360.
- D. Bléger and S. Hecht, *Angew. Chem., Int. Ed.*, 2015, 54, 11338–11349.
- B. L. Feringa, *Angew. Chem., Int. Ed.*, 2018, 56, 11060–11078.
- A. S. Dvornikov, E. P. Walker and P. M. Rentzepis, *J. Phys. Chem. A*, 2009, 113, 13633–13644.
- M. Hoshino, E. Uchida, Y. Norikane, R. Azumi, S. Nozawa, A. Tomita, T. Sato, S. Adachi and S. Koshihara, *J. Am. Chem. Soc.*, 2014, 136, 9158–9164.
- H. Zhou, C. Xue, P. Weis, Y. Suzuki, S. Huang, K. Koynov, G. K. Auernhammer, R. Berger, H.-J. Butt and S. Wu, *Nat. Chem.*, 2017, 9, 145–151.
- O. S. Bushuyev, M. Aizawa, A. Shishido and C. J. Barrett, *Macromol. Rapid Commun.*, 2018, 39, 1700253.
- L. Dong, Y. Feng, L. Wang and W. Feng, *Chem. Soc. Rev.*, 2018, 47, 7339–7368.
- W. R. Browne and B. L. Feringa, *Annu. Rev. Phys. Chem.*, 2009, 60, 407–428.
- Q. Bian, W. Wang, G. Han, Y. Chen, S. Wang and G. Wang, *ChemPhysChem*, 2016, 17, 2503–2508.
- K. G. Yager and C. J. Barrett, *J. Photochem. Photobiol., A*, 2006, 182, 250–261.
- H. M. D. Bandara and S. C. Burdette, *Chem. Soc. Rev.*, 2012, 41, 1809–1825.
- R. Siewertsen, H. Neumann, B. Buchheim-Stehn, R. Herges, C. Näther, F. Renth and F. Temps, *J. Am. Chem. Soc.*, 2009, 131, 15594–15595.
- C. Eisenbach, *Ber. Bunsen-Ges.*, 1980, 84, 680–690.
- F. Ercole, T. P. Davis and R. A. Evans, *Polym. Chem.*, 2010, 1, 37–54.
- C. E. Evans and P. A. Lovell, *Chem. Commun.*, 2009, 2305–2307.
- M. Irie and T. Suzuki, *Makromol. Chem., Rapid Commun.*, 1987, 8, 607–610.
- M. R. di Nunzio, P. L. Gentili, A. Romani and G. Favaro, *J. Phys. Chem. C*, 2010, 114, 6123–6131.
- T. Gushiken, M. Saito, T. Ubukata and Y. Yokoyama, *Photochem. Photobiol. Sci.*, 2010, 9, 162–171.
- N. Ishii and J. Abe, *Appl. Phys. Lett.*, 2013, 102, 163301.
- T. Kumpulainen, B. Lang, A. Rosspointner and E. Vauthey, *Chem. Rev.*, 2017, 117, 10826–10939.
- C. García-Iriepa, M. Marazzi, L. M. Frutos and D. Sampedro, *RSC Adv.*, 2013, 3, 6241.
- M. Quick, A. L. Dobryakov, M. Gerecke, C. Richter, F. Berndt, I. N. Ioffe, A. A. Granovsky, R. Mahrwald, N. P. Ernsting and S. A. Kovalenko, *J. Phys. Chem. B*, 2014, 118, 8756–8771.
- A. Nenov, R. Borrego-Varillas, A. Oriana, L. Ganzer, F. Segatta, I. Conti, J. Segarra-Martí, J. Omachi, M. Dapor, S. Taioli, C. Manzoni, S. Mukamel, G. Cerullo and M. Garavelli, *J. Phys. Chem. Lett.*, 2018, 9, 1534–1541.

- 27 J. Casellas, M. J. Bearpark and M. Reguero, *ChemPhysChem*, 2016, **17**, 3068–3079.
- 28 Y.-C. Lu, E. W.-G. Diau and H. Rau, *J. Phys. Chem. A*, 2005, **109**, 2090–2099.
- 29 T. Pancur, F. Renth, F. Temps, B. Harbaum, A. Krüger, R. Herges and Chr. Näther, *Phys. Chem. Chem. Phys.*, 2005, **7**, 1985–1989.
- 30 R. Siewertsen, J. B. Schönborn, B. Hartke, F. Renth and F. Temps, *Phys. Chem. Chem. Phys.*, 2011, **13**, 1054–1063.
- 31 T. A. Singleton, K. S. Ramsay, M. M. Barsan, I. S. Butler and C. J. Barrett, *J. Phys. Chem. B*, 2012, **116**, 9860–9865.
- 32 J. Bahrenburg, F. Renth, F. Temps, F. Plamper and W. Richtering, *Phys. Chem. Chem. Phys.*, 2014, **16**, 11549–11554.
- 33 K. Röttger, S. Wang, F. Renth, J. Bahrenburg and F. Temps, *Appl. Phys. B: Lasers Opt.*, 2015, **118**, 185–193.
- 34 G. S. Kumar and D. C. Neckers, *Chem. Rev.*, 1989, **89**, 1915–1925.
- 35 C. J. Barrett, J. Mamiya, K. G. Yager and T. Ikeda, *Soft Matter*, 2007, **3**, 1249–1261.
- 36 P. Weis and S. Wu, *Macromol. Rapid Commun.*, 2018, **39**, 1700220.
- 37 R. A. Evans, T. L. Hanley, M. A. Skidmore, T. P. Davis, G. K. Such, L. H. Yee, G. E. Ball and D. A. Lewis, *Nat. Mater.*, 2005, **4**, 249–253.
- 38 W. Zhang, K. Yoshida, M. Fujiki and X. Zhu, *Macromolecules*, 2011, **44**, 5105–5111.
- 39 C. Appiah, G. Woltersdorf and W. H. Binder, *Polym. Chem.*, 2017, **8**, 2752–2763.
- 40 K. Wang, L. Yin, T. Miu, M. Liu, Y. Zhao, Y. Chen, N. Zhou, W. Zhang and X. Zhu, *Mater. Chem. Front.*, 2018, **2**, 1112–1118.
- 41 *Silicon-containing polymers: the science and technology of their synthesis and applications*, ed. R. G. Jones, A. Waturo and J. Chojnowski, Springer Science + Business, Dordrecht, Boston, London, 2000.
- 42 C. J. Otolski, A. Mohan Raj, V. Ramamurthy and C. G. Elles, *J. Phys. Chem. Lett.*, 2019, **10**, 121–127.
- 43 C.-C. Hsu, Y.-T. Wang, A. Yabushita, C.-W. Luo, Y.-N. Hsiao, S.-H. Lin and T. Kobayashi, *J. Phys. Chem. A*, 2011, **115**, 11508–11514.
- 44 J. Strueben, P. J. Gates and A. Staubitz, *J. Org. Chem.*, 2014, **79**, 1719–1728.
- 45 J. Strueben, M. Lipfert, J.-O. Springer, C. A. Gould, P. J. Gates, F. D. Sönnichsen and A. Staubitz, *Chem. – Eur. J.*, 2015, **21**, 11165–11173.
- 46 J. Strüben, J. Hoffmann, D. Presa-Soto, C. Näther and A. Staubitz, *Acta Crystallogr., Sect. E: Crystallogr. Commun.*, 2016, **72**, 1590–1594.
- 47 P. R. Dvornic and R. W. Lenz, *J. Appl. Polym. Sci.*, 1980, **25**, 641–652.
- 48 V. Passarelli, F. Benetollo, P. Zanella, G. Carta and G. Rossetto, *Dalton Trans.*, 2003, 1411–1418.
- 49 S. Koltzenburg, M. Maskos and O. Nuyken, *Polymer Chemistry*, Springer-Verlag, Berlin Heidelberg, 2017.
- 50 P. R. Dvornic and R. W. Lenz, *J. Polym. Sci., Polym. Chem. Ed.*, 1982, **20**, 951–966.
- 51 P. R. Dvornic, *Polym. Bull.*, 1992, **28**, 339–344.
- 52 J. F. Rabek, T. A. Skowronski and B. Rånby, *Polymer*, 1981, **21**, 226–229.
- 53 F. A. Bovey and P. A. Mirau, *NMR of polymers*, Academic Press, San Diego, 1996.
- 54 I. H. M. Van Stokkum, D. S. Larsen and R. Van Grondelle, *Biochim. Biophys. Acta*, 2004, **1657**, 82–104.
- 55 F. Perrin, *J. Phys. Radium*, 1936, **7**, 1–11.
- 56 S. Harms, K. Rätzke, C. Pakula, V. Zaporozhchenko, T. Strunskus, W. Egger, P. Sperr and F. Faupel, *J. Polym. Sci., Part B: Polym. Phys.*, 2011, **49**, 404–408.
- 57 Z. Mahimwalla, K. G. Yager, J. Mamiya, A. Shishido, A. Priimagi and C. J. Barrett, *Polym. Bull.*, 2012, **69**, 967–1006.
- 58 R. Klajn, *Pure Appl. Chem.*, 2010, **82**, 2247–2279.
- 59 T. Naito, K. Horie and I. Mita, *Polymer*, 1993, **34**, 4140–4145.
- 60 H. Satzger, C. Root and M. Braun, *J. Phys. Chem. A*, 2004, **108**, 6265–6271.
- 61 C. Xu, L. Yu, F. L. Gu and C. Zhu, *Phys. Chem. Chem. Phys.*, 2018, **20**, 23885–23897.
- 62 I. K. Lednev, T. Q. Ye, P. Matousek, M. Towrie, P. Fogg, F. V. R. Neuwahl, S. Umopathy, R. E. Hester and J. N. Moore, *Chem. Phys. Lett.*, 1998, **290**, 68–74.

2.2. A Potentially Cross-Linkable Linear Poly(Azobenzene-siloxane)

This manuscript was submitted to *Chemistry of Materials*: Mathias Schulz-Senft, Sindu Shree, Jan Strüben, Xin Jin, David Presa Soto, Rainer Adelung, Anne Staubitz, Reversible Volume Switching of a Poly(silazobenzyl-siloxane), *submitted to Chem. Mater.* **2019**.

Abstract

Poly(silazobenzyl-siloxane)s are novel polymers that contain azobenzene groups in the main chain, alternating with siloxane units. While the latter impart a low stiffness, high flexibility, and high endurance on the polymer, azobenzene units can reversibly photoisomerize from E to Z. There are examples in which this movement on a molecular level has been translated into a macroscopically observable movement (photomechanical effect). This work provides the first example of a photoswitchable, linear polysiloxane with azobenzene in the main chain as a repeating unit as opposed to the side chain that can still switch in the solid state. Most known examples of photomechanical azobenzene-based polymers require a liquid crystalline arrangement of the switching moieties. Poly(silazobenzyl-siloxane) is amorphous and we show a reversible height change of a polymer film of 4% without any alignment of the azobenzenes. This photoexpansion was monitored by atomic force microscopy (AFM) for four irradiation series.

Scientific Contribution to this Manuscript

I synthesized all used compounds. Jan Strueben and David Presa Soto established and optimized the synthesis of the molecules **48**, **49**, **50**, **52**, and **53**. I established the synthesis of polymer **55**, by adapting the procedure presented in section 2.1. I conducted the UV and GPC analyses in solution. Sindu Shree prepared the film and measured its properties by UV spectroscopy, profilometry and AFM.

Reversible Volume Switching of a Poly(silazobenzene-siloxane)

Mathias Schulz-Senft,^{‡1,2,3} Sindu Shree,^{‡4} Jan Strueben,¹ Xin Jin,⁴ David Presa Soto,¹ Ruchira A. Colaco,^{2,3} Rainer Adelung,^{*4} Anne Staubitz^{*1,2,3}

¹Otto-Diels-Institute for Organic Chemistry, University of Kiel, Otto-Hahn-Platz 4, 24098 Kiel (Germany), ²Institute for Organic and Analytical Chemistry, University of Bremen, Leobener Str. 7, 28359 Bremen (Germany), ³MAPEX Center for Materials and Processes, University of Bremen, Bibliothekstraße 1, 28359 Bremen (Germany), ⁴Institute for Materials Science, University of Kiel, Kaiserstr. 2, 24143 Kiel (Germany).

ABSTRACT: Poly(silazobenzene-siloxane)s are novel polymers that contain azobenzene groups in the main chain, alternating with siloxane units. While the latter impart a high flexibility on the polymer, azobenzene units can change their shape by reversibly photo isomerizing from *E* to *Z* geometry. Both chemical entities are chemically and thermally robust, which make them ideal for materials applications. This work provides the first example of a photoswitchable, linear polysiloxane with azobenzene in the main chain as a repeating unit (as opposed to the side chain) that can still switch in the solid state. Most known examples of photomechanical azobenzene-based polymers require a liquid crystalline arrangement of the switching moieties. However, poly(silazobenzyl-siloxane) is amorphous and we show a substantial, macroscopic reversible height change of a polymer film of ~4% without any alignment of the azobenzenes. This photo expansion was monitored by atom force microscopy (AFM) for four irradiation cycles.

Introduction

Azobenzene chromophores can undergo reversible light induced *E/Z* isomerization. The thermodynamically stable *E* form isomerizes to the *Z* form upon irradiation with UV light. The reverse reaction can be induced by irradiation with visible light, typically with a wavelength of ca. 440 nm.¹ This photo isomerization of the double bond in the azo group occurs at a high quantum yield (0.25 for unsubstituted azobenzene; up to 0.84 for electron rich azobenzenes)¹ with high fatigue resistance.² The isomerization is accompanied by changes in dipole moment (from 0 D to 3.1 D),³ spatial orientation (the *E* isomer is planar,⁴ the *Z* isomer shows a dihedral angle of 173.5° of the central C-N=N-C moiety),⁵ length (the distance between the 4 and 4' position reduces from 0.99 nm⁶ to 0.55 nm³). In addition, the volume of the *Z* isomer is increased compared to the *E* isomer (switching azobenzenes in polymer matrices reduces the free volume^{7,8}). Especially the spatial and volumetric changes require a sufficiently flexible environment for effective switching. Depending on which switching mechanism one assumes (torsion, inversion and hula twist), the isomerization of azobenzenes is estimated to require volumes between 0.12 nm³ and 0.38 nm³.⁹

The facile synthetic access^{10,11} to azobenzenes was used to incorporate these photoswitches into various polymeric environments.⁹ Although applications in solution are numerous, for example light activated self-healing polymers,^{12,13} crown ether based ions traps,^{14,15} and they have been discussed for drug delivery,¹⁶ applications in the solid state are very rare. An exception, in which polymers containing azobenzenes can show macroscopically visible responses to UV light illumination in the solid state is the photomechanical effect in liquid crystalline elastomers:⁹ In

these, the light energy can be translated into a visible deformation of a polymer film or fiber, which enables applications such as photo-actuators.¹⁷⁻²⁰ Photo-controlled movement requires liquid crystalline arrangements of azobenzenes, which are immobilized during polymerization.²¹ If not located in mesogenic phases, switching of polymeric azobenzenes may result in changes of the glass transition temperature T_g .^{12,22} As T_g is a decisive parameter of several physical properties of the polymer such as stiffness, elasticity, hardness etc., a change in T_g is accompanied by changing film volumes²³ and/or softening of surfaces.²⁴ Even without crossing above T_g , photoinduced switching of azobenzenes polymers affects the polymers' volumes. Generally, in amorphous polymers, polymer chain length is a determining factor of the extent of chain entanglement and this in turn determines how a polymer behaves at or above its T_g . Short polymer chains show low entanglements and the polymer flows at T_g . Long polymer chains show high entanglements which makes the agglomerated polymer to expand at T_g . This has been observed in amorphous azobenzene polymers as well, in which switching (*E*→*Z*) of azobenzene moieties caused an expansion of 1-5%.²⁵ Switching azobenzene in liquid crystalline polymers induces a contraction along the alignment direction of the mesogens.²⁵ The combination of both, photoinduced expansion and compression can be utilized in the development of photoactuators or artificial muscles. E.g. the flight muscles of insects show only a change in length by 1-2%.²⁶

Poly(siloxanes) are amongst the most industrially important elastomers. They possess an advantageous combination of low glass transition temperatures (as low as -120 °C),²⁷ thermal stability, and low surface tension.²⁸ This is required in applications such as medical implants, elec-

tric insulators, sealants, etc.^{29–31} The free volume of the polymers drastically increases at temperatures above their T_g .³² The Si-O bond shows low energy barriers for rotation (approx. 2.5 kJ/mol) and for linearization of the Si-O-Si angle (1.3 kJ/mol), leading to the very flexible polysiloxane chains.²⁸ This flexibility makes polysiloxanes suitable scaffolds to tailor switchable azobenzenes into the side chains of these polymers.^{33–45} However, we reasoned that siloxane linkers should provide sufficient flexibility to maintain the photoswitchability of the azobenzenes even in the backbone of polymers.

Above 200 °C, polysiloxanes degrade into shorter cyclic siloxanes, which can be suppressed by introducing aryl groups into the so-called poly(silylene-siloxanes) (PSAS) main chain.^{46–48} In comparison to the linear polysiloxanes, PSAS possess more rigid chain elements and thus show higher glass transition temperatures.⁴⁹ Substitution of every third dimethylsilane unit in poly(dimethylsiloxane) (PDMS) by a phenyl ring increased the T_g from -120 °C to -25 °C.⁵⁰ Elongating the resulting disiloxane bridge between the phenyl groups by one siloxane unit decreased the T_g to -63 °C, further elongation of the bridge reduced the effect of additional siloxane units.⁵⁰ Therefore, short siloxanes are promising linkers to provide a sufficiently low glass transition to allow the switching of azobenzenes in the polymer backbone at room temperature in the condensed state.

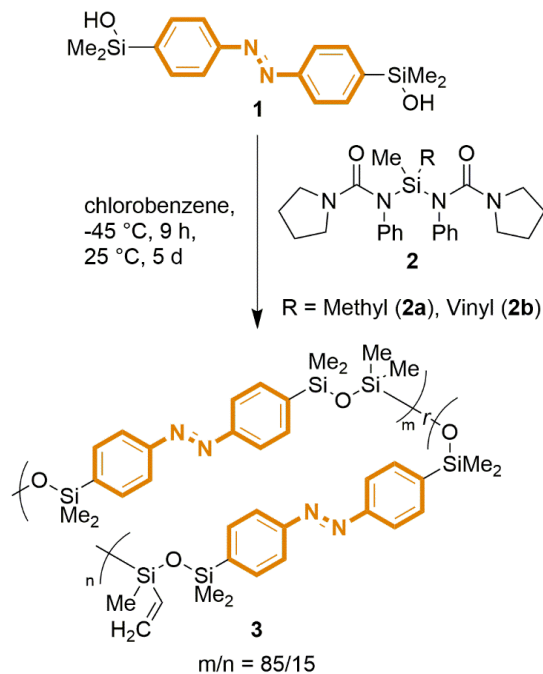
In this study, the advancement of linear alternating poly(silazobenzyl-siloxanes) is presented and the light induced switching of volume was investigated, specifically with the question whether a *macroscopically* measureable volume change was possible. Photo induced expansion of films of polyacrylate with azobenzene units in the side chains was measured before by ellipsometry, giving a reversible expansion effect of 3% upon laser irradiation.²³ However, to the best of our knowledge, this work is the first example of investigating the cyclic switching of such azobenzene-based polysiloxane films by AFM, with *main chain azobenzene* polymers.

Experimental Section

Materials

All used chemicals were purchased from Acros, Alfa Aesar, Grüssing, Merck and Sigma-Aldrich. Except for the dichlorosilanes, the chemicals were used without further purification. Dichlorodimethylsilane and dichloromethylvinylsilane were distilled from calcium hydride and were degassed before further use. Solvents and chemicals that were used in inert synthesis were dried (if not purchased anhydrous) and degassed prior to synthesis and stored under nitrogen either in J-Young glassware or a nitrogen filled glovebox from MBraun. Further details on the supplier of each chemical and solvent and the individual drying procedures are provided in the supporting information (SI).

Scheme 1. Synthesis of the poly(silazobenzyl-siloxane) 3 containing 15% vinyl functional groups by polycondensation.



Synthesis of the Polymer and its Precursors

Inert syntheses were carried out in nitrogen atmosphere using Schlenk techniques or inside a nitrogen filled glovebox. The cooling of inert syntheses was achieved by using a cooling block connected to a Julabo FP88 cryostat inside the glove box. Microwave assisted syntheses were performed on a Biotage Initiator+ SP Wave peptide synthesizer in the organic synthesis mode. A fixed hold time was turned off.

All synthesized air-stable precursors were characterized by melting points, IR and NMR (^1H , $^{13}\text{C}\{^1\text{H}\}$, $^{129}\text{Sn}\{^1\text{H}\}$, $^{29}\text{Si}\{^1\text{H}\}$) spectroscopy and high resolution mass spectrometry. The silane co-monomers **2a** and **2b** were too sensitive towards moisture to record more data than NMR spectra. NMR experiments were performed either on a Bruker Avance Neo 500 (^1H NMR: 500 MHz) or on a Bruker Avance II HD 600 (^1H NMR: 600 MHz) FT-NMR spectrometer at 300 K. and the assignment of peaks was performed with the help of two-dimensional NMR spectroscopy such as ^1H COSY, $^1\text{H}/^{13}\text{C}\{^1\text{H}\}$ HSQC, $^1\text{H}/^{13}\text{C}\{^1\text{H}\}$ HMBC or $^1\text{H}/^{29}\text{Si}\{^1\text{H}\}$ HMBC if possible. The spectra were referenced solvent residual proton signals (^1H) or the solvent itself (^{13}C , $^{129}\text{Sn}\{^1\text{H}\}$ and $^{29}\text{Si}\{^1\text{H}\}$ spectra were internally referenced against tetramethylsilane (TMS). Further details on the equipment used for analysis are provided in the supporting information.

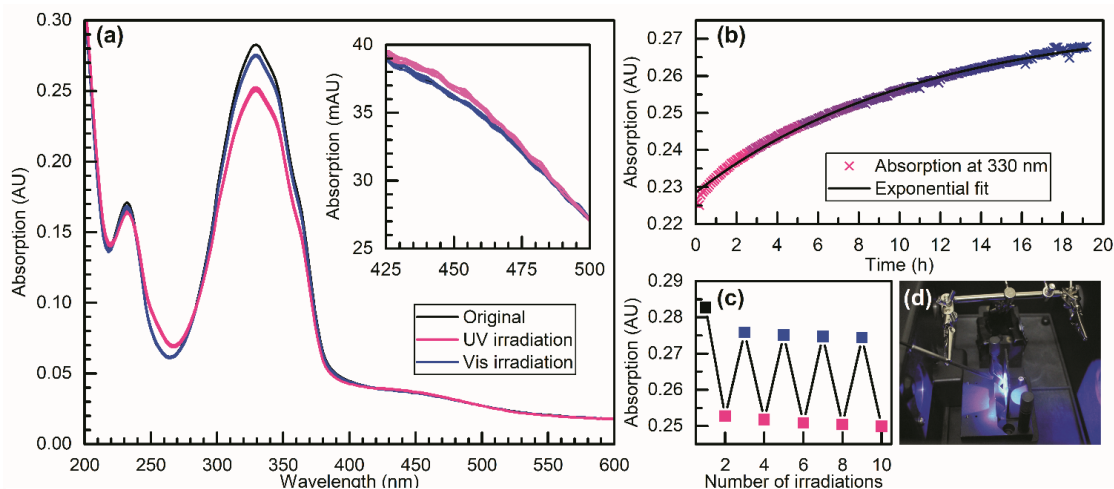


Figure 1. (a) Cyclic UV-visible spectra of polymer **3**. The thin film of **3** was irradiated with UV (365 nm) and blue (450 nm) back and forth for 5 cycles. Inset contains the zoomed-in spectra at the range of 425 – 500 nm. (b) Thermal relaxation after UV irradiation. The absorption at 330 nm was monitored in intervals of 5 minutes. Exponential fitting gave a half-life time of $7.37 \text{ h} \pm 9 \text{ min}$. (c) Shows stable cyclic behavior of **3** measured at 330 nm after every irradiation. (d) The measurement set-up for conducting UV-blue light irradiation before the UV-Visible spectrum was taken.

The polymer **3** was synthesized inside the glove box and analyzed by IR, NMR, UV-Visible spectroscopy and gel permeation chromatography (GPC) in solution. A film of **3** was investigated by AFM, profilometry and UV-Visible measurements.

Preparation of the Polymer Film

A film of the polymer **3** was prepared by spin coating onto a quartz substrate: A solution of **3** with a concentration of $214 \mu\text{M}$ in 10 mL THF was applied to a cleaned and dried quartz substrate in a spin coater at a rotational frequency of 2000 rpm. The polymer film was dried and stored in a desiccator at reduced pressure to remove residual solvent. Average surface roughness was determined to be $5.7 \text{ nm} \pm 0.5$ using AFM and the thickness was measured to be $110 \text{ nm} \pm 5$ by profilometry.

Thermal Analysis

The thermal properties of the polymer **3** were investigated by thermogravimetric analysis (TGA) and differential scanning calorimetry (DSC). TGA measurements were performed on a Mettler Toledo DSC 3/TGA+ STAR system using aluminum crucibles under a nitrogen flow of 20 mL/min and a temperature ramp of 10 K/min. DSC measurements were conducted on a Mettler Toledo DSC

3+ STAR system using aluminum crucibles under a nitrogen flow of 20 mL/min and a temperature ramp of 20 K/min.

The polymer **3** proved to be of remarkable thermal stability. While no weight loss was observed for temperatures below $320 \text{ }^\circ\text{C}$, the sample started to slowly lose weight with increasing temperatures. The onset temperature of the degradation was determined to be $376 \text{ }^\circ\text{C}$. At $500 \text{ }^\circ\text{C}$, the sample had lost almost 25% of its original weight. The glass transition was determined to occur at $17.1 \text{ }^\circ\text{C}$.¹

Irradiation Equipment

The irradiation experiments of solutions of **3** were carried out using LED light sources by Sahlmann Photochemical Solutions with an optical power of 1000 mW (365 nm) and 900 mW (450 nm). The distance between the light source and sample was 10 mm with horizontal alignment of the light source. Irradiation of the film for AFM and UV-Visible measurements was achieved using the fiber-coupled LEDs M365FP1 (365 nm, 15.5 mW) and M455F3 (455 nm, 24.5 mW) from Thorlabs with an angle of 30° .

In this work, we use the terms “UV light” and “blue light” to refer to the nominal peak wavelengths of the irradiation

¹ While it was attempted to obtain a T_g for the switched polymer, this was not feasible: In order to record a strong enough signal, the polymer film in the crucible was too thick for the

irradiation to switch throughout the sample. Switching in solution and evaporating the solvent was deemed unreliable as it is known that even small solvent impurities may lower the T_g .

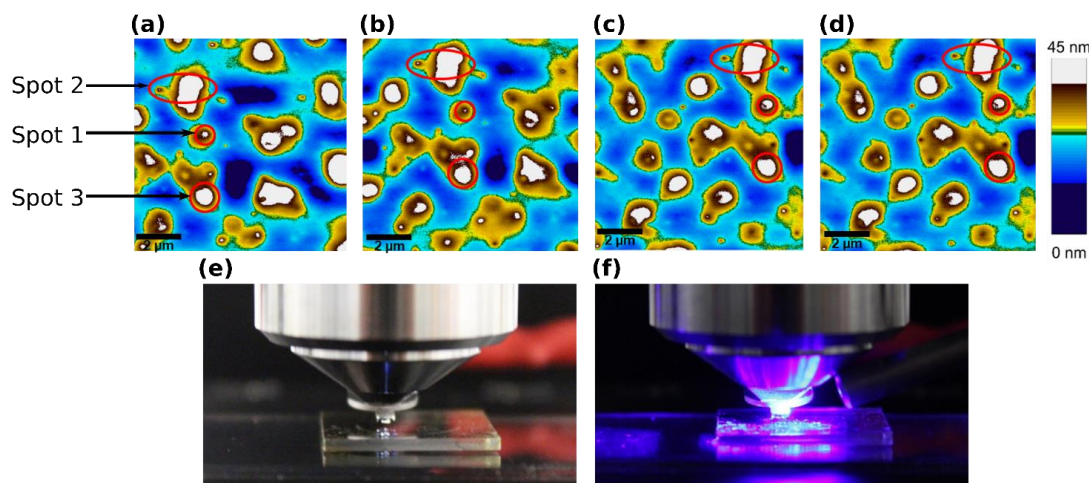


Figure 2. AFM topographical scans of the thin films of **3** coated on a quartz substrate. Each scan was acquired after 20 min of irradiation. (a) Surface scan after 1st UV light irradiation, (b) Surface scan after 1st blue light irradiation, (c) Surface scan after 2nd UV light irradiation and (d) Surface scan after 2nd UV light irradiation. Marked spots in the images are the common areas used for height measurement. On the far right is the scale bar representing the color profile of all scans. (d) Setup of the environmental AFM, with the probe head and tip on top of the quartz substrate with the polymer film. (e) Direct irradiation of the polymer film on the quartz substrate without removing the probe head.

equipment, 365 nm and 450 nm, respectively. The term “visible light” also refers to 450 nm.

UV-Visible Measurements

UV-Visible spectra of the film of polymer **3** were recorded in absorption mode in a Perkin Elmer Lambda 900 spectrometer. Spectra were recorded before and after irradiation with UV and blue light for five switching cycles. After the final UV irradiation, the thermal relaxation was followed by recording spectra every five minutes over the course of 19 hours. The according half-life time was determined using an exponential fit of the increase of the absorption at 330 nm over time.

In solution, the UV-Visible were recorded at 25 °C using a Perkin Elmer Lambda 14 UV-Visible spectrometer. Quartz cuvettes with a light path length of 10 mm from Hellma Analytics were used. The polymer was measured before and after irradiation with UV and visible light. To investigate the thermal relaxation after irradiation with UV light, repetitive measurements were performed every 15 minutes over the course of 40 hours. The half-life time of the relaxation was determined by an exponential fit of the increase of the absorption at 330 nm over time. Spectra of these measurements are provided in the supporting information.

AFM Measurements

Topographical AFM imaging were conducted resonance under the WITec RA 300 microscope with an Asylum cantilever with 2 Nm⁻¹, 70 kHz. To avoid damaging the thin film, the scans were performed in tapping mode, scanning an area of 100 μm². For this purpose, films of the polymer on quartz glass were irradiated with UV light (365 nm)

without retracting the AFM probe (Figure 1 (e and f)). Thus, it was possible to track the same area throughout the irradiation cycles. The obtained surface maps (Figure 1 (a-d)) still reveal a slight drift between the irradiation cycles. After four irradiations, the drift was too large for a comparative analysis. Within this area, the height profile of three distinctive spots was monitored.

The series of AFM surface scans started after irradiation with UV light, followed by alternating irradiation with blue light and UV light.

GPC Measurements

Gel permeation chromatography was performed on a Viscotek GPC max VE2001 equipped with a Viscotek VE3580 RI detector and a column set of LT5000 and LT4000 in THF (VWR, HPLC-grade) with a flow rate of 1 mL/min. Conventional calibration and analysis was done with OmniSEC 4.6.2 software using polystyrene standards. The number average molecular weight (M_n) and the weight average molecular weight (M_w) were determined and used to derive the poly dispersity index (PDI).

For analyzing the switching of **3**, the solution was irradiated with UV light for one hour. Again, M_n , M_w and the PDI were determined.

Results & Discussion

Synthesis of the Poly(silazobenzyl-siloxane) **3**

The polymer **3** was obtained via a polycondensation reaction using the azobenzyl hydroxysilane **1** and two urea derivatives **2a,b** as monomers (Scheme 1.). The synthesis of the azobenzene derivative **1** was reported previously by

us.⁵³ In order to investigate the influence of modifications of the backbone on the materials' behaviour, two urea functionalized silanes **2** that were to serve as co-monomers were also synthesized.⁵² While the compound **2a** connects two azobenzene monomers via a SiMe₂ unit, compound **2b** introduces a vinyl group into the backbone of polymer **3**. The bis(ureido)silanes **2** were added simultaneously to a solution of the azobenzene **1** at -45 °C, thus statistically distributing the vinyl moieties throughout the polymer.² The polymerization was monitored via GPC. After 8 d, the polymer was obtained with a M_n of 14.4 kDa, M_w of 23.3 kDa (corresponding to a polydispersity index (PDI) = 1.62). The number of repeating units bearing vinyl groups was determined by NMR spectroscopy to be 15%. Synthetic details of the polymerization, as well as of the synthetic routes to the monomers **1** and **2** are included in the supporting information, accompanied by their respective NMR spectra.

Analysis of the Switching in Film and Solution by UV-vis Spectroscopy

To investigate whether the azobenzene moieties were able to switch in the polymer film of **3**, a thin film (thickness = 110 ± 5 nm) was analyzed by UV-vis spectroscopy in transmission mode. Upon irradiation with UV light (365 nm), the absorption of the ππ* band at 330 nm decreased by 10%, whereas the change of the nπ* band at 450 nm was barely notable (Figure 1). This development of *Z* azobenzene could be reversed by irradiation with blue light (450 nm). After five cycles, the polymer film showed no signs of photodegradation (Figure 1(c)). The thermal relaxation after irradiation with UV light was monitored at intervals of five minutes over the course of 19 hours. For determination of the half-life time, the absorption at the ππ* band at 330 nm was plotted and an exponential fit was applied. The half-life time was 7:37 h ± 9 min (Figure 1(b)).

The UV-vis results of the film were complemented by UV-vis spectroscopy in solution. A solution of the polymer in THF was subjected to UV (365 nm) and visible light (450 nm). The measurements revealed under UV light irradiation a reduction of the ππ* band at 330 nm by approx. two thirds, which was fully reversible upon irradiation with blue light (450 nm). The half-life time of the thermal relaxation reaction was determined to be 21 h ± 18 min (see Supporting Information, Figure SI-4).

Thus, the thermal isomerization from *Z* to *E* azobenzene moieties was ca. 3 times faster in the film compared to solution. This behavior was unexpected and unusual. We hypothesize that this may be explained by the local environment of the switched azobenzene units in the film: Switching of azobenzene moieties to their *Z* states leads to a chain

contraction. However, contrary to the solution state, the remaining polymer chain cannot easily follow this movement as it is constrained by the surrounding film. Thus, mechanical energy builds up and favors relaxation in the mechanically unstrained *E*-state.

Moreover, the isomerization reaction of azobenzene units from their *E*- to the *Z*-isomer requires a flexible environment and a larger free volume than that taken up by the individual isomers.⁵³ Even in glassy polymers, the photoswitching of azobenzene increases the free volume.^{7,54} The resulting change in glass transition can lead to so-called photo-fluidity.²⁴ The larger space around the switched azobenzene units facilitates the thermal back reaction compared to the reaction in solution, where the change of the free volume during switching is immediately filled up with solvent molecules.^{55,56}

Measuring the Volume Switching of the Film by AFM

The photo-elastic behavior of the polymer **3** was tested by atomic force microscopy (AFM) in tapping mode, scanning an area of 100 μm². For this purpose, films of the polymer on quartz glass were irradiated with UV light (365 nm) without retracting the AFM probe. Thus, it was possible to track the same area throughout the irradiation cycles. The obtained surface maps (Figure 2) still revealed a slight drift between the irradiation cycles, however, four irradiation sequences could be measured and compared. Within this area, the height profile of three distinctive spots was monitored. From the height profiles and calculated relative height differences of spot 1 (Figure 3(a) and (b)) maximum height variations of 4 nm were observed. With a film thickness of ~110 nm, this translates to a thickness change of ~114 nm which corresponds to a volume change of 1.6 volume %. The series of AFM areal surface scans started after irradiation with UV light, followed by alternating irradiation with blue light and UV light. The film's height measured after UV light irradiation is significantly higher than after blue light irradiation. Compared to the initial UV irradiated state, the film height decreased throughout the common areas measured. The second irradiation sequence confirms the reversibility of the switching, partially leading to larger effects. In all three spots (Figure 3), the maximum height changed by 1 – 4 nm per cycle. These findings are consistent with other studies that prove a higher spatial demand for *Z*-azobenzene moieties in polymer films.^{8,57,58} The height profiles of spots 2 and 3 are provided in the Supporting Information, Figure SI-3 and SI-4.

² As a vinyl group is not expected to change the electrophilicity of the Si center by much, similar reaction kinetics were assumed for both monomers.

Measuring the Volume Switching of the Solution by GPC

The switching could also be monitored by GPC. A solution of **3** in THF was measured before and after UV irradiation and the apparent molecular weights were determined after calibration against polystyrene. Upon irradiation with UV light, the apparent molecular weight decreased from 14.4 to 11.8 kDa (M_n) and 23.3 to 19.9 kDa (M_w), corresponding to a reduction by 18% (M_n) and 15% (M_w), respectively. This observed decrease in the apparent molecular weight might appear contradictory to the increase in volume of the film that was determined by AFM measurements. However, the intrinsic helicity of *Z* azobenzenes facilitates the formation of dense coils, as we have recently investigated in depth.⁵¹ The GPC elugram and the weight distribution are shown in the Supporting Information, Figure SI-1.

Conclusion

In solution, a decrease in apparent molecular weight of 15 (M_w) to 18% (M_n) was determined by GPC analysis. The polymer was thermally stable up to 400 °C. Despite the two phenyl rings in the main chain per repeating unit, the glass transition occurred below room temperature at 18.4 °C. This results from the highly flexible trisiloxane units that connect the azobenzene moieties. Due to this highly flexible linkers, the azobenzenes' photoswitching could also be

observed in a film of **3**. UV-vis measurements in THF confirmed successful switching and the thermal half-life time of the back switching to be 21 h was observed.

A method of investigating a spin-coated film of the polymer throughout two irradiation cycles was successfully established under AFM. These measurements revealed a reversible height variation of the film by 10% and a 4% reversible film expansion. UV-Visible spectroscopy of the film showed the switching of a minority of the azobenzene units in the polymer backbone, while thermal relaxation occurs with a half-life time of approx. 7.5 hours. The film's photostability was proven by cyclic irradiations with UV and blue light, giving no evidence of degradation.

The presented study proves the potential of the photoswitchable polymer system. Though the azobenzene units are located in the backbone of the polymer, linked by only trisiloxane bridges, it was possible to reversibly induce a photo expansion without any signs of degradation. In the further development of these systems, the effect of cross-linking will be investigated.

ASSOCIATED CONTENT

Supporting Information. This material is available free of charge via the Internet at <http://pubs.acs.org>. Detailed list of used chemicals, solvents and equipment; synthetic details of **1**, **2a**, **2b**, **3** and their precursors; GPC and UV-vis (solution) spectra of **3**; ^1H , $^{13}\text{C}\{^1\text{H}\}$, $^{129}\text{Sn}\{^1\text{H}\}$ and $^{29}\text{Si}\{^1\text{H}\}$

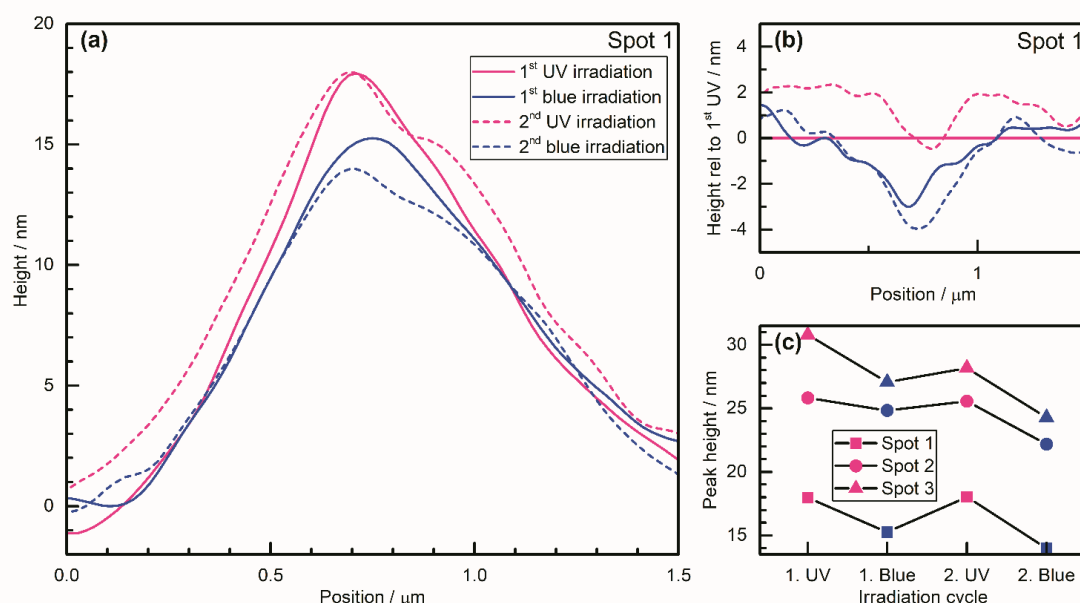


Figure 3. (a) Height profile of Spot 1 after the four irradiation stages. (b) Height differences relative to the 1st UV irradiation. (c) Maximum height values of all three spots after the four irradiation stages.

NMR spectra of all synthesized compounds; AFM height profiles of Spot 1, Spot 2 and Spot 3. TGA and DSC (3 cycles) traces of the polymer 3

AUTHOR INFORMATION

Corresponding Author

* Rainer Adelung, ra@tf.uni-kiel.de

* Anne Staubitz, staubitz@uni-bremen.de

Author Contributions

A. S. and R. A. conceived and supervised the project. J. S. and D. P. S. established the synthesis of monomers. M. S.-S. optimized the synthesis of monomers and polymers and conducted NMR, GPC, UV-vis (solution) and MS analyses of all compounds. S.S. carried out AFM and UV-Visible (thin film) measurements. M.S.-S., S.S. and A.S. wrote the manuscript and all authors have given approval to the final version of the manuscript. / ‡These authors contributed equally.

Notes

The authors declare no competing financial interests.

ACKNOWLEDGMENT

This work was funded by the German Research Foundation (DFG) in the context of the Collaborative Research Center 677 "Function by Switching", Project C14. This research has been supported by the Institutional Strategy of the University of Bremen, funded by the German Excellence Initiative. D.P.S. thanks the EU COST Action CM 1302: Smart Inorganic Polymers.

ABBREVIATIONS

AFM – Atomic force microscopy

DSC – Differential scanning calorimetry

GPC – Gel permeation chromatography

PDI – Polydispersity index

PDMS – Poly(dimethylsiloxane)

PSAS – Poly(silylene-siloxane)

TGA – Thermogravimetric analysis

REFERENCES

- (1) Bandara, H. M. D.; Burdette, S. C. Photoisomerization in Different Classes of Azobenzene. *Chem. Soc. Rev.* **2012**, *41* (5), 1809–1825. <https://doi.org/10.1039/C1CS15179G>.
- (2) Venkataramani, S.; Jana, U.; Dommaschk, M.; Sönnichsen, F. D.; Tucek, F.; Herges, R. Magnetic Bistability of Molecules in Homogeneous Solution at Room Temperature. *Science* **2011**, *331* (6016), 445–448. <https://doi.org/10.1126/science.1201180>.
- (3) Hartley, G. S. The Cis-Form of Azobenzene. *Nature* **1937**, *140*, 281.
- (4) Harada, J.; Ogawa, K.; Tomoda, S. Molecular Motion and Conformational Interconversion of Azobenzenes in Crystals as Studied by X-Ray Diffraction. *Acta Crystallogr. B* **1997**, *53* (4), 662–672. <https://doi.org/10.1107/S0108768197002772>.
- (5) Mostad, A.; Rømming, C. A Refinement of the Crystal Structure of Cis-Azobenzene. *Acta Chem. Scand.* **1971**, *25*, 3561–3568.
- (6) Brown, C. J. A Refinement of the Crystal Structure of Azobenzene. *Acta Crystallogr.* **1966**, *21* (1), 146–152. <https://doi.org/10.1107/S0365110X66002445>.
- (7) Naito, T.; Horie, K.; Mita, I. Photochemistry in Polymer Solids: 12. Effects of Main-Chain Structures and Formation of Hydrogen Bonds on Photoisomerization of Azobenzene in Various Polymer Films. *Polymer* **1993**, *34* (19), 4140–4145. [https://doi.org/10.1016/0032-3861\(93\)90680-9](https://doi.org/10.1016/0032-3861(93)90680-9).
- (8) Harms, S.; Rätzke, K.; Pakula, C.; Zaporojtchenko, V.; Strunskus, T.; Egger, W.; Sperr, P.; Faupel, F. Free Volume Changes on Optical Switching in Azobenzene-Polymethylmethacrylate Blends Studied by a Pulsed Low-Energy Positron Beam. *J. Polym. Sci. Part B Polym. Phys.* **2011**, *49* (6), 404–408. <https://doi.org/10.1002/polb.22201>.
- (9) Bushuyev, O. S.; Aizawa, M.; Shishido, A.; Barrett, C. J. Shape-Shifting Azo Dye Polymers: Towards Sunlight-Driven Molecular Devices. *Macromol. Rapid Commun.* **2018**, *39* (1), 1700253. <https://doi.org/10.1002/marc.201700253>.
- (10) García-Iriepa, C.; Marazzi, M.; Frutos, L. M.; Sampedro, D. E/Z Photochemical Switches: Syntheses, Properties and Applications. *RSC Adv.* **2013**, *3* (18), 6241. <https://doi.org/10.1039/c2ra22363e>.
- (11) Strueben, J.; Lipfert, M.; Springer, J.-O.; Gould, C. A.; Gates, P. J.; Sönnichsen, F. D.; Staubitz, A. High-Yield Lithiation of Azobenzenes by Tin-Lithium Exchange. *Chem. – Eur. J.* **2015**, *21* (31), 1165–1173. <https://doi.org/10.1002/chem.201500003>.
- (12) Weis, P.; Tian, W.; Wu, S. Photoinduced Liquefaction of Azobenzene-Containing Polymers. *Chem. – Eur. J.* **2018**, *24* (25), 6494–6505. <https://doi.org/10.1002/chem.201704162>.
- (13) Wang, C.; Fadeev, M.; Zhang, J.; Vázquez-González, M.; Davidson-Rozenfeld, G.; Tian, H.; Willner, I. Shape-Memory and Self-Healing Functions of DNA-Based Carboxymethyl Cellulose Hydrogels Driven by Chemical or Light Triggers. *Chem. Sci.* **2018**, *9* (35), 7145–7152. <https://doi.org/10.1039/C8SC02411A>.
- (14) Shinkai, S.; Nakaji, T.; Nishida, Y.; Ogawa, T.; Manabe, O. Photoresponsive Crown Ethers. 1. Cis-Trans Isomerism of Azobenzene as a Tool to Enforce Conformational Changes of Crown Ethers and Polymers. *J. Am. Chem. Soc.* **1980**, *102* (18), 5860–5865. <https://doi.org/10.1021/ja00538a026>.
- (15) Janus, K.; Sworakowski, J. Photochromism of Crown Ethers with Incorporated Azobenzene Moiety. *J. Phys. Chem. B* **2005**, *109* (1), 93–101. <https://doi.org/10.1021/jp0483268>.
- (16) Eom, T.; Yoo, W.; Kim, S.; Khan, A. Biologically Activatable Azobenzene Polymers Targeted at Drug Delivery and Imaging Applications. *Biomaterials* **2018**, *185*, 333–347. <https://doi.org/10.1016/j.biomaterials.2018.09.020>.
- (17) Nie, J.; Liu, X.; Yan, Y.; Zhang, H. Supramolecular Hydrogen-Bonded Photodriven Actuators Based on an Azobenzene-Containing Main-Chain Liquid Crystalline Poly(Ester-Amide). *J. Mater. Chem. C* **2017**, *5* (39), 10391–10398. <https://doi.org/10.1039/C7TC02943H>.
- (18) Xiong, Y.; Zhang, L.; Weis, P.; Naumov, P.; Wu, S. A Solar Actuator Based on Hydrogen-Bonded Azopolymers for Electricity Generation. *J. Mater. Chem. A* **2018**, *6* (8), 3361–3366. <https://doi.org/10.1039/C7TA1139H>.
- (19) Kizilkan, E.; Strueben, J.; Jin, X.; Schaber, C. F.; Adelung, R.; Staubitz, A.; Gorb, S. N. Influence of the Porosity on the Photoresponse of a Liquid Crystal Elastomer. *R. Soc. Open Sci.* **2016**, *3* (4), 150700. <https://doi.org/10.1098/rsos.150700>.
- (20) Kizilkan, E.; Strueben, J.; Staubitz, A.; Gorb, S. N. Bioinspired Photocontrollable Microstructured Transport Device. *Sci. Robot.* **2017**, *2* (2), eaak9454. <https://doi.org/10.1126/scirobotics.aak9454>.

- (21) Ikeda, T.; Nakano, M.; Yu, Y.; Tsutsumi, O.; Kanazawa, A. Anisotropic Bending and Unbending Behavior of Azobenzene Liquid-Crystalline Gels by Light Exposure. *Adv. Mater.* **2003**, *15* (3), 201–205. <https://doi.org/10.1002/adma.200390045>.
- (22) Zhou, H.; Xue, C.; Weis, P.; Suzuki, Y.; Huang, S.; Koynov, K.; Auernhammer, G. K.; Berger, R.; Butt, H.-J.; Wu, S. Photoswitching of Glass Transition Temperatures of Azobenzene-Containing Polymers Induces Reversible Solid-to-Liquid Transitions. *Nat. Chem.* **2017**, *9* (2), 145–151. <https://doi.org/10.1038/nchem.2625>.
- (23) Tanchak, O. M.; Barrett, C. J. Light-Induced Reversible Volume Changes in Thin Films of Azo Polymers: The Photomechanical Effect. *Macromolecules* **2005**, *38* (25), 10566–10570. <https://doi.org/10.1021/ma051564w>.
- (24) Karageorgiev, P.; Neher, D.; Schulz, B.; Stiller, B.; Pitsch, U.; Giersig, M.; Brehmer, L. From Anisotropic Photo-Fluidity towards Nanomanipulation in the Optical near-Field. *Nat. Mater.* **2005**, *4* (9), 699–703. <https://doi.org/10.1038/nmat1459>.
- (25) Barrett, C. J.; Mamiya, J.; Yager, K. G.; Ikeda, T. Photo-Mechanical Effects in Azobenzene-Containing Soft Materials. *Soft Matter* **2007**, *3*, 1249–1261.
- (26) Josephson, R. K. Comparative Physiology of Insect Flight Muscle. In *Nature's Versatile Engine: Insect Flight Muscle Inside and Out*; Vigoreaux, J. O., Ed.; Molecular Biology Intelligence Unit; Springer US: Boston, MA, 2006; pp 34–43. https://doi.org/10.1007/0-387-31213-7_3.
- (27) *Polymer Data Handbook*; Mark, J. E., Ed.; Oxford University Press: Oxford, 1999.
- (28) *Silicon-Containing Polymers: The Science and Technology of Their Synthesis and Applications*; Jones, R. G., Waturo, A., Chojnowski, J., Eds.; Springer Science+Business: Dordrecht; Boston; London, 2000.
- (29) Moretto, H.-H.; Schulze, M.; Wagner, G. Silicones. In *Ullmann's Encyclopedia of Industrial Chemistry*; Wiley-VCH Verlag GmbH & Co. KGaA, Ed.; Wiley-VCH Verlag GmbH & Co. KGaA: Weinheim, Germany, 2000. <https://doi.org/10.1002/14356007.a24.057>.
- (30) Chandrasekar, V. *Inorganic and Organometallic Polymers*; Springer Verlag: Berlin Heidelberg, 2005.
- (31) Mark, J. E.; Allcock, H. R.; West, R. *Inorganic Polymers*, Second Edition.; Oxford University Press: Oxford, New York, 2005.
- (32) White, R. P.; Lipson, J. E. G. Polymer Free Volume and Its Connection to the Glass Transition. *Macromolecules* **2016**, *49* (11), 3987–4007. <https://doi.org/10.1021/acs.macromol.6b00215>.
- (33) Ohm, C.; Brehmer, M.; Zentel, R. Liquid Crystalline Elastomers as Actuators and Sensors. *Adv. Mater.* **2010**, *22* (31), 3366–3387. <https://doi.org/10.1002/adma.200904059>.
- (34) Miller, L. S.; Walton, D. J.; Stone, P. J. W.; McRoberts, A. M.; Sethi, R. S. Langmuir-Blodgett Films for Nonlinear Optical Applications. *J. Mater. Sci. Mater. Electron.* **1994**, *5* (2), 75–82. <https://doi.org/10.1007/BF00187116>.
- (35) Miller, L. S.; McRoberts, A. M.; Walton, D. J.; Parry, D. A.; Newton, A. L. Optical Gas Sensing Using Langmuir-Blodgett Films. *Mater. Sci. Eng. C* **1995**, *3* (3), 257–262. [https://doi.org/10.1016/0928-4931\(95\)00084-4](https://doi.org/10.1016/0928-4931(95)00084-4).
- (36) Öge, T.; Zentel, R. Manipulation of the Ferroelectricity in LC Polymers via Photomechanical Isomerization of Azobenzene Moieties. *Macromol. Chem. Phys.* **1996**, *197* (6), 1805–1813. <https://doi.org/10.1002/macp.1996.021970602>.
- (37) Cviklinski, J.; Tajbakhsh, A. R.; Terentjev, E. M. UV Isomerisation in Nematic Elastomers as a Route to Photo-Mechanical Transducer. *Eur. Phys. J. E* **2002**, *9* (1), 427–434. <https://doi.org/10.1140/epje/i2002-10095-y>.
- (38) Liu, X.; Cai, M.; Liang, Y.; Zhou, F.; Liu, W. Photo-Regulated Stick-Slip Switch of Water Droplet Mobility. *Soft Matter* **2011**, *7* (7), 3331–3336. <https://doi.org/10.1039/C0SM01144D>.
- (39) Guo, S.; Sugawara-Narutaki, A.; Okubo, T.; Shimojima, A. Synthesis of Ordered Photoresponsive Azobenzene-Siloxane Hybrids by Self-Assembly. *J. Mater. Chem. C* **2013**, *1* (42), 6989–6995. <https://doi.org/10.1039/C3TC30587B>.
- (40) Wen, H.; Zhang, W.; Weng, Y.; Hu, Z. Photomechanical Bending of Linear Azobenzene Polymer. *RSC Adv.* **2014**, *4* (23), 11776–11781. <https://doi.org/10.1039/C3RA48035F>.
- (41) Garcia-Amorós, J.; Martínez, M.; Finkelmann, H.; Velasco, D. Photoactuation and Thermal Isomerisation Mechanism of Cyanoazobenzene-Based Liquid Crystalline Elastomers. *Phys. Chem. Chem. Phys.* **2014**, *16* (8), 8448–8454. <https://doi.org/10.1039/C4CP00446A>.
- (42) Guo, S.; Chaikittisilp, W.; Okubo, T.; Shimojima, A. Azobenzene-Siloxane Hybrids with Lamellar Structures from Bridge-Type Alkoxysilyl Precursors. *RSC Adv.* **2014**, *4* (48), 25319–25325. <https://doi.org/10.1039/C4RA01709A>.
- (43) Finkelmann, H.; Nishikawa, E.; Pereira, G. G.; Warner, M. A New Opto-Mechanical Effect in Solids. *Phys. Rev. Lett.* **2001**, *87* (1), 015501. <https://doi.org/10.1039/PhysRevLett.87.015501>.
- (44) Garcia-Amorós, J.; Finkelmann, H.; Velasco, D. Influence of the Photo-Active Azo Cross-Linker Spacer on the Opto-Mechanics of Polysiloxane Elastomer Actuators. *J. Mater. Chem.* **2011**, *21* (4), 1094–1101. <https://doi.org/10.1039/C0JM02502J>.
- (45) Camacho-Lopez, M.; Finkelmann, H.; Palfy-Muhoray, P.; Shelley, M. Fast Liquid-Crystal Elastomer Swims into the Dark. *Nat. Mater.* **2004**, *3* (5), 307–310. <https://doi.org/10.1038/nmat1118>.
- (46) Dvornic, P. R.; Lenz, R. W. Exactly Alternating Silarylene-Siloxane Polymers: 6. Thermal Stability and Degradation Behaviour. *Polymer* **1983**, *24* (6), 763–768. [https://doi.org/10.1016/0032-3861\(83\)90016-2](https://doi.org/10.1016/0032-3861(83)90016-2).
- (47) Dvornic, P. R.; Perpall, H. J.; Uden, P. C.; Lenz, R. W. Exactly Alternating Silarylene-Siloxane Polymers. VII. Thermal Stability and Degradation Behavior of p-Silphenylene-Siloxane Polymers with Methyl, Vinyl, Hydrido, and/or Fluoroalkyl Side Groups. *J. Polym. Sci. Part Polym. Chem.* **1989**, *27* (10), 3503–3514. <https://doi.org/10.1002/pola.1989.080271027>.
- (48) Chen, X.; Cui, Y.; Yin, G.; Liao, L. Thermooxidative Degradation Behavior of Poly(Silphenylene-Siloxane)s. *J. Appl. Polym. Sci.* **2010**, *117* (2), 926–933. <https://doi.org/10.1002/app.31429>.
- (49) *Inorganic Polymeric Nanocomposites and Membranes*; Becker, O., Ed.; Advances in polymer science; Springer: Berlin; New York, 2005.
- (50) Dvornic, P. R.; Lenz, R. W. Exactly Alternating Silarylene-Siloxane Polymers. 9. Relationships between Polymer Structure and Glass Transition Temperature. *Macromolecules* **1992**, *25* (14), 3769–3778. <https://doi.org/10.1021/ma00040a024>.
- (51) Schulz-Senft, M.; Bank, D.; Strube, J.; Presa-Soto, D.; Sönnichsen, F. D.; Renth, F.; Temps, F.; Staubit, A. Efficient Photoisomerisation and Size Switching in a Strictly Alternating Main-Chain Azobenzene-Trisiloxane Polymer with 45wt% Chromophore Load Rationalised by Ultrafast Dynamics. *Submit. J Mater Chem C* **2019**.
- (52) Dvornic, P. R.; Lenz, R. W. Exactly Alternating Silarylene-Siloxane Polymers. II. The Condensation Polymerization of Arylenedisilanol and Bisureidosilanes. *J. Polym. Sci. Polym. Chem. Ed.* **1982**, *20* (4), 951–966. <https://doi.org/10.1002/pol.1982.170200405>.
- (53) Singleton, T. A.; Ramsay, K. S.; Barsan, M. M.; Butler, I. S.; Barrett, C. J. Azobenzene Photoisomerization under High Ex-

ternal Pressures: Testing the Strength of a Light-Activated Molecular Muscle. *J. Phys. Chem. B* **2012**, *116* (32), 9860–9865. <https://doi.org/10.1021/jp3060872>.

(54) Vapaavuori, J.; Laventure, A.; Bazuin, C. G.; Lebel, O.; Pellerin, C. Submolecular Plasticization Induced by Photons in Azobenzene Materials. *J. Am. Chem. Soc.* **2015**, *137* (42), 13510–13517. <https://doi.org/10.1021/jacs.5b06611>.

(55) Airinei, A.; Rusu, E.; Barboiu, V. Responsive Behavior of 4-(N-Maleimido)Azobenzene in Polymers with Aromatic Main Chain and Side Chain Linked Units. *J. Braz. Chem. Soc.* **2010**, *21* (3), 489–495. <https://doi.org/10.1590/S0103-50532010000300014>.

(56) Grebenkin, S.; Meshalkin, A. B. Wavelength Dependence of the Reorientation Efficiency of Azo Dyes in Polymer Matrices. *J. Phys. Chem. B* **2017**, *121* (35), 8377–8384. <https://doi.org/10.1021/acs.jpcc.7b03171>.

(57) Yager, K. G.; Tanchak, O. M.; Godbout, C.; Fritzsche, H.; Barrett, C. J. Photomechanical Effects in Azo-Polymers Studied by Neutron Reflectometry. *Macromolecules* **2006**, *39* (26), 9311–9319. <https://doi.org/10.1021/ma0617320>.

(58) Yager, K. G.; Barrett, C. J. Photomechanical Surface Patterning in Azo-Polymer Materials. *Macromolecules* **2006**, *39* (26), 9320–9326. <https://doi.org/10.1021/ma061733s>.

3. A Macrocyclic Azobenzene-Siloxane Dimer

3.1. Background

By incorporation of azobenzenes into macrocycles, the photoisomerization of azobenzenes can be used to switch the functionality of the cycles.^[116,241,242] Bridging crown ethers with azobenzenes or azopyridines^[243] leads to photoswitching of the cryptands' ion binding capacities.^[243–246] Direct incorporation of azobenzenes into the macrocycle of cryptands resulted in photoswitchable pore sizes, again affecting the ion binding capacities.^[246–250] Similarly, the cavity size of calixarenes can be influenced by switching azobenzenes that are attached to or incorporated in the calixarene cone.^[251,252] Other examples of azobenzene units in macrocycles involve the incorporation a poly(*N*-isopropylacrylamide) (PNIPAM) chain that formed a rotaxane with cyclodextrin and was subsequently closed to form a catenane^[253] or the usage as photoswitching unit in carbohydrate-based macrocycles.^[254] The secondary structure of peptides can be switched by azobenzenes as side chains connecting two amino acids in the peptide sequence.^[255,256]

In all these examples, the azobenzene is a minor part of a flexible larger ring or ring system. Therefore, the photoinduced (*E*)→(*Z*) isomerization and the thermal (*Z*)→(*E*) isomerization occur as usually expected for non-cyclic azobenzenes.^[242,257,258]

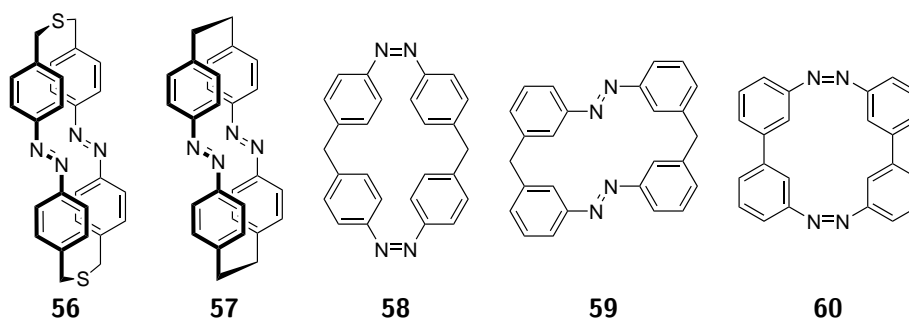


Figure III.1. Examples of azobenzophane dimers with short linkers. With shorter linkers, the ring strain increases. The stability of the switched form decreases in the *para* substituted dimers from **56**^[193] to **57**,^[259] while **58** shows reversed stability and fast thermal relaxation.^[260,261] Linked at the *meta*-positions, **59** is stable in the (*E*),(*E*)-form,^[262] whereas **60** demonstrated reversed stability.^[263] Both are photoswitchable.

Oligoazobenzophanes are cyclic oligomers of azobenzene units connected by short linkers.^[116,241,242] While some examples of trimers^[264–274] or tetramers^[267,271,272,274] were published, dimeric azobenzophanes^[193,259–263,266–268,271–277] have drawn more attention. In these relatively small cycles, the resulting ring strain alters the isomerization behavior.^[241] This effect can be illustrated with cyclic dimers that are connected at the azobenzenes' 4- and

4'-positions. The dimer **56** with dimethylene sulfide linkers can be switched by irradiation with UV light to its (Z),(Z)-isomer, which thermally isomerizes to the (E),(E)-isomer.^[193] The half-life time of the (Z),(Z)→(E),(Z) isomerization was determined to be ca. 5 d, the (E),(Z)→(E),(E) proceeds with a half-life time of 6.25 min.^[193] Shorter ethyl linkers in **57** lead to decreased half-life times of 42.5 h and 15 s for the (Z),(Z)→(E),(Z) and (E),(Z)→(E),(E) isomerization, respectively.^[259] Further reduction of the linker length to one methyl group results in reversed stabilities. The (Z),(Z)-isomer of **58** is thermodynamically stable and appeared not photoswitchable.^[260] However, the photoisomerization could later be proven, but the ring strains force the (E),(E)-isomer to switch back within milliseconds.^[261] In contrast, a linkage in the 3- and 3'-positions (*meta* to the azo group) does not result in reversed stability for a dimer linked by methyl groups.^[262] The dimer **59** undergoes photoisomerization and the thermal back reaction shows half-life times of 20 d and 6 d for (Z),(Z)→(E),(Z) and (E),(Z)→(E),(E) isomerization, respectively. Due to the smaller ring strain in dimers based on *meta* functionalized azobenzene, the directly linked dimer **60** can be synthesized. Again, the (Z),(Z)-configuration is thermodynamically stable, but can be switched to the (E),(E)-configuration.^[263]

Independent which isomer ((E),(E) or (Z),(Z)) is thermodynamically stable, the initial thermal isomerization from the PSS to the mixed (E),(Z)-intermediate is significantly slower than the subsequent relaxation to the thermodynamically stable isomer.^[241] With a half-life time of the (Z),(Z)-isomer of up to 400 d,^[277] azobenzophanes with short linkers are virtually bistable systems that can be utilized in long-term data storages.^[273] However, the thermal back reaction does not follow first order kinetics in films.^[273]

In addition to these basic designs, macrocycles with azocarbazoles were synthesized, leading to a visible colorchange upon photoswitching.^[278,279] It was also possible to synthesize a macrocycle containing one azobenzene and two dihydroazulene units retaining their individual switchability.^[280]

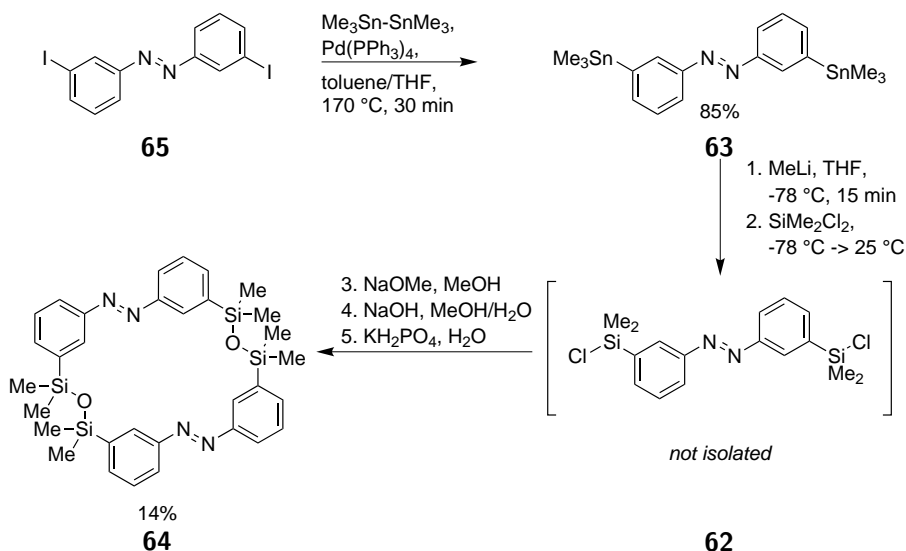
As presented in the previous chapters, short siloxane units possess the flexibility that is required to ensure efficient switching of azobenzenes in constrained polymeric environments. It is therefore feasible that an azobenzophane with siloxane linkers between the azobenzene moieties maintains the photoswitching properties of non-cyclic azobenzenes.

3.2. Synthesis & Properties

The Synthetic Route towards azobenzene bearing silanol groups was presented in chapter 2. The crucial step includes a tin-lithium-silicon exchange that yields an intermediate bis(chlorodimethylsilane)azobenzene (*para*: **61**, *meta*: **62**) that undergoes a controlled hydrolysis to the silanol **48**.^[115]

As discussed in Part I, subsection 1.2.4, the condensation of chlorosilanes to silanols is highly pH sensitive. The hydrochloric acid formed during the hydrolysis catalyzes condensation of the silanols to cyclic and linear oligomers and polymers.^[89,281] This consecutive reaction also occurs in aromatic silanes. The direct hydrolysis of chlorodimethylphenylsilane

with equimolar amounts of water yields a 1:1 mixture of chlorosilane and hydroxysilane after 20 s.^[282] In order to circumvent the condensation and isolate silanols in high yields, the hydrolysis can be carried out at the interface of two-phase ether/water systems^[283] or initial nucleophilic displacement of the chloride by methoxide, with subsequent cleavage of the ether bond.^[284] As presented in chapter 2, it was possible to synthesize the monomer **48** with hydroxysilane groups following this route.^[115] In contrast, applying the optimized hydrolysis procedure to 3,3'-bis(trimethylstannyl)azobenzene (**63**) yielded the diazobenzophane **64**.



Scheme III.5 Synthetic route to yield the cyclophane dimer **64**. Reported yield in the synthesis of **63**:^[114] 70%.

Analogous to the synthetic route to yield the silanol **48**, the synthesis of the cyclophane **64** commences from 3-iodoaniline (see Scheme III.5, details in Part V, chapter 7). It reacted in an oxidative azo coupling to the iodo azobenzene **65** with a yield of 68%. Stannylation via a Stille-Kelly coupling gave 3,3'-bis(trimethylstannyl)azobenzene **63** in a yield of 85%. The combined yield with 58% over two reactions was almost doubled in respect to the procedure that was established by Jan Strüben.^[114] Under strictly inert atmosphere, the tin-lithium exchange followed by quenching with dichlorodimethylsilane to the intermediate **62** was conducted. Due to the moisture sensitivity of **62**, it was not isolated, but subjected to a controlled hydrolysis. After removal of the solvent and excess of the quenching agent, the residue was re-dissolved in THF and slowly added to a solution of sodium methoxide in methanol. The methoxysilyl ether was cleaved in by sodium hydroxide in methanol/water and the final dehydration was carried out in monopotassium phosphate buffer. The azobenzene cyclophane **64** was isolated in a yield of 14% and a crystal structure of the (*E*),(*E*)-isomer could be obtained. The reaction conditions of the hydrolysis and subsequent dehydration were further optimized by Melanie Walther in the context of a MSc. Thesis to increase the yield to 24%.^[285]

The Photoswitching Behavior of the azobenzophane **64** was investigated using UV light (340 nm) to induce (*E*)→(*Z*) isomerization. ¹H NMR spectra proved the presence of solely (*E*),(*E*)-isomer **64a** under ambient conditions in THF-*d*₈ (See Part V, chapter 7). The UV spectrum (Figure III.2 a) of the (*E*),(*E*)-isomer **64a** in *n*-hexane featured a strong $\pi\pi^*$ band with a maximum at 318 nm and two shoulders at 336 nm and 352 nm, respectively. The $n\pi^*$ transition showed a maximum at 440 nm. After irradiation with UV light (340 nm) for 30 min, the $\pi\pi^*$ absorption decreased while the maximum underwent a hypsochromic shift to 286 nm. The $n\pi^*$ absorption increased upon irradiation with UV light. NMR spectroscopy confirmed that the PSS after irradiation with UV light (340 nm) contained 100% (*Z*),(*Z*)-isomer **64c**.^[285] The corresponding ¹H, ¹³C{¹H} and ²⁹Si{¹H} NMR spectra are shown in Part V, subsection 7.4.3, starting on page 404.

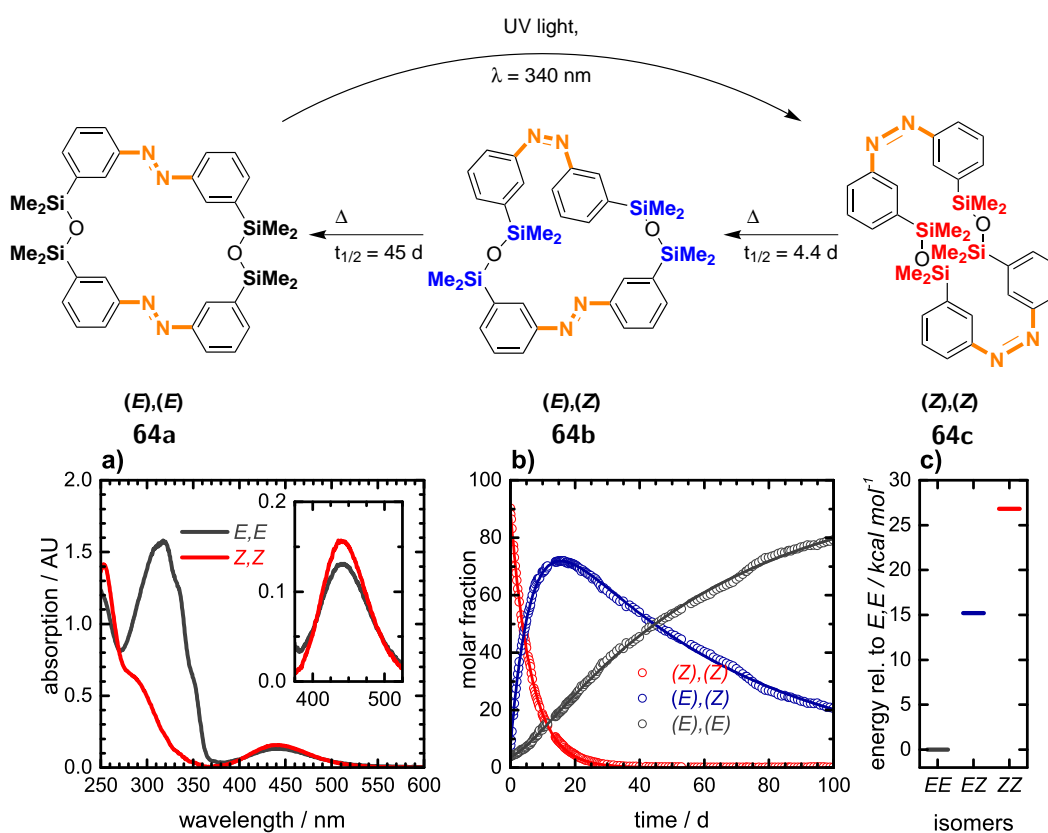


Figure III.2. Switching of the azobenzene cyclophane **64**. Top: Irradiation with UV light (340 nm) switches the (*E*),(*E*)-isomer **64a** to the (*Z*),(*Z*)-isomer **64c**. Thermal relaxation proceeds via the (*E*),(*Z*)-isomer **64b**. The dimethyl silyl groups are colored corresponding to their representation in the spectra a) and b). **a)** Absorption spectra of **64a** (black) and **64c** (red) in *n*-hexane. **b)** Thermal decay of **64c** (red) to **64b** (blue) with consecutive isomerization to **64a** (black) in THF-*d*₈. Circles represent the molar fractions as determined by ¹H NMR spectroscopy, lines represent the fitting curves. **c)** Difference of the ground state energies of the (*E*),(*E*)- (**64a**), (*E*),(*Z*)- (**64b**) and (*Z*),(*Z*)- (**64c**) isomers compared to **64a**.

The thermal back switching was investigated by ^1H NMR spectroscopy (see Figure III.2 b) and Figure III.3). The signals in the aliphatic region were assigned to the three switching states (E),(E) (**64a**), (E),(Z) (**64b**) and (Z),(Z) (**64c**) (see Part V, 404). The integrals of the dimethylsilyl groups were tracked over the course of 100 d. The progression of the corresponding molar fractions is shown in Figure III.2 b) and reveals the expected consecutive reaction (Z),(Z) \rightarrow (E),(Z) \rightarrow (E),(E). Exponential fitting provided the decay constants $\tau_1 = 4.4$ d for the initial decay (Z),(Z) \rightarrow (E),(Z) and $\tau_2 = 45$ d for the consecutive reaction (E),(Z) \rightarrow (E),(E). The evolution of the signals corresponding to the three switching states (Z),(Z) **64c**, (E),(Z) **64b**, and (E),(E) **64a** at ten different decay times is shown in Figure III.3.

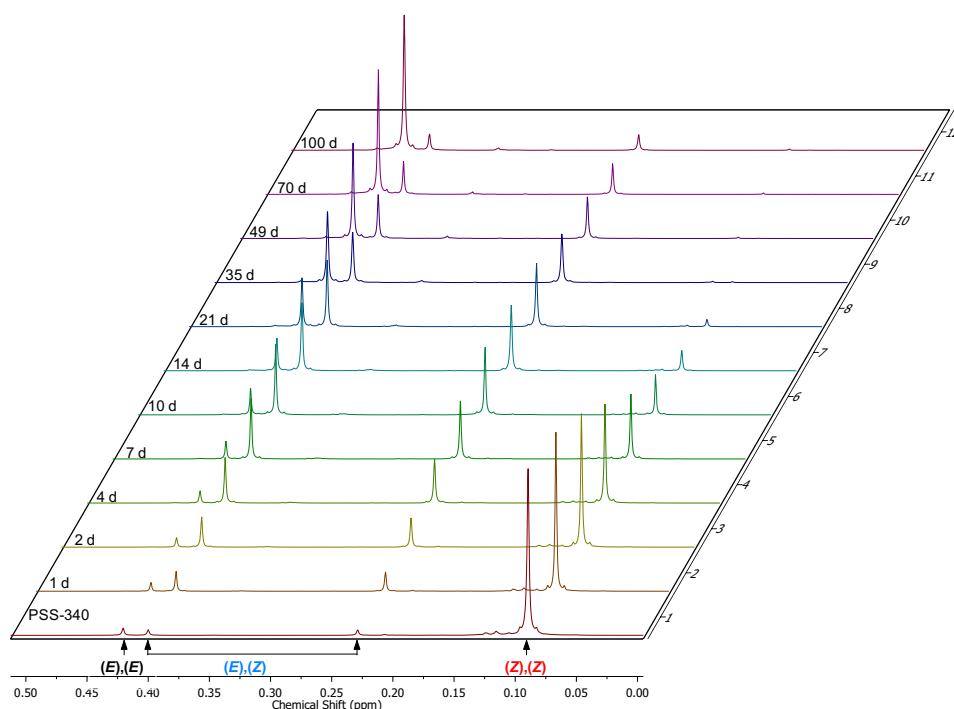


Figure III.3. Evolution of the SiMe_2 signals in the ^1H NMR spectra of the azobenzene cyclophane **64** after irradiation with UV light (340 nm). The signal corresponding to the (Z),(Z)-isomer decayed within 21 d, the two signals of the (E),(Z)-isomer pass a maximum at approximately the same time.

The PSS that contains only the (Z),(Z)-isomer **64c** proved the superior flexibility of the siloxane groups that enable quantitative isomerization of the azo groups. Still, the ring strain in **64** hindered the thermal relaxation. The first (Z) \rightarrow (E) isomerization showed a decay constant of 4.4 d, which is approximately four times longer than the relaxation of the (Z)-azobenzene units in the polymer **54** (see chapter 2). Opposed to the reported examples of other azobenzophanes,^[116,241,242] the intermediate (E),(Z)-isomer **64b** was significantly more stable than **64c** and decayed approximately ten times slower.

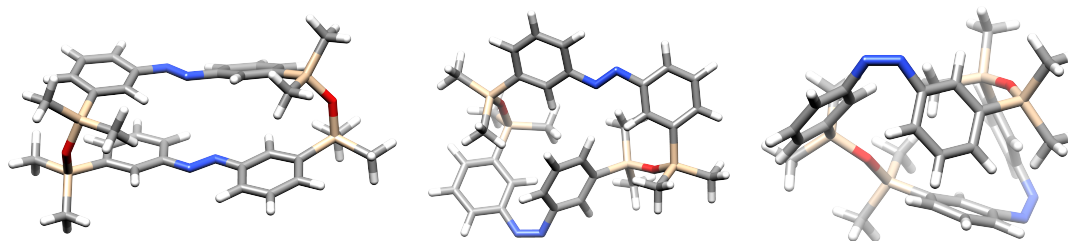


Figure III.4. DFT optimized structures of the switching states (*E*),(*E*) (left), (*E*),(*Z*) (left), and (*Z*),(*Z*) (right) of the azobenzene cyclophane **64**.

The stability of the three isomers **64a–c** was investigated by DFT modeling. The geometries and frequencies of the isomers were optimized at the B3LYP/6-311G* level of theory (see Figure III.4). Detailed results are presented in Part V section 7.3, starting on page 391. Comparison of the zero-point energy corrected energy (E_{ZPE}) revealed an increase in energy of $15.2 \text{ kcal mol}^{-1}$ in **64b** and of $26.8 \text{ kcal mol}^{-1}$ in **64c** compared to **64a**. The differences in energy were in the expected range, the (*E*)-isomer in unhindered azobenzenes is typically ca. 12 kcal mol^{-1} more stable than the (*Z*)-isomer.^[286] Recurrently, these findings prove an independent switching of both azobenzene moieties. An increased energy of the mixed isomer **64b** compared to both other isomers **64a,c** would be expected in case of bistable switching behavior as reported for the systems **56** and **60**.^[116]

Bibliography of Part III

- [10] E. Merino, *Chem. Soc. Rev.* **2011**, *40*, 3835–3853.
- [11] H. M. D. Bandara, S. C. Burdette, *Chem. Soc. Rev.* **2012**, *41*, 1809–1825.
- [89] W. Noll, *Chemistry and Technology of Silicones*, Academic Press, New York, **1968**.
- [107] C. J. Brown, *Acta Crystallogr.* **1966**, *21*, 146–152.
- [108] A. Mostad, C. Rømming, *Acta Chem. Scand.* **1971**, *25*, 3561–3568.
- [112] S. Venkataramani, U. Jana, M. Dommaschk, F. D. Sönnichsen, F. Tuczek, R. Herges, *Science* **2011**, *331*, 445–448.
- [114] J. Strueben, PhD thesis, Christian-Albrechts-Universität, Kiel, **2015**.
- [115] J. Strüben, J. Hoffmann, D. Presa-Soto, C. Näther, A. Staubitz, *Acta Crystallogr. Sect. E: Crystallogr. Commun.* **2016**, *72*, 1590–1594.
- [116] R. Reuter, H. A. Wegner, *Chem. Commun.* **2011**, *47*, 12267–12276.
- [185] *Industrial Dyes: Chemistry, Properties, Applications*, (Ed.: K. Hunger), Wiley-VCH, Weinheim, **2003**.
- [186] G. S. Hartley, *Nature* **1937**, *140*, 281.
- [187] J. Henzl, M. Mehlhorn, H. Gawronski, K.-H. Rieder, K. Morgenstern, *Angew. Chem. Int. Ed.* **2006**, *45*, 603–606.
- [188] K. Scheil, T. G. Gopakumar, J. Bahrenburg, F. Temps, R. J. Maurer, K. Reuter, R. Berndt, *J. Phys. Chem. Lett.* **2016**, *7*, 2080–2084.
- [189] T. Kumpulainen, B. Lang, A. Rosspeintner, E. Vauthey, *Chem. Rev.* **2017**, *117*, 10826–10939.
- [190] J. Harada, K. Ogawa, S. Tomoda, *Acta Crystallogr. Sect. B: Struct. Sci.* **1997**, *53*, 662–672.
- [191] G. S. Hartley, R. J. W. L. Fèvre, *J. Chem. Soc.* **1939**, *0*, 531–535.
- [192] M. Quick, A. L. Dobryakov, M. Gerecke, C. Richter, F. Berndt, I. N. Ioffe, A. A. Granovsky, R. Mahrwald, N. P. Ernsting, S. A. Kovalenko, *J. Phys. Chem. B* **2014**, *118*, 8756–8771.
- [193] H. Rau, E. Lüddecke, *J. Am. Chem. Soc.* **1982**, *104*, 1616–1620.
- [194] H. Rau, S. Yu-Quan, *J. Photochem. Photobiol. A* **1988**, *42*, 321–327.
- [195] Y.-C. Lu, E. W.-G. Diau, H. Rau, *J. Phys. Chem. A* **2005**, *109*, 2090–2099.

- [196] T. Pancur, F. Renth, F. Temps, B. Harbaum, A. Krüger, R. Herges, C. Näther, *Phys. Chem. Chem. Phys.* **2005**, *7*, 1985–1989.
- [197] R. Siewertsen, J. B. Schönborn, B. Hartke, F. Renth, F. Temps, *Phys. Chem. Chem. Phys.* **2011**, *13*, 1054–1063.
- [198] T. A. Singleton, K. S. Ramsay, M. M. Barsan, I. S. Butler, C. J. Barrett, *J. Phys. Chem. B* **2012**, *116*, 9860–9865.
- [199] R. S. H. Liu, G. S. Hammond, *Proc. Natl. Acad. Sci. U. S. A.* **2000**, *97*, 11153–11158.
- [200] C.-W. Jiang, R.-H. Xie, F.-L. Li, R. E. Allen, *The Journal of Physical Chemistry A* **2011**, *115*, 244–249.
- [201] M. Böckmann, N. L. Doltsinis, D. Marx, *The Journal of Chemical Physics* **2012**, *137*, 22A505.
- [202] B. Ortiz, P. Villanueva, F. Walls, *J. Org. Chem.* **1972**, *37*, 2748–2750.
- [203] H. Firouzabadi, B. Vessal, M. Naderi, *Tetrahedron Lett.* **1982**, *23*, 1847–1850.
- [204] R. Thorwirth, F. Bernhardt, A. Stolle, B. Ondruschka, J. Asghari, *Chem. Eur. J.* **2010**, *16*, 13236–13242.
- [205] H. K. Hombrecher, K. Lüdtkke, *Tetrahedron* **1993**, *49*, 9489–9494.
- [206] J. Hoffmann, T. Kuczmera, E. Lork, A. Staubitz, *Molecules* **2019**, *24*, 303.
- [207] E. Baer, A. L. Tosoni, *J. Am. Chem. Soc.* **1956**, *78*, 2857–2858.
- [208] K. Müller, J. Wadhwa, J. S. Malhi, L. Schöttner, A. Welle, H. Schwartz, D. Hermann, U. Ruschewitz, L. Heinke, *Chem. Commun.* **2017**, *53*, 8070–8073.
- [209] K. H. Pausacker, *J. Chem. Soc.* **1953**, 1989–1990.
- [210] K. Monir, M. Ghosh, S. Mishra, A. Majee, A. Hajra, *Eur. J. Org. Chem.* **2014**, 1096–1102.
- [211] K. Kinoshita, *Bull. Chem. Soc. Jpn.* **1959**, *32*, 783–787.
- [212] J. Strueben, P. J. Gates, A. Staubitz, *J. Org. Chem.* **2014**, *79*, 1719–1728.
- [213] J. Strueben, M. Lipfert, J.-O. Springer, C. A. Gould, P. J. Gates, F. D. Sönnichsen, A. Staubitz, *Chem. - Eur. J.* **2015**, *21*, 11165–11173.
- [214] S. Hiroto, *Chem. - Asian J.* **2019**, 10.1002/asia.201900213.
- [215] R. F. Nystrom, W. G. Brown, *J. Am. Chem. Soc.* **1948**, *70*, 3738–3740.
- [216] M. L. Di Gioia, A. Leggio, I. F. Guarino, V. Leotta, E. Romio, A. Liguori, *Tetrahedron Lett.* **2015**, *56*, 5341–5344.
- [217] R. O. Hutchins, D. W. Lamson, L. Rua, C. Milewski, B. Maryanoff, *J. Org. Chem.* **1971**, *36*, 803–806.
- [218] K. Pothula, L. Tang, Z. Zha, Z. Wang, *RSC Adv.* **2015**, *5*, 83144–83148.
- [219] W.-h. Wei, T. Tomohiro, M. Kodaka, H. Okuno, *J. Org. Chem.* **2000**, *65*, 8979–8987.

- [220] L. Wang, H. Neumann, M. Beller, *Angew. Chem. Int. Ed.* **2019**, *58*, 5417–5421.
- [221] A. Khan, S. Hecht, *Chem. - Eur. J.* **2006**, *12*, 4764–4774.
- [222] W. Moormann, D. Langbehn, R. Herges, *Synthesis* **2017**, *49*, 3471–3475.
- [223] X. Chi, W. Cen, J. A. Queenan, L. Long, V. M. Lynch, N. M. Khashab, J. L. Sessler, *J. Am. Chem. Soc.* **2019**, *141*, 6468–6472.
- [224] D. Formenti, F. Ferretti, F. K. Scharnagl, M. Beller, *Chem. Rev.* **2019**, *119*, 2611–2680.
- [225] I. Szele, H. Zollinger in *Preparative Organic Chemistry*, Topics in Current Chemistry, Springer, Berlin Heidelberg, **1983**, pp. 1–66.
- [226] A. Tsuge, T. Moriguchi, S. Mataka, M. Tashiro, *J. Chem. Soc. Perkin Trans. 1* **1993**, 2211–2215.
- [227] J. Y. Kim, G. Kim, C. R. Kim, S. H. Lee, J. H. Lee, J. S. Kim, *J. Org. Chem.* **2003**, *68*, 1933–1937.
- [228] C. A. Hunter, L. D. Sarson, *Tetrahedron Lett.* **1996**, *37*, 699–702.
- [229] C. Schütt, G. Heitmann, T. Wendler, B. Krahwinkel, R. Herges, *J. Org. Chem.* **2016**, *81*, 1206–1215.
- [230] G. Heitmann, C. Schütt, R. Herges, *Eur. J. Org. Chem.* **2016**, *2016*, 3817–3823.
- [231] M. H. Davey, V. Y. Lee, R. D. Miller, T. J. Marks, *J. Org. Chem.* **1999**, *64*, 4976–4979.
- [232] I. D. Entwistle, T. Gilkerson, R. A. Johnstone, R. P. Telford, *Tetrahedron* **1978**, *34*, 213–215.
- [233] D. A. Fletcher, B. G. Gowenlock, K. G. Orrell, *J. Chem. Soc. Perkin Trans. 2* **1997**, 2201–2206.
- [234] M. Dommaschk, M. Peters, F. Gutzeit, C. Schütt, C. Näther, F. D. Sönnichsen, S. Tiwari, C. Riedel, S. Boretius, R. Herges, *J. Am. Chem. Soc.* **2015**, *137*, 7552–7555.
- [235] H. Caro, *Angew. Chem.* **1898**, *11*, 845–846.
- [236] K. M. Ibne-Rasa, C. G. Lauro, J. O. Edwards, *J. Am. Chem. Soc.* **1963**, *85*, 1165–1167.
- [237] B. G. Gowenlock, G. B. Richter-Addo, *Chem. Rev.* **2004**, *104*, 3315–3340.
- [238] S. Spyroudis, A. Varvoglis, *Synthesis* **1975**, *1975*, 445–447.
- [239] P. Groves, *Polym. Chem.* **2017**, *8*, 6700–6708.
- [240] M. Dowds, D. Bank, J. Strueben, D. P. Soto, F. D. Sönnichsen, F. Renth, F. Temps, A. Staubitz, *J. Mater. Chem. C* **2020**, 10.1039.C9TC05193G.
- [241] Y. Norikane, *J. Photopolym. Sci. Technol.* **2012**, *25*, 153–158.

- [242] E. Wagner-Wysiecka, N. Łukasik, J. F. Biernat, E. Luboch, *J. Inclusion Phenom. Macrocyclic Chem.* **2018**, *90*, 189–257.
- [243] S. Shinkai, T. Kouno, Y. Kusano, O. Manabe, *J. Chem. Soc. Perkin Trans. 1* **1982**, 2471–2477.
- [244] S. Shinkai, T. Nakaji, Y. Nishida, T. Ogawa, O. Manabe, *J. Am. Chem. Soc.* **1980**, *102*, 5860–5865.
- [245] S. Shinkai, Y. Honda, K. Ueda, O. Manabe, *Bull. Chem. Soc. Jpn.* **1984**, *57*, 2144–2149.
- [246] S. Shinkai, Y. Honda, K. Ueda, O. Manabe, *Isr. J. Chem.* **1984**, *24*, 302–306.
- [247] S. Shinkai, T. Minami, Y. Kusano, O. Manabe, *J. Am. Chem. Soc.* **1983**, *105*, 1851–1856.
- [248] S. Shinkai, Y. Honda, T. Minami, K. Ueda, O. Manabe, M. Tashiro, *Bull. Chem. Soc. Jpn.* **1983**, *56*, 1700–1704.
- [249] S. Shinkai, K. Miyazaki, O. Manabe, *J. Chem. Soc. Perkin Trans. 1* **1987**, 449–456.
- [250] A. Lyapunov, T. Kirichenko, C. Kulygina, R. Zubatyuk, M. Fonari, A. Kyrychenko, A. Doroshenko, *J. Inclusion Phenom. Macrocyclic Chem.* **2015**, *81*, 499–508.
- [251] M. Tlustý, P. Slavík, H. Dvořáková, V. Eigner, P. Lhoták, *Tetrahedron* **2017**, *73*, 1230–1237.
- [252] H. Galán, G. Henrich, J. de Mendoza, P. Prados, *Eur. J. Org. Chem.* **2010**, *2010*, 1249–1257.
- [253] X.-P. Qiu, E. V. Korchagina, J. Rolland, F. M. Winnik, *Polym. Chem.* **2014**, *5*, 3656–3665.
- [254] G. Despras, J. Hain, S. O. Jaeschke, *Chem. - Eur. J.* **2017**, *23*, 10838–10847.
- [255] D. G. Flint, J. R. Kumita, O. S. Smart, G. A. Woolley, *Chem. Biol.* **2002**, *9*, 391–397.
- [256] S. Bellotto, S. Chen, I. Rentero Rebollo, H. A. Wegner, C. Heinis, *J. Am. Chem. Soc.* **2014**, *136*, 5880–5883.
- [257] A. A. Beharry, G. A. Woolley, *Chem. Soc. Rev.* **2011**, *40*, 4422–4437.
- [258] X. Zhang, X. Ma, K. Wang, S. Lin, S. Zhu, Y. Dai, F. Xia, *Macromol. Rapid Commun.* **2018**, *39*, 1800142.
- [259] N. Tamaoki, K. Koseki, T. Yamaoka, *Angew. Chem. Int. Ed. Engl.* **1990**, *29*, 105–106.
- [260] A. Heindl, L. Schweighauser, C. Logemann, H. Wegner, *Synthesis* **2017**, *49*, 2632–2639.
- [261] C. Slavov, C. Yang, A. H. Heindl, T. Stauch, H. A. Wegner, A. Dreuw, J. Wachtveitl, *J. Phys. Chem. Lett.* **2018**, *9*, 4776–4781.
- [262] Y. Norikane, K. Kitamoto, N. Tamaoki, *Org. Lett.* **2002**, *4*, 3907–3910.

- [263] Y. Norikane, R. Katoh, N. Tamaoki, *Chem. Commun.* **2008**, 1898.
- [264] R. Reuter, N. Hostettler, M. Neuburger, H. A. Wegner, *Eur. J. Org. Chem.* **2009**, 2009, 5647–5652.
- [265] R. Reuter, N. Hostettler, M. Neuburger, H. A. Wegner, *Chimia* **2010**, 64, 180–183.
- [266] H.-W. Losensky, H. Spelthann, A. Ehlen, F. Vögtle, J. Bargon, *Angew. Chem. Int. Ed. Engl.* **1988**, 27, 1189–1191.
- [267] Y. Norikane, K. Kitamoto, N. Tamaoki, *J. Org. Chem.* **2003**, 68, 8291–8304.
- [268] Y. Norikane, Y. Hirai, M. Yoshida, *Chem. Commun.* **2011**, 47, 1770–1772.
- [269] R. Reuter, H. A. Wegner, *Chem. - Eur. J.* **2011**, 17, 2987–2995.
- [270] R. Reuter, H. A. Wegner, *Org. Lett.* **2011**, 13, 5908–5911.
- [271] N. Tamaoki, K. Ogata, K. Koseki, T. Yamaoka, *Tetrahedron* **1990**, 46, 5931–5942.
- [272] N. Tamaoki, T. Yamaoka, *J. Chem. Soc. Perkin Trans. 2* **1991**, 873–878.
- [273] N. Tamaoki, S. Yoshimura, T. Yamaoka, *Thin Solid Films* **1992**, 221, 132–139.
- [274] A. H. Heindl, J. Becker, H. A. Wegner, *Chem. Sci.* **2019**, 10.1039.C9SC02347J.
- [275] K. Takaishi, A. Muranaka, M. Kawamoto, M. Uchiyama, *Org. Lett.* **2012**, 14, 276–279.
- [276] G. Ritter, G. Haefelinger, E. Lueddecke, H. Rau, *J. Am. Chem. Soc.* **1989**, 111, 4627–4635.
- [277] D. Röttger, H. Rau, *J. Photochem. Photobiol. A* **1996**, 101, 205–214.
- [278] L. Schweighauser, H. A. Wegner, *Chem. Commun.* **2013**, 49, 4397–4399.
- [279] L. Schweighauser, D. Häussinger, M. Neuburger, H. A. Wegner, *Org. Biomol. Chem.* **2014**, 12, 3371.
- [280] A. Vlasceanu, M. Koerstz, A. B. Skov, K. V. Mikkelsen, M. B. Nielsen, *Angew. Chem. Int. Ed.* **2018**, 57, 6069–6072.
- [281] *Silicon-containing polymers: the science and technology of their synthesis and applications*, (Eds.: R. G. Jones, A. Waturo, J. Chojnowski), Springer Science+Business, Dordrecht; Boston; London, **2000**.
- [282] R. Lehnert, A. Porzel, K. Rühlmann, *Z. Chem.* **1988**, 28, 190–192.
- [283] J. A. Cella, J. C. Carpenter, *J. Organomet. Chem.* **1994**, 480, 23–26.
- [284] H. Matsumoto, K. Shono, Y. Nagai, *Org. Prep. Proced. Int.* **1981**, 13, 118–123.
- [285] M. Walther, Master Thesis, Christian-Albrechts-Universität, Kiel, **2018**.
- [286] K. G. Yager, C. J. Barrett, *J. Photochem. Photobiol. A* **2006**, 182, 250–261.

Part IV.

Summary & Future Directions

Recapitulation

This thesis aimed for advancing the field of stimuli-responsive materials by applying two switchable systems: spiropyrans (Part II) and azobenzenes (Part III). Spiropyrans were implemented as additive in composite materials (Part II, section 1.2) and bound covalently to the main chain of conjugated polymers (Part II, chapter 3). Azobenzene dyes were to be incorporated into the repeating units of linear polymers with strictly alternating azobenzene and siloxane units in the main chain (Part III, chapter 2 and chapter 3).

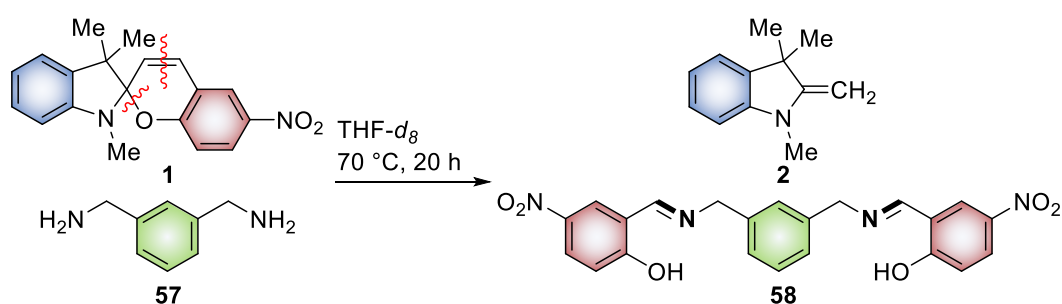
Spiropyrans in Polymer Materials

Composites

When applied as additives in composites based on PTU, spiropyrans retained their ability to switch upon irradiation with UV light. In addition, the ring-opening to MC can be induced by heating. When tetrapodal zinc oxide is used as ceramic filler (S. Shree et al., *ACS Appl. Mater. Interfaces* **2017**, *9*, 38000-38007), the composite samples show mechanically induced switching appearing when the sample breaks. However, this represents the first example for mechanochromism in spiropyran-based polymer systems.^[287]

The mechanoswitching properties of PTU composites could be improved by using glass-fibers as reinforcement (S. Shree et al., *Mater. Horiz.* **2019**, *submitted*), so that the mechanically induced colorchange occurs *before* structural failure of the samples. Broadening the scope of applicable matrix materials resulted in an unexpected finding. While the mechanical properties of spiropyran composites in epoxy resin as matrix and glassfibers as reinforcements are within the expected range, the samples lost their mechano- and photoswitchability.

In-depth investigation of the reactions during the curing process of the epoxy resins revealed a degradation of the spiropyran to methylene indole and a condensation of the chromene fragment with xylylenediamine (**5**), a curing additive. The amine-induced ring-



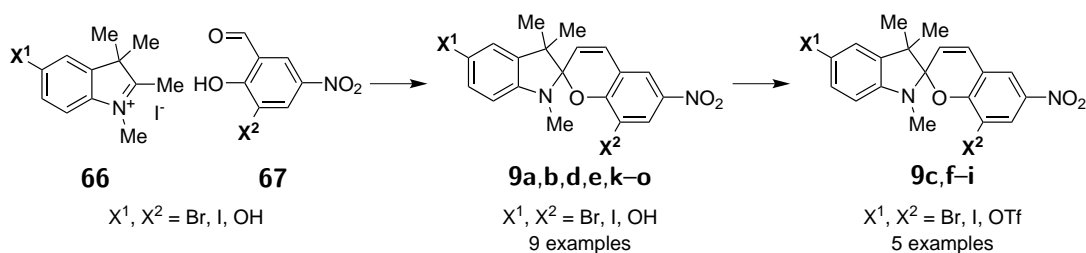
Scheme IV.1 During curing of the epoxy resin, the embedded spiropyran **1** degraded. The curing additive **5** caused cleavage of two bonds in **1** (red wavy lines). The benzene rings are colored according to their derivation. Blue: indole fragment of **1**; Red: chromene fragment of **1**; Green: **5**. The imine groups of **6** are highlighted in bold.

opening of spiropyrans and degradation of the ethylene bridge followed by imine formation of the product **6** have not been reported before (see Scheme IV.1).

These results pave the road to the use of spiropyrans as mechanochromic damage indicator in large-scale applications using PTU composites. However, a broader variety of applicable matrices is desirable. Future research will mostly focus on the materials' scientific aspects of composites with spiropyrans and transferring the composite system to various matrices. To avoid the discovered undesirable degradation of spiropyrans, the underlying reactivity should be explored further. Variation of the base (pK_a , other functional groups than primary amines) and the spiropyran (electron density, substitution pattern) should reveal whether the cleavage of the styrene motif or the imine formation is the driving force in this reaction.

Conjugated Polymers

For the intended electrophile-selective cross-coupling, spiropyrans with 14 different substitution patterns **9** were synthesized and analyzed in respect to their photochromic properties (Schulz-Senft et al., *Dyes Pigm.* **2017**, *136*, 292-301). This was achieved by functionalizing the indole **66** and benzaldehyde **67** precursors of the spiropyrans with bromide, iodide and hydroxy substituents. For the use in cross-coupling reactions, the hydroxy groups of **9k-o** were converted into trifluoromethanesulfonyl (OTf) groups. The obtained spiropyrans **9c,f-i** were the first reported examples of spiropyrans with OTf substituents. The photochromic properties of these spiropyrans are remarkable: introducing the OTf substituent in the 5' position at the indole side (X^1 in Scheme IV.2) of spiropyrans resulted in short half-life times of the MC form of less than five minutes. In contrast, OTf substituents at the chromene site (X^2) enhance the stability of the open form, so that it was the predominant species in acetonitrile under dark conditions. When both sides bear OTf substituents (**9c**), the contrary effects level out and the photochromic properties remain as expected: under dark conditions, an equilibrium between SP and MC with predominantly SP forms. Irradiation with UV light enriches the open MC form; irradiation with green light enriches the closed SP form.



Scheme IV.2 Spiropyrans with nine different substitution patterns were synthesized (X^1 and X^2 : Br, I, OH; **9a,b,d,e,k-o**) from the precursors **66** and **67**. The hydroxy groups were subsequently converted into OTf groups in five examples **9c,f-i**.

The symmetrically functionalized spiropyrans with bromo (**9a**), iodo (**9b**) and OTf (**9c**) substituents were used as electrophile in Stille cross-coupling reactions. In all tested conditions, the indole site (X^1) remained inert, whereas the chromene site (X^2) underwent

a reaction. Unexpectedly, not the phenyl group of trimethylphenylstannane (**16**), but one of the methyl groups was transferred in yields up to 86%. This finding was attributed to sterical restraints at the reaction site. However, the substituents showed the following relative reactivity: OTf < Br < I.

Since the attempts of using spiropyran in cross-coupling reactions to connect them with conjugated polymers failed at this early stage, it was necessary to consider a different route. Apparently, the disruptive factors are the high electron density at the X¹ position and the sterical hindrance at the X² position. This was circumvented by connecting the indole and chromene moieties *prior* to the formation of spiropyrans. As a proof of principle, 3-hexylthiophene was introduced at both, indolene and chromene sites. During the synthetic route, the Suzuki cross-coupling of 3-iodo-2-methoxy-5-nitrobenzaldehyde (**25**) with a boron-functionalized thiophene **20** was accompanied by an *in situ* deprotection of the hydroxy group. This finding was evaluated by DFT studies and could be attributed to the thiophene's electron donating properties. The obtained spiropyran **19** was the first reported example of covalently connecting spiropyrans and thiophenes at these positions. Analysis of the photochemical properties of **19** revealed a dominating effect of the electron donating thiophene unit at the chromene site. After photoswitching, the open form **19b** underwent cyclization to the closed **19a** with a half-life time of less than 30 s. Besides the expected red fluorescence corresponding to merocyanine, the dye showed blue fluorescence upon excitation with UV light (365 nm), indicating delocalization of electrons throughout the thiophenes and adjacent phenyl rings. This assumption is supported by DFT simulations of spiropyran with 3-methylthiophene as substituents. The HOMO or HOMO-1 orbitals spread throughout thiophene and the neighboring phenyl rings. However, the thiophene rings are significantly twisted towards their direct neighbors, increasing the band gap.^[65]

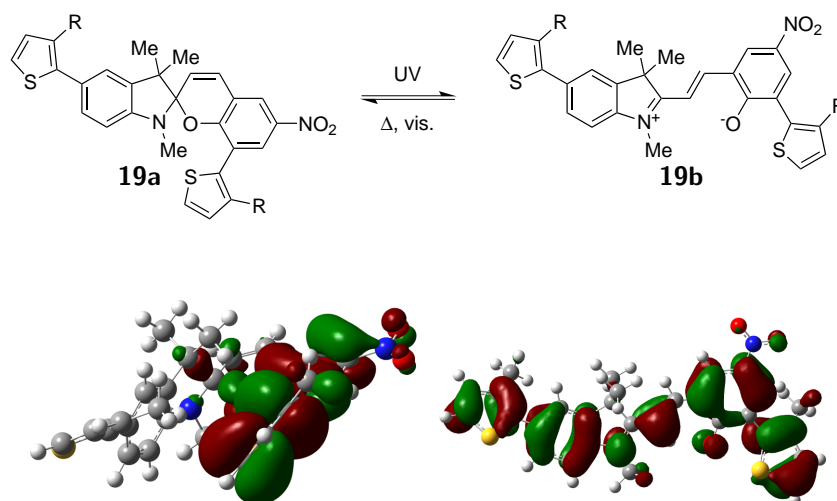
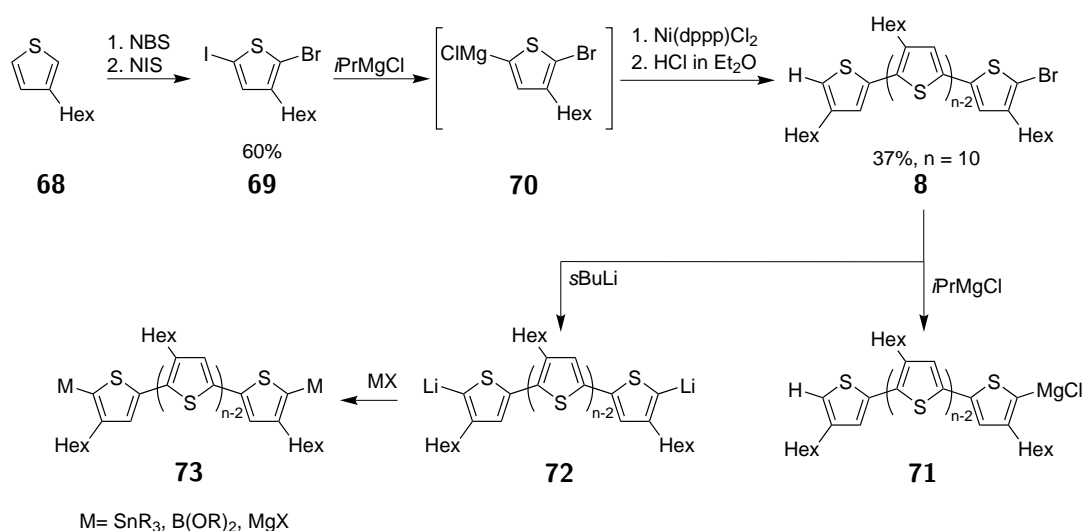


Figure IV.1. The synthesized spiropyran **19** (R = *n*-Hex) represents the first reported example of spiropyran bearing hexylthiophene substituents. The calculated HOMO-1 orbitals (R = Me) reveal delocalization of electrons through the thiophenes and neighboring phenyl rings. In the closed form **19a**, the conjugation is interrupted by the central spiro atom. The open form **19b** showed conjugation throughout the complete molecule.

The described synthesis and analysis of a spiropyran **19** with two hexylthiophene substituents represent only a proof of principle and open the door to photoresponsive organic electronics. Within the synthetic route, the conditions of the Suzuki cross-coupling reactions and the nitration bear the potential to be optimized. In the context of a three-month research internship,¹ Ashley Kim already synthesized a short regioregular P3HT **8** with a proton and bromide as defined end groups (see Scheme IV.3) starting from 3-hexylthiophene (**68**).^[288] The dielectrophilic thiophene **69** was first selectively transferred into the Grignard compound **70**, which was then polymerized by Grignard metathesis. This polymerization follows a chain growth mechanism, which allowed good control over the chain lengths ($\overline{X}_n = 10$, $\overline{D} = 1.03$) while only one tail-tail coupling was observed per chain.^[288] The end groups of this polythiophene can be selectively transferred into MgCl/H **71** or Li/Li **72** (see Scheme IV.3).^[289] This would allow the synthesis of P3HT with two metal substituents, such as Grignard salts, stannanes, or boronic esters as end groups. Such bimetal P3HTs **73** could be used in subsequent cross-coupling reactions. When P3HT was successfully functionalized with the spiropyran precursors, the condensation of spiropyran connects two or multiple P3HT chains.



Scheme IV.3 Starting from 3-hexylthiophene (**68**), the dielectrophilic monomer **69** was synthesized by Ashley Kim under my supervision. Subsequently, she metallated the monomer **69** to the Grignard compound **70** that was polymerized by Grignard metathesis to give P3HT **8** with defined H/Br end groups.^[288] Such a polythiophene can be functionalized selectively with one Grignard (**71**) or two lithium (**72**) end groups.^[289]

After obtaining the poly(thiophene) functionalized spiropyran **7**, the effect of the spiropyran isomerization on the band gap can be investigated by cyclic voltammetry. A potential mechanically induced switching of the central spiropyran should be tested in solution (ultrasound irradiation) and in solid materials (tensile tests). To obtain a mechanoswitching of the spiropyran in the poly(thiophene) chains, an elongation of the attached P3HT chains

¹Funded by the German Academic Exchange Service (DAAD) and the American Chemical Society (ACS) by an "International Research for Undergraduates" scholarship.

might be required. The expected change in conductivity can be utilized in devices like OFETs. Photoswitching of **7** also effected the fluorescence. This could lead OLEDs that can be switched photochemically or mechanically (see Figure IV.2).

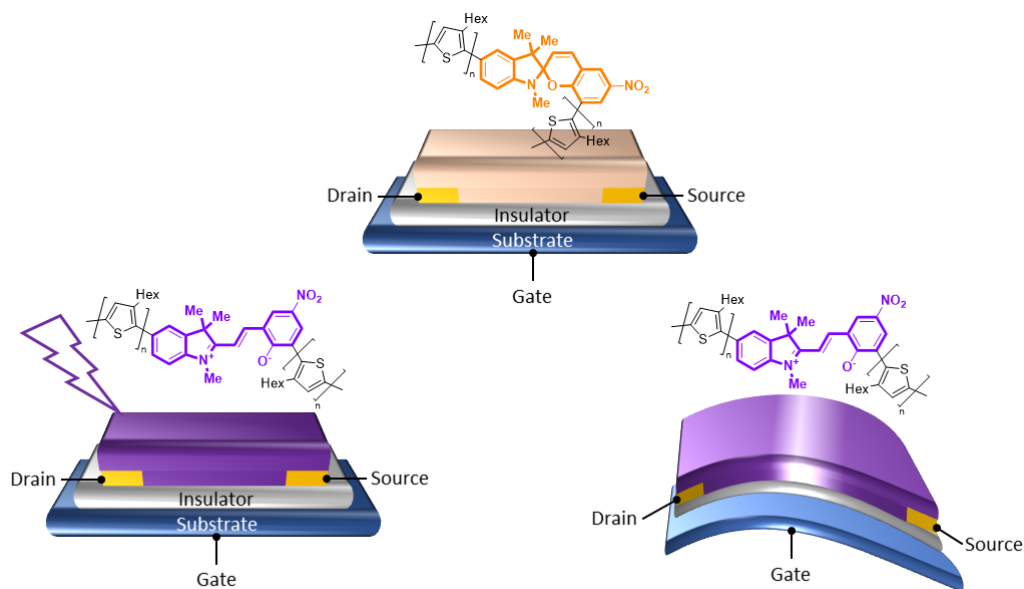


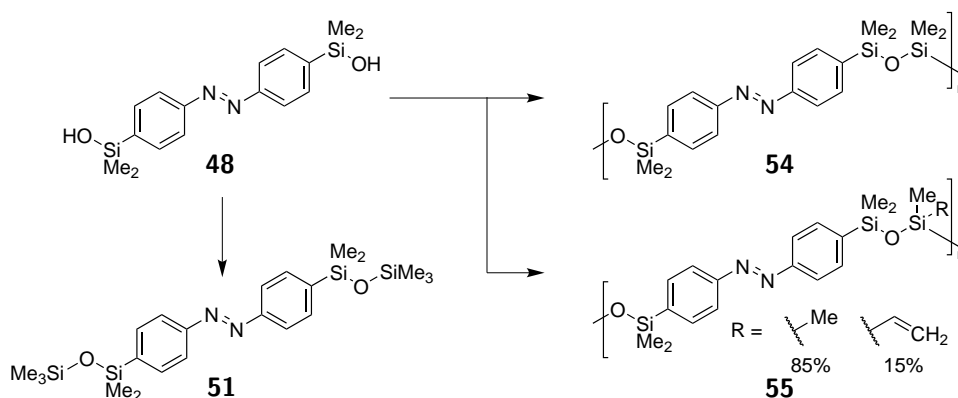
Figure IV.2. An OFET with P3HT functionalized spiropyran as the semiconducting layer (**top**) can potentially be switched by irradiation with UV light (**bottom left**), or by applying mechanical stress (**bottom right**).

To increase the conjugation between the thiophene chains and adjacent phenyl rings, removal of the hexyl chain at the first thiophene ring would be advisable. The DFT optimizations of the benzaldehyde derivatives in section 3.3 revealed a significantly decreased twisting of an unsubstituted thiophene as substituent compared to 3-methyl-thiophene. Synthetically, this could be achieved by using a thiophene with two different metal groups (e.g. alkylstannane and boronic ester)^[290,291] at the 2- and 5- positions as spacer between P3HT and spiropyran.

Azobenzene and Siloxanes

Linear Azobenzene-Siloxane Copolymers by Polycondensation

The polycondensation of arylsilanols with ureasilanes is an effective method of synthesizing silyl-siloxanes in high yields.^[292] The procedure was utilized by Jan Strüben to synthesize an exactly alternating azobenzene-trisiloxane copolymer.^[114] This thesis presents the improved syntheses of the azobenzene-disilanol monomer **48** and the polymer **54** (Part III, section 2.1). In addition, it was possible to synthesize a linear polymer **55** that contained vinyl side chains (Part III, section 2.2, see Scheme IV.4).



Scheme IV.4 The azobenzene-silanol **48** was used to synthesize azobenzene-trisiloxane copolymers **54** and **55** and the reference compound **51**.

Thorough investigation of the linear polymer **54** proved the excellent switching capacities of this polymer architecture (M. Schulz-Senft et al., *J. Mater. Chem. C* **2020**). The PSS of the azobenzene units in the polymer main chains showed a ratio of (*Z*)/(*E*)-azobenzenes that was similar to a reference azobenzene **51** with two disiloxane substituents. Another indication of the efficient switching mechanism were the surprisingly fast isomerization dynamics that were obtained by FTAS measurements. The polymer **54** with $\overline{X}_n = 130$ switched only 1.3 times slower than the reference molecule **51** with only one azobenzene unit. Further insights were gained by DOSY NMR spectroscopy. It could be proven that switching of the azobenzene units occurred in every chain. In the PSS, the polymer showed a volume decrease of approximately 25%.

While linear polymers are well soluble and can be easily applied, long term applications such as coatings require durable materials. Introducing cross-linkers after polymerization and after processing provides the possibility to achieve durable coatings. For this purpose, one methyl group was substituted by a vinyl group in 15% of the repeating units in polymer **55** (Schulz-Senft et al., *Chem. Mater.* **2019**, *submitted*). Thus, it should be possible to implement silane cross-linkers by hydrosilylation reactions. The polymer **55** showed similar size switching effects in solution like **54**. When spin-coated on quartz substrate, the resulting film showed reversed behavior. Upon irradiation with UV light, the film responded by an increase in height. This effect was reversible and could be followed by AFM for two cycles.

However, due to the low intensity of the light source that was used in the AFM microscope, only a minor fraction of the azobenzene units switched, as was also indicated by UV/vis measurements. Interestingly, the thermal half-life of the switched polymer is shorter in the film (7.5 h) than in solution (21 h).

This project proved the efficient switching behavior of azobenzene-siloxane copolymers. The flexible siloxane linkers are capable of rearranging in both, solution and film to allow the movement of the azobenzene units. The switching in films and solid states can be investigated in future research. Also, the cross-linking can be used to tailor the material's properties by variation of the amount of cross-links and the length of the linkers.

A Macrocyclic Azobenzene for Ring-Opening Polymerization

It was possible to establish the synthesis of a macrocyclic azobenzene-siloxane **64** that contained two azobenzene units in the cycle (Figure IV.3, left). In **64**, the azobenzenes are connected by Si-O-Si bridges in the 3 and 3' positions. Although the formation of macrocycles by condensation competes with the formation of oligomers, it was possible to isolate the cycle **64** in a relatively high yield of 14%, even without applying the high dilution principle.^[293] In the context of a MSc thesis, Melanie Walther was able to improve the yield to 24%.^[285]

The (*E*),(*E*)-isomer of **64** is highly crystalline, allowing easy purification. It was possible to obtain a single crystal, which structure was determined by Prof. Näther from the Institute for Inorganic Chemistry, University Kiel. The crystal structure revealed two major features: I) the Si-O-Si bridges are almost perpendicular to one azobenzyl plane and twisted towards the other, leading to twist of the azobenzene planes by approximately 45° (Figure IV.3, middle). II) the azobenzene units are crossed by an angle of 70° (Figure IV.3, right). These effects cause axial chirality of the macrocycle. While Figure IV.3 depicts only the *M*-helix, however, the crystal structure contained equal amounts of *P*-helices as well.

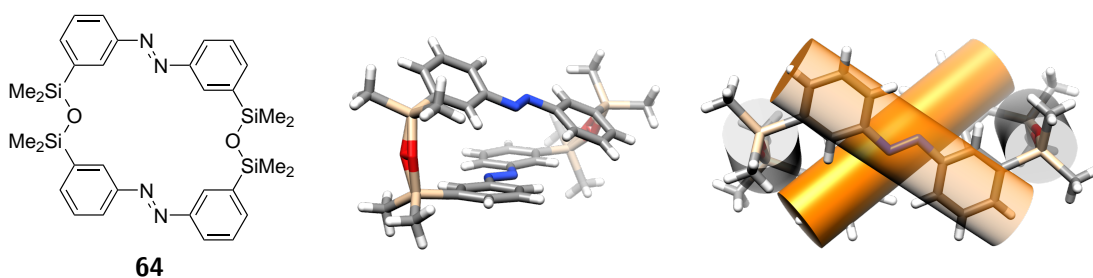


Figure IV.3. Crystal structure of the azobenzene-siloxane macrocycle **64**. Orange tubes symbolize the azobenzene units, gray tubes visualize the orientation of the Si-O-Si axes in the siloxane linkers. The opposing orientation of the azobenzene units in the macrocycle induce helical chirality. In this example, the *M*-helix is depicted, the crystal structure was a racemic mixture of *M*- and *P*-helices.

Photoswitching of the macrocycle was possible by irradiation with UV light (340 nm) and blue light (450 nm). In solution, the PSS at 340 nm contained only (*Z*),(*Z*)-isomer, which underwent slow (*Z*)→(*E*) isomerization with decay times of 4.5 d for the first and 45 d for

the second isomerization. This resembles an independent switching of both azobenzenes and proves the high flexibility of the siloxane linkers. Currently, the ultrafast dynamics of the azobenzene switching are being investigated by the group of Prof. Friedrich Temps at the Institute of Physical Chemistry, University Kiel.

These findings open several potential aspects of future research. Establishing a method for the ring-opening polymerization of the macrocycle would provide access to the controlled synthesis of linear azobenzene-siloxanes. The macrocycle's structure can be altered by changing the substituents in the SiR_2 groups, to introduce potential cross-linking sites into the polymer. Additionally, the position of the linkers could be varied to the 4 and 4' or the 2 and 2' positions. Since the Si-O-Si axes point out of the azobenzene plane, different positions of the linkers should not hinder the formation of similar macrocycles.

Bibliography of Part IV

- [65] S. S. Zade, M. Bendikov, *Chem. - Eur. J.* **2007**, *13*, 3688–3700.
- [114] J. Strueben, PhD thesis, Christian-Albrechts-Universität, Kiel, **2015**.
- [285] M. Walther, Master Thesis, Christian-Albrechts-Universität, Kiel, **2018**.
- [287] D. J. Fisher, *Mechanochromism*, Materials Research Forum LLC, Millersville, **2019**.
- [288] A. Kim, M. Schulz, A. Staubitz in, 249th ACS National Meeting & Exposition, American Chemical Society, Denver, **2015**.
- [289] L. Zhang, K. Hashimoto, K. Tajima, *Polym. J.* **2012**, *44*, 1145–1148.
- [290] J. Linshoef, A. C. J. Heinrich, S. A. W. Segler, P. J. Gates, A. Staubitz, *Org. Lett.* **2012**, *14*, 5644–5647.
- [291] A. C. J. Heinrich, B. Thiedemann, P. J. Gates, A. Staubitz, *Org. Lett.* **2013**, *15*, 4666–4669.
- [292] P. R. Dvornic, R. W. Lenz, *J. Polym. Sci. Polym. Chem. Ed.* **1982**, *20*, 951–966.
- [293] L. Rossa, F. Vögtle in *Cyclophanes I*, (Ed.: F. Vögtle), Topics in Current Chemistry, Springer, Berlin, Heidelberg, **1983**, pp. 1–86.

Part V.

Experimental Part

1. General Methods & Materials for Unpublished Synthesis

The experimental details on the published or submitted results were comprised in supporting informations for the respective manuscript. These contain lists of the equipment and materials that were used in the respective context. Molecular sieve was activated by heating to 300 °C and at reduced pressure (0.03 mbar) and stored in a nitrogen filled glove box. If an inert atmosphere was required for the synthesis, the reactions were performed on a Schlenk-line under nitrogen atmosphere. When argon (grade "N46") was used as protective gas, it was dried by passing it through activated molecular sieve (3 Å) (column diameter: 5 cm, length: 40 cm). All glassware that was used for syntheses under protective atmosphere was dried by heating (200 °C), evacuation (0.03 mbar) and flushing with protective gas at least three times before use. Syringes were flushed with protective gas at least three times prior to use.

1.1. Equipment Used for Synthesis & Analysis of Unpublished Substances

Microwave (MW) assisted syntheses were performed on a Biotage Initiator+ SP Wave peptide synthesizer in the organic synthesis mode. The times given in the experimental procedures include the heating time to reach the desired temperature.

Reactions that required inert workup were conducted in a labmaster 130 glove box by MBraun, filled with nitrogen. Air sensitive compounds were stored either in a labmaster 130 glovebox by MBraun or in J-Young's glassware under a nitrogen atmosphere.

For parallel cross-coupling reactions, a Carousel 12 Plus reaction setup by Radley was used and connected to a nitrogen filled Schlenk line.

All formerly unpublished NMR spectra were either recorded on a Bruker Avance Neo 500 (^1H NMR: 500 MHz) with a triple resonance (^1H , ^{13}C and ^nX with X being any nucleus and its corresponding nucleon number n) probe head or on a Bruker Avance II HD 600 (^1H NMR: 600 MHz) with a triple resonance (^1H , ^{13}C and ^{15}N) cryo probe head FT-NMR spectrometer at 298 K. ^1H NMR and $^{13}\text{C}\{^1\text{H}\}$ NMR spectra were referenced using tetramethyl silane (TMS). $^{29}\text{Si}\{^1\text{H}\}$ and $^{129}\text{Sn}\{^1\text{H}\}$ spectra were referenced indirectly according to the IUPAC recommendations for the frequency ratio to ^1H .^[294]

The exact assignment of the peaks was performed by two-dimensional NMR spectroscopy such as ^1H , ^1H COSY, $^1\text{H}, ^1\text{H}$ NOESY, $^1\text{H}, ^{13}\text{C}\{^1\text{H}\}$ HSQC, $^1\text{H}, ^{13}\text{C}\{^1\text{H}\}$ HMBC and $^1\text{H}, ^{29}\text{Si}\{^1\text{H}\}$ HMBC if possible. The following abbreviations were used to assign the signals'

multicplities: apparent triplet (at), doublet (d), doublet of doublets (dd), doublet of doublet of doublets (ddd), multiplet (m), singlet (s), triplet (t), triplet of triplets (tt)

Mass spectrometric measurements were performed in the positive ion collection mode using a JEOL Accu TOF 4GGCV electron ionization (EI) mass spectrometer or a Thermo Fisher Q Exactive Plus with a quadruple orbitrap electrospray ionization (ESI) mass spectrometer. Electron ionization was performed using an ionization potential of 70 eV.

Infrared spectroscopy (IR) was measured using a Perkin Elmer Paragon 1000 FT-IR spectrometer equipped with an A531-G Golden-Gate attenuated total reflection (ATR) unit.

Melting points were measured on a Gallenkamp MPD 350 BM 2.5 or an electrothermal IA6304 capillary melting point apparatus.

Thin layer chromatography (TLC) was performed using pre-coated TLC-sheets from Macherey-Nagel with silica gel 60 and fluorescent indicator UV₂₅₄.

Flash column chromatography was performed on an Interchim Puriflash 430 column machine.

UV light illuminations were carried out using either an array of three Seoul CUD4AF1B LEDs (340 nm, optical performance: 55 mW each) or one Nichia NVSU233A-U365 LED (365 nm, optical performance: 1030 mW), assembled by Sahlmann Photochemical Solutions. Illuminations with visible light were carried out using one Luxeon LXML-PX01 LED (450 nm, optical performance: 900 mW), or one Luxeon LXML-PX02 LED (565 nm, optical performance: 350 mW), assembled by Sahlmann Photochemical solutions.

1.2. Chemicals & Solvents Used in the Synthesis and Analysis of Unpublished Substances

Aqueous solutions of hydrochloric acid were prepared by dilution of concentrated acid (37%). Saturated solutions of sodium chloride (brine), were prepared from the solid salts. Phenyltrimethylstannane was prepared following a literature procedure.^[295] Nitrating acid was prepared from fuming nitric acid (100%) and concentrated sulfuric acid (98%) as a 3/4 volumetric mixture. All reagents or solvents which were dried and/or degassed were stored under a nitrogen atmosphere over molecular sieve 3 Å either in a glovebox or in J. Young's glassware. Reagents or solvents which were purchased dry in septum-sealed bottles were kept under a nitrogen atmosphere.

Unless noted otherwise, all reagents were used as received without further purification. All solvents which were purchased as "technical grade" were purified by rotary evaporation prior to use. If necessary, the solvents were dried either via a PS-MD-5 solvent purification system by Innovative Technology or a procedure as noted in Table V.2. Solvents for the use in protective atmosphere were degassed by at least three freeze-pump-thaw cycles, before the flask was refilled with protective gas. Water and aqueous solutions were degassed by bubbling nitrogen through the liquid via a cannula (diameter: 0.8 mm) for one hour.

Table V.1. List of Chemicals and Reagents.

Reagent	Supplier	Purity	Notes
Calcium hydride	Acros Organics	ca. 93%	
Copper(I) bromide	Sigma-Aldrich	98%	
Copper(I) iodide	Aldrich	99.9%	
Dichlorodimethylsilane	Acros Organics	99%	Purified by distillation, stored under nitrogen
Hexamethylbenzene	TCI	99%	
Hexamethyldistannane	ABCR	99%	Stored at -30°C in a glovebox
3-Hexylthiophene-2-boronic acid pinacol ester	TCI	>97%	Stored in a glovebox
Hydrochloric acid	Grüssing	37%	
3-Iodoaniline	ABCR	98%	
Iodomethane	Sigma-Aldrich	>99%	
2-Iodophenol	ABCR	98%	
Lithium chloride	Acros Organics	>99%	Anhydrous, stored in a glovebox
Magnesium chloride	Acros Organics	99.9%	Anhydrous, stored in a glovebox
Magnesium sulfate	Grüssing	99%	
Methyl lithium	Acros Organics	3%	1.6 mol L^{-1} in cumene/ 2-Me-THF
Monopotassium phosphate	Merck	>98%	
Nitric acid	Merck	100%	Fuming
$\text{Pd}(\text{dppf})\text{Cl}_2$	Sigma-Aldrich	>98%	Stored in a glovebox
$\text{Pd}(\text{PPh}_3)_4$	Sigma-Aldrich	99%	Stored in a glovebox
$\text{Pd}(\text{Pt-Bu}_3)_2$	TCI	98%	Stored in a glovebox
Pd_2dba_3	Strem Chemicals	98%	Stored in a glovebox
Piperidine	Acros Organics	99.5%	Stored under nitrogen
Potassium carbonate	ABCR	98%	
Sodium chloride	Grüssing	99.5%	
Sodium hydroxide	Grüssing	99%	
Sodium methoxide	TCI	>97%	Stored in a glovebox
Sodium methoxide		4.5 mol L^{-1}	Solution in MeOH
SPhos	Strem Chemicals	>98%	
Sulfuric acid	Grüssing	98%	

Continued on next page

Continued from previous page

Reagent	Supplier	Purity	Notes
Triethylamine (TEA)	Acros Organics	99.5%	Predried over KOH, distilled from CaH ₂
Tripotassium phosphate	ABCR	97%	Anhydrous, stored in a glovebox

Table V.2. List of Solvents.

Solvent	Supplier	Purity	Notes
Acetonitrile	Sigma-Aldrich	HPLC grade	
Chloroform	VWR	Technical grade	
DCM	VWR	HPLC grade	Drying: PS-MD-5, degassed
Diethyl ether	BCD	Technical grade	
Diethyl ether	AlfaAesar	Spectrophotometric grade, inhibitor-free, 99.9%	Degassed, stored over molecular sieve
DMF	Acros Organics	99.8%, extra dry,	stored over molecular sieve, AcroSeal [®]
Ethanol	CMP Walter	Techn. Grade, denaturated with benzine	Distilled from CaO, degassed
Ethyl acetate	CMP Walter	Technical grade	
Hexane	CMP Walter	Technical grade	
Methanol	Acros Organics	99.8%	Purchased extra dry, AcroSeal [®]
Pentane	VWR	Technical grade	
Pyridine	Grüssing	99.5%	
THF	VWR	HPLC grade	Predrying: PS-MD-5, drying: sodium/benzophenone
Toluene	VWR	Technical grade	
Water		Deionized	

2. Spiropyran in Composites

2.1. Supporting Information for *ACS Mat. Interfaces*
2017, *9*, 38000-38007.

Supporting Information for am-2017-095982

Light, Force and Heat: A Multi-Stimuli Composite that Reveals its Violent Past

Sindu Shree,^{†} Mathias Schulz-Senft,[‡] Nils H. Alsleben,[†] Yogendra Kumar Mishra,^{†*} Anne
Staubitz,^{‡,§,*} Rainer Adelung^{†,*}*

[†]Institute for Materials Science, Functional Nanomaterials, University of Kiel, Kaiserstr. 2, 24143
Kiel, Germany

[‡]Otto-Diels-Institute for Organic Chemistry, University of Kiel, Otto-Hahn-Platz 4, 24118 Kiel,
Germany

[¥]Institute for Organic and Analytical Chemistry, University of Bremen, Leobener Str. NW2 C,
28359 Bremen, Germany

[§]MAPEX Center for Materials and Processes, University of Bremen Bibliothekstraße 1, 28359
Bremen, Germany

SS (sisi@tf.uni-kiel.de), YKM (ykm@tf.uni-kiel.de), AS (staubitz@uni-bremen.de) RA (ra@uni-
kiel.de)

S-1

1. Abbreviations

The use of abbreviations follows the conventions from the ACS Style guide. In addition, the following abbreviations were used.

Abbreviation	Meaning
ATR	Attenuated total reflection (IR)
COSY	Correlation spectroscopy
dd (NMR)	Doublet of doublets
EI	Electron ionization
FT	Fourier transform
HMBC	Heteronuclear multiple bond correlation
HPLC	High performance liquid chromatography
HSQC	Heteronuclear single quantum coherence
NOESY	Nuclear Overhauser enhancement spectroscopy
TOF	Time-of-flight mass detector

2. Analytical Equipment

NMR spectra were either recorded on a Bruker DRX 500 (^1H NMR: 500 MHz) FT-NMR spectrometer. ^1H NMR and $^{13}\text{C}\{^1\text{H}\}$ NMR spectra were referenced against the solvent residual proton signals (^1H) or the solvent itself (^{13}C).

The exact assignment of the peaks was performed by two-dimensional NMR spectroscopy such as ^1H COSY, ^1H NOESY, $^1\text{H}/^{13}\text{C}$ HSQC or $^1\text{H}/^{13}\text{C}$ HMBC if possible.

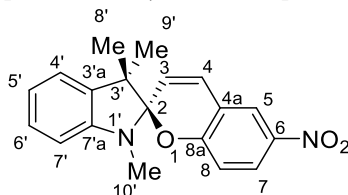
Mass spectrometric measurements were performed in the positive ion collection mode using a JEOL-Accu TOF 4GGCV EI mass spectrometer. Electron ionization was performed using an ionization potential of 70 eV.

UV spectra were recorded at 20 °C using a Perkin Elmer Lambda 900 UV spectrometer.

Melting points were measured on an electrothermal IA6304 capillary melting point apparatus and are uncorrected.

The irradiation experiments were carried out using LED light sources with an optical power of 680 mW (360-370 nm) and 20 W (520-530 nm).

Materials

1',3',3'-Trimethyl-6-nitrospiro[chromene-2,2'-indoline]

Molecular structures of 1',3',3'-Trimethyl-6-nitrospiro[chromene-2,2'-indoline]

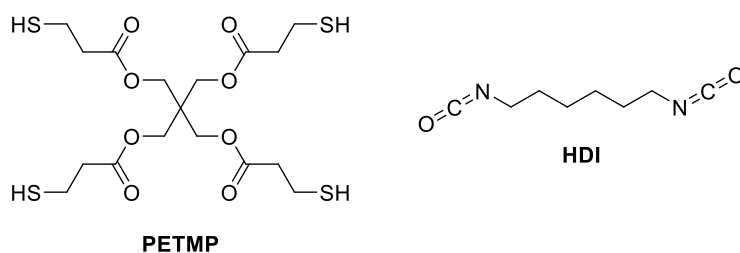
Melting point: $T = 160\text{ }^{\circ}\text{C}$, Lit:¹ 178 – 179 $^{\circ}\text{C}$

¹H NMR (500 MHz, CDCl₃, 300 K): $\delta = 8.03 - 7.99$ (m, 2H, H-5, H-7), 7.21 (ddd, ³ $J = 7.7$ Hz, ³ $J = 7.4$ Hz, ⁴ $J = 1.0$ Hz, 1H, H-6'), 7.09 (dd, ³ $J = 7.2$ Hz, ⁴ $J = 1.0$ Hz, 1H, H-4'), 6.93 (d, ³ $J = 10.3$ Hz, 1H, H-4), 6.89 (ddd, ³ $J = 7.4$ Hz, ³ $J = 7.2$ Hz, ⁴ $J = 1.0$ Hz, 1H, H-5'), 6.77 (d, ³ $J = 8.5$ Hz, 1H, H-8), 6.56 (d, ³ $J = 7.7$ Hz, 1H, H-7'), 5.86 (d, ³ $J = 10.3$ Hz, 1H, H-3), 2.75 (s, 3H, H-10'), 1.30 (s, 3H, H-8'), 1.19 (s, 3H, H-9') ppm.

¹³C NMR (126 MHz, CDCl₃, 300 K): $\delta = 160.0$ (C-6), 147.8 (C-7'a), 141.1 (C-4a), 136.3 (C-3'a), 128.4 (C-4), 128.0 (C-6'), 126.0 (C-7), 122.8 (C-5), 121.8 (C-3), 121.7 (C-4'), 119.9 (C-5'), 118.8 (C-8a), 115.6 (C-8), 107.2 (C-7'), 106.5 (C-2), 52.4 (C-3'), 29.0 (C-10'), 26.0 (C-9'), 20.1 (C-8') ppm.

IR (ATR): $\tilde{\nu} = 3068$ (w), 2963 (m), 2866 (m), 1656 (w), 1609 (m), 1575 (m), 1509 (m), 1488 (s), 1441 (m), 1382 (w), 1364 (m), 1330 (s), 1301 (m), 1269 (s), 1184 (m), 1122 (m), 1089 (s), 1022 (m), 1016 (m), 949 (s), 916 (s), 838 (m), 807 (s), 782 (m), 750 (vs), 681 (s), 627 (m), 573 (m), 550 (m) cm⁻¹

HRMS (EI-TOF): m/z (%): [M]⁺ calcd for [C₁₉H₁₈N₂O₃]⁺ 322.13174; found 322.13148 (56), 159.10 (100) [M-Ph-O-NO₂-C₂H₂]⁺.

Monomers for the Synthesis of Polythiourethane (PTU)

Molecular structures of the two components pentaerythritol tetrakis(3-mercaptopropionate) (PETMP) and hexamethylenediisocyanate (HDI) of polythiourethane (PTU).

Figure S1

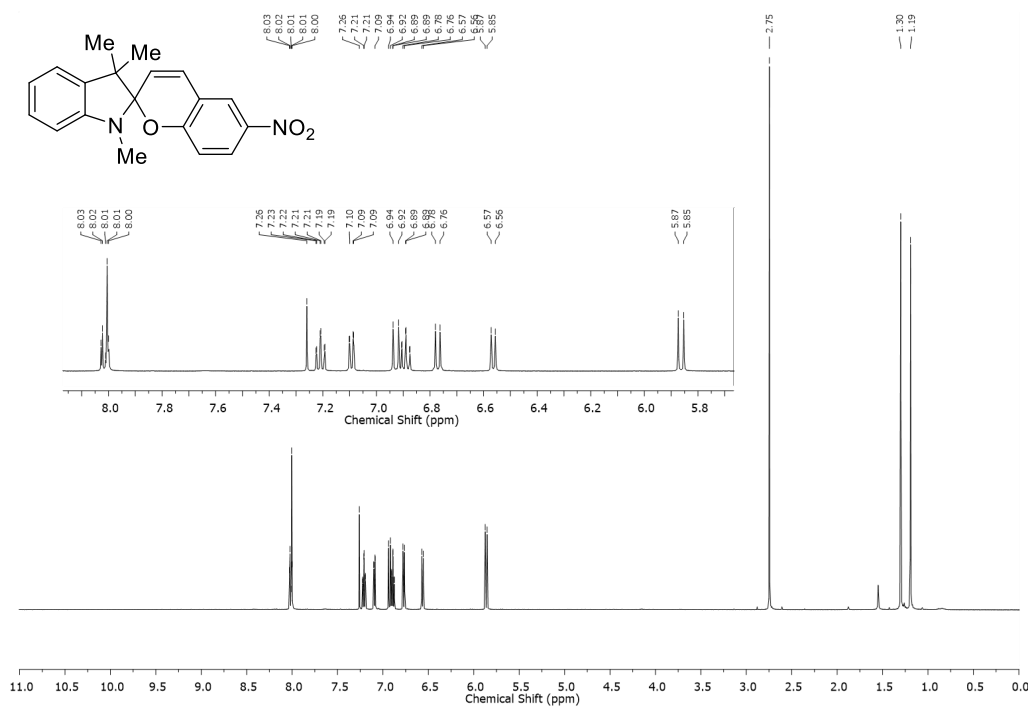


Figure S1: ^1H NMR spectrum of 1',3',3'-trimethyl-6-nitrospiro[chromene-2,2'-indoline] in CDCl_3 .

Figure S2

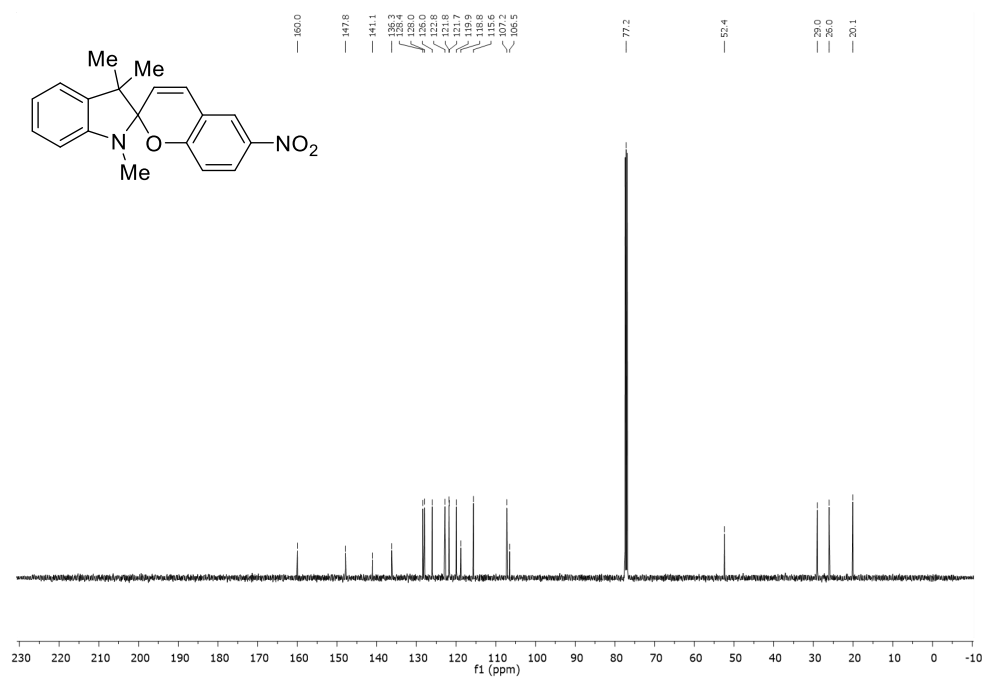


Figure S2: $^{13}\text{C}\{^1\text{H}\}$ NMR spectrum of 1',3',3'-trimethyl-6-nitrospiro[chromene-2,2'-indoline] in CDCl_3 .

Figure S3

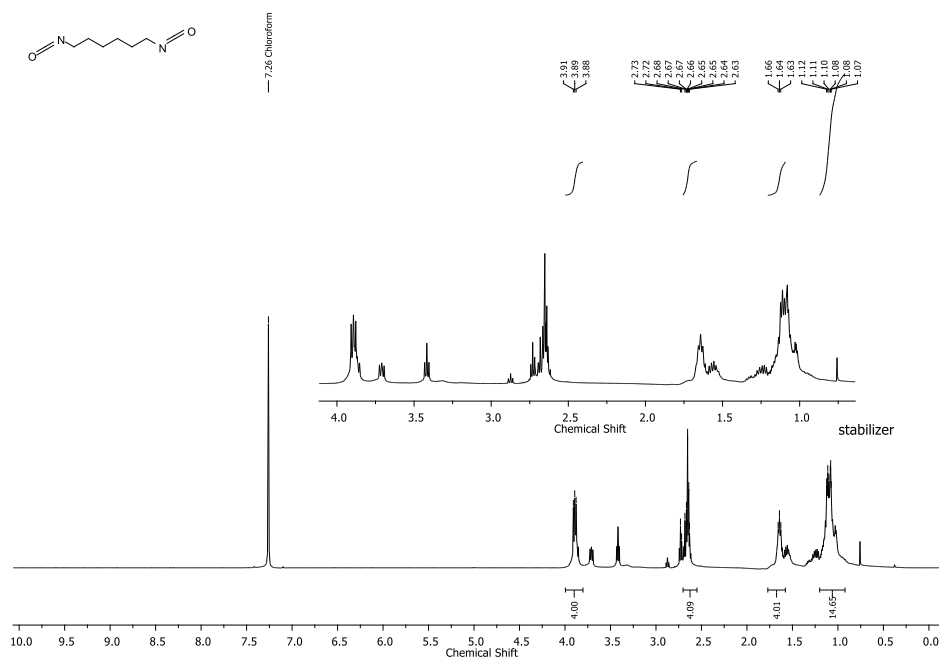
**Figure S3:** ^1H NMR spectrum of hexamethylenediisocyanate (HDI) in CDCl_3 (PTU-Monomer).

Figure S4

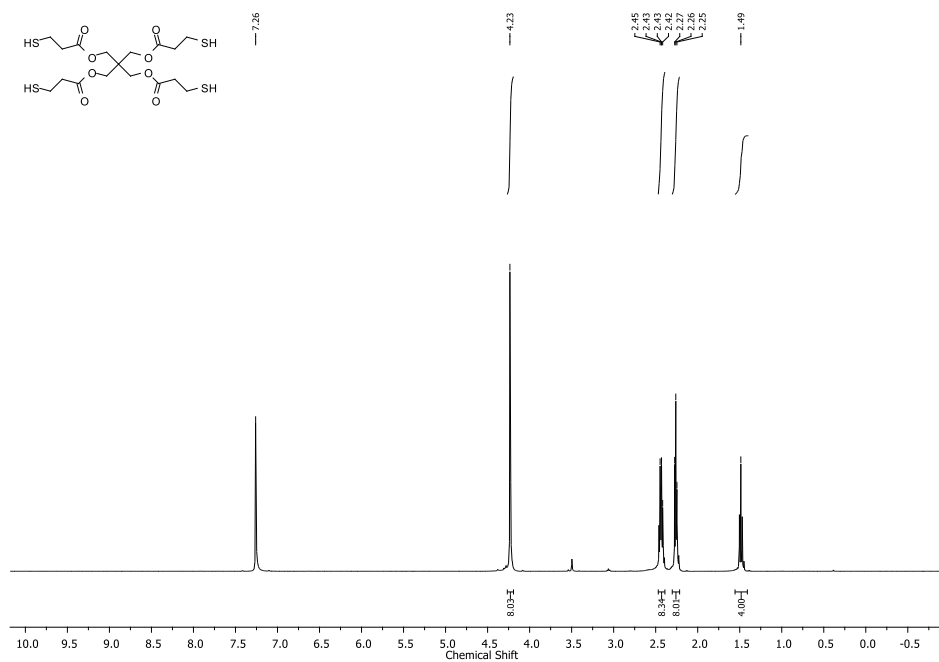


Figure S4: ¹H NMR spectrum of pentaerythritol tetrakis(3-mercaptopropionate) (PETMP) in CDCl₃ (PTU-Monomer).

Figure S5

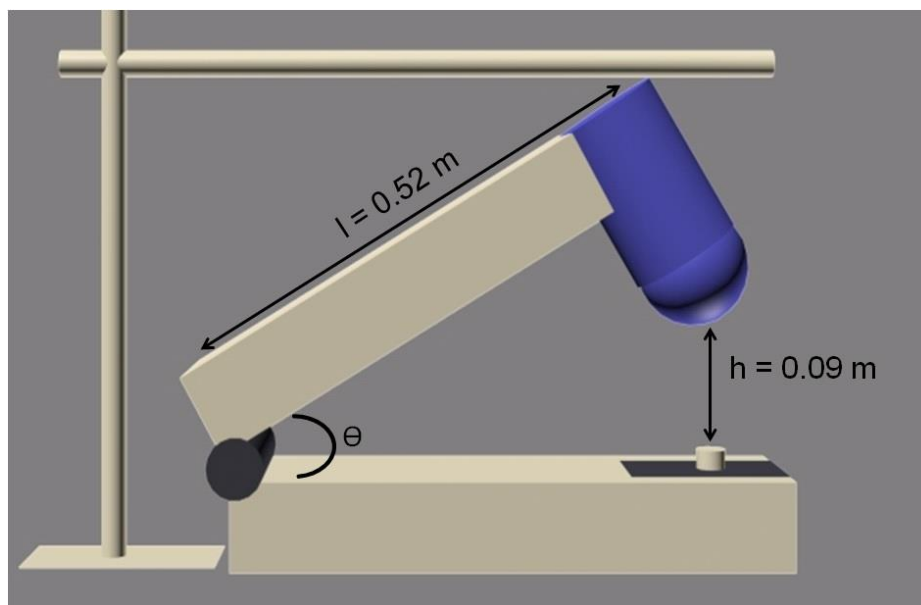


Figure S5: Schematic drawing of the “Hammer test”. The hammer is pulled up to a pre set height and released to fall on the sample freely.

Table T1: The average impact force measured required to damage the polymer matrix causing a color change

Sample name	Average impact pressure to cause switching (kPa)	Standard error (yEr±)
SP	106.252	8.064
P ₁	115.434	8.296
P ₂	144.293	18.643
P ₃	162.657	14.956
P ₄	232.18	3.935

References

- (1) Roxburgh, C. J.; Sammes, P. G.; Abdullah, A. Steric and Substituent Effects on the Photoreversibility of Novel Indolospirobenzopyrans: Acid Deuterolysis, UV and ¹H NMR Spectroscopy. *Dyes Pigments* **2009**, 82 (2), 226–237.

2.2. Supporting Information for *Mater. Horiz.* 2019
submitted

Please do not adjust margins

Electronic Supporting Information

Self-Reporting Mechanochromic Coating: Glassfiber Reinforced Polymer Composites That Predict Impact Induced DamageSindu Shree^{a*}, Mathias Schulz-Senft^b, Alina Kuntze^a, Yogendra Kumar Mishra^{a*}, Anne Staubitz^{b,c,d}, and Rainer Adelung^{a*}^a Functional Nanomaterials, Institute for Materials Science, Kiel University, Kaiserstr. 2, D-24143, Kiel, Germany.^b Otto-Diels-Institute for Organic Chemistry, Kiel University, Otto-Hahn-Platz 4, 24118 Kiel, Germany.^c Institute for Organic and Analytical Chemistry, University of Bremen, Leobener Str. 7, 28359 Bremen, Germany.^d MAPEX Center for Materials and Processes, University of Bremen Bibliothekstr. 1, 28359 Bremen, Germany**Keywords:** Glassfiber, polythiourethane, polymer composite, spiropyran, self-reporting, mechanochromic**Contents**

1. Analytical Equipment	2
2. Materials.....	2
1',3',3'-Trimethyl-6-nitrospiro[chromene-2,2'-indoline]	2
3. Sample preparation.....	3
4. Hammer Test.....	3
5. Image Analysis.....	3
6. Infrared Imaging	4
7. Analysis of the Spiropyran Failure in the Epoxy Matrix	4
8. Plotted NMR Spectra.....	9
¹ H and ¹³ C{ ¹ H} NMR Spectra of 1',3',3'-Trimethyl-6-nitrospiro[chromene-2,2'-indoline] in CDCl ₃	9
¹ H NMR Spectra of SP, Isopropyl glucidyl ether (iPr-Epoxy) and the Reaction Mixture in THF- <i>d</i> ₈	10
¹ H NMR Spectra of SP, Phenyl Glucidyl Ether (Ph-Epoxy) and the Reaction Mixture in THF- <i>d</i> ₈	11
¹ H NMR Spectra of SP, 2-Hydroxybenzoic acid (HBA) and the Reaction Mixture in THF- <i>d</i> ₈	12
¹ H and ¹³ C{ ¹ H} NMR Spectra of SP, Xylylenediamine (XDA), 1,3,3-Trimethyl-2-methyleneindoline (Ind) and the Reaction Mixture in THF- <i>d</i> ₈	12
References	14

Please do not adjust margins

Please do not adjust margins

ARTICLE

Journal Name

Abbreviations

The use of abbreviations follows the conventions from the ACS Style guide.^[1] In addition, the following abbreviations were used.

Abbreviation	Meaning
ATR	Attenuated total reflection (IR)
COSY	Correlation spectroscopy
dd (NMR)	Doublet of doublets
EI	Electron ionization
FT	Fourier transform
HMBC	Heteronuclear multiple bond correlation
HSQC	Heteronuclear single quantum coherence

1. Analytical Equipment

NMR spectra were recorded on a Bruker Avance Neo 500 (¹H NMR: 500 MHz) FT-NMR spectrometer at 300 K. ¹H NMR and ¹³C{¹H} NMR spectra were referenced against the solvent residual proton signals (¹H) or the solvent itself (¹³C).

The exact assignment of the peaks was performed by two-dimensional NMR spectroscopy such as ¹H COSY, ¹H NOESY, ¹H/¹³C HSQC and ¹H/¹³C HMBC.

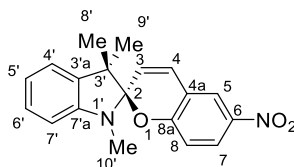
Mass spectrometric measurements were performed in the positive ion collection mode using a JEOL-Accu TOF 4GGCV EI mass spectrometer. For electron spray ionization (ESI), a Thermo Fisher Q Exactive Plus mass spectrometer with a quadrupole orbitrap was used in positive and negative ion collection mode with an ionization potential of 3.2 kV.

FTIR spectra were measured using a Perkin Elmer Paragon 1000 FT-IR spectrometer equipped with an A531-G Golden-Gate-ATR-unit.

The irradiation experiments were carried out using LED light sources with an optical power of 680 mW (360-370 nm) and 20 W (520-530 nm) at the LED.

A scanning electron microscope (SEM) from Carl Zeiss (10 kV, 10 μA) was used to investigate the samples in the presented work.

Infrared (IR) images were obtained using a FLIR ONE camera. The images were processed and temperatures were extracted using the software FLIR Tools.

2. Materials**1',3',3'-Trimethyl-6-nitrospiro[chromene-2,2'-indoline]**

Materials: 1,3,3-Trimethyl-2-methyleneindoline was purchased from Sigma-Aldrich Co. (Aldrich, 97%), 2-hydroxy-5-nitrobenzaldehyde was purchased from TCI Co. (>97%) and ethanol was purchased from Acros (anhydrous, ≥99.5%, stored over molecular sieves). All reagents were used without further purification.^[2]

1,3,3-Trimethyl-2-methyleneindoline (7.80 g, 45.0 mmol) and 2-hydroxy-5-nitrobenzaldehyde (7.52 g, 45.0 mmol) were dissolved in EtOH (125 mL) and heated to 78 °C for 3 h. Then the reaction mixture was cooled to -25 °C and the crystallized product was obtained after filtration as a green powder (12.7 g, 39.4 mmol, 88 %, Lit.: 89 %).^[2]

Melting point: *T* = 176 °C, Lit: 178 – 179 °C^[2]

¹H NMR (500 MHz, CDCl₃, 300 K): δ = 8.03 – 7.99 (m, 2H, H-5, H-7), 7.21 (ddd, ³J = 7.7 Hz, ³J = 7.4 Hz, ⁴J = 1.0 Hz, 1H, H-6'), 7.09 (dd, ³J = 7.2 Hz, ⁴J = 1.0 Hz, 1H, H-4'), 6.93 (d, ³J = 10.3 Hz, 1H, H-4), 6.89 (ddd, ³J = 7.4 Hz, ³J = 7.2 Hz, ⁴J = 1.0 Hz, 1H, H-5'), 6.77 (d, ³J = 8.5 Hz, 1H, H-8), 6.56 (d, ³J = 7.7 Hz, 1H, H-7'), 5.86 (d, ³J = 10.3 Hz, 1H, H-3), 2.75 (s, 3H, H-10'), 1.30 (s, 3H, H8'), 1.19 (s, 3H, H-9') ppm.

¹³C{¹H} NMR (126 MHz, CDCl₃, 300 K): δ = 160.0 (C-6), 147.8 (C-7'a), 141.1 (C-4a), 136.3 (C-3'a), 128.4 (C-4), 128.0 (C-6'), 126.0 (C-7), 122.8 (C-5), 121.8 (C-3), 121.7 (C-4'), 119.9 (C-5'), 118.8 (C-8a), 115.6 (C-8), 107.2 (C-7'), 106.5 (C-2), 52.4 (C-3'), 29.0 (C-10'), 26.0 (C-9'), 20.1 (C-8') ppm.

IR (ATR): $\tilde{\nu}$ = 3069 (w), 2966 (w), 2866 (w), 1655 (w), 1610 (m), 1575 (m), 1509 (s), 1488 (s), 1443 (m), 1364 (m), 1333 (vs), 1303 (s), 1271 (vs), 1185 (m), 1123 (s), 1089 (vs), 1022 (s), 950 (vs), 930 (s), 913 (s), 807 (vs), 752 (vs), 681 (s), 628 (m), 575 (m), 550 (m), 518 (m) cm⁻¹.

Please do not adjust margins

Please do not adjust margins

Materials Horizons

ARTICLE

HRMS (EI-TOF): m/z (%): $[M]^+$ calcd. for $[C_{19}H_{18}N_2O_3]^+$ 322.1317; found 322.1292 (67), 159.10 (100) $[M-Ph-O-NO_2-C_2H_2]^+$.

3. Sample Preparation

The “epoxy resin L”, the “hardener S” and the woven glassfibers with an areal density of 163 gm^{-2} used for the reinforcement were purchased from R&G Faserverbundwerkstoffe GmbH. The components for the PTU matrix, were bought from FPT Fluid- & Prozesstechnik GmbH. Both matrices were used and processed without further treatment, following the suppliers’ instructions.

Polymer composites with and without glassfibers were produced as explained in this section. Spiropyran (SP) was used in all the samples as a stress indicator to compare the mechanochromicity and the impact resistance of the composite system. In all the samples, SP was used at a concentration of 0.5 wt% and the glassfiber concentration was at $\sim 8 \text{ wt\%}$. The PTU/spiropyran (PTU/SP) was coated onto the woven glassfibers as explained in the following procedure. The monomers pentaerythritol tetrakis(3-mercaptopropionate) (PETMP) and hexamethylene diisocyanate (HDI) were mixed at a weight ratio of 1:1.4 with SP. After 15 min of degassing in a decicator, 20% of the total volume of this mixture was cast into a mold so that a uniform layer was obtained. A rectangular woven glassfiber mat ($70 \times 70 \text{ mm}^2$) was placed over the unpolymerized layer and the remaining 80% of the mixture was poured over the glassfiber mat. The sample was then placed for 20 h in a furnace at $80 \text{ }^\circ\text{C}$. To compare the GFPS composite system to the commercially available epoxy polymer, epoxy/spiropyran coated glassfiber (GFES) samples were prepared similarly: PTU/SP was first hand-dispersed into the hardener and the epoxy resin (45:100 parts by volume of hardener : epoxy) was later added to the dispersion, the unpolymerized mixture was coated onto the glassfiber mat as explained earlier. PTU/SP, GFPS and GFES i.e., sheets with and without glassfiber mats (thickness, 5 mm) were then cut into smaller samples of the size $20 \times 20 \text{ mm}^2$ for further investigations.

4. Hammer Test

The “Hammer test” test (Figure SI-1) involved a hammer weighing 2.141 kg with a hinge at its base falling freely on the samples. The test was repeated periodically until a color change was observed. The force required to damage the system was determined by the number of hits needed to cause a color change from orange to purple.

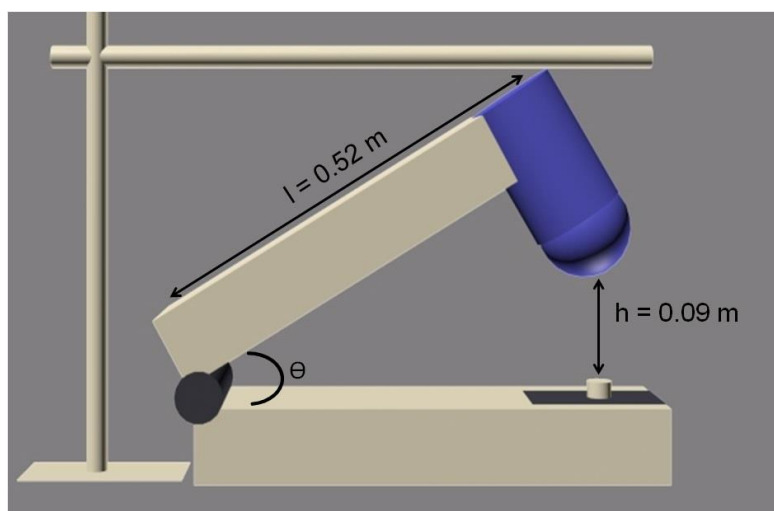


Figure SI-1: Sketch of the “Hammer test”. The hammer shaft is drawn to a defined height and released on to the sample freely.

The impact force was calculated using the following equation $F = m \cdot g \cdot \sin\theta = m \cdot g \cdot \frac{h}{l}$ where F is Force, m is weight of the hammer head, g is acceleration due to gravity, h is height of fall, and l is length of the hammer. Pressure per impact was calculated using $P = F/a$ where a is the area of impact or point of contact. The measured area of impact was $1.53 \times 10^{-4} \text{ m}^2$.

5. Image Analysis

Corresponding videos of the periodic impact test were created with ImageJ by stacking the images taken after each hit under periodic impact test of the samples PTU/SP and GFPS. An RGB hyper stack was created using ImageJ for the purpose of quantitative analysis. Videos

Please do not adjust margins

Please do not adjust margins

ARTICLE

Journal Name

of the impact test of the sample PTU/SP with separated red, blue and green filter served to observe which color showed the most transformation under impact and was thus most suited for the analysis. These videos are attached separately.

6. Infrared Imaging

To monitor the temperature changes occurring at the point of impact on a sample due to periodic impact (Hammer test) IR imaging was employed. The resulting temperatures at and around the point of impact differed by maximally $\sim 6\text{--}8\text{ }^{\circ}\text{C}$ (Figure SI-2).

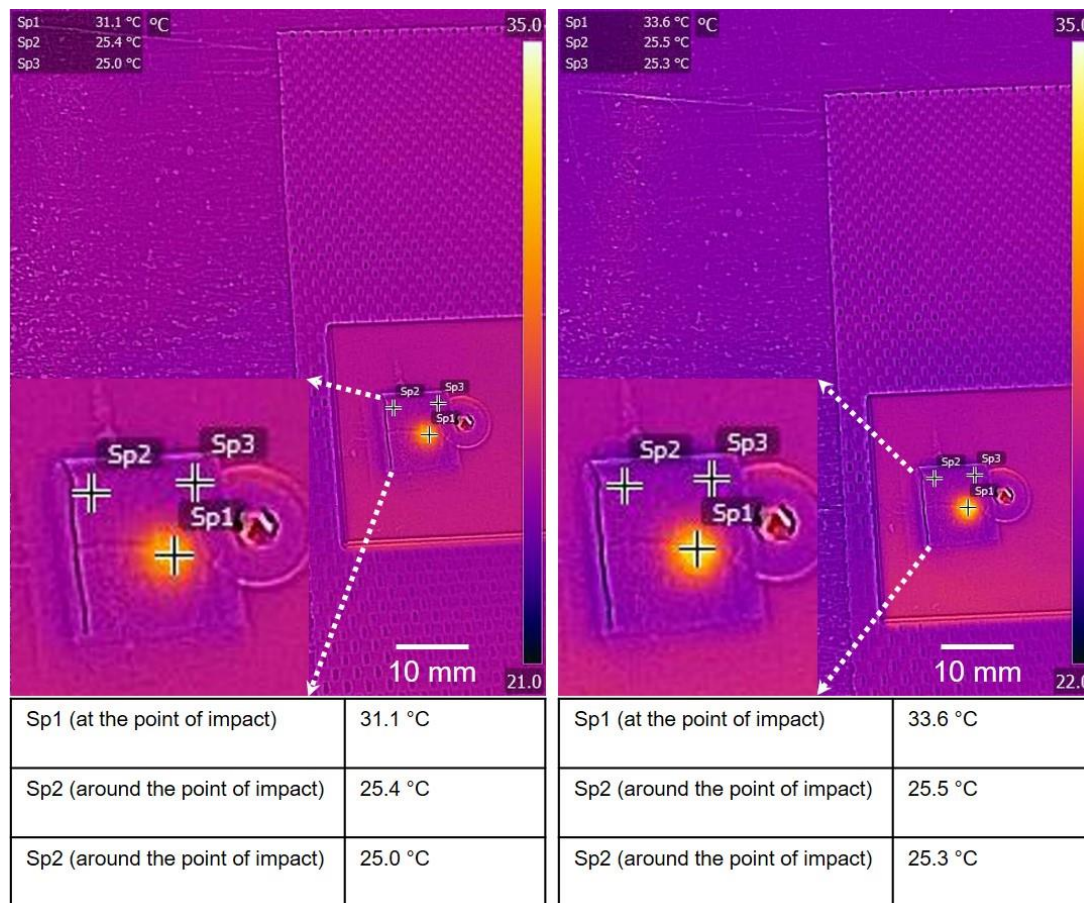


Figure SI-2: Images of GFPS samples were taken by an infrared camera at the end of the periodic impact test. Temperatures at different spots (Sp) were measured for comparison.

7. Analysis of Spiropyran Degradation in the Epoxy Matrix

SP in the epoxy matrix could not be used as a stress indicator. SP is a molecule with several functional groups and the components for the synthesis of the epoxy polymer also comprise a high number of compounds with various functional groups. It is plausible that undesired reactions between these components and the SP take place and thus render the molecule inactive. In order to shed some light on this, several experiments were performed:

The supplier of epoxy system that was used, R&G Faserverbundwerkstoffe GmbH, specifies the "Epoxy Resin L" as a three-component mixture, consisting of an epoxy resin as pre-polymer, phenylglycidyl ether formaldehyde resin as reactive pre-polymer and 1,6-hexanediol diglycidyl ether as reactive monomer (shown in Figure SI-3). The "Hardener S" is a mixture of six components. Two styrenated phenols, 2-

Please do not adjust margins

Please do not adjust margins

Materials Horizons

ARTICLE

hydroxy benzoic acid and three primary amines are combined to ensure complete curing within 24 h above 5 °C. Since the supplier specifies only percentage ranges for each component, accurate investigation of the reaction of SP with the hardener and resin during the curing was not feasible. Instead, four model compounds representing the functional groups in both resin and hardener were chosen. Isopropyl glucidyl ether (**iPr-Epoxy**) and phenyl glucidyl ether (**Ph-Epoxy**) represent the reactive components in the "Epoxy Resin L". The "Hardener S" contains phenol groups, benzoic acid groups and amines. Here 2-hydroxybenzoic acid (**HBA**) and *m*-xylylenediamine (**XDA**) was chosen as representative components.

The four reference compounds (**iPr-Epoxy**, 98%; **Ph-Epoxy**, 99%; **HBA**, ≥99% and **XDA**, 99%) were purchased from TCI Co and used without further purification.

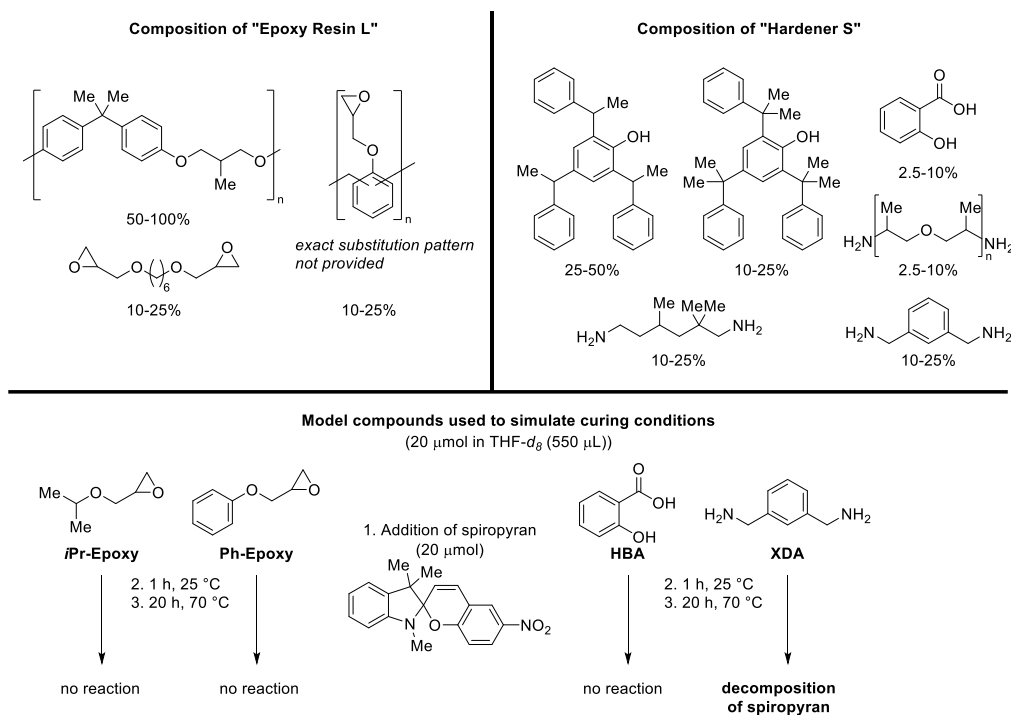


Figure SI-3: Composition of the commercial epoxy system. Top: Composition of the purchased Epoxy Resin L and Hardener S from R&G Faserverbundwerkstoffe GmbH. Bottom: Four model compounds were selected for the investigation of the possible reaction of **SP** during the curing process. The compounds were dissolved in THF-*d*₈, before adding SP. Only the sample with **XDA** lead to decomposition of the SP as shown by NMR spectroscopy.

Each of the four compounds (20 μmol) were mixed with SP (20 μmol) in THF-*d*₈ and placed in sealable NMR tubes in a nitrogen filled glove box. To understand the interaction between SP and the components three ¹H NMR spectra were obtained: a) immediately after mixing, b) after resting for 1 h at 25 °C, and c) after resting for 20 h at 70 °C.

The ¹H spectra of the SP and the four equimolar mixtures after the complete heating cycle is displayed **Figure SI-4**. All spectra were recorded using the same settings and were not individually rescaled. The signals corresponding to the protons of the SP can be found in all spectra, however, they are notably less intense in the top spectrum, corresponding to the mixture with **XDA**. The signals of the proton *H*-3 and the methyl groups *H*-8' and *H*-9' (compare section 4) are the most distinct ones to control the SP's stability and they are highlighted in **Figure SI-4**.

Please do not adjust margins

Please do not adjust margins

ARTICLE

Journal Name

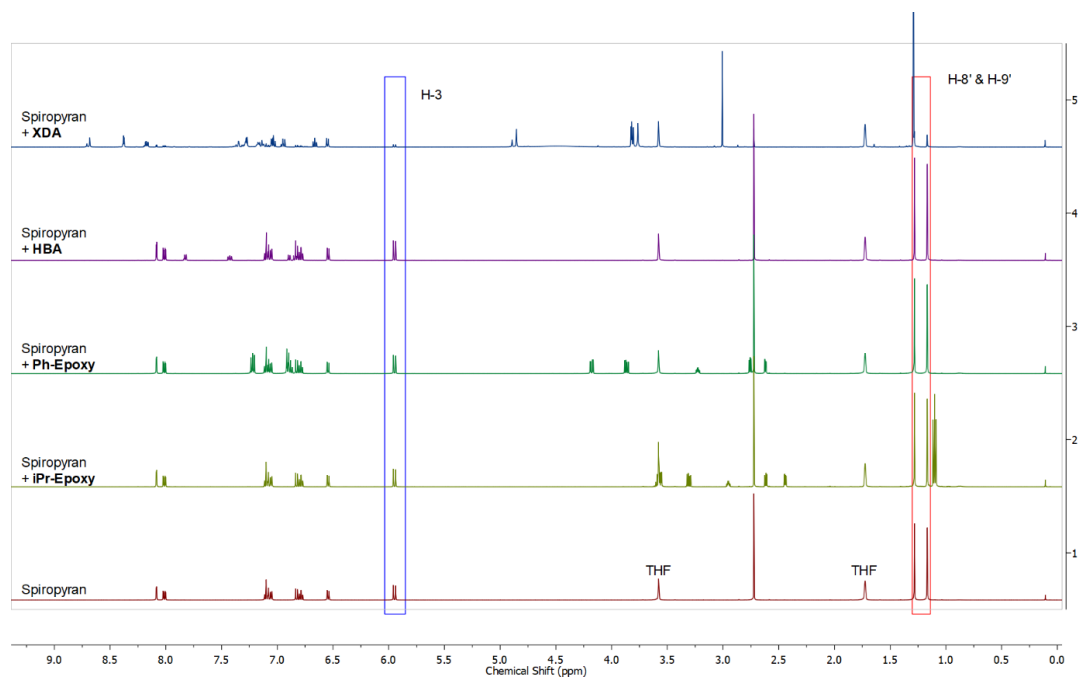
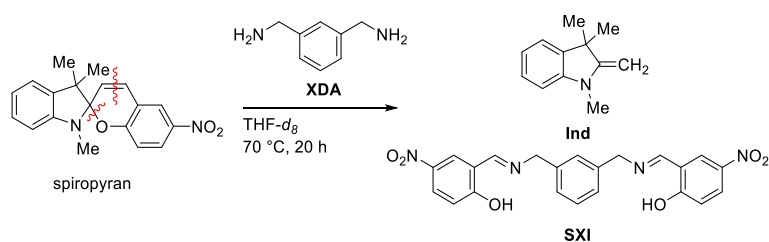


Figure SI-4: Overview of the stability test. The ^1H spectra of (bottom to top) SP, SP + *iPr*-Epoxy, SP + Ph-Epoxy, SP + HBA, SP + XDA after resting at 70 °C for 20 h are shown. All spectra were recorded with the same settings and were not rescaled. The blue box highlights the signal of the proton *H*-3 and the red box highlights the signal of the methyl protons *H*-8' and *H*-9' (compare section 4) of the SP. The intensity of these signals is drastically reduced in the top spectrum, corresponding to the mixture of SP and XDA. The signals corresponding to the solvent THF- d_6 are labeled in the bottom spectrum.

In order to reveal the kind of reaction that could have occurred with XDA, the sample with SP and XDA was fully investigated using NMR methods. First, a switching to the open merocyanine form could be excluded as the characteristic signal of the ethylene bridge was absent. Whereas the coupling constant of the protons (*H*-3 and *H*-4, compare to **Chapter 2** in this SI) is approx. 10 Hz in the closed form, it increases to approx. 15 Hz in the open form.^[3] It was possible to identify 1,3,3-trimethyl-2-methyleneindoline (**Ind**) and 5-nitrosalicylaldehyde-1,3-xylylenediimine (**SXI**) as products, proving a cleavage of the ethylene bridge in the SP. ESI mass spectrometry in high resolution of the reaction mixture proved the presence of the four mentioned compounds. An additional set of signals was detected in ^1H and $^{13}\text{C}\{^1\text{H}\}$ NMR. As in **SXI**, it contained signals corresponding to imine bridges. However, it might be structurally similar to **SXI** and could not be assigned this set of signals to a reasonable product.



Scheme SI-1: Confirmed ring opening reaction of SP in presence of xylylenediamine (XDA). 1,3,3-Trimethyl-2-methyleneindolene (**Ind**) and 5-nitrosalicylaldehyde-1,3-xylylenediimine were identified as products. The broken SP bonds are indicated as red wavy lines.

Please do not adjust margins

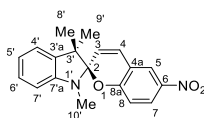
Please do not adjust margins

Materials Horizons

ARTICLE

The NMR shift data were obtained by measuring the reaction mixture. Assignment of the peaks was performed by using spectra of the pure compounds SP, XDA and Ind as reference. The ESI measurement was performed using an ionization potential of 3.2 kV. SP, XDA and Ind were detected in positive ion mode; SXI was detected in negative ion mode.

Signals assigned to SP:

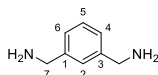


$^1\text{H NMR}$ (500 MHz, THF- d_6 , 300 K): δ = 8.08 (d, 4J = 2.8 Hz, 1H, H-5), 8.01 (dd, 3J = 9.0 Hz, 4J = 2.8 Hz, 1H, H-7), 7.12 – 7.08 (m, 2H, H-4, H-6'), 7.05 (dd, 3J = 7.4 Hz, 4J = 1.3 Hz, H-4'), 6.83 (d, 3J = 9.0 Hz, 1H, H-8), 6.79 (ddd, 3J = 7.4 Hz, 3J = 7.4 Hz, 3J = 1.0 Hz, 1H, H-5'), 6.54 (d, 3J = 7.7 Hz, 1H, H-7'), 5.95 (d, 3J = 10.3 Hz, 1H, H-3), 2.72 (s, 3H, H-10'), 1.28 (s, 3H, H-8'), 1.17 (s, 3H, H-9') ppm.

$^{13}\text{C}\{^1\text{H}\}$ NMR (126 MHz, THF- d_6 , 300 K): δ = 160.6 (C-8a), 148.8 (C-7a'), 142.1 (C-6), 137.0 (C-3a'), 129.3 (C-4), 128.4 (C-6'), 126.3 (C-7), 123.3 (C-5), 122.3 (C-3), 122.1 (C-4'), 120.4 (C-5'), 120.0 (C-4a), 116.1 (C-8), 107.7 (C-7'), 107.3 (C-2), 52.9 (C-3'), 28.9 (C-10'), 26.2 (C-8'), 20.2 (C-9') ppm.

HRMS (ESI-Sector): m/z : [M+H] $^+$ calcd. for [C₁₉H₁₉N₂O₃] $^+$ 323.1390; found 323.1385.

Signals assigned to xylylenediamine (XDA):

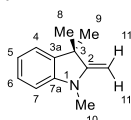


$^1\text{H NMR}$ (500 MHz, THF- d_6 , 300 K): δ = 7.30 – 7.27 (m, 1H, H-2), 7.19 – 7.11 (m, 3H, H-4, H-5, H-6), 3.76 (s, 4H, H-7), 1.39 (s, 4H, NH₂) ppm.

$^{13}\text{C}\{^1\text{H}\}$ NMR (126 MHz, THF- d_6 , 300 K): δ = 145.3 (C-1, C-3), 128.6 (C-5), 126.4 (C-2), 125.6 (C-4, C-6), 47.4 (C-7) ppm.

HRMS (ESI-Sector): m/z : [M+H] $^+$ calcd. for [C₈H₁₃N₂] $^+$ 137.1073; found 137.1072.

Signals assigned to 1,3,3-trimethyl-2-methyleneindoline (Ind):



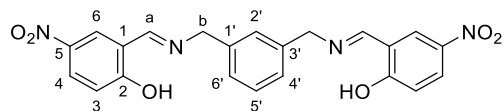
$^1\text{H NMR}$ (500 MHz, THF- d_6 , 300 K): δ = 7.06 – 7.01 (m, 2H, H-4, H-6), 6.67 (ddd, 3J = 7.4 Hz, 3J = 7.4 Hz, 3J = 1.0 Hz, 1H, H-5), 6.55 (d, 3J = 7.8 Hz, 1H, H-7), 3.82 (d, 5J = 1.9 Hz, 2H, H-11, H-11'), 3.01 (s, 3H, H-10), 1.29 (s, 6H, H-8, H-9) ppm.

$^{13}\text{C}\{^1\text{H}\}$ NMR (126 MHz, THF- d_6 , 300 K): δ = 163.4 (C-2), 147.3 (C-7a), 138.2 (C-3a), 128.2 (C-6), 122.3 (C-4), 119.1 (C-5), 105.7 (C-7), 73.5 (C-11), 44.7 (C-3), 30.2 (C-8, C-9), 28.7 (C-10) ppm.

HRMS (ESI-Sector): m/z : [M+H] $^+$ calcd. for [C₁₂H₁₆N] $^+$ 174.1277; found 174.1275

Please do not adjust margins

Please do not adjust margins

Signals assigned to 5-nitrosalicylaldehyde-1,3-xylylenediimine (SX1):

$^1\text{H NMR}$ (500 MHz, THF- d_8 , 300 K):¹ δ = 8.68 (m, 2H, H-a), 8.38 (d, 4J = 2.9 Hz, 2H, H-6), 8.17 (dd, 3J = 9.2 Hz, 4J = 2.9 Hz, 2H, H-4), 7.35 (m, 1H, H-2'), 7.28 (m, H-5'), 7.18 (m, H-4', H-6'), 6.94 (d, 3J = 9.2 Hz, 2H, H-3), 4.85 (m, 4H, H-b) ppm.

$^{13}\text{C}\{^1\text{H}\}$ NMR (126 MHz, THF- d_8 , 300 K): δ = 169.5 (C-2), 166.4 (C-a), 139.9 (C-5), 138.2 (C-1', C-3'), 129.1 (C-6), 128.5 (C-4), 127.5 (C-2'), 127.1 (C-5'), 126.7 (C-4', C-6'), 119.2 (C-3), 118.4 (C-1), 62.45 (C-b) ppm.

HRMS (ESI-Sector): m/z : [M-H]⁻ calcd. for [C₂₂H₁₇N₄O₆]⁻ 433.1154; found 433.1152.

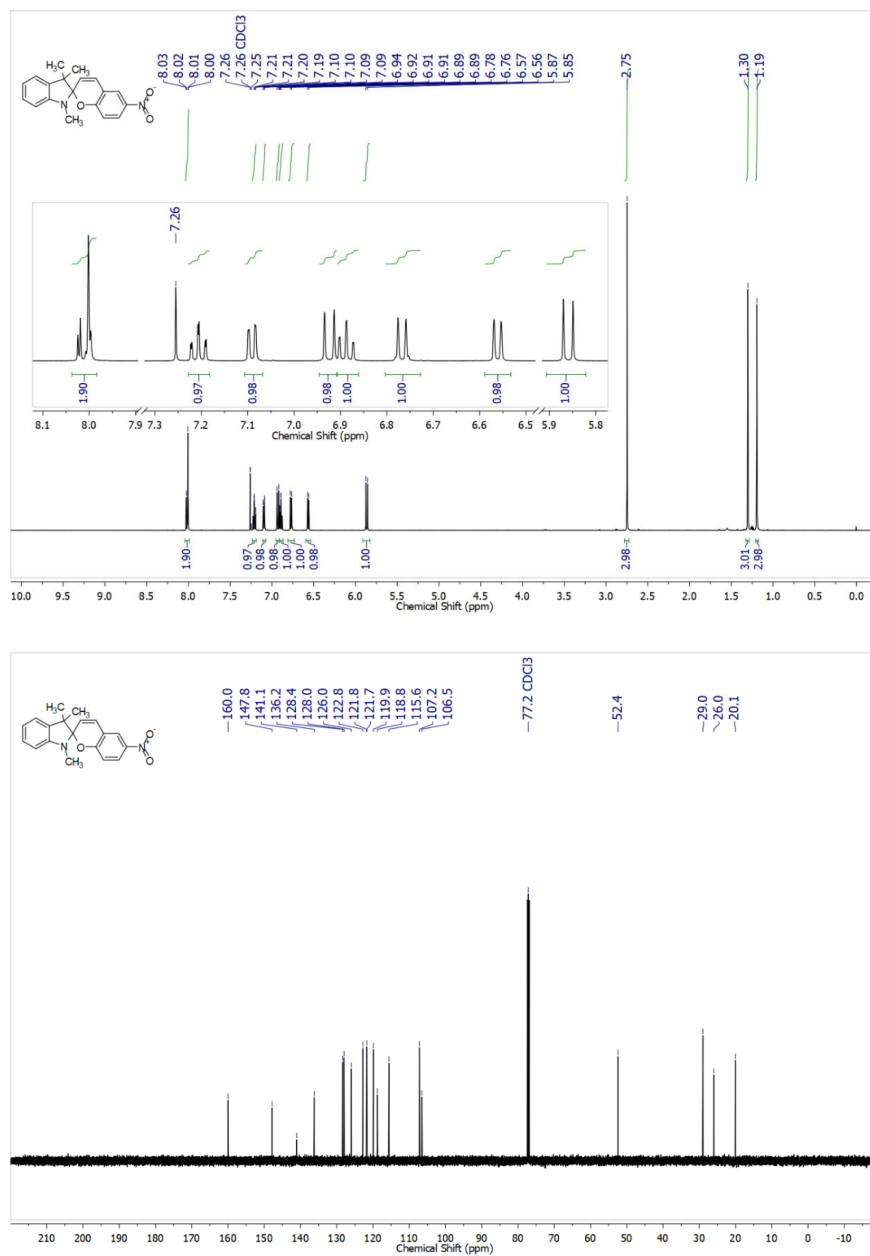
¹ Due to the intensive overlap of signals with a chemical shift of 7.3 – 7.0 ppm in the $^1\text{H NMR}$ spectrum, it was not possible to integrate reliably.

Please do not adjust margins

Please do not adjust margins

Materials Horizons

ARTICLE

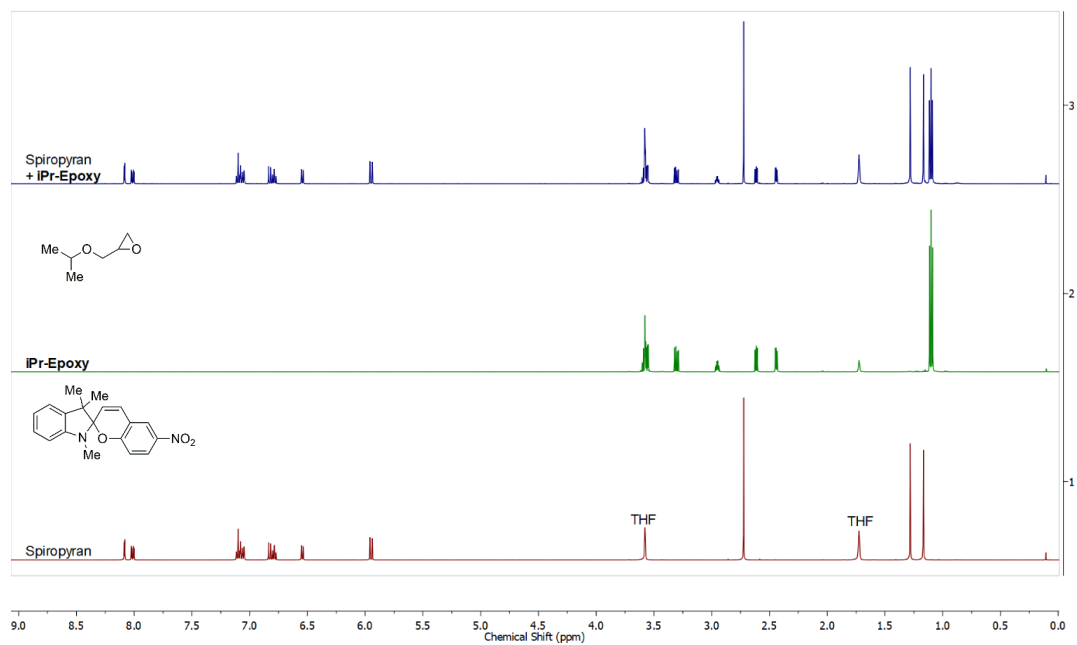
8. Plotted NMR Spectra**¹H and ¹³C{¹H} NMR Spectra of 1',3',3'-Trimethyl-6-nitrospi[chromene-2,2'-indoline] in CDCl₃**

Please do not adjust margins

Please do not adjust margins

ARTICLE

Journal Name

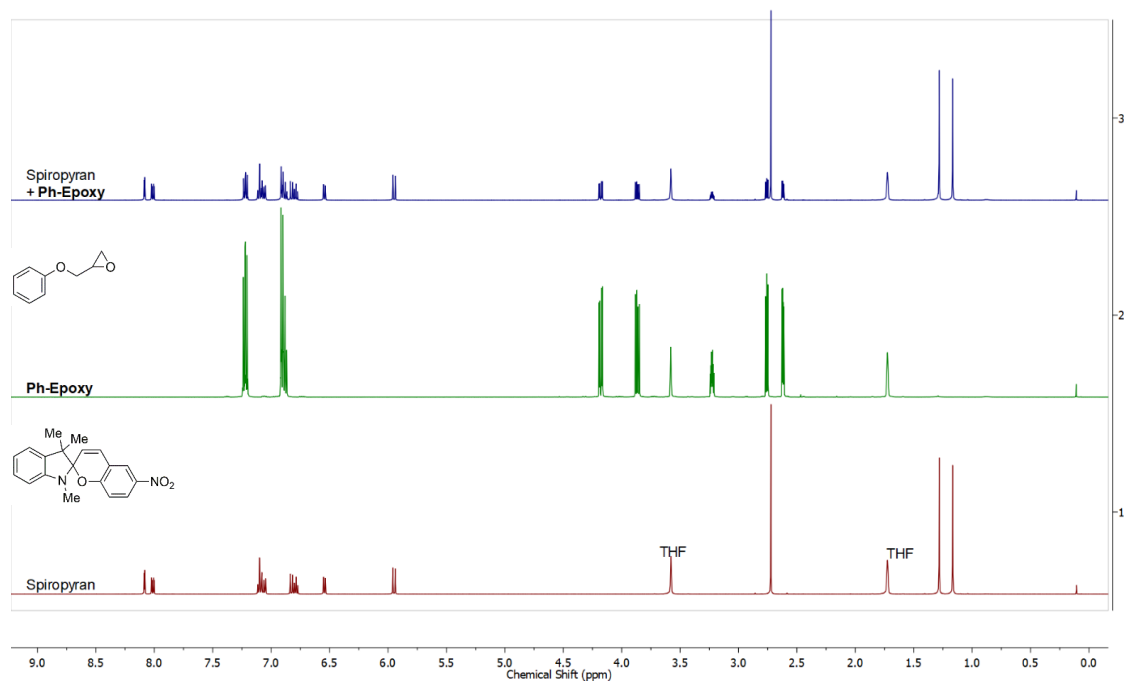
¹H NMR Spectra of SP, Isopropyl Glucidyl Ether (*i*Pr-Epoxy) and the Reaction Mixture in THF-*d*₈

Please do not adjust margins

Please do not adjust margins

Materials Horizons

ARTICLE

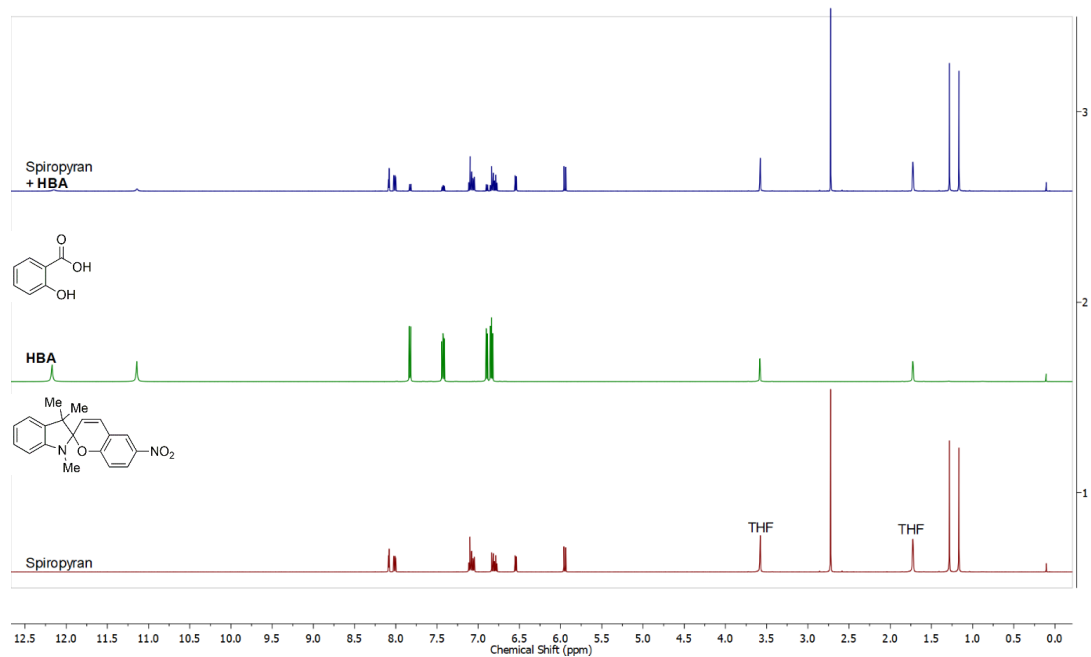
¹H NMR Spectra of SP, Phenyl Glucidyl Ether (Ph-Epoxy) and the Reaction Mixture in THF-*d*₈

Please do not adjust margins

Please do not adjust margins

ARTICLE

Journal Name

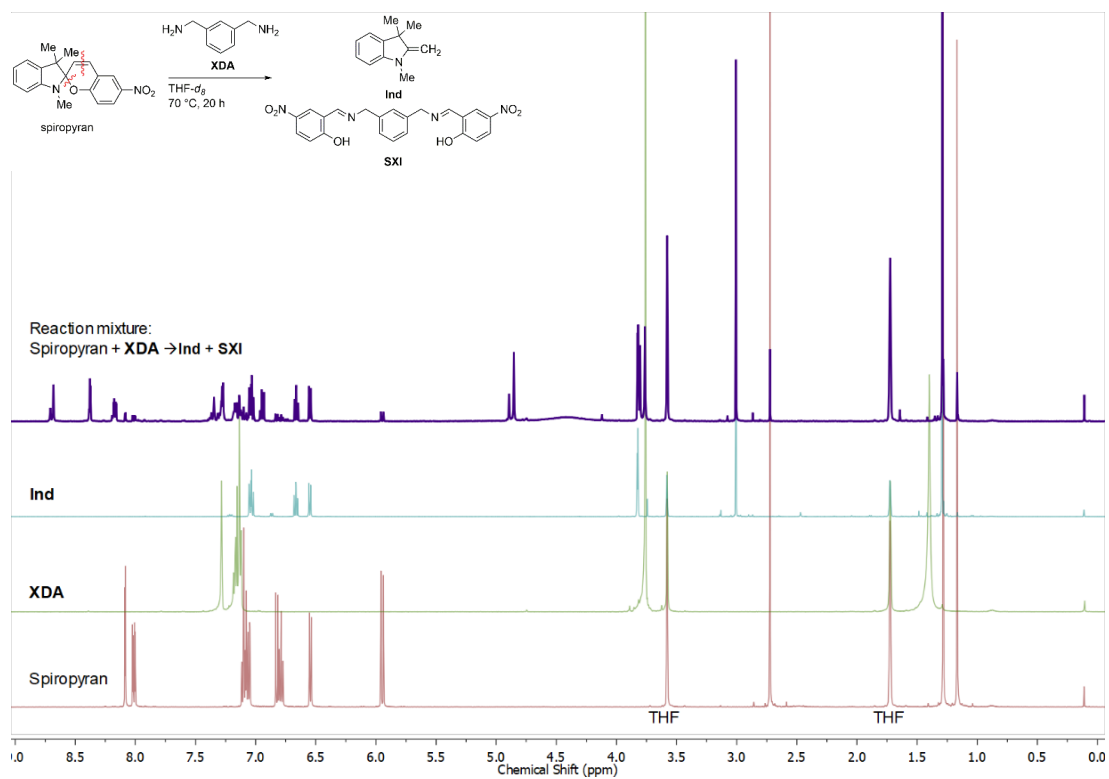
¹H NMR Spectra of SP, 2-Hydroxybenzoic acid (HBA) and the Reaction Mixture in THF-*d*₆**¹H and ¹³C{¹H} NMR Spectra of SP, Xylylenediamine (XDA), 1,3,3-Trimethyl-2-methyleneindoline (Ind) and the Reaction Mixture in THF-*d*₆**

Please do not adjust margins

Please do not adjust margins

Materials Horizons

ARTICLE

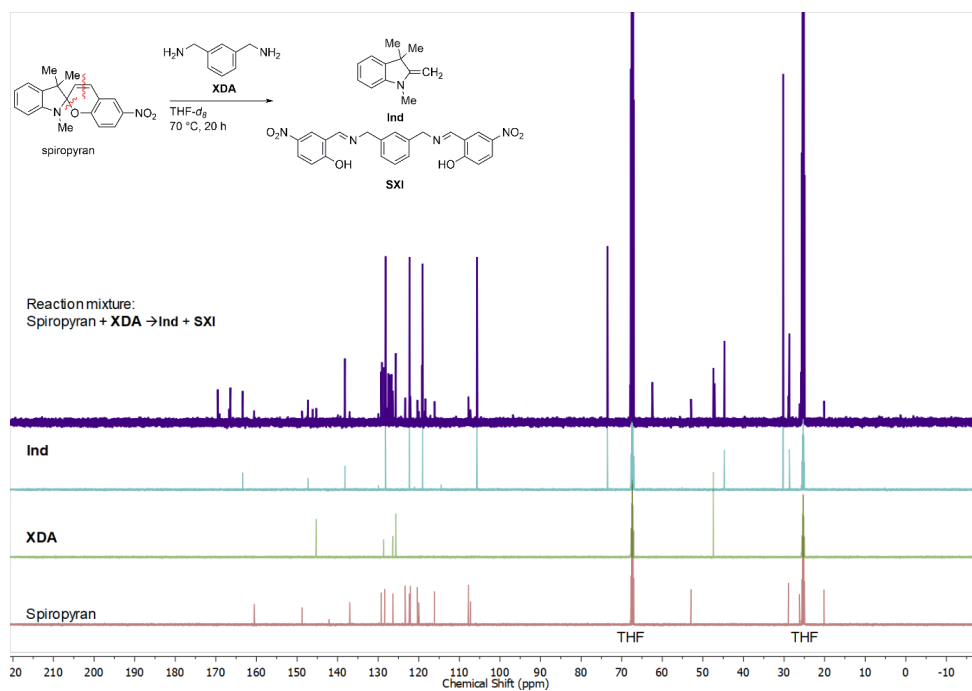
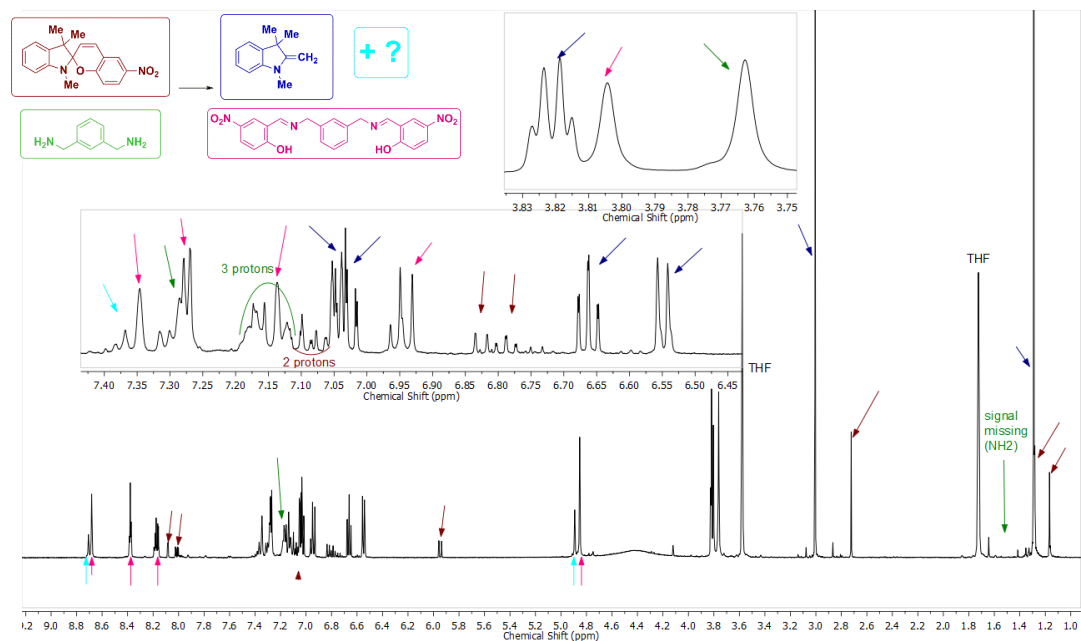


Please do not adjust margins

Please do not adjust margins

ARTICLE

Journal Name



References

1. M. Coghill, L. R. Garson, Eds., *The ACS Style Guide: Effective Communication of Scientific Information*, American Chemical Society, Washington, DC, 2006.
2. C. J. Roxburgh, P. G. Sammes, A. Abdullah, *Dye. Pigment.* 2011, **90**, 146.
3. M. Schulz-Senft, P. J. Gates, F. D. Sönnichsen, A. Staubitz, *Dye. Pigment.* 2017, **136**, 292.

Please do not adjust margins

3. Spiropyran Dyes with Halide and Pseudohalide Groups

Most syntheses in this context were published in the Supplementary Material of the publication in *Dyes and Pigments*.^[174]

3.1. Supporting Information for *Dyes and Pigments* 2017, 136, 292-301.

Supplementary Material

for

Diversely Halogenated Spiropyrans - Useful Synthetic Building Blocks for a Versatile Class of Molecular Switches

Mathias Schulz-Senft¹, Paul J. Gates², Frank D. Sönnichsen¹, and Anne Staubitz^{*,1,3,4}

¹ *Otto-Diels-Institute for Organic Chemistry, University of Kiel, Otto-Hahn-Platz 4, 24098 Kiel (Germany)*

² *School of Chemistry, University of Bristol, Cantock's Close, Bristol BS8 1TS (UK)*

³ *Institute for Organic and Analytical Chemistry, University of Bremen, Leobener Str. NW2 C, 28359 Bremen (Germany).*

⁴ *MAPEX Center for Materials and Processes, University of Bremen Bibliothekstraße 1, 28359 Bremen (Germany)*

* astaubitz@oc.uni-kiel.de and staubitz@uni-bremen.de

Abbreviations	2
Analytical Equipment and Equipment for Syntheses	2
Reagents	3
Solvents.....	4
References	5
Experimental Procedures	6
UV/vis Measurements and Determination of Attenuation Coefficients by ¹ H NMR Spectroscopy.....	28
UV/vis Spectra and Corresponding ¹ H NMR Spectra	33
¹ H NMR and ¹³ C{ ¹ H} NMR Spectra.....	46

Abbreviations

The use of abbreviations follows the conventions from the ACS Style guide.[1] In addition, the following abbreviations are used.

Abbreviation	Long form
at (NMR)	Apparent triplet
ATR	Attenuated total reflection (IR)
CI	Chemical ionization
COSY	Correlation spectroscopy
DCM	Dichloromethane
dd (NMR)	Doublet of doublets
DMSO	Dimethyl sulfoxide
EI	Electron ionization
ESI	Electrospray ionization
FT	Fourier transform
HMBC	Heteronuclear multiple bond correlation
HPLC	High performance liquid chromatography
HSQC	Heteronuclear single quantum coherence
NOESY	Nuclear Overhauser enhancement spectroscopy
PSS	Photostationary state
THF	Tetrahydrofuran
TOF	Time-of-flight mass detector
v/v	Volume concentration (volume/volume)

Analytical Equipment and Equipment for Syntheses

NMR spectra were either recorded on a Bruker DRX 500 (^1H NMR: 500 MHz) or on a Bruker Avance 600 (^1H NMR: 600 MHz) FT-NMR spectrometer. ^1H NMR and $^{13}\text{C}\{^1\text{H}\}$ NMR spectra were referenced against the solvent residual proton signals (^1H) or the solvent itself (^{13}C). ^{19}F NMR spectra were referenced internally against CCl_3F . The exact assignment of the peaks was performed by two-dimensional NMR spectroscopy such as ^1H COSY, ^1H NOESY, $^1\text{H}/^{13}\text{C}$ HSQC or $^1\text{H}/^{13}\text{C}$ HMBC if possible.

^1H NMR spectra for the determination of the ratio between spirocyanine and merocyanine form were recorded on a Bruker Avance 600 MHz FT-NMR spectrometer. Due to the low concentration of the samples (ca. 50 $\mu\text{mol/L}$), excitation sculpting was used to suppress residual solvent lines and 1024 scans were recorded. Mass spectrometric measurements were performed in the positive ion mode using a JEOL-Accu TOF 4GGCV EI mass spectrometer, a Bruker Daltonics micrOTOF II ESI mass spectrometer or a VG Analytical Autospec apparatus for CI. Electron ionization (EI) and Chemical ionization (CI) were performed using an ionization potential of 70 eV. In the case of CI ionization, methane was used as the reagent gas.

IR spectra were measured using a Perkin Elmer Paragon 1000 FT-IR spectrometer equipped with an A531-G Golden-Gate-ATR-unit.

UV spectra were recorded at 25 °C using a Perkin Elmer Lambda 14 UV spectrometer. Quartz cuvettes with a light path length of 10 mm from Hellma Analytics were used.

Melting points were measured on an electrothermal IA6304 capillary melting point apparatus and are uncorrected.

The irradiation experiments were carried out using LED light sources with an optical power of 1050 mW (Nichia NC4U033A; 365 nm) and 350 mW (Luxeon LXML-PX02; 565 nm).

Reagents

If not noted otherwise, all reagents were used as received.

Reagent	Supplier	Purity/concentration	Notes
2-Bromophenol	ABCR	98%	
2-Iodophenol	Sigma-Aldrich	98%	
3-Methyl-2-butanone	ABCR	98%	
4-Bromophenyl hydrazine hydrochloride	Sigma-Aldrich	99%	
4-Iodophenyl hydrazine	Maybridge	95%	
4-Methoxyphenyl hydrazine hydrochloride	TCI	>98%	
Hydrobromic acid	Sigma-Aldrich	48%	Reagent grade
Hydrochloric acid	Grüssing	37%	
Iodomethane	Sigma-Aldrich	99%	Contains copper as stabilizer
Magnesium chloride	Acros	99.9%	Anhydrous
Magnesium sulfate	Grüssing	99%	
Nitric acid	Merck	100% (fuming)	
o-Vanillin	AlfaAesar	99%	
Paraformaldehyde	ABCR	97%	
Piperidine	Acros	>99.5%	
Potassium hydroxide	Grüssing	85%	
Pyridine	Acros	99.5%	Extra dry, over molecular sieve
Silica gel 60	Merck		15-40 µm
Sodium chloride	Grüssing	99.5%	
Sodium hydroxide	Grüssing	98%	
Sodium sulfate	Grüssing	98%	
Trichlorofluoromethane	Sigma-Aldrich	>99%	
Triethylamine	Acros	99.5%	Predried over KOH, distilled from CaH ₂
Trifluoromethanesulfonic anhydride	ABCR	>99%	

Solvents

All solvents which were purchased in technical grade were purified by evaporation prior to use. Solvents of purities higher than 99% were not purified further. Some solvents were degassed by three freeze-pump-thaw cycles, backfilled with nitrogen and stored over molecular sieve 3 Å.

The following solvents were dried in a solvent purification system PS-MD-5 by Innovative Technology: dichloromethane, diethyl ether, tetrahydrofuran.

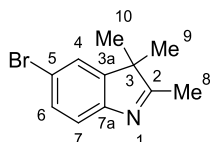
Solvent	Supplier	Purity	Drying procedure	Degassed
Acetic acid	Grüssing	99.5%	Distilled from copper(II) sulfate	No
Acetone	Walter-CMP	Technical grade	none	No
Acetonitrile	Sigma-Aldrich	>99.9%, HPLC grade	none	No
Acetonitrile- <i>d</i> ₃	Deutero	99.8% D	none	No
Chloroform- <i>d</i>	Euriso-top	99.8% D	none	No
Dichloromethane	VWR	HPLC grade	PS-MD-5	Yes
Dichloromethane- <i>d</i> ₂	Deutero	99.6% D	none	No
Diethyl ether	VWR	HPLC grade	PS-MD-5	Yes
Dimethyl sulfoxide- <i>d</i> ₆	Euriso-top	99.8% D	none	No
Ethanol	VWR	Technical grade, denaturated with petroleum oil	Distilled from calcium oxide	No
Ethyl acetate	Walter-CMP	Technical grade	none	No
<i>n</i> -Heptane	AlfaAesar	>99%	none	No
<i>n</i> -Hexane	Sigma-Aldrich	>99.9%, HPLC grade	none	No
Tetrahydrofuran	VWR	HPLC grade	PS-MD-5	Yes
Toluene	VWR	Technical grade	none	No

References

- [1] Coghill AM, Garson LR, editors. *The ACS Style Guide: Effective Communication of Scientific Information*. 3rd ed. Washington, DC: American Chemical Society; 2006.
- [2] Völker SF, Renz M, Kaupp M, Lambert C. Squaraine Dyes as Efficient Coupling Bridges between Triarylamine Redox Centres. *Chem - Eur J* 2011;17:14147–63. doi:10.1002/chem.201102227.
- [3] Tomasulo M, Sortino S, Raymo FM. Bichromophoric Photochromes Based on the Opening and Closing of a Single Oxazine Ring. *J Org Chem* 2008;73:118–26. doi:10.1021/jo7017119.
- [4] Hall LM, Gerowska M, Brown T. A highly fluorescent DNA toolkit: synthesis and properties of oligonucleotides containing new Cy3, Cy5 and Cy3B monomers. *Nucleic Acids Res* 2012;40:e108–e108. doi:10.1093/nar/gks303.
- [5] Gerowska M, Hall L, Richardson J, Shelbourne M, Brown T. Efficient reverse click labeling of azide oligonucleotides with multiple alkynyl Cy-Dyes applied to the synthesis of HyBeacon probes for genetic analysis. *Tetrahedron* 2012;68:857–64. doi:10.1016/j.tet.2011.11.041.
- [6] Zimmermann T, Hennig L. Ring transformations of heterocyclic compounds. XXII. Pyrido[1,2-a]indolium salts from 2-methyl-3H-indoles by pyrylium mediated three carbon annelation. *J Heterocycl Chem* 2002;39:263–9. doi:10.1002/jhet.5570390203.
- [7] Fegan A, Shirude PS, Balasubramanian S. Rigid cyanine dyenucleic acid labels. *Chem Commun* 2008:2004–6. doi:10.1039/B801629A.
- [8] Potisek SL, Davis DA, Sottos NR, White SR, Moore JS. Mechanophore-Linked Addition Polymers. *J Am Chem Soc* 2007;129:13808–9. doi:10.1021/ja076189x.
- [9] Davis DA, Hamilton A, Yang J, Cremar LD, Van Gough D, Potisek SL, et al. Force-induced activation of covalent bonds in mechanoresponsive polymeric materials. *Nature* 2009;459:68–72. doi:10.1038/nature07970.
- [10] Brady RM, Hatzis E, Connor T, Street IP, Baell JB, Lessene G. Synthesis of conformationally constrained benzoylureas as BH3-mimetics. *Org Biomol Chem* 2012;10:5230–7. doi:10.1039/c2ob25618e.
- [11] Lee CK, Davis DA, White SR, Moore JS, Sottos NR, Braun PV. Force-Induced Redistribution of a Chemical Equilibrium. *J Am Chem Soc* 2010;132:16107–11. doi:10.1021/ja106332g.

Experimental Procedures

5-Bromo-2,3,3-trimethyl-3*H*-indole[2] (8a)



A solution of *p*-bromophenylhydrazine hydrochloride (1.50 g, 6.72 mmol), 3-methyl-2-butanone (1.16 g, 13.4 mmol) in dry glacial AcOH (120 mL) was heated to 130 °C under a nitrogen atmosphere for 6 h. The reaction mixture was allowed to cool to ambient temperature and subsequently the solvent was removed under reduced pressure. After dissolving the residue in Et₂O (150 mL) and addition of water (100 mL), the aqueous layer was extracted with *n*-hexane (2 × 100 mL) and Et₂O (1 × 150 mL). The organic phases were combined and washed with KOH (10%, 3 × 100 mL) and water (3 × 100 mL). Removal of the solvent and drying in vacuo gave the product as dark brown oil (1.34 g, 5.65 mmol, 84%, Lit.[2] 97%).^a

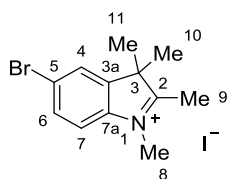
¹H NMR (500 MHz, CDCl₃): δ = 7.42 – 7.36 (m, 3H, *H*-4, *H*-6, *H*-7), 2.25 (s, 3H, *H*-8), 1.28 (s, 6H, *H*-9, *H*-10) ppm.

¹³C NMR (126 MHz, CDCl₃): δ = 188.6 (C-2), 152.8 (C-5), 147.9 (C-7a), 130.8 (C-4), 125.0 (C-6), 121.4 (C-7), 119.0 (C-3a), 54.3 (C-3), 23.1 (C-9, C-10), 15.5 (C-8) ppm.

IR (ATR): $\tilde{\nu}$ = 2964 (m), 2927 (w), 1574 (s), 1462 (m), 1446 (s), 1428 (s), 1416 (m), 1376 (m), 1315 (w), 1245 (m), 1199 (m), 1083 (w), 1051 (w), 937 (w), 866 (m), 821 (vs), 707 (w), 677 (m), 634 (w), 537 (m) cm⁻¹.

HRMS (EI-TOF): *m/z* (%): [M]⁺ calcd for [C₁₁H₁₂⁷⁹BrN]⁺ 237.0153; found 237.0145 (98); calcd for [C₁₁H₁₂⁸¹BrN]⁺ 239.0133; found 239.01411 (100); 231.99 (80) [M-CH₃]⁺; 170.97 (83) [M-C(CH₃)₂C(CH₃)]⁺.

5-Bromo-1,2,3,3-tetramethyl-3*H*-indolium iodide (3a)



5-Bromo-2,3,3-trimethyl-3*H*-indole (1.34 g 5.65 mmol) was dissolved in iodomethane (15.0 mL, 240 mmol) and heated to 45 °C for 9 h. After allowing the reaction mixture to cool to ambient temperature, the dispersion was diluted with Et₂O (1 × 15 mL), filtered and rinsed with Et₂O (1 × 15 mL) to yield 5-bromo-1,2,3,3-tetramethyl-3*H*-indolium iodide as light purple solid (1.87 g, 4.92 mmol, 87%).

^a The ¹H NMR data are in agreement with reference[2]. Further data were not provided in this reference.

Melting point: $T = 245\text{ }^{\circ}\text{C}$.

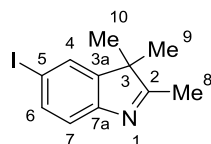
$^1\text{H NMR}$ (500 MHz, $\text{DMSO-}d_6$): $\delta = 8.16$ (s, 1H, *H-4*), 7.88-7.84 (m, 2H, *H-6*, *H-7*), 3.95 (s, 3H, *H-8*), 2.75 (s, 3H, *H-9*), 1.53 (s, 6H, *H-10*, *H-11*) ppm.

$^{13}\text{C NMR}$ (126 MHz, $\text{DMSO-}d_6$): $\delta = 196.6$ (*C-2*), 143.9 (*C-3a*), 141.4 (*C-7a*), 131.7 (*C-7*), 126.7 (*C-4*), 122.6 (*C-5*), 117.1 (*C-6*), 54.2 (*C-3*), 34.8 (*C-8*), 21.5 (*C-10*, *C-11*), 15.5 (*C-9*) ppm.

IR (ATR): $\tilde{\nu} = 3042$ (w), 2966 (m), 2926 (w), 2869 (w), 1628 (m), 1606 (m), 1583 (m), 1469 (s), 1450 (s), 1406 (s), 1365 (m), 1336 (m), 1319 (m), 1254 (m), 1234 (m), 1134 (s), 1079 (s), 992 (m), 935 (s), 879 (m), 824 (vs), 795 (s), 747 (m), 556 (s) cm^{-1} .

HRMS (ESI-TOF): m/z (%): $[\text{M-I}]^+$ calcd for $[\text{C}_{12}\text{H}_{15}^{79}\text{BrN}]^+$ 252.0382; found 252.0382 (100); calcd for $[\text{C}_{12}\text{H}_{15}^{81}\text{BrN}]^+$ 254.0367; found 254.0362 (99).

5-Iodo-2,3,3-trimethyl-3*H*-indole (**8b**)



4-Iodophenylhydrazine (1.30 g, 5.55 mmol), 3-methyl-2-butanone (956 mg, 11.1 mmol) and dry glacial AcOH (30 mL) were heated to $130\text{ }^{\circ}\text{C}$ under a nitrogen atmosphere for 3 h. After allowing the reaction mixture to cool to ambient temperature, the solvent was removed in vacuo and the residue was dissolved in Et_2O (150 mL) and water (100 mL) was added. After phase separation, the aqueous phase was extracted with *n*-hexane (2 x 100 mL) and Et_2O (1 x 100 mL). The combined organic phases were then washed with aqueous KOH solution (10%, 3 x 100 mL) and water (3 x 100 mL). After drying over MgSO_4 , the solvent was removed and the remaining product was dried *in vacuo* to give a dark brown oil (1.35 g, 4.73 mmol, 85%).^a

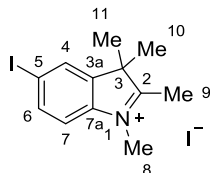
$^1\text{H NMR}$ (500 MHz, CDCl_3): $\delta = 7.62$ (dd, $^3J = 8.1\text{ Hz}$, $^4J = 1.7\text{ Hz}$, 1H, *H-6*), 7.59 (d, $^4J = 1.7\text{ Hz}$, 1H, *H-4*), 7.29 (d, $^3J = 8.1\text{ Hz}$, 1H, *H-7*), 2.27 (s, 3H, *H-8*), 1.29 (s, 6H, *H-9*, *H-10*) ppm.

$^{13}\text{C NMR}$ (126 MHz, CDCl_3): $\delta = 188.6$ (*C-2*), 153.2 (*C-5*), 148.2 (*C-7a*), 136.9 (*C-6*), 130.8 (*C-4*), 121.9 (*C-7*), 90.2 (*C-3a*), 54.2 (*C-3*), 23.1 (*C-9*, *C-10*), 15.5 (*C-8*) ppm.

IR (ATR): $\tilde{\nu} = 2962$ (m), 2924 (m), 2867 (w), 1690 (w), 1604 (w), 1579 (s), 1460 (s), 1445 (s), 1258 (s), 1200 (s), 878 (m), 861 (m), 820 (vs), 805 (vs) cm^{-1} .

HRMS (ESI-TOF): m/z (%): $[\text{M+H}]^+$ calcd for $[\text{C}_{11}\text{H}_{12}\text{IN+H}]^+$ 286.0087; found 286.0091 (100).

^a This compound has been prepared previously by different routes in yields of 79%[3], 81%[4], 96%[5] and 94%[6], respectively. $^1\text{H NMR}$ data agree with reported values of references[4,6], but not with references[3,5]. $^{13}\text{C NMR}$ data are in agreement with the reported values of references[3,5] references[4,6] did not provide $^{13}\text{C NMR}$ data. HRMS and IR data were not reported by these references.

5-Iodo-1,2,3,3-tetramethyl-3H-indolium iodide (3b)

5-Iodo-2,3,3-trimethyl-3H-indole (1.35 g, 4.73 mmol) was dissolved in iodomethane (15.0 mL, 240 mmol) and heated to 45 °C for 15 h. After allowing the reaction mixture to cool to ambient temperature and filtration and washing with Et₂O (2 mL), the product was obtained as light brown solid (1.75 g, 4.09 mmol, 86%).^a

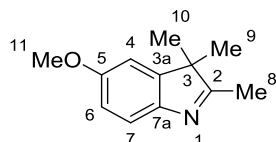
Melting point: *T* = 255 °C.

¹H NMR (500 MHz, DMSO-*d*₆): δ = 8.28 (d, ⁴*J* = 1.5 Hz, 1H, *H*-4), 7.99 (dd, ³*J* = 8.4 Hz, ⁴*J* = 1.5 Hz, 1H, *H*-6), 7.72 (d, ³*J* = 8.4 Hz, 1H, *H*-7), 3.94 (s, 3H, *H*-8), 2.74 (s, 3H, *H*-9), 1.52 (s, 6H, *H*-10, *H*-11) ppm.

¹³C NMR (126 MHz, DMSO-*d*₆): δ = 196.1 (C-2), 143.8 (C-3a), 141.9 (C-7a), 137.4 (C-6), 132.2 (C-4), 117.1 (C-7), 96.0 (C-5), 54.0 (C-3), 34.8 (C-8), 21.5 (C-10, C-11), 14.2 (C-9) ppm.

IR (ATR): $\tilde{\nu}$ = 3057 (w), 2969 (w), 2926 (w), 1628 (m), 1605 (m), 1583 (m), 1463 (s), 1442 (m), 1411 (s), 1398 (s), 1317 (m), 1256 (m), 1134 (s), 984 (m), 937 (m), 862 (m), 817 (vs), 789 (s), 760 (m), 745 (m), 613 (m), 556 (s), 449 (m) cm⁻¹.

HRMS (ESI-TOF): *m/z* (%): [M-I]⁺ calcd for [C₁₂H₁₅N]⁺ 300.0244; found 300.0244 (100).

5-Methoxy-2,3,3-trimethyl-3H-indole[8] (8c)

(4-Methoxy)-phenyl hydrazine hydrochloride (**26**) (10.0 g, 57.3 mmol) and 3-methyl-2-butanone (**7**) (4.93 g, 57.3 mmol) were dissolved in abs. EtOH (260 mL) and heated to reflux under a N₂ atmosphere for 5 h. Then the solution was allowed to cool to 24 °C and was filtered through silica gel (eluent: EtOAc). The product **27** was obtained as reddish-brown viscous oil (8.44 g, 44.6 mmol, 78 %, Lit.[8] 76 %)^b

^a This compound has been prepared previously by different routes in yields of 70%[7] and 74%[5]. ¹H NMR data do agree with reported values of references[5,7]. ¹³C NMR data are in agreement with the reported values of reference[5]. Reference[7] did not provide ¹³C NMR data. HRMS and IR data were not reported by these references.

^b ¹H NMR, ¹³C NMR, HRMS and mp data are in agreement with reference[8]. IR data were not reported.

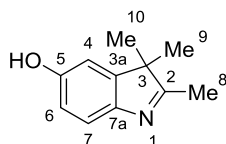
¹H NMR (500 MHz, CDCl₃): δ = 7.42 (d, ³J = 8.3 Hz, 1H, H-7), 6.84 – 6.80 (m, 2H, H-4, H-6), 3.82 (s, 3H, H-11), 2.24 (s, 3H, H-8), 1.28 (s, 6H, H-9, H-10) ppm.

¹³C NMR (126 MHz, CDCl₃): δ = 185.9 (C-2), 158.1 (C-5), 147.5 (C-7a), 147.4 (C-3a), 120.2 (C-7), 112.2 (C-4), 108.3 (C-6), 55.8 (C-11), 53.9 (C-3), 23.4 (C-9, C-10), 15.4 (C-8) ppm.

IR (ATR): $\tilde{\nu}$ = 3248 (w, b), 2961 (m), 2928 (m), 2864 (s), 2833 (s), 1713 (w), 1613 (m), 1580 (m), 1462 (vs), 1431 (s), 1380 (m), 1287 (s), 1212 (s), 1199 (s), 1178 (s), 1144 (m), 1068 (s), 1028 (s), 866 (m), 817 (s), 749 (m), 697 (w), 617 (m), 587 (m) cm⁻¹.

HRMS (EI-TOF): *m/z* (%): [M]⁺ calcd for [C₁₂H₁₅NO]⁺ 189.1154; found 189.1154 (100); 174.10 (100) [M-CH₃]⁺.

5-Hydroxy-2,3,3-trimethyl-3*H*-indole[9] (**8d**)



5-Methoxy-2,3,3-trimethyl-3*H*-indole (3.00 g, 15.9 mmol) was dissolved in hydrobromic acid (48%, 53.0 mL, 477 mmol). After heating at 140 °C for 2 h, the solution was allowed to cool, and diluted with water (200 mL). Solid NaOH was added until the mixture reached pH = 8. The aqueous solution was extracted with DCM (4 x 100 mL). The combined organic layers were washed with brine (300 mL), dried over Na₂SO₄, filtered, and the solvent was removed *in vacuo* to yield **8** as a brown solid (2.46 g, 13.4 mmol, 79%, Lit.[9] 97%).^a

Melting point: *T* = 175 °C.

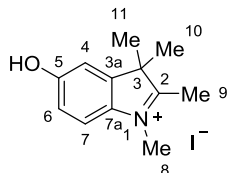
¹H NMR (600 MHz, CDCl₃): δ = 7.32 (d, ³J = 8.3 Hz, 1 H, H-7), 6.85 (d, ⁴J = 2.3 Hz, 1H, H-4), 6.78 (dd, ³J = 8.3 Hz, ⁴J = 2.3 Hz, 1H, H-6), 2.26 (s, 3H, H-8), 1.28 (s, 6H, H-9, H-10) ppm.

¹³C NMR (151 MHz, CDCl₃): δ = 186.0 (C-2), 155.7 (C-5), 147.4 (C-7a), 145.2 (C-3a), 120.0 (C-7), 114.3 (C-6), 109.9 (C-4), 53.8 (C-3), 23.3 (C-9, C-10), 15.1 (C-8) ppm.

IR (ATR): $\tilde{\nu}$ = 3248 (w, b), 2961 (m), 2928 (m), 2864 (s), 2833 (s), 1713 (w), 1613 (m), 1580 (m), 1462 (vs), 1431 (s), 1380 (m), 1287 (s), 1212 (s), 1199 (s), 1178 (s), 1144 (m), 1068 (s), 1028 (s), 866 (m), 817 (s), 749 (m), 697 (w), 617 (m), 587 (m) cm⁻¹.

HRMS (EI-TOF): *m/z* (%): [M]⁺ calcd. for C₁₁H₁₃NO⁺ 175.0997; found 175.0995 (95); 160.0 (100) [M-CH₃]⁺.

^a This compound has also been prepared via a different route in a yield of 91%[8]. ¹H NMR, ¹³C NMR, HRMS and mp data are in agreement with reference[8]. IR data were not reported. In reference[9], no analytical data were reported.

5-Hydroxy-1,2,3,3-tetramethyl-3*H*-indolium iodide[8] (3c)

5-Hydroxy-2,3,3-trimethyl-3*H*-indole (2.37 g, 13.5 mmol) was dissolved in iodomethane (25.0 mL, 400 mmol) in a nitrogen atmosphere and heated at 50 °C for 17 h. After allowing the reaction mixture to cool to ambient temperature, the dispersion was diluted with Et₂O (10 mL) and filtered. After drying in vacuo, 5-hydroxy-1,2,3,3-tetramethyl-3*H*-indolinium iodide was obtained as a brown solid (4.02 g, 12.7 mmol, 94%, Lit.[8] 64%) without further purification.^a

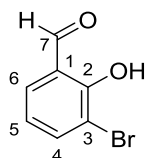
Melting point: $T = 242$ °C.

¹H NMR (500 MHz, DMSO-*d*₆): $\delta = 10.24$ (s, 1H, OH), 7.68 (d, ³*J* = 8.7 Hz, 1H, H-7), 7.12 (d, ⁴*J* = 2.3 Hz, 1H, H-4), 6.94 (dd, ³*J* = 8.7 Hz, ⁴*J* = 2.3 Hz, 1H, H-6), 3.90 (s, 3H, H-8), 2.67 (s, 3H, H-9), 1.47 (s, 6H, H-10, H-11) ppm.

¹³C NMR (126 MHz, DMSO-*d*₆): $\delta = 191.9$ (C-2), 159.0 (C-5), 143.7 (C-3a), 134.1 (C-7a), 116.1 (C-7), 115.0 (C-6), 110.3 (C-4), 53.4 (C-3), 34.5 (C-8), 21.9 (C-10, C-11), 13.6 (C-8) ppm.

IR (ATR): $\tilde{\nu} = 3178$ (m, b), 3023 (w), 2973 (w), 1619 (m), 1597 (m), 1495 (m), 1471 (m), 1356 (m), 1296 (s), 1194 (s), 1055 (w), 947 (w), 993 (w), 899 (m), 800 (s), 648 (s), 551 (m) cm⁻¹.

HRMS (ESI-TOF): *m/z* (%): [M-I]⁺ calcd. for [C₁₂H₁₆NO]⁺ 190.1226; found 190.1233 (100).

3-Bromo-2-hydroxybenzaldehyde (5a)

Anhydrous MgCl₂ (1.90 g, 20.0 mmol) and 2-bromophenol (1.73 g, 10.0 mmol) were dissolved in dry THF (50 mL), before dry TEA (2.8 mL, 2.02 g, 20.0 mmol) and paraformaldehyde (1.20 g, 40.0 mmol) were added. The reaction mixture was heated to 90 °C for 6 h. During this period, the color of the solution changed from white to yellow. After cooling to 22 °C, Et₂O (50 mL) was added and the organic phase was washed with hydrochloric acid (2 N, 2 x 50 mL) and water (2 x 50 mL). After phase

^a ¹H NMR, ¹³C NMR, HRMS and mp data are in agreement with reference[8]. IR data were not reported.

separation and drying over MgSO_4 , the solvent was removed *in vacuo* and the crude product was dissolved in DCM/*n*-heptane (1/1, v/v 30 mL) and crystallized after removal of DCM at $-25\text{ }^\circ\text{C}$. Drying *in vacuo* gave the 3-bromo-2-hydroxybenzaldehyde as colorless crystalline needles (1.48 g, 7.35 mmol, 73%).

Melting point: $T = 53\text{ }^\circ\text{C}$.

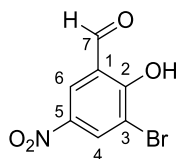
$^1\text{H NMR}$ (500 MHz, CDCl_3): $\delta = 11.61$ (d, $^5J = 0.5$ Hz, 1H, OH), 9.87 (s, 1H, H-7), 7.79 (ddd, $^3J = 7.9$ Hz, $^4J = 1.6$ Hz, $^5J = 0.5$ Hz, 1H, H-4), 7.55 (dd, $^3J = 7.7$ Hz, $^4J = 1.6$ Hz, 1H, H-6), 6.95 (at, $^3J = 7.8$ Hz, 1H, H-5) ppm.

$^{13}\text{C NMR}$ (126 MHz, CDCl_3): $\delta = 196.2$ (C-7), 158.3 (C-2), 140.2 (C-4), 133.1 (C-6), 121.5 (C-3), 120.9 (C-5), 111.4 (C-1) ppm.

IR (ATR): $\tilde{\nu} = 3071$ (w), 3022 (w), 2856 (m), 2755 (w), 1644 (vs), 1610 (s), 1568 (m), 1473 (m), 1436 (vs), 1383 (vs), 1339 (m), 1309 (m), 1291 (vs), 1268 (s), 1216 (vs), 1171 (vs), 1127 (vs), 1072 (s), 900 (s), 818 (s), 778 (s), 772 (vs), 666 (vs), 591 (vs), 546 (m) cm^{-1}

HRMS (EI-TOF): m/z (%): $[\text{M}]^+$ calcd for $[\text{C}_7\text{H}_5^{79}\text{BrO}_2]^+$ 199.9473; found 199.9467 (68); calcd for $[\text{C}_7\text{H}_5^{81}\text{BrO}_2]^+$ 201.9453; found 201.94472 (67); 118.99 (100) $[\text{M}-\text{Br}]^+$.

3-Bromo-2-hydroxy-5-nitrobenzaldehyde (2a)



3-Bromo-2-hydroxybenzaldehyde (9.00 g, 44.8 mmol) was dissolved in glacial AcOH (225 mL) and cooled to $15\text{ }^\circ\text{C}$. A mixture of glacial AcOH and fuming nitric acid (1/1 v/v; 3.75 mL) was added over the course of 30 min while the internal temperature was kept at $15\text{ }^\circ\text{C}$. Then the reaction mixture was stirred at $15\text{ }^\circ\text{C}$ for another 1 h. Subsequently, the cooling bath was removed and the reaction stirred for 18 h at $35\text{ }^\circ\text{C}$. After diluting the solution with water (200 mL), the formed yellow precipitate was filtered and washed with AcOH (20 mL). Subsequent crystallization from DCM/*n*-hexane (100 mL/100 mL) gave the product as yellow solid (6.47 g, 26.3 mmol, 59%).

Melting point: $T = 144\text{ }^\circ\text{C}$.

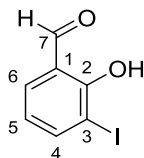
$^1\text{H NMR}$ (500 MHz, CDCl_3): $\delta = 12.23$ (s, 1H, OH), 9.98 (s, 1H, H-7), 8.69 (d, $^4J = 2.6$ Hz, 1H, H-4), 8.54 (d, $^4J = 2.6$ Hz, 1H, H-6) ppm.

$^{13}\text{C NMR}$ (126 MHz, CDCl_3): $\delta = 195.1$ (C-7), 163.1 (C-2), 140.8 (C-5), 134.6 (C-4), 128.4 (C-2), 119.6 (C-1), 112.5 (C-3) ppm.

IR (ATR): $\tilde{\nu} = 3300$ (w), 3087 (m), 3073 (m), 2884 (w), 1657 (s), 1613 (s), 1537 (s), 1426 (s), 1339 (s), 1283 (s), 1210 (s), 1162 (s), 1096 (s), 947 (s), 918 (s), 902 (s), 759 (s), 742 (vs), 714 (vs), 694 (vs), 488 (m), 478 (m) cm^{-1} .

HRMS (EI-TOF): m/z (%): $[\text{M}]^+$ calcd for $[\text{C}_7\text{H}_4^{79}\text{BrNO}_4]^+$ 244.9324; found 244.9316 (100); calcd for $[\text{C}_7\text{H}_4^{81}\text{BrNO}_4]^+$ 246.9303; found 246.9296 (98); 216.94 (13) $[\text{M}-\text{CO}]^+$.

SI-11

2-Hydroxy-3-iodobenzaldehyde[10] (5b)

To a stirred solution of 2-iodophenol (15.0 g, 68.2 mmol) in dry THF (340 mL), anhydrous $MgCl_2$ (12.9 g, 136 mmol), dry TEA (18.9 mL, 136 mmol) and paraformaldehyde (8.20 g, 273 mmol) were added under an atmosphere of dry nitrogen. The reaction mixture was heated to reflux for 12 h. The color of the reaction mixture changed from colorless via yellow to a reddish ochre. After cooling to 20 °C, Et_2O (200 mL) was added. After phase separation, the organic phase was washed with hydrochloric acid (2 N, 3 x 150 mL), water (1 x 150 mL) and brine (1 x 150 mL). The hydrochloric washings were combined and extracted with Et_2O (1 x 200 mL). The organic phases were combined and after drying over $MgSO_4$, the solvent was removed *in vacuo*. The residue was taken up with EtOAc (40 mL), crystallized at -20 °C and filtered. The filtrate was concentrated in vacuo and recrystallized another time from EtOAc (10 mL). The product was obtained as yellow crystals (8.20 g, 33.1 mmol, 49%, Lit.[10] 84%).^a

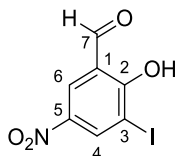
Melting point: $T = 72$ °C.

¹H NMR (500 MHz, $CDCl_3$): $\delta = 11.82$ (s, 1H, OH), 9.77 (s, 1H, H-7), 8.00 – 7.98 (m, 1H, H-4), 7.58 (dd, $^3J = 7.7$ Hz, $^4J = 1.6$ Hz, 1H, H-6), 6.84 (at, $^3J = 7.7$ Hz, 1H, H-5) ppm.

¹³C NMR (126 MHz, $CDCl_3$): $\delta = 196.1$ (C-7), 160.6 (C-2), 146.3 (C-4), 134.1 (C-6), 121.8 (C-3), 120.7 (C-5), 85.6 (C-1) ppm.

IR (ATR): $\tilde{\nu} = 3061$ (w, b), 3022 (w), 2853 (m), 1639 (vs), 1603 (s), 1469 (m), 1431 (s), 1382 (s), 1296 (s), 1282 (s), 1264 (s), 1213 (s), 1170 (s), 1117 (vs), 892 (s), 730 (vs), 662 (vs), 585 (vs) cm^{-1} .

HRMS (EI-TOF): m/z (%): $[M]^+$ calcd for $[C_7H_5IO_2]^+$ 247.9334; found 247.9337 (100); 126.90 (15) $[I]^+$; 92.03 (25) $[M-I-CHO]^+$.

Hydroxy-3-iodo-5-nitrobenzaldehyde (2b)

^a ¹H NMR, ¹³C NMR, IR and mp data are in agreement with reference[10]. HRMS data were not reported.

2-Hydroxy-3-iodobenzaldehyde (8.20 g, 33.1 mmol) was dissolved in glacial AcOH (160 mL) and cooled to 15 °C. A mixture of glacial AcOH and fuming nitric acid (1/1 v/v; 5.52 mL) was added over the course of 30 min while the internal temperature was kept at 15 °C and then the reaction mixture was stirred at 15 °C for another 1 h. The solution turned dark red. Subsequently, the cooling bath was removed and the reaction stirred at 40 °C for 14 h. After diluting with water (160 mL), the solution was filtered. The filtrate was diluted with more water (160 mL) and filtered again. The combined precipitates were washed with Et₂O (30 mL), giving a yellow powder which was dried *in vacuo* to obtain the product (3.80 g, 13.0 mmol, 39%).

Melting point: $T = 150\text{ °C}$.

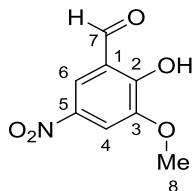
¹H NMR (500 MHz, DMSO-*d*₆): $\delta = 10.09$ (s, 1H, *H*-7), 8.77 (d, ⁴ $J = 2.7$ Hz, 1H, *H*-6), 8.67 (d, ⁴ $J = 2.7$ Hz, 1H, *H*-4) ppm.

¹³C NMR (126 MHz, DMSO-*d*₆): $\delta = 194.5$ (C-7), 164.7 (C-5), 140.9 (C-4), 139.5 (C-2), 128.5 (C-6), 120.9 (C-1), 89.1 (C-3) ppm.

IR (ATR): $\tilde{\nu} = 3086$ (m), 3071 (m), 2874 (w), 1653 (s), 1646 (s), 1608 (s), 1527 (s), 1422 (s), 1341 (s), 1333 (vs), 1299 (s), 1282 (vs), 1270 (s), 1210 (s), 1155 (s), 1104 (s), 744 (vs), 713 (vs), 682 (vs), 486 (s) cm⁻¹.

HRMS (CI-TOF, methane): m/z (%): [M+H]⁺ calcd for [C₇H₄INO₄+H]⁺ 293.9263; found 293.9267 (100); 308.0 (35) [M+CH₄]⁺.

2-Hydroxy-3-methoxy-5-nitrobenzaldehyde[9] (5c)



o-Vanillin (30.0 g, 197 mmol) was dissolved in glacial AcOH (138 mL) and water (7 mL) and cooled to 15 °C. A mixture of glacial AcOH and fuming nitric acid (2/1 v/v; 30 mL) was added over the course of 45 min at a temperature of 15 °C. The reaction mixture was stirred at 15 °C for another 90 min. Subsequently, the solution was diluted with water (300 mL).

The yellow precipitate which formed was filtered and washed with water (20 mL). After washing the precipitate with Et₂O (30 mL), it was dried *in vacuo* to obtain the product as a yellow powder (21.6 g, 110 mmol, 56%, Lit.[9] 50%).^a

Melting point: $T = 131\text{ °C}$.

¹H NMR (500 MHz, DMSO-*d*₆): $\delta = 10.32$ (s, 1H, *H*-7), 8.09 (d, ⁴ $J = 2.7$ Hz, 1H, *H*-6), 7.92 (d, ⁴ $J = 2.7$ Hz, 1H, *H*-4), 3.99 (s, 3H, *H*-8) ppm.

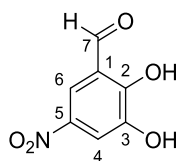
^a ¹H NMR, ¹³C NMR, HRMS spectroscopic and mp data are in agreement with reference[9]. IR data were not reported.

^{13}C NMR (126 MHz, $\text{DMSO}-d_6$): δ = 189.3 (C-7), 156.4 (C-5), 149.1 (C-3), 139.4 (C-2), 121.6 (C-1), 115.7 (C-6), 110.3 (C-4), 56.8 (C-8) ppm.

IR (ATR): $\tilde{\nu}$ = 3168 (w, b), 3093 (m), 1667 (s), 1520 (s), 1480 (s), 1447 (s), 1393 (s), 1340 (vs), 1267 (vs), 1199 (s), 1092 (vs), 953 (vs), 885 (s), 765 (s), 722 (vs), 581 (s) cm^{-1} .

HRMS (EI-TOF): m/z (%): $[\text{M}]^+$ calcd for $[\text{C}_8\text{H}_7\text{NO}_5]^+$ 197.0324; found 197.0328 (100); 151.02 (42) $[\text{M}-\text{NO}_2]^+$.

2,3-Dihydroxy-5-nitrobenzaldehyde[9] (2c)



2-Hydroxy-3-methoxy-5-nitrobenzaldehyde (13.8 g, 70.0 mmol) was dissolved in hydrobromic acid (48%, 233 mL) and heated at 140 °C for 5 h. Subsequently, the solution was diluted with water (500 mL), cooled to 0 °C and filtered. The precipitate was washed with water (100 mL) and was dried *in vacuo* to yield 2,3-dihydroxy-5-nitrobenzaldehyde as brown powder without further purification (12.1 g, 66.3 mmol, 95%, Lit:[9] 86%).^a

Melting point: T = 191 °C.

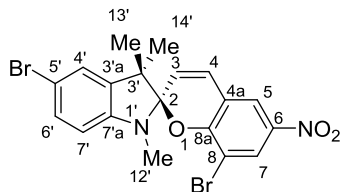
^1H NMR (500 MHz, $\text{DMSO}-d_6$): δ = 11.10 (s, OH), 10.30 (s, 1H, H-7), 7.98 (d, 4J = 2.8 Hz, 1H, H-6), 7.78 (d, 4J = 2.8 Hz, 1H, H-4) ppm.

^{13}C NMR (126 MHz, $\text{DMSO}-d_6$): δ = 189.8 (C-7), 155.9 (C-2), 147.2 (C-3), 139.3 (C-5), 121.8 (C-1), 114.6 (C-6), 113.2 (C-4) ppm.

IR (ATR): $\tilde{\nu}$ = 3259 (m, b), 3088 (m), 1663 (s), 1518 (s), 1456 (s), 1341 (vs), 1262 (vs), 1181 (vs), 950 (s), 903 (s), 754 (vs), 742 (vs), 595 (vs), 563 (vs), 542 (vs) cm^{-1} .

HRMS (EI-TOF): m/z (%): $[\text{M}]^+$ calcd for $[\text{C}_7\text{H}_5\text{NO}_5]^+$ 183.0168; found 183.0172 (100); 168.98 (25) $[\text{M}-\text{O}]^+$.

5'8-Dibromo-1',3',3'-trimethyl-6-nitrospiro[chromene-2,2'-indoline] (9a)



^a ^1H NMR, ^{13}C NMR, HRMS and mp data are in agreement with reference[9]. IR data were not reported.

5-Bromo-1,2,3,3-tetramethyl-3*H*-indolium iodide (1.00 g, 2.63 mmol), 3-bromo-2-hydroxybenzaldehyde (647 mg, 2.63 mmol) and dry piperidine (0.520 mL, 5.26 mmol) were dissolved in EtOH (45 mL) and heated to reflux under a nitrogen atmosphere for 5 h. After cooling down to -25 °C, the product had crystallized. The crude product was dissolved in a mixture of DCM (25 mL) and *n*-heptane (25 mL) and crystallized by removal of DCM under reduced pressure. The product was obtained as dark blue solid (979 mg, 2.04 mmol, 78%).

Melting point: $T = 252$ °C.

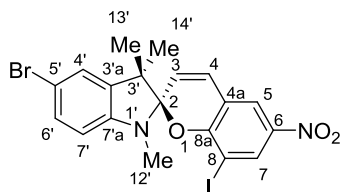
¹H NMR (500 MHz, CD₂Cl₂, 300 K): $\delta = 8.28$ (d, $^4J = 2.6$ Hz, 1 H, H-5), 7.98 (d, $^4J = 2.6$ Hz, 1 H, H-7), 7.30 (dd, $^3J = 8.2$ Hz, $^4J = 1.9$ Hz, 1 H, H-6'), 7.19 (d, $^4J = 1.9$ Hz, 1 H, H-4'), 6.95 (d, $^3J = 10.3$ Hz, 1 H, H-4), 6.47 (d, $^3J = 8.2$ Hz, 1 H, H-7'), 5.89 (d, $^3J = 10.3$ Hz, 1 H, H-3), 2.71 (s, 3 H, H-12'), 1.28 (s, 3 H, H-13'), 1.19 (s, 3H, H-14') ppm.

¹³C NMR (126 MHz, CD₂Cl₂, 300 K): $\delta = 156.4$ (C-8a), 147.3 (C-7'a), 141.6 (C-6), 139.1 (C-3'a), 130.9 (C-6'), 129.2 (C-7), 129.0 (C-4), 125.4 (C-4'), 122.4 (C-3), 122.1 (C-5), 120.2 (C-4a), 112.0 (C-5'), 109.8 (C-8), 109.2 (C-7'), 108.5 (C-2), 53.0 (C-3'), 29.2 (C-12'), 26.0 (C-14'), 20.1 (C-13') ppm.

IR (ATR): $\tilde{\nu} = 3101$ (w), 3072 (w), 2984 (w), 2936 (w), 1597 (s), 1507 (vs), 1440 (s), 1397 (s), 1286 (s), 1254 (s), 1201 (vs), 1165 (vs), 1117 (vs), 1078 (vs), 1040 (vs), 959 (vs), 886 (s), 871 (s), 852 (s), 822 (s), 801 (s), 772 (s), 745 (s), 729 (s), 696 (vs) cm⁻¹.

HRMS (EI-TOF): m/z (%): [M]⁺ calcd for [C₁₉H₁₆N₂⁷⁹Br₂O₃]⁺ 477.9528; found 477.9515 (38); calcd for [C₁₉H₁₆N₂⁷⁹Br⁸¹BrO₃]⁺ 479.9507; found 479.9497 (75); calcd for [C₁₉H₁₆N₂⁸¹Br₂O₃]⁺ 481.9687; found 481.9500 (38); 237.00 (100) [M-(PhBrONO₂C₂H)]⁺.

5'-Bromo-8-iodo-1',3',3'-trimethyl-6-nitrospiro[chromene-2,2'-indoline] (9b)



5-Bromo-1,2,3,3-tetramethyl-3*H*-indolium iodide (3.80 g, 10.0 mmol), 3-iodo-2-hydroxybenzaldehyde (2.93 g, 10.0 mmol) and dry piperidine (1.17 g, 20.0 mmol) were dissolved in EtOH (170 mL) and heated to reflux under a nitrogen atmosphere for 4.5 h. After cooling to -20 °C, the product had crystallized and was filtered to be obtained as dark blue solid (2.66 g, 5.04 mmol, 50%).^a

Melting point: $T = 187$ °C

^a The color suggests that the compound was obtained in the merocyanine form, but in CDCl₃, which was used for NMR spectroscopy, the spiropyran was detected.

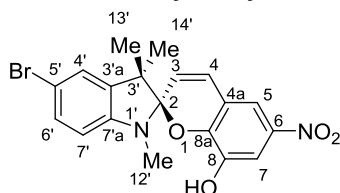
¹H NMR (600 MHz, CDCl₃, 300 K): δ = 8.48 (d, ⁴J = 2.6 Hz, 1 H, H-5), 7.99 (d, ⁴J = 2.6 Hz, 1 H, H-7), 7.29 (dd, ³J = 8.2 Hz, ⁴J = 2.0 Hz, 1 H, H-6'), 7.18 (d, ⁴J = 2.0 Hz, 1 H, H-4'), 6.87 (d, ³J = 10.3 Hz, 1 H, H-4), 6.44 (d, ³J = 8.2 Hz, 1 H, H-7'), 5.84 (d, ³J = 10.3 Hz, 1 H, H-3), 2.67 (s, 3 H, H-12'), 1.28 (s, 3 H, H-13'), 1.20 (s, 3H, H-14') ppm.

¹³C NMR (151 MHz, CDCl₃, 300 K): δ = 158.0 (C-6), 146.8 (C-5'), 141.7 (C-8a), 138.5 (C-7'a), 134.8 (C-5), 130.6 (C-6'), 128.7 (C-4), 125.0 (C-4'), 122.5 (C-7), 121.8 (C-3), 118.5 (C-8), 112.0 (C-3'a), 108.9 (C-7'), 108.4 (C-2), 82.7 (C-4a), 52.4 (C-3'), 29.1 (C-12'), 25.8 (C-14'), 20.2 (C-13') ppm.

IR (ATR): $\tilde{\nu}$ = 3071 (w), 2996 (w), 2960 (m), 2927 (w), 1653 (w), 1599 (m), 1511 (s), 1479 (s), 1431 (s), 1333 (vs), 1275 (s), 1261 (s), 1225 (m), 1186 (m), 1110 (m), 1092 (s), 1071 (m), 1016 (s), 963 (s), 913 (m), 897 (m), 846 (s), 809 (s), 779 (m), 752 (s), 741 (s), 722 (s), 710 (s), 655 (s), 579 (m), 503 (m) cm⁻¹

HRMS (ESI-TOF): *m/z* (%): [M+H]⁺ calcd for [C₁₉H₁₆N₂⁷⁹BrIO₃+H]⁺ 526.9462; found 526.9473 (98); calcd for [C₁₉H₁₆N₂⁸¹BrIO₃+H]⁺ 528.9447; found 528.9452 (100).

5'-Bromo-8-hydroxy-1',3',3'-trimethyl-6-nitrospiro[chromene-2,2'-indoline] (9c)



5-Bromo-1,2,3,3-tetramethyl-3*H*-indolium iodide (3.80 g, 10.0 mmol), 2,3-dihydroxy-5-nitrobenzaldehyde (1.83 g, 10.0 mmol) and dry piperidine (1.17 g, 20.0 mmol) were dissolved in dry EtOH (170 mL) under a nitrogen atmosphere and heated to reflux for 4.5 h. After cooling to -20 °C, the product had crystallized and was filtered to be obtained as dark blue solid (3.68 g, 8.82 mmol, 88%).^a

Melting point: *T* = 275 °C.

¹H NMR (500 MHz, DMSO-*d*₆, 300 K): δ = 10.18 (s, 1 H, OH), 7.73 (d, ⁴J = 2.7 Hz, 1 H, H-5), 7.56 (d, ⁴J = 2.7 Hz, 1 H, H-7), 7.30-7.27 (m, 2 H, H-4', H-7'), 7.15 (d, ³J = 10.3 Hz, 1 H, H-4), 6.59 (dd, ³J = 7.4 Hz, ⁴J = 2.5 Hz, 1 H, H-6'), 5.93 (d, ³J = 10.3 Hz, 1 H, H-3), 2.67 (s, 3H, H-12'), 1.21 (s, 3H, H-13'), 1.11 (s, 3H, H-14') ppm.

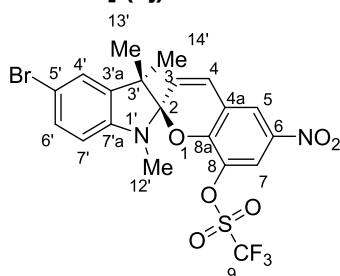
¹³C NMR (126 MHz, DMSO-*d*₆, 300 K): δ = 147.7 (C-6), 146.8 (C-7'a), 144.7 (C-8), 139.9 (C-4a), 138.8 (C-3'a), 130.0 (C-6'), 128.6 (C-4), 124.7 (C-7'), 120.8 (C-3), 118.8 (C-8a), 113.6 (C-5), 110.9 (C-7), 110.2 (C-5'), 108.8 (C-4'), 105.4 (C-2), 51.9 (C-3'), 28.4 (C-12'), 25.4 (C-13'), 19.2 (C-14') ppm.

^a The color suggests that the compound was obtained in the merocyanine form, but in DMSO, which was used for NMR spectroscopy, the spiropyran was detected.

IR (ATR): $\tilde{\nu}$ = 3214 (m, b), 3082 (w), 2976 (w), 1615 (w), 1590 (m), 1568 (m), 1510 (s), 1432 (s), 1400 (s), 1287 (s), 1190 (vs), 1171 (vs), 877 (vs), 789 (vs), 746 (vs), 539 (vs), 459 (vs) cm^{-1} .

HRMS (EI-TOF): m/z (%): $[\text{M}]^+$ calcd for $[\text{C}_{19}\text{H}_{17}\text{N}_2^{79}\text{BrO}_4]^+$ 416.0372; found 416.0365 (51); calcd for $[\text{C}_{19}\text{H}_{17}\text{N}_2^{81}\text{BrO}_4]^+$ 418.0351; found 418.0345 (50); 237.00/239.00 (100/98) $[\text{M}-(\text{PhO}_2\text{HNO}_2\text{C}_2\text{H}_2)]^+$.

5'-Bromo-8-trifluoromethylsulfonyl-1',3',3'-trimethyl-6-nitrospiro[chromene-2,2'-indoline] (9)



Trifluoromethanesulfonic anhydride (2.85 g, 10.0 mmol) was added to a solution of 5'-bromo-8-hydroxy-1',3',3'-trimethyl-6-nitrospiro[chromene-2,2'-indoline] (3.50 g, 8.39 mmol) and anhydrous pyridine (2.6 mL) in anhydrous DCM (33 mL) over the course of 10 min at 0 °C under a nitrogen atmosphere. The reaction mixture was stirred at 0 °C for 1.5 h, the cooling bath was removed and the reaction mixture stirred at 24 °C for 1 h before heating it to 40 °C for 2 h. The reaction mixture was purified by filtration through silica gel (eluent: EtOAc) and after removal of the solvent *in vac.*, the residue was dissolved in toluene (20 mL) and dried *in vacuo* again to remove remaining pyridine as azeotropic mixture to give the product as dark blue solid (3.42 g, 6.22 mmol, 74%).^{ab}

Melting point: $T = 195$ °C.

^1H NMR (500 MHz, CDCl_3 , 300 K): δ = 8.06 (d, $^4J = 2.6$ Hz, 1H, H-5), 7.99 (d, $^4J = 2.6$ Hz, 1H, H-7), 7.29 (dd, $^3J = 8.2$ Hz, $^4J = 2.0$ Hz, 1H, H-6'), 7.17 (d, $J = 2.0$ Hz, 1H, H-4'), 7.01 (d, $J = 10.5$ Hz, 1H, H-4), 6.43 (d, $^3J = 8.2$ Hz, 1H, H-7'), 5.98 (d, $^3J = 10.5$ Hz, 1H, H-3), 2.72 (s, 3H, H-12'), 1.31 (s, 3H, H-13'), 1.22 (s, 3H, H-14') ppm.

^{13}C NMR (126 MHz, CDCl_3 , 300 K): δ = 151.7 (C-6), 146.3 (C-7'a), 140.0 (C-8), 137.9 (C-3'a), 135.3 (C-4a), 130.7 (C-6'), 128.2 (C-4), 124.9 (C-4'), 122.5 (C-3),

^a The color suggested that the compound was obtained in the merocyanine form, but in CDCl_3 , which was used for NMR spectroscopy, a mixture of spiropyran:merocyanine was detected in a ratio of 1:0.14 (in the plotted spectrum, 5 peaks of the merocyanine species which do not overlay with spiropyran peaks were integrated).

^b The carbon atom of the trifluoromethanesulfonic ester (C-9) was not detectable via ^{13}C NMR spectroscopy, due to the large coupling constant of approx. 400 Hz, the quadruplet peaks are expected to be distributed over a range of 13 ppm and be lower in their intensity.

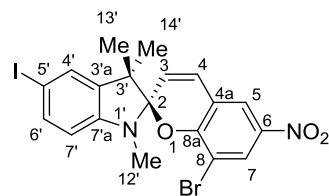
122.0 (C-5), 120.8 (C-8a), 119.0 (C-7), 112.2 (C-5'), 109.0 (C-2), 108.9 (C-7'), 52.6 (C-3'), 28.7 (C-12'), 26.0 (C-14'), 19.7 (C-13') ppm.

^{19}F NMR (471 MHz, CDCl_3 , 300 K): $\delta = -73.8$ ppm.^a

IR (ATR): $\tilde{\nu} = 3098$ (w), 2969 (w), 2938 (w), 2871 (w), 1604 (w), 1517 (m), 1475 (m), 1416 (m), 1336 (s), 1281 (s), 1215 (vs), 1132 (s), 1039 (s), 809 (vs), 729 (vs), 574 (s), 495 (s) cm^{-1} .

HRMS (EI-TOF): m/z (%): $[\text{M}]^+$ calcd for $[\text{C}_{20}\text{H}_{16}\text{N}_2^{79}\text{BrF}_3\text{O}_6\text{S}]^+$ 547.9865 found 547.9857 (40); calcd for $[\text{C}_{20}\text{H}_{16}\text{N}_2^{81}\text{BrF}_3\text{O}_6\text{S}]^+$ 549.9844; found 549.9839 (42); 417.02 (100) $[\text{M}-(\text{SO}_2\text{CF}_3)]^+$.

5'-Iodo-8-bromo-1',3',3'-trimethyl-6-nitrospiro[chromene-2,2'-indoline] (9d)



5-Iodo-1,2,3,3-tetramethyl-3*H*-indolium iodide (1.12 g, 2.63 mmol), 3-bromo-2-hydroxybenzaldehyde (647 mg, 2.63 mmol) and dry piperidine (0.520 mL, 5.26 mmol) were dissolved in EtOH (45 mL) and heated to reflux under a nitrogen atmosphere for 5 h. After cooling down to -20 °C, the product had crystallized and was filtered to be obtained as dark brown solid (1.09 g, 2.07 mmol, 79%).

Melting point: $T = 228$ °C.

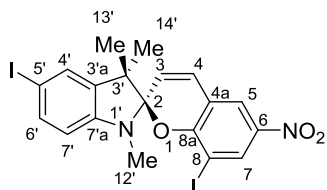
^1H NMR (500 MHz, CD_3Cl , 300 K): $\delta = 8.28$ (d, $^4J = 2.5$ Hz, 1H, H-5), 7.95 (d, $^4J = 2.5$ Hz, 1H, H-7), 7.47 (dd, $^3J = 8.1$ Hz, $^4J = 1.4$ Hz, 1H, H-6'), 7.32 (d, $^4J = 1.4$ Hz, 1H, H-4'), 6.91 (d, $^3J = 10.3$ Hz, 1H, H-4), 6.35 (d, $^3J = 8.1$ Hz, 1H, H-7'), 5.86 (d, $^3J = 10.3$ Hz, 1H, H-3), 2.71 (s, H-12'), 1.27 (s, 3H, H-13'), 1.19 (s, 3H, H-14') ppm.

^{13}C NMR (126 MHz, CD_3Cl , 300 K): $\delta = 155.9$ (C-8a), 147.4 (C-7a'), 141.1 (C-6), 138.8 (C-3a'), 136.7 (C-6'), 130.6 (C-4'), 129.0 (C-7), 128.4 (C-4), 122.0 (C-3), 121.6 (C-5), 119.4 (C-4a), 109.6 (C-8), 109.6 (C-7'), 107.7 (C-2), 81.3 (C-5'), 52.4 (C-3'), 29.0 (C-12'), 25.9 (C-14'), 20.1 (C-13') ppm.

IR (ATR): $\tilde{\nu} = 3081$ (w), 3066 (w), 2965 (w), 2925 (w), 1661 (w), 1591 (s), 1513 (s), 1442 (m), 1399 (m), 1265 (vs), 1201 (vs), 1171 (s), 1115 (s), 1078 (s), 962 (s), 810 (s), 790 (s), 774 (s), 747 (s), 727 (s), 697 (s), 662 (s) cm^{-1} .

HRMS (EI-TOF): m/z (%): $[\text{M}]^+$ calcd for $[\text{C}_{19}\text{H}_{16}\text{N}_2^{79}\text{Br}^{127}\text{IO}_3]^+$ 525.9389; found 525.9411 (61); calcd for $[\text{C}_{19}\text{H}_{16}\text{N}_2^{81}\text{Br}^{127}\text{IO}_3]^+$ 527.9369; found 527.9394 (60); 285.00 (100) $[\text{M}-(\text{PhIONO}_2\text{C}_2\text{H})]^+$.

^a The ^{19}F NMR spectrum of this compound was obtained without adding an internal standard.

5',8-Diiodo-1',3',3'-trimethyl-6-nitrospiro[chromene-2,2'-indoline] (9e)

5-Iodo-1,2,3,3-tetramethyl-3*H*-indolium iodide (3.42 g, 8.00 mmol), 3-iodo-2-hydroxybenzaldehyde (2.33 g, 8.00 mmol) and dry piperidine (1.60 mL, 16.0 mmol) were dissolved in dry EtOH (150 mL) and heated to reflux under a nitrogen atmosphere for 3 h. After cooling down to -30 °C, the product had crystallized. The crude product was dissolved in a mixture of acetone (25 mL) and *n*-heptane (25 mL) and crystallized by removal of acetone under reduced pressure. The product was obtained as dark violet solid (3.08 g, 5.36 mmol, 67 %).

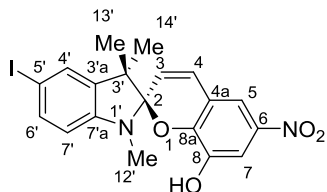
Melting point: $T = 231$ °C.

¹H NMR (500 MHz, CD₃Cl, 300 K): $\delta = 8.48$ (d, $^4J = 2.6$ Hz, 1H, H-5), 7.99 (d, $^4J = 2.6$ Hz, 1H, H-7), 7.48 (dd, $^3J = 8.1$ Hz, $^4J = 1.8$ Hz, 1H, H-6'), 7.34 (d, $^4J = 1.8$ Hz, 1H, H-4'), 6.87 (d, $^3J = 10.3$ Hz, 1H, H-4), 6.36 (d, $^3J = 8.1$ Hz, 1H, H-7'), 5.84 (d, $^3J = 10.3$ Hz, 1H, H-3), 2.67 (s, 3H, H-12'), 1.27 (s, 3H, H-13'), 1.20 (s, 3H, H-14') ppm.

¹³C NMR (126 MHz, CD₃Cl, 300 K): $\delta = 157.9$ (C-8a), 147.2 (C-7'a), 141.4 (C-6)^a, 138.7 (C-3'a), 136.5 (C-6'), 134.7 (C-7), 130.4 (C-4'), 128.5 (C-4), 122.4 (C-5), 121.6 (C-3), 118.3 (C-2), 109.5 (C-7'), 108.0 (C-4a), 82.6 (C-8), 81.2 (C-5'), 52.1 (C3'), 28.9 (C-12'), 25.6 (C-14'), 20.1 (C-13') ppm.

IR (ATR): $\tilde{\nu} = 3083$ (w), 3054 (w), 2983 (w), 2958 (w), 1583 (s), 1515 (s), 1497 (s), 1477 (m), 1444 (m), 1390 (m), 1282 (vs), 1265 (vs), 1203 (vs), 1173 (vs), 1081 (vs), 948 (vs), 810 (s), 726 (s), 681 (s), 489 (s) cm⁻¹.

HRMS (EI-TOF): m/z (%): [M]⁺ calcd for [C₁₉H₁₆N₂¹²⁷I₂O₃]⁺ 573.9250; found 573.9241 (80); 283.99 (100) iu⁺.

5'-Iodo-8-hydroxy-1',3',3'-trimethyl-6-nitrospiro[chromene-2,2'-indoline] (9f)

Iodoindoliniumiodide (1.12 g, 2.63 mmol), 2,3-dihydroxybenzaldehyde (482 mg, 2.63 mmol, 1 eq) and dry piperidine (0.520 mL, 5.26 mmol) were dissolved in dry EtOH (25 mL) and heated to reflux under a nitrogen atmosphere for 4.5 h, followed

^a The ¹³C NMR spectroscopic signal of the atom 4a was only observed and assigned by a ¹H/¹³C HMBC experiment. The signal's intensity in the ¹H decoupled ¹³C NMR is too low for an assignment.

by stirring at 20 °C for 16 h. After crystallization at -30 °C, the product was obtained as dark purple solid (1.09 g, 2.33 mmol, 89%).

Melting point: $T = 240$ °C.

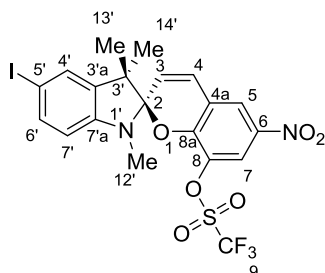
$^1\text{H NMR}$ (500 MHz, $\text{DMSO-}d_6$, 300 K): $\delta = 7.72$ (d, $^4J = 2.7$ Hz, 1H, H-5), 7.56 (d, $^4J = 2.7$ Hz, 1H, H-7), 7.44 (dd, $^3J = 8.1$ Hz, $^4J = 1.7$ Hz, 1H, H-6'), 7.41 (d, $^4J = 1.7$ Hz, 1H, H-4'), 7.14 (d, $^3J = 10.4$ Hz, 1H, H-4), 6.49 (d, $^3J = 8.1$ Hz, 1H, H-7'), 5.92 (d, $^3J = 10.4$ Hz, 1H, H-3), 2.66 (s, 3H, H-12'), 1.19 (s, 3H, H-13'), 1.10 (s, 3H, H-14') ppm.

$^{13}\text{C NMR}$ (126 MHz $\text{DMSO-}d_6$, 300 K): $\delta = 147.8$ (C-6), 147.4 (C-7'a), 144.7 (C-8a), 139.9 (C-8a), 139.1 (C-3'a), 135.9 (C-6'), 130.0 (C-4'), 128.6 (C-4), 120.8 (C-3), 118.8 (C-8a), 113.6 (C-5), 110.9 (C-7), 109.6 (C-7'), 105.3 (C-2), 80.6 (C-5'), 51.8 (C-3'), 28.3 (C-12'), 25.2 (C-14'), 19.2 (C-13') ppm.

IR (ATR): $\tilde{\nu} = 3219$ (w, b), 3082 (w), 2973 (w), 2932 (w), 1615 (m), 1588 (m), 1568 (m), 1509 (s), 1431 (s), 1399 (s), 1283 (s), 1211 (s), 1189 (vs), 1168 (vs), 1113 (vs), 1048 (vs), 957 (vs), 876 (vs), 789 (vs), 745 (s), 663 (s), 536 (s), 458 (s) cm^{-1} .

HRMS (EI-TOF): m/z (%): $[\text{M}]^+$ calcd for $[\text{C}_{19}\text{H}_{17}\text{N}_2^{127}\text{IO}_4]^+$ 464.0233; found 464.0217 (80); 285.00 (100) $[\text{M}-(\text{PhO}_2\text{HNO}_2\text{C}_2\text{H})]^+$.

5'-Iodo-8-trifluoromethylsulfonyl-1',3',3'-trimethyl-6-nitrospiro[chromene-2,2'-indoline] (9k)



Trifluoromethanesulfonic anhydride (367 mg, 0.22 μL , 1.30 mmol) was added to a solution of 8-hydroxy-5'-iodo-1',3',3'-trimethyl-6-nitrospiro[chromene-2,2'-indoline] (464 mg, 1.00 mmol) and anhydrous pyridine (396 mg, 400 μL , 5.00 mmol) in anhydrous DCM (10 mL) over the course of 10 min at 0 °C under a nitrogen atmosphere. The reaction mixture was stirred at 0 °C for 1.5 h, the cooling bath was removed and the reaction mixture stirred at 20 °C for 1 h before heating it to reflux for 2 h. The reaction mixture was purified by filtration through silica gel (eluent: EtOAc) and after removal of the solvent *in vacuo*, the residue was dissolved in toluene (20 mL) and dried *in vacuo* again to remove remaining pyridine as azeotropic mixture. The crude product was dissolved in a mixture of DCM (20 mL) and *n*-

heptane (20 mL) and crystallized by removal of DCM under reduced pressure. The product was obtained as orange solid (335 mg, 561 μmol , 56%).^a

Melting point: $T = 205\text{ }^\circ\text{C}$.

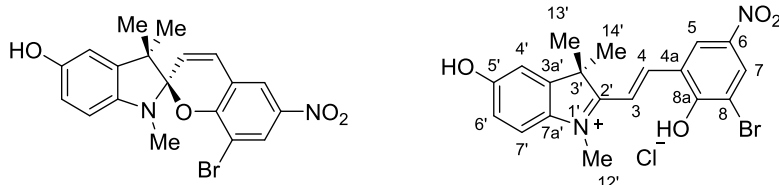
¹H NMR (500 MHz, CD_3Cl , 300 K): $\delta = 8.05$ (d, $^4J = 2.6$ Hz, 1H, H-7), 7.99 (d, $^4J = 2.6$ Hz, 1H, H-5), 7.48 (dd, $^3J = 8.2$ Hz, $^4J = 1.7$ Hz, 1H, H-6'), 7.33 (d, $^4J = 1.7$ Hz, 1H, H-4'), 7.01 (d, $^3J = 10.5$ Hz, 1H, H-4), 6.35 (d, $^3J = 8.2$ Hz, 1H, H-7'), 5.97 (d, $^3J = 10.5$ Hz, 1H, H-3), 2.72 (s, 3H, H-12'), 1.30 (s, 3H, H-13'), 1.21 (s, 3H, H-14') ppm.

¹³C NMR (126 MHz, CD_3Cl , 300 K): $\delta = 151.7$ (C-8a), 146.9 (C-7'a), 140.0 (C-6), 138.3 (C-3'a), 136.7 (C-6'), 135.3 (C-8), 130.4 (C-4'), 128.1 (C-4), 122.5 (C-3), 122.0 (C-5), 120.8 (C-4a), 119.0 (C-7), 109.6 (C-7'), 108.8 (C-2), 81.5 (C-5'), 52.5 (C-3'), 28.7 (C-12'), 26.0 (C-14'), 19.7 (C-13') ppm.

IR (ATR): $\tilde{\nu} = 3097$ (w), 2976 (w), 2936 (w), 2872 (w), 1601 (m), 1515 (s), 1515 (s), 1422 (s), 1336 (s), 1280 (s), 1233 (s), 1213 (vs), 1181 (s), 1133 (s), 1081 (s), 1039 (s), 952 (s), 899 (s), 881 (s), 815 (s), 806 (vs), 743 (s), 728 (vs), 593 (s), 572 (s), 497 (s) cm^{-1} .

HRMS (EI-TOF): m/z (%): $[\text{M}]^+$ calcd for $[\text{C}_{20}\text{H}_{16}\text{N}_2^{127}\text{IF}_3\text{O}_6\text{S}]^+$ 595.9726; found 595.9721 (60); 463.00 (100) $[\text{M}-(\text{SO}_2\text{CF}_3)]^+$.

5'-Hydroxy-8-bromo-1',3',3'-trimethyl-6-nitrospiro[chromene-2,2'-indoline] (9g)



5-Hydroxy-1,2,3,3-tetramethyl-3*H*-indolium iodide (834 mg, 2.63 mmol), 3-bromo-2-hydroxybenzaldehyde (647 mg, 2.63 mmol) and dry piperidine (0.52 mL, 5.26 mmol) were dissolved in dry EtOH (45 mL) and heated to reflux under a nitrogen atmosphere for 3 h. After cooling down to $-30\text{ }^\circ\text{C}$, the product had crystallized and was filtered to be obtained as dark brown solid (990 mg, 2.37 mmol, 90%). ¹H NOESY NMR experiments confirmed the species present in solution ($\text{DMSO}-d_6$, HCl) as merocyanine form in the *trans* conformation; likely in its protonated form.

Melting point: $T = 268\text{ }^\circ\text{C}$.

¹H NMR (500 MHz, $\text{DMSO}-d_6$, 300 K): $\delta = 8.82$ (d, $^4J = 2.7$ Hz, 1H, H-5), 8.41-8.35 (m, 2H, H-4, H-7), 7.67 (d, $^3J = 8.8$ Hz, 1H, H-7'), 7.62 (d, $^3J = 16.4$ Hz, 1H, H-3), 7.13 (d, $^4J = 2.3$ Hz, 1H, H-4'), 7.02 (dd, $^3J = 8.8$ Hz, $^4J = 2.3$ Hz, 1H, H-6'), 4.06 (s, 3H, H-12'), 1.62 (s, 6H, H-13', H-14') ppm.

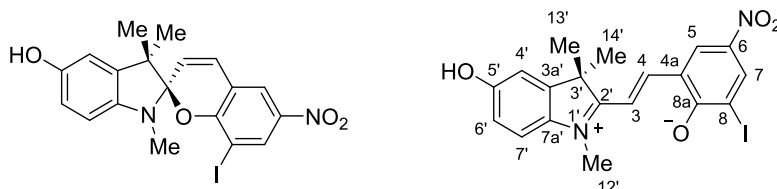
^a The carbon atom of the trifluoromethanesulfonic ester (C-9) was not detectable via ¹³C NMR spectroscopy. Due to the large coupling constant of approx. 400 Hz, the quadruplet peaks are expected to be distributed over a range of 13 ppm and be decreased in their intensity.

^{13}C NMR (126 MHz DMSO- d_6 , 300 K): δ = 179.0 (C-2'), 161.0 (C-5'), 160.4 (C-9), 147.0 (C-3a'), 143.8 (C-4), 141.5 (C-6), 134.5 (C-7a'), 131.4 (C-7), 125.5 (C-4a), 124.6 (C-5), 117.7 (C-7'), 117.0 (C-3), 116.7 (C-6'), 114.8 (C-8), 110.7 (C-4'), 52.8 (C-3'), 36.0 (C-12'), 26.1 (C-13', C-14') ppm.

IR (ATR): $\tilde{\nu}$ = 3166 (w,b), 3048 (w), 2989 (w), 2971 (w), 2929 (w), 1617 (m), 1584 (s), 1516 (s), 1429 (s), 1401 (s), 1358 (s), 1306 (s), 1277 (vs), 1226 (vs), 1206 (vs), 1172 (s), 1122 (s), 1071 (s), 1039 (s), 970 (s), 894 (s), 849 (s), 810 (s), 747 (vs), 701 (vs), 638 (s), 461 (s) cm^{-1} .

HRMS (EI-TOF): m/z (%): $[\text{M}]^+$ calcd for $[\text{C}_{19}\text{H}_{17}\text{N}_2^{79}\text{BrO}_4]^+$ 416.0372; found 416.0359 (31); calcd for $[\text{C}_{19}\text{H}_{17}\text{N}_2^{81}\text{BrO}_4]^+$ 418.0351; found 418.0342 (30); 175.09 (100) $[\text{M}-(\text{PhOBrNO}_2\text{C}_2\text{H})]^+$.

5'-Hydroxy-8-iodo-1',3',3'-trimethyl-6-nitrospiro[chromene-2,2'-indoline] (9h)



5-Hydroxy-1,2,3,3-tetramethyl-3*H*-indolium iodide (834 mg, 2.63 mmol), 3-iodo-2-hydroxybenzaldehyde (771 mg, 2.63 mmol) and dry piperidine (0.520 mL, 5.26 mmol) were dissolved in dry EtOH (45 mL) and heated to reflux under a nitrogen atmosphere for 3 h. After cooling down to -20 $^{\circ}\text{C}$, the product had crystallized and was filtered to be obtained as dark solid (1.08 g, 2.32 mmol, 88%).

Melting point: $T = 259$ $^{\circ}\text{C}$.

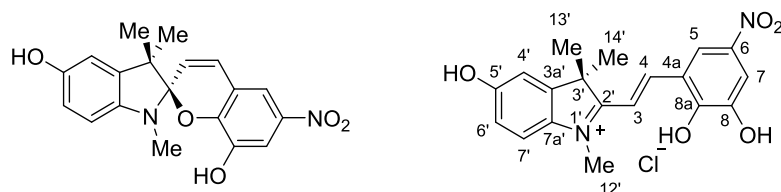
^1H NMR (500 MHz, DMSO- d_6 , 300 K): δ = 8.68 (d, $^4J = 3.0$ Hz, 1H, H-5), 8.45 (d, $^4J = 3.0$ Hz, 1H, H-7), 8.36 (d, $^3J = 15.5$ Hz, 1H, H-4), 8.24 (d, $^3J = 15.5$ Hz, 1H, H-3), 7.57 (d, $^3J = 8.7$ Hz, 1H, H-7'), 7.11 (d, $^4J = 2.2$ Hz, 1H, H-4'), 6.92 (dd, $^3J = 8.7$ Hz, $^4J = 2.2$ Hz, 1H, H-6'), 3.88 (s, 3H, H-12'), 1.70 (s, 6H, H-13', H-14') ppm.

^{13}C NMR (126 MHz DMSO- d_6 , 300 K): δ = 179.3 (C-2'), 174.8 (C-8a), 158.3 (C-5'), 151.7 (C-4), 145.1 (C-3a'), 135.6 (C-5), 134.1 (C-7a'), 132.7 (C-7), 131.8 (C-6), 118.5 (C-4a), 115.2 (C-6'), 115.0 (C-7'), 109.8 (C-4'), 109.0 (C-3), 99.8 (C-8), 50.9 (C-3'), 33.3 (C-12'), 26.2 (C-13', 14') ppm.

IR (ATR): $\tilde{\nu}$ = 3112 (m, b), 2974 (w), 1595 (m), 1573 (w), 1507 (s), 1475 (m), 1455 (m), 1397 (m), 1368 (s), 1283 (vs), 1254 (vs), 1202 (vs), 1084 (vs), 956 (s), 833 (s), 771 (m), 743 (s), 685 (vs), 648 (s), 552 (m) cm^{-1} .

HRMS (EI-TOF): m/z (%): $[\text{M}]^+$ calcd for $[\text{C}_{19}\text{H}_{17}\text{N}_2^{127}\text{IO}_4]^+$ 464.0233; found 464.0217 (62); 175.10 (100) $[\text{M}-(\text{PhOINO}_2\text{C}_2\text{H})]^+$.

5',8-Dihydroxy-1',3',3'-trimethyl-6-nitrospiro[chromene-2,2'-indoline][11] and its corresponding merocyanine form (9i)



5-Hydroxy-1,2,3,3-tetramethyl-3*H*-indolium iodide (1.79 g, 5.64 mmol) and 2,3-dihydroxy-5-nitrobenzaldehyde (735 mg, 4.04 mmol) were dissolved in EtOH (55 mL) and piperidine (790 μ L, 8.0 mmol) under a nitrogen atmosphere. The reaction mixture was heated to 80 $^{\circ}$ C for 3 h and cooled down to -20 $^{\circ}$ C subsequently. After filtration and washing with EtOH (30 mL, -20 $^{\circ}$ C), the wet filter cake was dried *in vacuo* to yield 5',8-dihydroxy-1',3',3'-trimethyl-6-nitrospiro[chromene-2,2'-indoline] as dark green solid (1.41 g, 3.97 mmol, 98%, Lit.[11] 99%). 1 H NOESY NMR experiments confirmed the species present in solution (DMSO- d_6 , HCl) as merocyanine form in the *trans* conformation; likely in its protonated form.

mp: > 300 $^{\circ}$ C

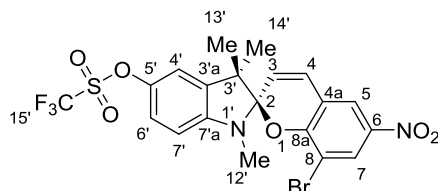
1 H NMR (500 MHz, DMSO- d_6 , 300 K): δ = 8.51 (d, 4J = 2.7 Hz, 1 H, H-7), 8.31 (d, 3J = 16.5 Hz, 1 H, H-4), 7.96 (d, 4J = 2.7 Hz, 1 H, H-5), 7.74 (d, 3J = 16.6 Hz, 1 H, H-3), 7.72 (d, 3J = 8.7 Hz, 1 H, H-7'), 7.22 (d, 4J = 2.7 Hz, 1 H, H-4'), 7.07 (dd, 3J = 8.7 Hz, 4J = 2.7 Hz, 1 H, H-6'), 4.09 (s, 3H, H-12'), 1.70 (s, 6H, H-13', H-14') ppm.

13 C NMR (126 MHz, DMSO- d_6 , 300 K): δ = 178.5 (C-4a), 160.1 (C-5'), 153.3 (C-6), 146.6 (C-3a'), 146.0 (C-8), 143.9 (C-4), 139.9 (C-8a), 133.9 (C-7a'), 121.2 (C-2'), 116.7 (C-7, C-7'), 115.9 (C-6'), 114.8 (C-3), 112.1 (C-5), 110.0 (C-4'), 51.9 (C-3'), 34.8 (C-12'), 25.9 (C-13', C-14') ppm.

IR (ATR): $\tilde{\nu}$ = 3203 (w, b), 2981 (w), 1596 (m), 1513 (m), 1454 (m), 1411 (m), 1359 (m), 1273 (s), 1244 (m), 1215 (s), 1180 (s), 1061 (s), 961 (s), 899 (m), 863 (s), 800 (s), 788 (m), 764 (m), 739 (s), 544 (s) cm^{-1} .

HRMS (EI-TOF): m/z (%): $[M]^+$ calcd for $[\text{C}_{19}\text{H}_{18}\text{N}_2\text{O}_5+\text{H}]^+$ 354.1216; found 354.1214 (40); 175.09 (100) $[\text{M}-(\text{PhO}_2\text{HNO}_2\text{C}_2\text{H}_2)]^+$.

5'-Trifluoromethylsulfonyl-8-bromo-1',3',3'-trimethyl-6-nitrospiro[chromene-2,2'-indoline] (9l)



Trifluoromethanesulfonic anhydride (500 mg, 1.77 mmol) was added to a solution of 5'-bromo-8-hydroxy-1',3',3'-trimethyl-6-nitrospiro[chromene-2,2'-indoline] (417 mg, 1.00 mmol) and anhydrous pyridine (0.4 mL, 396 mg, 5 mmol) in anhydrous DCM (10 mL) over the course of 6 min at 0 °C. The reaction mixture was stirred at 0 °C for 1.5 h, before the cooling bath was removed and the reaction mixture stirred at 24 °C for 1 h followed by heating it to 40 °C for 2 h. After the reaction cooled down, the mixture was diluted with DCM (10 mL) and the remaining anhydride was deactivated by addition of water (20 mL). The phases were separated, the aqueous phase was extracted with DCM (2 x 10 mL) and the solvent was removed *in vacuo*. The remaining solid was dissolved in EtOAc (20 mL), which was then washed with hydrochloric acid (1 mol/L, 2 x 20 mL) and water (20 mL). After drying over MgSO₄ and removal of solvent, the crude product was dissolved in chloroform (20 mL) and the solution was filtered. Removal of the solvent gave the product as dark purple solid (239 mg, 435 μmol, 43%).

Melting point: $T = 87$ °C.

¹H NMR (500 MHz, CDCl₃, 300 K): $\delta = 8.29$ (d, $^4J = 2.6$ Hz, 1H, H-7), 7.97 (d, $^4J = 2.6$ Hz, 1H, H-5), 7.09 (dd, $^3J = 8.5$ Hz, $^4J = 2.5$ Hz, 1H, H-6'), 6.97 (d, $^4J = 2.5$ Hz, 1H, H-4'), 6.94 (d, $^3J = 10.3$ Hz, 1H, H-4), 6.53 (d, $^3J = 8.5$ Hz, 1H, H-7'), 5.88 (d, $^3J = 10.3$ Hz, 1H, H-3), 2.74 (s, 3H, H-12'), 1.30 (s, 3H, H-13'), 1.22 (s, 3H, H-14') ppm.

¹³C NMR (126 MHz, CDCl₃, 300 K): $\delta = 155.8$ (C-8a), 147.2 (C-7'a), 143.2 (C-5'), 141.3 (C-4a), 138.2 (C-3'a), 129.1 (C-7), 128.7 (C-4), 121.7 (C-3), 121.6 (C-5), 120.9 (C-6'), 115.5 (H-4'), 109.6 (C-8), 108.0 (C-2), 107.5 (C-7'), 52.5 (C-3'), 29.1 (C-12'), 25.6 (C-14'), 19.9 (C-13') ppm.^a

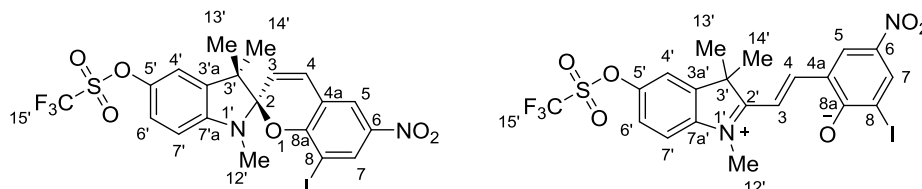
¹⁹F NMR (471 MHz, CDCl₃, 300 K): $\delta = -78.6$ ppm.^b

IR (ATR): $\tilde{\nu} = 3091$ (w), 2966 (w), 2926 (w), 2852 (w), 1599 (w), 1520 (m), 1486 (m), 1419 (s), 1336 (s), 1269 (m), 1243 (s), 1205 (vs), 1139 (vs), 1091 (s), 1019 (m), 966 (m), 923 (m), 900 (s), 858 (m), 832 (s), 810 (s), 743 (s), 712 (s), 615 (s) cm⁻¹.

HRMS (EI-TOF): m/z (%): [M]⁺ calcd for [C₂₀H₁₆⁷⁹BrF₃N₂O₆S]⁺ 547.9865; found 547.9856 (20); calcd for [C₂₀H₁₆⁸¹BrF₃N₂O₆S]⁺ 549.9844; found 549.9846 (21); 415.03/417.03 (100) [M-(CF₃SO₂)]⁺.

^a The carbon atom of the trifluoromethanesulfonic ester (C-9) was not detectable via ¹³C NMR spectroscopy, due to the large coupling constant of approx. 400 Hz, the quadruplet peaks are expected to be distributed over a range of 13 ppm and be lower in their intensity.

^b The ¹⁹F NMR spectrum of this compound was obtained without adding an internal standard.

5'-Trifluoromethylsulfonyl-8-iodo-1',3',3'-trimethyl-6-nitrospiro[chromene-2,2'-indoline] (9m)

Trifluoromethanesulfonic anhydride (635 mg, 1.3 mmol) was added to a solution of 5'-hydroxy-8-iodo-1',3',3'-trimethyl-6-nitrospiro[chromene-2,2'-indoline] (464 mg, 1.00 mmol) in anhydrous DCM (10 mL) over the course of 2 min at 0 °C. The reaction mixture was stirred at 0 °C for 1 h, the cooling bath was removed and the reaction mixture stirred at 20 °C for 1 h before heating it to reflux for 2 h. The reaction mixture was purified by filtration through silica gel (Macherey-Nagel, eluent: EtOAc) and after removal of the solvent *in vacuo*, the residue was dissolved in toluene (20 mL) and dried *in vacuo* again to remove remaining pyridine as azeotropic mixture. The crude product was purified by column chromatography (silica gel, MeOH/EtOAc 5/95 v/v) to obtain a dark purple solid (259 mg, 434 μ mol, 43%).

TLC (MeOH/EtOAc, 5/95): R_f = 0.15

Melting point: T = 85 °C.

¹H NMR (600 MHz, CD₂Cl₂, 300 K):

Signals assigned to the *spiro[chromene-2,2'-indoline]* (closed) form: δ = 8.29 (d, ⁴J = 2.6 Hz, 1H, H-5), 7.99 (d, ⁴J = 2.6 Hz, 1H, H-7), 7.11 (dd, ³J = 8.5 Hz, ⁴J = 2.5 Hz, 1H, H-6'), 7.00 (d, ⁴J = 2.5 Hz, 1H, H-4'), 6.97 (d, ³J_Z = 10.3 Hz, 1H, H-4), 6.57 (d, ³J = 8.5 Hz, 1H, H-7'), 5.90 (d, ³J_Z = 10.3 Hz, 1H, H-3), 2.76 (s, 3H, H-12'), 1.30 (s, 3H, H-13'), 1.21 (s, 3H, H-14') ppm.

Signals assigned to the *merocyanine* (open) form: δ = 9.12 (d, ⁴J = 2.6 Hz, 1H, H-5), 8.75 (⁴J = 2.6 Hz, 1H, H-7), 8.28 (d, ³J_E = 16.3 Hz, 1H, H-4), 7.86 (d, ³J = 8.8 Hz, 1H, H-7'), 7.83 (d, ³J_E = 16.3 Hz, 1H, H-3), 7.62 (dd, ³J = 8.8 Hz, ⁴J = 2.3 Hz, 1H, H-6'), 7.58 (d, ⁴J = 2.3 Hz, 1H, H-4'), 4.37 (s, 3H, H-12'), 1.88 (s, 6H, H-13', H-14') ppm.

¹³C NMR (151 MHz, CD₂Cl₂, 300 K):^a

Signals assigned to the *spiro[chromene-2,2'-indoline]* (closed) form: δ = 147.9 (C-8a), 147.5 (C-3'a), 143.4 (C-5'), 141.7 (C-6), 138.8 (C-7'a), 129.3 (C-5), 129.2 (C-4), 123.2 (C-8), 122.1 (C-7, C-3), 121.2 (C-6'), 120.1 (C-4a), 115.9 (C-4'), 108.6 (C-2), 107.7 (C-7'), 52.9 (C-3'), 30.3 (C-12'), 25.8 (C-14'), 20.0 (C-13') ppm.

Signals assigned to the *merocyanine* (open) form: δ = 184.7 (C-2'), 151.5 (C-5'), 148.1 (C-6), 146.9 (C-8a), 146.5 (C-3'a), 143.6 (C-4), 141.2 (C-7'a), 133.3 (C-7),

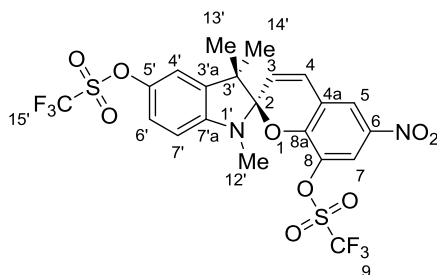
^a The carbon atom of the trifluoromethanesulfonic ester (C-9) was not detectable via ¹³C NMR spectroscopy, due to the large coupling constant of approx. 400 Hz, the quadruplet peaks are expected to be distributed over a range of 13 ppm and be lower in their intensity.

124.7 (C-5), 124.1 (C-6'), 120.6 (C-3), 119.4 (C-8), 118.4 (C-7'), 117.4 (C-4'), 109.8 (C-4a), 54.7 (C-3'), 37.0 (C-12'), 25.9 (C-13', C-14') ppm.

IR (ATR): $\tilde{\nu}$ = 3085 (w), 2973 (w), 1604 (m), 1538 (w), 1420 (s), 1342 (m), 1257 (vs), 1231 (vs), 1170 (vs), 1137 (vs), 1035 (vs), 905 (s), 870 (s), 832 (s), 765 (s), 743 (s), 632 (vs), 616 (vs), 600 (vs), 512 (vs) cm^{-1}

HRMS (EI-TOF): m/z (%): $[M]^+$ calcd for $[\text{C}_{20}\text{H}_{16}\text{F}_3^{127}\text{IN}_2\text{O}_6\text{S}]^+$ 595.97258; found 595.97047 (16); 463.07 (100) $[\text{M}-(\text{CF}_3\text{SO}_2)]^+$.

Bis-5',8-(trifluoromethylsulfonyl)-1',3',3'-trimethyl-6-nitrospiro[chromene-2,2'-indoline] (9n)



Trifluoromethanesulfonic anhydride (1.69 g, 1.01 mL, 6.00 mmol) was added to a solution of 5',8-dihydroxy-1',3',3'-trimethyl-6-nitrospiro[chromene-2,2'-indoline] (886 mg, 2.50 mmol) and anhydrous pyridine (791 mg, 0.81 mL, 10.0 mmol) in anhydrous DCM (10 mL) over the course of 10 min at 0 °C under a nitrogen atmosphere. The reaction mixture was stirred at 0 °C for 1.5 h, the cooling bath was removed and the reaction mixture stirred at 20 °C for 1 h before heating it to 50 °C for 2 h. The reaction mixture was filtered through silica gel (silica gel, eluent: EtOAc) and after removal of the solvent *in vac.*, the residue was dissolved in toluene (20 mL) and dried *in vac.* again to remove remaining pyridine as azeotropic mixture. The crude product was purified by column chromatography (silica gel, eluent: TEA/DCM 5% *v/v*). After removal of the solvent *in vacuo*, the product was obtained as purple solid (1.37 g, 2.22 mmol, 89%).

TLC (silica gel, UV, TEA/DCM 5% *v/v*): R_f = 1.0 – 0.5

Melting point: T = 96 °C

$^1\text{H NMR}$ (500 MHz, CDCl_3 , 300 K): δ = 8.07 (d, 4J = 2.5 Hz, 1 H, H-5), 8.00 (d, 4J = 2.5 Hz, 1 H, H-7), 7.10 (dd, 4J = 2.5 Hz, 3J = 8.5 Hz, 1 H, H-6'), 7.05 (d, 3J = 10.5 Hz, 1 H, H-4), 6.99 (d, 4J = 2.5 Hz, 1 H, H-4'), 6.53 (d, 3J = 8.5 Hz, 1 H, H-7'), 6.01 (d, 3J = 10.5 Hz, 1 H, H-3), 2.75 (s, 3H, H-12'), 1.34 (s, 3H, H-13'), 1.25 (s, 3H, H-14') ppm.

$^{13}\text{C NMR}$ (126 MHz, CDCl_3 , 300 K): δ = 151.5 (C-6), 146.8 (C-7'a), 143.5 (C-5'), 140.2 (C-8), 137.8 (C-3'a), 135.1 (C-4a), 128.5 (C-4), 122.1 (C-7), 121.9 (C-3), 120.9

(C-6'), 120.7 (C-8a), 119.6 (C-9), 119.1 (C-5), 117.5 (C-15'), 115.4 (C-4'), 108.9 (C-2), 107.7 (C-7'), 52.4 (C-3'), 28.8 (C-12'), 25.9 (C-13'), 19.5 (C-14') ppm.^a

¹⁹F NMR (471 MHz, CDCl₃, 300 K): δ = -72.7, -74.0 ppm.

IR (ATR): $\tilde{\nu}$ = 3104 (w), 2966 (w), 1647 (w), 1615 (m), 1588 (w), 1531 (m), 1476 (m), 1416 (s), 1345(s), 1301 (m), 1223 (vs), 1209 (vs), 1136 (vs), 1103 (s), 1082 (s), 1047 (m), 1017 (m), 1001 (m), 955 (m), 942 (m), 905 (vs), 876 (s), 837 (s), 815 (vs), 772 (m), 730 (s), 657 (m), 620 (s), 595 (s), 587 (s), 503 (s) cm⁻¹.

HRMS (ESI-TOF): *m/z* (%): [M+H]⁺ calcd for [C₂₁H₁₆N₂F₆O₉S₂+H]⁺ 619.0274; found 619.0278 (75); 641.01 (100) [M+Na]⁺.

^a The carbon atom of the trifluoromethanesulfonic ester (C-9) was not detectable via ¹³C NMR spectroscopy, due to the large coupling constant of approx. 400 Hz, the quadruplet peaks are expected to be distributed over a range of 13 ppm and be lower in their intensity.

UV/vis Measurements and Determination of Attenuation Coefficients by ^1H NMR Spectroscopy

Sample Preparation

Of each new spiropyran, a stock solution was prepared in acetonitrile (HPLC-grade, 100 mL, circa 0.1 mmol/L). A defined volume (1 – 5 mL) was taken out of this solution and diluted to give a final volume of 10 mL to obtain the desired various sample concentrations (circa 10 – 50 $\mu\text{mol/L}$).

For the determination of the ratio between the spiropyran and merocyanine species in a dark environment by ^1H NMR spectroscopy, 500 μL of the most concentrated solution (circa 50 $\mu\text{mol/L}$) and 50 μL of deuterated acetonitrile were combined.

Table i: Preparation of stock solutions.

<i>Compound</i>	<i>Mol. Weight (g/mol)</i>	<i>Targeted conc. stock solution (mol/L)</i>	<i>Targeted weight (mg)</i>	<i>Actual sample weight (mg)</i>	<i>Volume stock solution (mL)</i>	<i>Conc. stock solution (mol/L)</i>
9a	480.16	1.00E-04	4.80	4.86	100	1.01E-04
9b	527.16	1.00E-04	5.27	5.65	100	1.07E-04
9c	417.26	1.00E-04	4.17	2.98	100	7.14E-05
9j	549.32	1.00E-04	5.49	5.91	100	1.08E-04
9d	527.16	1.00E-04	5.27	5.45	100	1.03E-04
9e	574.16	1.00E-04	5.74	4.35	100	7.58E-05
9f	464.26	1.00E-04	4.64	2.76	100	5.94E-05
9k	596.32	1.00E-04	5.96	6.91	100	1.16E-04
9g	417.26	1.00E-04	4.17	5.86	100	1.40E-04
9h	464.26	1.00E-04	4.64	3.76	100	8.10E-05
9l	549.32	1.00E-04	5.49	5.34	100	9.72E-05
9m	596.32	1.00E-04	5.96	6.86	100	1.15E-04
9n	618.47	1.00E-04	6.18	6.25	100	1.01E-04

Summarized Results

For all new spiropyrans, 5 different dilutions were investigated by UV/vis spectroscopy under the following conditions: **(a)** after illumination with green light (565 nm), until a photostationary state was reached, in which mostly spiropyran form was present; **(b)** after irradiation with UV light (365 nm), until a photostationary state was reached, in which the merocyanine forms are enriched; **(c)** after keeping the sample solutions dark for at least 24 hours, the measurement was carried out under red light (i.e. no absorption possible); **(d)** time dependent measurements after

PSS³⁶⁵; typically, 120 scans were taken with a time interval of less than 2 min,^a **(e)** time dependent measurements after PSS⁵⁶⁵, typically, 120 scans were taken with a time interval of 6 min.^b

The graphs **(a-c)** contain a plot of the measured intensities at the absorption maxima and a linear fit; the results are summarized in table ii. Plots of time dependent measurements **(d, e)** contain a plot of the measured absorption at the maximum which corresponds to the merocyanine state and an exponential fit. These results are summarized in table iii.

For the determination of the ratio between merocyanine and spiropyran, ¹H NMR spectra of the most concentrated samples from **(c)** were recorded and plotted in **(f)**. The signals used to determine the ratio are marked with green (merocyanine) and orange (spiropyran) boxes. Table iv shows the obtained results.

^a The intervals were: 2 min for **9a**, 1 min for **9b,d,e,m**, 15 s for **9c,f,l**.

^b For **9b** and **9e**, 2 min and 1 min were used, respectively.

Table ii: Absorption maxima and calculated attenuation coefficients from a linear fit (using a fixed intercept at 0;0) including errors.

Name	Wavelength of abs. max. (nm)		Attenuation ($L(\text{mol cm})^{-1}$)					
	SP form	MC form	PSS (565 nm)		PSS (365 nm)		Equilibrium in dark conditions	
			Slope (linear fit)	Std. error	Slope (linear fit)	Std. error	Slope (linear fit)	Std. error
9a	315	556	9168	50	30591	381	1858	37
9b	306	559	7709	129	11500	98	1082	15
9c	355	568	8765	37	27520	221	2424	26
9j	308	536	8699	74	6885	183	21876	335
9d	308	559	8826	69	19770	103	1576	10
9e	314	561	5534	36	8320	82	828	24
9f	355	570	7849	67	24215	511	2209	20
9k	311	538	8881	72	5274	52	23936	224
9g	320	547	9948	107	1747	13	31621	330
9h	320	549	7583	160	1972	51	15851	658
9l	331	561	7364	40	23266	277	336	1.5
9m	335	557	4948	166	6292	210	289	13
9n	304	537	6483	49	11532	97	6879	33

Table iii: The half-life times $t_{1/2}$ refer to samples, which, after illumination, were allowed to isomerize in the dark. The absorption maximum of merocyanine was plotted in dependence on time, before an exponential fit ($y = y_0 + A_1 e^{-x/t_1}$) was applied.

Name	Decay after PSS (365 nm)			Decay after PSS (565 nm)		
	t_1 (min)	Std. error	$t_{1/2}$ (hh:mm:ss)	t_1 (min)	Std. error	$t_{1/2}$ (hh:mm:ss)
	Exp. fit	Exp. fit		Exp. fit	Exp. fit	
9a	22.15155	0.00964	00:15:21	33.3562 2		00:23:07
9b	16.54166	0.0599	00:11:28	32.1321 5	0.09491	00:22:16
9c	1.3287	0.00237	00:00:55	n.n. ^b		
9j	n.n. ^a			365.409 87	1.33004	04:13:17
9d	20.75646	0.01001	00:14:23	36.2259 8	0.29487	00:25:07
9e	19.24909	0.19885	00:13:21	12.7739 9	0.02188	00:08:51
9f	1.73289	0.00153	00:01:12	n.n. ^b		
9k	n.n. ^a			300.356 14	1.07554	03:28:11
9g	n.n. ^a			411.942 73	1.57521	04:45:32
9h	n.n. ^a			392.056 5	0.55513	04:31:45
9l	3.87585	0.01548	00:02:41	n.n. ^b		
9m			00:00:00	n.n. ^b		
9n	81.52332	0.27588	00:56:30	175.046 44	0.66688	02:01:20

^a A decay measurement was not performed, because the concentration of merocyanine was lower at the PSS₃₆₅ compared to dark conditions. This is because the merocyanine form also absorbs at this wavelength, leading to the formation of the spiropyran form, an effect that is not present in the dark equilibrium.

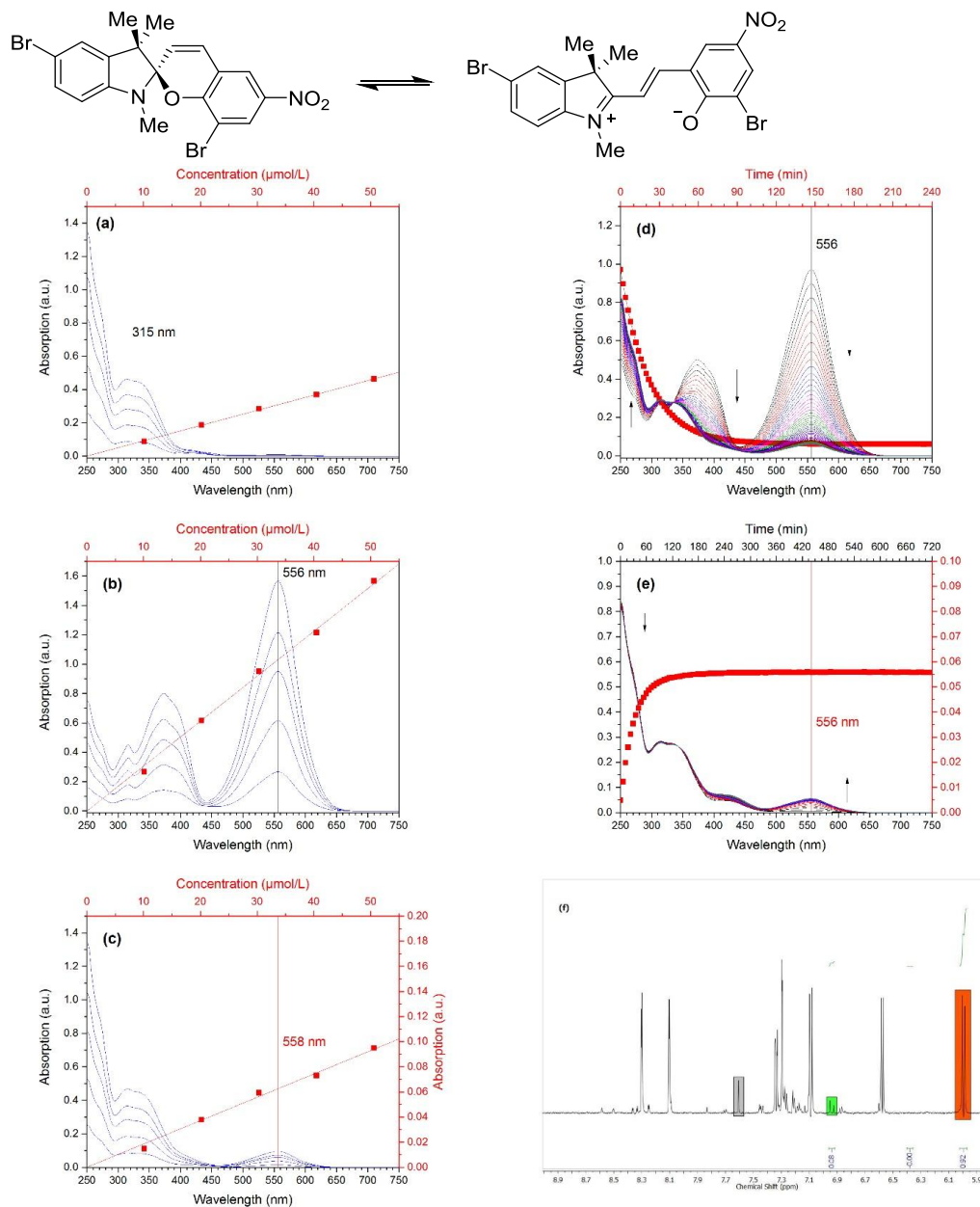
^b A decay measurement was not performed, because the concentration of merocyanine at the PSS₅₆₅ was the same compared to dark conditions.

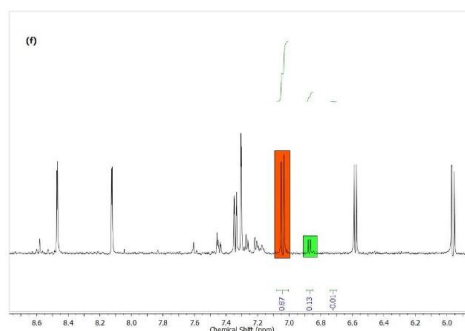
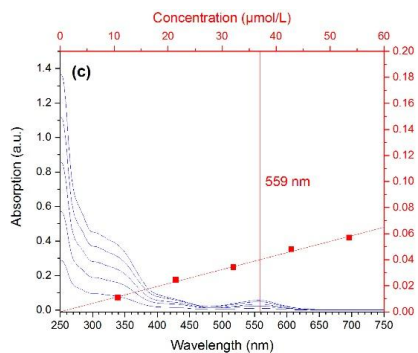
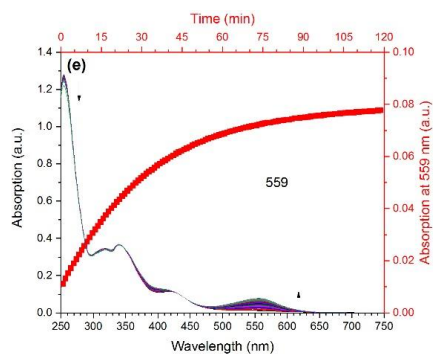
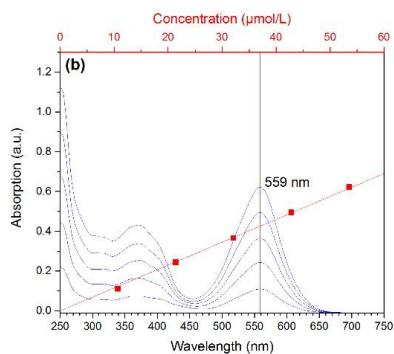
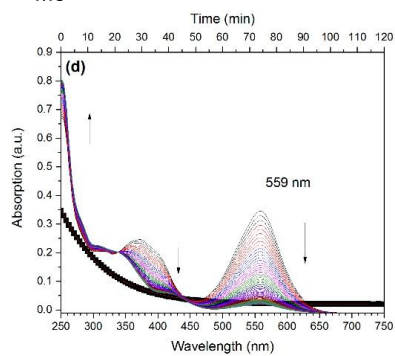
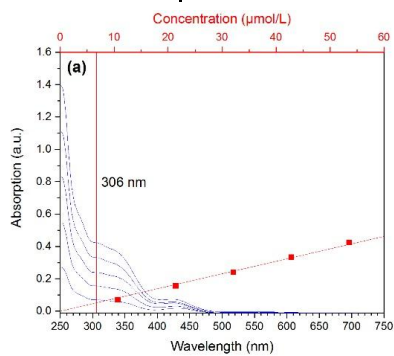
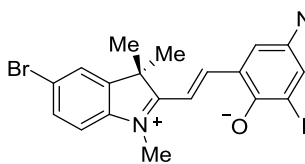
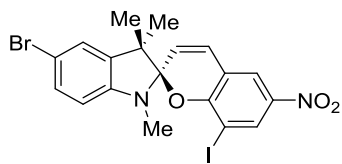
Table iviv: Determination of the absolute attenuation coefficient ϵ_{MC} of merocyanine form by combined UV/vis and $^1\text{H NMR}$ spectral analysis and calculation of the ratio between merocyanine and spiropyran forms in the photostationary state after irradiation with 365 nm for 30 sec.

Compound	Equilibrium in dark conditions						Photostationary state (365 nm)					
	Attenuation ($\text{L}(\text{mol cm})^{-1}$)		Ratio [MC]:[SP]		ϵ_{MC} ($\text{L}(\text{mol cm})^{-1}$)		Attenuation ($\text{L}(\text{mol cm})^{-1}$)		Calculated Ratio [MC]:[SP]			
	Slope (linear fit)	Std. error	Integration of $^1\text{H NMR}$	Integration error	Calculated $\epsilon_{\text{dark}}/\text{Int.}$	Error	Slope (linear fit)	Std. error	[MC]	[SP]		
9a	1858	37	08:92	0.02	24447	6434	30591	381	125	-25		
9b	1082	15	12:88	0.01	9328	804	11500	98	123	-23		
9c	2424	26	07:93	0.00	34629	0	27520	221	79	21		
9j	21876	335	59:41	0.01	37078	628	6885	183	19	81		
9d	1576	10	07:93	0.01	22514	3216	19770	103	88	12		
9e	828	24	04:96	0.01	20700	5175	8320	82	40	60		
9f	2209	20	06:94	0.00	36817	0	24215	511	66	34		
9k	23936	224	52:48	0.00	46031	0	5274	52	11	89		
9g	31621	330	58:42	0.00	54519	0	1747	13	03	97		
9h	15851	658	56:44	0.00	28305	0	1972	51	07	93		
9l	336	1.5	02:98	0.00	16800	0	24402	268	138	-38		
9m	289	556	48:52	0.00	556	0	6292	210	348	-248		
9n	6879	33	27:73	0.02	25478	1887	11532	97	45	55		

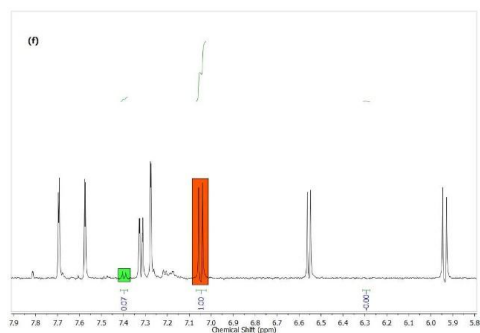
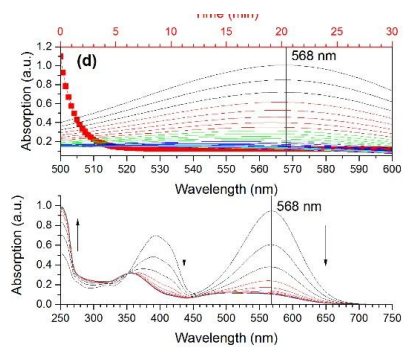
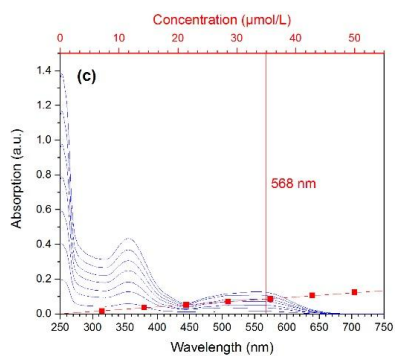
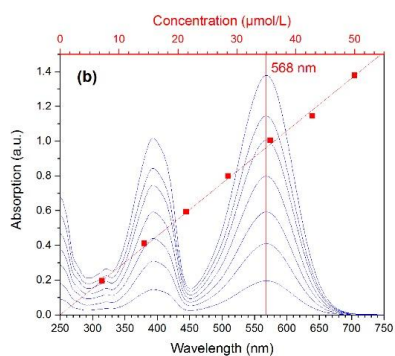
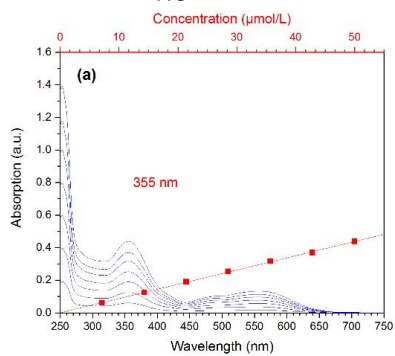
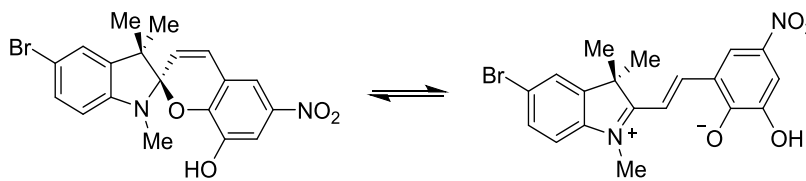
UV/vis Spectra and Corresponding ¹H NMR Spectra

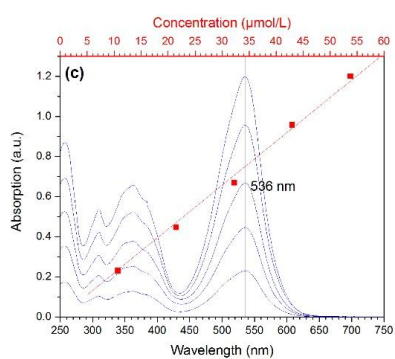
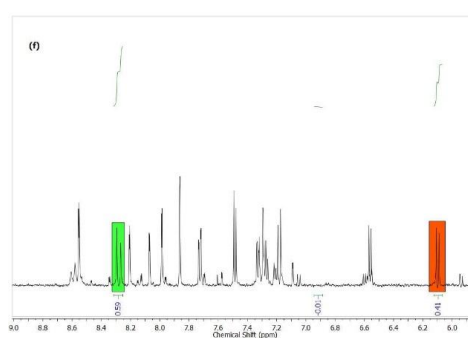
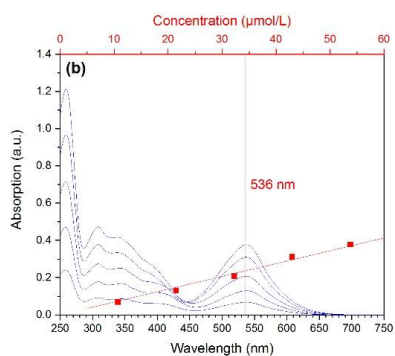
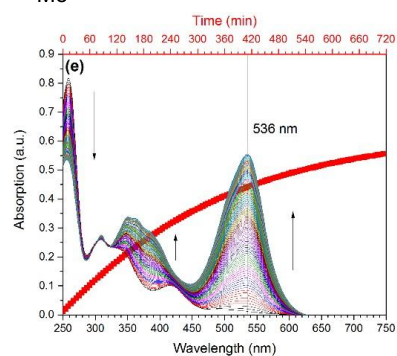
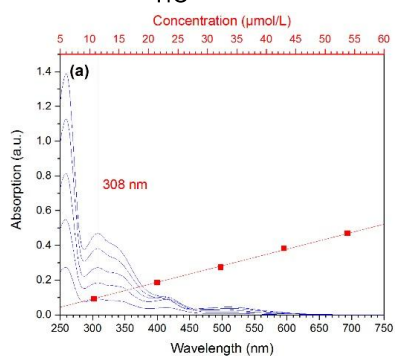
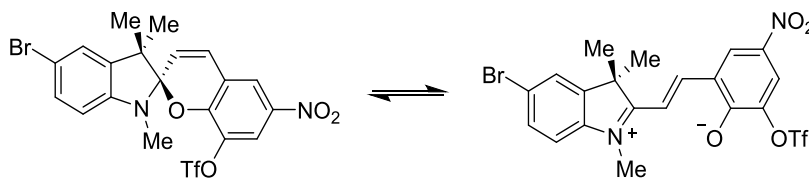
5'8-Dibromo-1',3',3'-trimethyl-6-nitrospiro[chromene-2,2'-indoline] (9a)



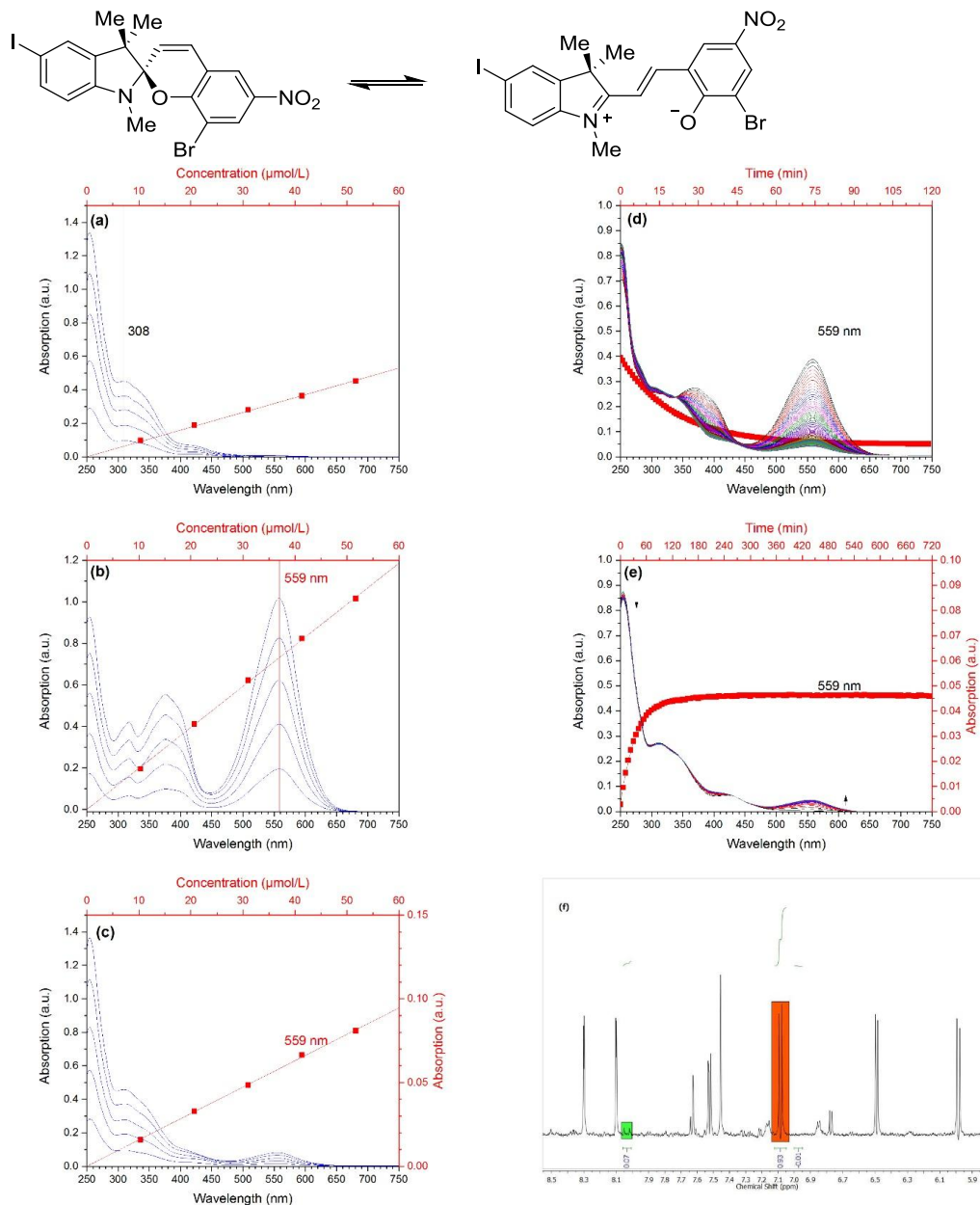
5'-Bromo-8-iodo-1',3',3'-trimethyl-6-nitrospiropyran[chromene-2,2'-indoline] (9b)

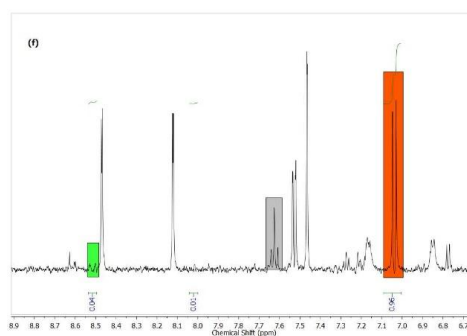
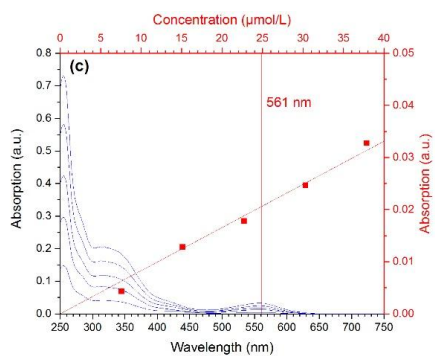
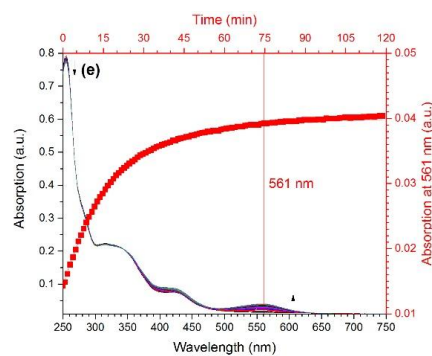
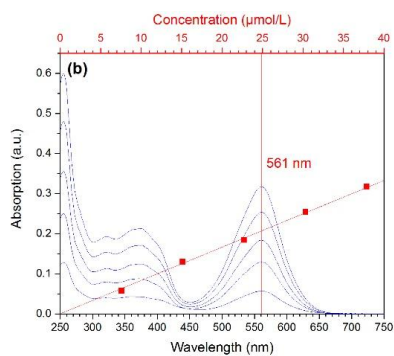
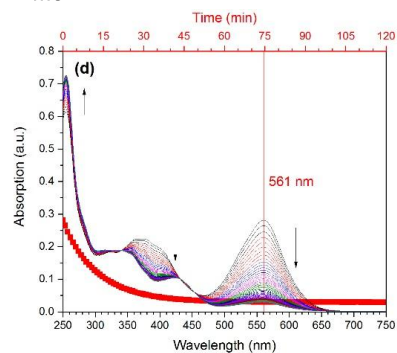
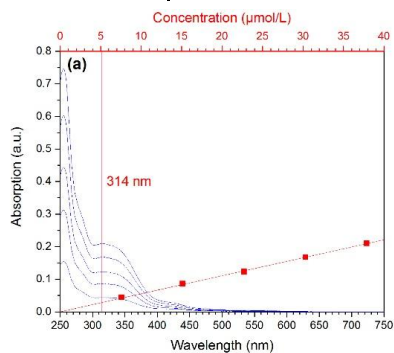
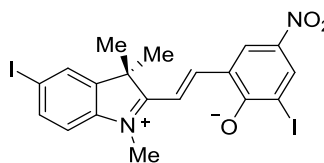
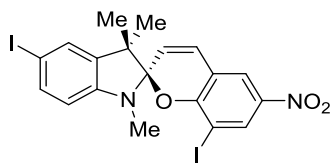
5'-Bromo-8-hydroxy-1',3',3'-trimethyl-6-nitrospiro[chromene-2,2'-indoline] (9c)



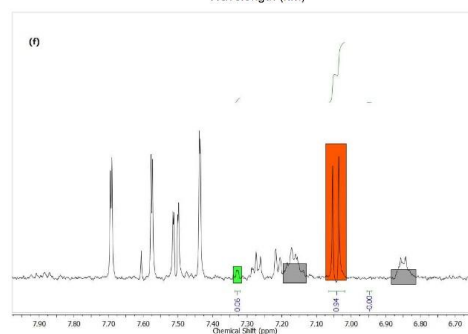
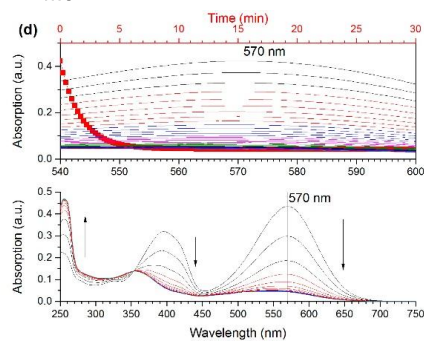
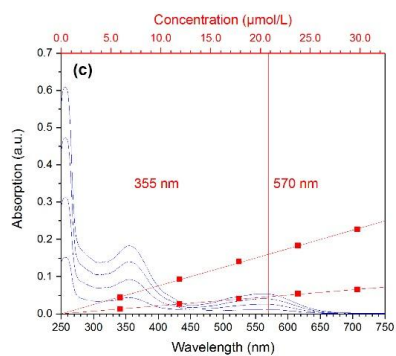
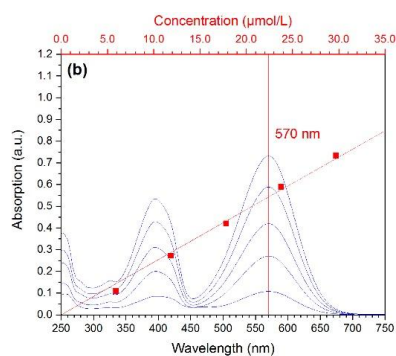
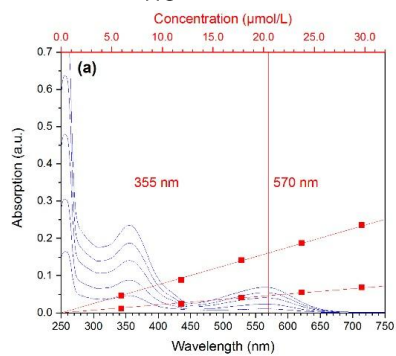
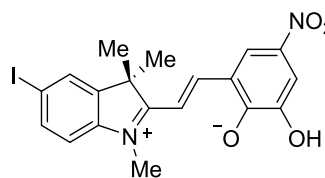
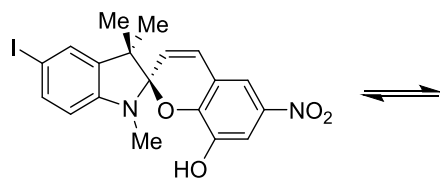
5'-Bromo-8-trifluoromethylsulfonyl-1',3',3'-trimethyl-6-nitrospiro[chromene-2,2'-indoline] (9)

5'-Iodo-8-bromo-1',3',3'-trimethyl-6-nitrospiro[chromene-2,2'-indoline] (9d)

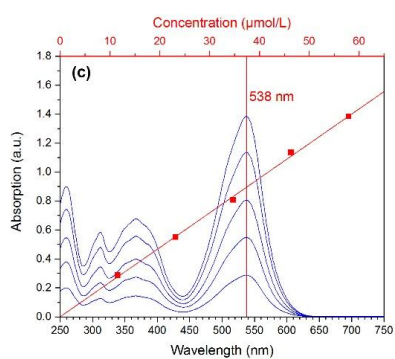
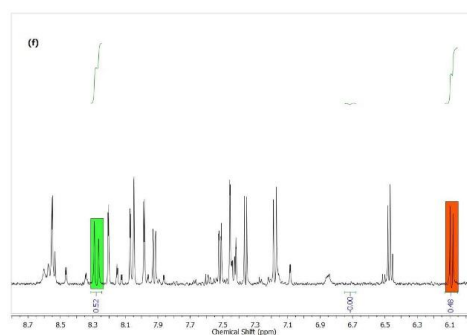
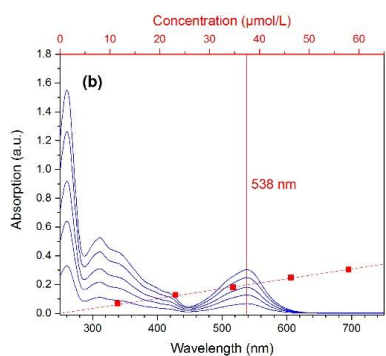
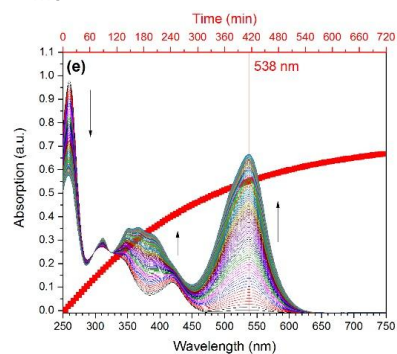
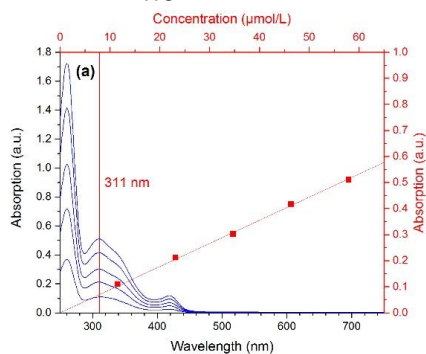
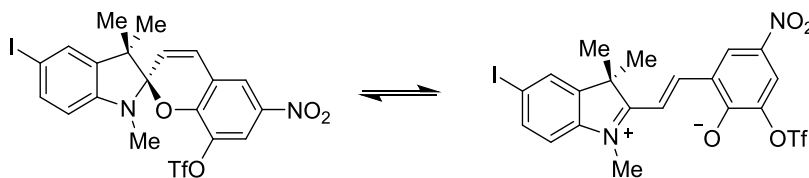


5',8-Diiodo-1',3',3'-trimethyl-6-nitrospiro[chromene-2,2'-indoline] (9e)

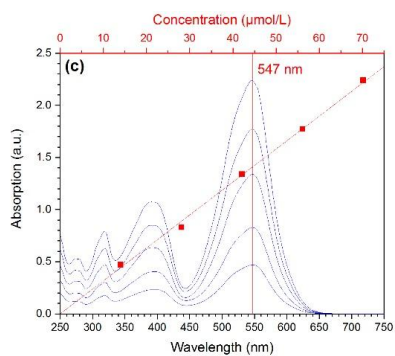
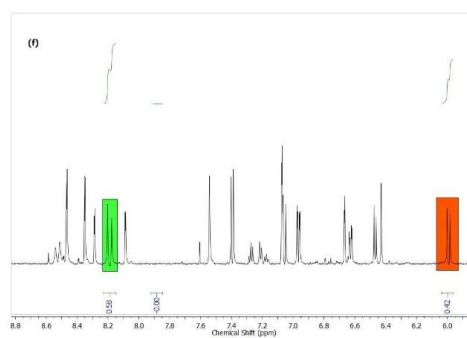
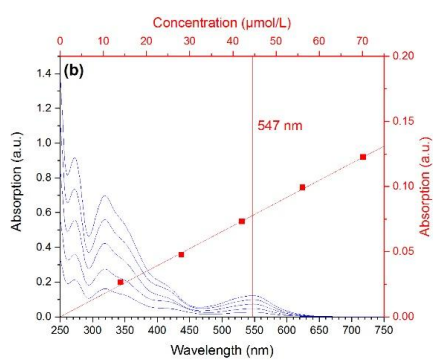
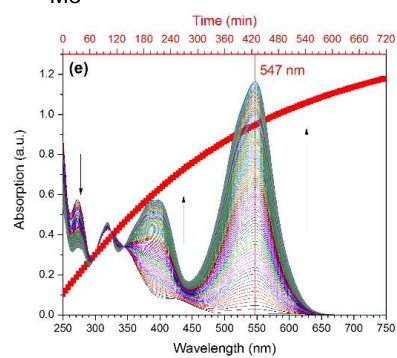
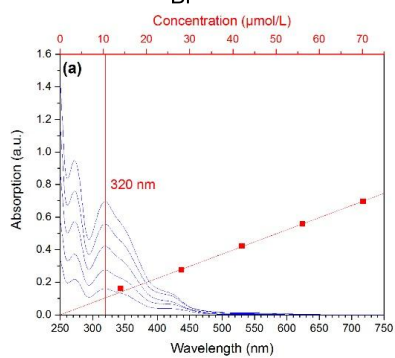
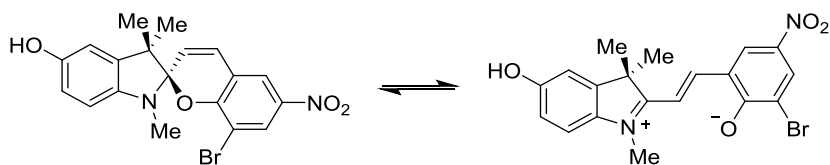
5'-Iodo-8-hydroxy-1',3',3'-trimethyl-6-nitrospiro[chromene-2,2'-indoline] (9f)



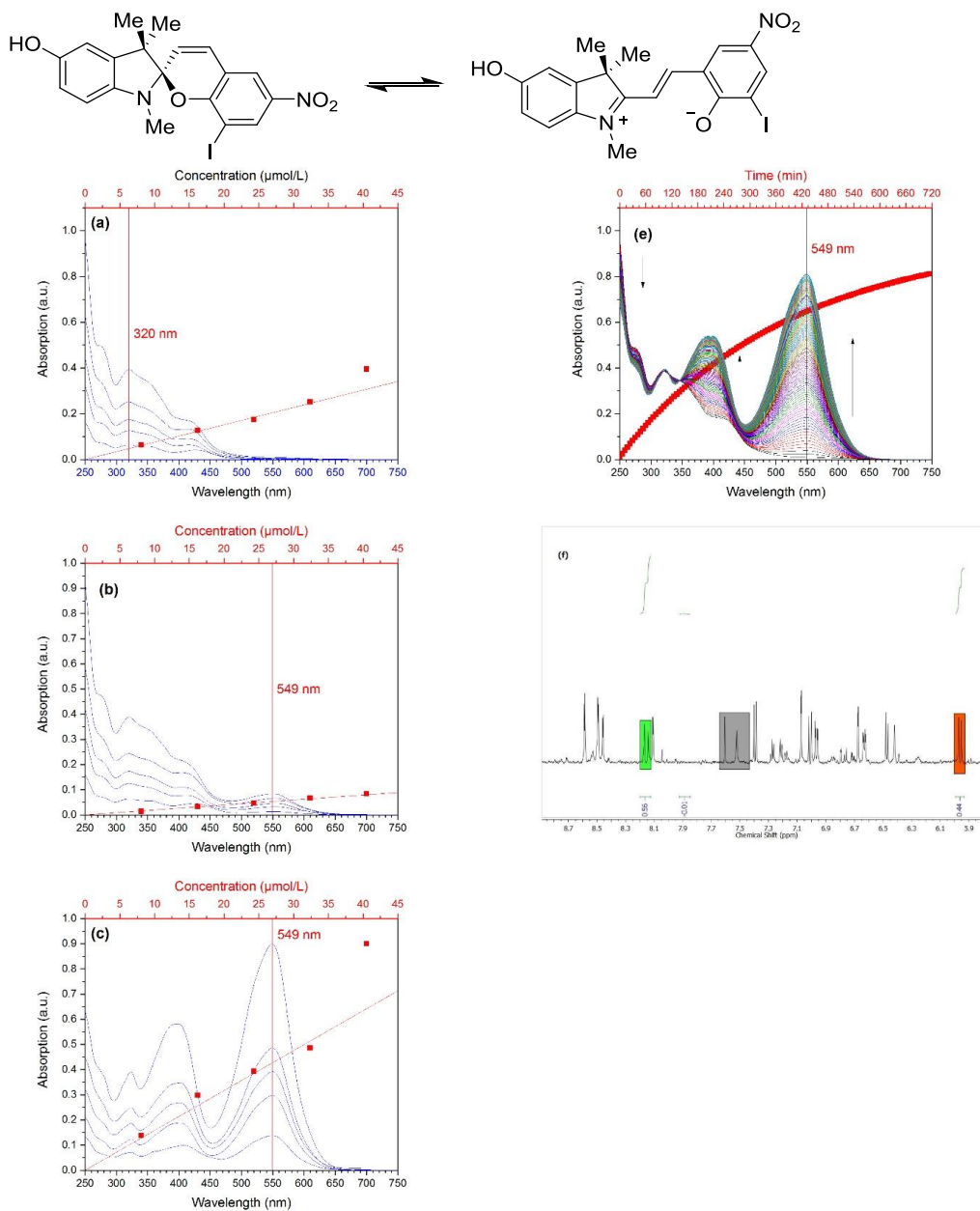
5'-Iodo-8-trifluoromethylsulfonyl-1',3',3'-trimethyl-6-nitrospiro[chromene-2,2'-indoline] (9k)



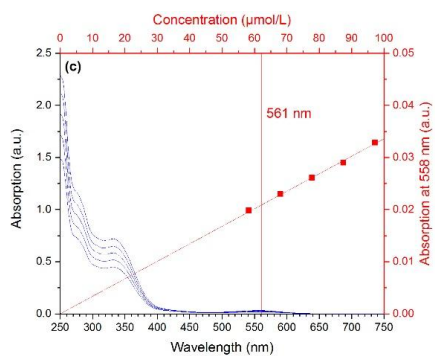
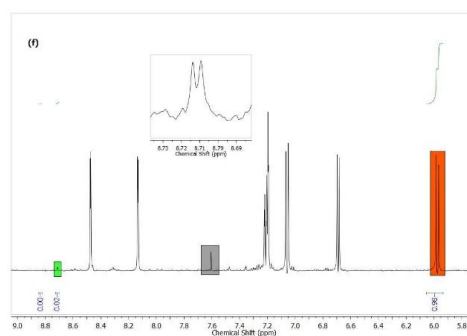
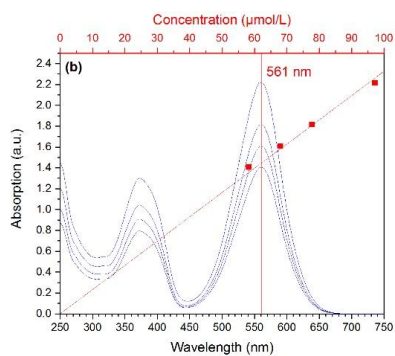
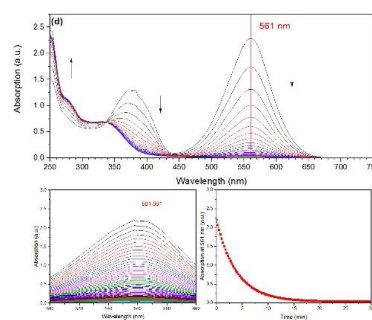
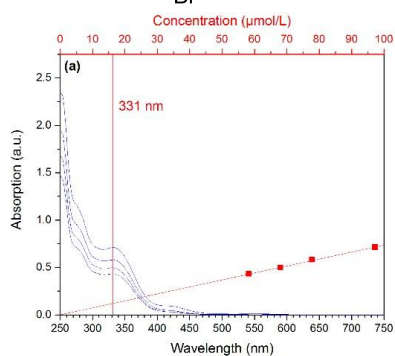
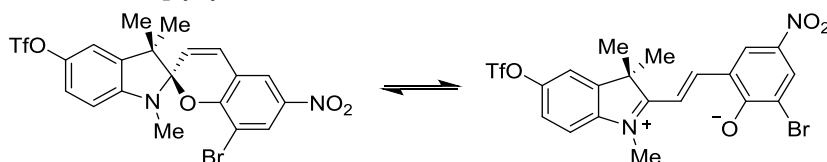
5'-Hydroxy-8-bromo-1',3',3'-trimethyl-6-nitrospiro[chromene-2,2'-indoline] (9g)



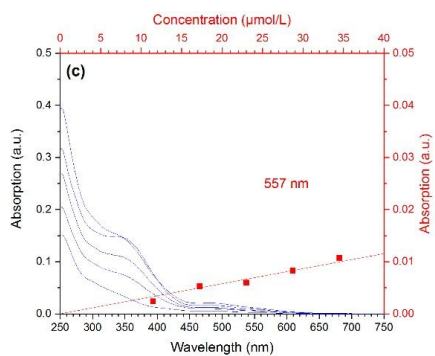
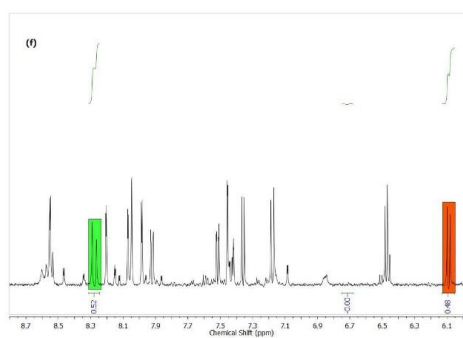
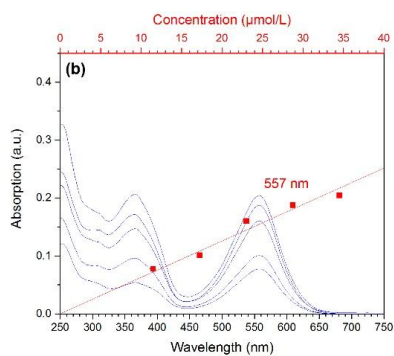
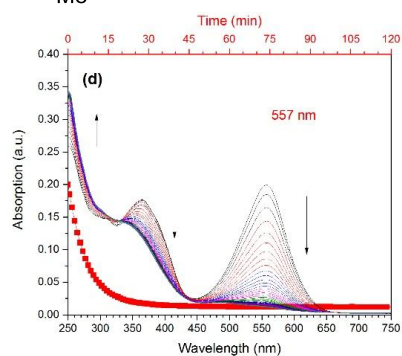
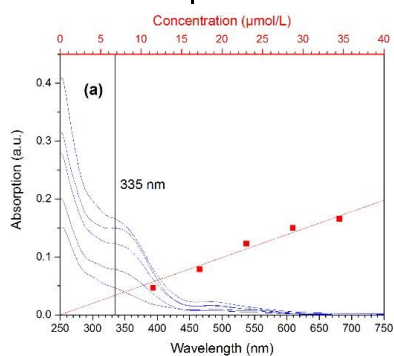
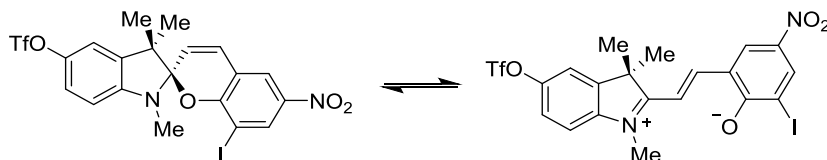
5'-Hydroxy-8-iodo-1',3',3'-trimethyl-6-nitrospiro[chromene-2,2'-indoline] (9h)



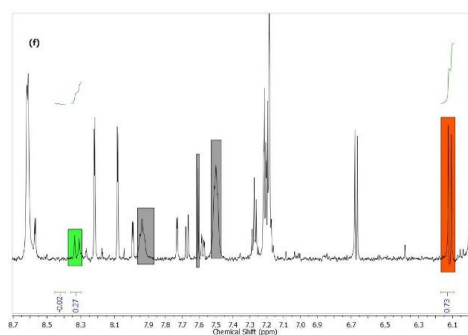
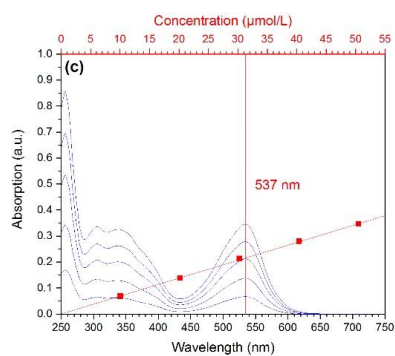
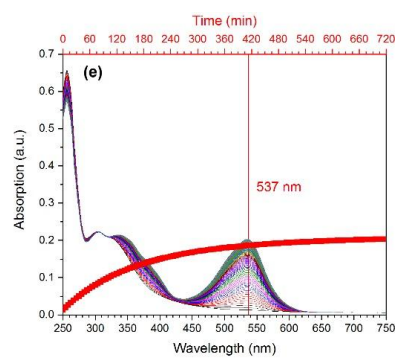
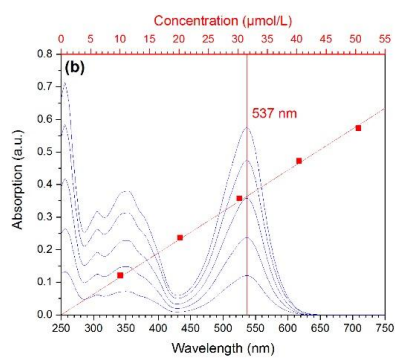
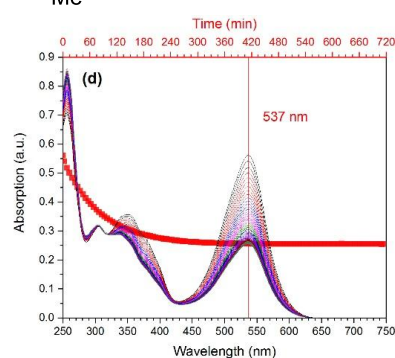
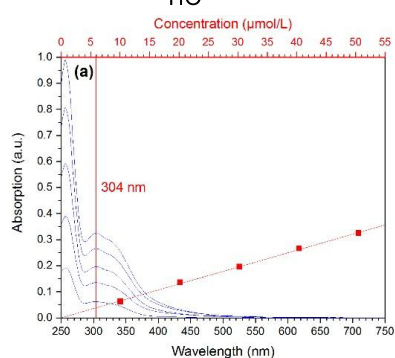
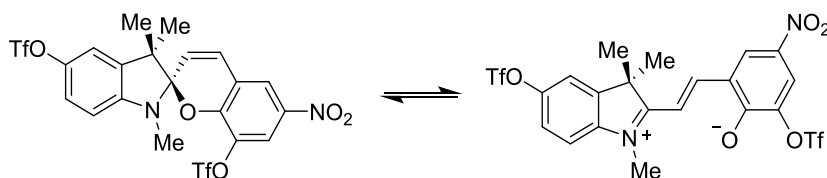
5'-Trifluoromethylsulfonyl-8-bromo-1',3,3'-trimethyl-6-nitrospiro[chromene-2,2'-indoline] (9I)



5'-Trifluoromethylsulfonyl-8-iodo-1',3',3'-trimethyl-6-nitrospiro[chromene-2,2'-indoline] (9m)

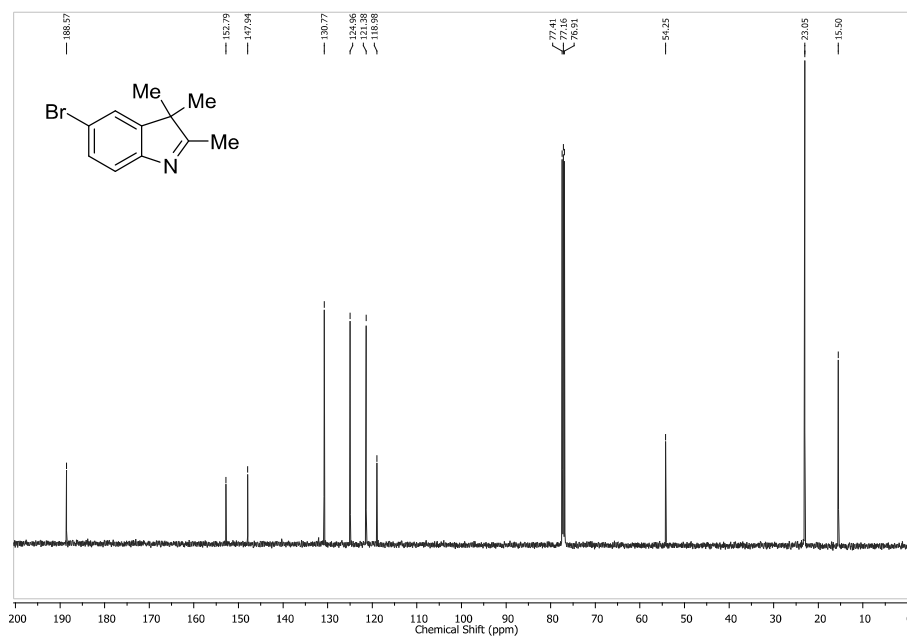
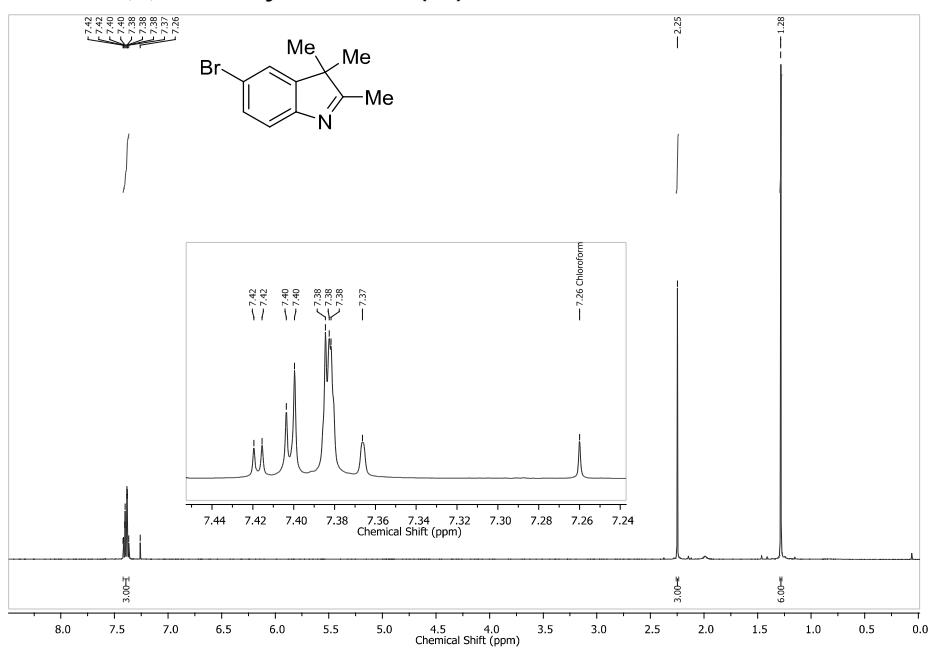


Bis-5',8-(trifluoromethylsulfonyl)-1',3',3'-trimethyl-6-nitrospiro[chromene-2,2'-indoline] (9n)



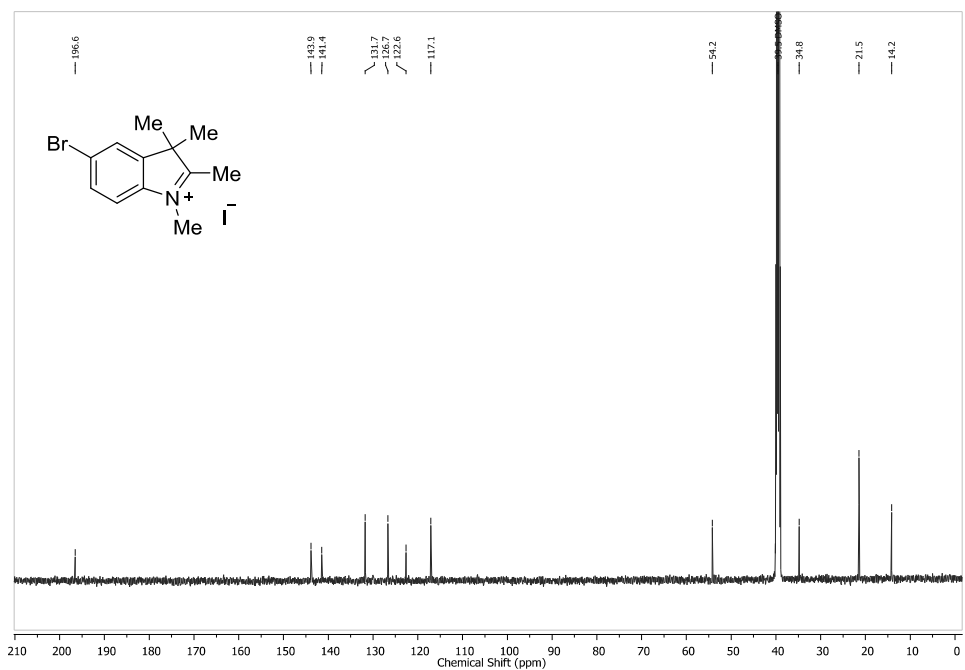
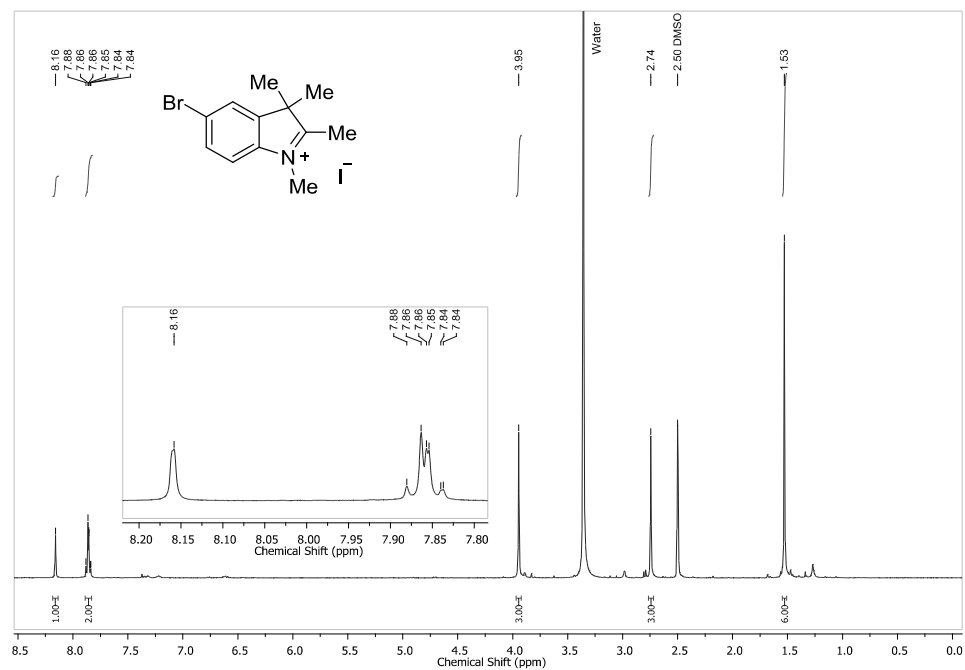
^1H NMR and $^{13}\text{C}\{^1\text{H}\}$ NMR Spectra

5-Bromo-2,3,3-trimethyl-3H-indole (8a)



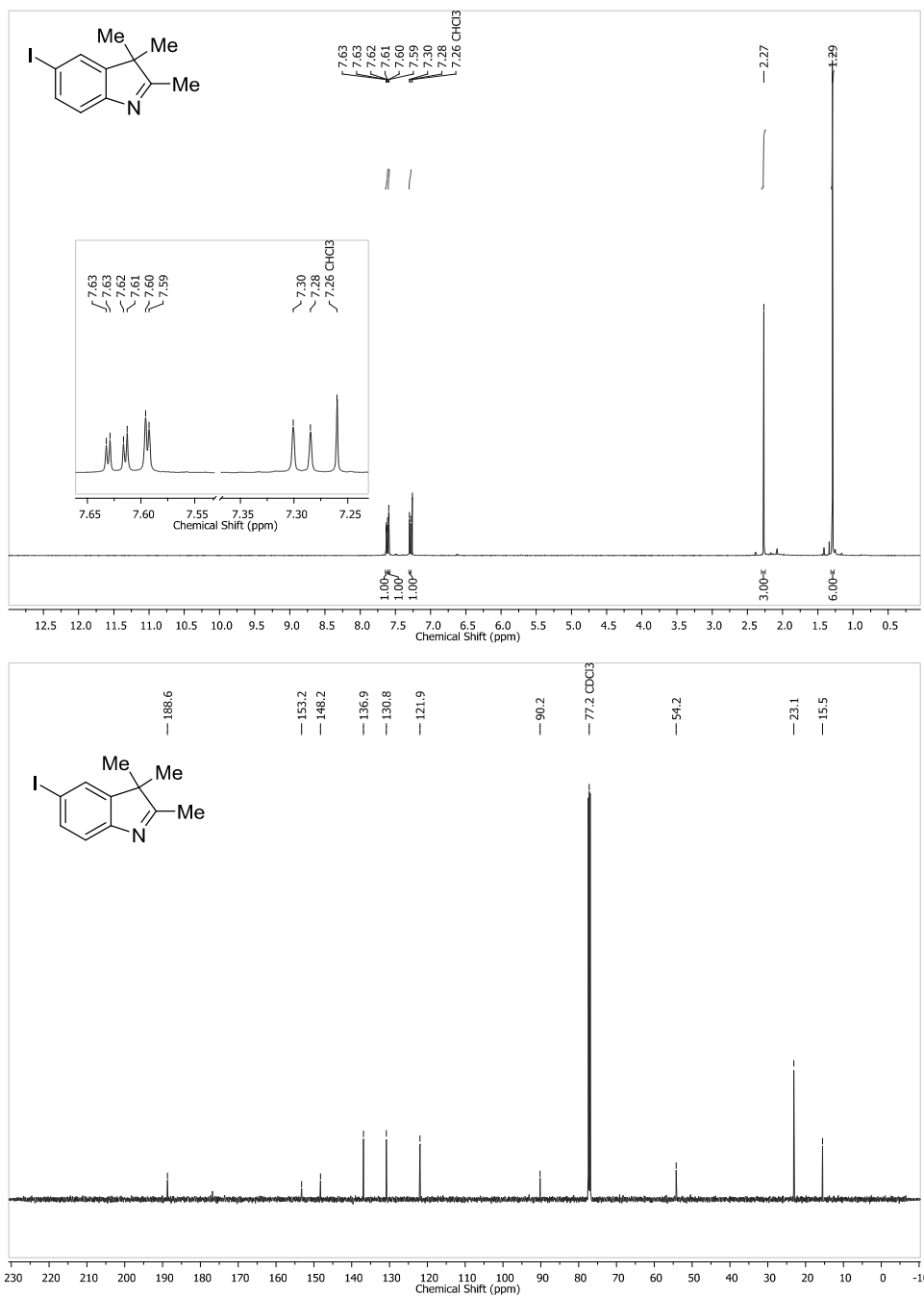
SI-46

5-Bromo-1,2,3,3-tetramethyl-3H-indolium iodide (3a)



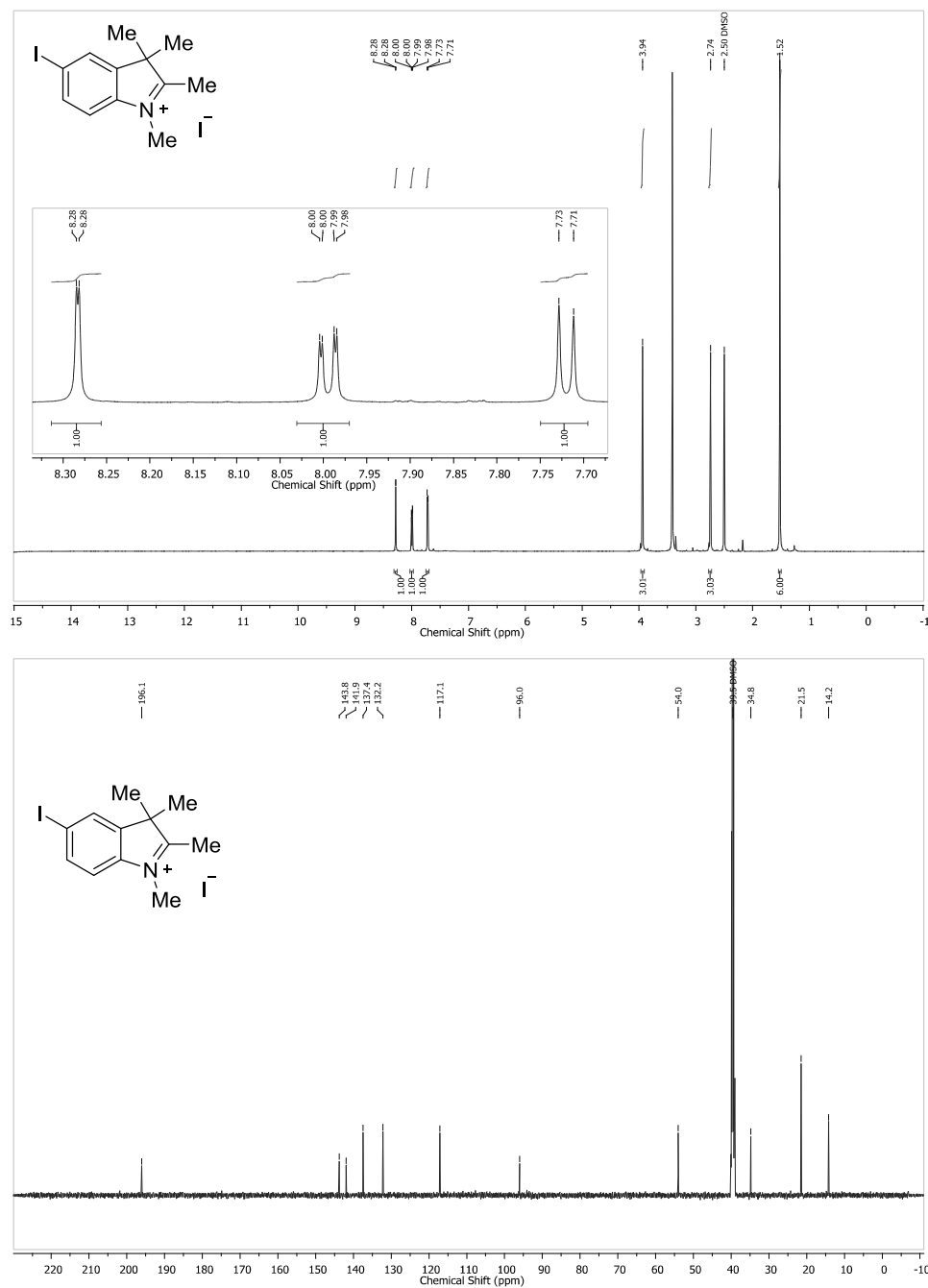
SI-47

5-Iodo-2,3,3-trimethyl-3H-indole (8b)



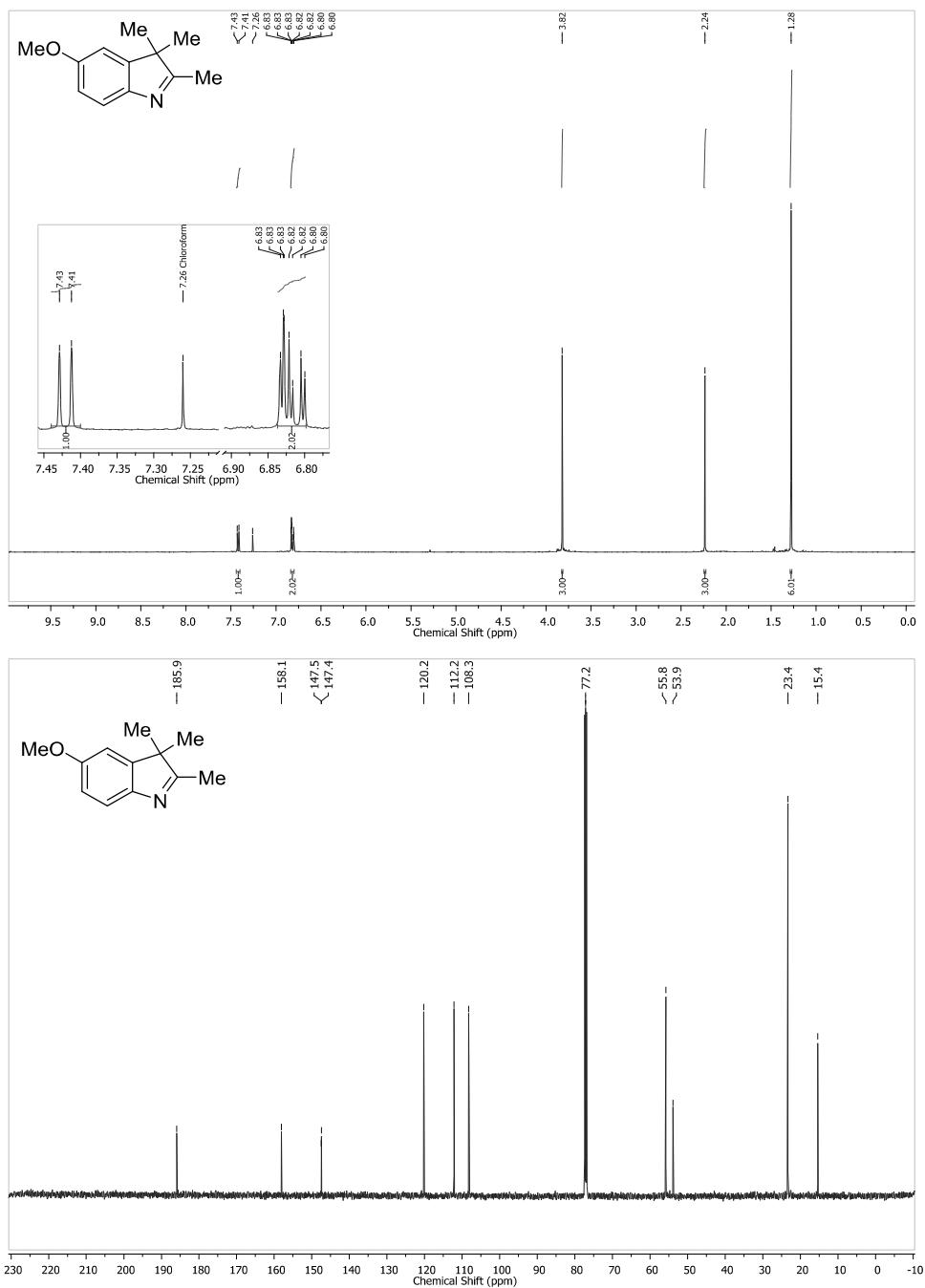
SI-48

5-Iodo-1,2,3,3-tetramethyl-3H-indolium iodide (3b)



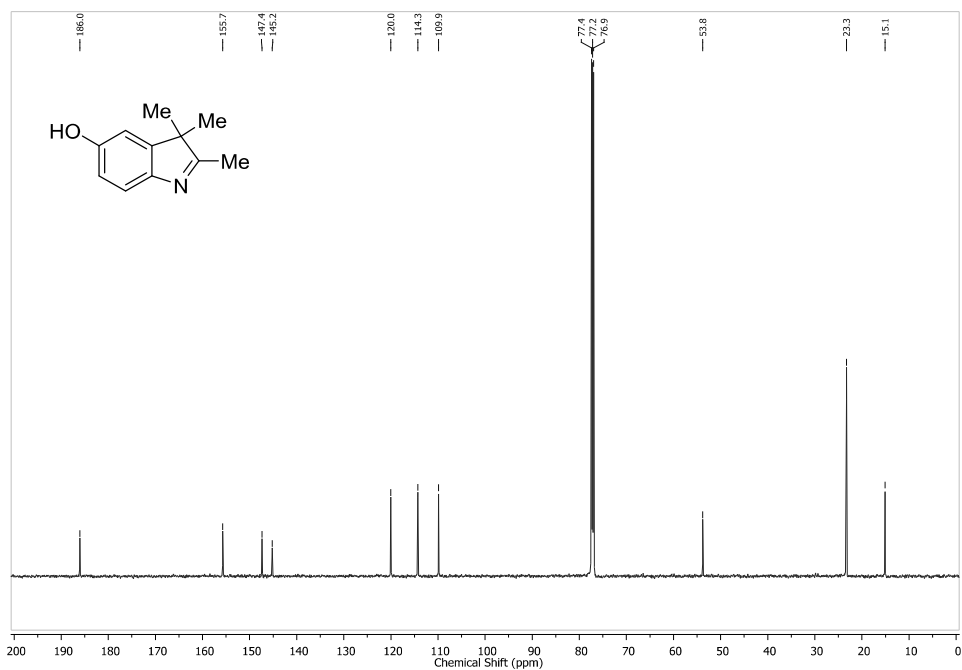
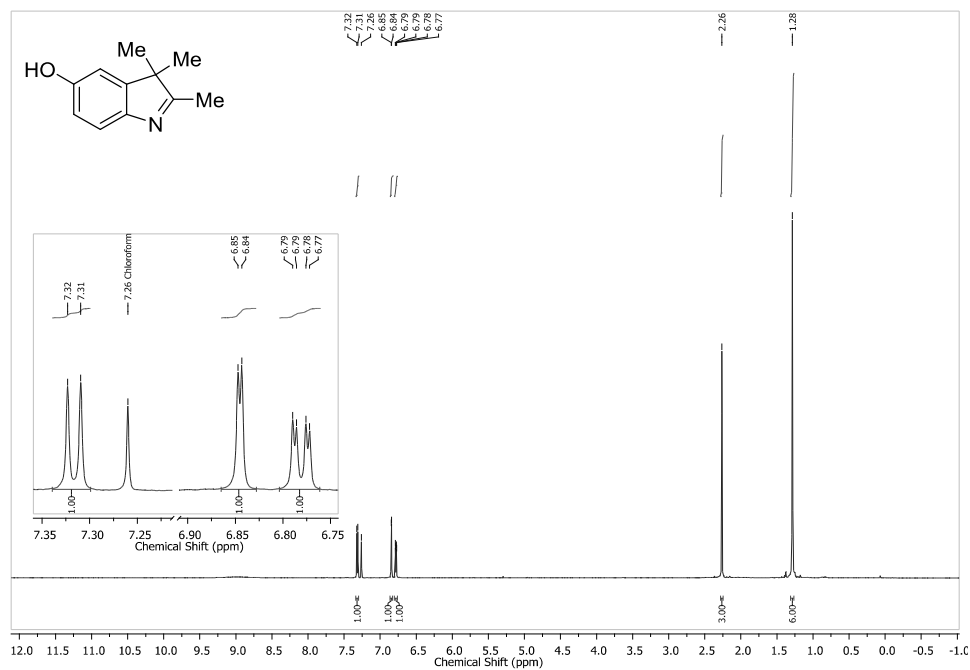
SI-49

5-Methoxy-2,3,3-trimethyl-3H-indole (8c)

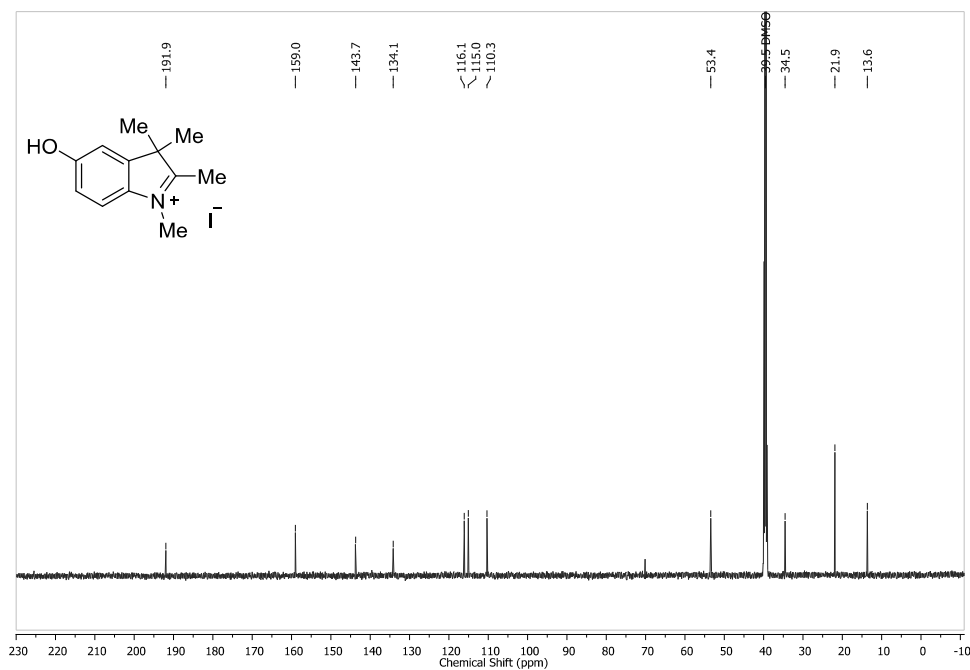
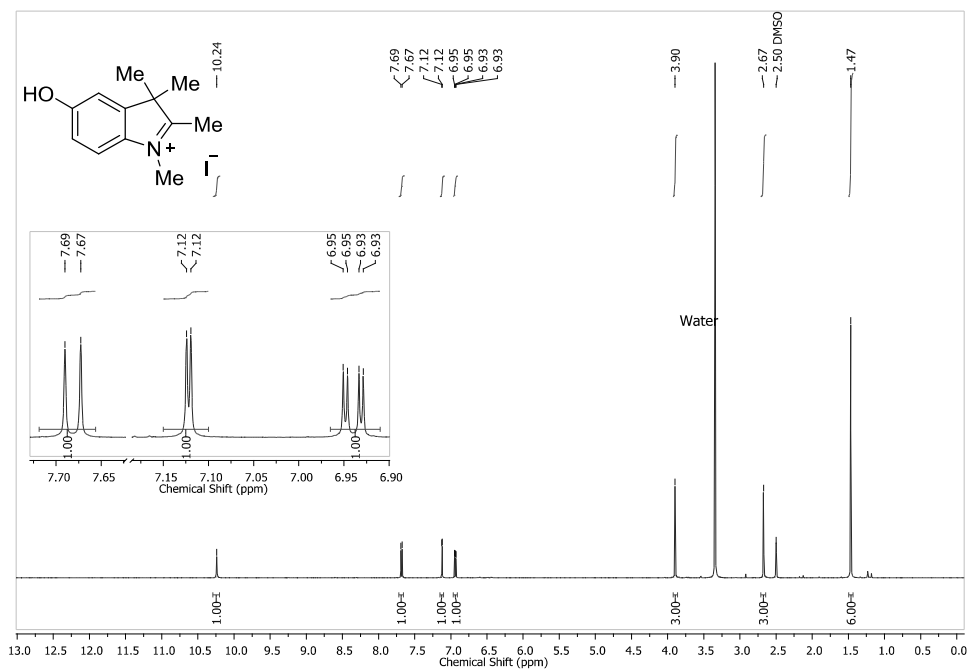


SI-50

5-Hydroxy-2,3,3-trimethyl-3H-indole (8d)

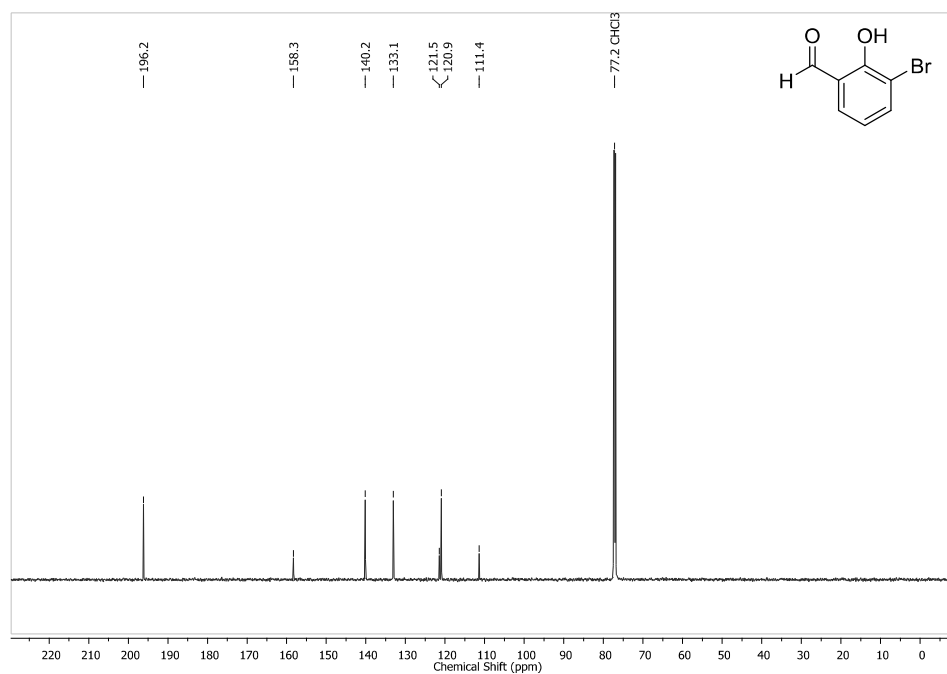
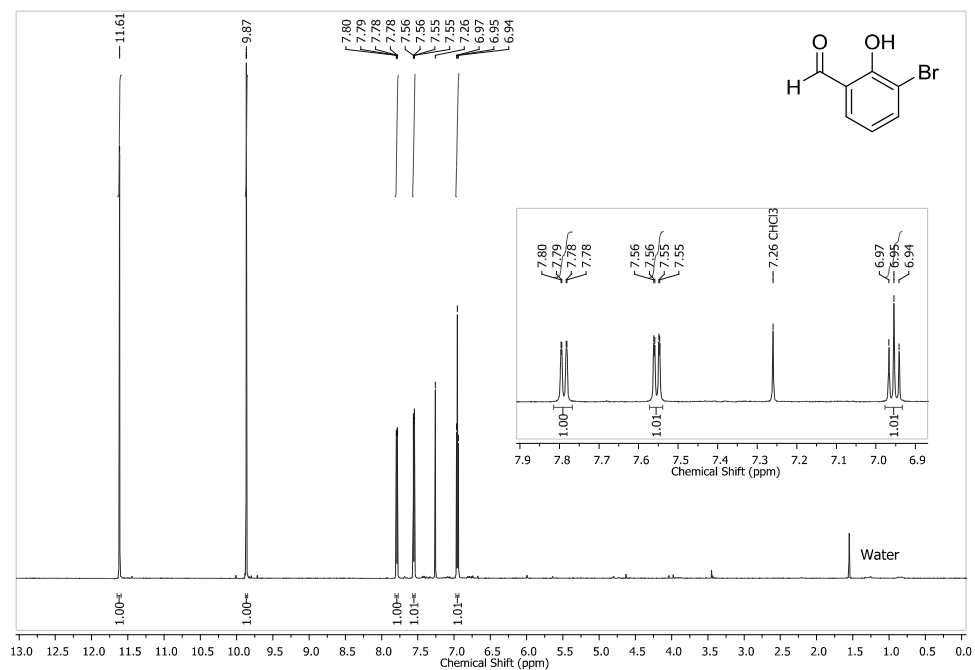


SI-51

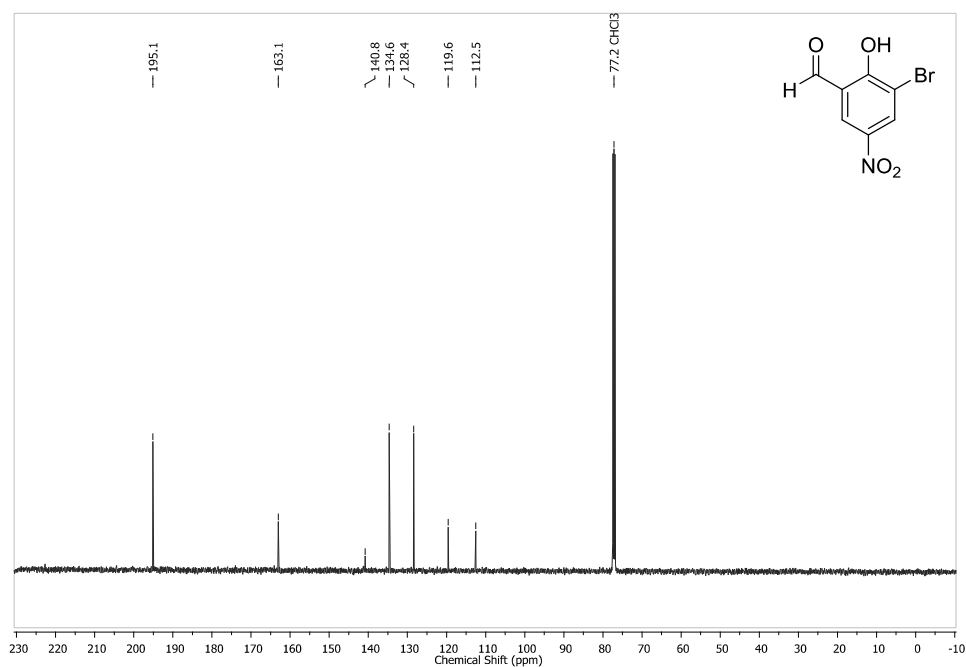
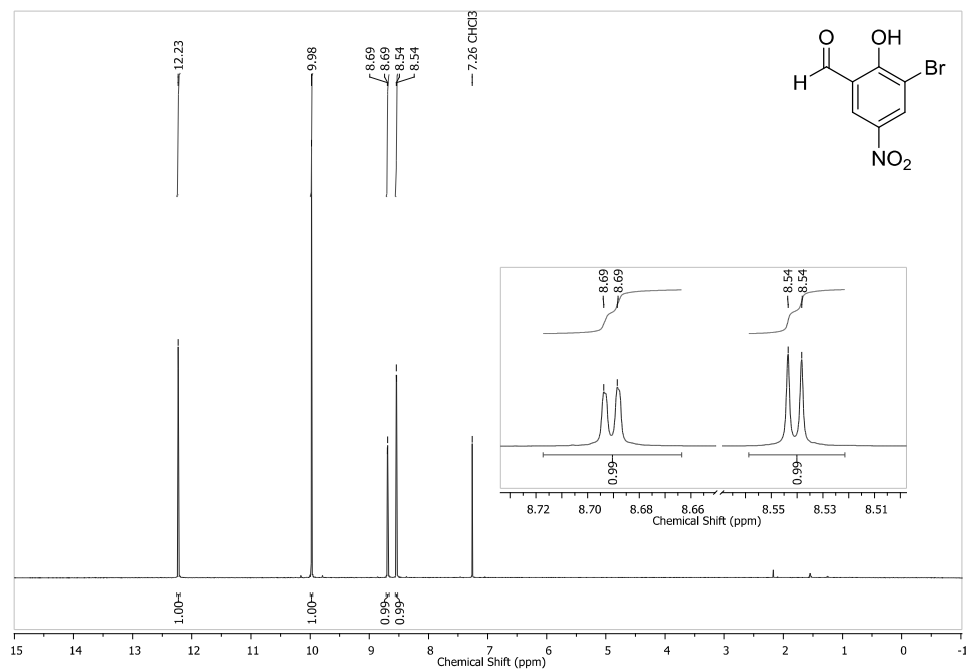
5-Hydroxy-1,2,3,3-tetramethyl-3*H*-indolium iodide (3c)

SI-52

3-Bromo-2-hydroxybenzaldehyde (5a)

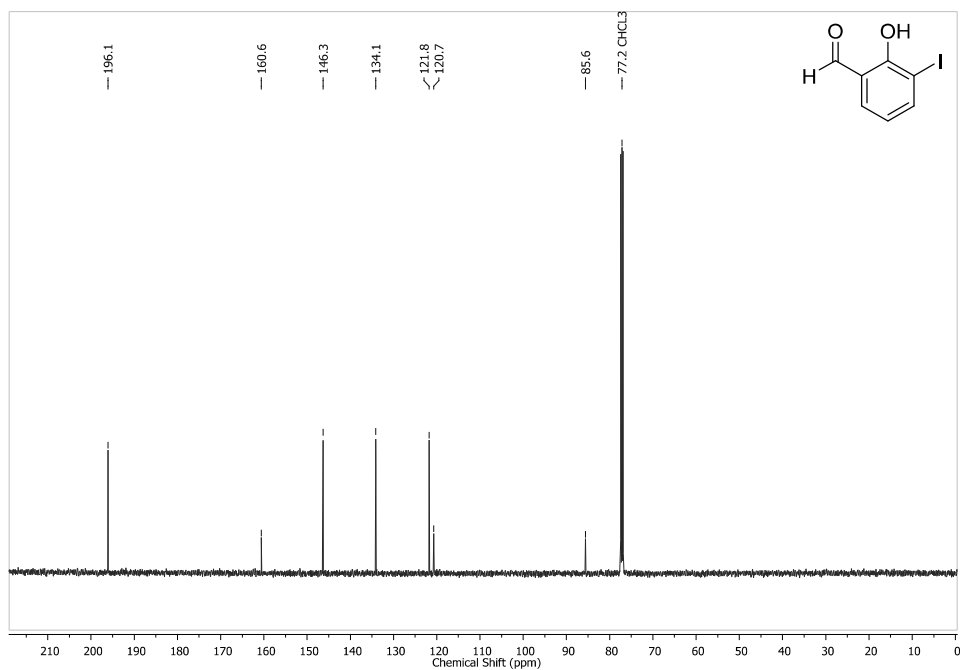
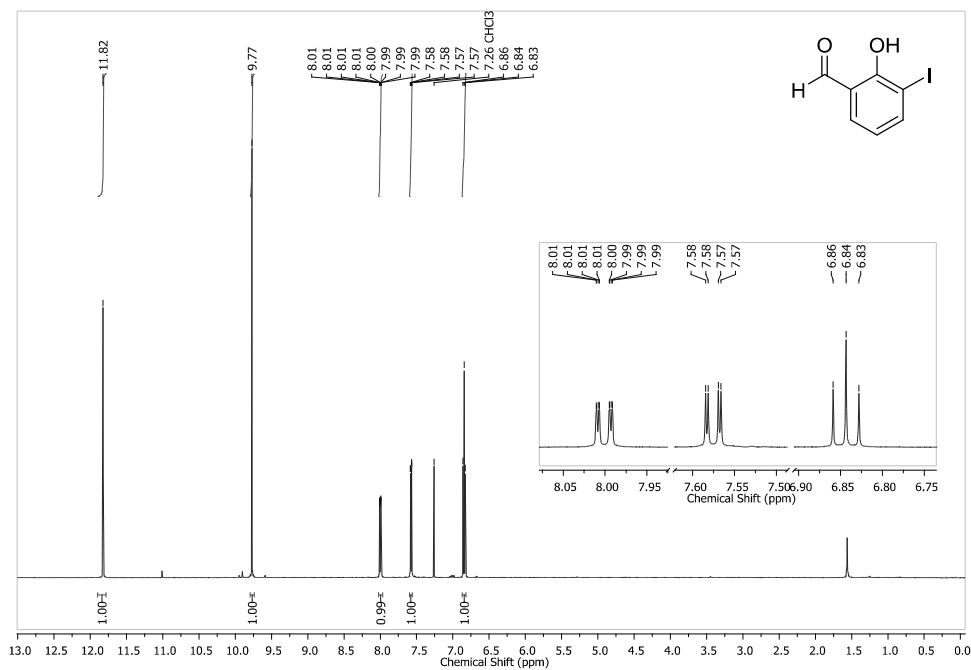


SI-53

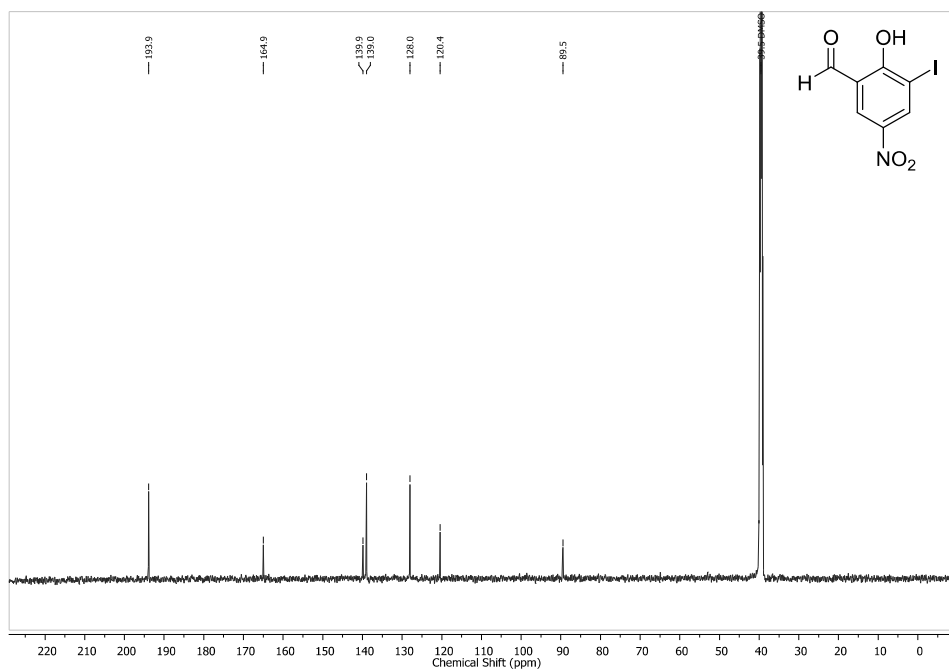
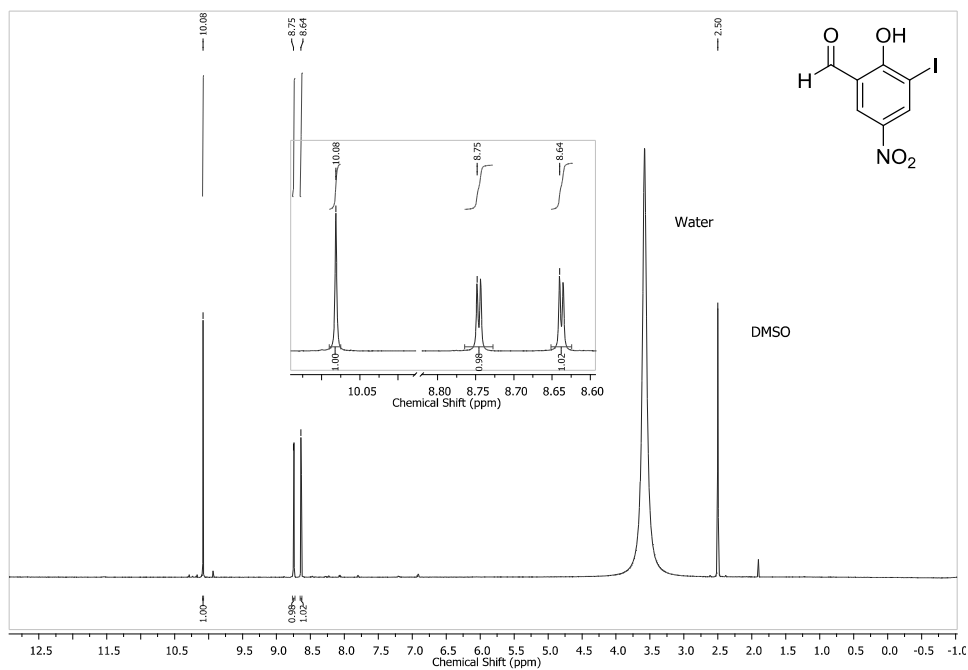
3-Bromo-2-hydroxy-5-nitrobenzaldehyde (2a)

SI-54

2-Hydroxy-3-iodobenzaldehyde (5b)

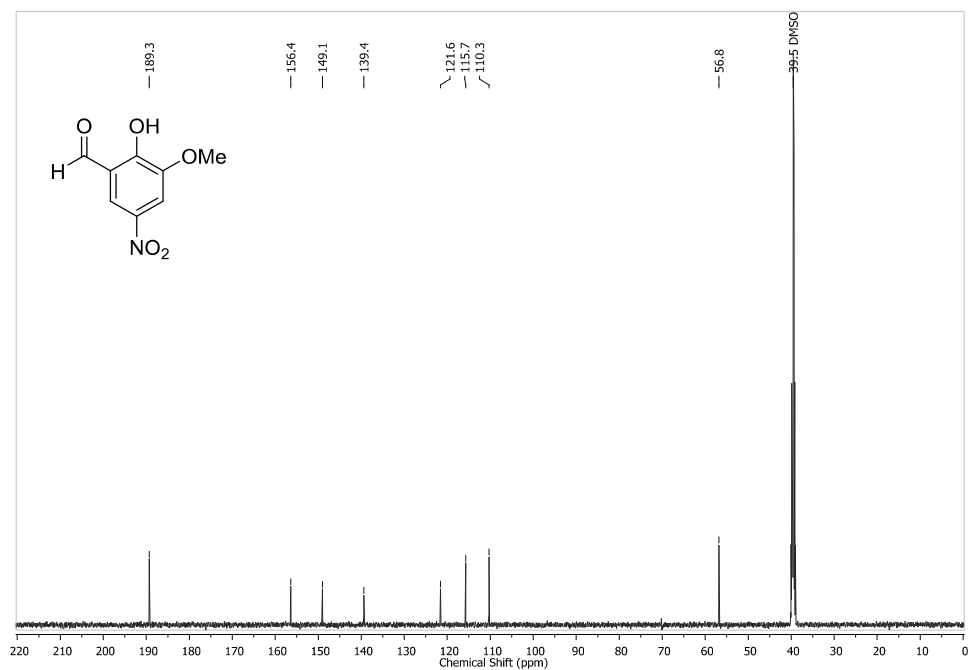
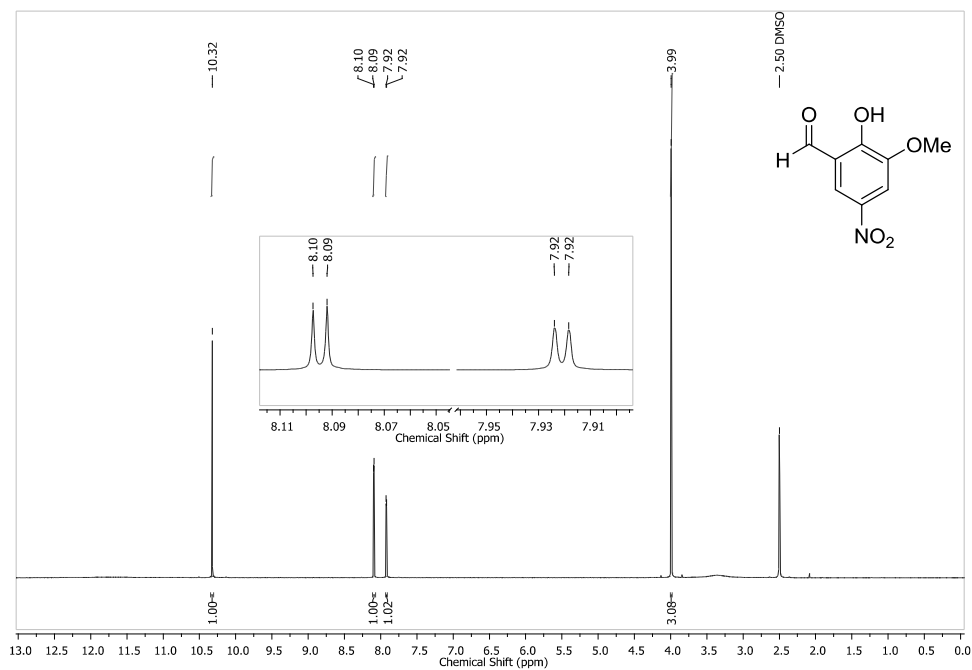


SI-55

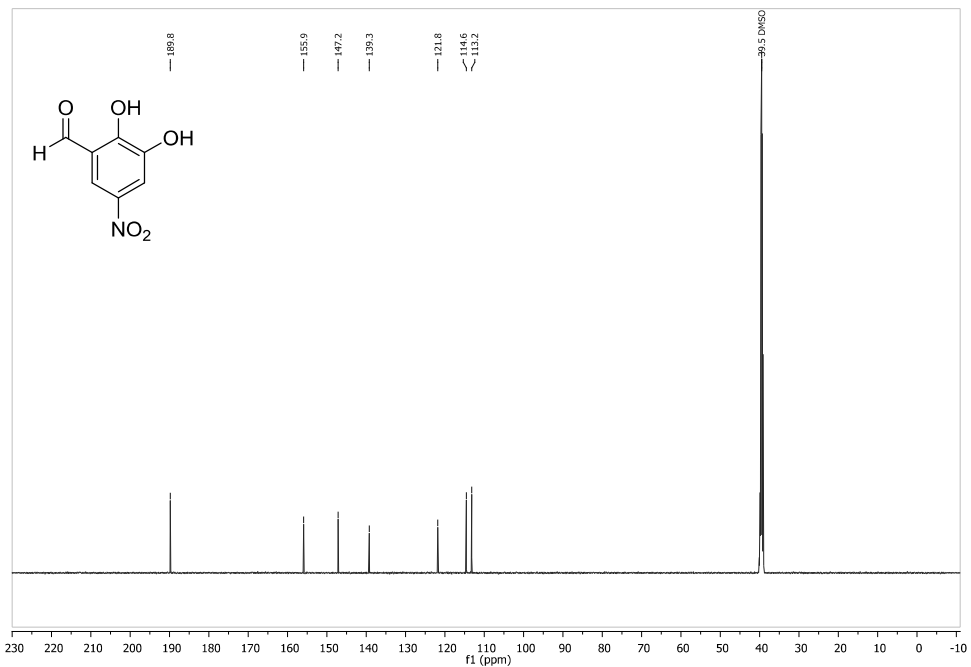
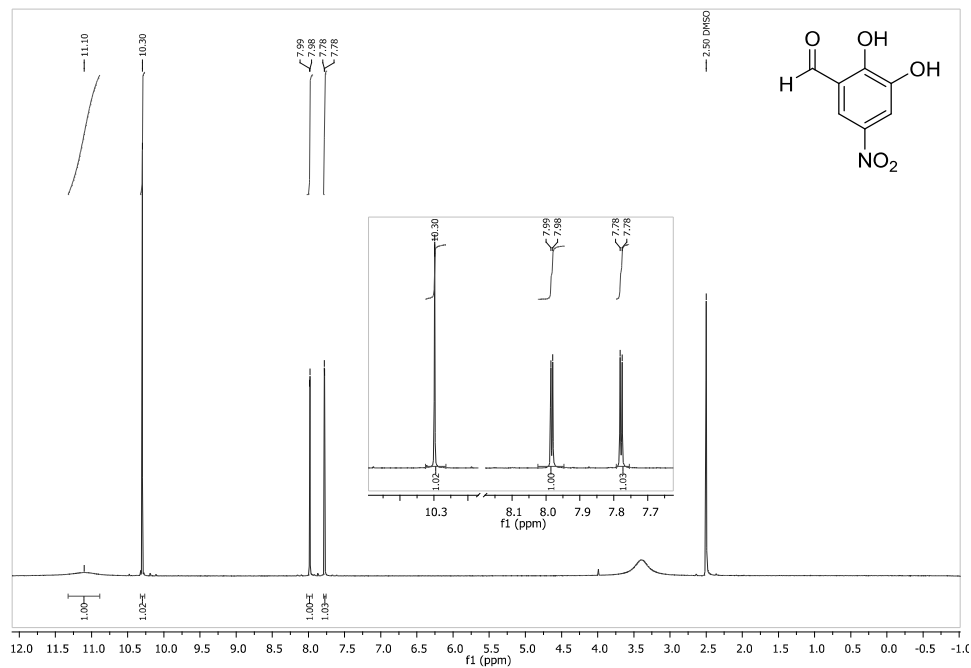
2-Hydroxy-3-iodo-5-nitrobenzaldehyde (2b)

SI-56

2-Hydroxy-3-methoxy-5-nitrobenzaldehyde (5c)

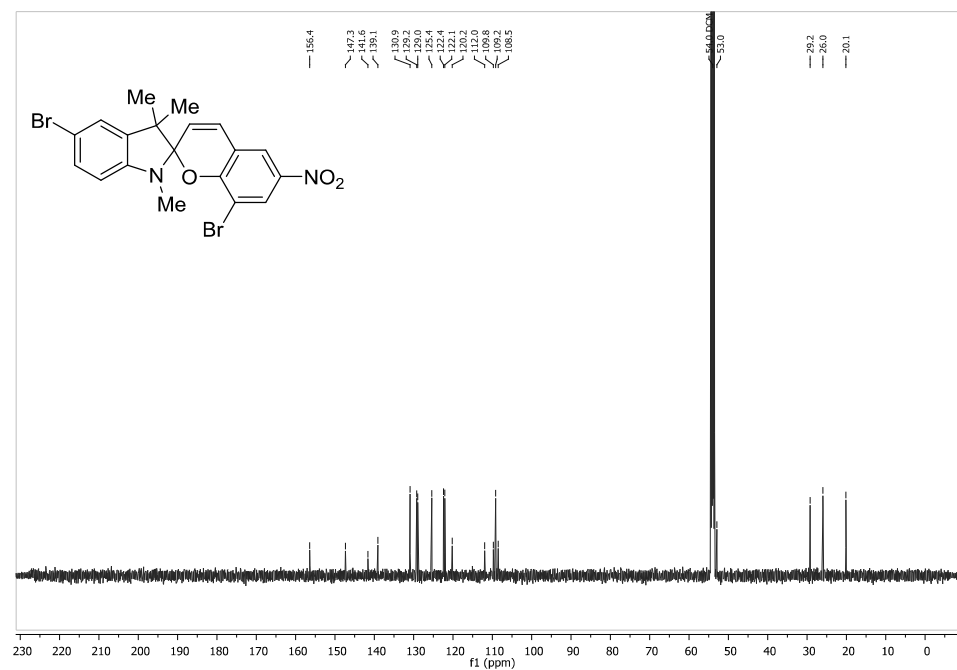
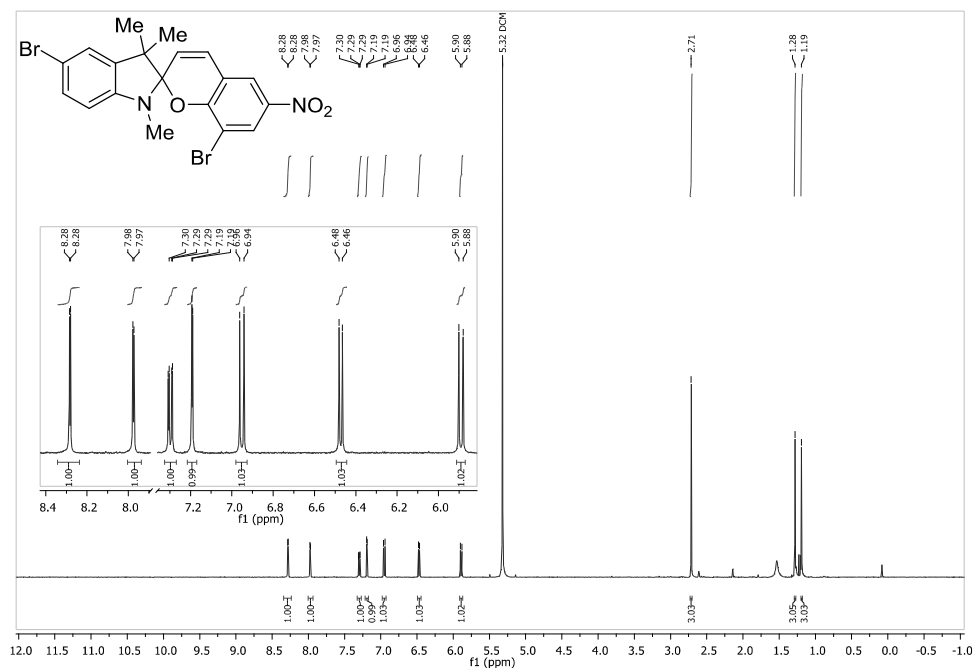


SI-57

2,3-Dihydroxy-5-nitrobenzaldehyde (2c)

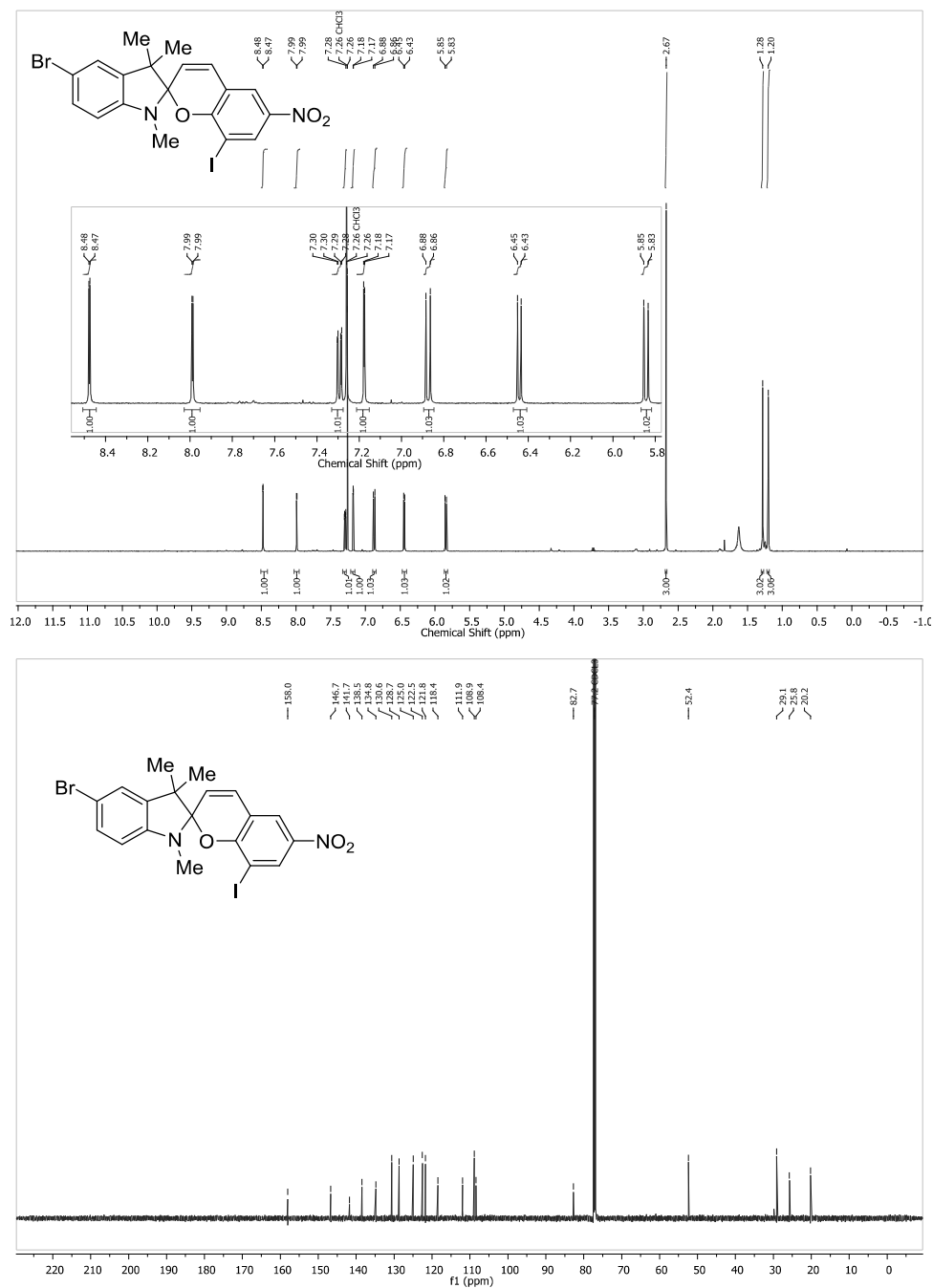
SI-58

5'8-Dibromo-1',3',3'-trimethyl-6-nitrospiro[chromene-2,2'-indoline] (9a)



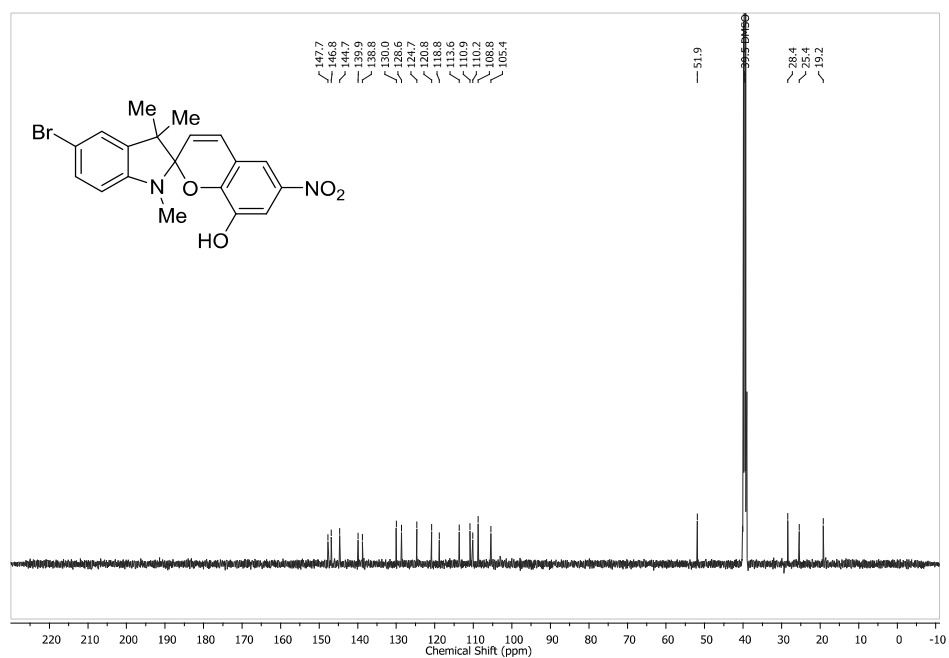
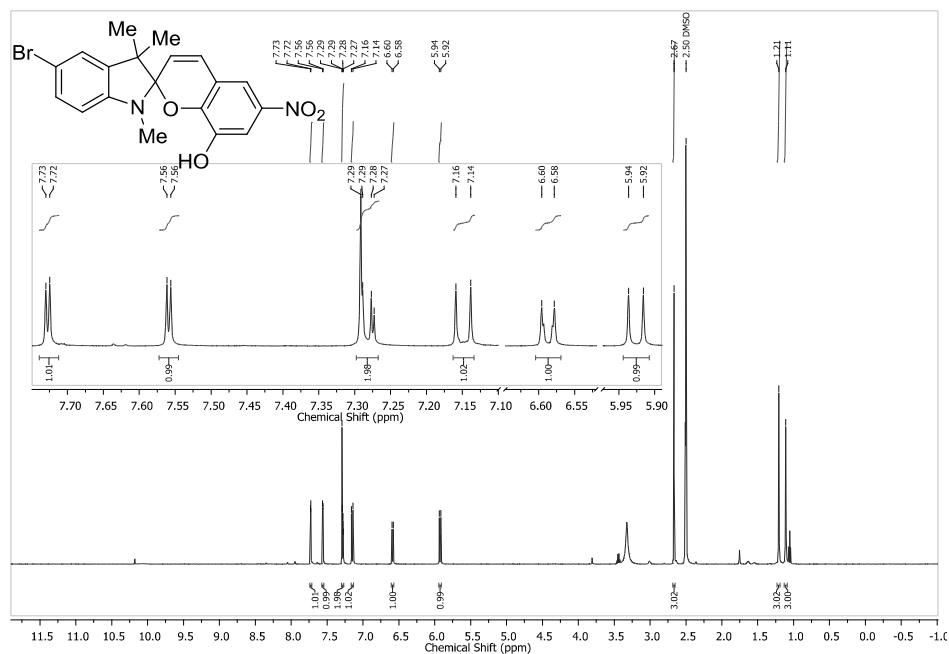
SI-59

5'-Bromo-8-iodo-1',3',3'-trimethyl-6-nitrospiro[chromene-2,2'-indoline] (9b)



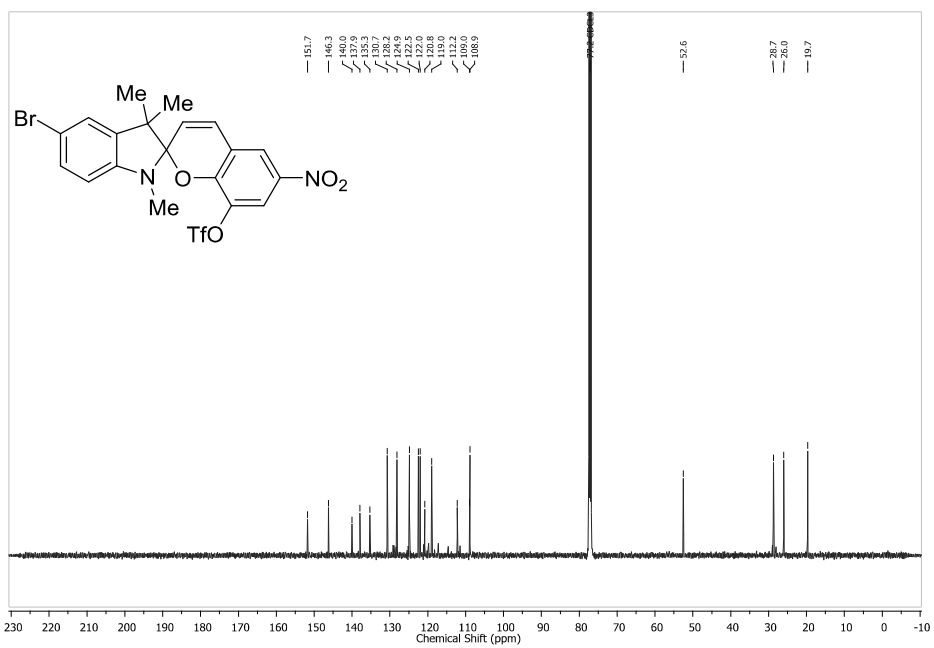
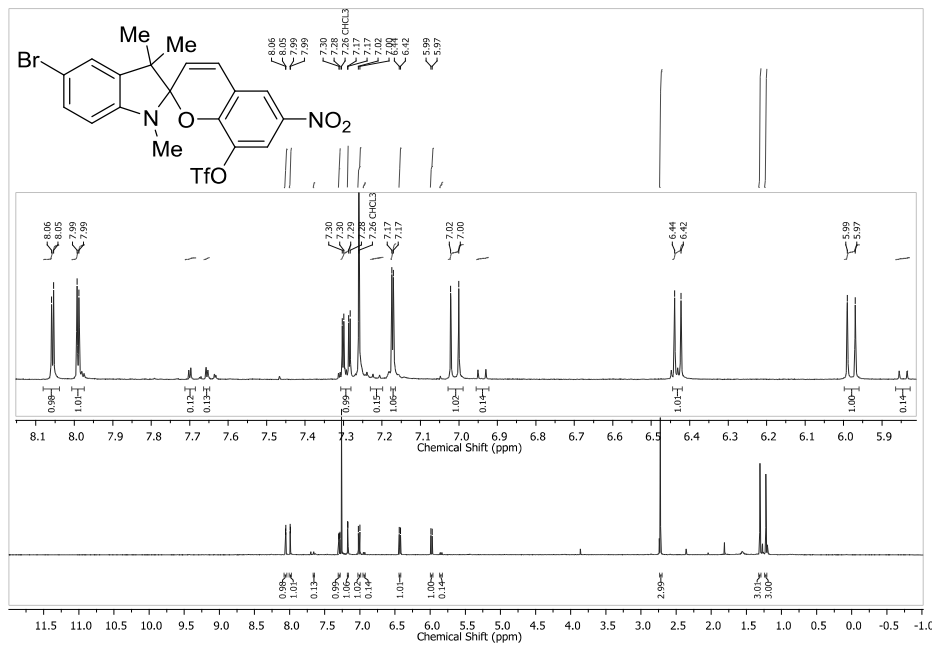
SI-60

5'-Bromo-8-hydroxy-1',3',3'-trimethyl-6-nitrospiro[chromene-2,2'-indoline] (9c)

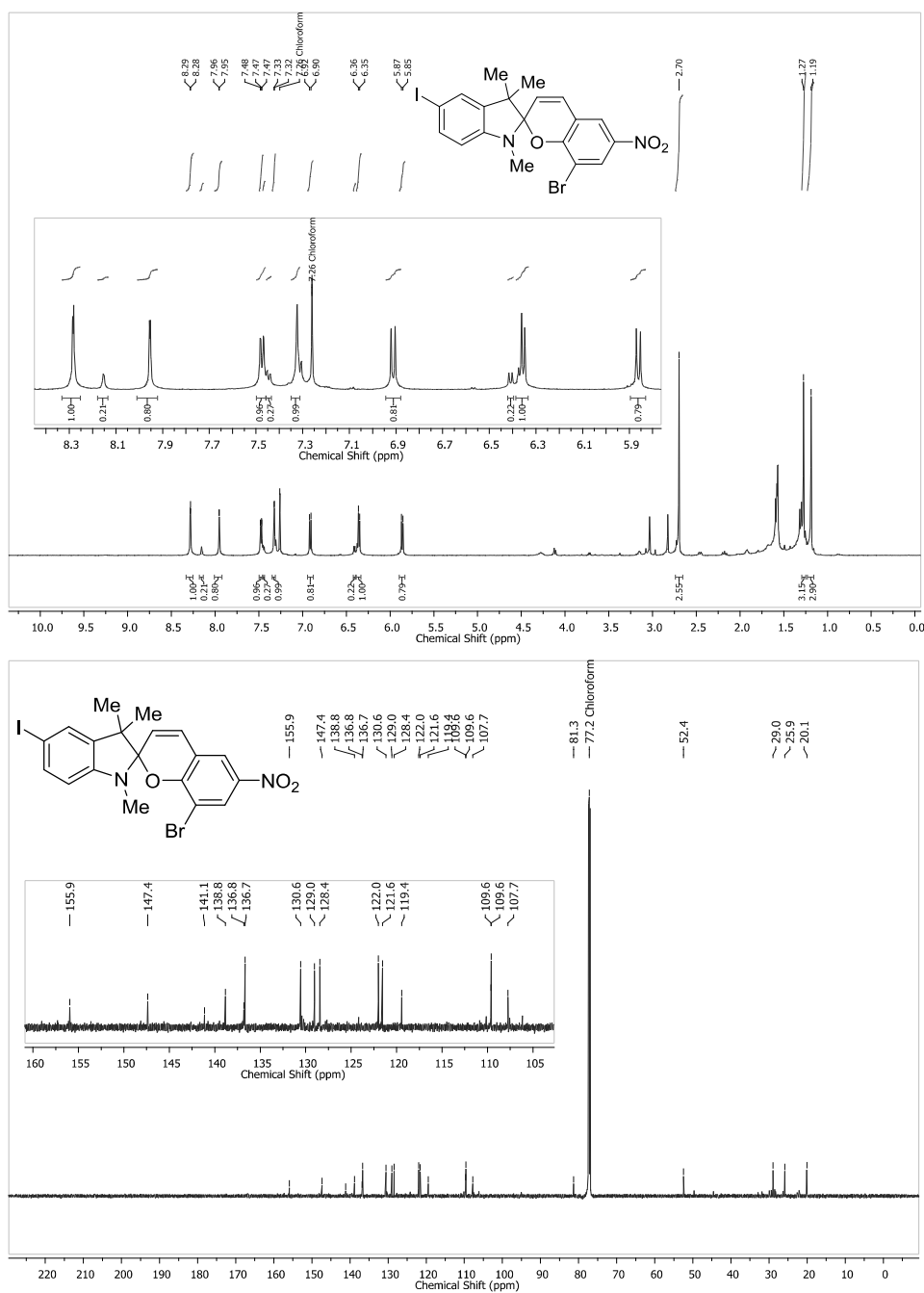


SI-61

5'-Bromo-8-trifluoromethylsulfonyl-1',3',3'-trimethyl-6-nitrospiro[chromene-2,2'-indoline] (9j)

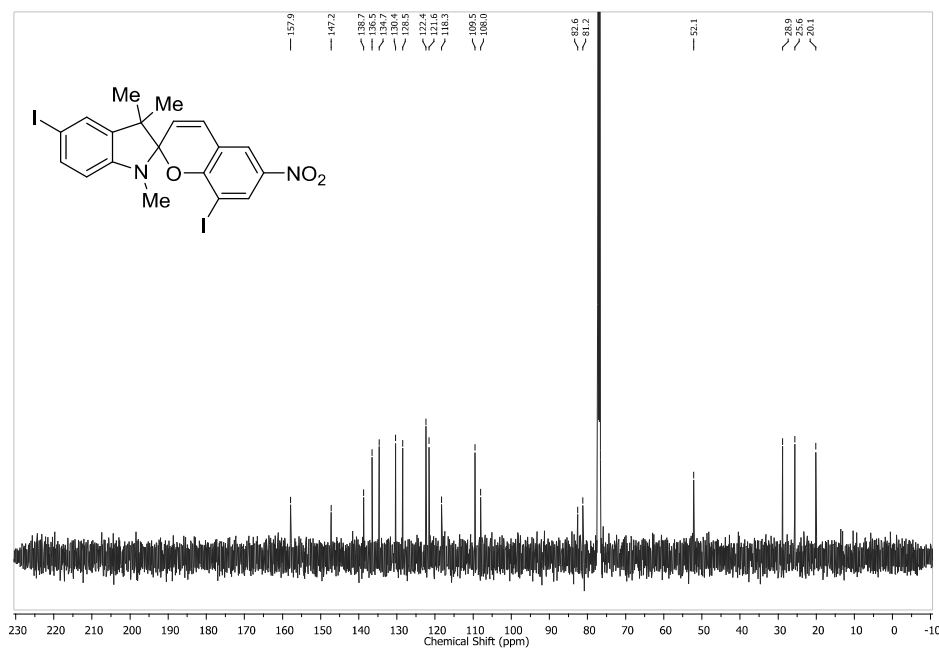
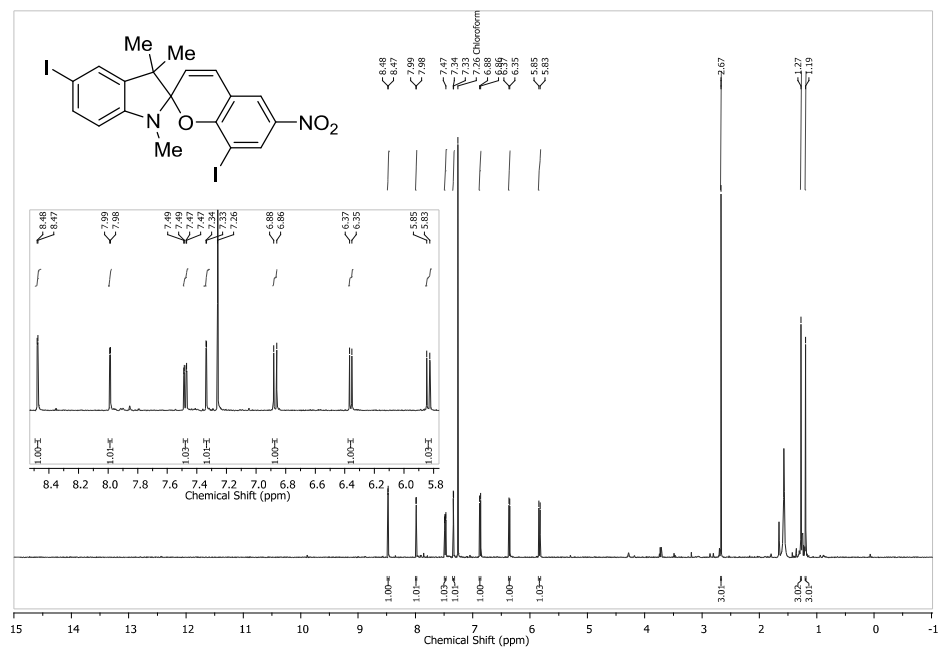


5-Iodo-8-bromo-1',3',3'-trimethyl-6-nitrospiro[chromene-2,2'-indoline] (9d)

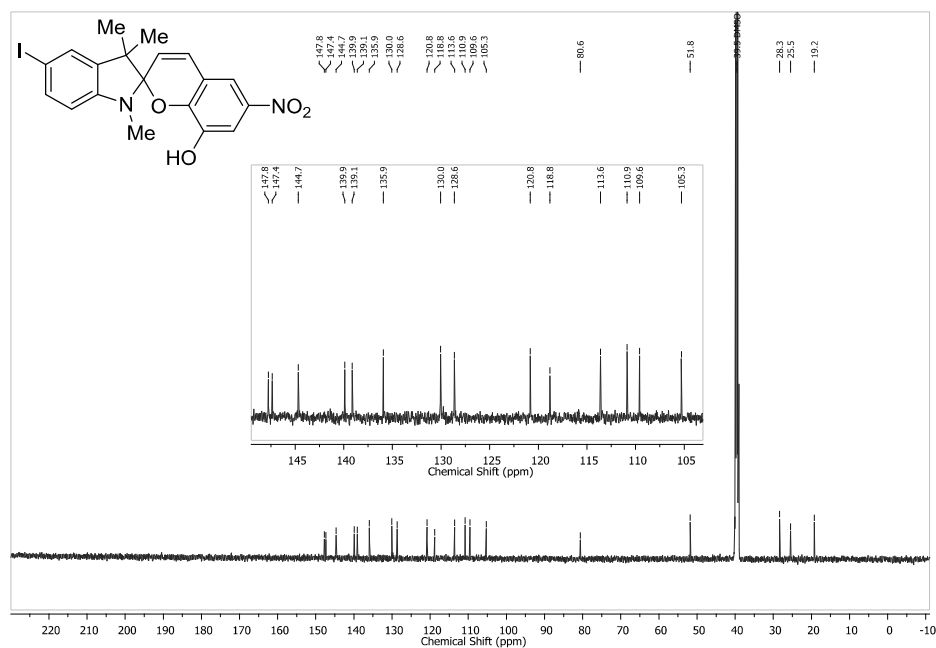
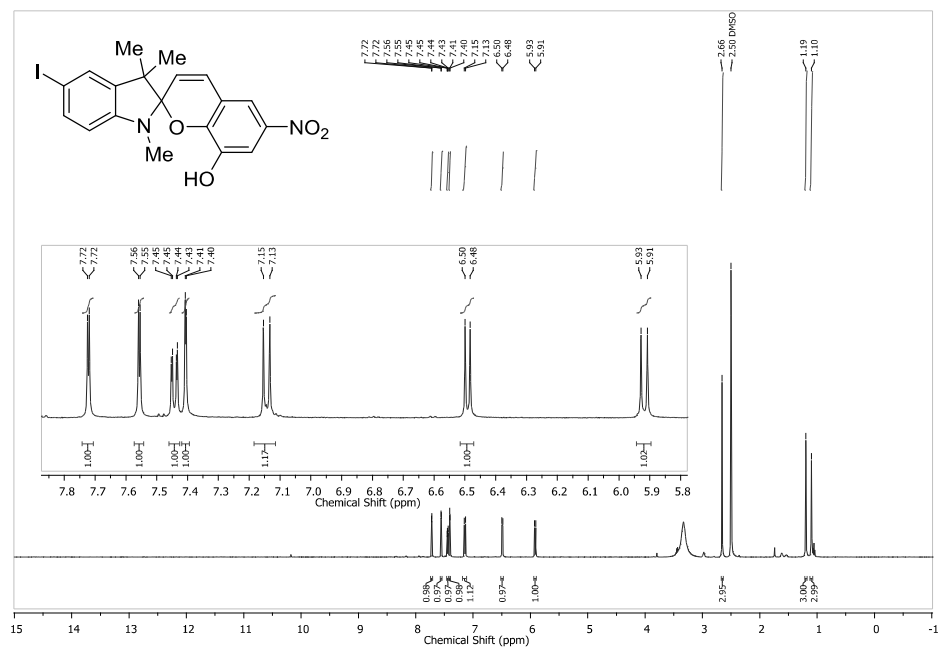


SI-63

5',8-Diiodo-1',3',3'-trimethyl-6-nitrospiro[chromene-2,2'-indoline] (9e)

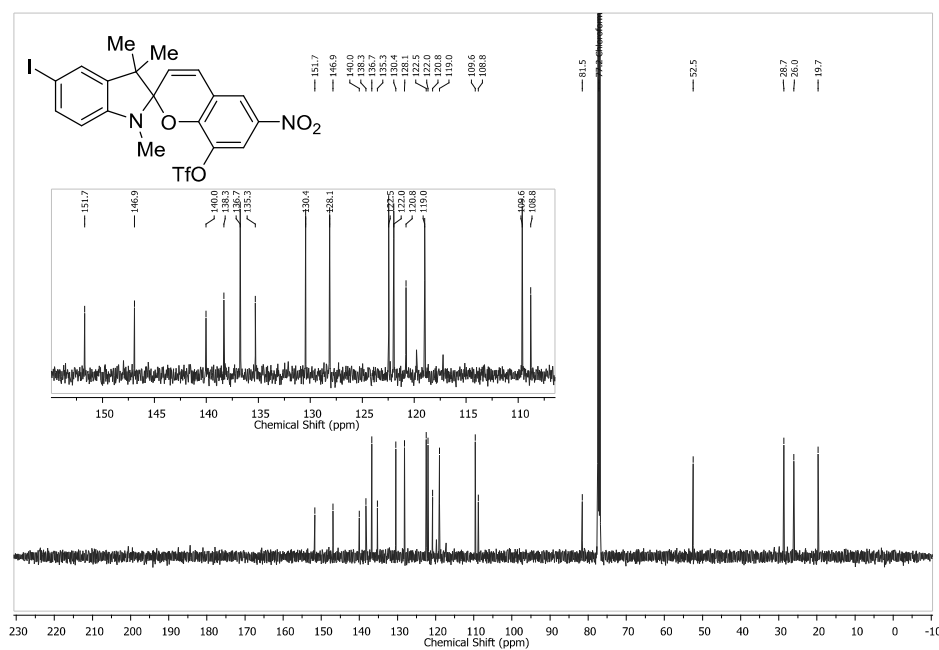
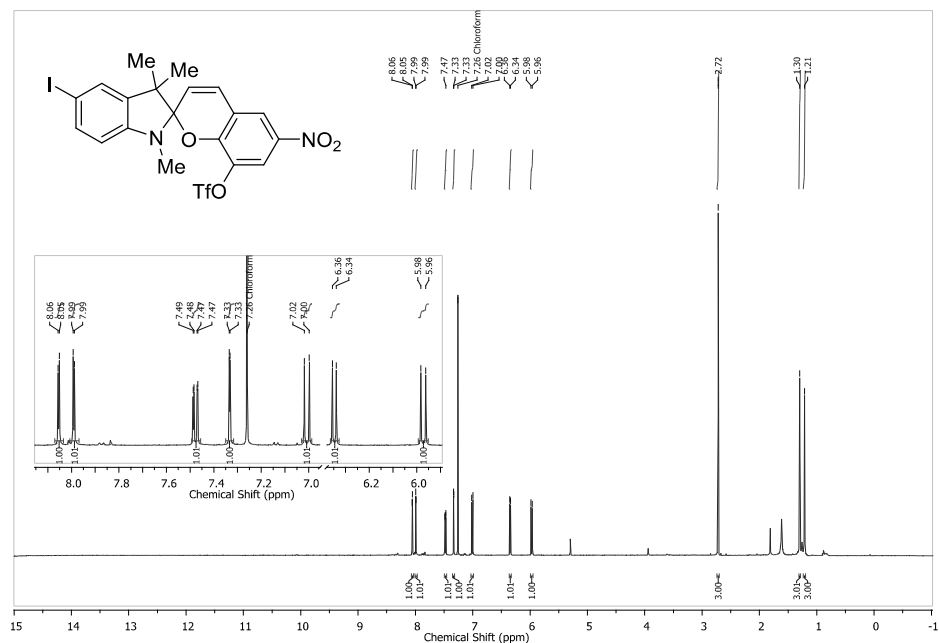


5'-Iodo-8-hydroxy-1',3',3'-trimethyl-6-nitrospiro[chromene-2,2'-indoline] (9f)



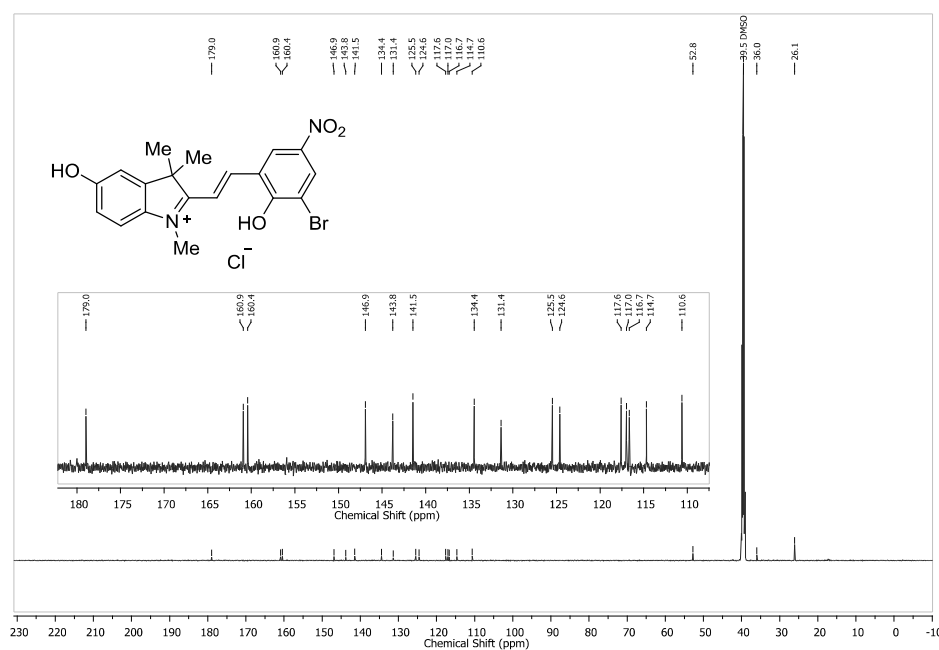
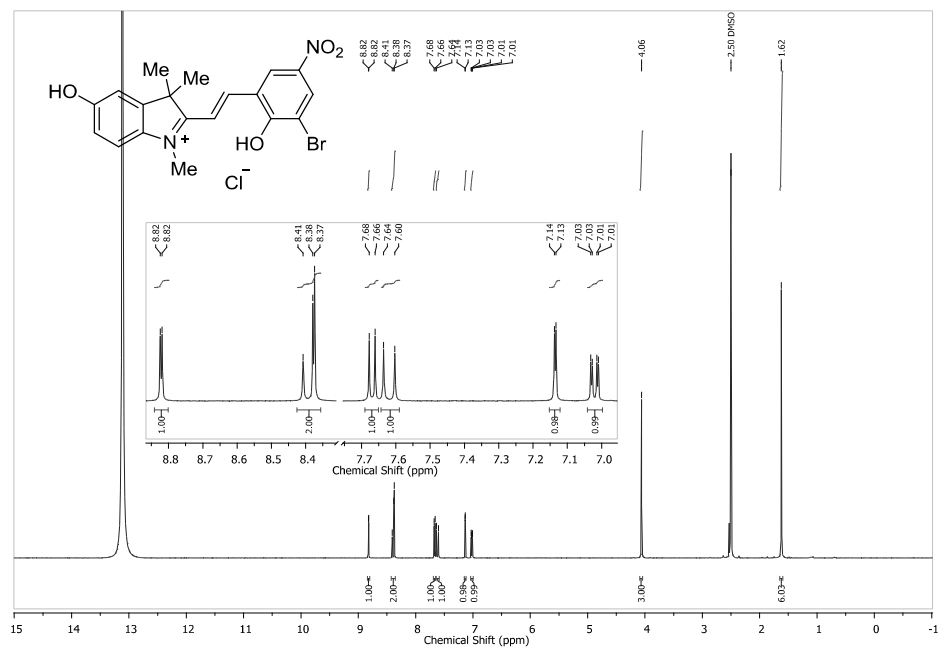
SI-65

5'-Iodo-8-trifluoromethylsulfonyl-1',3',3'-trimethyl-6-nitrospiro[chromene-2,2'-indoline] (9k)

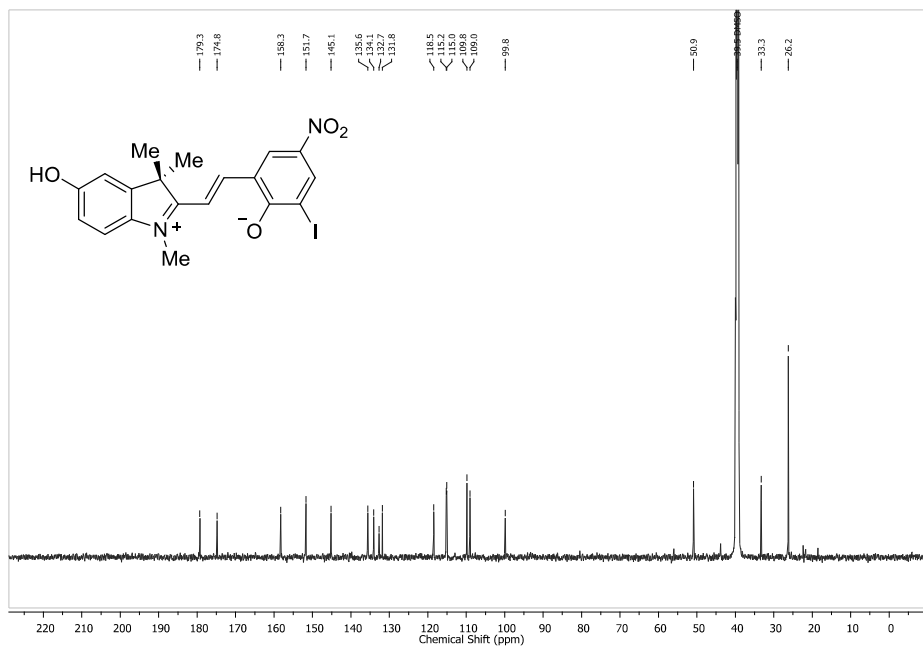
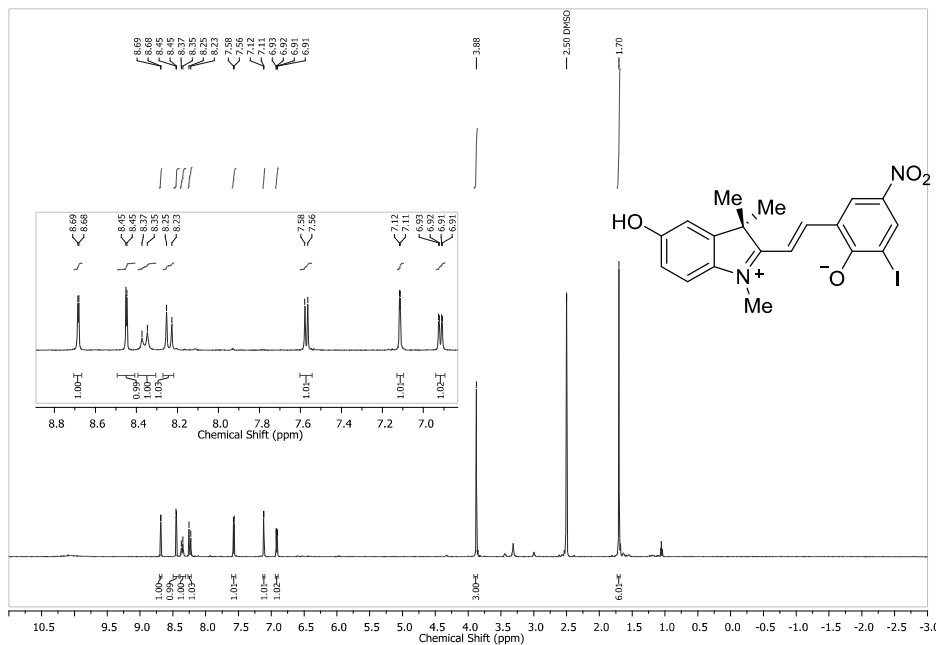


SI-66

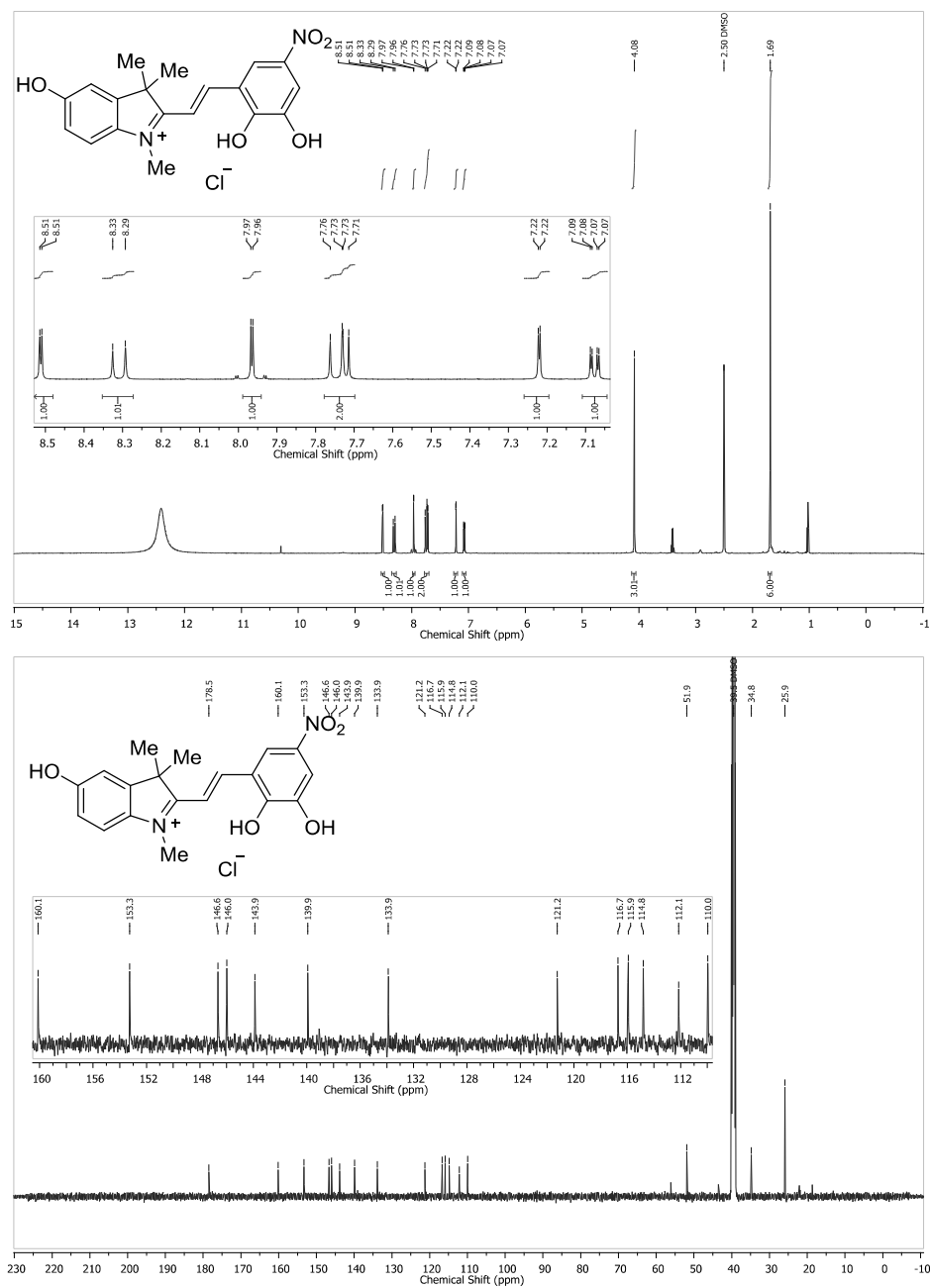
5'-Hydroxy-8-bromo-1',3',3'-trimethyl-6-nitrospiro[chromene-2,2'-indoline] (9g)



SI-67

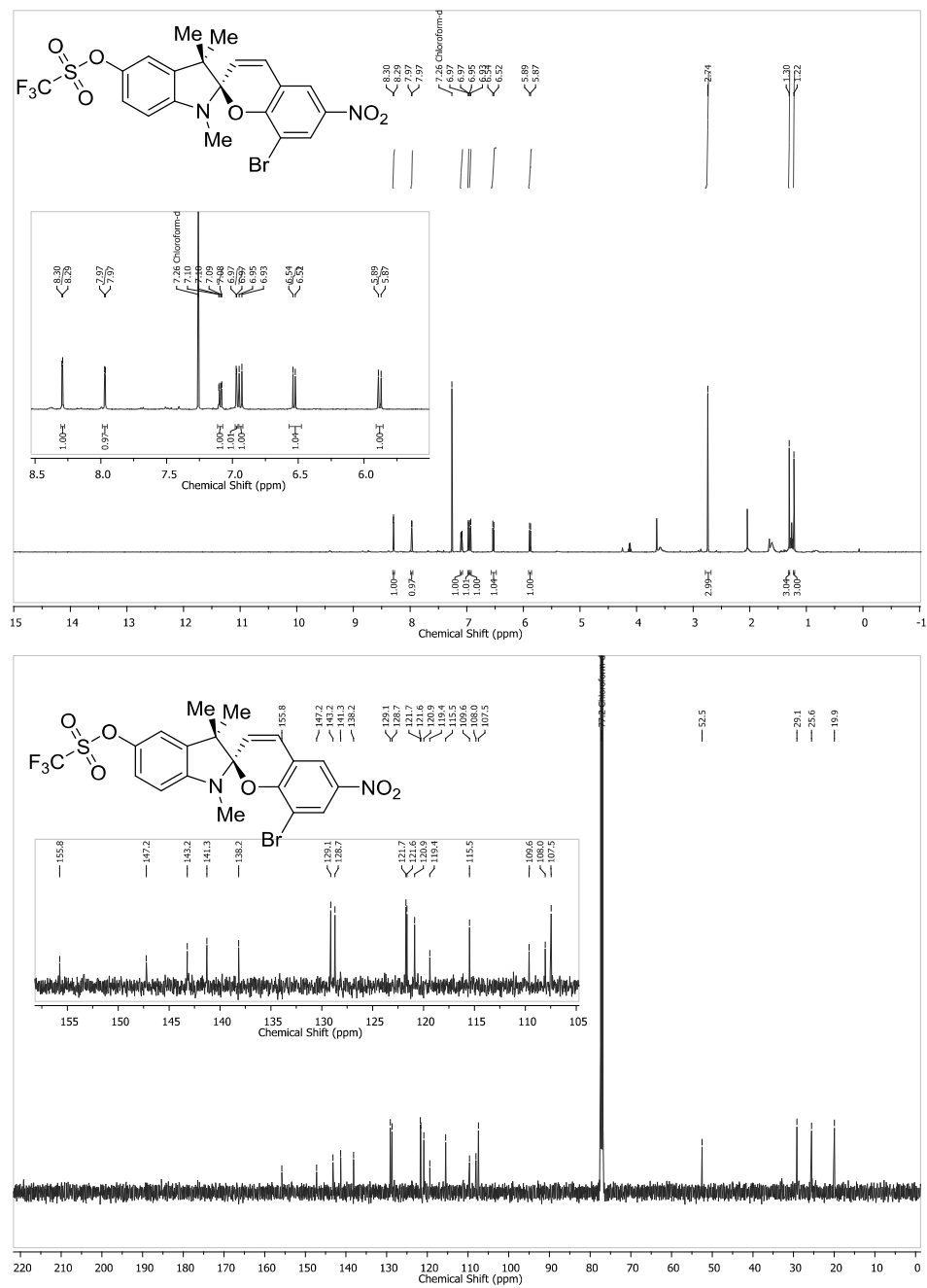
5'-Hydroxy-8-iodo-1',3',3'-trimethyl-6-nitrospiro[chromene-2,2'-indoline] (9h)

5',8-Dihydroxy-1',3',3'-trimethyl-6-nitrospiro[chromene-2,2'-indoline][11] (9i)



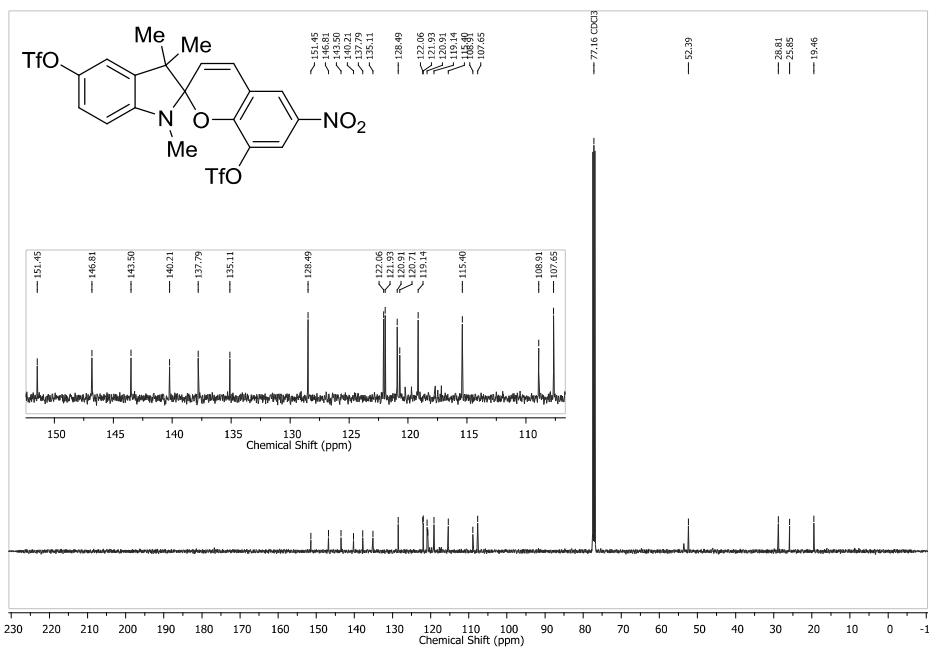
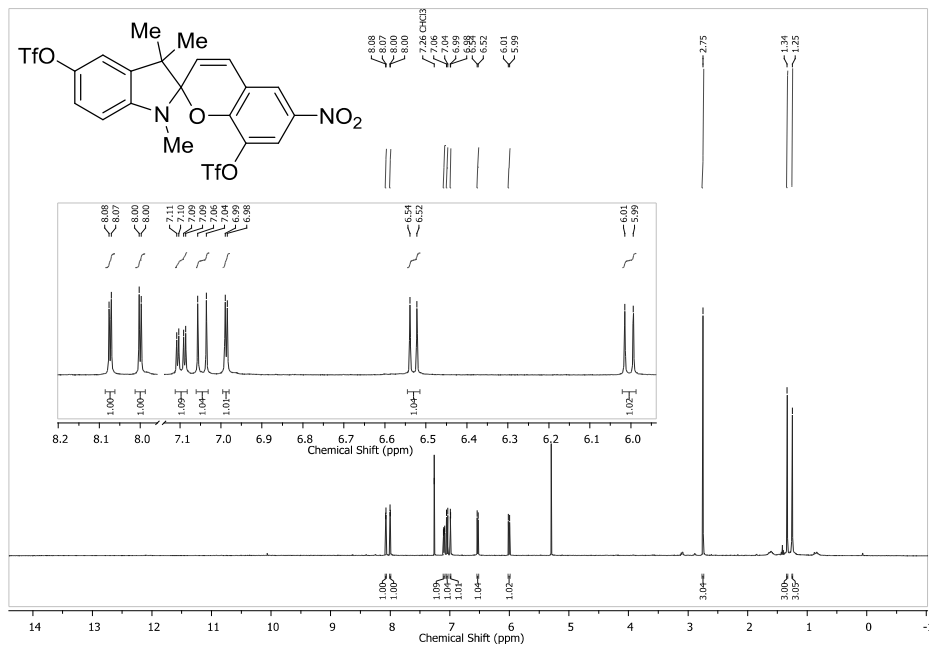
SI-69

5'-Trifluoromethylsulfonyl-8-bromo-1',3',3'-trimethyl-6-nitrospiro[chromene-2,2'-indoline] (9I)



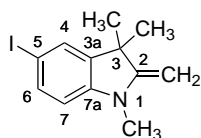
SI-70

Bis-5',8-(trifluoromethylsulfonyl)-1',3',3'-trimethyl-6-nitrospiro[chromene-2,2'-indoline] (9n)



3.2. Unpublished Syntheses

3.2.1. Synthesis of 5-Iodo-1,3,3-trimethyl-2-methylene-3*H*-indolene (13)



5-Iodo-1,2,3,3-tetramethyl-3*H*-indolium iodide (**14** 1.49 g, 3.50 mmol) was dissolved in toluene (35 mL) and a solution of sodium hydroxide (14.0 g, 350 mmol) in water (17.5 mL) was added. The mixture stirred at 50 °C for 3 h. After cooling to 25 °C, the organic phase was separated, dried over magnesium sulfate and filtered. After removing the solvent, the product **13** was obtained as brown oil (1.04 g, 3.46 mmol, 99%) and was pure without further purification.

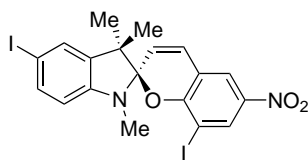
¹H NMR (600 MHz, CDCl₃): δ = 7.39 (dd, ³*J* = 8.2 Hz, ⁴*J* = 1.7 Hz, 1 H, H-6), 7.30 (d, ⁴*J* = 1.7 Hz, 1 H, H-4), 6.32 (³*J* = 8.2 Hz, 1 H, H-7), 3.87-3.84 (m, 2 H, C=CH₂), 3.00 (s, 3 H, N-CH₃), 1.31 (s, 6 H, C-(CH₃)₂) ppm.

¹³C{¹H} NMR (151 MHz, CDCl₃): δ = 161.9 (C-2), 146.1 (C-7a), 140.4 (C-3a), 136.1 (C-6), 130.6 (C-4), 107.1 (C-7), 79.3 (C-5), 74.1 (C=CH₂), 44.1 (C-3), 29.9 C-(CH₃)₂, 28.8 (N-CH₃) ppm.

IR (ATR): $\tilde{\nu}$ = 2962 (m), 2923 (w), 2864 (w), 1651 (s), 1596 (s), 1560 (w), 1486 (vs), 1453 (w), 1435 (w), 1414 (m), 1366 (s), 1334 (s), 1275 (s), 1263 (w), 1231 (s), 1133 (s), 1071 (m), 945 (w), 933 (w), 878 (w), 795 (s), 782 (s), 771 (s), 642 (w), 565 (m), 556 (m), 527 (m) cm⁻¹.

HRMS (EI-time-of-flight (TOF)): *m/z* = [M]⁺ (%) calculated (calcd) for [C₁₂H₁₄¹²⁷IN]⁺ 299.01709, found 299.01711 (73); 283.99 (100) [M-CH₃]⁺.

3.2.2. Synthesis of 5',8-Diiodo-1',3',3'-trimethyl-6-nitrospiro[chromene-2,2'-indoline] (9b)



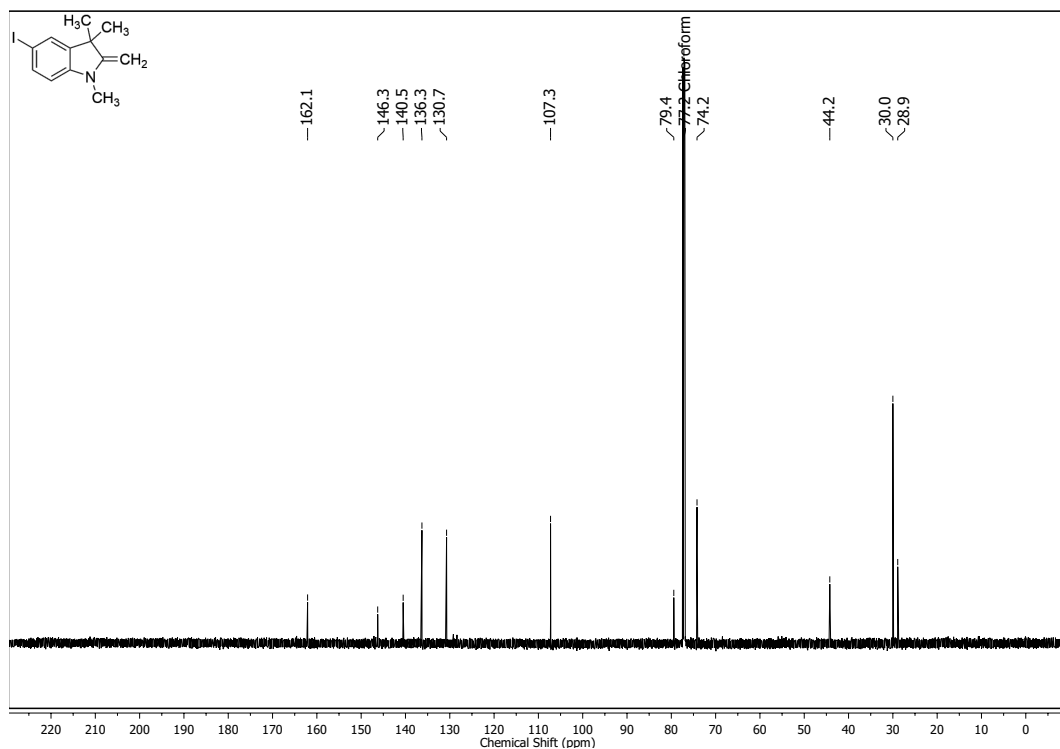
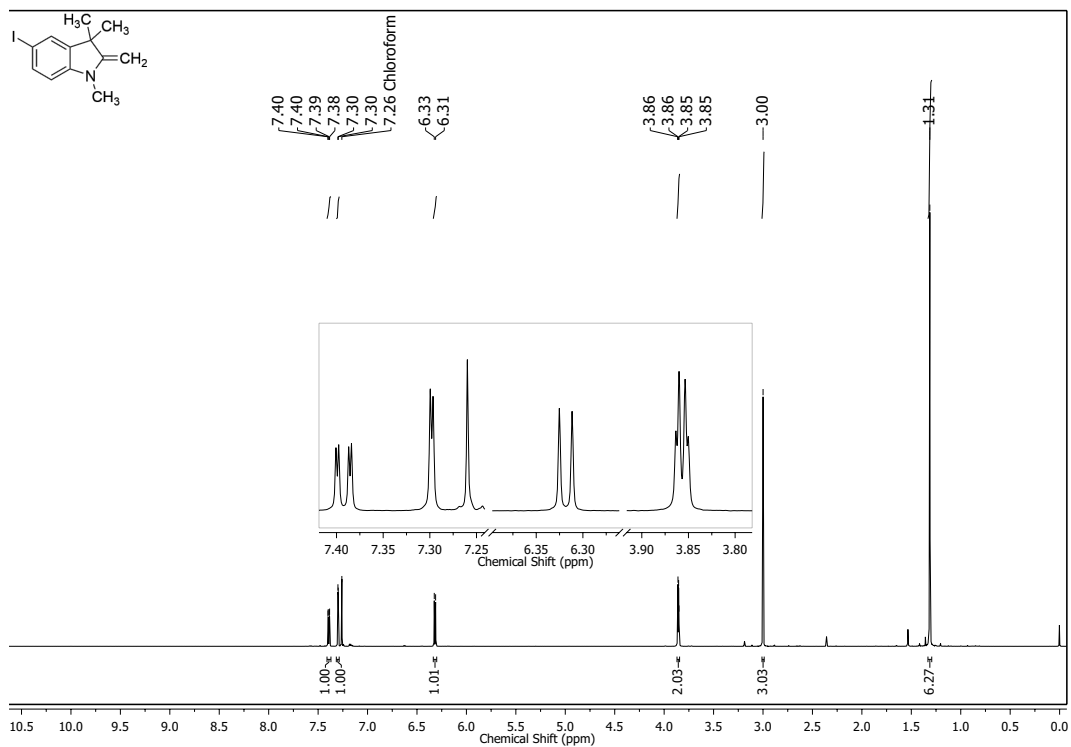
A solution of 3-iodo-2-hydroxy-5-nitrobenzaldehyde (**74** 756 mg, 2.58 mmol) and the indolene (**13** 772 mg, 2.58 mmol) in dry ethanol (25 mL) was heated to 78 °C for 3 h. After cooling to -32 °C, the product **9b** had precipitated as violet solid (1.28 g, 2.23 mmol, 86%, Lit.:^[174] 67%) and was pure without further purification.

The analytical data were in agreement with the procedure that was published in *Dyes and Pigments*.^[174]

3.3. NMR Spectra of Unpublished Substances

3.3.1. ^1H and $^{13}\text{C}\{^1\text{H}\}$ Spectra of

5-Iodo-1,3,3-trimethyl-2-methylene-3*H*-indolene (13) in CDCl_3



4. Stille Coupling Reactions of Spiropyrans **9a–c**

4.1. Standardized Synthetic Procedure

The dielectrophilic spiropyrans **9a–c** (100 μmol , see Figure V.1) were placed into a 20 mL Radley Carousel 12 Plus reaction vessel, that was transferred into a nitrogen filled glove box. Toluene (5 mL), the catalyst (5 μmol , 2.5% per reaction site) and a solution of trimethylphenylstannane (**16**, 1.00 mL, 0.1 mol L⁻¹, 100 μmol) in toluene, the additive lithium chloride (400 μmol) or copper(I) iodide (10.0 μmol) (where applicable) and a solution of hexamethylbenzene (100 μL , 0.1 mol L⁻¹, 10 μmol) in toluene as an internal standard were added consecutively, before the vial was closed (For exact weighed portions, see Table V.3). The reaction mixtures were transferred out of the glove box, placed in a preheated "Radley Carousel 12 Plus" and connected to a nitrogen-filled Schlenk line.

The progress of the reaction was monitored by collecting samples (150 μL) from the hot reaction mixture. These samples were passed through a column of silica gel (diameter: 5 mm, length: 20 mm; eluent: EtOAc) to remove the catalyst and most tin species from the mixtures. After the solvent was removed *in vacuo*, the residues were dissolved in CDCl₃ and analyzed by ¹H and, if necessary, ¹³C{¹H} and 2D NMR spectra.

Signals corresponding to the starting materials **9a–c** were found in all reaction samples. In the reactions that showed a conversion of **9a–c**, the signals of the formed product could be assigned to the compounds **18a–c**. In the reaction of the spiropyran **9b** with iodo substituents, the protons at the 5- and 7-positions (*ortho* to the nitro group) experience a high field shift from 8.48 ppm to 7.92 ppm and 7.99 ppm to 7.87 ppm, respectively. This indicates a new substituent at the 8-position. By ¹H and ¹H,¹H NOESY NMR spectroscopy, it was possible to identify a methyl group (instead of the expected phenyl group) as new substituent at the 8-position in all examples that showed the formation of a product (compare Figure II.1 in Part II, 87). The composition of the products **18a–c** was confirmed by HRMS measurements.

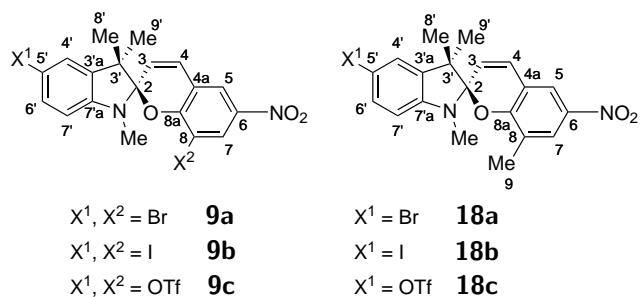


Figure V.1. Overview of the identified substances by ^1H NMR spectroscopy after Stille coupling. The reaction mixtures contained either **9** or a mixture of **9** and **18**.

Table V.3. Weighed portions of the solid substances used in the Stille coupling reactions.

Entry No.	Substance	Amount / μmol	Mass / mg
1	9a	100	48.0
2	9b	100	57.2
3	9c	100	61.9
4	$\text{Pd}(\text{PPh}_3)_4$	5.00	5.78
5	$\text{Pd}(\text{P}t\text{-Bu}_3)_2$	5.00	2.55
6	Pd_2dba_3	3.00	2.75
7	$\text{Pd}(\text{dppf})\text{Cl}_2$	5.00	3.65
8	SPhos	18.0	7.39
9	LiCl	400	17.0
10	CuI	10.0	1.9

4.1.1. Reaction of 5',8-Dibromo-1',3',3'-trimethyl-6-nitrospiro--[chromene-2,2'-indoline] (**9a**)

Only one reaction using **9a** with $\text{Pd}(\text{PPh}_3)_4$ as catalyst and without additives was performed. After a reaction time of 5 d and the short workup, 12% of the starting material were converged to the product **18a**.

Signals assigned to the starting material 9a The recorded ^1H NMR data of **9a** are in agreement with the data published for compound **9a** in *Dyes and Pigments*.^[174]

^1H NMR (500 MHz, CDCl_3): $\delta = 8.29$ (d, $^4J = 2.6$ Hz, 1H, H-5), 7.96 (d, $^4J = 2.6$ Hz, 1H, H-7), 7.29 (dd, $^3J = 8.2$ Hz, $^4J = 2.0$ Hz, 1H, H-6'), 7.17 (d, $^4J = 2.0$ Hz, 1H, H-4'), 6.92 (d, $^3J = 10.3$ Hz, 1H, H-4), 6.44 (d, $^3J = 8.2$ Hz, 1H, H-7'), 5.87 (d, $^3J = 10.3$ Hz, 1H, H-3), 2.70 (s, 3H, N- CH_3), 1.28 (s, 3H, H-8'), 1.20 (s, 3H, H-9') ppm.

Signals assigned to the product 18a **^1H NMR** (500 MHz, CDCl_3): $\delta =$ ppm. 7.92 (d, $^4J = 2.8$ Hz, 1H, H-5), 7.87 (d, $^4J = 2.8$ Hz, 1H, H-7), 7.27 – 7.25 (m, 1H, H-6'),¹ 7.15

¹This signal was overlaid by the residual solvent CHCl_3 .

(d, $^4J = 2.0$ Hz, 1H, H-4'), 6.92 (d, $^3J = 10.3$ Hz, 1H, H-4),^{II} 6.41 (d, $^3J = 8.2$ Hz, 1H, H-7'), 5.81 (d, $^3J = 10.3$ Hz, 1H, H-3), 2.67 (s, 3H, N-CH₃), 2.03 (s, 3H, H-9), 1.25 (s, 3H, H-8'), 1.19 (s, 3H, H-9') ppm.

4.1.2. Reaction of 5',8-Diiodo-1',3',3'-trimethyl-6-nitrospiro-[chromene-2,2'-indoline] (**9b**)

The Stille reactions of **9b** are shown in Table V.4.

Table V.4. Reaction conditions of the Stille coupling of **9b**.

Entry No.	Catalyst System	Additive	Reaction Time	Conversion
1	Pd(PPh ₃) ₄	–	5 d	29%
2	Pd(PPh ₃) ₄	LiCl	15 h	17%
3	Pd(PPh ₃) ₄	CuI	48 h	15%
4	Pd(Pt-Bu ₃) ₂	LiCl	5 d	36%
5	Pd ₂ dba ₃ /SPhos	LiCl	5 d	86%
6	Pd(dppf)Cl ₂	LiCl	5 d	32%

Signals assigned to the starting material **9b**

The recorded ¹H NMR data of **9b** are in agreement with the data published for compound **9e** in *Dyes and Pigments*.^[174]

¹H NMR (500 MHz, CDCl₃): $\delta = 8.48$ (d, $^4J = 2.6$ Hz, 1H, H-5), 7.99 (d, $^4J = 2.6$ Hz, 1H, H-7), 7.48 (dd, $^3J = 8.2$ Hz, $^4J = 1.8$ Hz, 1H, H-6'), 7.34 (d, $^4J = 1.8$ Hz, 1H, H-4'), 6.87 (d, $^3J = 10.3$ Hz, 1H, H-4), 6.36 (d, $^3J = 8.2$ Hz, 1H, H-7'), 5.84 (d, $^3J = 10.3$ Hz, 1H, H-3), 2.67 (s, 3H, N-CH₃), 1.28 (s, 3H, H-8'), 1.19 (s, 3H, H-9') ppm.

Signals assigned to the product **18b**

¹H NMR (500 MHz, CDCl₃): $\delta = 7.92$ (d, $^4J = 2.8$ Hz, 1H, H-5), 7.87 (d, $^4J = 2.8$ Hz, 1H, H-7), 7.46 (dd, $^3J = 8.1$ Hz, $^4J = 1.8$ Hz, 1H, H-6'), 7.31 (d, $^4J = 1.8$ Hz, 1H, H-4'), 6.91 (d, $^3J = 10.3$ Hz, 1H, H-4), 6.33 (d, $^3J = 8.1$ Hz, 1H, H-7'), 5.81 (d, $^3J = 10.3$ Hz, 1H, H-3), 2.67 (s, 3H, N-CH₃), 2.04 (s, 3H, H-9), 1.24 (s, 3H, H-8'), 1.18 (s, 3H, H-9') ppm.

Mass Spectrometry of the Crude Product

HRMS (EI-TOF): Starting material **9b**: $m/z = [M]^+$ (%) calcd for [C₁₉H₁₆¹²⁷I₂N₂O₃]⁺ 573.92503, found 573.92503 (24); Product **18b** calcd for [C₂₀H₁₉¹²⁷IN₂O₃]⁺ 462.04403, found 462.04430 (53); 284.99 (100) [C₁₁H₁₂¹²⁷IN]⁺; .

^{II}This signal had not shifted and fully superimposed with the signal corresponding to H-4 of the starting material **9a**.

4.1.3. Reaction of Bis-5',8-(trifluoromethylsulfonyl)-1',3',3'-trimethyl-6-nitrospiro-[chromene-2,2'-indoline] (9c)

The Stille reactions of **9c** are shown in Table V.5.

Table V.5. Reaction conditions of the Stille coupling of **9c**.

Entry No.	Catalyst System	Additive	Reaction Time	Conversion
1	Pd(PPh ₃) ₄	–	24 h	0%
2	Pd(PPh ₃) ₄	LiCl	15 h	18%
3	Pd(PPh ₃) ₄	CuI	48 h	0%
4	Pd(Pt-Bu ₃) ₂	LiCl	5 d	0%
5	Pd ₂ dba ₃ /SPhos	LiCl	5 d	11%
6	Pd(dppf)Cl ₂	LiCl	5 d	7%

Signals assigned to the starting material **9c**

The recorded ¹H NMR data of **9c** are in agreement with the data published for compound **9n** in *Dyes and Pigments*.^[174]

¹H NMR (500 MHz, CDCl₃): δ = 8.07 (d, ⁴J = 2.5 Hz, 1H, H-5), 8.00 (d, ⁴J = 2.5 Hz, 1H, H-7), 7.10 (dd, ³J = 8.5 Hz, ⁴J = 2.5 Hz, 1H, H-6'), 7.05 (d, ³J = 10.3 Hz, 1H, H-4), 6.99 (d, ⁴J = 2.5 Hz, 1H, H-4'), 6.53 (d, ³J = 8.5 Hz, 1H, H-7'), 6.00 (d, ³J = 10.3 Hz, 1H, H-3), 2.75 (s, 3H, N-CH₃), 1.34 (s, 3H, H-8'), 1.25 (s, 3H, H-9') ppm.

Signals assigned to the product **18c**

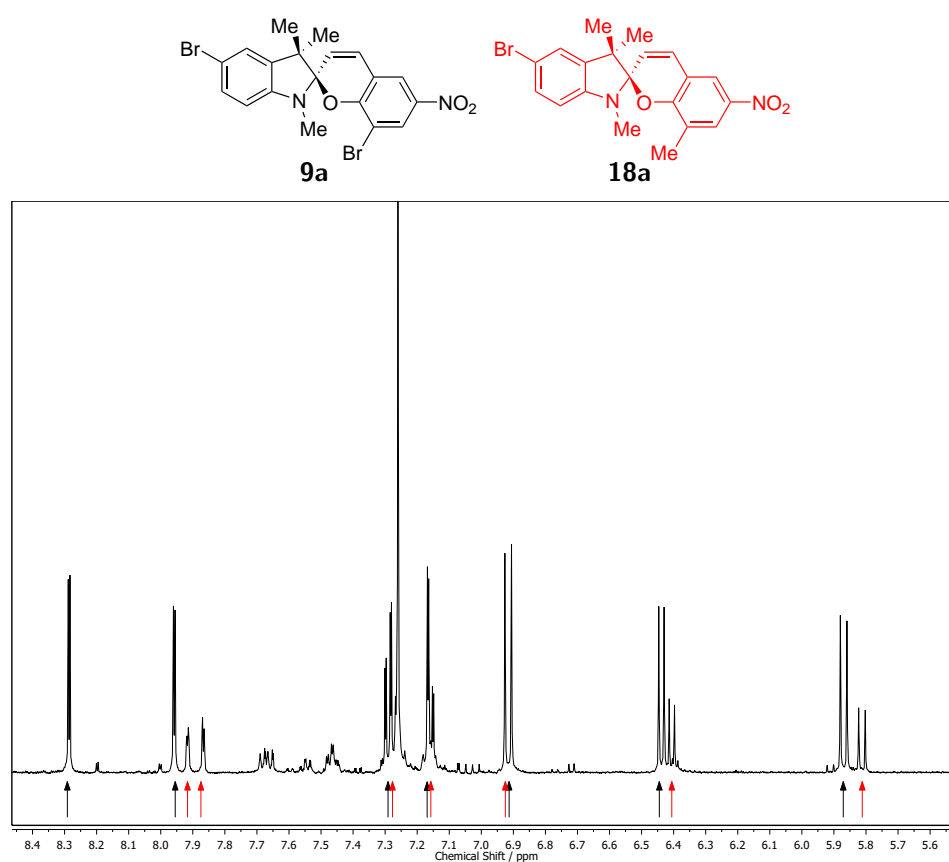
¹H NMR (500 MHz, CDCl₃): δ = 7.93 (d), 7.88 (d), 7.09 – 7.06 (m, 1H, H-6'),^{III} 6.95 (d, ⁴J = 2.6 Hz, 1H, H-4'), 6.94 (d, ³J = 10.3 Hz, 1H, H-4), 6.49 (d, ³J = 8.5 Hz, 1H, H-7'), 5.82 (d, ³J = 10.3 Hz, 1H, H-3), 2.71 (s, 3H, N-CH₃), 2.04 (s, 3H, H-9), 1.27 (s, 3H, H-8'), 1.21 (s, 3H, H-9') ppm.

^{III}This signal was overlaid by the signal corresponding to H-6' of **9c**. One coupling constant could be assigned to be ⁴J = 2.6 Hz, the coupling constant corresponding to the ³J coupling one could not be assigned.

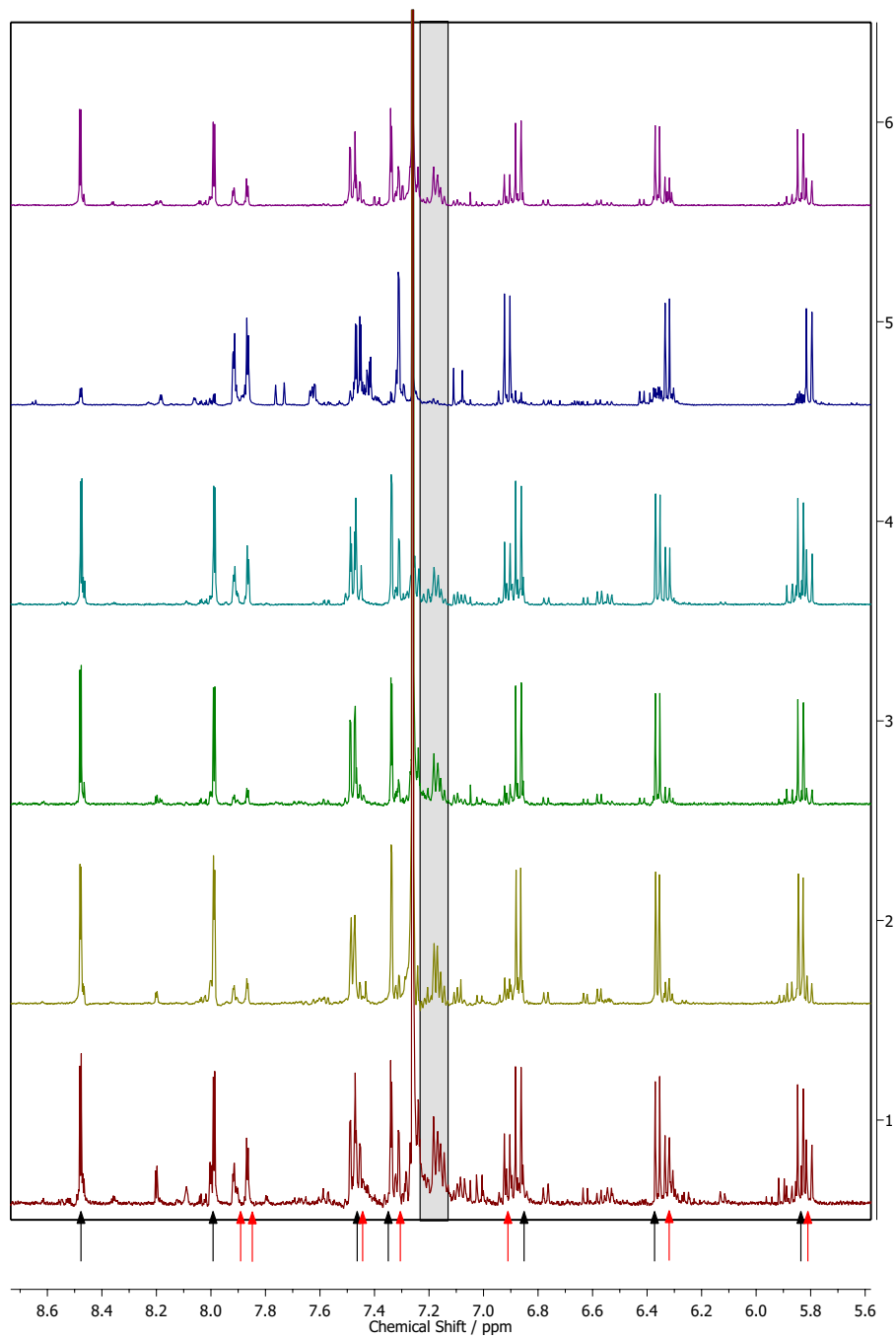
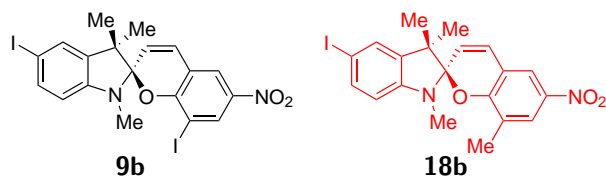
4.2. Aromatic Regions of the ^1H NMR Spectra of the Stille Coupling Reactions of **9a–c** in CDCl_3

For all product mixtures, the signals could be assigned to the starting materials **9a–c** and the products **18a–c** by 2D experiments. In all spectra, black arrows indicate signals corresponding to the starting materials **9a–c** and red arrows indicate signals corresponding to the products **18a–c**. Signals indicating remaining toluene are highlighted by a grey box. The row numbers in the stacked spectra of the reaction of **9b** and **9c** correspond to the entry numbers in Table V.4 or Table V.5, respectively.

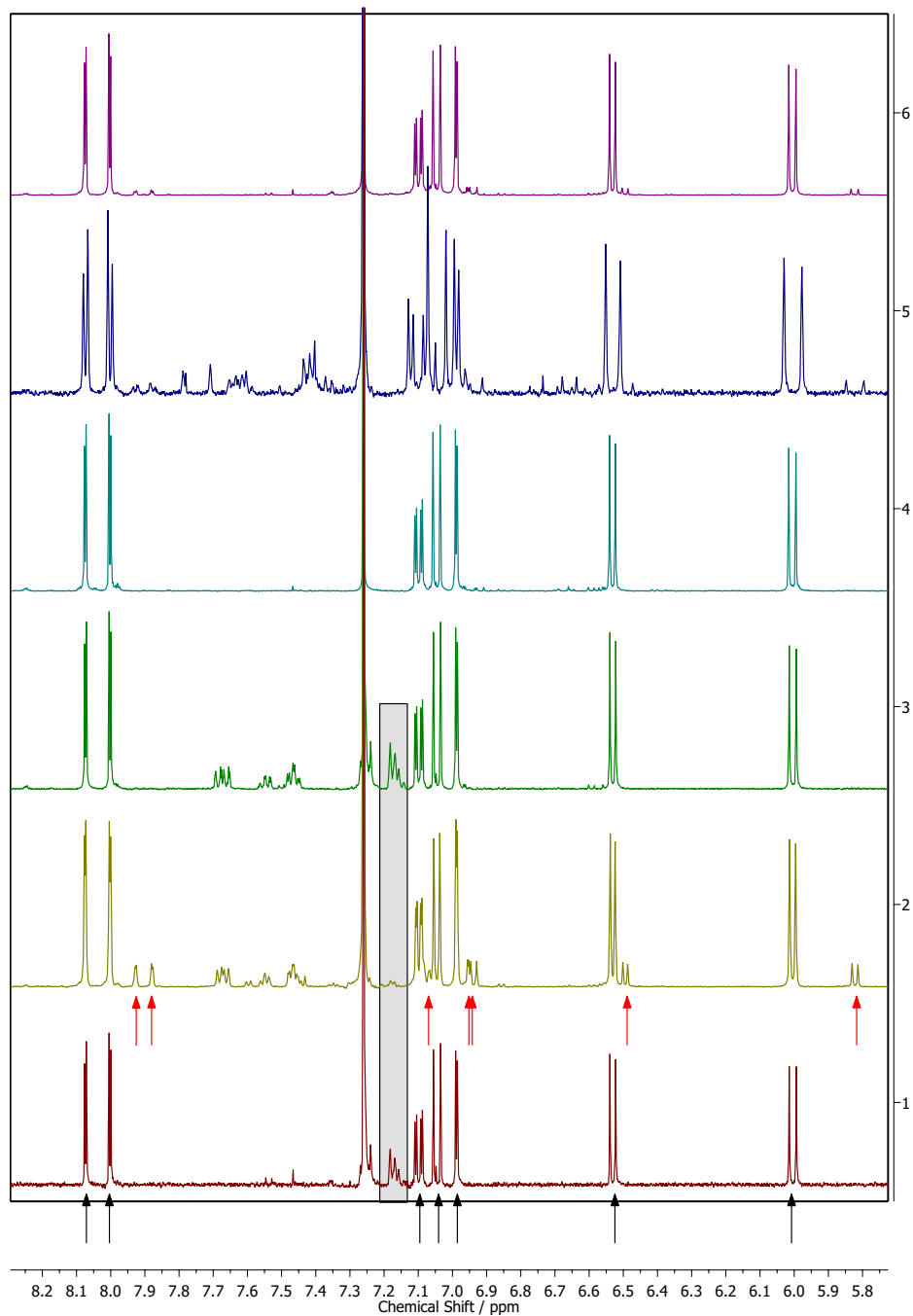
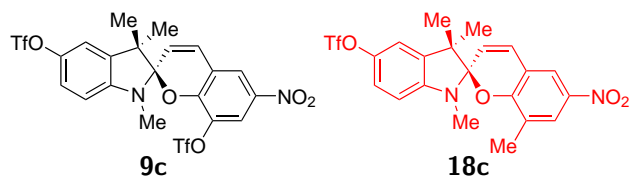
4.2.1. Reaction of **9a**



4.2.2. Reactions of 9b



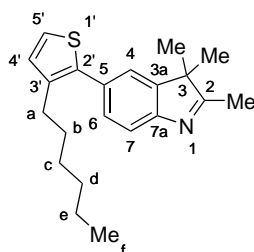
4.2.3. Reactions of **9c**



5. Spiropyran Dyes for the Incorporation into Poly(thiophenes)

5.1. Syntheses

5.1.1. Synthesis of 5-(3-Hexylthien-2-yl)-2,3,3-trimethyl-3*H*-indole (27)



A mixture of 5-iodo-2,3,3-trimethyl-3*H*-indole (**23** 214 mg, 750 μmol), 3-hexylthiophene-2-boronic acid pinacol ester (**20** 219 μL , 221 mg, 750 μmol) and tetrakis(triphenylphosphine)-palladium(0) (26.0 mg, 22.5 μmol) was dissolved in DMF (3.9 mL) and the MW vial was closed inside a glovebox. Under Schlenk conditions, a degassed aqueous solution of tripotassium phosphate (1.13 mL, 1.0 mol L⁻¹, 1.13 mmol) was added, before the reaction mixture was heated to 150 °C for 3 h. Subsequently, the reaction mixtures of two syntheses were combined, diluted with water (50 mL) and extracted with dichloromethane (DCM) (6 mL \times 25 mL). After drying over magnesium sulfate, the solvent was removed. The crude product was purified by flash chromatography (*n*-hexane/EtOAc) to give the product **27** as red oil (290 mg, 891 μmol , 59%).

TLC (UV, *n*-hexane/EtOAc = 3/1): R_f = 0.2.

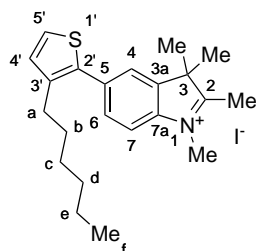
¹H NMR (500 MHz, CDCl₃): δ = 7.55 (dd, ³*J* = 7.9 Hz, ⁵*J* = 0.6 Hz, 1H, H-7), 7.36 (dd, ³*J* = 7.9 Hz, ⁴*J* = 1.8 Hz, 1H, H-6), 7.32 (dd, ⁴*J* = 1.8 Hz, ⁵*J* = 0.6 Hz, 1H, H-4), 7.21 (d, ³*J* = 5.2 Hz, 1H, H-5'), 6.98 (d, ³*J* = 5.2 Hz, 1H, H-4'), 2.64 (dd, ³*J* = 7.9 Hz, ³*J* = 7.9 Hz, 2H, H-a), 2.31 (s, 3H, C2-CH₃), 1.61 (tt, ³*J* = 7.9 Hz, ³*J* = 7.5 Hz, 2H, H-b), 1.34 (s, 6H, C3-(CH₃)₂), 1.32-1.20 (m, 6H, H-c,d,e), 0.85 (t, ³*J* = 6.9 Hz, 1H, H-f) ppm.

¹³C{¹H} NMR (126 MHz, CDCl₃): δ = 188.6 (C-2), 153.1 (C-3a), 146.0 (C-7a), 138.7 (C-2'), 138.2 (C-3'), 131.9 (C-5), 129.7 (C-4'), 129.1 (C-6), 123.6 (C-5'), 122.6 (C-4), 119.8 (C-7), 53.9 (C-3), 31.8 (C-c), 31.2 (C-b), 29.3 (C-d), 28.8 (C-a), 23.3 (C-3-(CH₃)₂), 22.7 (C-e), 15.6 (C-2-CH₃), 14.2 (C-f) ppm.

IR (ATR): $\tilde{\nu}$ = 2958 (m), 2925 (s), 2856 (m), 1576 (m), 1462 (s), 1426 (m), 1205 (m), 1120 (w), 1087 (w), 887 (m), 834 (vs), 806 (m), 725 (s), 656 (s) cm⁻¹.

HRMS (EI-TOF): $m/z = [M]^+$ (%) calcd for $[C_{21}H_{27}S]^+$ 325.18642, found 325.18626 (100).

5.1.2. Synthesis of 5-(3-Hexylthien-2-yl)-1,2,3,3-tetramethyl-3*H*-indolium Iodide (**28**)



5-(3-Hexylthienyl)-2,3,3-trimethyl-3*H*-indole (**27** 290 mg, 891 μ mol) was dissolved in acetonitrile (5.0 mL) in a MW vial. After addition of iodomethane (111 μ L, 253 mg, 1.78 mmol), the vial was crimped and the reaction was heated (MW) to 100 °C for 24 h. The volatile matter was removed *in vacuo* and the product **28** was obtained without further purification as red solid (412 mg, 882 μ mol, 99%).

melting point (Mp): T = 182 °C.

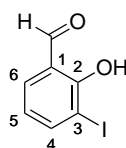
^1H NMR (500 MHz, CDCl_3): $\delta = 7.71$ (d, $^3J = 8.4$ Hz, 1H, H-7), 7.64 (dd, $^3J = 8.4$ Hz, $^4J = 1.7$ Hz, 1H, H-6), 7.55 (d, $^4J = 1.7$ Hz, 1H, H-4), 7.32 (d, $^3J = 5.1$ Hz, 1H, H-5'), 7.03 (d, $^3J = 5.1$ Hz, 1H, H-4'), 4.32 (s, 3H, N- CH_3), 3.14 (s, 3H, C- CH_3), 2.64 (dd, $^3J = 7.8$ Hz, $^3J = 7.8$ Hz, 2H, H-a), 1.72 (s, 6H, C-(CH_3)₂), 1.61 (tt, $^3J = 7.8$ Hz, $^3J = 7.5$ Hz, 2H, H-b), 1.35 – 1.23 (m, 6H, H-c,d,e), 0.86 (t, $^3J = 6.7$ Hz, 3H, H-f) ppm.

$^{13}\text{C}\{^1\text{H}\}$ NMR (126 MHz, CDCl_3): $\delta = 195.5$ (C-2), 141.7 (C-3a), 140.6 (C-7a), 140.4 (C-3'), 137.7 (C-5), 135.2 (C-2'), 130.5 (C-6), 129.9 (C-4'), 125.3 (C-5'), 123.8 (C-4), 115.3 (C-7), 54.7 (C-3), 37.5 (N- CH_3), 31.6 (C-d), 31.0 (C-b), 29.2 (C-c), 28.8 (C-a), 23.3 (C-(CH_3)₂), 22.6 (C-e), 17.3 (C- CH_3), 14.1 (C-f) ppm.

IR (ATR): $\tilde{\nu} = 3086$ (w), 2965 (m), 2923 (s), 2873 (m), 2857 (m), 1622 (m), 1610 (m), 1589 (m), 1528 (m), 1483 (s), 1473 (s), 1460 (s), 1421 (s), 1396 (m), 1372 (m), 1358 (m), 1074 (s), 991 (m), 937 (m), 882 (m), 842 (s), 831 (vs), 749 (vs), 729 (m), 706 (s), 674 (s) cm^{-1} .

HRMS (ESI-sector): $m/z = [M-I]^+$ (%) calcd for $[C_{22}H_{30}NS]^+$ 340.20935, found 340.20899 (100).

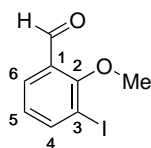
5.1.3. Synthesis of 2-Hydroxy-3-iodobenzaldehyde (**22**)



To a stirred solution of 2-iodophenol (22.0 g, 100 mmol) in dry THF (500 mL), anhydrous magnesium chloride (19.0 g, 200 mmol), dry TEA (27.7 mL, 20.2 g, 200 mmol) and paraformaldehyde (12.0 g, 400 mmol) were added. The reaction mixture was heated to reflux for 17 h. The color of the reaction mixture changed from colorless over yellow to a reddish ocre. After cooling to 20 °C, Et₂O (300 mL) and water (200 mL) were added followed by phase separation. The organic phase was washed with hydrochloric acid (2 mol/L, 3 × 200 mL), water (1 × 200 mL) and brine (1 × 100 mL). The hydrochloric washings were combined and extracted with Et₂O (3 × 300 mL). The organic phases were combined and the solvent was removed in vacuo. The residue was taken up with EtOAc (30 mL) and crystallized at -24 °C and filtered. The filtrate was concentrated in vacuo and recrystallized from EtOAc (10 mL); this recrystallization of the filtrate was repeated until no further crystallization occurred. The product **22** was obtained as yellow crystals (14.7 g, 59.2 mmol, 59%, Lit.:^[296] 84%, Lit.:^[174] 49%).

The analytical data were in agreement with the ones published in *Dyes and Pigments*^[174] and presented in Part V, section 3.1.

5.1.4. Synthesis of 3-Iodo-2-methoxybenzaldehyde (**24**)



Potassium carbonate (2.76 g, 20.0 mmol) was added to a solution of 2-hydroxy-3-iodobenzaldehyde (**22**, 2.48 g, 10.0 mmol) in DMF (10 mL), followed by addition of iodomethane (1.24 mL, 2.82 g, 20.0 mmol). The reaction mixture stirred at 23 °C for 30 min and was heated to 40 °C for 24 h, before it was diluted with water (400 mL). The resulting mixture was extracted with Et₂O (5 × 200 mL). After drying over magnesium sulfate and removing the solvent *in vacuo*, the product **24** was obtained as brown solid (2.42 g, 9.24 mmol, 92%) and was pure without further purification.

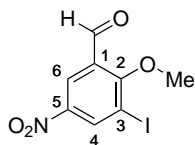
Mp: T = 35.0 °C.

¹H NMR (500 MHz, CDCl₃): δ = 10.33 (d, ⁵J = 0.8 Hz, 1H, CHO), 8.04 (dd, ³J = 7.7 Hz, ⁴J = 1.7 Hz, 1H, H-4), 7.83 (dd, ³J = 7.7 Hz, ⁴J = 1.7 Hz, 1H, H-6), 7.02 (at, ³J = 7.7 Hz, ⁵J = 0.8 Hz, 1H, H-5), 3.96 (s, 3H, OCH₃) ppm.

¹³C{¹H} NMR (126 MHz, CDCl₃): δ = 189.5 (CHO), 162.9 (C-2), 145.7 (C-4), 130.45 (C-1), 129.3 (C-6), 126.7 (C-5), 93.1 (C-3), 64.2 (OCH₃) ppm.

IR (ATR): $\tilde{\nu}$ = 3065 (w), 3007 (w), 2963 (w), 2937 (w), 2859 (m), 2742 (w), 1676 (s), 1580 (s), 1449 (s), 1416 (s), 1382 (s), 1241 (vs), 1230 (vs), 1107 (s), 1070 (s), 995 (vs), 847 (s), 798 (s), 782 (vs), 752 (s), 689 (s) cm⁻¹.

HRMS (EI-TOF): m/z = [M]⁺ (%) calcd for [C₈H₇¹²⁷IO₂]⁺ 261.94907, found 261.94867 (100).

5.1.5. Synthesis of 3-Iodo-2-methoxy-5-nitrobenzaldehyde (**25**)

2-Methoxy-3-iodobenzaldehyde (**24**, 2.62 g, 10.0 mmol) was dissolved in DCM (25 mL) and cooled to 0 °C. To the cooled solution, nitrating acid (1.5 mL, HNO₃/H₂SO₄ = 3/4, *v/v*, 20.0 mmol) was added with a dropping speed of 0.1 mL/min. The cooling bath was allowed to warm to 23 °C within 20 h. The reaction was quenched with water (100 mL) and DCM (75 mL) was added. After phase separation, the aqueous phase was extracted with DCM (3 x 100 mL). The obtained crude product was purified by flash chromatography (EtOAc/*n*-pentane) and recrystallized from EtOAc and *n*-pentane at -25 °C to give the product **25** as yellow solid (463 mg, 1.51 mmol, 15%).¹

TLC (UV, *n*-hexane/EtOAc = 4/1): R_f = 0.60.

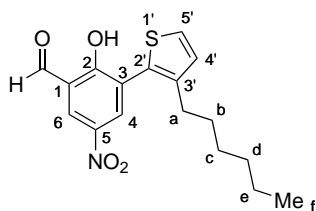
Mp: T = 36.5 °C.

¹H NMR (600 MHz, CDCl₃): δ = 10.31 (s, 1H, CHO), 8.88 (d, ⁴J = 2.8 Hz, 1H, H-4), 8.69 (d, ⁴J = 2.8 Hz, 1H, H-6), 4.06 (s, 3H, OCH₃) ppm.

¹³C{¹H} NMR (151 MHz, CDCl₃): δ = 187.2 (CHO), 167.1 (C-2), 145.0 (C-5), 139.7 (C-4), 129.8 (C-1), 124.9 (C-6), 93.3 (C-3), 64.6 (OCH₃) ppm.

IR (ATR): $\tilde{\nu}$ = 3057 (m), 2952 (w), 2858 (w), 2752 (w), 1705 (s), 1589 (s), 1503 (s), 1462 (s), 1342 (vs), 1297 (s), 1255 (s), 1208 (s), 1101 (s), 976 (vs), 937 (s), 907 (s), 848 (m), 785 (m), 758 (s), 741 (s), 710 (s), 659 (s) cm⁻¹.

HRMS (EI-TOF): *m/z* = [M]⁺ (%) calcd for [C₈H₆¹¹⁷INO₄]⁺ 306.93415, found 306.93388 (100).

5.1.6. Synthesis of 3-(3-Hexylthien-2-yl)-2-hydroxy-5-nitrobenzaldehyde (**26**)

3-Iodo-2-methoxy-5-nitrobenzaldehyde (**25**, 230 mg, 750 μmol), 3-hexylthiophene-2-boronic acid pinacol ester (**20**, 219 μL, 221 mg, 750 μmol) and Pd(PPh₃)₄ (26.0 mg, 22.5 μmol) were dissolved in DMF (3.9 mL) in a MW vial inside a glove box. After transferring the vial out, a degassed solution of tripotassium phosphate in water (1.13 mL, 1.13 mmol, 1.0 mol/L)

¹The crude product (2.25 g) contained approximately 50% of product, suggesting a conversion of approximately 37%.

was added and the vial was heated in to 150 °C for 45 min. The vial was opened and the reaction mixture was diluted with water (50 mL) and brine (25 mL) and extracted with DCM (15 × 25 mL). The combined organic phases were washed with brine (100 mL), dried over magnesium sulfate and the solvent was removed *in vacuo*. The crude product was purified by chromatography (*n*-pentane/EtOAc) and the product **26** was obtained as yellow solid (143 mg, 429 μmol, 57%).

TLC (UV, *n*-hexane/EtOAc = 4/1): $R_f = 0.62$.

Mp: $T = 119\text{ }^\circ\text{C}$.

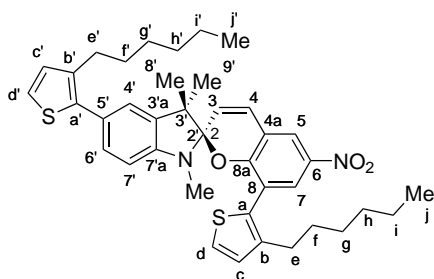
^1H NMR (500 MHz, CDCl_3): $\delta = 12.08$ (d, $^5J = 0.6$ Hz, 1H, OH), 10.05 (s, 1H, CHO), 8.57 (d, $^4J = 2.8$ Hz, 1H, H-6), 8.44 (dd, $^4J = 2.8$ Hz, $^5J = 0.6$ Hz, H-4), 7.41 (d, $^3J = 5.2$ Hz, 1H, H-5'), 7.04 (d, $^3J = 5.2$ Hz, 1H, H-4'), 2.49 (dd, $^3J = 7.6$ Hz, $^3J = 7.6$ Hz, 2H, H-a), 1.58 (tt, $^3J = 7.6$ Hz, $^3J = 7.6$ Hz, 2H, H-b),^{II} 1.31-1.16 (m, 6H, H-c,d,e), 0.86-0.80 (t, $^3J = 7.0$ Hz 3H, H-f) ppm.

$^{13}\text{C}\{^1\text{H}\}$ NMR (126 MHz, CDCl_3): $\delta = 195.7$ (CHO), 164.3 (C-2), 142.7 (C-3'), 140.3 (C-5), 133.6 (C-4), 129.1 (C-6), 129.0 (C-4'), 128.0 (C-2'), 126.4 (C-5'), 126.0 (C-3), 119.7 (C-1), 31.7 (c-d), 30.6 (C-b), 29.3 (C-a), 29.2 (C-c), 22.7 (C-e), 14.2 (C-f) ppm.

IR (ATR): $\tilde{\nu} = 3079$ (w), 2954 (m), 2926 (s), 2856 (m), 1656 (s), 1619 (m), 1591 (m), 1526 (s), 1438 (s), 1339 (vs), 1311 (vs), 1202 (s), 1099 (s), 956 (m), 915 (m), 835 (m), 745 (s), 720 (vs), 647 (m), 506 (s) cm^{-1} .

HRMS (EI-TOF): $m/z = [M]^+$ (%) calcd for $[\text{C}_{17}\text{H}_{19}\text{NO}_4\text{S}]^+$ 333.10348, found 333.10409 (51), 263.0 (100) $[\text{M}-\text{C}_5\text{H}_{10}]$.

5.1.7. Synthesis of 5',8-Di(3-hexylthien-2-yl)-1',3',3'-trimethyl-6-nitrospiro-chromene-2,2'-indoline (19)



3-(3-Hexylthiophen-2-yl)-2-hydroxy-5-nitrobenzaldehyde (**26**, 83.4 mg, 250 μmol), 5-(3-hexyl-thien-2-yl)-1,2,3,3-tetramethyl-3*H*-indolium iodide (**28**, 117 mg, 250 μmol) and piperidine (50 uL, 43 mg, 500 μmol) were dissolved in EtOH (2 mL) and heated to 78 °C for 2 h. After the solvent was removed *in vacuo*, the crude product was purified by flash chromatography (EtOAc/*n*-pentane) and the product **19** was obtained as dark purple solid (96.7 mg, 148 μmol, 59%).

Besides the predominant closed SP form, the ^1H NMR spectrum revealed the presence of approximately 33% open MC form **19b** in THF- d_8 , which could be identified by the signal

^{II}Due to an overlay with residual water from the NMR solvent, the integral was larger in the spectrum.

corresponding to the open ethylene bridge (H-3 and H-4). Most other MC signals showed an overlap with signals of the SP form. Thus, only the signals arising from the SP form **19a** were assigned.

TLC (UV, EtOAc/*n*-pentane, 1/3): $R_f = 0.88$.

Mp: $T = 85\text{ }^\circ\text{C}$.

$^1\text{H NMR}$ (500 MHz, THF- d_8): $\delta = 8.12$ (d, $^4J = 2.8$ Hz, 1H, H-5), 8.07 (d, $^4J = 2.8$ Hz, 1H, H-7), 7.18 (d, $^3J = 10.3$ Hz, 1H, H-4), ^{III} 7.17 (d, $^3J = 5.2$ Hz, 1H, H-d'), 7.13 (dd, $^3J = 7.9$ Hz, $^4J = 1.8$ Hz, 1H, H-6'), 7.13 (d, $^3J = 5.2$ Hz, H-d), 7.02 (d, $^4J = 1.8$ Hz, 1H, H-4'), 6.92 (dd, $^3J = 5.2$ Hz, $^4J = 1.4$ Hz, H-c'), ^{IV} 6.79 (d, $^3J = 5.2$ Hz, H-c), 6.55 (d, $^3J = 7.9$ Hz, 1H, H-7'), 6.03 (d, $^3J = 10.3$ Hz, 1H, H-3), 2.77 (s, 3H, N-CH₃), 2.68-2.50 (m, 4H, H-e,e'), 1.64-1.56 (m, 4H, H-f,f'), 1.35-1.22 (m, 12H, H-g,h,i,g',h',i'), 1.22 (s, 3H, H-8'), 1.21 (s, 3H, H-9'), 0.90-0.85 (m, 6H, H-j,j') ppm.

$^{13}\text{C NMR}$ (126 MHz, THF- d_8): $\delta = 157.2$ (C-8a), 147.9 (C-7'a), 141.7 (C-a), 141.4 (C-6), 139.5 (C-a'), 138.2 (C-b'), 137.3 (C-3'a), 130.2 (C-b), 129.6 (C-c'), 129.6 (C-4), 129.5 (C-6'), 128.5 (C-c), 127.6 (C-7), 126.9 (C-5'), 125.8 (C-d), 123.2 (C-d'), 122.5 (C-5), 121.5 (C-3), 120.3 (C-4a), 108.0 (C-2,2'), 107.4 (C-7'), 52.3 (C-3'), 32.6 (C-g,h,i,g',h' or i'), 32.4 (C-g,h,i,g',h' or i'), 31.9 (C-f,f'), 30.4 (C-g,h,i,g',h' or i'), 30.0 (C-g,h,i,g',h' or i'), 29.8 (C-e or e'), 29.3 (C-e or e'), 28.9 (N-CH₃), 25.6 (C-9'), 23.4 (C-g,h,i,g',h' or i'), 23.3 (C-g,h,i,g',h' or i'), 20.1 (C-8'), 14.3 (C-j, or j'), 14.2 (C-j, or j') ppm.

IR (ATR): $\tilde{\nu} = 2956$ (m), 2924 (s), 2854 (m), 1718 (w), 1655 (w), 1612 (m), 1587 (m), 1519 (s), 1493 (s), 1459 (s), 1432 (s), 1382 (m), 1333 (vs), 1272 (s), 1230 (s), 1184 (m), 1132 (s), 1107 (s), 1088 (s), 1063 (m), 1015 (s), 969 (m), 927 (m), 909 (m), 874 (m), 863 (m), 809 (s), 746 (m), 720 (s), 691 (m), 657 (s) cm^{-1} .

HRMS (EI-TOF): $m/z = [\text{M}]^+$ (%) calcd for $[\text{C}_{39}\text{H}_{46}\text{N}_2\text{O}_3\text{S}_2]^+$ 654.29498, found 654.29526 (100).

^{III}Between 7.20 and 7.10 ppm, four signals of the SP-isomer and several signals of the MC-isomer were overlapping. Thus, the integral in the plotted spectrum was too high.

^{IV}This signal was overlapping with signals of the MC isomer.

5.2. DFT Calculations of 5',8-Di(3-methylthiophen-2-yl)-1',3',3'-trimethyl-6- nitrospiro-[chromene-2,2'-indoline] (40)

Using Gaussian 09,^[297] the geometry and IR-frequencies of the molecules **40a–c** were optimized. Dispersive interactions were considered using the D3 version of Grimme's empirical dispersion correction.^[298] The absence of negative frequencies indicated true minima. The calculations were fully converged. For comparison, the electronic energies (E) and the zero-point energy corrected energies (E_{ZPE}) are given in Hartree accompanied by the point group. Visualization of the optimized structures was performed using UCSF Chimera.^[299] The orbital geometries were visualized using GaussView 6.0.16.^[300]

Table V.6. Energies of Frontier Orbitals of **40a**, **40b** and **40c** as Obtained by DFT Optimization. Energy levels and calculated HOMO-LUMO gap ΔE_{H-L} as derived by DFT. The geometrically compatible orbitals that were used for the calculation of the HOMO-LUMO gap are highlighted in bold.

Orbital	SP 40a	(Z)-MC 40b	(E)-MC 40c
LUMO+1	−1.85 eV	−1.77 eV	−1.72 eV
LUMO	−2.41 eV	−3.06 eV	−3.01 eV
HOMO	−5.55 eV	−5.46 eV	−5.32 eV
HOMO−1	−6.18 eV	−5.96 eV	−5.97 eV
ΔE_{H-L}	3.77 eV	2.40 eV	2.31 eV

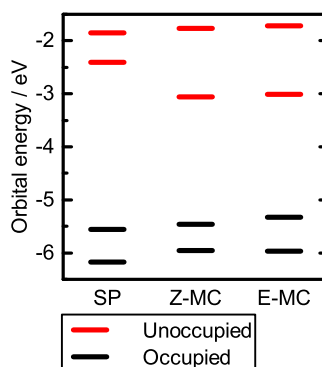
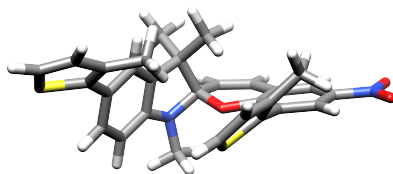


Figure V.2. Energies of frontier orbitals of **40a**, **40b** and **40c** as obtained by DFT optimization. Visualization of the orbital energies. Occupied orbitals are depicted as black lines and unoccupied orbitals are depicted as red lines.

5.2.1. Closed Form 40a



Optimized at the B3LYP/6-311G* level of theory.

E -2252.637222 Hartree

E_{ZPE} -2252.151473 Hartree

Point Group C_1

Lowest Unoccupied Molecular Orbitals

Highest Occupied Molecular Orbitals

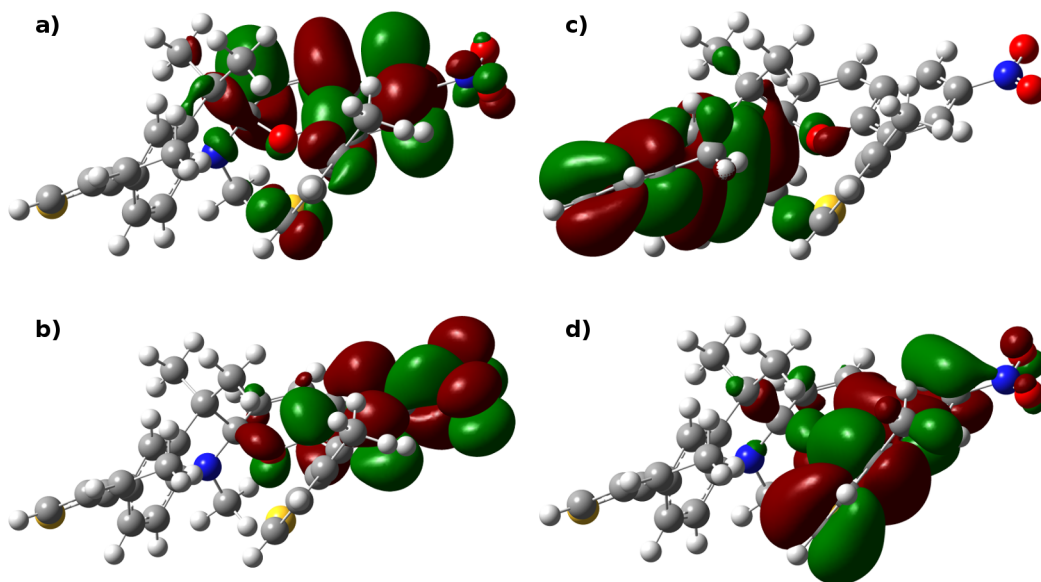


Figure V.3. Frontier orbitals of **40a**. **left:** Unoccupied molecular orbitals. **right:** Occupied molecular orbitals. **a)** LUMO+1; **b)** LUMO; **c)** HOMO; **d)** HOMO-1

Table V.7. Atom Coordinates of **40a** after DFT Optimization.

Coordinates				
Atom Count	Symbol	X	Y	Z
1	C	-3.5823510	-0.5515444	0.0759384
2	C	-3.5088102	-1.1732543	1.3286554
3	C	-2.4256576	-1.9794716	1.6911058
4	C	-1.4048884	-2.1590453	0.7665421
5	C	-1.4757157	-1.5739339	-0.5032951

Continued on next page

Continued from previous page

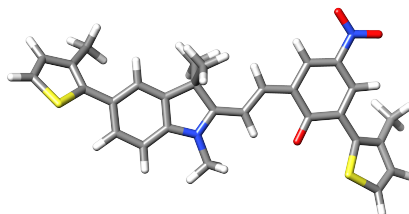
Atom Count	Symbol	X	Y	Z
6	C	-2.5461576	-0.7820755	-0.8537046
7	N	-0.1919768	-2.8561652	0.9095470
8	C	0.7188505	-2.3220432	-0.0776258
9	C	-0.2289190	-1.9515203	-1.2809353
10	O	1.2036199	-1.0456550	0.4891189
11	C	2.4187556	-0.5434296	0.2241634
12	C	3.4598763	-1.3801232	-0.2178771
13	C	3.1324391	-2.7797734	-0.4586984
14	C	1.8734051	-3.2260395	-0.3886622
15	C	2.5992722	0.8429363	0.4190740
16	C	3.8917817	1.3465103	0.2461059
17	C	4.9276783	0.5115392	-0.1622407
18	C	4.7287593	-0.8422660	-0.4082968
19	C	-0.5088033	-3.1968405	-2.1467944
20	C	0.3321013	-0.8219058	-2.1476090
21	C	0.3123936	-3.1579776	2.2396653
22	C	-4.6840659	0.3602128	-0.2661087
23	C	1.4683601	1.7363125	0.7152925
24	C	-4.6126979	1.6271949	-0.8020959
25	C	-5.9075851	2.2040860	-0.9978317
26	C	-6.9339916	1.3937698	-0.6148784
27	S	-6.3505597	-0.1203318	-0.0081940
28	S	0.1978127	1.2952447	1.8435429
29	C	-0.6058977	2.8003569	1.6052782
30	C	0.0415092	3.5818554	0.6937896
31	C	1.2311628	2.9878295	0.1745122
32	C	-3.3369708	2.3636872	-1.1142066
33	C	2.0698286	3.6716004	-0.8722078
34	N	6.2717145	1.0810658	-0.3438508
35	O	7.1675578	0.3239764	-0.7012470
36	O	6.4199350	2.2790378	-0.1303875
37	H	-4.2935062	-0.9875640	2.0546270
38	H	-2.3765354	-2.4113792	2.6840268
39	H	-2.5962246	-0.3208613	-1.8338671
40	H	3.9424301	-3.4578742	-0.7101234
41	H	1.6265756	-4.2634211	-0.5781930
42	H	4.1027132	2.3905957	0.4237827

Continued on next page

Continued from previous page

Atom Count	Symbol	X	Y	Z
43	H	5.5560528	-1.4571043	-0.7380845
44	H	-1.2899048	-2.9653123	-2.8737918
45	H	0.3840169	-3.5065312	-2.6972115
46	H	-0.8540302	-4.0353976	-1.5387312
47	H	0.4174469	0.1094552	-1.5880508
48	H	1.3151688	-1.0850581	-2.5481747
49	H	-0.3308831	-0.6444848	-2.9977908
50	H	0.4557358	-2.2525710	2.8416172
51	H	-0.3872782	-3.8196494	2.7529882
52	H	1.2670161	-3.6773379	2.1543495
53	H	-6.0562680	3.2007401	-1.3981449
54	H	-7.9952139	1.5931025	-0.6514563
55	H	-1.5293502	3.0073217	2.1267278
56	H	-0.3199398	4.5534891	0.3781593
57	H	-2.4922860	1.9845829	-0.5370979
58	H	-3.0719141	2.2859561	-2.1746257
59	H	-3.4419425	3.4286569	-0.8889205
60	H	2.8165945	4.3374463	-0.4270363
61	H	2.6056589	2.9574316	-1.4999430
62	H	1.4407826	4.2841023	-1.5226896

5.2.2. Open Form, TTC-Geometry 40b



Optimized at the B3LYP/6-311G* level of theory.

E -2252.623391 Hartree

E_{ZPE} -2252.138857 Hartree

Point Group C_1

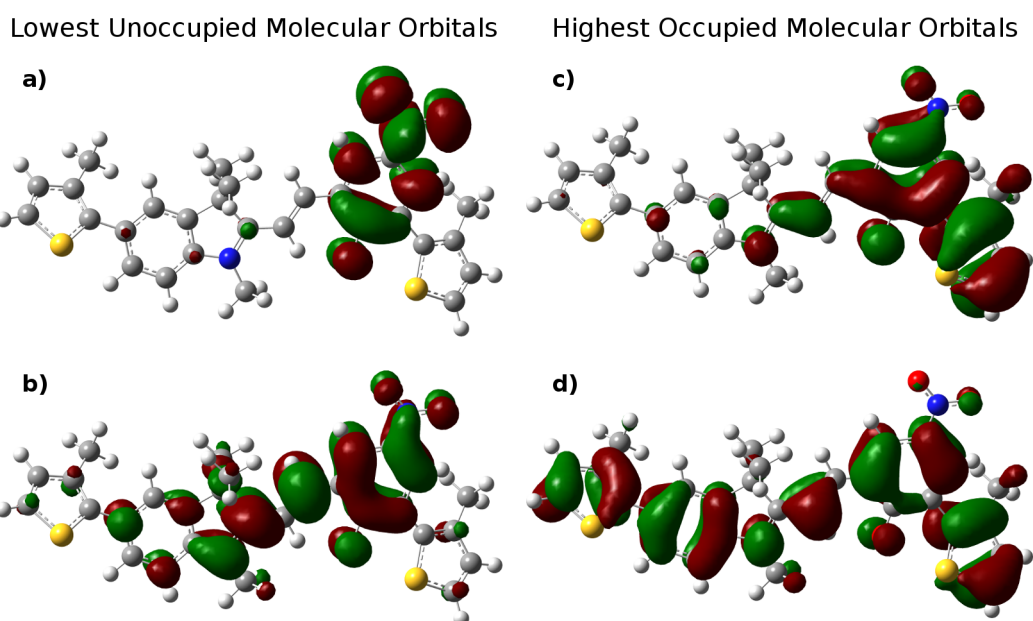


Figure V.4. Frontier orbitals of **40b**. **left:** Unoccupied molecular orbitals. **right:** Occupied molecular orbitals. **a)** LUMO+1; **b)** LUMO; **c)** HOMO; **d)** HOMO-1

Table V.8. Atom Coordinates of **40b** after DFT Optimization.

Coordinates					
Atom Count	Symbol	X	Y	Z	
1	C	5.6473779	-0.5349469	0.0525475	
2	C	5.3445734	-1.9057802	0.1062598	
3	C	4.0321363	-2.3752938	0.0926086	
4	C	3.0090496	-1.4362232	0.0319705	

Continued on next page

Continued from previous page

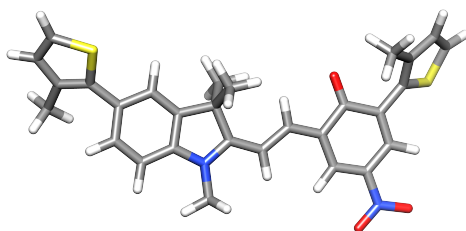
Atom Count	Symbol	X	Y	Z
5	C	3.2802956	-0.0690107	-0.0255115
6	C	4.5831396	0.3860525	-0.0232646
7	N	1.6146019	-1.6245545	0.0108881
8	C	0.9464843	-0.4399021	-0.0611516
9	C	1.9740195	0.7007986	-0.0965677
10	C	1.8949778	1.4968585	-1.4177414
11	C	1.8398431	1.6318506	1.1281588
12	C	0.9526396	-2.9208910	0.0551278
13	C	7.0379322	-0.0607182	0.0674743
14	C	7.5933450	0.9774846	0.7845336
15	C	8.9900926	1.1291803	0.5190962
16	C	9.4799675	0.2264465	-0.3763406
17	S	8.2428823	-0.8442059	-0.9386360
18	C	6.8619473	1.8443371	1.7740695
19	C	-0.4375259	-0.3938336	-0.0931417
20	C	-1.2055381	0.7710952	-0.1634332
21	C	-2.6024273	0.8758757	-0.1825476
22	C	-3.4987229	-0.3067668	-0.1182086
23	C	-4.9553497	-0.0432299	-0.0690643
24	C	-5.4099079	1.2420980	-0.2132358
25	C	-4.5164198	2.3443123	-0.3042226
26	C	-3.1611470	2.1766005	-0.2769931
27	O	-3.0620146	-1.4644317	-0.1198510
28	C	-5.8873569	-1.1574757	0.1081213
29	C	-7.1324764	-1.1398219	0.7199131
30	C	-7.8006446	-2.3949815	0.6245320
31	C	-7.0829438	-3.3452851	-0.0412876
32	S	-5.5400704	-2.7565465	-0.5390729
33	C	-7.7445874	0.0194660	1.4608858
34	N	-5.0677322	3.6920378	-0.4284529
35	O	-4.2841821	4.6361530	-0.5105105
36	O	-6.2909985	3.8111043	-0.4418483
37	H	6.1557734	-2.6215722	0.1794343
38	H	3.8392542	-3.4403580	0.1383578
39	H	4.7964876	1.4459217	-0.1011609
40	H	0.9560638	2.0436688	-1.5058987
41	H	2.7137406	2.2189629	-1.4600723

Continued on next page

Continued from previous page

Atom Count	Symbol	X	Y	Z
42	H	1.9842525	0.8339061	-2.2803590
43	H	0.9015757	2.1868107	1.1165725
44	H	1.8869944	1.0638668	2.0592808
45	H	2.6607378	2.3529645	1.1298141
46	H	0.2939059	-2.9821052	0.9237656
47	H	0.3554616	-3.0743483	-0.8460657
48	H	1.6984313	-3.7078022	0.1224062
49	H	9.6041721	1.8831288	0.9980494
50	H	10.4916482	0.1264817	-0.7418781
51	H	5.9703138	1.3517553	2.1655462
52	H	7.5076439	2.0906858	2.6206959
53	H	6.5456585	2.7928878	1.3260003
54	H	-0.9898968	-1.3215231	-0.0646462
55	H	-0.6841283	1.7222146	-0.2075649
56	H	-6.4659676	1.4555635	-0.2767110
57	H	-2.5189910	3.0470821	-0.3396315
58	H	-8.7787554	-2.5754549	1.0558733
59	H	-7.3554207	-4.3748359	-0.2266123
60	H	-6.9866197	0.6606144	1.9156688
61	H	-8.3562859	0.6538834	0.8102150
62	H	-8.3982096	-0.3451232	2.2573747

5.2.3. Open Form, TTT-Geometry 40c



Optimized at the B3LYP/6-311G* level of theory.

E -2252.621185 Hartree

E_{ZPE} -2252.136979 Hartree

Point Group C_1

Lowest Unoccupied Molecular Orbitals

Highest Occupied Molecular Orbitals

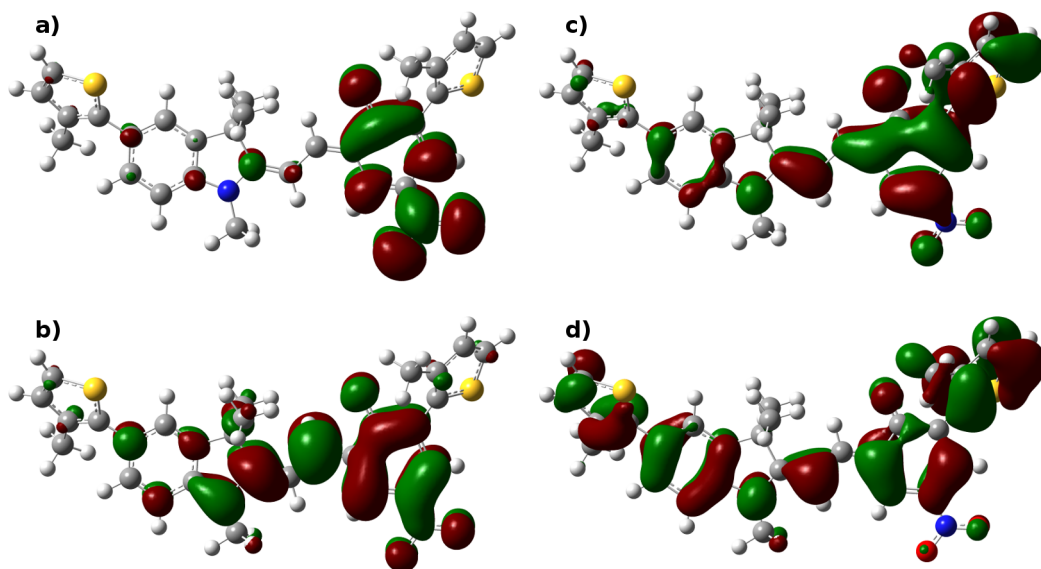


Figure V.5. Frontier orbitals of **40c**. **left:** Unoccupied molecular orbitals. **right:** Occupied molecular orbitals. **a)** LUMO+1; **b)** LUMO; **c)** HOMO; **d)** HOMO-1

Table V.9. Atom Coordinates of **40c** after DFT Optimization.

Coordinates				
Atom Count	Symbol	X	Y	Z
1	C	-5.6314696	0.1077041	-0.0318671
2	C	-5.6836222	1.5053248	-0.1571578
3	C	-4.5302419	2.2873730	-0.2146041
4	C	-3.3036141	1.6368834	-0.1578576

Continued on next page

Continued from previous page

Atom Count	Symbol	X	Y	Z
5	C	-3.2210960	0.2489887	-0.0448823
6	C	-4.3678185	-0.5155388	0.0209499
7	N	-2.0003693	2.1682557	-0.1980075
8	C	-1.0542640	1.1893997	-0.1131506
9	C	-1.7625734	-0.1707689	-0.0033067
10	C	-1.4485234	-0.8766319	1.3349810
11	C	-1.4396299	-1.0862146	-1.2055359
12	C	-1.6921871	3.5842372	-0.3160087
13	C	-6.8669987	-0.6849840	0.0318578
14	C	-8.0138786	-0.4552605	0.7611641
15	C	-8.9991948	-1.4697566	0.5495848
16	C	-8.6065169	-2.4451154	-0.3169268
17	S	-7.0105977	-2.1539162	-0.9179579
18	C	-8.2284805	0.6900207	1.7134493
19	C	0.3011711	1.4650302	-0.1278466
20	C	1.3055605	0.4952407	-0.0431696
21	C	2.6857789	0.6806674	-0.0489871
22	C	3.5148653	-0.5564084	0.0554929
23	C	4.9850254	-0.3653234	0.0196003
24	C	5.5055244	0.8956102	-0.0633318
25	C	4.6667190	2.0478284	-0.1348772
26	C	3.3049608	1.9514479	-0.1350033
27	O	2.9981709	-1.6676371	0.1753934
28	C	5.8532440	-1.5421718	0.1351251
29	C	5.8279174	-2.7219577	-0.5744388
30	C	6.8582671	-3.6201298	-0.1582836
31	C	7.6429629	-3.1330769	0.8453703
32	S	7.1437085	-1.5484100	1.3236241
33	C	4.8656181	-3.0408741	-1.6834689
34	N	5.2858477	3.3695197	-0.2279119
35	O	6.5124844	3.4266573	-0.2383954
36	O	4.5502479	4.3537954	-0.2900358
37	H	-6.6494389	1.9900716	-0.2340988
38	H	-4.6129831	3.3632025	-0.3131254
39	H	-4.3047836	-1.5929498	0.1316541
40	H	-0.4075022	-1.1939621	1.3941321
41	H	-1.6568533	-0.2204064	2.1824084

Continued on next page

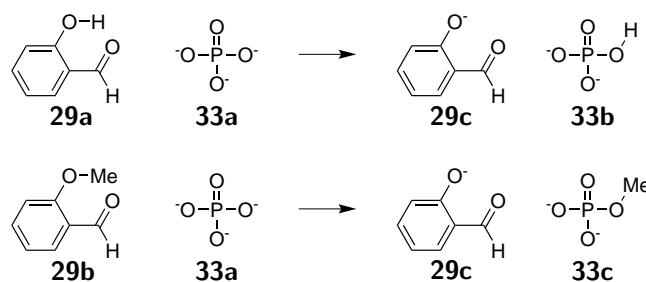
Continued from previous page

Atom Count	Symbol	X	Y	Z
42	H	-2.0778599	-1.7641294	1.4326815
43	H	-0.3970719	-1.4037286	-1.2061085
44	H	-2.0649534	-1.9808588	-1.1591907
45	H	-1.6455646	-0.5796758	-2.1506452
46	H	-1.1073571	3.7745134	-1.2189808
47	H	-2.6143192	4.1552483	-0.3749673
48	H	-1.1254108	3.9277204	0.5526742
49	H	-9.9629592	-1.4698151	1.0456946
50	H	-9.1580681	-3.3155969	-0.6411870
51	H	-7.2843086	1.1062933	2.0683305
52	H	-8.7931690	1.5043232	1.2461779
53	H	-8.8006039	0.3629832	2.5854111
54	H	0.5994641	2.5044401	-0.2082487
55	H	1.0202651	-0.5461593	0.0388341
56	H	6.5769603	1.0481048	-0.0885212
57	H	2.7224625	2.8612756	-0.2011504
58	H	7.0081679	-4.5950222	-0.6083426
59	H	8.4814031	-3.6101311	1.3319931
60	H	4.5608920	-2.1403982	-2.2206298
61	H	5.3176104	-3.7280798	-2.4037389
62	H	3.9556012	-3.4962581	-1.2872021

5.3. DFT Calculations of Phenol and Anisole Derivatives and the Corresponding Phenolates for the Estimation of Intramolecular Hydrogen Bonds

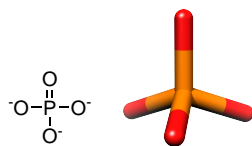
Using Gaussian 09,^[297] the geometry and IR-frequencies of phosphate (**33a**), hydrogen phosphate (**33a**), methyl phosphate (**33a**), and the molecules **3a–c**, **30a–c**, **31a–c**, and **32a–c** were optimized. Dispersive interactions were considered using the D3 version of Grimme's empirical dispersion correction to take hydrogen bonds into account.^[298] The absence of negative frequencies indicated true minima. The calculations were fully converged. For comparison, the electronic energies (E) and the zero-point energy corrected energies (E_{ZPE}) are given in Hartree accompanied by the point group. Visualization of the optimized structures was performed using UCSF Chimera.^[299]

As described in Part II, section 3.3, ΔE_{rct} was calculated from the E_{ZPE} s and describes the reaction energy of the transfer of a proton or a methyl group from the phenols **3a**, **29a**, **30a**, **31a**, and **32a** or anisoles **3b**, **29b**, **30b**, **31b**, and **32b** to phosphate (**33a**).

Table V.10. Calculated energies of starting materials and products of the deprotonation of phenols and the demethylation of anisoles with phosphate and derived reaction energy differences.

Entry No.	Structure	Starting Materials OR =	Starting Materials		Products		Reaction ΔE_{rct} / kcal mol ⁻¹
				E_{ZPE} / kcal mol ⁻¹		E_{ZPE} / kcal mol ⁻¹	
1		O ⁻	33a	-402909.4	33b 33c	-403481.6 -428136.0	- -
2		OH	29a	-192924.9	29c	-192583.2	-230.5
		OMe	29b	-217577.4			-232.4
3		OH	30a	-264061.1	30c	-263721.8	-232.8
		OMe	30b	-288706.3			-242.1
4		OH	3a	-392428.1	3c	-392110.0	-254.1
		OMe	3b	-417073.1			-263.5
5		OH	31a	-738706.6	31c	-738393.6	-259.1
		OMe	31b	-763349.5			-270.7
6		OH	32a	-763367.9	32c	-763052.9	-257.2
		OMe	32b	-788011.3			-268.2

5.3.1. Phosphate (33a)



Optimized at the B3LYP/6-311+G* level of theory.

E -642.089537 Hartree

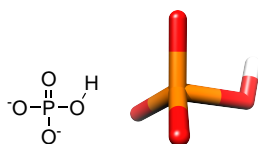
E_{ZPE} -642.076996 Hartree

Point Group TD

Table V.11. Atom Coordinates of **33a** after DFT Optimization.

Coordinates				
Atom Count	Symbol	X	Y	Z
1	P	0.000000	0.000000	0.000000
2	O	0.925483	0.925483	0.925483
3	O	-0.925483	-0.925483	0.925483
4	O	-0.925483	0.925483	-0.925483
5	O	0.925483	-0.925483	-0.925483

5.3.2. Hydrogen Phosphate (33b)



Optimized at the B3LYP/6-311+G* level of theory.

E -643.013038 Hartree

E_{ZPE} -642.988797 Hartree

Point Group C₁

Table V.12. Atom Coordinates of **33b** after DFT Optimization.

Coordinates				
Atom Count	Symbol	X	Y	Z
1	P	-0.159817	-0.025923	-0.060238
2	O	0.437051	-0.484154	-1.421506

Continued on next page

Continued from previous page

Atom Count	Symbol	X	Y	Z
3	O	-0.954657	1.291734	-0.080302
4	O	-0.781015	-1.157062	0.784503
5	O	1.346910	0.402417	0.798640
6	H	2.010940	-0.034635	0.252897

5.3.3. Methyl Phosphate (33c)



Optimized at the B3LYP/6-311+G* level of theory.

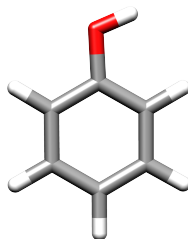
E -682.330021 Hartree

E_{ZPE} -682.278140 HartreePoint Group C₁

Table V.13. Atom Coordinates of 33c after DFT Optimization.

Coordinates				
Atom Count	Symbol	X	Y	Z
1	P	0.555329	-0.060924	0.000010
2	O	0.464249	-0.889973	1.299034
3	O	1.561651	1.096978	-0.000044
4	O	0.464369	-0.890200	-1.298876
5	O	-1.001421	0.837010	-0.000136
6	C	-2.137675	0.038613	-0.000008
7	H	-2.187462	-0.616677	0.889551
8	H	-3.039524	0.684999	0.000094
9	H	-2.187678	-0.616676	-0.889563

5.3.4. Phenol (29a)



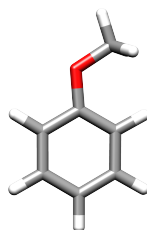
Optimized at the B3LYP/6-311+G* level of theory.

E -307.549512 Hartree
 E_{ZPE} -307.445452 Hartree
 Point Group C₁

Table V.14. Atom Coordinates of **29a** after DFT Optimization.

Coordinates				
Atom Count	Symbol	X	Y	Z
1	C	-0.9381000	-0.0217000	0.0000000
2	C	-0.2229000	-1.2202000	0.0000000
3	C	1.1681000	-1.1905000	0.0000000
4	C	1.8558000	0.0246000	0.0000000
5	C	1.1339000	1.2162000	0.0000000
6	C	-0.2605000	1.1994000	0.0000000
7	O	-2.3054000	-0.1099000	0.0000000
8	H	-2.6994000	0.7704000	0.0002000
9	H	-0.7701000	-2.1561000	0.0000000
10	H	1.7190000	-2.1257000	0.0000000
11	H	2.9402000	0.0414000	0.0000000
12	H	1.6538000	2.1689000	0.0000000
13	H	-0.8187000	2.1326000	0.0000000

5.3.5. Anisole (29b)



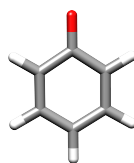
Optimized at the B3LYP/6-311+G* level of theory.

E -346.864445 Hartree
 E_{ZPE} -346.731696 Hartree
 Point Group C₁

Table V.15. Atom Coordinates of **29b** after DFT Optimization.

Coordinates				
Atom Count	Symbol	X	Y	Z
1	C	0.4528554	-0.2704730	-0.0000558
2	C	-0.4951848	-1.3013771	-0.0000006
3	C	-1.8503367	-0.9996763	0.0000444
4	C	-2.2826306	0.3296728	0.0000398
5	C	-1.3373109	1.3495496	-0.0000130
6	C	0.0305246	1.0622615	-0.0000640
7	O	1.7593871	-0.6690287	-0.0001220
8	C	2.7730640	0.3242257	0.0001162
9	H	-0.1435321	-2.3271890	0.0000078
10	H	-2.5754529	-1.8075235	0.0000883
11	H	-3.3419744	0.5627757	0.0000780
12	H	-1.6571967	2.3870317	-0.0000195
13	H	0.7443657	1.8762995	-0.0001159
14	H	3.7187550	-0.2151115	0.0002261
15	H	2.7171732	0.9554922	-0.8939462
16	H	2.7168805	0.9553549	0.8942560

5.3.6. Phenolate (29c)

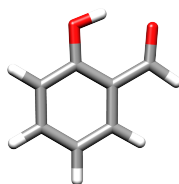


Optimized at the B3LYP/6-311G* level of theory.

E -306.990816 Hartree
 E_{ZPE} -306.900916 Hartree
 Point Group C₁

Table V.16. Atom Coordinates of **29c** after DFT Optimization.

Coordinates				
Atom Count	Symbol	X	Y	Z
1	C	-1.0780683	0.0002336	0.0000027
2	C	-0.2873360	-1.2115416	0.0000037
3	C	1.1004692	-1.2004580	0.0000070
4	C	1.8281254	0.0001044	0.0000066
5	C	1.1005048	1.2002698	-0.0000010
6	C	-0.2876487	1.2115739	-0.0000046
7	O	-2.3476639	-0.0001986	-0.0000117
8	H	-0.8334094	-2.1532928	0.0000032
9	H	1.6381902	-2.1500592	0.0000106
10	H	2.9152480	-0.0000363	0.0000098
11	H	1.6378724	2.1500661	-0.0000037
12	H	-0.8328671	2.1538191	-0.0000125

5.3.7. 2-Hydroxybenzaldehyde (**30a**)

Optimized at the B3LYP/6-311+G* level of theory.

E -420.922681 Hartree

E_{ZPE} -420.808141 Hartree

Point Group C₁

Table V.17. Atom Coordinates of **30a** after DFT Optimization.

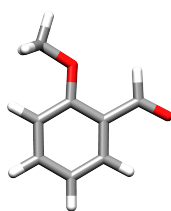
Coordinates				
Atom Count	Symbol	X	Y	Z
1	C	0.0596852	0.8428515	0.0000065
2	C	-1.2710382	1.2767773	0.0000430
3	C	-2.3023131	0.3498486	0.0000368
4	C	-2.0434108	-1.0294860	-0.0000093

Continued on next page

Continued from previous page

Atom Count	Symbol	X	Y	Z
5	C	-0.7310563	-1.4649275	-0.0000428
6	C	0.3376760	-0.5487817	-0.0000281
7	O	1.0295710	1.7706029	-0.0000689
8	C	1.7101416	-1.0324863	0.0000184
9	O	2.7035784	-0.3117586	0.0000833
10	H	1.9013228	1.3215483	-0.0002119
11	H	-1.4651817	2.3431730	0.0000659
12	H	-3.3289144	0.7022894	0.0000663
13	H	-2.8614772	-1.7405420	-0.0000146
14	H	-0.5066670	-2.5281350	-0.0000661
15	H	1.8376154	-2.1318633	-0.0001029

5.3.8. 2-Methoxybenzaldehyde (30b)



Optimized at the B3LYP/6-311+G* level of theory.

E -460.224898 Hartree

E_{ZPE} -460.082690 HartreePoint Group C₁Table V.18. Atom Coordinates of **30b** after DFT Optimization.

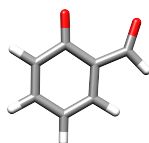
Coordinates				
Atom Count	Symbol	X	Y	Z
1	C	0.6527843	0.0713128	0.0000070
2	C	1.1828840	-1.2237707	0.0002299
3	C	0.3256322	-2.3226424	0.0001163
4	C	-1.0592641	-2.1551943	-0.0001151
5	C	-1.5830279	-0.8695456	-0.0001909
6	C	-0.7484049	0.2536952	-0.0001363

Continued on next page

Continued from previous page

Atom Count	Symbol	X	Y	Z
7	O	1.4131186	1.1988663	0.0000356
8	C	-1.3507309	1.6067504	-0.0000351
9	O	-2.5482417	1.8125461	0.0002338
10	C	2.8307528	1.0818435	-0.0001242
11	H	2.2526699	-1.3867544	0.0004335
12	H	0.7516566	-3.3210249	0.0002023
13	H	-1.7166359	-3.0174690	-0.0002404
14	H	-2.6540045	-0.6984135	-0.0002868
15	H	-0.6411097	2.4516707	-0.0002950
16	H	3.1873332	0.5620532	-0.8952136
17	H	3.2097885	2.1018881	-0.0001444
18	H	3.1875345	0.5620572	0.8948804

5.3.9. 2-Formylphenolate (30c)



Optimized at the B3LYP/6-311G* level of theory.

E -420.366931 Hartree

E_{ZPE} -420.267389 HartreePoint Group C₁

Table V.19. Atom Coordinates of 30c after DFT Optimization.

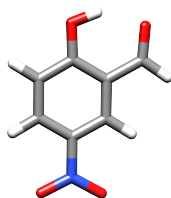
Coordinates				
Atom Count	Symbol	X	Y	Z
1	C	-0.0291319	0.9818636	-0.0000257
2	C	1.4184795	1.1818787	-0.0000286
3	C	2.3223608	0.1494152	-0.0000163
4	C	1.8972804	-1.2029025	0.0000059
5	C	0.5388109	-1.4524677	0.0000182
6	C	-0.4388881	-0.4314413	0.0000028
7	O	-0.8126022	1.9540403	-0.0000061

Continued on next page

Continued from previous page

Atom Count	Symbol	X	Y	Z
8	C	-1.8196819	-0.8739631	0.0000136
9	O	-2.8605652	-0.2298421	0.0000219
10	H	1.7506257	2.2173923	-0.0000426
11	H	3.3898149	0.3718722	-0.0000247
12	H	2.6189240	-2.0149374	0.0000171
13	H	0.1892668	-2.4861206	0.0000384
14	H	-1.8986706	-1.9960891	0.0000654

5.3.10. 2-Hydroxy-5-nitrobenzaldehyde (3a)



Optimized at the B3LYP/6-311+G* level of theory.

E -625.490790 Hartree
 E_{ZPE} -625.373929 Hartree
 Point Group C₁

Table V.20. Atom Coordinates of **3a** after DFT Optimization.

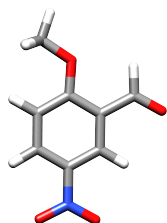
Coordinates				
Atom Count	Symbol	X	Y	Z
1	C	-1.4479146	0.8948937	0.0000143
2	C	-0.4197113	1.8506839	-0.0001791
3	C	0.9016242	1.4504115	-0.0001881
4	C	1.2164506	0.0841751	-0.0000292
5	C	0.2242055	-0.8786409	0.0000904
6	C	-1.1194588	-0.4891685	0.0001478
7	O	-2.7079057	1.3295603	0.0001277
8	C	-2.1701320	-1.5040531	0.0000789
9	O	-3.3676645	-1.2483061	-0.0000911
10	N	2.6263888	-0.3334770	0.0000303
11	O	2.8649219	-1.5362166	-0.0003160

Continued on next page

Continued from previous page

Atom Count	Symbol	X	Y	Z
12	O	3.4793723	0.5465696	0.0003530
13	H	-3.3182929	0.5596201	-0.0001429
14	H	-0.6903889	2.8995856	-0.0003215
15	H	1.7031472	2.1775135	-0.0002964
16	H	0.4936877	-1.9283307	0.0001820
17	H	-1.8330498	-2.5567173	0.0001683

5.3.11. 2-Methoxy-5-nitrobenzaldehyde (3b)



Optimized at the B3LYP/6-311G* level of theory.

E -664.792754 Hartree
 E_{ZPE} -664.648257 Hartree
 Point Group C₁

Table V.21. Atom Coordinates of **3b** after DFT Optimization.

Coordinates				
Atom Count	Symbol	X	Y	Z
1	C	-1.4211162	-0.4372147	0.0000009
2	C	-0.6531586	-1.6119640	0.0000013
3	C	0.7317336	-1.5360639	0.0000009
4	C	1.3536101	-0.2887352	0.0000001
5	C	0.6132381	0.8836744	0.0000006
6	C	-0.7786462	0.8239795	0.0000010
7	O	-2.7702081	-0.4245528	0.0000003
8	C	-1.5548763	2.0923905	0.0000011
9	O	-1.0380791	3.1882434	0.0000002
10	N	2.8255556	-0.2199200	-0.0000006
11	O	3.3442363	0.8887545	-0.0000036

Continued on next page

Continued from previous page

Atom Count	Symbol	X	Y	Z
12	O	3.4430637	-1.2800853	0.0000018
13	C	-3.4899114	-1.6577599	-0.0000028
14	H	-1.1247610	-2.5851822	0.0000024
15	H	1.3354713	-2.4340559	0.0000016
16	H	1.1006264	1.8504130	0.0000004
17	H	-2.6527813	1.9874145	0.0000021
18	H	-3.2666812	-2.2437767	-0.8961085
19	H	-3.2666884	-2.2437770	0.8961046
20	H	-4.5414161	-1.3803142	-0.0000069

5.3.12. 2-Formyl-4-nitrophenolate (3c)



Optimized at the B3LYP/6-311G* level of theory.

E -624.969691 Hartree

E_{ZPE} -624.867022 HartreePoint Group C₁

Table V.22. Atom Coordinates of 3c after DFT Optimization.

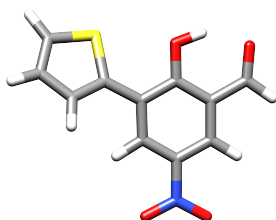
Coordinates				
Atom Count	Symbol	X	Y	Z
1	C	1.5380205	1.0197854	0.0000327
2	C	0.3791874	1.9176367	0.0001067
3	C	-0.9101108	1.4795549	0.0000873
4	C	-1.1896920	0.0840627	0.0000025
5	C	-0.1324528	-0.8265370	-0.0000548
6	C	1.1967180	-0.4187000	-0.0000377
7	O	2.6934589	1.4659593	0.0000426
8	C	2.1925399	-1.4893129	-0.0000904
9	O	3.4075024	-1.4126539	-0.0000465

Continued on next page

Continued from previous page

Atom Count	Symbol	X	Y	Z
10	N	-2.5347686	-0.3780951	-0.0000226
11	O	-2.7591005	-1.6036915	-0.0000721
12	O	-3.4565687	0.4610145	0.0000527
13	H	0.6067914	2.9794300	0.0001725
14	H	-1.7417661	2.1739747	0.0001368
15	H	-0.3685277	-1.8860445	-0.0001141
16	H	1.7192839	-2.5046607	-0.0001286

5.3.13. 2-Hydroxy-5-nitro-3-thien-2-ylbenzaldehyde (31a)



Optimized at the B3LYP/6-311+G* level of theory.

E -1177.367842 Hartree
 E_{ZPE} -1177.203916 Hartree
 Point Group C₁

Table V.23. Atom Coordinates of **31a** after DFT Optimization.

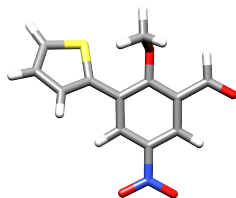
Coordinates				
Atom Count	Symbol	X	Y	Z
1	C	0.0877650	1.2116980	0.0840710
2	C	-0.3586120	-0.1348410	0.0474210
3	C	0.6159280	-1.1298780	-0.0317570
4	C	1.9768360	-0.8207550	-0.0342800
5	C	2.4209440	0.4866210	0.0142000
6	C	1.4758470	1.5146290	0.0697500
7	C	-1.7761900	-0.5078590	0.1042320
8	O	-0.8294340	2.1773540	0.1323540
9	C	1.9325090	2.9019650	0.1117700
10	O	1.1870750	3.8733300	0.1529100

Continued on next page

Continued from previous page

Atom Count	Symbol	X	Y	Z
11	S	-3.0811290	0.4927610	-0.5040770
12	C	-4.2496580	-0.7270940	-0.1489830
13	C	-3.6829670	-1.8309860	0.4268220
14	C	-2.2772420	-1.7056500	0.5682950
15	H	-0.3838170	3.0549650	0.1488070
16	N	2.9606530	-1.9136010	-0.1120810
17	O	4.1480050	-1.6088810	-0.1324480
18	O	2.5354110	-3.0623520	-0.1487370
19	H	0.3259570	-2.1685660	-0.1089090
20	H	3.4820160	0.7037050	0.0007970
21	H	3.0271180	3.0525760	0.1038230
22	H	-5.2937210	-0.5470530	-0.3625190
23	H	-4.2476650	-2.6972610	0.7477000
24	H	-1.6558280	-2.4700390	1.0182140

5.3.14. 2-Methoxy-5-nitro-3-thien-2-ylbenzaldehyde (31b)



Optimized at the B3LYP/6-311G* level of theory.

E -1216.665646 Hartree

E_{ZPE} -1216.474780 HartreePoint Group C₁Table V.24. Atom Coordinates of **31b** after DFT Optimization.

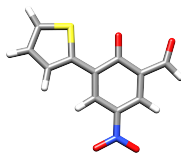
Coordinates				
Atom Count	Symbol	X	Y	Z
1	C	0.1112410	1.0885650	-0.0450700
2	C	-0.3713990	-0.2388840	-0.0031750
3	C	0.5703160	-1.2721930	-0.0008940
4	C	1.9320480	-0.9857900	-0.0261300

Continued on next page

Continued from previous page

Atom Count	Symbol	X	Y	Z
5	C	2.4098970	0.3110410	-0.0824340
6	C	1.4885360	1.3608740	-0.0924660
7	C	-1.8020570	-0.5706870	0.0393910
8	O	-0.7681080	2.1353980	-0.0827620
9	C	1.9882530	2.7620200	-0.1534710
10	O	3.1641490	3.0498430	-0.1437940
11	S	-3.0217230	0.3009920	-0.8678880
12	C	-4.2610360	-0.7804380	-0.3321260
13	C	-3.7730260	-1.7471010	0.5018640
14	C	-2.3717870	-1.6291060	0.7087490
15	C	-1.3144270	2.5253690	1.1901430
16	N	2.8946110	-2.1116830	-0.0178910
17	O	4.0846000	-1.8400250	-0.0907920
18	O	2.4391360	-3.2461170	0.0657320
19	H	0.2487140	-2.3046760	-0.0057160
20	H	3.4706120	0.5222150	-0.1206400
21	H	1.2134800	3.5451680	-0.2154110
22	H	-5.2810000	-0.6298150	-0.6560520
23	H	-4.3890400	-2.5121700	0.9573390
24	H	-1.7987620	1.6797990	1.6849140
25	H	-0.5239610	2.9284380	1.8310500
26	H	-2.0512590	3.2969310	0.9775590
27	H	-1.8010620	-2.2947830	1.3450260

5.3.15. 2-Formyl-4-nitro-6-(thien-2-yl)phenolate (31c)

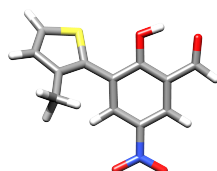


Optimized at the B3LYP/6-311G* level of theory.

E -1176.854414 Hartree
 E_{ZPE} -1176.704982 Hartree
 Point Group C₁

Table V.25. Atom Coordinates of **31c** after DFT Optimization.

Coordinates				
Atom Count	Symbol	X	Y	Z
1	C	0.0142185	1.2482658	-0.0006625
2	C	-0.3756328	-0.1791707	0.0055469
3	C	0.5899358	-1.1607120	-0.0133619
4	C	1.9652327	-0.8453694	-0.0087074
5	C	2.3787807	0.4863358	0.0111462
6	C	1.4578333	1.5230139	0.0191108
7	C	-1.7957474	-0.5313502	0.0242126
8	O	-0.8498748	2.1365714	-0.0260722
9	C	2.0175789	2.8770135	0.0432246
10	O	1.4426566	3.9478763	0.0591934
11	S	-3.0763612	0.6721551	-0.0970699
12	C	-4.3022164	-0.5554770	-0.0258655
13	C	-3.7685701	-1.8101909	0.0954353
14	C	-2.3503973	-1.7935357	0.1252828
15	N	2.9365796	-1.8951615	-0.0265961
16	O	4.1441959	-1.5992031	-0.0242806
17	O	2.5430915	-3.0743794	-0.0430769
18	H	0.3221727	-2.2086362	-0.0352694
19	H	3.4418609	0.7020446	0.0184801
20	H	3.1370033	2.8667159	0.0493870
21	H	-5.3476657	-0.2794250	-0.0625626
22	H	-4.3602008	-2.7165172	0.1670247
23	H	-1.7540973	-2.6923923	0.2239502

5.3.16. 2-Hydroxy-5-nitro-3-(3-methylthien-2-yl)benzaldehyde (**32a**)

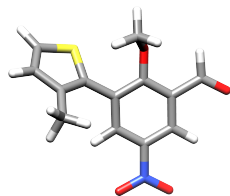
Optimized at the B3LYP/6-311+G* level of theory.

E -1216.696000 Hartree
 E_{ZPE} -1216.504138 Hartree
 Point Group C₁

Table V.26. Atom Coordinates of **32a** after DFT Optimization.

Coordinates				
Atom Count	Symbol	X	Y	Z
1	C	0.3052056	1.3368336	0.1284713
2	C	-0.2677522	0.0495142	-0.0402247
3	C	0.5989517	-1.0278890	-0.2036157
4	C	1.9858171	-0.8598292	-0.1707899
5	C	2.5545994	0.3871030	-0.0009146
6	C	1.7179457	1.4975465	0.1466345
7	C	-1.7205217	-0.1752662	-0.0308837
8	O	-0.5122148	2.3775951	0.2740974
9	C	2.3128274	2.8196516	0.3268381
10	O	1.6695880	3.8531165	0.4648079
11	S	-2.8128792	0.8079852	-0.9865204
12	C	-4.1633523	-0.1579353	-0.5172925
13	C	-3.8002413	-1.1587383	0.3360556
14	C	-2.4010999	-1.1849084	0.6218070
15	C	-1.7928443	-2.1982831	1.5537510
16	H	0.0195864	3.1988534	0.3780711
17	N	2.8556866	-2.0348911	-0.3342434
18	O	4.0680304	-1.8511257	-0.3273992
19	O	2.3177446	-3.1286807	-0.4639808
20	H	0.1998352	-2.0181367	-0.3718269
21	H	3.6322997	0.4969004	0.0137521
22	H	3.4172835	2.8575948	0.3344455
23	H	-5.1516326	0.0823040	-0.8825914
24	H	-4.5051167	-1.8609579	0.7655797
25	H	-0.8514874	-1.8511832	1.9833423
26	H	-2.4758598	-2.4156431	2.3786259
27	H	-1.5910445	-3.1472958	1.0454113

5.3.17. 2-Methoxy-5-nitro-3-(3-methylthien-2-yl)benzaldehyde (32b)



Optimized at the B3LYP/6-311G* level of theory.

E -1255.994653 Hartree
 E_{ZPE} -1255.775889 Hartree
 Point Group C₁

Table V.27. Atom Coordinates of **32b** after DFT Optimization.

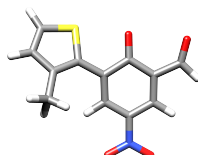
Coordinates				
Atom Count	Symbol	X	Y	Z
1	C	-0.3027723	-1.2148163	-0.0067346
2	C	0.2742840	0.0736758	-0.0971050
3	C	-0.5864846	1.1702470	-0.1708832
4	C	-1.9670734	0.9884994	-0.1532911
5	C	-2.5381431	-0.2691200	-0.0882754
6	C	-1.6988822	-1.3832803	-0.0137401
7	C	1.7297674	0.2935916	-0.1343416
8	O	0.4796042	-2.3321126	0.0323234
9	C	-2.3077477	-2.7395694	0.0700072
10	O	-3.5032189	-2.9299714	0.1031562
11	S	2.7514393	-0.5794901	-1.2610782
12	C	4.1493500	0.2846172	-0.7267027
13	C	3.8481827	1.1783980	0.2584969
14	C	2.4614285	1.1982079	0.6066763
15	C	1.9108684	2.1015984	1.6764250
16	C	1.2055932	-2.5630027	1.2530849
17	N	-2.8415987	2.1798801	-0.2252694
18	O	-4.0494214	1.9948527	-0.2758031
19	O	-2.3014094	3.2802498	-0.2253901
20	H	-0.1859374	2.1696768	-0.2681407
21	H	-3.6121552	-0.4031490	-0.0892040
22	H	-1.5979395	-3.5832635	0.0983069
23	H	5.1139507	0.0759079	-1.1669857

Continued on next page

Continued from previous page

Atom Count	Symbol	X	Y	Z
24	H	4.5879638	1.8091353	0.7373870
25	H	0.9524177	1.7494785	2.0613653
26	H	2.6061108	2.1707103	2.5170465
27	H	1.7583598	3.1192245	1.3017401
28	H	1.8220902	-1.7019482	1.5190974
29	H	0.5065957	-2.7871368	2.0649368
30	H	1.8420454	-3.4243828	1.0625953

5.3.18. 2-Formyl-4-nitro-6-(3-methylthien-2-yl)phenolate (32c)



Optimized at the B3LYP/6-311G* level of theory.

E -1216.179792 Hartree
 E_{ZPE} -1216.002134 Hartree
 Point Group C₁

Table V.28. Atom Coordinates of **32c** after DFT Optimization.

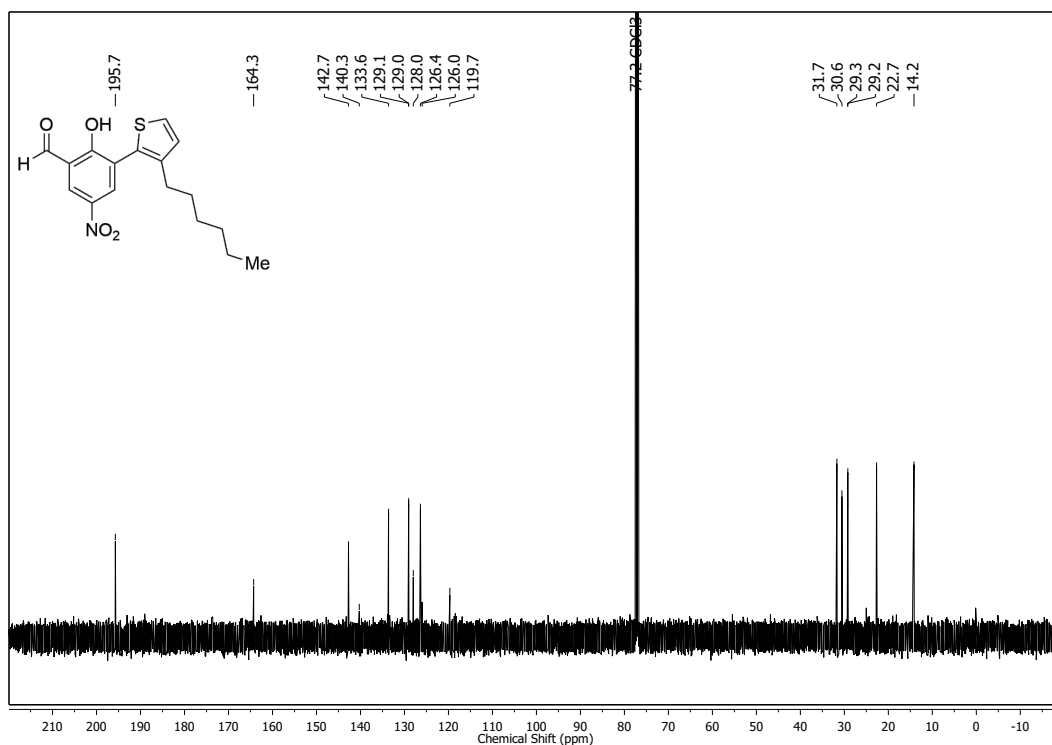
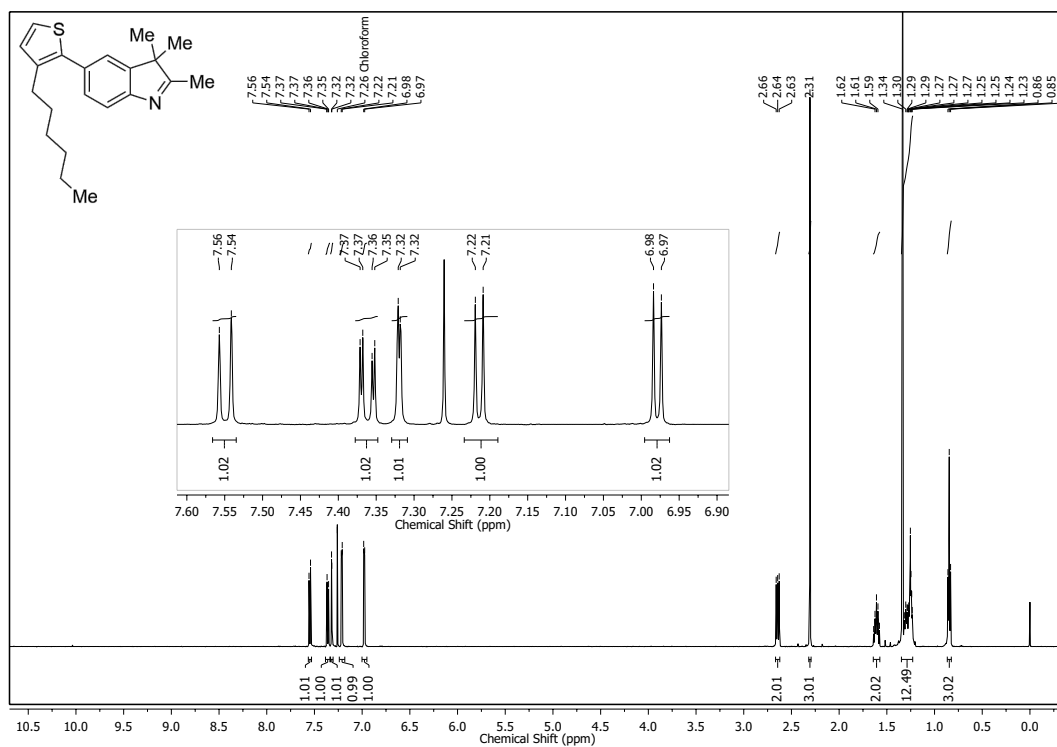
Coordinates				
Atom Count	Symbol	X	Y	Z
1	C	0.2670879	1.4112694	0.0316634
2	C	-0.2838453	0.0346253	-0.0401707
3	C	0.5659071	-1.0393964	-0.1785686
4	C	1.9706970	-0.8842381	-0.1401755
5	C	2.5292494	0.3802836	0.0378678
6	C	1.7308643	1.5099038	0.1405839
7	C	-1.7350893	-0.1581097	-0.0130719
8	O	-0.4787797	2.3970275	-0.0225381
9	C	2.4360113	2.7772979	0.3439072
10	O	1.9834086	3.8964094	0.4900406
11	S	-2.8280445	1.0793454	-0.6296415
12	C	-4.2062777	0.0713962	-0.3532214

Continued on next page

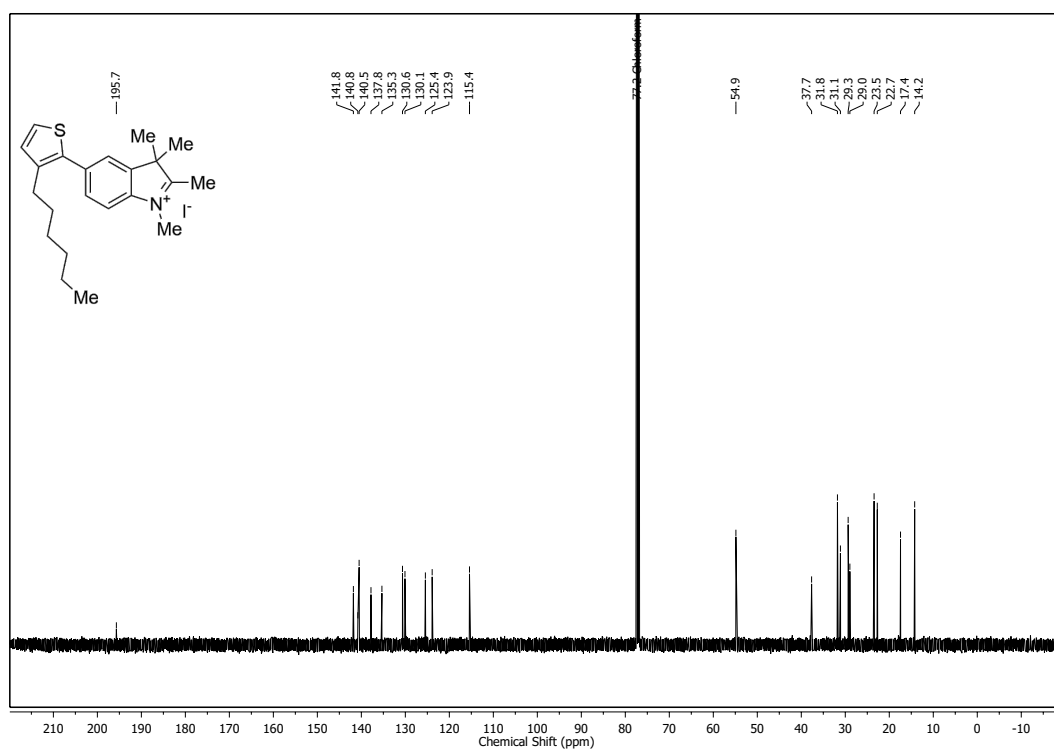
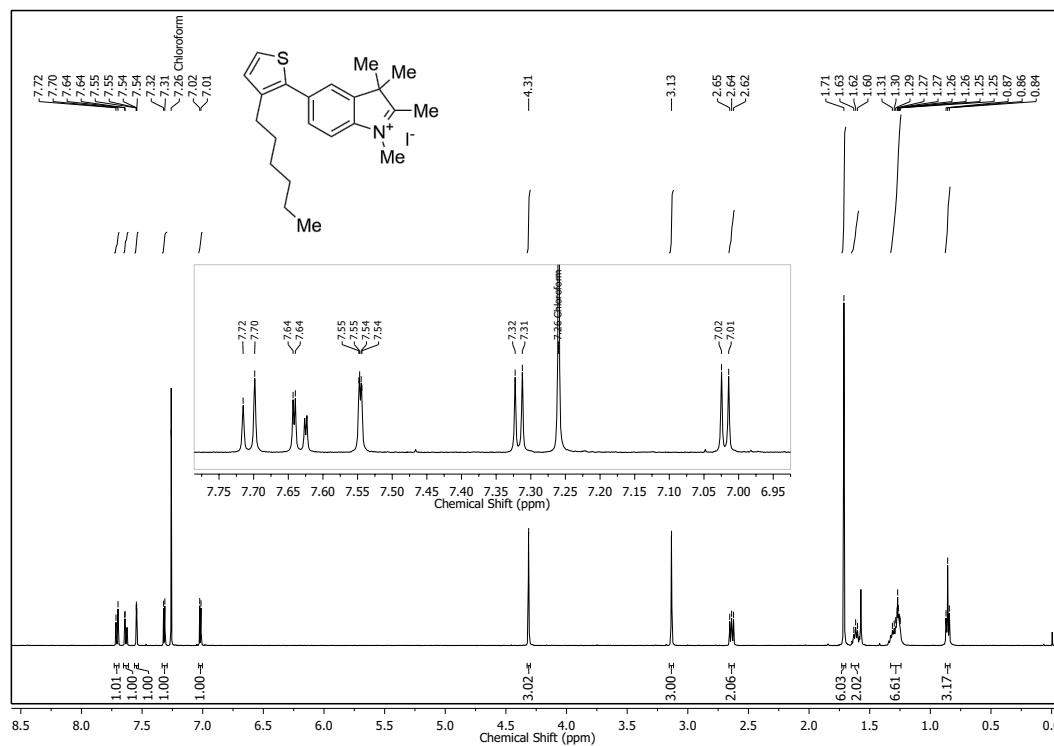
Continued from previous page

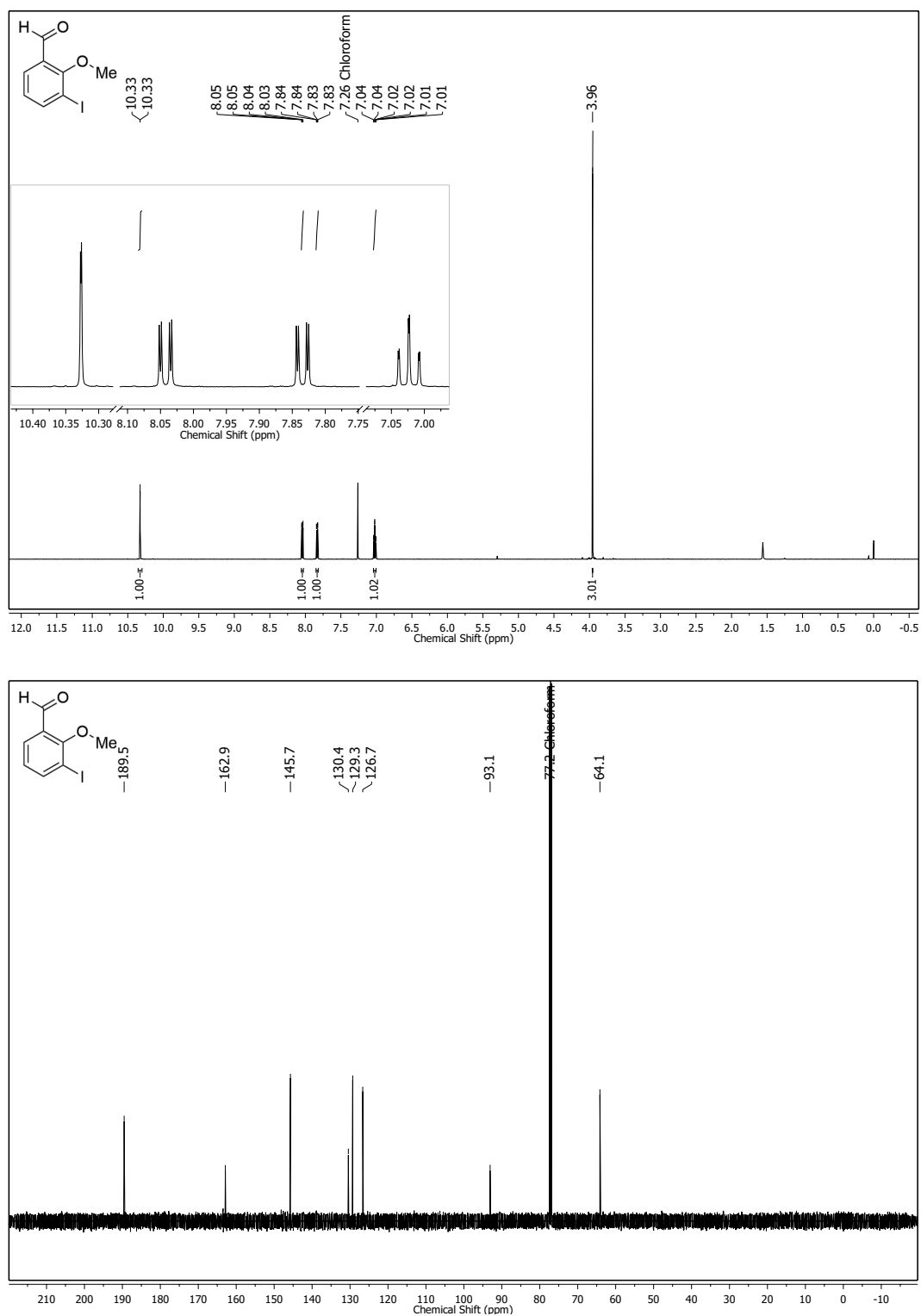
Atom Count	Symbol	X	Y	Z
13	C	-3.8587827	-1.1147333	0.2290524
14	C	-2.4541270	-1.2592144	0.4324784
15	C	-1.8845832	-2.4757143	1.1147281
16	N	2.8146596	-2.0278867	-0.2766792
17	O	4.0489126	-1.8751725	-0.2477791
18	O	2.2890320	-3.1466634	-0.4185453
19	H	0.1816556	-2.0345930	-0.3444418
20	H	3.6092044	0.4712274	0.0898154
21	H	3.5465280	2.6379318	0.3718388
22	H	-5.2005814	0.4342999	-0.5764706
23	H	-4.5771182	-1.8700426	0.5317689
24	H	-0.9920598	-2.2344236	1.6964118
25	H	-2.6251084	-2.9085200	1.7946513
26	H	-1.5996846	-3.2632266	0.4075813

5.4. NMR Spectra

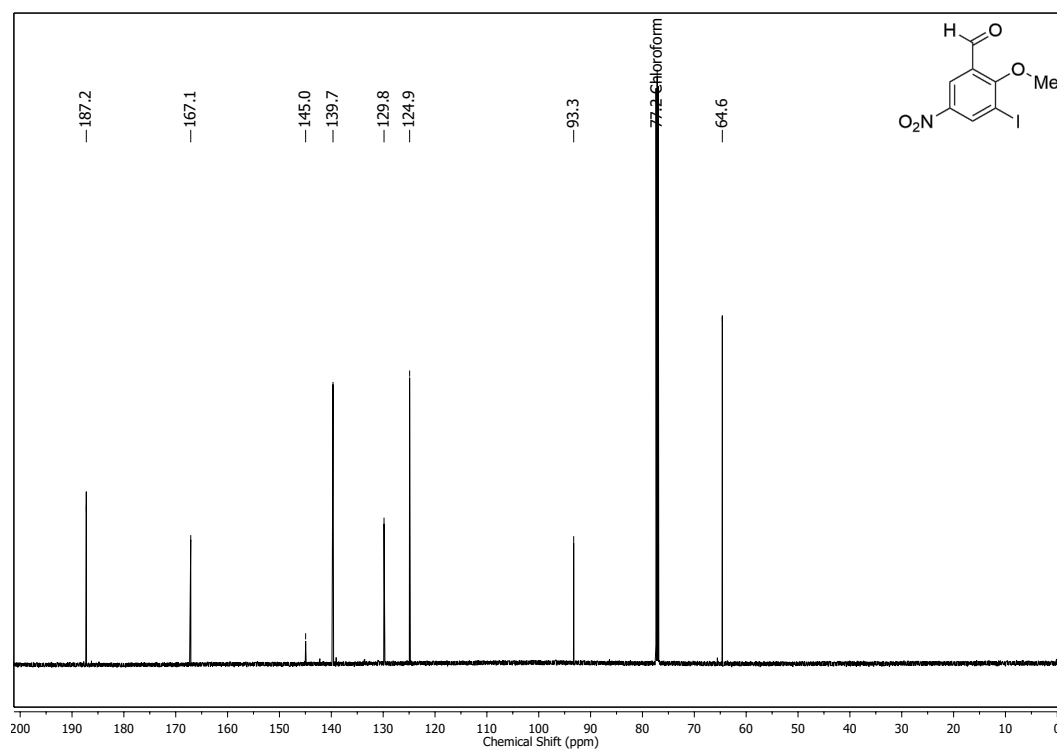
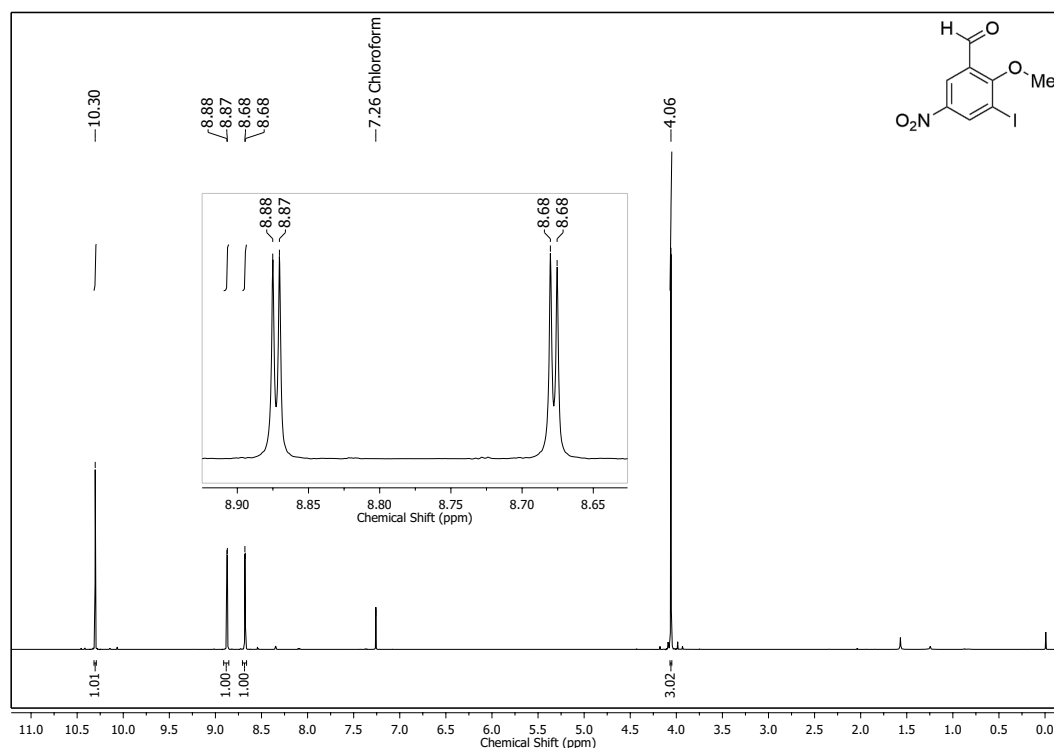
5.4.1. ^1H and $^{13}\text{C}\{^1\text{H}\}$ NMR Spectra of 5-(3-Hexylthien-2-yl)-2,3,3-trimethyl-3*H*-indole (27) in CDCl_3 

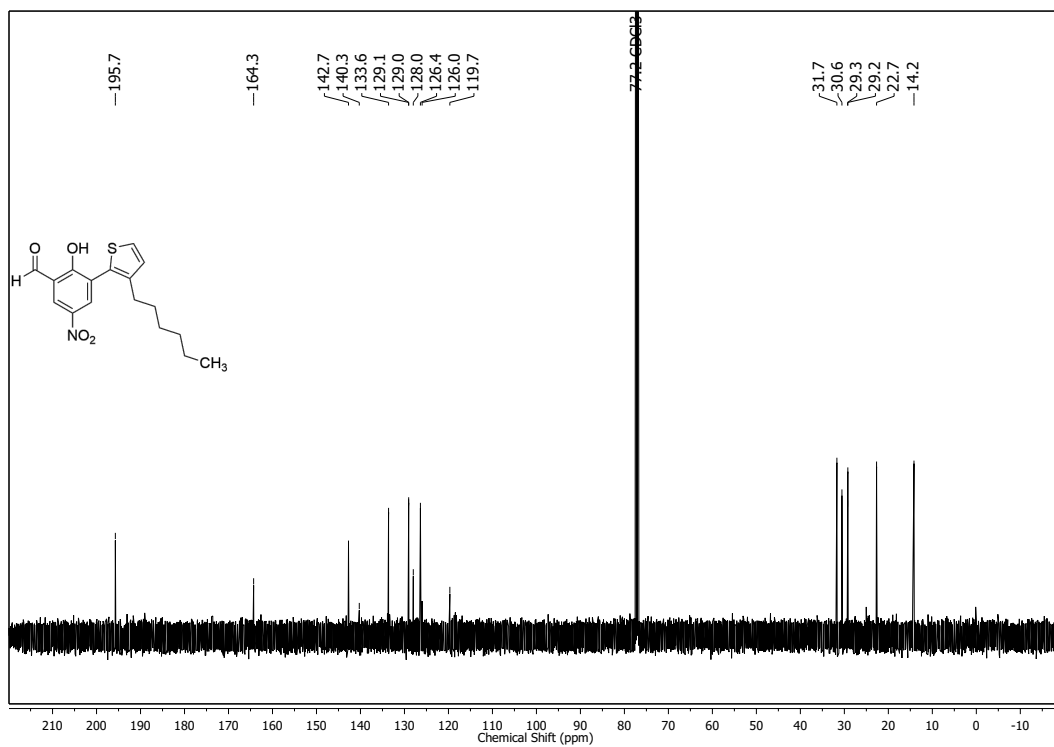
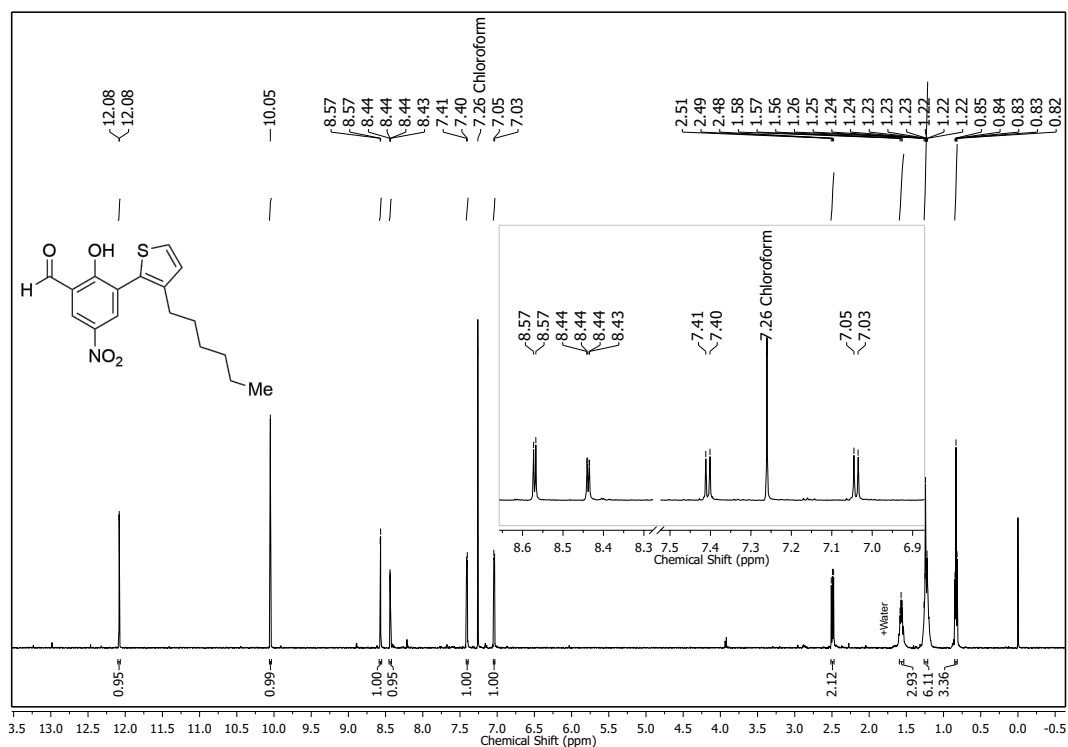
5.4.2. ^1H and $^{13}\text{C}\{^1\text{H}\}$ NMR Spectra of
5-(3-Hexylthienyl)-1,2,3,3-tetramethyl-3*H*-indolium Iodide (28)
in CDCl_3



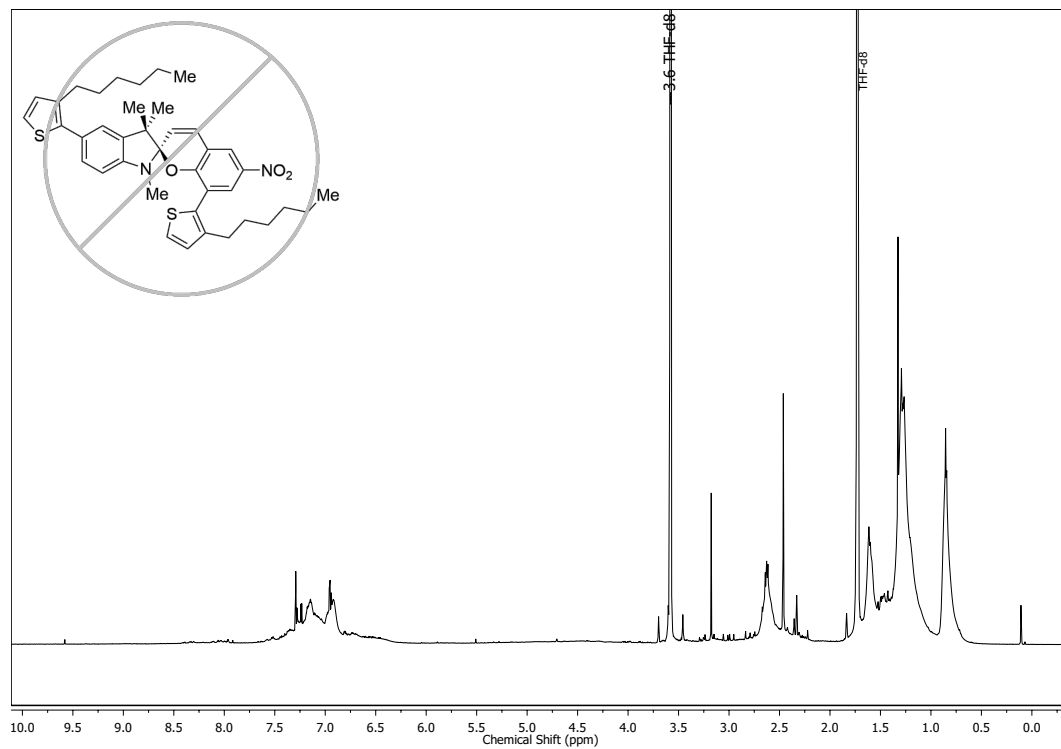
5.4.3. ^1H and $^{13}\text{C}\{^1\text{H}\}$ NMR Spectra of 3-Iodo-2-methoxy-benzaldehyde (24) in CDCl_3 

5.4.4. ^1H and $^{13}\text{C}\{^1\text{H}\}$ NMR Spectra of
3-Iodo-2-methoxy-5-nitro-benzaldehyde (25) in CDCl_3



5.4.5. ^1H and $^{13}\text{C}\{^1\text{H}\}$ NMR Spectra of 3-(3'-Hexylthien-2-yl)-2-hydroxy-5-nitro-benzaldehyde (26) in CDCl_3 

5.4.7. ^1H NMR Spectrum of 5',8-Di(3-hexylthiophen-2-yl)-1',3',3'-trimethyl-6-nitrospiro-[chromene-2,2'-indoline] (19) After Irradiation with UV Light for 50 min in $\text{TFH-}d_8$



6. Azobenzene as Repeating Unit in a Polymer

6.1. Synthesis of an Alternating Poly-(Azobenzene-Trisiloxane) and its Characterization in Solution

Electronic Supplementary Material (ESI) for Journal of Materials Chemistry C.
This journal is © The Royal Society of Chemistry 2019

Electronical Supporting Information

for

Efficient reversible photoisomerisation with large hydrodynamic size-switching of a main-chain poly(azobenzene-trisiloxane)

Mathias Dowds,^{†a,b,c} Dennis Bank,^{†d} Jan Strueben,^a David Presa Soto,^e Frank D. Sönnichsen,^a Falk
Renth,^{*d} Friedrich Temps^{*d} and Anne Staubitz^{*a,b,c}

^a Otto-Diels-Institute for Organic Chemistry, University of Kiel, Otto-Hahn-Platz 4, D-24098 Kiel, Germany.

^b University of Bremen, Institute for Analytical and Organic Chemistry, Leobener Straße 7, D-28359 Bremen, Germany. E-mail: staubitz@uni-bremen.de

^c University of Bremen, MAPEX Center for Materials and Processes, Bibliothekstraße 1, D-28359 Bremen, Germany

^d Institute for Physical Chemistry, University of Kiel, Max-Eyth-Str. 1, D-24098 Kiel, Germany. E-mail: temps@phc.uni-kiel.de

^e Universidad de Oviedo, Facultad de Química, Departamento de Química Orgánica e Inorgánica, Julián Clavería s/n, 33006, Oviedo, Spain.

* corresponding authors

† These authors contributed equally.

Table of Contents

Abbreviations	2
Analytical Equipment and Equipment for Syntheses	2
Reagents	3
Solvents	4
References	5
Synthetic Procedures	6
4,4'-Bis(iodo)azobenzene (S1)	6
4,4'-Bis(trimethylstannyl)azobenzene (1)	6
4,4'-Bis(hydroxydimethylsilane)azobenzene (2)	7
4,4'-Bis(1,1,3,3,3-pentamethyldisiloxanyl)azobenzene (5)	8
Bis(pyrrolidin-1-yl)dimethylsilane (S2)	8
Bis(<i>N</i> -phenyl- <i>N</i> -pyrrolidinecarbonylamino)dimethylsilane (4)	9
Poly(4,4'-azobenzene- <i>alt</i> -hexamethyl-trisiloxane) (6)	9
Investigation of the Switching Behaviour of the Monomers and the Polymer	11
¹ H NMR measurements: PSS and DOSY	11
GPC measurement	12
Femtosecond Transient Electronic Absorption Spectroscopy (TEAS)	13
SVD-based global analysis of the transient electronic absorption data	14
Photostability tests of compound 5 and polymer 6	15
Cyclic UV-Vis measurements of polymer 6	15

Repeated switching cycles of compound 5 by irradiation with 365 nm and 450 nm light monitored by ^1H NMR measurements.....	16
Repeated switching cycles of polymer 6 by irradiation with 365 nm and 450 nm light monitored by ^1H NMR measurements.....	17
Supplementary Plots of UV-VIS Spectra of all Azobenzene Derivatives	18
Plotted ^1H , $^{13}\text{C}\{^1\text{H}\}$ NMR and $^{29}\text{Si}\{^1\text{H}\}$ or $^{119}\text{Sn}\{^1\text{H}\}$ NMR spectra for all compounds	23

Abbreviations

The use of abbreviations follows the conventions from the ACS Style guide.¹ In addition, the following abbreviations are used.

Abbreviation	Long form
at (NMR)	Apparent triplet
DCM	Dichloromethane
dd (NMR)	Doublet of doublets
HMBC	Heteronuclear multiple bond correlation
HSQC	Heteronuclear single quantum coherence
MeTHF	2-Methyltetrahydrofuran
PSS	Photostationary state

Analytical Equipment and Equipment for Syntheses

NMR spectra were either recorded on a Bruker Avance Neo 500 (^1H NMR: 500 MHz) or on a Bruker Avance II HD 600 (^1H NMR: 600 MHz) FT-NMR spectrometer at 298 K. ^1H NMR and $^{13}\text{C}\{^1\text{H}\}$ NMR spectra were referenced using tetramethyl silane (TMS).

The exact assignment of the peaks was performed by two-dimensional NMR spectroscopy such as ^1H COSY, ^1H NOESY, $^1\text{H}/^{13}\text{C}\{^1\text{H}\}$ HSQC, $^1\text{H}/^{13}\text{C}\{^1\text{H}\}$ HMBC and $^1\text{H}/^{29}\text{Si}\{^1\text{H}\}$ HMBC if possible. ^1H DOSY experiments were analysed with the Bruker Topspin 4.03 software to determine the T1/T2 dynamics.

Mass spectrometric measurements were performed in the positive ion collection mode using a JEOL-Accu TOF 4GGCV EI mass spectrometer, or a Thermo Fisher Q Exactive Plus with a quadruple Orbitrap ESI mass spectrometer. Electron ionisation (EI) was performed using an ionization potential of 70 eV. IR spectra were measured using a Perkin Elmer Paragon 1000 FT-IR spectrometer equipped with an A531-G Golden-Gate-ATR-unit.

UV spectra of the compounds 4,4'-bis(iodo)azobenzene, 4,4'-bis(trimethylstannyl)azobenzene and 4,4'-bis(hydroxydimethylsilane)azobenzene were recorded at 25 °C using a Perkin Elmer Lambda 14 UV spectrometer in acetonitrile. Quartz cuvettes with a light path length of 10 mm from Hellma Analytics were used.

Melting points were measured on an electrothermal IA6304 capillary melting point apparatus and are uncorrected.

Elemental analysis was performed on a EURO EA elemental analyzer by EURO VECTOR Instruments.

Conventional gel permeation chromatography was performed on a Viscotek GPC max VE2001 equipped with a Viscotek VE3580 RI detector and a column set of LT5000 and LT4000 in THF (VWR,

HPLC-grade) with a flow rate of 1 mL/min. Calibration and analysis was done with OmniSEC 4.6.2 software using polystyrene standards. Origin 2016 was used for plotting the chromatograms.

The irradiation experiments were carried out using a square array (diameter = 50 mm) of 12 LEDs (365 nm) with an individual optical power of 300 mW or one Luxeon LXML-PR01 LED (450 nm) with an optical power of 900 mW. The irradiation equipment was assembled by Sahlmann Photochemical Solutions. NMR and GPC samples were irradiated for 90 minutes.

Reactions that required inert workup were conducted in a labmaster 130 glove box by MBraun, flushed with nitrogen.

Microwave assisted syntheses were performed on a Biotage Initiator+ SP Wave peptide synthesiser in the organic synthesis mode. The times given in the experimental procedures include the heating time to reach the given temperature.

The cooling of inert syntheses was achieved by using a cooling block connected to a Julabo FP88 cryostat inside the glove box.

Viscosities were determined at 298 K using a capillary viscometer ("Ostwald viscometer") with a capillary diameter of $d = 0.3$ mm and capillary constant of approx. $K = 6.25 \cdot 10^{-9} \text{ m}^2/\text{s}^2$ by SI Analytics. The capillary constant was determined by reference measurements with water at 20 °C.

Reagents

If not noted otherwise, all reagents were used as received. Hydrochloric acid solutions were prepared by diluting the concentrated acid.

Reagent	Supplier	Purity or concentration	Notes
[Pd(PPh ₃) ₄]	Aldrich	99%	
4-Iodoaniline	Acros	98%	
Copper (I) bromide	Sigma-Aldrich	98%	
Dichlorodimethylsilane	Acros	99%	Distilled from CaH ₂ and degassed before use
Hexamethyldistannane	Acros	99%	
Hydrochloric acid	Grüssing	37.5%	
Magnesium sulphate	Grüssing		
Methyl lithium	Acros	3% in MeTHF / Cumol	Exact concentration was determined by titration against menthol and 1,10-phenanthroline as indicator. ²
Monopotassium phosphate	Merck	Extra pure	
Phenyl isocyanate	Alfa Aesar	>98%	Degassed before use
Pyridine	Grüssing	99.5%	
Pyrrolidine	Alfa Aesar	99%	Degassed before use
Sodium hydroxide	Grüssing	99%	

Solvents

All solvents that were purchased in technical grade were purified by distillation prior to use. Solvents of purities higher than 99% were not purified further. Some solvents were degassed by three freeze-pump-thaw cycles, then the flask was again filled with nitrogen and the solvent stored over molecular sieves with the pore size 3 Å.

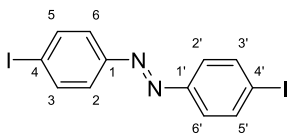
The following solvents were dried in a solvent purification system PS-MD-5 by Innovative Technology: dichloromethane, tetrahydrofuran.

Solvent	Supplier	Purity	Drying procedure	Degassed
Acetonitrile	Sigma-Aldrich	>99.9%, HPLC grade	none	No
Benzene-<i>d</i>₆	Deutero	99.5% D	Distilled from CaH ₂ , stored over molecular sieve 3 Å	Yes
Chlorobenzene	Acros	99.9%, HPLC grade	Distilled from CaH ₂ , stored over molecular sieve 3 Å	Yes
Chloroform	VWR	Techn. grade	none	No
Chloroform-<i>d</i>	Euriso-top	99.8% D	none	No
Dichloromethane	VWR	HPLC grade	PS-MD-5	Yes
Dichloromethane	BCD	Techn. grade	none	No
Dichloromethane-<i>d</i>₂	Deutero	99.6% D	none	No
Diethyl ether	Alfa-Aesar	Spectrophotometric grade, >99%, inhibitor free	Molecular sieve 3 Å	Yes
Diethyl ether	BCD	Techn. grade	none	No
Ethanol	CMP Walther	Techn. grade, denatured with benzene	none	No
<i>n</i>-Hexane	CMP Walther	Techn. grade	none	No
<i>n</i>-Hexane	CMP Walther	Techn. grade	Distilled from CaH ₂ , stored over molecular sieve 3 Å	Yes
Methanol	Acros	99.8%, anhydrous, stored over molecular sieve 3 Å		No
<i>n</i>-Pentane	CMP Walther	Techn. grade	none	No
Tetrahydrofuran	VWR	HPLC grade	PS-MD-5, followed by distillation from Na	Yes
Toluene	Acros	99.85%, Extra dry, stored over molecular sieves	none	Yes
Water (for viscosity measurements)	Honeywell	Chromasolv™ Plus, HPLC grade	none	No

References

- 1 A. M. Coghill and L. R. Garson, Eds., *The ACS Style Guide: Effective Communication of Scientific Information*, American Chemical Society, Washington, DC, 3rd edn., 2006.
- 2 H.-S. Lin and L. A. Paquette, *Synth. Commun.*, 1994, **24**, 2503–2506.
- 3 J. Strueben, P. J. Gates and A. Staubitz, *J. Org. Chem.*, 2014, **79**, 1719–1728.
- 4 G. M. K. Hughes and B. C. Saunders, *J. Chem. Soc. Resumed*, 1954, **0**, 4630–4634.
- 5 J. Strüben, J. Hoffmann, D. Presa-Soto, C. Näther and A. Staubitz, *Acta Crystallogr. Sect. E Crystallogr. Commun.*, 2016, **72**, 1590–1594.
- 6 V. Passarelli, F. Benetollo, P. Zanella, G. Carta and G. Rossetto, *Dalton Trans.*, 2003, 1411–1418.
- 7 P. R. Dvornic and R. W. Lenz, *J. Appl. Polym. Sci.*, 1980, **25**, 641–652.
- 8 K. Röttger, S. Wang, F. Renth, J. Bahrenburg and F. Temps, *Appl. Phys. B Lasers Opt.*, 2015, **118**, 185–193.
- 9 S. Wang, S. Schatz, M. C. Stuhldreier, H. Böhnke, J. Wiese, C. Schröder, T. Raeker, B. Hartke, J. K. Keppler, K. Schwarz, F. Renth and F. Temps, *Phys. Chem. Chem. Phys.*, 2017, **19**, 30683–30694.
- 10 F. Renth, M. Foca, A. Petter and F. Temps, *Chem. Phys. Lett.*, 2006, **428**, 62–67.
- 11 F. Renth, R. Siewertsen, F. Strübe, J. Mattay and F. Temps, *Phys. Chem. Chem. Phys.*, 2014, **16**, 19556–19563.
- 12 I. H. M. Van Stokkum, D. S. Larsen and R. Van Grondelle, *Biochim. Biophys. Acta*, 2004, **1657**, 82–104.
- 13 E. R. Henry and J. Hofrichter, in *Essential Numerical Computer Methods*, ed. M. Johnson, 1st edn., 2010, pp. 81–139.

Synthetic Procedures

4,4'-Bis(iodo)azobenzene (**S1**)

This compound has been synthesised before,³ the procedure was optimised as follows:

CuBr (7.24 g, 45.7 mmol) was dissolved in pyridine (90 mL), and stirred for 30 min, before the precipitate was removed by filtration. The filtrate was diluted with pyridine (20 mL). 4-Iodoaniline (14.3 g, 65.3 mmol) was added in one portion and the mixture was stirred for 20 h at 24 °C while bubbling air through the solution via a syringe (0.2 bar, 250 L/h, diameter: 1 mm). Hydrochloric acid (2 N, 200 mL) was added to the solution and the aqueous phase was extracted with diethyl ether (1 x 300 mL) and dichloromethane (2 x 200 mL). The combined organic phases were washed with hydrochloric acid (2 N, 2 x 200 mL) and the solvents were removed in vacuo. The crude solid product was purified by washing it with boiling ethanol (300 mL). After drying the product in vacuo, an orange solid was obtained without further purification (9.24 g, 21.3 mmol, 65%, Lit.:³ 61%).

Mp: 237 °C (Lit.:³ 210 °C, Lit.:⁴ 237-238 °C).

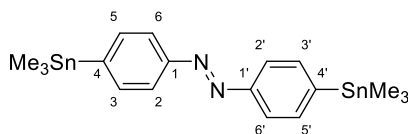
¹H NMR (500 MHz, CDCl₃): δ = 7.87 (d, ³J = 8.7 Hz, 4H, H-3,3',5,5'), 7.64 (d, ³J = 8.7 Hz, 4H, H-2,2',6,6')

¹³C{¹H} NMR (126 MHz, CDCl₃): δ = 151.9 (C-1,1'), 138.6 (C-3,3',5,5'), 124.7 (C-2,2',6,6'), 98.3 (C-4,4')

IR (ATR): $\tilde{\nu}$ = 3079 (w), 1575 (m), 1561 (m), 1470 (m), 1393 (s), 1297 (s), 1280 (s), 1156 (m), 1097 (s), 1051 (s), 1002 (s), 833 (vs), 811 (vs), 714 (vs), 539 (vs), 525 (vs) cm⁻¹.

HRMS (EI-TOF) *m/z* (%): [M]⁺ calcd. for [C₁₂H₈N₂I₂]⁺ 433.8777, found 433.8767 (60), 230.94 (100) [M-C₆H₄I]⁺, 202.93 (100) [M-C₆H₄IN₂]⁺.

UV-VIS (acetonitrile, 25 °C): *E* isomer: $\lambda_{\pi-\pi^*}$ = 350 nm, $\lambda_{\nu-\pi^*}$ = 443 nm; PSS (365 nm): $\lambda_{\pi-\pi^*}$ = 301 nm, $\lambda_{\nu-\pi^*}$ = 442 nm; thermal half-life time *Z*→*E*: 65.5 ± 0.5 h.

4,4'-Bis(trimethylstannyl)azobenzene (**1**)

This compound has been before,³ the procedure was optimised as follows:

Under a nitrogen atmosphere, 4,4''-bis(iodo-)azobenzene (**S1**, 1.30 g, 3.00 mmol), hexamethyldistannane (2.29 g, 7.00 mmol) and [Pd(PPh₃)₄] (139 mg, 120 μ mol, 4 mol%) were dissolved in toluene (18 mL) and THF (2 mL) in a microwave reaction vessel. The reaction mixture was heated for 30 min to 170 °C. Five such reaction batches were combined for the work-up. Then, the solvent was removed under reduced pressure followed by purification by column chromatography (eluent: *n*-pentane, R_f = 0.65). The product was obtained as orange solid (7.23 g, 14.3 mmol, 95%, Lit.:³ 81%).

Mp: 54 °C (Lit.:³ 54 °C).

^1H NMR (500 MHz, CDCl_3): δ = 7.87 (d, 3J = 8.2 Hz, 4 H, H-3,3',5,5'), 7.65 (d, 3J = 8.2 Hz, 4 H, H-2,2',6,6'), 0.34 (s, 18 H, $\text{Sn}(\text{CH}_3)_3$) ppm.

$^{13}\text{C}\{^1\text{H}\}$ NMR (126 MHz, CDCl_3): δ = 152.9 (C-4,4'), 147.2 (C-1, 1'), 136.6 (C-2,2',6, 6'), 122.1 (C-3,3',5,5'), -9.3 ($\text{Sn}(\text{CH}_3)_3$) ppm.

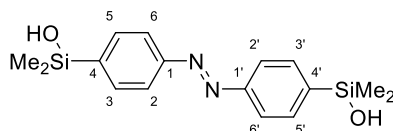
$^{119}\text{Sn}\{^1\text{H}\}$ NMR (187 MHz, CDCl_3): δ = -25.03 ppm.

IR (ATR): $\tilde{\nu}$ = 3067 (w), 3024 (w), 2987 (w), 2917 (w), 1925 (w), 1437 (m), 1383 (m), 1306 (m), 1067 (m), 1011 (m), 831 (s), 761 (s), 583 (s), 508 (s) cm^{-1} .

HRMS (ESI-FTMS) m/z : $[\text{M}+\text{H}]^+$ calcd. for $[\text{C}_{18}\text{H}_{26}\text{N}_2\text{Sn}_2+\text{H}]^+$ 511.0213, found 511.0227.

UV-VIS (acetonitrile, 25 °C): *E* isomer: $\lambda_{\pi-\pi^*}$ = 334 nm, $\lambda_{\nu-\pi^*}$ = 443 nm; PSS (365 nm): $\lambda_{\pi-\pi^*}$ = 289 nm, $\lambda_{\nu-\pi^*}$ = 447 nm; thermal half-life time $Z \rightarrow E$: 48.7 ± 1.2 h.

4,4'-Bis(hydroxydimethylsilane)azobenzene (**2**)



This compound has been synthesised before,⁵ the procedure was optimised as follows:

Under argon atmosphere, 4,4'-bis(trimethylstannyl)-azobenzene (**1**, 3.00 g, 5.91 mmol) was dissolved in dry THF (70 mL). Methyl lithium (20 mL) was added at -78 °C. The orange solution turned dark and was stirred 15 min. Then, dichlorodimethylsilane (24 mL, 25.7 g, 199 mmol) was added. The reaction was allowed to warm to 25 °C by removing the cooling bath. The solvent and the excess of dichlorodi-methylsilane were removed *in vacuo*. The residual orange solid was dissolved in THF (40 mL) and added (rate: 1 mL/min) to a solution of sodium methoxide in methanol (13.5 mL of 4.5 N solution, diluted with 20 mL MeOH). Inert conditions were maintained until this point. The mixture was opened to air and a solution of sodium hydroxide in methanol and water (24 mL, 5 mol/L, MeOH:H₂O 10:1) was added. The resulting mixture was stirred 15 minutes, before a solution of sodium hydroxide in water (24 mL, 5 mol/L) was added. The reaction mixture was stirred 5 h, for all these steps, the temperature was held at 25 °C. This mixture was poured into a vigorously stirred solution of mono potassium phosphate in water (150 mL, 1 mol/L). The resulting solution was extracted with chloroform (4 x 50 mL). The combined organic phases were dried over MgSO_4 and the solvent was removed *in vacuo*. The crude product was purified by solvent diffusion crystallisation: A saturated solution in chloroform was overlaid with *n*-hexane and cooled to -30 °C for 48 h. After three crystallisation cycles, the product was obtained as orange solid (845 mg, 2.56 mmol, 43%, Lit.:⁵ 35%).

Mp.: T = 141 °C, Lit.:⁵ 141 °C.

^1H NMR (500 MHz, CDCl_3): δ = 7.91 (d, 3J = 8.3 Hz, 4 H, H-3,3',5,5'), 7.75 (d, 3J = 8.3 Hz, 4 H, H-2,2',6,6'), 1.99 (s, 1H, OH), 0.46 (s, 12 H, $\text{Si}(\text{CH}_3)_2$) ppm.

$^{13}\text{C}\{^1\text{H}\}$ NMR (126 MHz, CDCl_3): δ = 153.6 (C-1,1'), 143.0 (C-4,4'), 134.0 (C-3,3'), 122.3 (C-2,2'), 0.2 ($\text{Si}(\text{CH}_3)_2$) ppm.

$^{29}\text{Si}\{^1\text{H}\}$ NMR (99 MHz, CDCl_3): δ = 7.77 ppm.

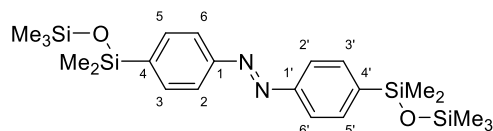
IR (ATR): $\tilde{\nu}$ = 141 (m), 2956 (w), 1385 (m), 1251 (m), 1106 (w), 859 (s), 833 (s), 815 (s), 776 (s), 667 (s), 553 (s), 529 (m), 491 (m) cm^{-1} .

HRMS (EI-TOF) m/z : $[\text{M}]^+$ calcd. for $[\text{C}_{16}\text{H}_{22}\text{N}_2\text{O}_2\text{Si}_2]^+$ 330.12198, found 330.12163 (35), 151.06 (100) $[\text{M}-\text{HOSi}(\text{CH}_3)_2\text{C}_6\text{H}_4\text{N}_2]^+$.

SI-7

UV-VIS (acetonitrile, 25 °C): *E* isomer: $\lambda_{\pi-\pi^*} = 331$ nm, $\lambda_{\nu-\pi^*} = 444$ nm; PSS (365 nm): $\lambda_{\pi-\pi^*} = 291$ nm, $\lambda_{\nu-\pi^*} = 444$ nm; thermal half-life time $Z \rightarrow E$: 34.7 ± 0.3 h.

4,4'-Bis(1,1,3,3,3-pentamethyldisiloxanyl)azobenzene (5)



Compound **2** (100 mg, 303 μ mol) was dissolved in dry DCM (2 mL), deprotonated with triethyl amine (90 μ L, 67 mg, 670 μ mol) and stirred at 0 °C for 1 h, before trimethylsilyl chloride (90 μ L, 75 mg, 670 μ mol) was added and the mixture was stirred at 0 °C for another 2 h. The reaction mixture was diluted with dry *n*-hexane and filtered through celite. After column chromatography (DCM:*n*-hexane 10:90), the product was obtained as orange liquid (102 mg, 216 μ mol, 71%).

^1H NMR (600 MHz, CDCl_3): $\delta = 7.89$ (d, $^3J = 8.2$ Hz, 4 H, H-2,2',6,6'), 7.70 (d, $^3J = 8.2$ Hz, 4 H, H-3,3',5,5'), 0.36 (s, Si-(CH_3)₂, 12 H), 0.11 (s, 18H) ppm.

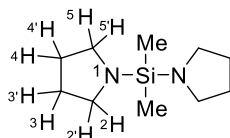
$^{13}\text{C}\{^1\text{H}\}$ NMR (151 MHz, CDCl_3): $\delta = 153.4$ (C-1,1'), 144.1 (C-4,4'), 133.9 (C-3,3',5,5'), 122.1 (C-2,2',6,6'), 2.1 (Si-(CH_3)₃), 1.0 (Si-(CH_3)₂) ppm.

$^{29}\text{Si}\{^1\text{H}\}$ NMR (99 MHz, CDCl_3): $\delta = 9.2$ (Si-(CH_3)₃), -2.6 (Si-(CH_3)₂) ppm.

IR (ATR): $\tilde{\nu} = 3025$ (w), 2957 (m), 2898 (w), 1591 (w), 1387 (w), 1252 (s), 1110 (s), 1043 (vs), 1014 (s), 835 (vs), 798 (vs), 780 (vs), 751 (s), 686 (s), 611 (m), 556 (m), 529 (m) cm^{-1} .

HRMS (EI-TOF) m/z : $[\text{M}]^+$ (%) calcd. for $[\text{C}_{22}\text{H}_{38}\text{N}_2\text{O}_2\text{Si}_4]^+$ 474.20103, found 474.20058 (40), 147.06 (100) $[\text{Si}(\text{CH}_3)_3\text{-O-Si}(\text{CH}_3)_2]^+$.

Bis(pyrrolidin-1-yl)dimethylsilane (S2)



This reaction was performed entirely under nitrogen atmosphere. To a solution of dichlorodimethylsilane (80.0 mL, 85.6 g, 663 mmol) in *n*-hexane (150 mL), pyrrolidine (230 mL, 196 g, 2.76 mol) was added dropwise over the course of 1 h at 0 °C. After completion of the addition, the ice bath was removed and the reaction was stirred for 15 h. A precipitate of the amino hydrochloride, which had formed, was removed by filtration under inert conditions. The liquid was placed in a J. Young's flask and the remaining solvent was removed *in vacuo*. A colourless liquid (116 g, 585 mmol, 88%, Lit.:⁶ 95%) was obtained.

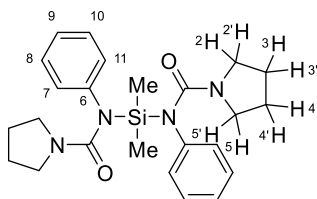
^1H NMR (500 MHz, CDCl_3): $\delta = 2.93 - 2.88$ (m, 8 H, H-2,2',5,5'), 1.67 - 1.62 (m, 8 H, H-3,3',4,4'), 0.04 (s, 6 H, Si- CH_3) ppm.

$^{13}\text{C}\{^1\text{H}\}$ NMR (126 MHz, CDCl_3): $\delta = 46.8$ (C-2,5), 26.9 (C-3,4), -3.3 (Si- CH_3) ppm

$^{29}\text{Si}\{^1\text{H}\}$ NMR (187 MHz, CDCl_3): $\delta = -8.11$ ppm.

HRMS (ESI-FTMS): m/z : $[\text{M}+\text{H}]^+$ calcd. for $[\text{C}_{10}\text{H}_{23}\text{N}_2^{28}\text{Si}]^+$ 199.16250; found 199.16255.

Elem. Anal. Calcd. for $\text{C}_{10}\text{H}_{22}\text{N}_2\text{Si}$: C 60.54, H 11.18, N 14.12; found: C 60.61, H 11.27, N 14.27.

Bis(*N*-phenyl-*N*-pyrrolidinecarbonylamino)dimethylsilane (4)

The reaction was performed entirely under inert conditions. Bis(pyrrolidinyl)dimethyl silane (**S2**, 40.0 g, 201 mmol) was dissolved in dry diethyl ether (250 mL) and cooled in an ice bath to 0 °C. Then phenyl isocyanate (45.0 mL, 49.3 g, 410 mmol) was added dropwise at 0 °C over the course of 3 h and the reaction mixture was allowed to warm to 25 °C over the course of 15 h. The white precipitate of bis(*N*-phenyl-*N*'-pyrrolidinyl)dimethylsilane was collected by filtration under inert conditions. The product was washed with dry diethyl ether (20 mL) and dried at 0.05 mbar for 12 h to receive the product as colourless solid (79.6 g, 182 mmol, 91%, Lit.:⁷ 85%).

Mp.: T = 72 °C.

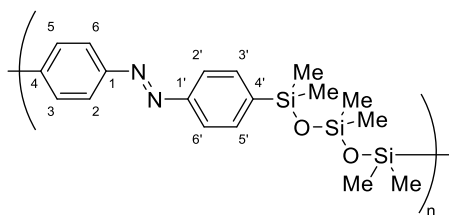
¹H NMR (500 MHz, CDCl₃): δ = 7.20 – 7.15 (m, H-8,10), 7.07 (t, ³J = 7.5 Hz, 2 H, H-9,9'), 6.95 – 6.91 (m, 4 H, H-7,11), 2.88 (m, 8 H, H-2,5), 1.58 (m, 8 H, H-3,4), 0.37 (s, 6 H, Si-CH₃) ppm.

¹³C{¹H} NMR (126 MHz, CDCl₃): δ = 159.7 (C=O), 143.0 (C-6), 128.9 (C-7,11), 128.5 (C-8,10), 125.1 (C-9), 47.7 (C-2,5), 25.4 (C-3,4), -1.5 (Si-CH₃) ppm.

²⁹Si{¹H} NMR (99 MHz, CDCl₃): δ = -3.57 ppm.

HRMS (ESI): Despite inert sample preparation, no traces of the [M+H]⁺ peak could be detected. Instead, the free urea ligand was found: *m/z* (%): [M+H]⁺ calcd. for [C₁₁H₁₄N₂O+H]⁺ 191.11789; found 191.11789 (90); [M+K]⁺ calcd. for [C₁₁H₁₄N₂O+K]⁺ 229.07377; found 229.07381 (100).

Elem. Anal. Calcd. for C₂₅H₃₅N₄O₂Si: C 66.48, H 7.81, N 12.40, O 7.08; found: C 66.60, H 7.90, N 12.56, O 7.13.

Poly(4,4'-azobenzene-*alt*-hexamethyl-trisiloxane) (6)

This reaction was performed in a nitrogen filled glove box. 4,4'-bis(Hydroxydimethylsilane)-azobenzene (**2**, 317 mg, 960 μmol), was dissolved in chlorobenzene (2 mL). A solution of bis(*N*-phenyl-*N*-pyrrolidinecarbonylamino)dimethyl silane (419 mg, 960 μmol) in chlorobenzene (8 mL) was added with a rate of 0.015 mL/min at -45 °C. The solution was stirred for 5 d at 25 °C, while the reaction progress was monitored by GPC. Once the retention volume measured by GPC remained unchanged, the solvent was evaporated and the polymer was purified by dissolving it in THF and precipitation into methanol (10 fold excess) for three times. The product was obtained as orange solid (227 mg, 61%).

¹H NMR (500 MHz, CDCl₃): δ = 7.88 (d, ³J = 8.2 Hz, 4 H, H-2,2'), 7.69 (d, ³J = 8.2 Hz, 4 H, H-3,3'), 0.40 – 0.35 (m, 12 H, C-Si(CH₃)₂-O), 0.11 – 0.07 (m, 6H, O-Si(CH₃)₂-O) ppm.

¹³C{¹H} NMR (126 MHz, CDCl₃): δ = 153.4 (C-1,1'), 143.6 (C-4,4'), 134.0 (C-3,3'), 122.1 (C-2,2'), 1.5 (C-Si(CH₃)₂-O), 0.9 (O-Si(CH₃)₂-O) ppm.

²⁹Si{¹H} NMR (99 MHz, CDCl₃): δ = -2.33 (C-Si(CH₃)₂-O), -18.93 (O-Si(CH₃)₂-O) ppm.

IR (ATR): $\tilde{\nu}$ = 3026 (w), 2958 (m), 1591 (w), 1386 (w), 1257 (s), 1161 (w), 1109 (s), 1030 (vs), 1012 (s), 958 (w), 835 (s), 817 (s), 781 (vs), 720 (m), 702 (m), 686 (m), 665 (m), 623 (m), 555 (s), 528 (m) cm⁻¹.

GPC (THF, 1 mL/min, conv. calibration (PS), ambient light): M_n = 25.9 kDa; M_w = 50.6 kDa; PDI = 1.95.

Investigation of the Switching Behaviour of the Monomers and the Polymer

¹H NMR measurements: PSS and DOSY

Similar to the GPC analysis, the sample solutions were measured directly after dissolving and after irradiation with UV light for 90 minutes (PSS-365). To compare the data with the results from GPC and ultrafast measurements, three different solvents were used: chloroform-*d*, THF-*d*₈ and *n*-hexane-*d*₁₄. In chloroform and THF, the sample concentration was approx. 3 mg/mL. As the polymer tends to form aggregates in *n*-hexane, the sample concentration was reduced to 0.3 mg/mL.

For the analysis of the composition and the diffusion constants, the signals corresponding to the aromatic azobenzene units were used. In all three solvents, the polymer's azo groups were found to be almost quantitatively (min. 98%) in the *E*-form at ambient conditions. In the PSS, the *Z*-isomer was enriched to 50% (*n*-hexane), 58% (THF) and 67% (chloroform). In the "all-*E*-state", the polymer's signals showed negligible line broadening due to the geometric regularity of the adjacent monomers. Upon switching, the local environment of each azobenzene unit varied, leading to significant line broadening. The diffusion constants were obtained using the T1/T2 fitting with the "Topspin 4" software. In the PSS, the diffusion constant and thus the hydrodynamic radii differ significantly from the values before UV irradiation. However, the signals of *E*- and *Z*-azobenzene units show the same diffusion behaviour, indicating an incomplete switching of the azobenzene units in each chain. For plotting, the data were treated with the dosy2d command.

The hydrodynamic radii *r* were calculated using the Stokes-Einstein equation with the diffusion constant *D*, Boltzmann constant *k*_B, Temperature *T* = 298 K and the dynamic viscosity *η*:

$$r = \frac{k_B T}{6\pi\eta D}$$

To determine the dynamic viscosities *η* of the deuterated solvents, a capillary viscometer with a capillary constant *K* = 6.25 10⁻⁹ m²/s^{2a} was used. The solvents' flow time *t* was measured and the viscosities could be calculated by multiplication of the flow time with the capillary constant *K* and the solvents density *ρ*^b:

$$\eta = \rho \times K \times t$$

The calculated radii *r* were used to calculate the corresponding hydrodynamic volumes:

$$V = \frac{4}{3}\pi r^3$$

Table S1 Measured viscosities of the deuterated solvents that were used in ¹H DOSY NMR measurements. Capillary constant *K* = 6.25 10⁻⁹ m²/s². The temperature was 298 K. Flow times are averages of five measurements; the standard deviation for the last counting digit is given in brackets.

Solvent	Density ^c ρ / kg m ⁻³	Flow time t / s	Viscosity η / 10 ⁻⁴ Pa s
Chloroform- <i>d</i>	1500	56.5 (6)	5.30 (5)
THF- <i>d</i> ₈	985	78.6 (7)	4.84 (4)
<i>n</i> -Hexane- <i>d</i> ₁₄	767	62.8 (3)	3.01 (1)

Table S2 Overview of ¹H DOSY NMR results of the disiloxane functionalised azobenzene 5. Under the given irradiation conditions, the diffusion constants were determined for aromatic signals assigned to *E* and *Z* iso-

^a Determined by calibration measurements with water. (20 °C, kinematic viscosity *v* = 10⁻⁶ m²/s).

^b As provided by the supplier.

^c As provided by the supplier.

mers and used to calculate the corresponding hydrodynamic volume via the hydrodynamic radius. The ratio between *E*- and *Z*-azobenzene was determined by integration of the aromatic signals.

No.	Solvent	Irradiation	Diffusion constant / $10^{-10} \text{ m}^2/\text{s}$		Hydrodynamic radius / nm		Hydrodynamic volume / nm^3		<i>E</i> : <i>Z</i> Ratio
			<i>E</i> -Azo	<i>Z</i> -Azo	<i>E</i> -Azo	<i>Z</i> -Azo	<i>E</i> -Azo	<i>Z</i> -Azo	
1	CDCl_3	None	7.77	-	0.530	-	0.625	-	98:2
2	CDCl_3	PSS-365	7.46	8.67	0.552	0.475	0.705	0.450	33:67
3	THF	None	8.52	-	0.529	-	0.620	-	96:4
4	THF	PSS-365	8.65	9.11	0.521	0.495	0.593	0.508	36:64
5	Hexane	None	13.4	-	0.543	-	0.669	-	95:5
6	Hexane	PSS-365	13.6	14.9	0.532	0.486	0.630	0.479	54:46

Table S3 Overview of ^1H DOSY NMR results of the azobenzene-trisiloxane copolymer **6**. Under the given irradiation conditions, the diffusion constants were determined for aromatic signals assigned to *E* and *Z* isomers and used to calculate the corresponding hydrodynamic volume via the hydrodynamic radius. The ratio between *E*- and *Z*-azobenzene was determined by integration of the aromatic signals.

No.	Solvent	Irradiation	Diffusion constant / $10^{-10} \text{ m}^2/\text{s}$		Hydrodynamic radius / nm		Hydrodynamic volume / nm^3		<i>E</i> : <i>Z</i> Ratio
			<i>E</i> -Azo	<i>Z</i> -Azo	<i>E</i> -Azo	<i>Z</i> -Azo	<i>E</i> -Azo	<i>Z</i> -Azo	
1	CDCl_3	None	0.928	-	4.44	-	366	-	98:2
2	CDCl_3	5 min UV	1.02	1.10	4.05	3.75	278	221	60:40
3	CDCl_3	7 min UV	1.03	1.09	4.01	3.78	270	227	47:53
4	CDCl_3	11 min UV	1.03	1.07	4.00	3.86	267	242	36:63
5 ^a	CDCl_3	90 min UV	1.05	1.07	-	3.89	-	246	33:67
6 ^a	CDCl_3	20 min blue	0.979	0.995	-	4.20	-	310	86:14
7	THF	None	1.02	-	4.42	-	363	-	100:0
8 ^a	THF	90 min UV	1.09	1.13	-	4.05	-	279	42:58
9	Hexane	None	2.32	-	3.13	-	128	-	100:0
10 ^a	Hexane	90 min UV	3.64	3.26	-	2.10	-	39	50:50

a) The diffusion rates corresponding to the *E* and *Z* signals in the ^1H NMR spectrum were averaged to calculate the hydrodynamic radius and volume.

GPC measurement

The polymer was dissolved in THF (ca. 1 mg/mL) in a brown-glass GC vial and immediately, the GPC run was performed. Determination of the molecular weights was performed using a refraction index detector by conventional calibration. Linear poly(styrene) with narrow PDI standards were used for calibration. For switching, a stock solution of the polymer was prepared (1 mg/mL) and split into four samples. These samples were measured without irradiation, before the sample solutions were transferred to UV cuvettes and subjected to UV light (365 nm) for 90 minutes, before each sample was measured again. The results were averaged and the standard deviation was derived. The number

average molecular weight (M_n) decreased from 25.9 ± 0.5 to 19.4 ± 0.8 kDa, the weight average molecular weight (M_w) decreases from 50.6 ± 0.8 to 37.2 ± 1.9 kDa (Figure S1).

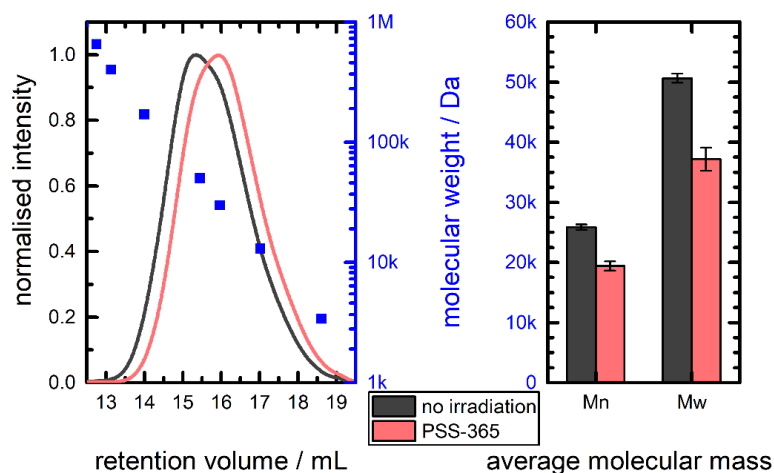


Figure S1 GPC results of switching the polymer **6**. Left: GPC traces (THF, 1 mL/min) of the polymer **6** before (grey) and after (light red) irradiation with UV light (365 nm) for 90 min. The curves are averaged over four measurements and normalised for better clarity. Black squares represent narrow polystyrene standards that were used for the calibration. For the corresponding molecular weight see the right Y-axis. Right: Comparison of the apparent molecular weights of the **6** sample before (grey) and after (light red) irradiation. The number average molecular weight (M_n) decreased from 25.9 ± 0.5 to 19.4 ± 0.8 kDa, the weight average molecular weight (M_w) decreases from 50.6 ± 0.8 to 37.2 ± 1.9 kDa. The error bars indicate the standard deviation

Femtosecond Transient Electronic Absorption Spectroscopy (TEAS)

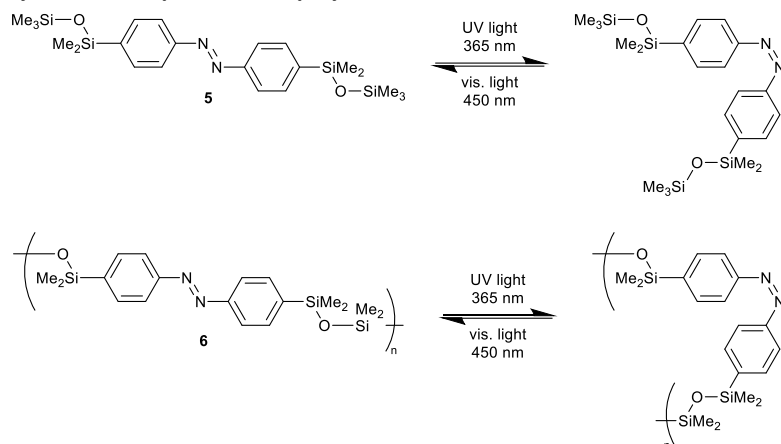
The setup for transient electronic absorption spectroscopy was based on a regeneratively amplified Ti:Sa laser system (Clark MXR CPA 2001) and has been described before.^{8–11} Pulses for the excitation of the azobenzene chromophores at $\lambda_{\text{exc}} = 320$ nm with < 100 fs pulse duration (FWHM) were generated by frequency doubling of compressed 640 nm pulses from a non-collinear optical parametric amplifier. For broadband detection in a range of $\lambda_{\text{probe}} = 325 - 675$ nm, spectrally broad pulses were obtained by supercontinuum generation (SCG) in a 1 mm CaF_2 plate using the 775 nm Ti:Sa laser fundamental, split into probe and reference beams and focused into the sample cell so that the probe and pump beams overlapped spatially. Spectrally resolved detection was done using a prism spectrograph equipped with two fast frame transfer CCD cameras (S7030-0906, Hamamatsu). The molecules were excited with pump energies of 250 nJ/pulse under magic angle conditions, i.e., rotating the relative angle between the polarization of the pump and probe beams to 54.7° using a Berek variable wave plate. All measurements were done at room temperature using solutions with an optical density of ~ 0.3 in *n*-hexane (UVASOL®, purity $> 99\%$) as solvent and pumped through a home-built flow cell with an optical path length of 1 mm to avoid accumulation of the photo product.

SVD-based global analysis of the transient electronic absorption data

The quantitative analysis of the transient electronic absorption data was based on the singular value decomposition (SVD) of the time-zero corrected data matrices,¹² where background and solvent contributions had been subtracted before. The SVD of the pre-processed data matrix D is given by

$$D = USV^T,$$

where the columns of the matrices U and V correspond to orthonormal SVD time traces $U_i(t)$ and SVD spectra $V_i(\lambda)$, and S is a diagonal matrix containing the non-negative singular values s_i in decreasing order.^{12,13} The number of relevant SVD components n , which identifies the number of recoverable spectroscopical species within the experimental errors, was determined using a scree plot of the singular values, by inspection of the SVD time traces and SVD spectra, and by checking the reconstructed reduced transient absorption matrices of rank n versus the input data matrices for remaining systematic deviations. The optimal global decay time constants and corresponding decay-associated difference spectra (DADS) describing the data were then extracted by simultaneous non-linear least-squares fitting to the SVD time profiles using a sum of exponential decay functions convoluted with the instrument response function (IRF) and a convoluted step function corresponding to a decay time of infinity to account for the permanent absorption changes.

Photostability tests of compound **5** and polymer **6**

The concentration of **5** and **6** in the NMR measurements was approximately 0.5 mg/mL, the irradiation times for the alternating irradiation with 365 nm and 450 nm light were three minutes for each cycle.

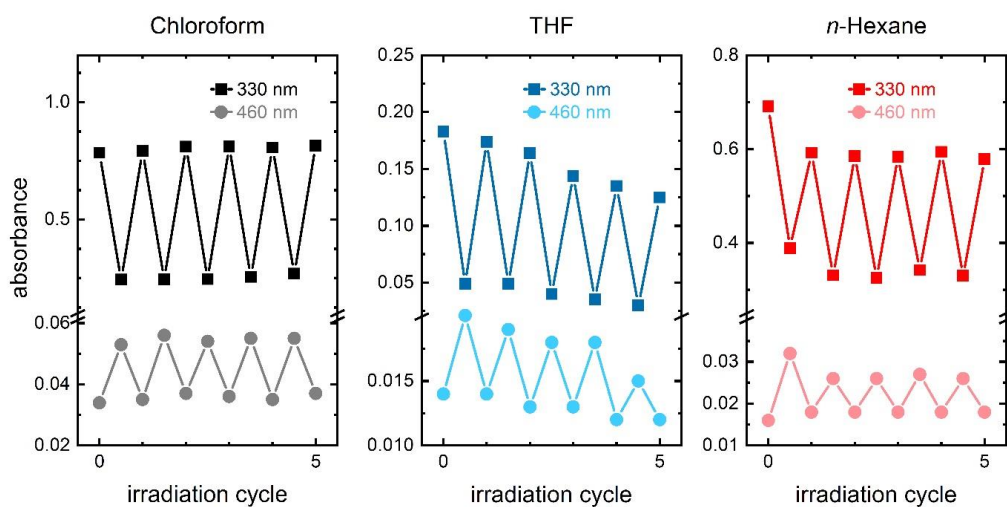
Cyclic UV-Vis measurements of polymer **6**

Figure S2. Photoswitching and photostability of polymer **6** as monitored by UV-VIS spectroscopy. The symbols show the normalised absorbances at 330 nm and 460 nm obtained after alternating irradiation of polymer **6** with 365 nm and 450 nm light into the respective photostationary states in chloroform (left panel, black), THF (center panel, blue) and *n*-hexane (right panel, red). The chosen wavelengths represent the absorption behaviour of the S_2 ($\pi\pi^*$) bands (dark squares) and S_1 ($n\pi^*$) bands (light circles). The first symbol corresponds to the thermal equilibrium, thereafter each cycle consists of two data points representing the PSS_{365} and PSS_{450} , respectively.

Repeated switching cycles of compound **5** by irradiation with 365 nm and 450 nm light monitored by ^1H NMR measurements

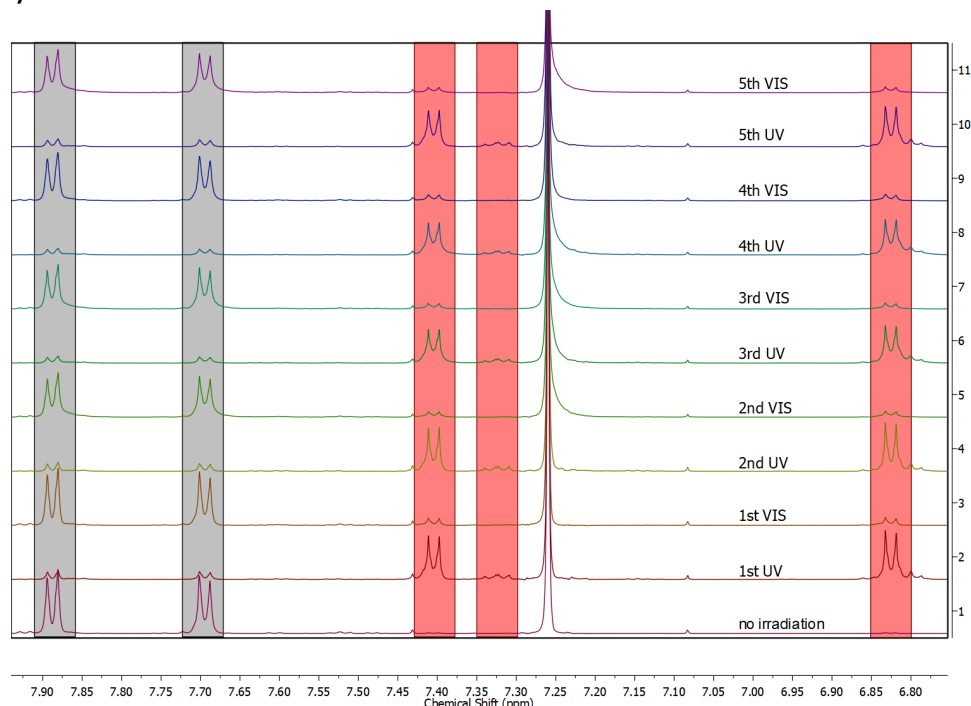


Figure S3. Aromatic region of the ^1H NMR spectra of **5** before and after alternating irradiation into the PSS with 365 nm and 450 nm light. Signals corresponding to *E*-isomers are highlighted in grey, signals of *Z*-isomers are highlighted in pink.

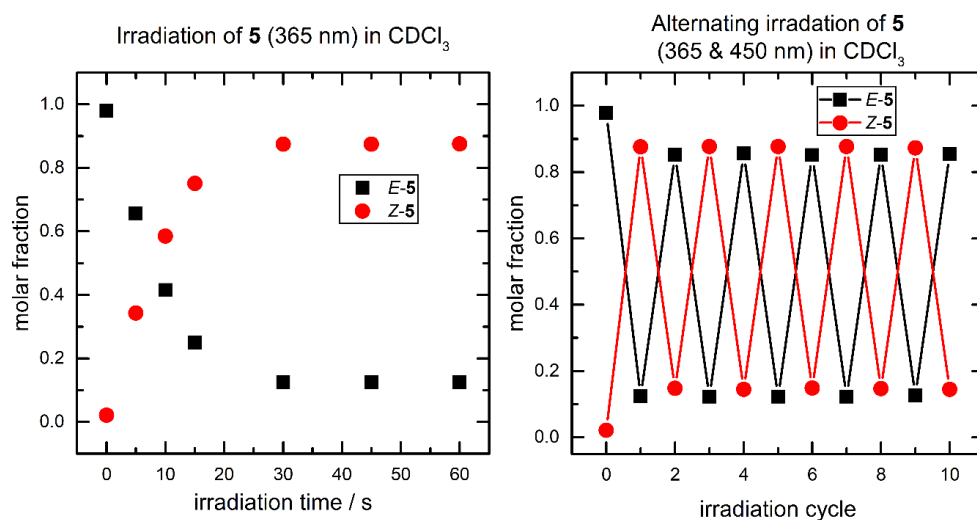


Figure S4. Left: molar fractions of *E*-isomers of **5** (black squares) and *Z*-isomers of **5** (red circles) for a series of consecutive irradiations with 365 nm light in CDCl_3 . Right: molar fractions of *E*-isomers of **5** (black squares) and *Z*-azobenzene units of **5** (red circles) upon alternating irradiation with 365 nm light and 450 nm light.

Repeated switching cycles of polymer **6** by irradiation with 365 nm and 450 nm light monitored by ^1H NMR measurements

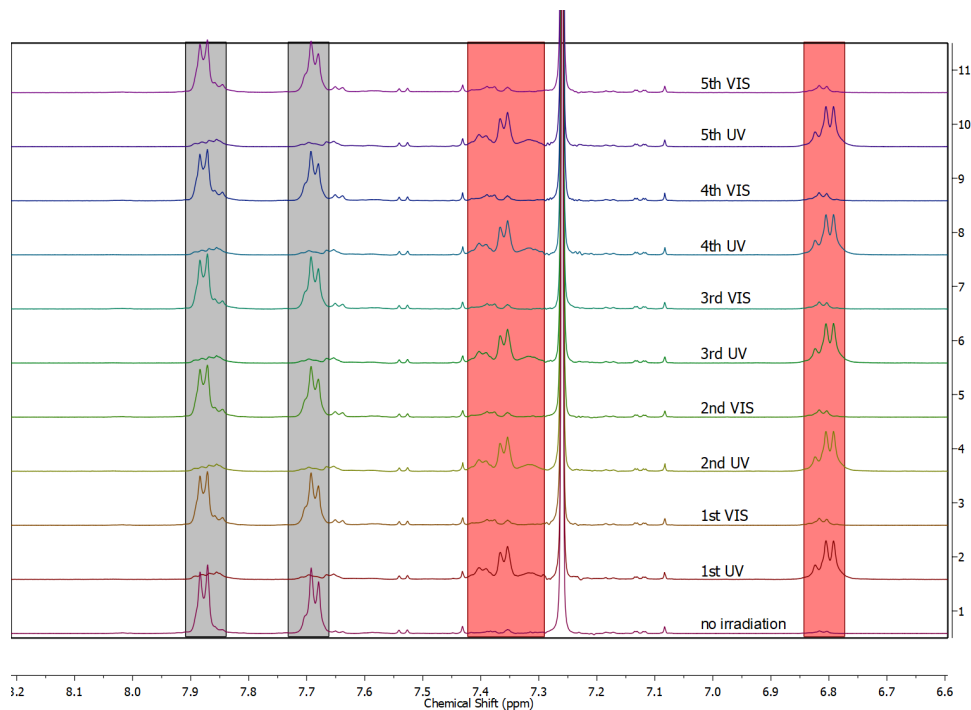


Figure S5. Aromatic region of the ^1H NMR spectra of **6** before and after alternating irradiation into the PSS₃₆₅ and PSS₄₅₀. Signals corresponding to *E*-isomers are highlighted in grey, signals of *Z*-isomers are in pink.

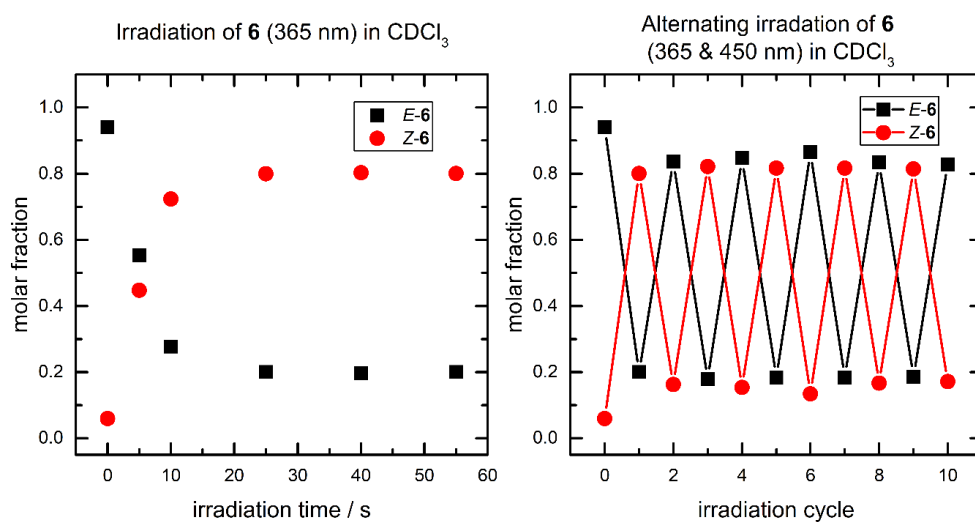


Figure S6. **Left:** molar fractions of *E*-azobenzene units of **6** (black squares) and *Z*-azobenzene units of **6** (red circles) for a series of consecutive irradiations with 365 nm light in CDCl_3 . **Right:** molar fractions of *E*-azobenzene units of **6** (black squares) and *Z*-isomer units of **6** (red circles) upon alternating irradiation (365 nm and 450 nm light).

Supplementary Plots of UV-VIS Spectra of all Azobenzene Derivatives

4,4'-Bis(iodo)azobenzene in acetonitrile

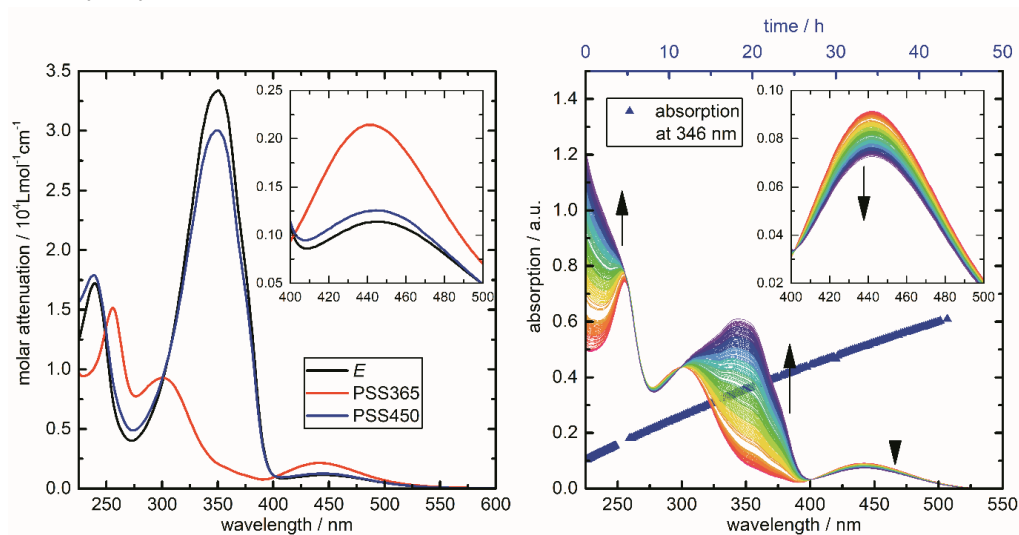


Figure S7. UV-VIS analysis of 4,4'-bis(iodo)azobenzene. Left: absorption spectra of the molecule without irradiation (black), of the PSS after irradiation with UV light (365 nm) (red) and of the PSS after irradiation with blue light (450 nm) (blue). Right: thermal relaxation after irradiation with UV light. Red represents the starting point, violet represents the end point. The spectra were recorded with a delay of 15 min over the course of 44 h. The time profile of the thermal relaxation of the $\pi\pi^*$ band is shown as blue triangles and was used to determine the half-life time via an exponential fit to be 65.5 ± 0.5 h. Arrows indicate the change in absorption of the $n\pi^*$ (<250 nm), $\pi\pi^*$ (ca. 350 nm) and $n\pi^*$ (ca.450 nm) bands.

4,4'-Bis(trimethylstannyl)azobenzene (1) in acetonitrile

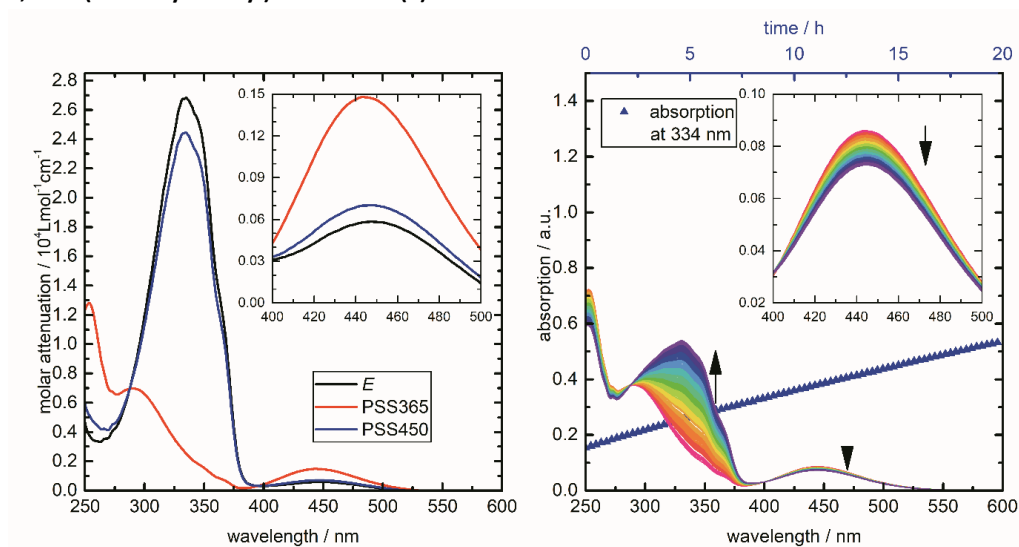


Figure S8. UV-VIS analysis of 4,4'-bis(trimethylstannyl)azobenzene (1). Left: absorption spectra of the molecule without irradiation (black), of the PSS after irradiation with UV light (365 nm) (red) and of the PSS after irradiation with blue light (450 nm) (blue). Right: thermal relaxation after irradiation with UV light. Red represents the starting point, violet represents the end point. The spectra were recorded with a delay of 15 min over the course of 20 h. The time profile of the thermal relaxation of the $\pi\pi^*$ band is shown as blue triangles and was used to determine the half-life time via an exponential fit to be 48.7 ± 1.2 h. Arrows indicate the change in absorption of the $\pi\pi^*$ (ca. 330 nm) and $n\pi^*$ (ca. 450 nm) bands.

4,4'-Bis(hydroxydimethylsilane)azobenzene (2) in acetonitrile

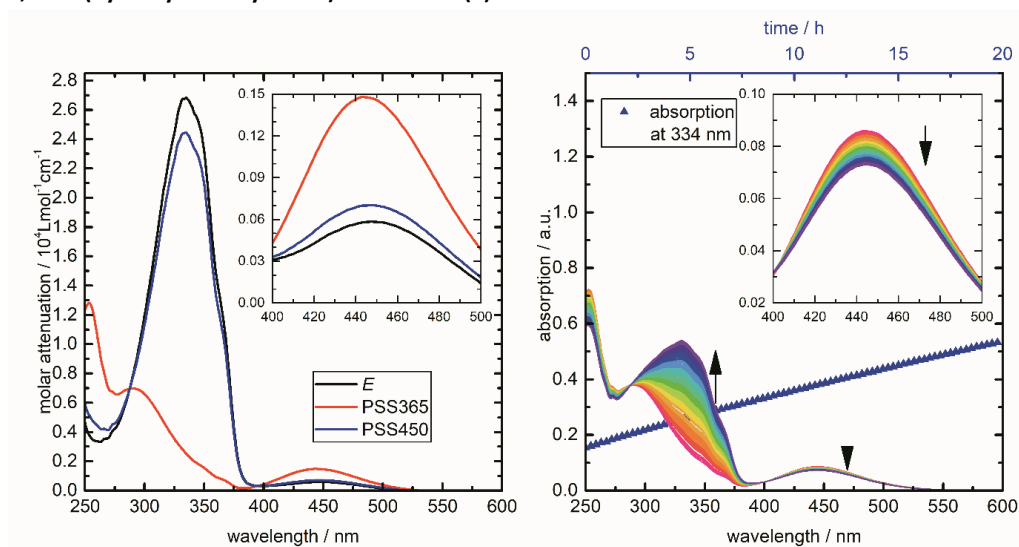


Figure S9. UV-VIS analysis of 4,4'-bis(hydroxydimethylsilane)azobenzene (2). Left: absorption spectra of the molecule without irradiation (black), of the PSS after irradiation with UV light (365 nm) (red) and of the PSS after irradiation with blue light (450 nm) (blue). Right: thermal relaxation after irradiation with UV light. Red represents the starting point, violet represents the end point. The spectra were recorded with a delay of 15 min over the course of 11.5 h. The time profile of the thermal relaxation of the $\pi\pi^*$ band is shown as blue triangles and was used to determine the half-life time via an exponential fit to be 34.7 ± 0.3 h. Arrows indicate the change in absorption of the $\pi\pi^*$ (ca. 330 nm) and $n\pi^*$ (ca. 450 nm) bands.

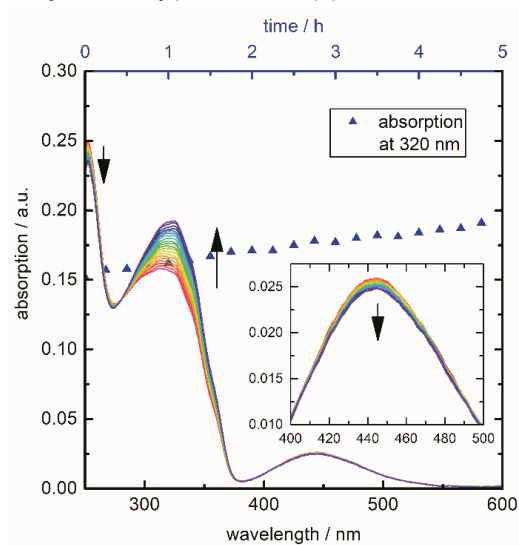
4,4'-Bis(1,1,3,3,3-pentamethyldisiloxanyl)azobenzene (5) in *n*-hexane

Figure S10. UV-VIS analysis of 4,4'-Bis(1,1,3,3,3-pentamethyldisiloxanyl)azobenzene (5) in *n*-hexane. Thermal relaxation after irradiation with UV light. Red represents the starting point, violet represents the end point. The spectra were recorded with a delay of 15 min over the course of 5 h. The time profile of the thermal relaxation of the $\pi\pi$ band is shown as blue triangles and was used to determine the half-life time via an exponential fit to be 15 ± 2 h. Arrows indicate the change in absorption of the $\pi\pi^*$ (ca. 330 nm) and $n\pi^*$ (ca. 450 nm) bands.

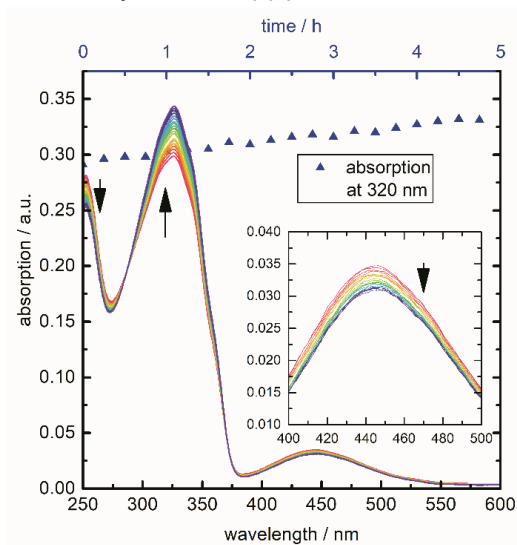
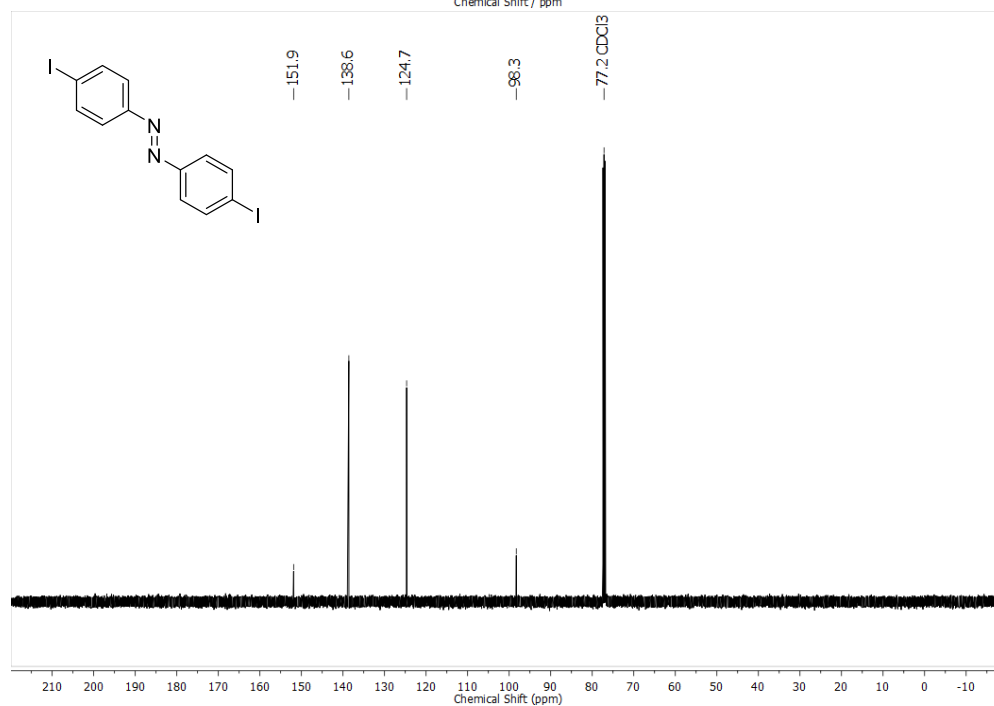
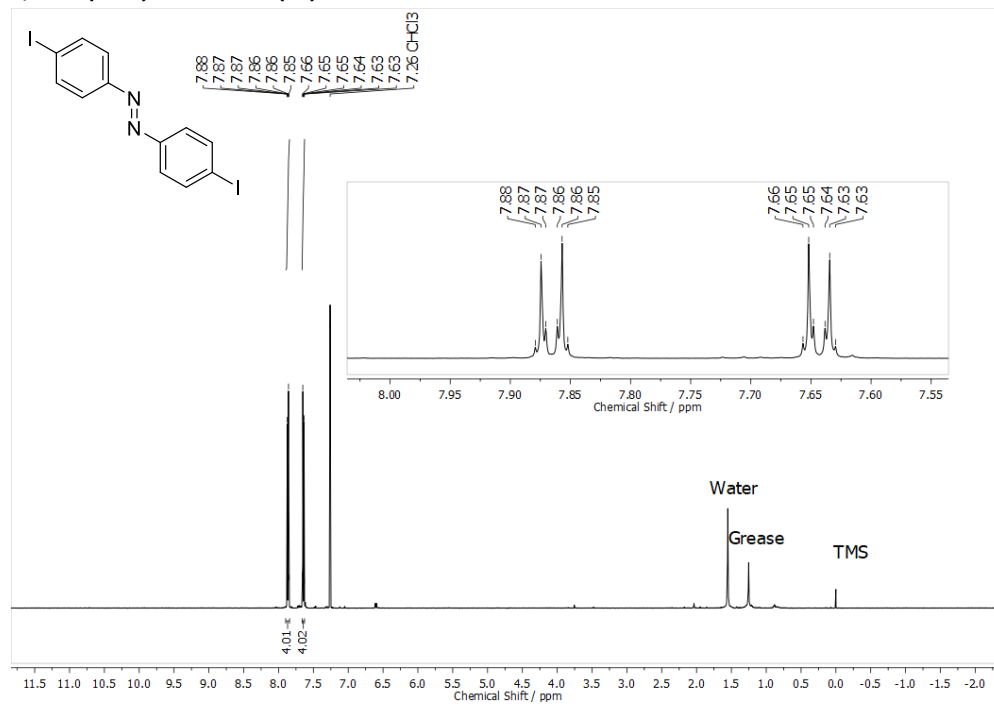
Poly(4,4'-azobenzene-*alt*-hexamethyl-trisiloxane) (6) in *n*-hexane

Figure S11. UV-VIS analysis of Poly(4,4'-azobenzene-*alt*-hexamethyl-trisiloxane) (6) in *n*-hexane. Thermal relaxation after irradiation with UV light. Red represents the starting point, violet represents the end point. The spectra were recorded with a delay of 15 min over the course of 5 h. The time profile of the thermal relaxation of the $\pi\pi$ band is shown as blue triangles and was used to determine the half-life time via an exponential fit to be 25 ± 2 h. Arrows indicate the change in absorption of the $\pi\pi^*$ (ca. 330 nm) and $n\pi^*$ (ca. 450 nm) bands.

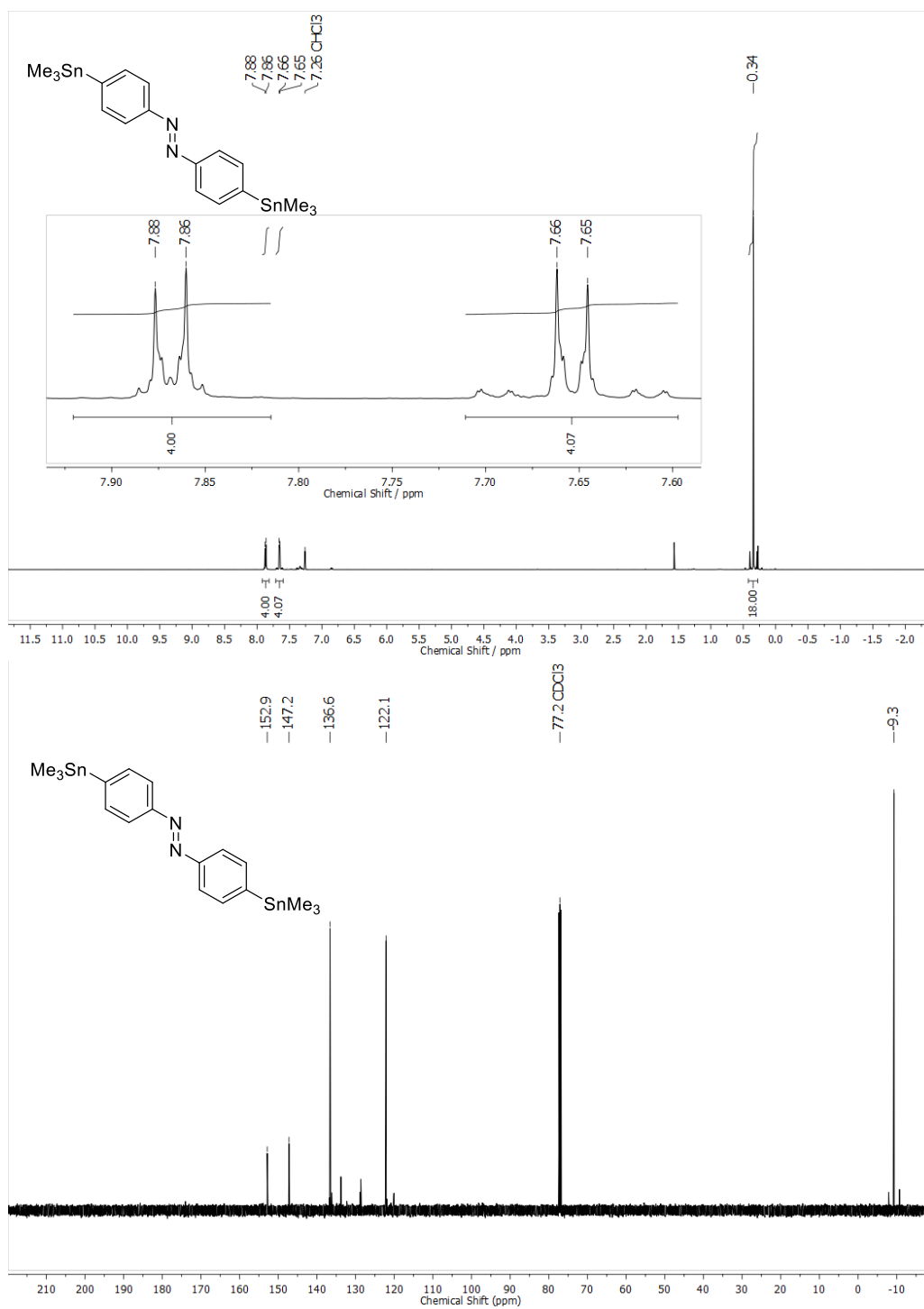
Plotted ^1H , $^{13}\text{C}\{^1\text{H}\}$ NMR and $^{29}\text{Si}\{^1\text{H}\}$ or $^{119}\text{Sn}\{^1\text{H}\}$ NMR spectra for all compounds

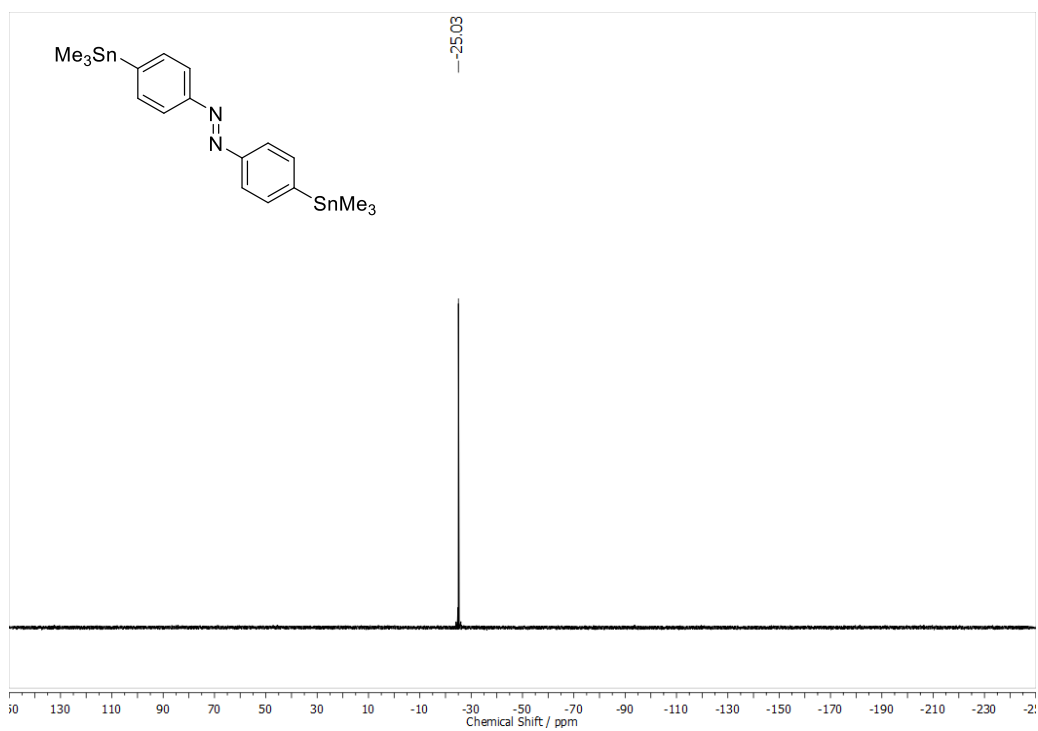
4,4'-Bis(iodo)azobenzene (S1) in chloroform-*d*



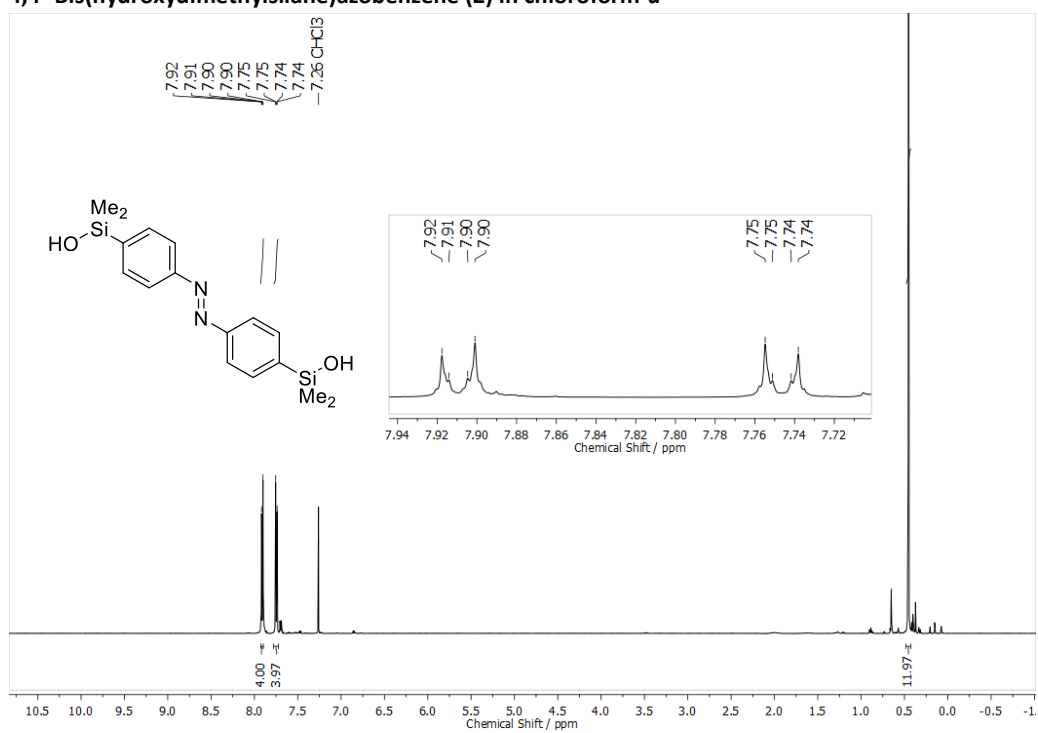
4,4'-Bis(trimethylstannyl)azobenzene (1) in chloroform-*d*

SI-23

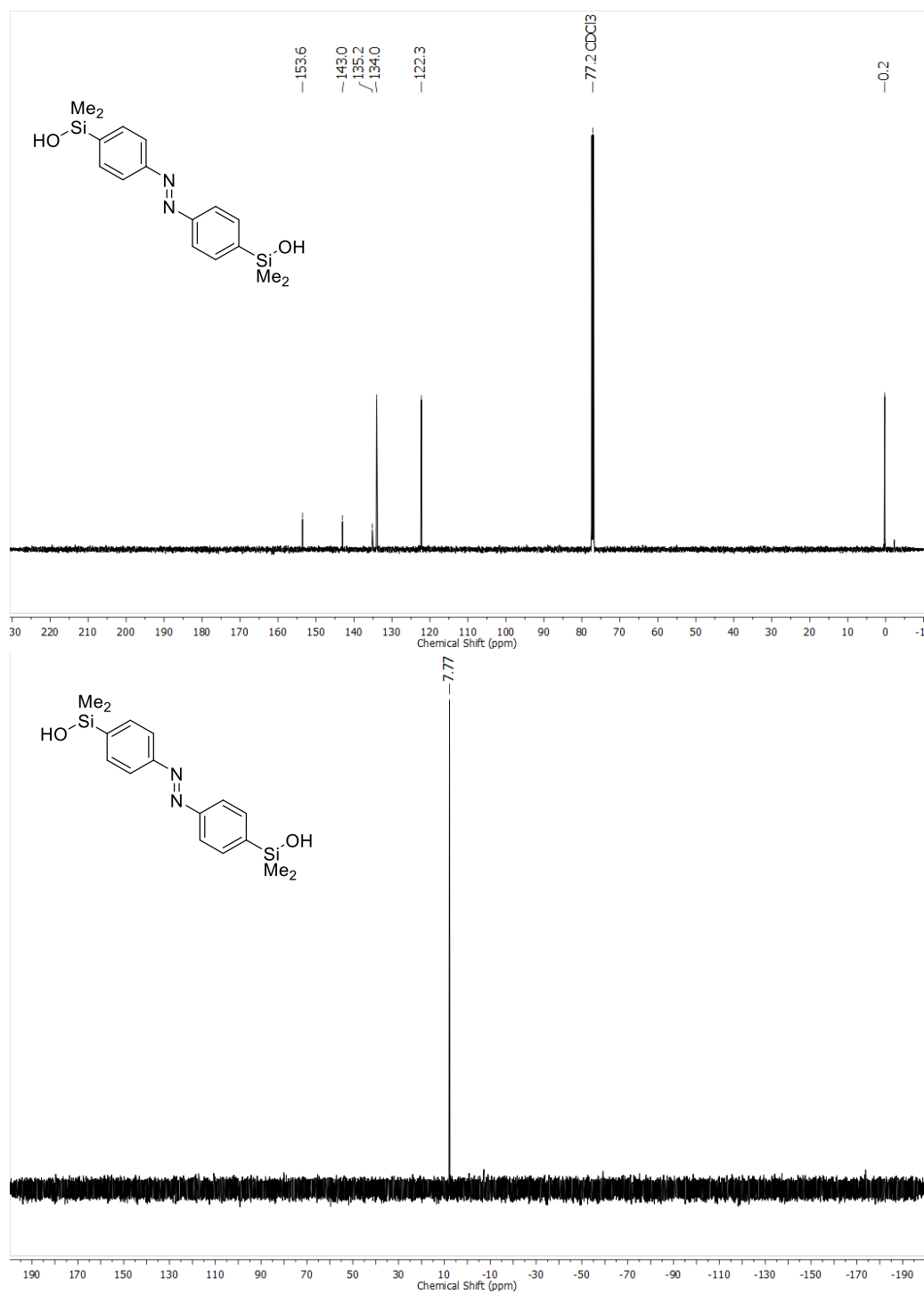




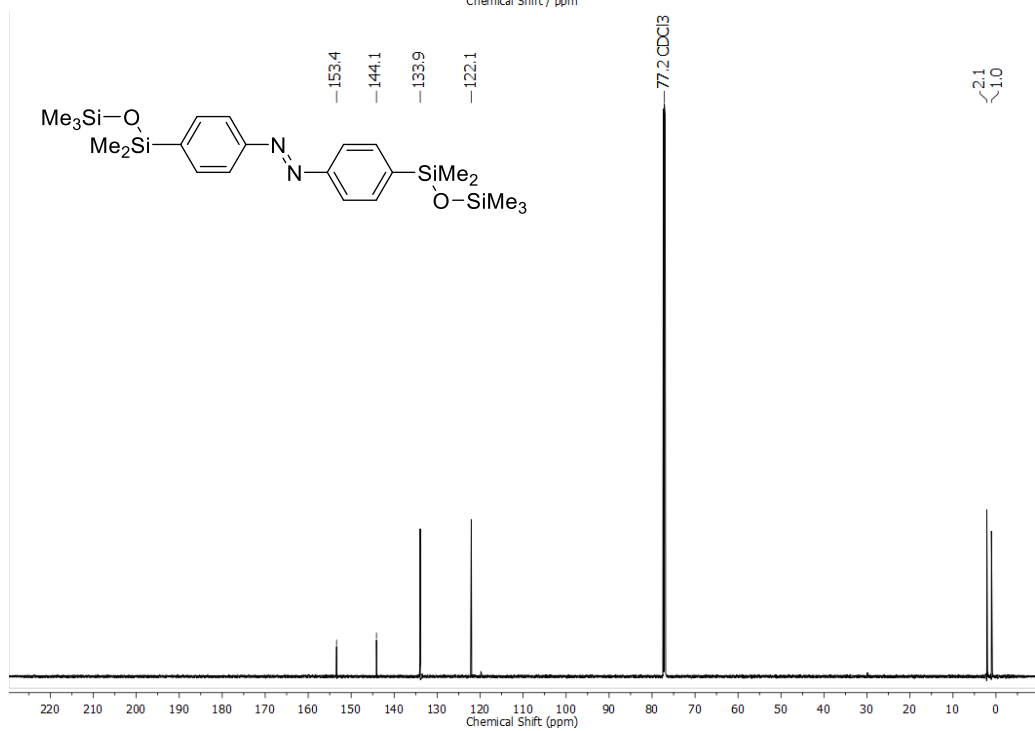
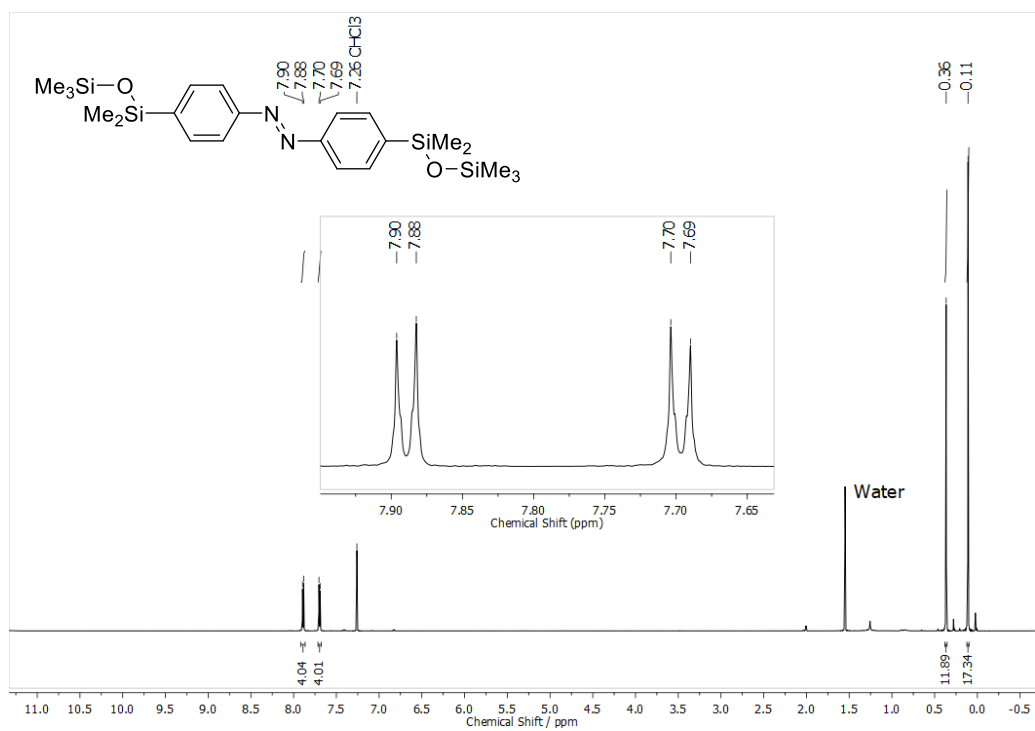
4,4'-Bis(hydroxydimethylsilane)azobenzene (2) in chloroform-*d*



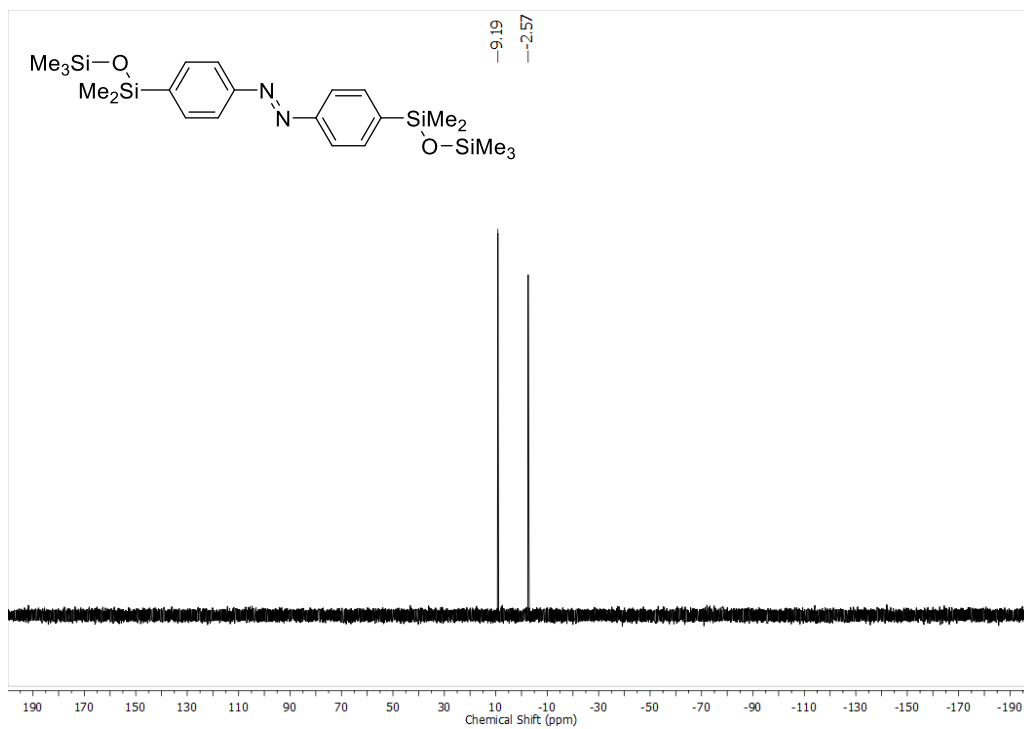
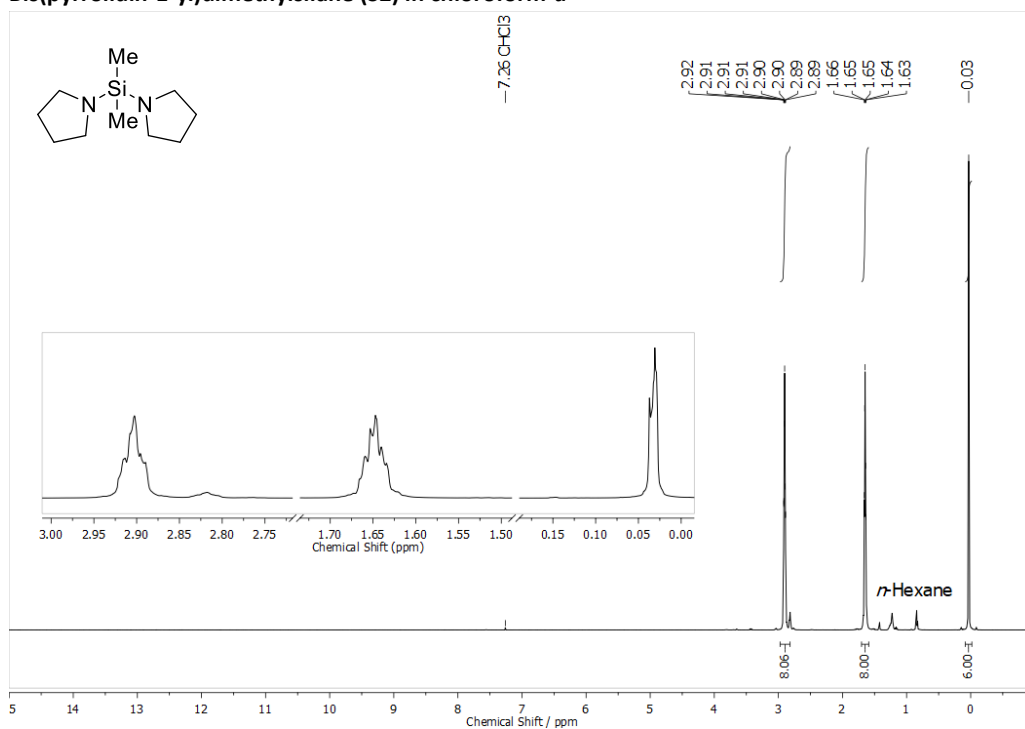
SI-25

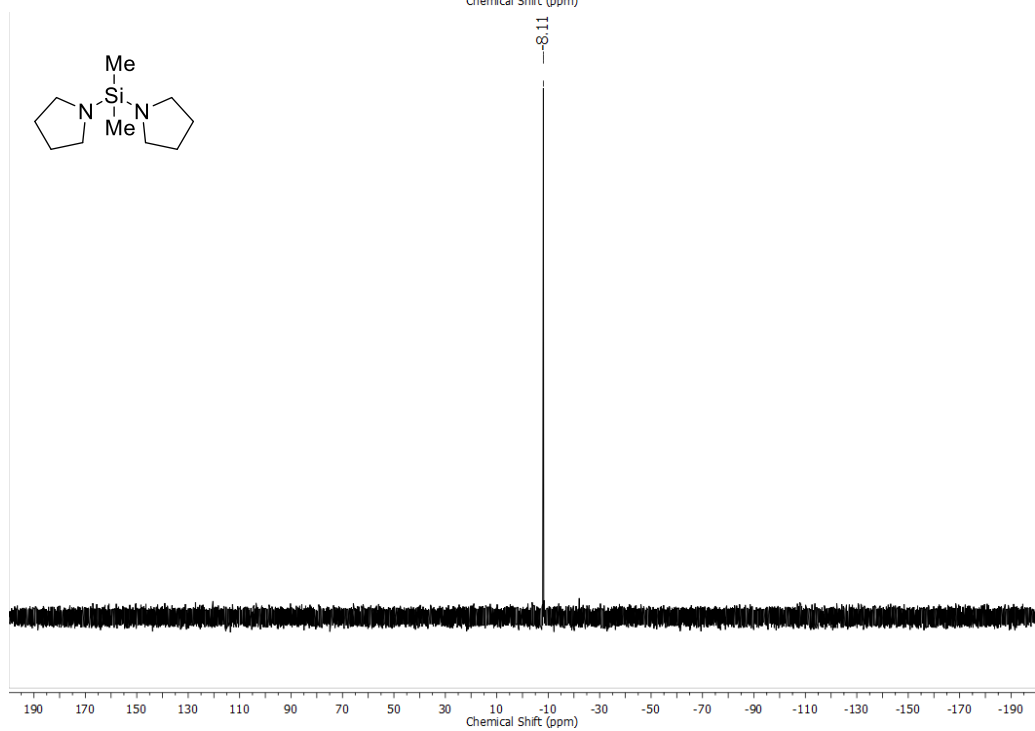
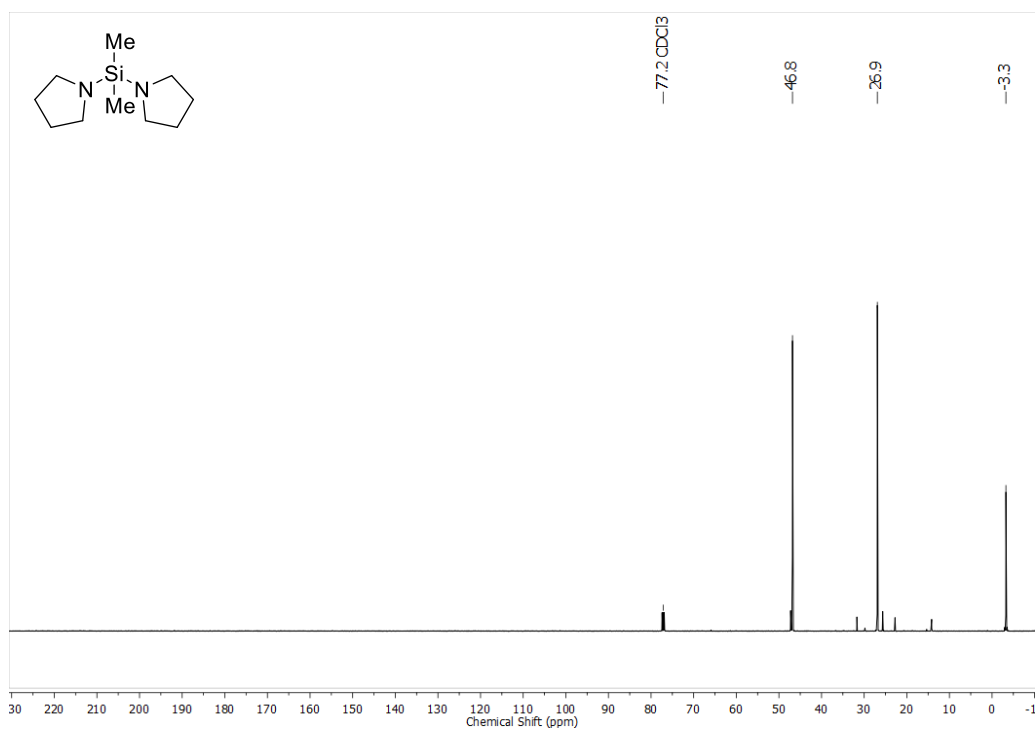
**4,4'-Bis(1,1,3,3,3-pentamethyldisiloxany)azobenzene (5) chloroform-*d***

SI-26



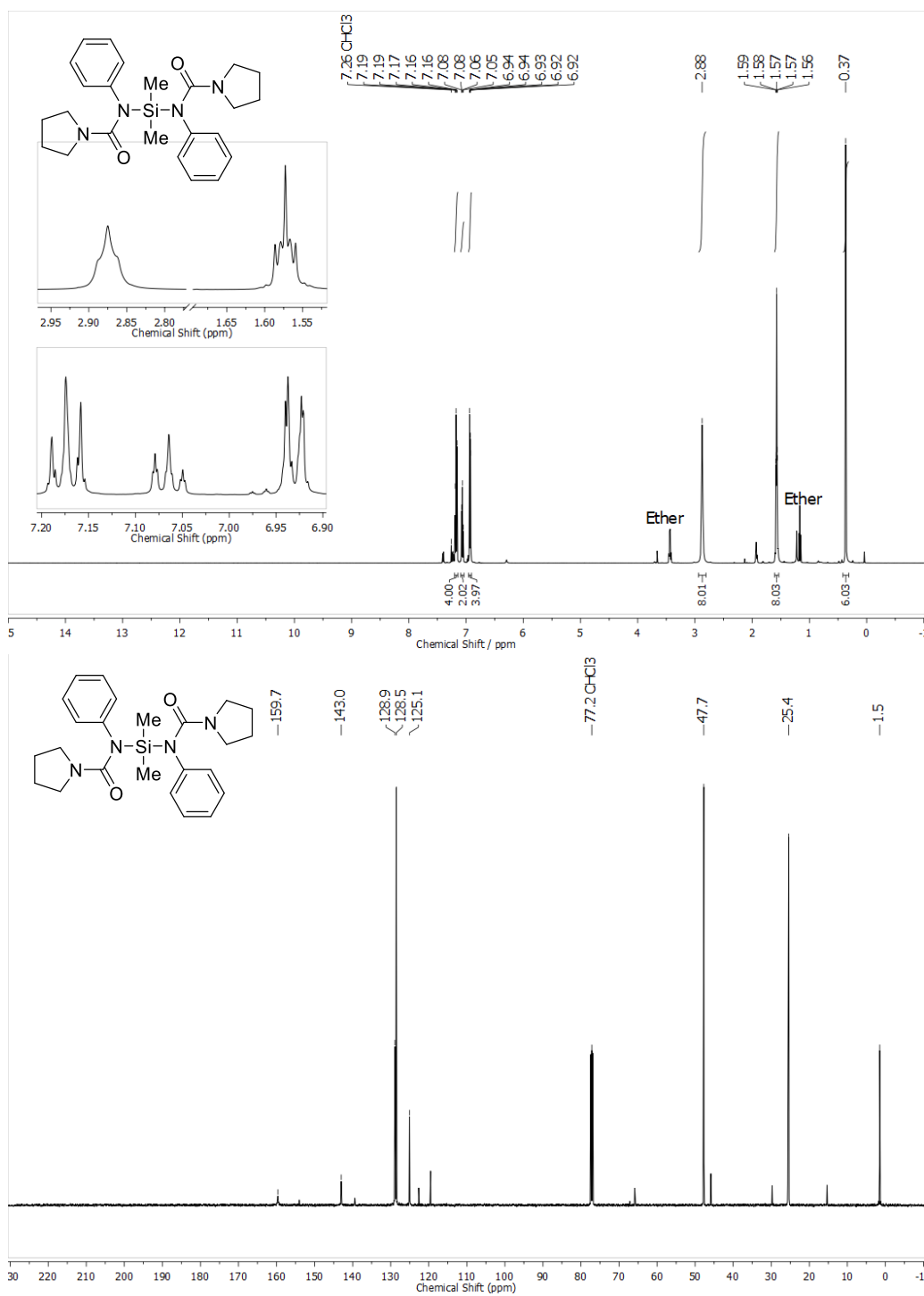
SI-27

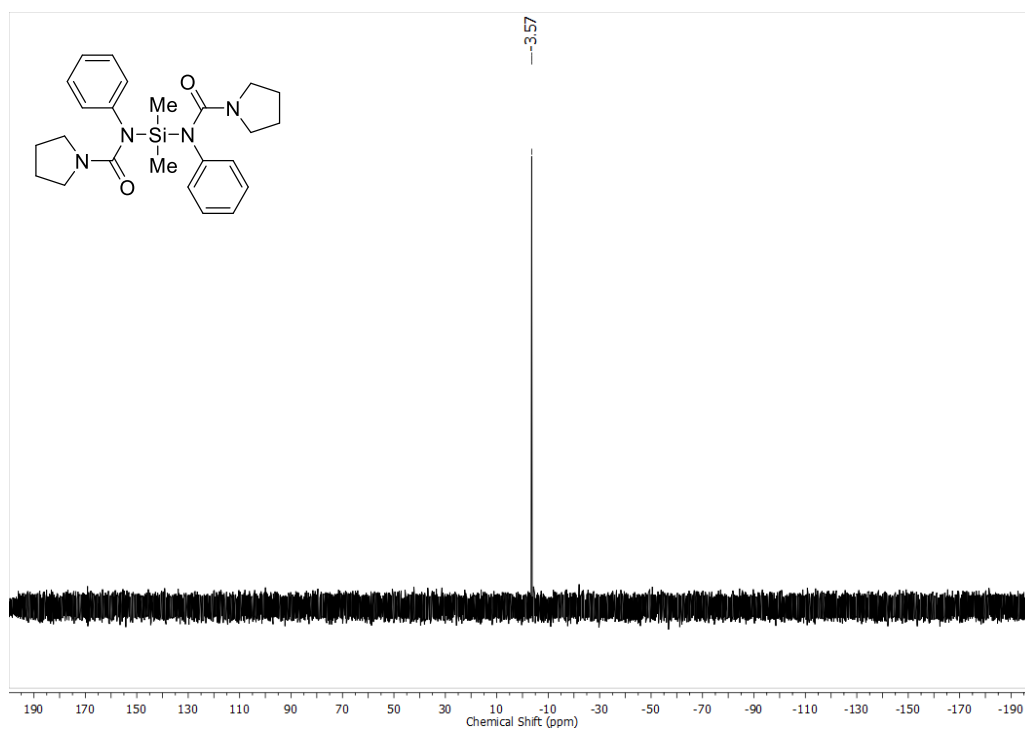
Bis(pyrrolidin-1-yl)dimethylsilane (S2) in chloroform-*d*



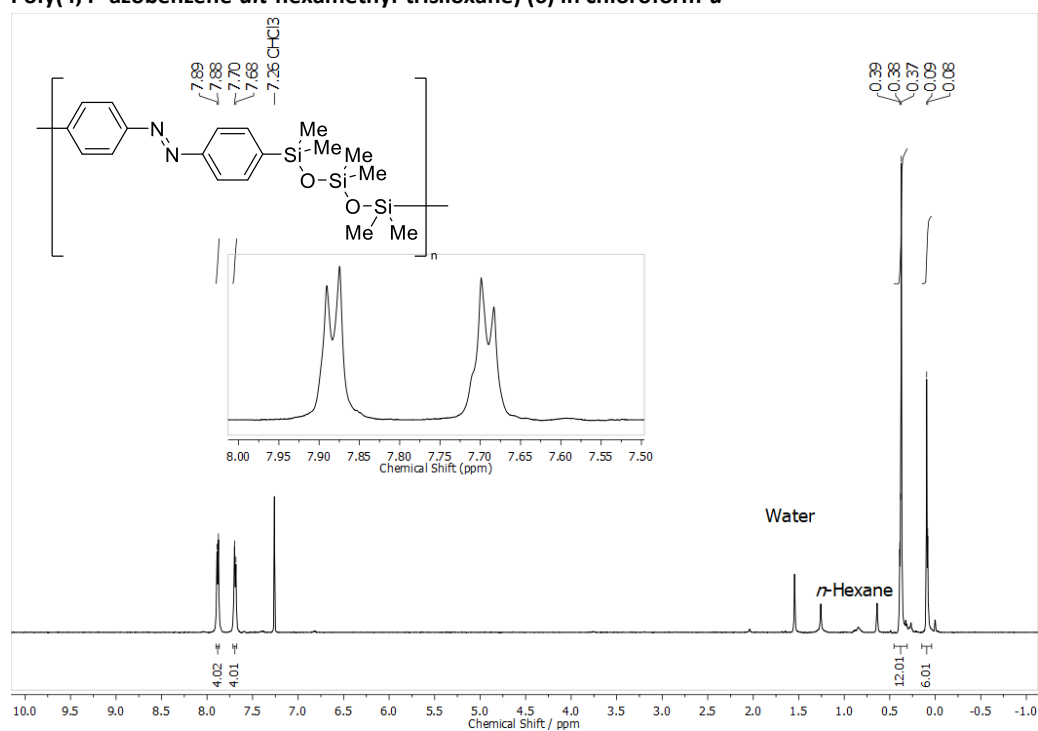
Bis(*N*-phenyl-*N*-pyrrolidinecarbonylamino)dimethylsilane (4) in chloroform-*d*

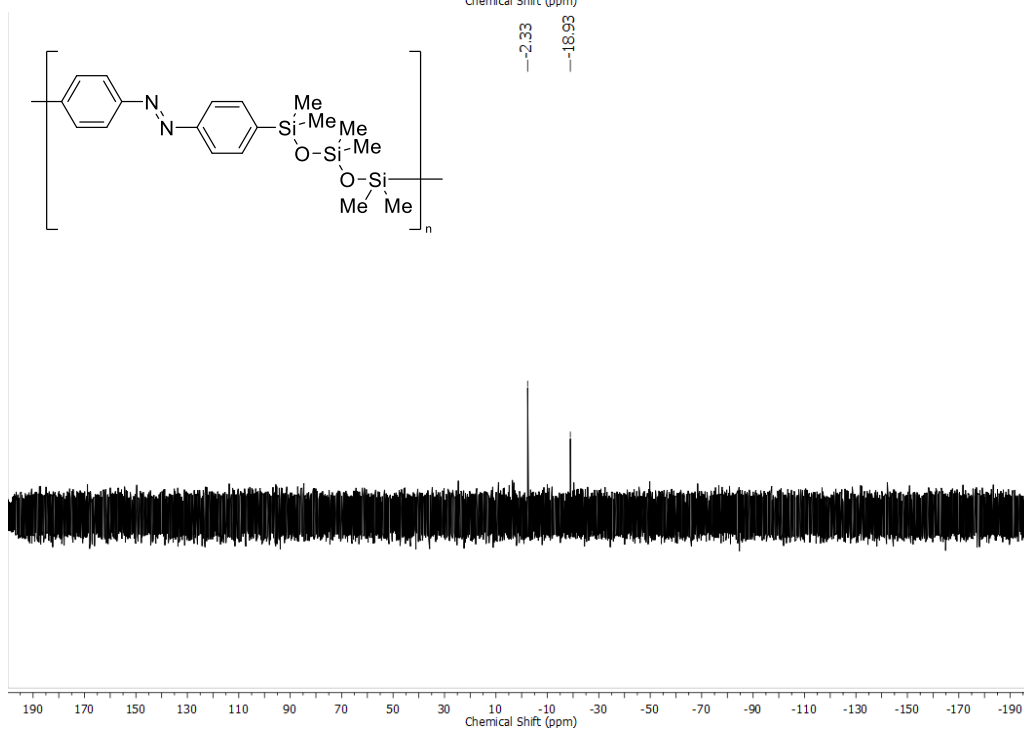
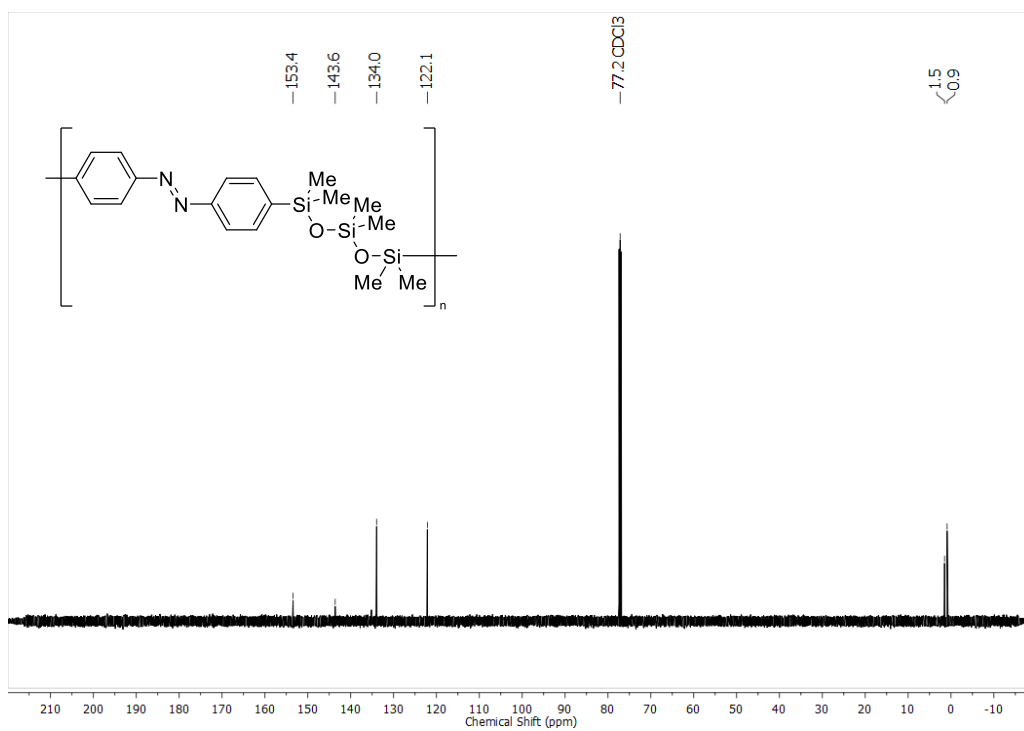
SI-29





Poly(4,4'-azobenzene-*alt*-hexamethyl-trisiloxane) (6) in chloroform-*d*





6.2. Synthesis of a Cross-Linkable Alternating Poly-(Azobenzene-Trisiloxane) and its Characterization in a Freestanding Film

Supporting Information

for

Reversible Volume Switching of a Poly(silazobenzene-siloxane).

Mathias Schulz-Senft,^{†1,2,3} Sindu Shree,^{†4} Jan Strueben,¹ Xin Jin,⁴ David Presa Soto,¹ Ruchira

A. Colaco,^{2,3} Rainer Adelung,^{*4} Anne Staubitz^{*1,2,3}

¹Otto-Diels-Institute for Organic Chemistry, University of Kiel, Otto-Hahn-Platz 4, 24098 Kiel (Germany), ²Institute for Organic and Analytical Chemistry, University of Bremen, Leobener Str. 7 NW2 C, 28359 Bremen (Germany), ³MAPEX Center for Materials and Processes, University of Bremen Bibliothekstraße 1, 28359 Bremen (Germany), ⁴Institute for Materials Science, University of Kiel, Kaiserstr. 2, 24143 Kiel (Germany).

ra@tf.uni-kiel.de; staubitz@uni-bremen.de

Abbreviations	2
Analytical Equipment and Equipment for Syntheses.....	2
Reagents.....	3
Solvents	4
References.....	5
Synthetic Procedures	6
4,4'-Bis(iodo)azobenzene (SI-1)	6
4,4'-Bis(trimethylstannyl)azobenzene (SI-2)	6
4,4'-Bis(hydroxydimethylsilane)azobenzene (1).....	7
Bis(pyrrolidinyl)dimethylsilane (SI-3a).....	8
Bis(<i>N</i> -phenyl- <i>N</i> -pyrrolidinecarbonylamino)dimethyl silane (2a).....	8
Bis(pyrrolidinyl)methylvinylsilane (SI-3b)	9
Bis(<i>N</i> -phenyl- <i>N</i> -pyrrolidinecarbonylamino)methylvinyl silane (2b).....	9
Poly(4,4'-azobenzene- <i>alt</i> -(hexamethyl-trisiloxane)- <i>stat</i> -(1,1,3,5,5-pentamethyl-3-vinyl-trisiloxane)) (3)	10
GPC Measurements	11
AFM Measurements	12
Plotted UV-Vis Spectra of the Polymer 3 in THF.....	14
Plotted TGA Spectrum of Polymer 3.....	15
Plotted DSC Spectrum (3 Cycles) of Polymer 3.....	15
Plotted ¹ H, ¹³ C{ ¹ H} and hetero NMR Spectra for All Compounds	16

SI-1

Abbreviations

The use of abbreviations follows the conventions from the ACS Style guide.¹ In addition, the following abbreviations are used.

Abbreviation	Long form
at (NMR)	Apparent triplet
ATR	Attenuated total reflection (IR)
CI	Chemical ionization
COSY	Correlation spectroscopy
DCM	Dichloromethane
dd (NMR)	Doublet of doublets
DMSO	Dimethyl sulfoxide
EI	Electron ionization
ESI	Electrospray ionization
FT	Fourier transform
HMBC	Heteronuclear multiple bond correlation
HPLC	High performance liquid chromatography
HSQC	Heteronuclear single quantum coherence
NOESY	Nuclear Overhauser enhancement spectroscopy
PSS	Photostationary state
THF	Tetrahydrofuran
TOF	Time-of-flight mass detector
v/v	Volume concentration (volume/volume)

Analytical Equipment and Equipment for Syntheses

NMR spectra were either recorded on a Bruker Avance Neo 500 (¹H NMR: 500 MHz) or on a Bruker Avance II HD 600 (¹H NMR: 600 MHz) FT-NMR spectrometer at 300 K. ¹H NMR and ¹³C{¹H} NMR spectra were referenced against the solvent residual proton signals (¹H) or the solvent itself (¹³C).

The exact assignment of the peaks was performed by two-dimensional NMR spectroscopy such as ¹H COSY, ¹H NOESY, ¹H/¹³C HSQC or ¹H/¹³C HMBC if possible.

Mass spectrometric measurements were performed in the positive ion collection mode using a JEOL-Accu TOF 4GGCV EI mass spectrometer, a Bruker Daltonics Apex IV FT Ion Cyclotron Resonance ESI mass spectrometer or a VG Analytical Autospec apparatus for CI. Electron ionization (EI) was performed using an ionization potential of 70 eV.

IR spectra were measured using a Perkin Elmer Paragon 1000 FT-IR spectrometer equipped with an A531-G Golden-Gate-ATR-unit.

UV-vis spectra were recorded at 25 °C using a Perkin Elmer Lambda 900 spectrometer for the film that was spin-coated on quartz glass and a Perkin Elmer Lambda 14 UV spectrometer in solution. Quartz cuvettes with a light path length of 10 mm from Hellma Analytics were used.

Melting points were measured on an electrothermal IA6304 capillary melting point apparatus and are uncorrected.

Gel permeation chromatography was performed on a Viscotek GPC max VE2001 equipped with a Viscotek VE3580 RI detector and a column set of LT5000 and LT4000 in THF (VWR, HPLC-grade) with a flow rate of 1 mL/min. Conventional calibration and analysis was done with OmniSEC 4.6.2 software using polystyrene standards.

Topographical AFM imaging were conducted under the WITec RA 300 microscope with an Asylum cantilever with 2 Nm^{-1} , 70 kHz. The same setup was also used for the determination of average surface roughness.

TGA measurements were performed on a Mettler Toledo DSC 3/TGA+ STAR system using aluminum crucibles under a nitrogen flow of 20 mL/min and a temperature ramp of 10 K/min.

DSC measurements were conducted on a Mettler Toledo DSC 3+ STAR system using aluminum crucibles under a nitrogen flow of 20 mL/min and a temperature ramp of 20 K/min.

The polymer film was prepared by spin coating 10 mL of a solution of the polymer (214 $\mu\text{mol/L}$) in THF at 2000 rpm. Quartz glass was used as substrate. The film thickness was verified by Ambios Xp2 profilometer.

The irradiation experiments were carried out using LED light sources assembled by Sahlmann Photochemical Solutions with an optical power of 1000 mW (365 nm) and 900 mW (450 nm) in solution. Irradiation of the film for AFM and UV-visible measurements was achieved using the fiber-coupled (400 μm in diameter) LEDs M365FP1 (365 nm, min. output: 9.8 mW, typical output: 15.5 mW) and M455F1 (455 nm, min. output: 9.5 mW, typical output: 11.0 mW) from Thorlabs with an angle of 30° .

Reactions that required inert workup were conducted in a labmaster 130 glove box by MBraun, flushed with nitrogen.

Microwave assisted syntheses were performed on a Biotage Initiator+ SP Wave peptide synthesizer in the organic synthesis mode. A fixed hold time was turned off.

The cooling of inert syntheses was achieved by using a cooling block connected to a Julabo FP88 cryostate inside the glove box.

Reagents

If not noted otherwise, all reagents were used as received. Hydrochloric acid solutions were prepared by diluting the concentrated acid.

Reagent	Supplier	Purity or concentration	Notes
[Pd(PPh ₃) ₄]	Aldrich	99%	
4-Iodoaniline	Acros	98%	
Copper (I) bromide	Sigma-Aldrich	98%	
Dichlorodimethylsilane	Acros	99%	Distilled from CaH ₂ and degassed before use
Dichloromethylvinylsilane	Aldrich	97%	Distilled from CaH ₂ and degassed before use
Hexamethyldistannane	Acros	99%	
Hydrochloric acid	Grüssing	37.5%	
Magnesium sulfate	Grüssing		

SI-3

Methyl lithium	Acros	3% in MeTHF / Cumol	Exact concentration was determined by titration against menthol.
Monopotassium phosphate	Merck	Extra pure	
Phenyl isocyanate	Alfa Aesar	>98%	Degassed before use
Pyridine	Grüssing	99.5%	
Pyrrolidine	Alfa Aesar	99%	Degassed before use
Sodium hydroxide	Grüssing	99%	

Solvents

All solvents that were purchased in technical grade were purified by distillation prior to use. Solvents of purities higher than 99% were not purified further. Some solvents were degassed by three freeze-pump-thaw cycles, then the flask was again filled with nitrogen and the solvent stored over molecular sieves with the pore size 3 Å.

The following solvents were dried in a solvent purification system PS-MD-5 by Innovative Technology: dichloromethane, tetrahydrofuran.

Solvent	Supplier	Purity	Drying procedure	Degassed
Acetonitrile	Sigma-Aldrich	>99.9%, HPLC grade	none	No
Benzene-<i>d</i>₆	Deutero	99.5% D	Distilled from CaH ₂ , stored over molecular sieves 3 Å	yes
Chlorobenzene	Acros	99.9%, HPLC grade	Distilled from CaH ₂ , stored over molecular sieves 3 Å	yes
Chloroform	VWR	Techn. grade	none	No
Chloroform-<i>d</i>	Euriso-top	99.8% D	none	No
Dichloromethane	VWR	HPLC grade	PS-MD-5	Yes
Dichloromethane	BCD	Techn. grade	none	No
Dichloromethane-<i>d</i>₂	Deutero	99.6% D	none	No
Diethyl ether	Alfa-Aesar	Spectrophotometric grade, >99%, inhibitor free	Molecular sieves 3 Å	Yes
Diethyl ether	BCD	Techn. grade	none	No
Ethanol	CMP Walther	Techn. grade, denaturated with benzine	none	No
<i>n</i>-Hexane	CMP Walther	Techn. grade	none	No
<i>n</i>-Hexane	CMP Walther	Techn. grade	Distilled from CaH ₂ , stored over molecular sieve 3 Å	Yes
Methanol	Acros	99.8%, anhydrous, stored over molecular sieves 3 Å		No
<i>n</i>-Pentane	CMP Walther	Techn. grade	none	No
Tetrahydrofuran	VWR	HPLC grade	PS-MD-5	Yes

SI-4

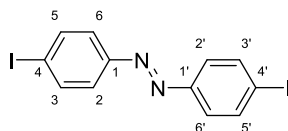
Toluene	Acros	99.85%, Extra dry, none stored over molecular sieves	Yes
----------------	-------	--	-----

References

- (1) *The ACS Style Guide: Effective Communication of Scientific Information*, 3rd ed.; Coghill, A. M., Garson, L. R., Eds.; American Chemical Society: Washington, DC, 2006.
- (2) Strueben, J.; Gates, P. J.; Staubitz, A. Tin-Functionalized Azobenzenes as Nucleophiles in Stille Cross-Coupling Reactions. *J. Org. Chem.* **2014**, *79* (4), 1719–1728. <https://doi.org/10.1021/jo402598u>.
- (3) Hughes, G. M. K.; Saunders, B. C. Studies in Peroxidase Action. Part IX. Reactions Involving the Rupture of the C–F, C–Br, and C–I Links in Aromatic Amines. *J. Chem. Soc. Resumed* **1954**, *0* (0), 4630–4634. <https://doi.org/10.1039/JR9540004630>.
- (4) Strüben, J.; Hoffmann, J.; Presa-Soto, D.; Näther, C.; Staubitz, A. Crystal Structures of 3,3'-Bis-(Hy-droxy-dimethylsilan-yl)Azo-benzene and 4,4'-Bis-(Hy-droxy-dimethyl-silane)Azo-benzene. *Acta Crystallogr. Sect. E Crystallogr. Commun.* **2016**, *72* (11), 1590–1594. <https://doi.org/10.1107/S2056989016016297>.
- (5) Passarelli, V.; Benetollo, F.; Zanella, P.; Carta, G.; Rossetto, G. Synthesis and Characterisation of Novel Zirconium(IV) Derivatives Containing the Bis-Amido Ligand SiMe₂(NRR')₂. *Dalton Trans.* **2003**, No. 7, 1411–1418. <https://doi.org/10.1039/B212705A>.
- (6) Dvornic, P. R.; Lenz, R. W. Exactly Alternating Silarylene–Siloxane Polymers. I. The Synthesis and Stability of Bis(1,1-tetramethylene-3-phenylureido)Dimethylsilane. *J. Appl. Polym. Sci.* **1980**, *25* (4), 641–652. <https://doi.org/10.1002/app.1980.070250411>.
- (7) Hedaya, E.; Kawakami, J. H.; Kopf, P. W.; Kwiatkowski, G. T.; McNeil, D. W.; Owen, D. A.; Peters, E. N.; Tulis, R. W. D2-meta-carborane-siloxanes. IV. Synthesis of Linear, High Molecular Weight Polymers. *J. Polym. Sci. Polym. Chem. Ed.* **1977**, *15* (9), 2229–2238. <https://doi.org/10.1002/pol.1977.170150914>.

Synthetic Procedures

4,4'-Bis(iodo)azobenzene (SI-1)



CuBr (7.24 g, 45.7 mmol) was dissolved in pyridine (90 mL), and stirred for 30 min, before the precipitate was removed by filtration. The filtrate was diluted with pyridine (20 mL). 4-Iodoaniline (14.3 g, 65.3 mmol) was added in one portion and the mixture was stirred for 20 h at 24 °C while bubbling air through the solution via a syringe (0.2 bar, 250 L/h, diameter: 1 mm). Hydrochloric acid (2 N, 200 mL) was added to the solution and the aqueous phase was extracted with diethyl ether (1 x 300 mL) and dichloromethane (2 x 200 mL). The combined organic phases were washed with hydrochloric acid (2 N, 2 x 200 mL) and the solvents were removed in vacuo. The crude solid product was purified by washing it with boiling ethanol (300 mL). After drying the product in vacuo, an orange solid was obtained without further purification (9.24 g, 21.3 mmol, 65%, Lit.:² 61%).

Mp: 237 °C (Lit.:² 210 °C, Lit.:³ 237-238 °C).

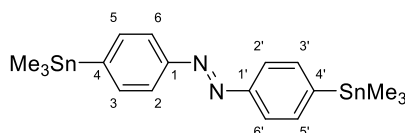
¹H NMR (500 MHz, CDCl₃): δ = 7.87 (d, ³J = 8.7 Hz, 4H, H-3,3',5,5'), 7.64 (d, ³J = 8.7 Hz, 4H, H-2,2',6,6') ppm.

¹³C{¹H} NMR (126 MHz, CDCl₃): δ = 151.9 (C-1,1'), 138.6 (C-3,3',5,5'), 124.7 (C-2,2',6,6'), 98.3 (C-4,4') ppm.

IR (ATR): $\tilde{\nu}$ = 3079 (w), 1575 (m), 1561 (m), 1470 (m), 1393 (s), 1297 (s), 1280 (s), 1156 (m), 1097 (s), 1051 (s), 1002 (s), 833 (vs), 811 (vs), 714 (vs), 539 (vs), 525 (vs) cm⁻¹.

HRMS (EI-TOF) *m/z* (%): [M]⁺ calcd. for [C₁₂H₈N₂I₂]⁺ 433.8777, found 433.8767 (60), 230.94 (100) [M-C₆H₄I]⁺, 202.93 (100) [M-C₆H₄IN₂]⁺.

4,4'-Bis(trimethylstannyl)azobenzene (SI-2)



This compound has been synthesized before,² the procedure was optimized as follows:

Under a nitrogen atmosphere, 4,4''-bis(iodo)-azobenzene (1.30 g, 3.00 mmol), hexamethyldistannane (2.29 g, 7.00 mmol) and [Pd(PPh₃)₄] (139 mg, 120 μmol, 4 mol%) were dissolved in toluene (18 mL) and THF (2 mL) in a microwave reaction vessel. The reaction mixture was heated for 30 min to 170 °C. Five such reaction batches were combined for the work-up. Then, the solvent was removed under reduced pressure followed by purification by column chromatography (eluent: *n*-pentane, R_f = 0.65). The product was obtained as orange solid (7.23 g, 14.3 mmol, 95%, Lit.:² 81%).

Mp: 54 °C (Lit.:² 54 °C).

¹H NMR (500 MHz, CDCl₃): δ = 7.87 (d, ³J = 8.2 Hz, 4 H, H-3, 3', 5, 5'), 7.65 (d, ³J = 8.2 Hz, 4 H, H-2, 2', 6, 6'), 0.34 (s, 18 H, Sn(CH₃)₃) ppm.

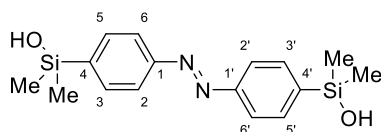
$^{13}\text{C}\{^1\text{H}\}$ NMR (126 MHz, CDCl_3): $\delta = 152.9$ (C-4, 4'), 147.2 (C-1, 1'), 136.6 (C-2, 2', 6, 6'), 122.1 (C-3, 3', 5, 5'), -9.3 ($\text{Sn}(\text{CH}_3)_3$) ppm.

$^{119}\text{Sn}\{^1\text{H}\}$ NMR (187 MHz, CDCl_3): $\delta = -25.03$ ppm.

IR (ATR): $\tilde{\nu} = 3067$ (w), 3024 (w), 2987 (w), 2917 (w), 1925 (w), 1437 (m), 1383 (m), 1306 (m), 1067 (m), 1011 (m), 831 (s), 761 (s), 583 (s), 508 (s) cm^{-1} .

HRMS (ESI-FTMS) m/z : $[\text{M}+\text{H}]^+$ calcd. for $[\text{C}_{18}\text{H}_{26}\text{N}_2\text{Sn}_2+\text{H}]^+$ 511.0213, found 511.0227.

4,4'-Bis(hydroxydimethylsilane)azobenzene (1)



This compound has been synthesized already,⁴ the procedure was optimized as follows:

Under argon atmosphere, 4,4'-bis(trimethylstannyl)-azobenzene (3.00 g, 5.91 mmol) was dissolved in dry THF (70 mL). Methyl lithium (20 mL) was added at -78°C . The orange solution turned dark and was stirred 15 min. Then, dichlorodimethylsilane (24 mL, 25.7 g, 199 mmol) was added. The reaction was allowed to warm to 25°C by removing the cooling bath. The solvent and the excess of dichlorodi-methylsilane were removed *in vacuo*. The residual orange solid was dissolved in THF (40 mL) and added (rate: 1 mL/min) to a solution of sodium methoxide in methanol (13.5 mL of 4.5 N solution, diluted with 20 mL MeOH). Inert conditions were maintained until this point. The mixture was opened to air and a solution of sodium hydroxide in methanol and water (24 mL, 5 mol/L, MeOH:H₂O 10:1) was added. The resulting mixture was stirred 15 minutes, before a solution of sodium hydroxide in water (24 mL, 5 mol/L) was added. The reaction mixture was stirred 5 h, for all these steps, the temperature was held at 25°C . This mixture was poured into a vigorously stirred solution of mono potassium phosphate in water (150 mL, 1 mol/L). The resulting solution was extracted with chloroform (4 x 50 mL). The combined organic phases were dried over MgSO_4 and the solvent was removed *in vacuo*. The crude product was purified by solvent diffusion crystallization: A saturated solution in chloroform was overlaid with *n*-hexane and cooled to -30°C for 48 h. After three crystallization cycles, the product was obtained as orange solid (845 mg, 2.56 mmol, 43%, Lit.:⁴ 35%).

Mp.: $T = 141^\circ\text{C}$, Lit.:⁴ 141°C .

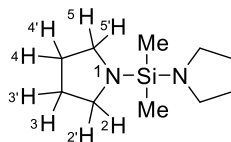
^1H NMR (500 MHz, CDCl_3): $\delta = 7.91$ (d, $^3J = 8.3$ Hz, 4 H, H-3,3',5,5'), 7.75 (d, $^3J = 8.3$ Hz, 4 H, H-2,2',6,6'), 1.99 (s, 1H, OH), 0.46 (s, 12 H, $\text{Si}(\text{CH}_3)_2$) ppm.

$^{13}\text{C}\{^1\text{H}\}$ NMR (126 MHz, CDCl_3): $\delta = 153.6$ (C-1,1'), 143.0 (C-4,4'), 134.0 (C-3,3'), 122.3 (C-2,2'), 0.2 ($\text{Si}(\text{CH}_3)_2$) ppm.

$^{29}\text{Si}\{^1\text{H}\}$ NMR (99 MHz, CDCl_3): $\delta = 7.77$ ppm.

IR (ATR): $\tilde{\nu} = 3141$ (m), 2956 (w), 1385 (m), 1251 (m), 1106 (w), 859 (s), 833 (s), 815 (s), 776 (s), 667 (s), 553 (s), 529 (m), 491 (m) cm^{-1} .

HRMS (EI-TOF) m/z (%): $[\text{M}]^+$ calcd for $[\text{C}_{16}\text{H}_{22}\text{N}_2\text{O}_2\text{Si}_2]^+$ 330.12198, found 330.12163 (35), 151.06 (100) $[\text{M}-\text{HOSi}(\text{CH}_3)_2\text{C}_6\text{H}_4\text{N}_2]^+$.

Bis(pyrrolidinyl)dimethylsilane (SI-3a)

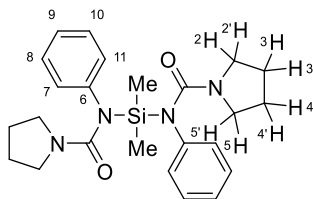
This reaction was performed entirely under nitrogen atmosphere. To a solution of dichlorodimethylsilane (80.0 mL, 85.6 g, 663 mmol) in *n*-hexane (150 mL), pyrrolidine (230 mL, 196 g, 2.76 mol) was added dropwise over the course of 1 h at 0 °C. After completion of the addition, the ice bath was removed and the reaction was stirred for 15 h. A precipitate of the amino hydrochloride, which had formed, was removed by filtration under inert conditions. The liquid was placed in a J. Young's flask and the remaining solvent was removed *in vacuo*. A colorless liquid (116 g, 585 mmol, 88%, Lit.:⁵ 95%) was obtained.

¹H NMR (500 MHz, CDCl₃): δ = 2.93 – 2.88 (m, 8 H, H-2,2',5,5'), 1.67 – 1.62 (m, 8 H, H-3,3',4,4'), 0.04 (s, 6 H, Si-CH₃) ppm.

¹³C{¹H} NMR (126 MHz, CDCl₃): δ = 46.8 (C-2,5), 26.9 (C-3,4), -3.3 (Si-CH₃) ppm

²⁹Si{¹H} NMR (187 MHz, CDCl₃): δ = -8.11 ppm.

HRMS (ESI-FTMS): *m/z*: [M+H]⁺ calcd for [C₁₀H₂₃N₂²⁸Si]⁺ 199.16250; found 199.16255.

Bis(*N*-phenyl-*N'*-pyrrolidinecarbonylamino)dimethyl silane (2a)

The reaction was performed entirely under inert conditions. Bis(pyrrolidinyl)dimethyl silane (40.0 g, 201 mmol) was dissolved in dry diethyl ether (250 mL) and cooled in an ice bath to 0 °C. Then phenyl isocyanate (45.0 mL, 49.3 g, 410 mmol) was added dropwise at 0 °C over the course of 3 h and the reaction mixture was allowed to warm to 25 °C over the course of 15 h. The white precipitate of bis(*N*-phenyl-*N'*-pyrrolidinyl)dimethylsilane was collected by filtration under inert conditions. The product was washed with dry diethyl ether (20 mL) and dried at 0.05 mbar for 12 h to receive the product as colourless solid (79.6 g, 182 mmol, 91%, Lit.:⁶ 85%).^a

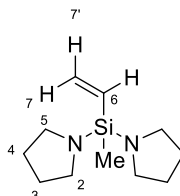
Mp.: T = 72 °C.

¹H NMR (500 MHz, CDCl₃): δ = 7.20 – 7.15 (m, H-8,10), 7.07 (t, ³J = 7.5 Hz, 2 H, H-9,9'), 6.95 – 6.91 (m, 4 H, H-7,11), 2.88 (m, 8 H, H-2,5), 1.58 (m, 8 H, H-3,4), 0.37 (s, 6 H, Si-CH₃) ppm.

¹³C{¹H} NMR (126 MHz, CDCl₃): δ = 159.7 (C=O), 143.0 (C-6), 128.9 (C-7,11), 128.5 (C-8,10), 125.1 (C-9), 47.7 (C-2,5), 25.4 (C-3,4), -1.5 (Si-CH₃) ppm.

²⁹Si{¹H} NMR (99 MHz, CDCl₃): δ = -3.57 ppm.

^a Due to the very high sensitivity of this compound, no IR or MS data could be obtained.

Bis(pyrrolidinyl)methylvinylsilane (SI-3b)

This compound has been synthesized already,⁷ the procedure was altered as follows:

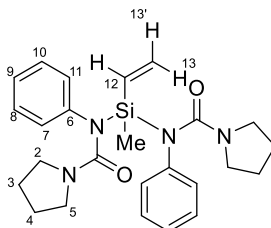
The reaction was performed entirely under inert conditions. A solution of pyrrolidine (11.3 mL, 9.60 g, 135 mmol) and *n*-hexane (60 mL) was cooled to -10 °C. To the cooled solution, dichloromethylvinylsilane (3.92 mL, 4.23 g, 30.0 mmol) was added with a rate of 0.1 mL/min. After complete addition, the mixture was heated to 25 °C and stirred for 3 h at 25 °C. The formed precipitate of pyrrolidine hydrochloride was removed by filtration and washed with *n*-hexane (100 mL). The solvent was removed under reduced pressure from the filtrate and after drying at 0.5 mbar for 10 h, the product was received as colorless liquid (4.24 g, 20.2 mmol, 67%, Lit.:⁷ 87%). The product is unstable under moisture.

¹H NMR (500 MHz, C₆D₆): δ = 6.29 (dd, ³J_E = 20.4 Hz, ³J_Z = 14.7 Hz, 1H, H-6), 6.03 (dd, ³J_Z = 14.7 Hz, ²J = 4.3 Hz, 1H, H-7'), 5.85 (dd, ³J_E = 20.4 Hz, ²J = 4.3 Hz, 1H, H-7), 3.06 – 2.98 (m, 8H, H-2,5), 1.64 – 1.56 (m, 8H, H-3,4), 0.27 (s, 3H, Si-CH₃) ppm.

¹³C{¹H} NMR (126 MHz, C₆D₆): δ = 137.7 (C-6), 132.2 (C-7), 47.1 (C-2,5), 27.2 (C-3,4), -4.1 (Si-CH₃)

²⁹Si{¹H} NMR (99 MHz, C₆D₆): δ = -19.1 ppm.

HRMS (EI-TOF) *m/z* (%): [M]⁺ calcd. for [C₁₁H₂₂N₂²⁸Si]⁺ 210.1534, found 210.15522 (40), 139.09 (100) [M-NH(CH₂)₄]⁺.

Bis(*N*-phenyl-*N'*-pyrrolidinecarbonylamino)methylvinyl silane (2b)

This compound has been synthesized previously,⁷ the procedure was optimized as follows:

The reaction was performed entirely under inert conditions. Bis(pyrrolidinyl)methylvinylsilane (3.37 mL, 3.05 g, 14.5 mmol) was dissolved in diethyl ether (15 mL) and cooled to -10 °C, before phenyl isocyanate (3.59 mL, 3.93 g, 33.0 mmol) was added with a rate of 0.10 mL/min. After complete addition, the cooling bath was removed and the reaction stirred at 25 °C for 15 h. The crude product was recrystallized from diethyl ether (60 mL) at -30 °C, filtered and washed with diethyl ether (30 mL) to obtain the product as white solid (5.47 g, 12.2 mmol, 84%, Lit.:⁷ 62%) after drying at 0.5 mbar for 20 h.^a

Mp.: T = 46 °C.

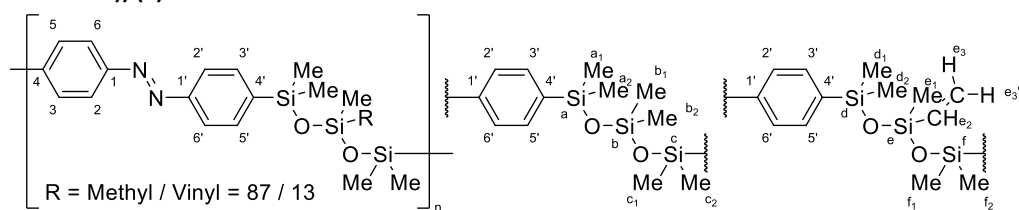
^a Due to the very high sensitivity of this compound, no IR or MS data could be obtained.

$^1\text{H NMR}$ (500 MHz, CDCl_3): $\delta = 7.15$ (t, $^3J = 7.8$, 4H, H-8,10), 7.06 (t, $^3J = 7.8$ Hz, 2H, H-9), 6.97 (t, $^3J = 7.8$ Hz, 4H, H-7,11), 6.35 (dd, $^3J = 20.5$ Hz, $^3J = 14.8$ Hz, 1H, H-12), 5.82 (dd, $^3J = 14.8$ Hz, $^2J = 3.1$ Hz, 1H, H-13'), 5.64 (dd, $^3J = 20.5$ Hz, $^2J = 3.1$ Hz, 1H, H-13), 2.87 (m, 8 H, H-2,5), 1.55 (m, 8 H, H-3,4), 0.37 (s, 3 H, Si- CH_3) ppm.

$^{13}\text{C}\{^1\text{H}\}$ NMR (126 MHz, CDCl_3): $\delta = 159.6$ (C=O), 142.6 (C-6), 137.1 (C-12), 131.3 (C-13,13'), 129.0 (C-7,11), 128.4 (C-8,10), 125.1 (C-9), 47.6 (C-2,5), 25.1 (C-3,4), -2.0 (Si- CH_3) ppm.

$^{29}\text{Si}\{^1\text{H}\}$ NMR (99 MHz, CDCl_3): $\delta = -18.31$ ppm.

Poly(4,4'-azobenzene-*alt*-(hexamethyl-trisiloxane)-*stat*-(1,1,3,5,5-pentamethyl-3-vinyl-trisiloxane)) (3)



This reaction was performed in a nitrogen filled glove box. 4,4'-Bis(hydroxydimethylsilane)-azobenzene (317 mg, 960 μmol), was dissolved in chlorobenzene (2 mL). A solution of bis(*N*-phenyl-*N*-pyrrolidinecarbonylamino)dimethyl silane (**2a**) (398 mg, 912 μmol) and bis(*N*-phenyl-*N*-pyrrolidinecarbonylamino)methylvinyl silane (**2b**) (21.5 mg, 48.0 μmol) in chlorobenzene (8 mL) was added with a rate of 15 $\mu\text{L}/\text{min}$ at -45°C . The solution was stirred for 8 d at 25°C , while the reaction progress was monitored by GPC. After 3 d, another portion of **2b** (22.4 mg, 50.0 μmol) was added and a portion of **1** (8.3 mg, 25 μmol) was added after 6 d. Once the measured retention volume remained unchanged, the solvent was evaporated and the polymer was purified by dissolving in THF and precipitation into methanol (10 fold excess) for three times. After drying at 0.05 mbar and 70°C for 20 h, the product was obtained as orange solid (369 mg). The ratio of methyl and vinyl substitution at the marked R group was determined to be 87 / 13. The NMR integrals are normalized per repeating unit.

$^1\text{H NMR}$ (600 MHz, CDCl_3):^a $\delta = 7.88$ (d, $^3J = 8.2$ Hz, 4.00H, H-2,6,2',6'), 7.69 (d, $^3J = 8.2$ Hz, 3.98 H, H-3,5,3',5'), 6.05 – 5.93 (m, 0.28 H, H-e2, H-e3), 5.79 (dd, $^3J = 19.3$ Hz, $^3J = 5.0$ Hz, 0.14 H, H-e3'), 0.65 (s, 1.08 H, H-d1,2,f2), 0.39 (s, 9.44 H, H-a1,2,c1,2), 0.32 (s, 0.39 H, H-f1), 0.17 (s, 0.37 H-e1), 0.10 (s, 4.28 H, H-b1,2) ppm.

$^{13}\text{C}\{^1\text{H}\}$ NMR (151 MHz, CDCl_3):^a $\delta = 153.4$ (C-1,1'), 144.5 (C-4,4' if R=vinyl), 143.6 (C-4,4' if R=Me), 141.9 (C-4,4' if R=Me),^b 141.7 (C-4,4' if R=Me),^a 137.0 (C-e2), 135.2,^c 135.1,^c 134.0,^c 133.9 (C-3,5,3',5'

^a Since the distribution of vinyl groups throughout the chain is random, partially very low intensities, overlapping signals in $^1\text{H NMR}$ and small chemical shift differences in all spectra made the full assignment of all signals to structural units impossible.

^b The repeating unit corresponding to these signals is probably neighboring one or more repeating units with a vinyl group.

^c The signals at 135.2, 135.1 and 134.0 could not be assigned by 2D experiments. However, they probably correspond to C-3,5,3',5' with a vinyl group in the same or adjacent repeating units.

if R=Me), 133.5 (C-e3), 122.2 (C-2,6,2',6' if R=vinyl) 122.1 (C-2,6,2',6' if R=Me), 1.5 (C-b1,2), 1.4, 1.03, 0.95, 0.91, -0.15, -0.3 (C-e1), -1.0 (C-f1), -2.2 (C-d1,2,f2) ppm.

$^{29}\text{Si}\{^1\text{H}\}$ NMR (99 MHz, CDCl_3): δ = -2.4 (Si-a,c), -3.5 (Si-a,c)^a -7.2 (Si-d,f), -18.9 (Si-b), -33.0 (Si-e) ppm.

IR (ATR): $\tilde{\nu}$ = 3025 (w), 2958 (m), 2900 (w), 1670 (w), 1591 (w), 1407 (w), 1389 (m), 1309 (w), 1257 (s), 1109 (s), 1031 (vs), 1012 (vs), 835 (vs), 781 (vs), 687 (s), 665 (s), 622 (m), 555 (s), 529 (m) cm^{-1} .

GPC (THF, 1 mL/min, conv. calibration (PS), ambient light): M_n = 14.4 kDa; M_w = 23.3 kDa; PDI = 1.62.

GPC (THF, 1 mL/min, conv. calibration (PS), 365 nm, 60 min): M_n = 11.8 kDa; M_w = 19.9 kDa; PDI = 1.69.

GPC Measurements

The polymer was dissolved in THF (ca. 1 mg/mL) and GPC spectra were recorded both without and after irradiation with UV light (365 nm, 60 min). Upon switching with UV light, the apparent molecular weight changes from 14.4 kDa to 11.8 kDa in case of M_n and from 23.3 kDa to 19.9 kDa in case of M_w (Figure SI-1). This corresponds to a decrease in apparent weight by 18% (M_n) and 15% (M_w), while the PDI remains almost constant, being 1.62 before and 1.69 after UV irradiation.

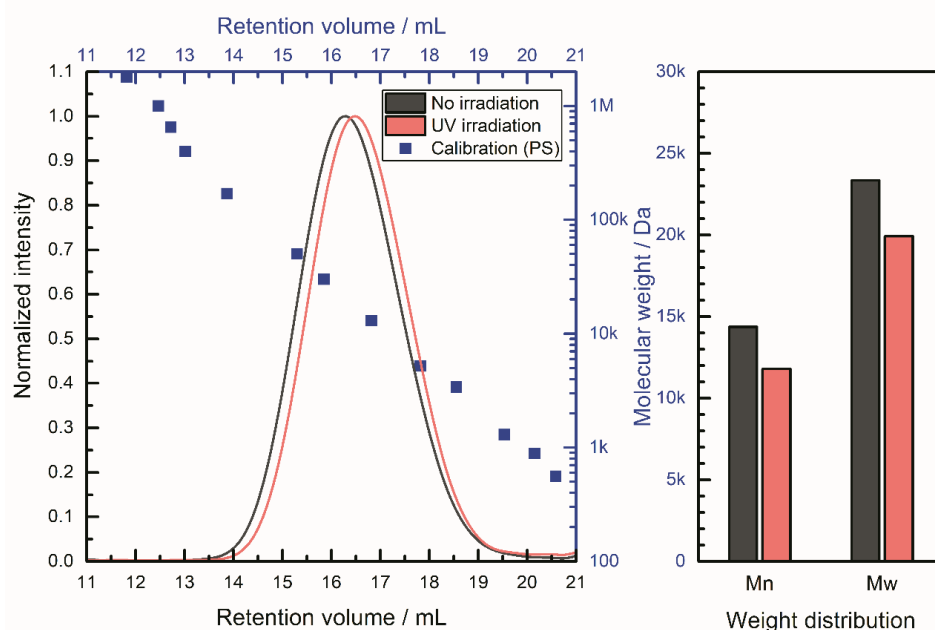


Figure SI-1. Analysis of the switching behavior of polymer **3** dissolved in THF (1 mg/mL). Left: the GPC chromatograms corresponding to the polymer without (grey) and after UV irradiation (red). The intensities were normalized for clarity. Blue squares indicate the retention volumes of the polystyrene standards used for calibration. Right: Comparison of the assigned apparent molecular weights. Shown are number average (M_n) and weight average (M_w) of the polymer without (grey) and after UV irradiation (red).

^a This repeating unit is probably adjacent to one with a vinyl group.

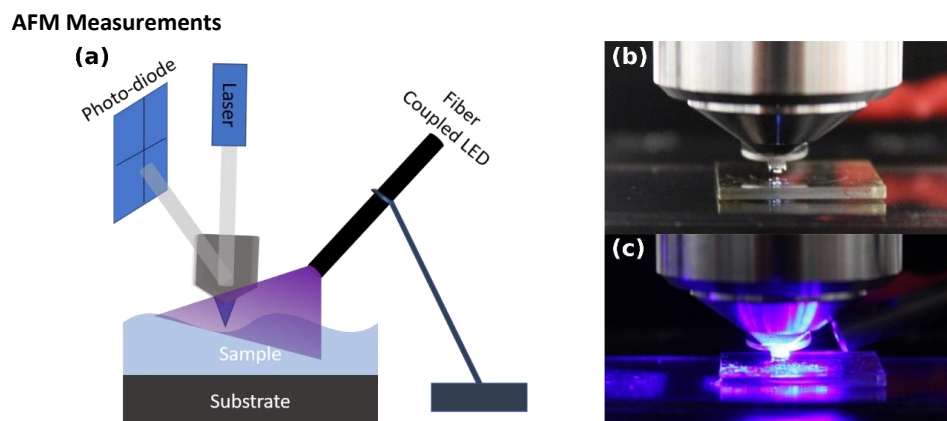


Figure SI-2. (a) Setup of the AFM experiments. The sample film was spin coated on a quartz glass slide. In addition to the conventional setup of the environmental AFM, the sample was illuminated through a fiber coupled LED in an angle of 30°. (b) Photograph of the setup without illumination in ambient light. (c) Photograph of the setup during illumination with UV light.

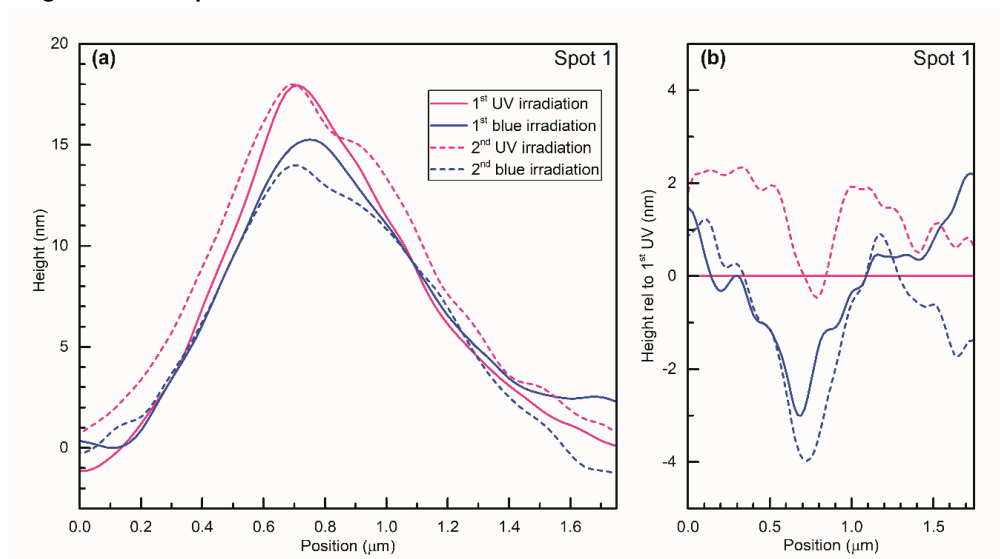
Height Profile of Spot 1

Figure SI-2. AFM analysis of Spot 1. (a) Height profile obtained from the AFM micrographs. (b) Height variations upon irradiation. Plotted are the differences in height relative to the 1st UV irradiation.

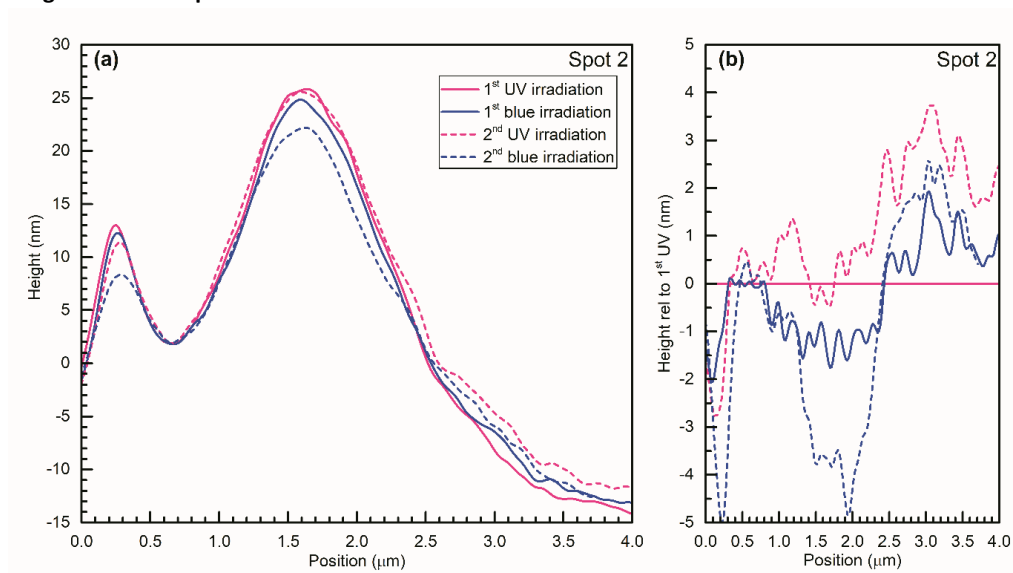
Height Profile of Spot 2

Figure SI-3. AFM analysis of Spot 2. (a) Height profile obtained from the AFM micrographs. (b) Height variations upon irradiation. Plotted are the differences in height relative to the 1st UV irradiation.

Height Profile of Spot 3

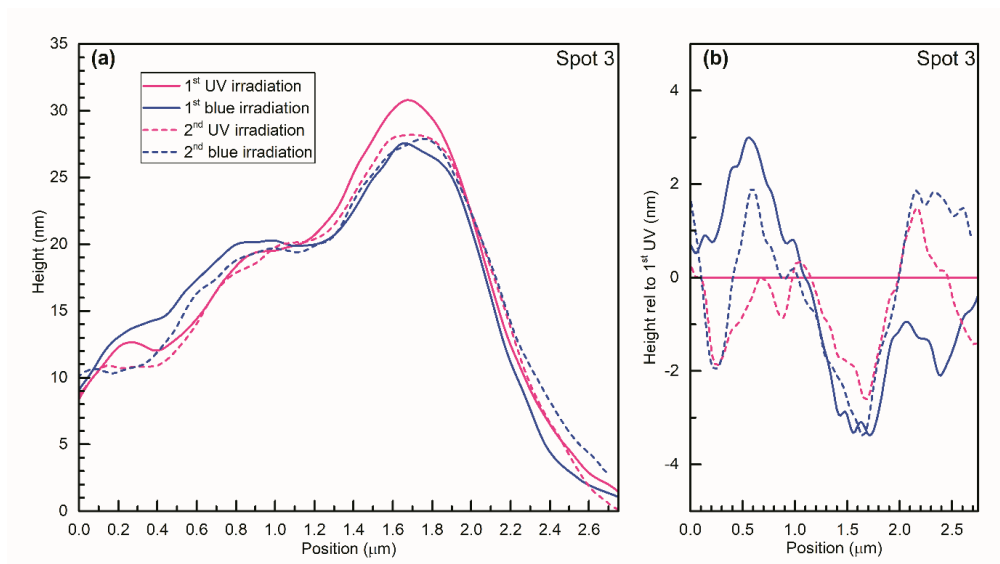


Figure SI-4. AFM analysis of Spot 3. (a) Height profile obtained from the AFM micrographs. (b) Height variations upon irradiation. Plotted are the differences in height relative to the 1st UV irradiation.

Plotted UV-Vis Spectra of the Polymer 3 in THF

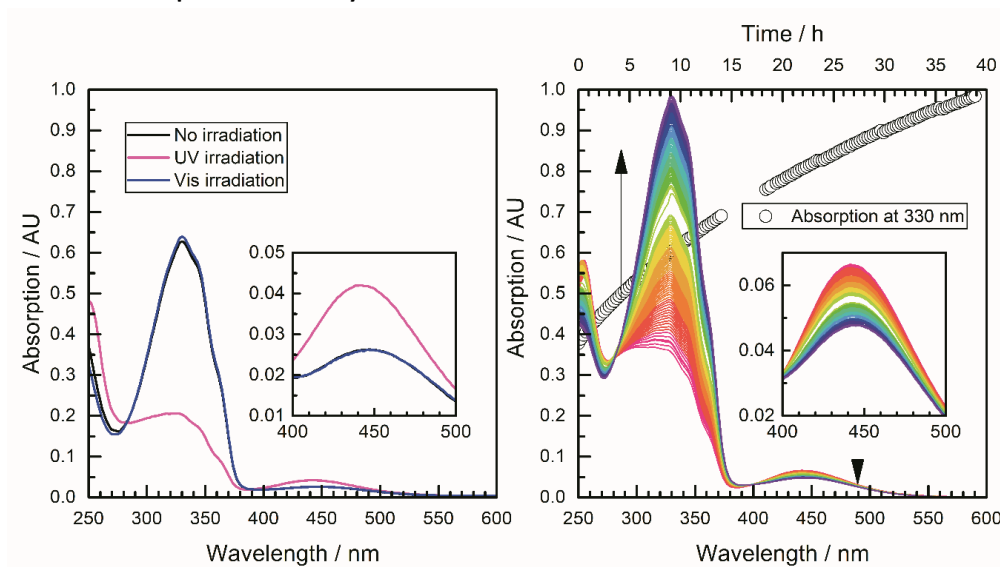
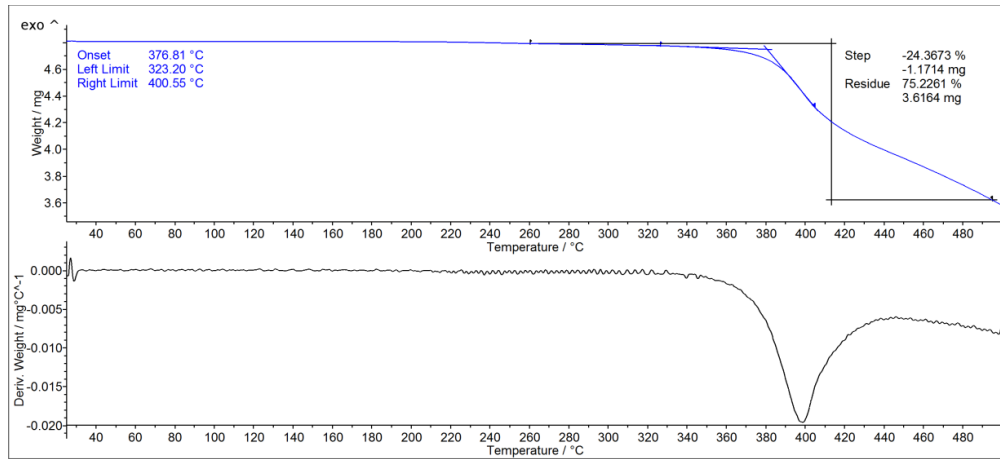
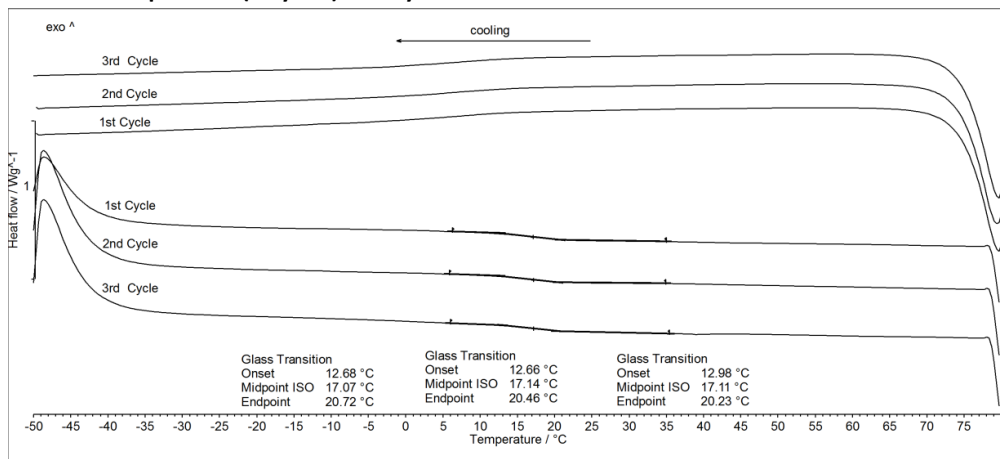


Figure SI-5. UV-vis spectra of the polymer **3** dissolved in THF. Left: comparison of without (black line), after UV- (pink line) and visible irradiation (blue line). The concentration of azobenzene moieties in the solution in acetonitrile was approx. 0.02 mmol/L. Right: Thermal relaxation after irradiation with UV light over the course of 40 h. The spectra were recorded with a delay of 15 min. The development of the absorption at 330 nm is shown as black circles. The concentration of azobenzene moieties in the solution was approx. 0.05 mmol/L. The half-life time was determined by an exponential fit to be $21 \text{ h} \pm 18 \text{ min}$.

Plotted TGA Spectrum of Polymer 3

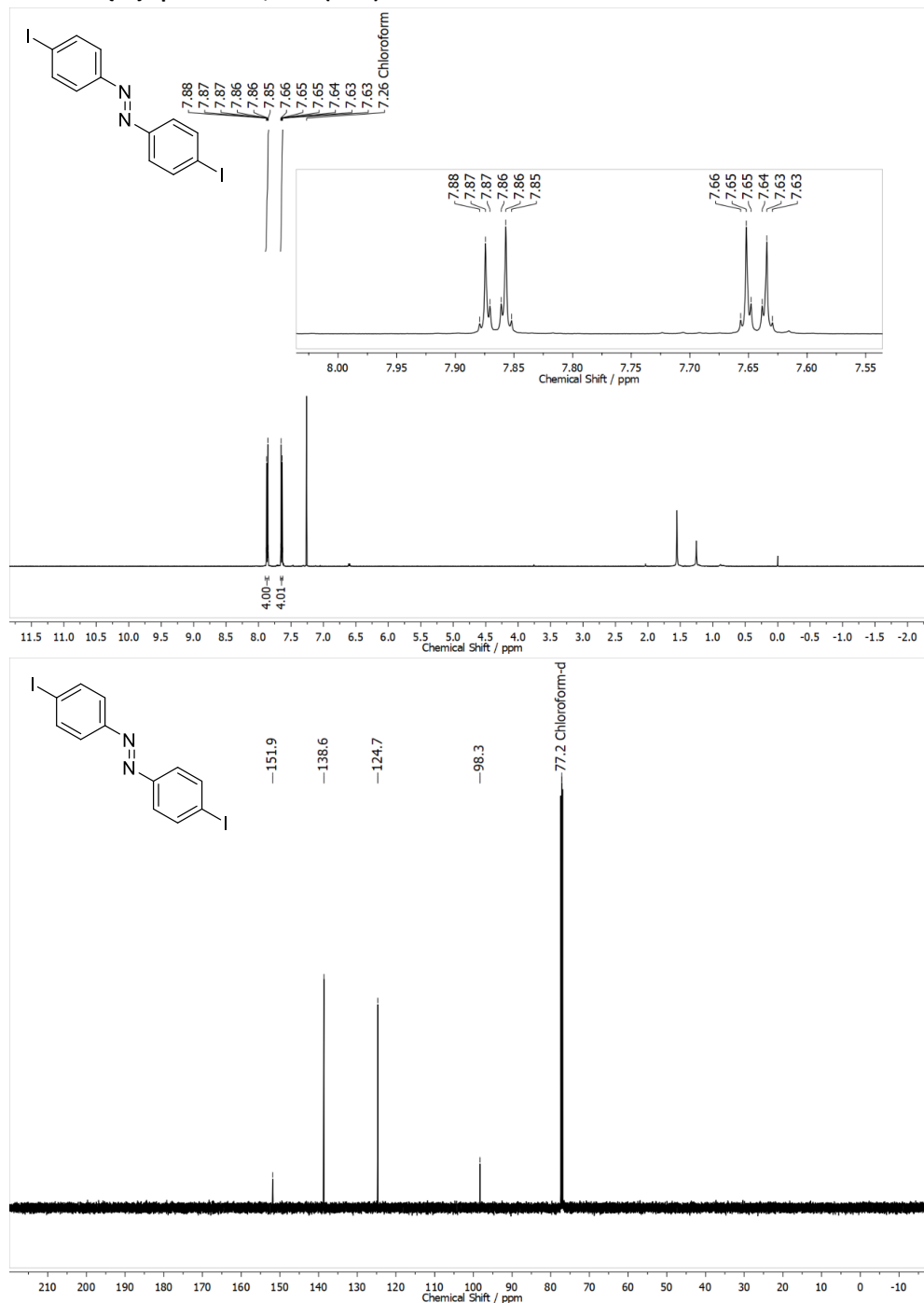


Plotted DSC Spectrum (3 Cycles) of Polymer 3

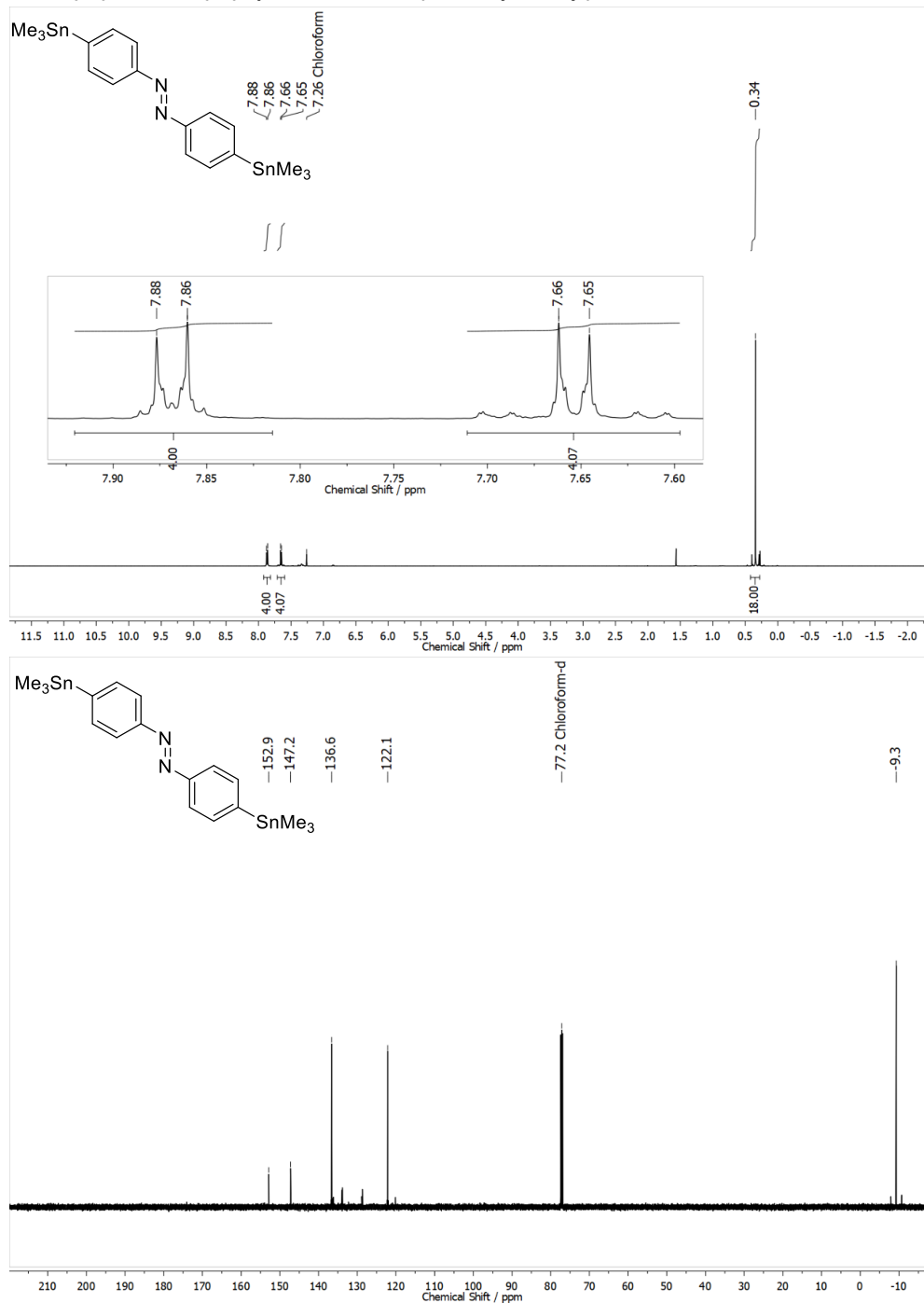


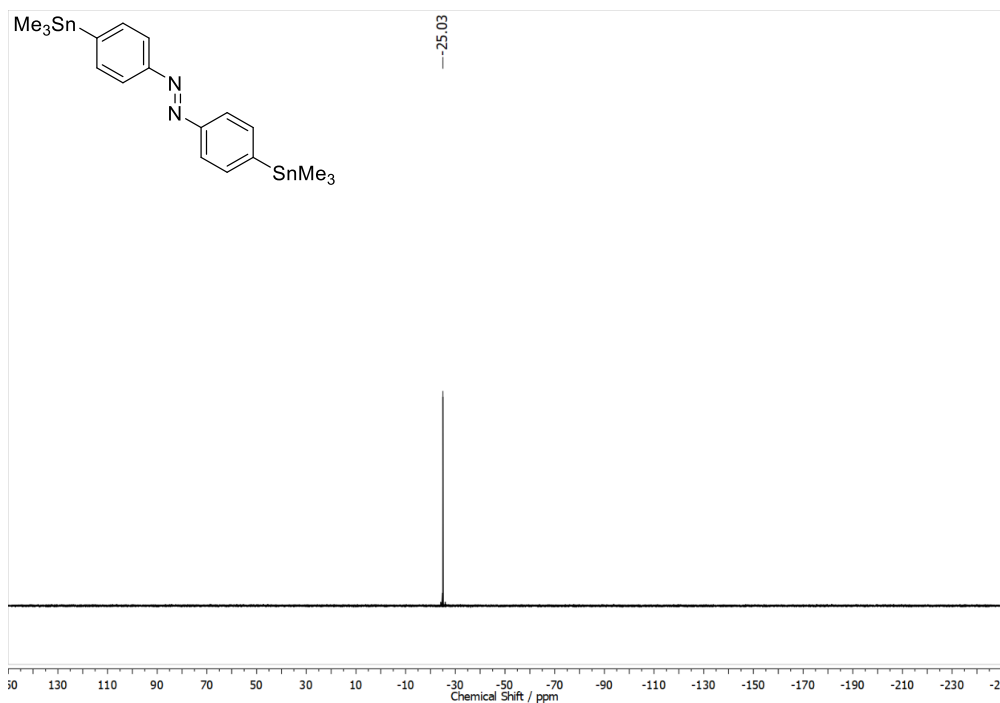
Plotted ^1H , $^{13}\text{C}\{^1\text{H}\}$ and hetero NMR Spectra for All Compounds

^1H and $^{13}\text{C}\{^1\text{H}\}$ Spectra of 4,4'-Bis(iodo)azobenzene in Chloroform-*d*

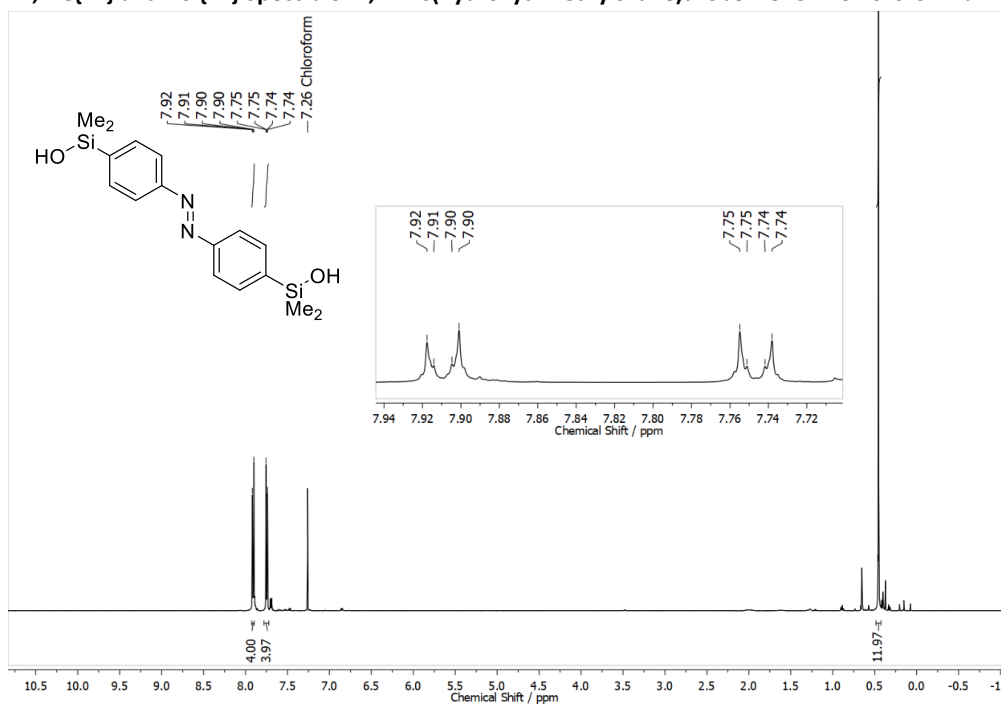


SI-16

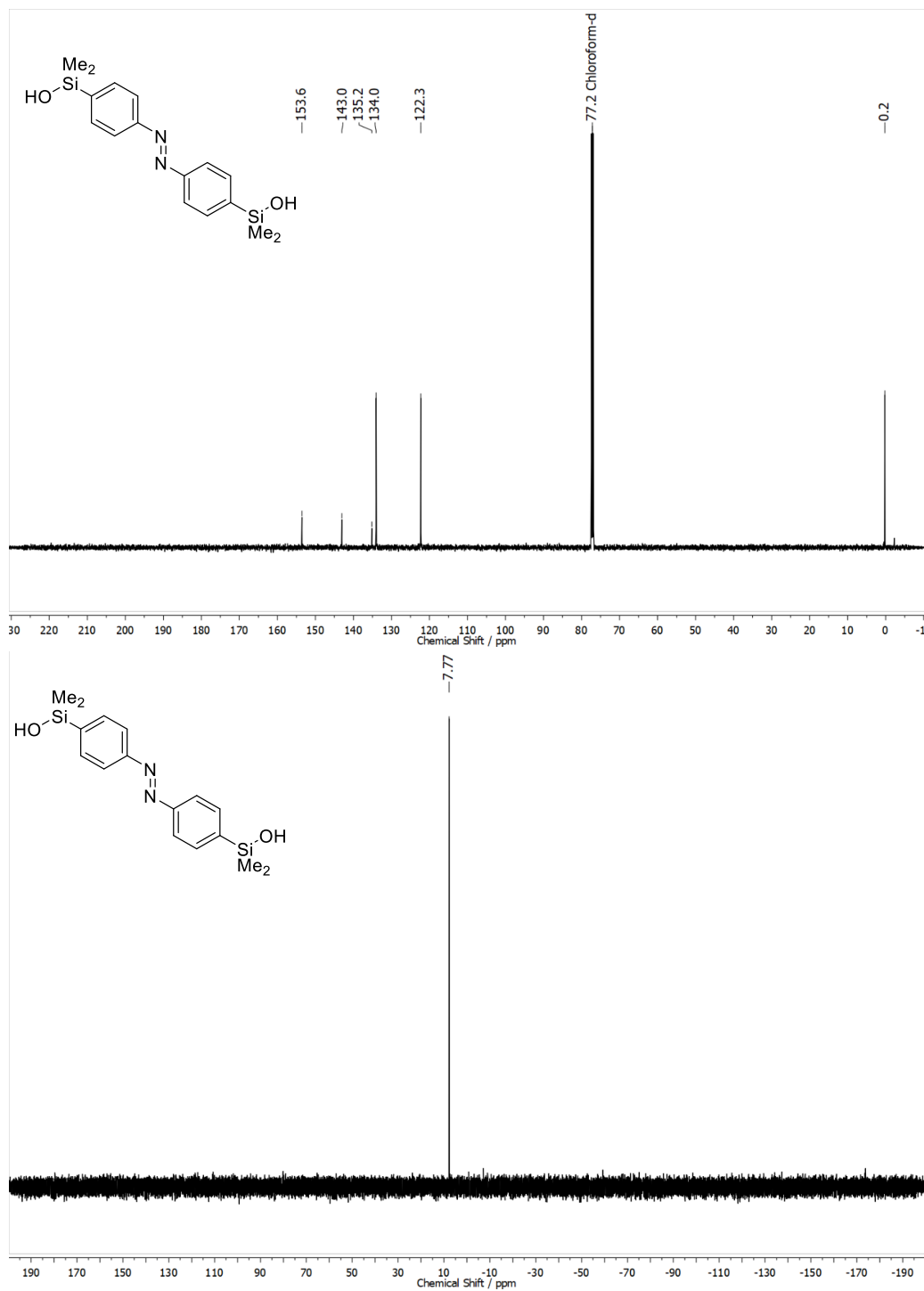
^1H , $^{13}\text{C}\{^1\text{H}\}$ and $^{129}\text{Sn}\{^1\text{H}\}$ Spectra of 4,4'-Bis(trimethylstannyl)azobenzene in Chloroform-d



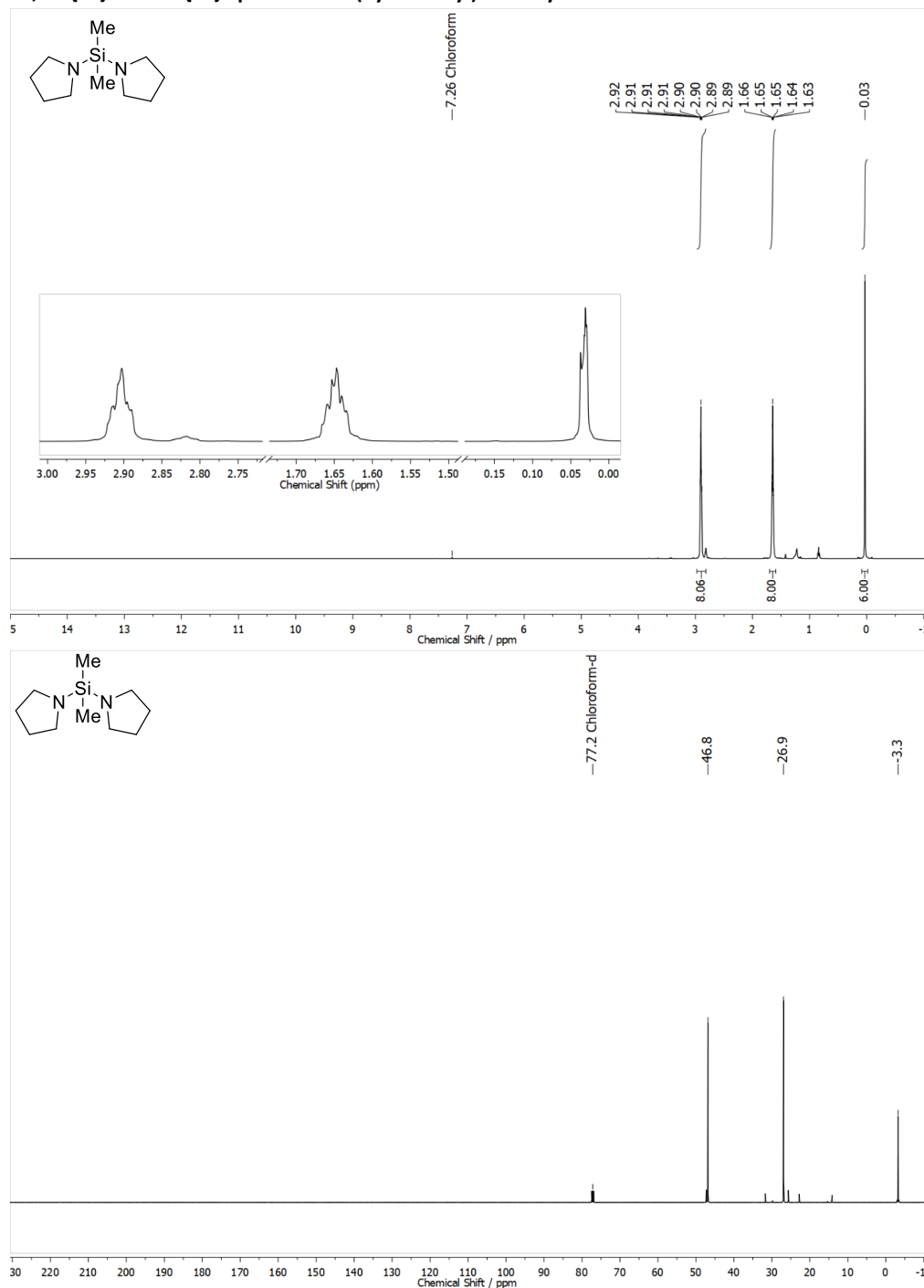
¹H, ¹³C{¹H} and ²⁹Si{¹H} Spectra of 4,4'-Bis(hydroxydimethylsilane)azobenzene in Chloroform-*d*



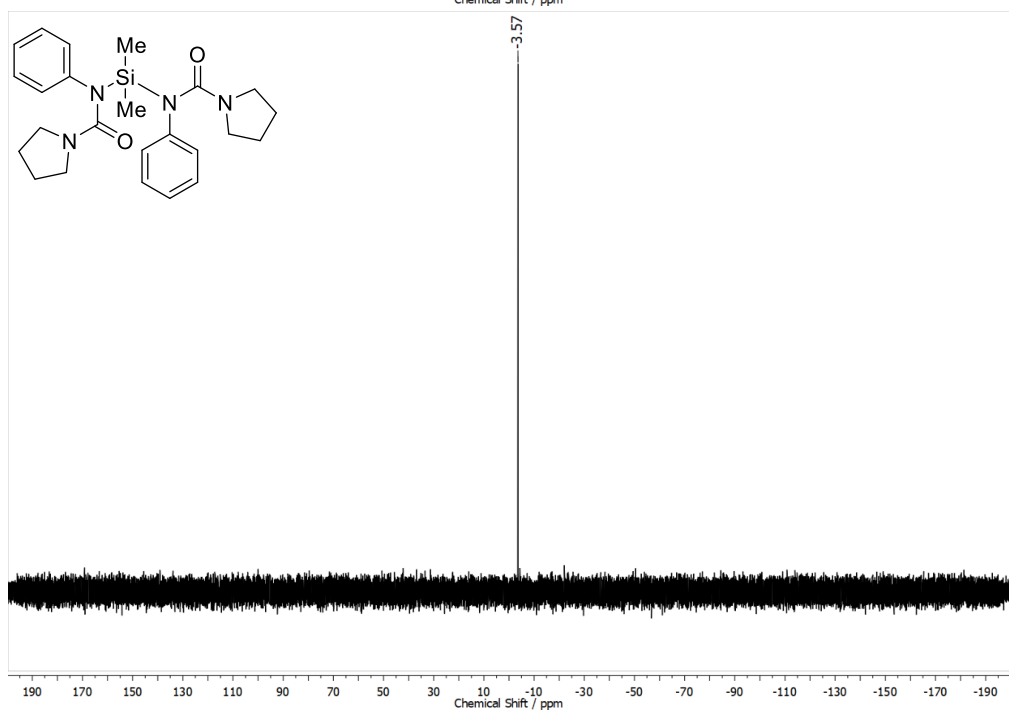
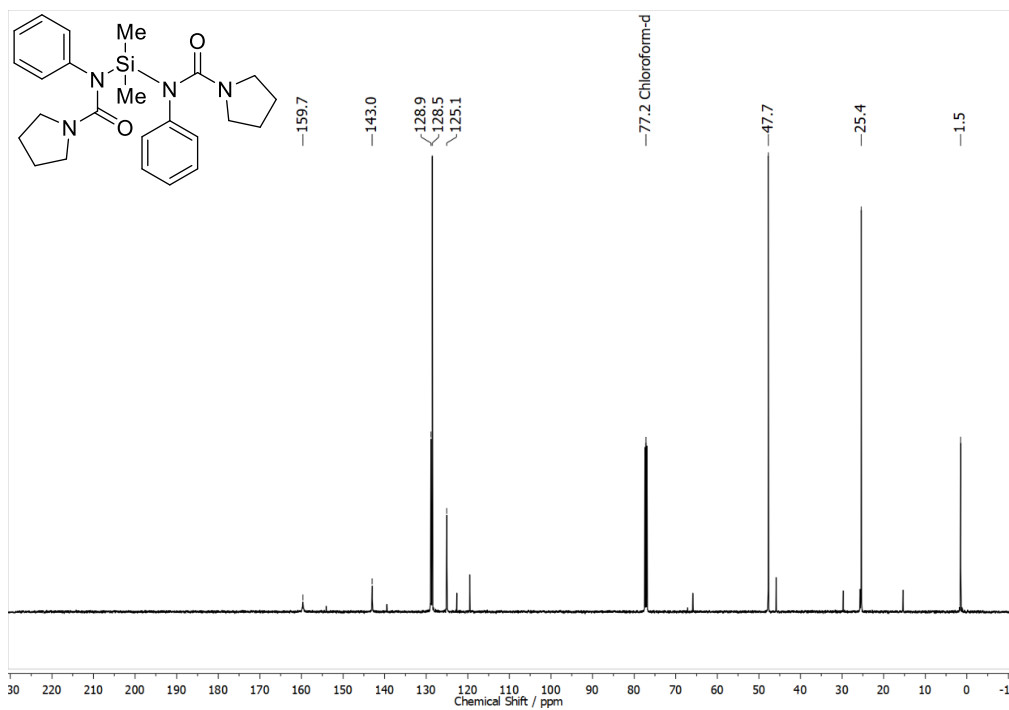
SI-18



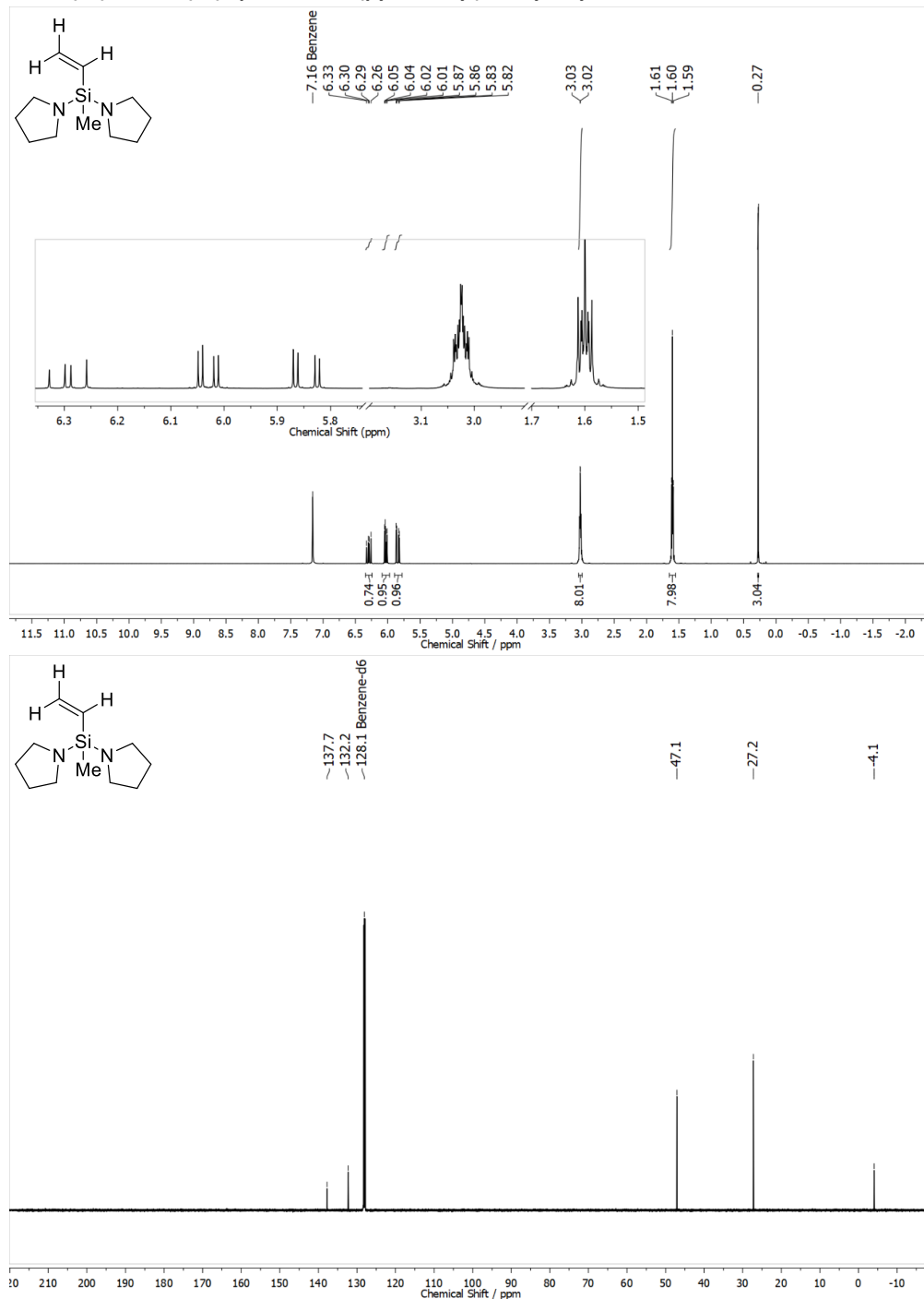
¹H, ¹³C{¹H} and ²⁹Si{¹H} Spectra of Bis(Pyrrolidinyl)dimethylsilane in Chloroform-d

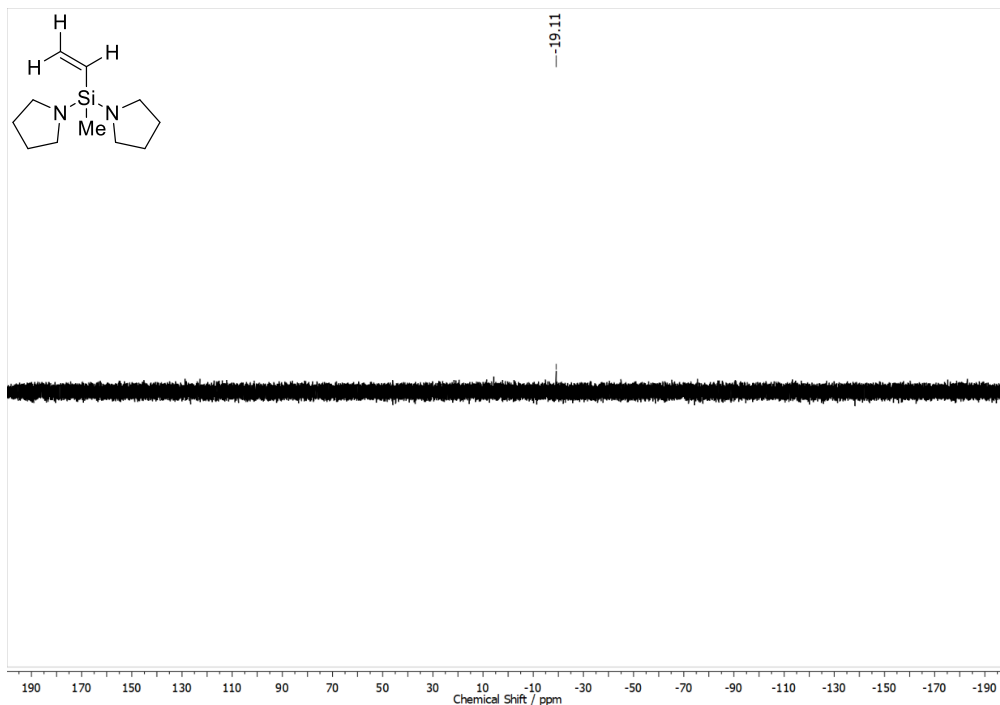


SI-20

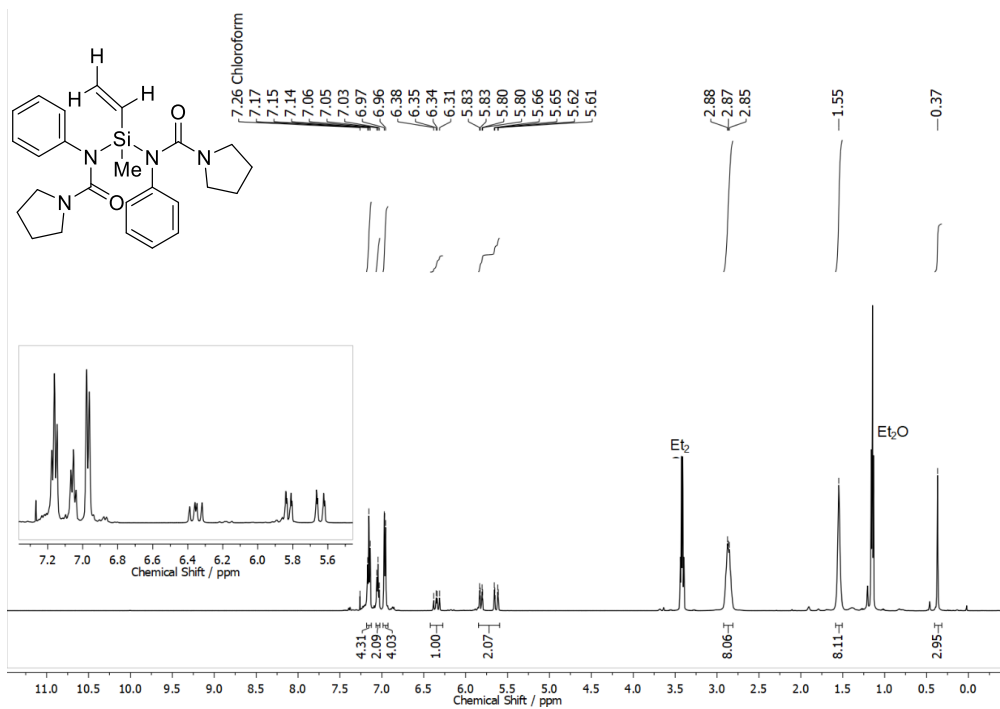


SI-22

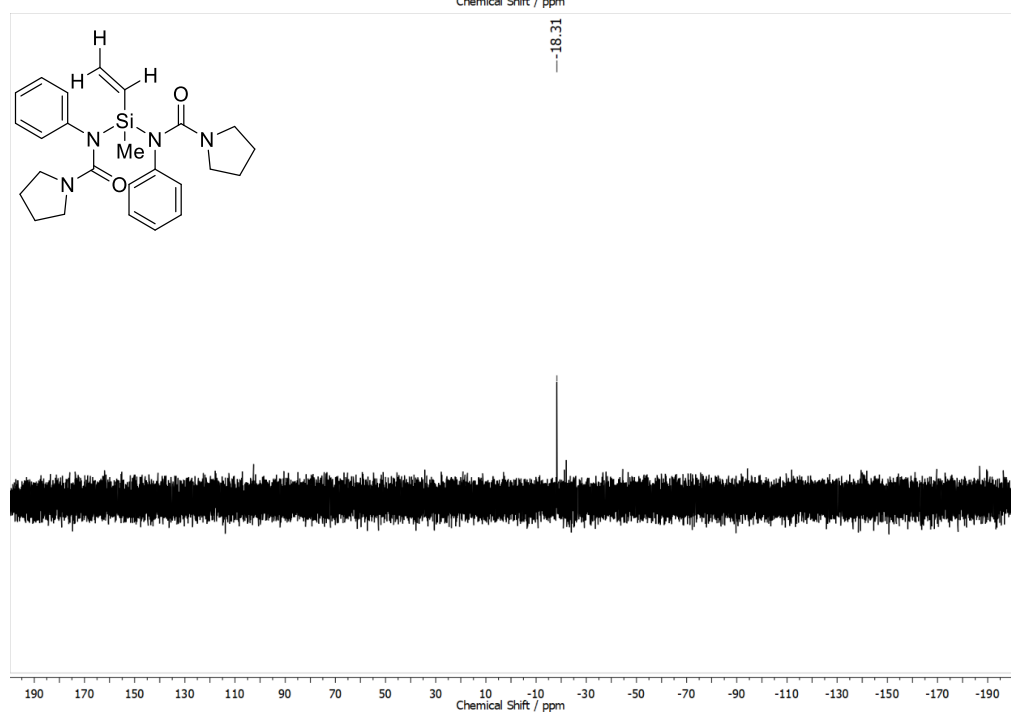
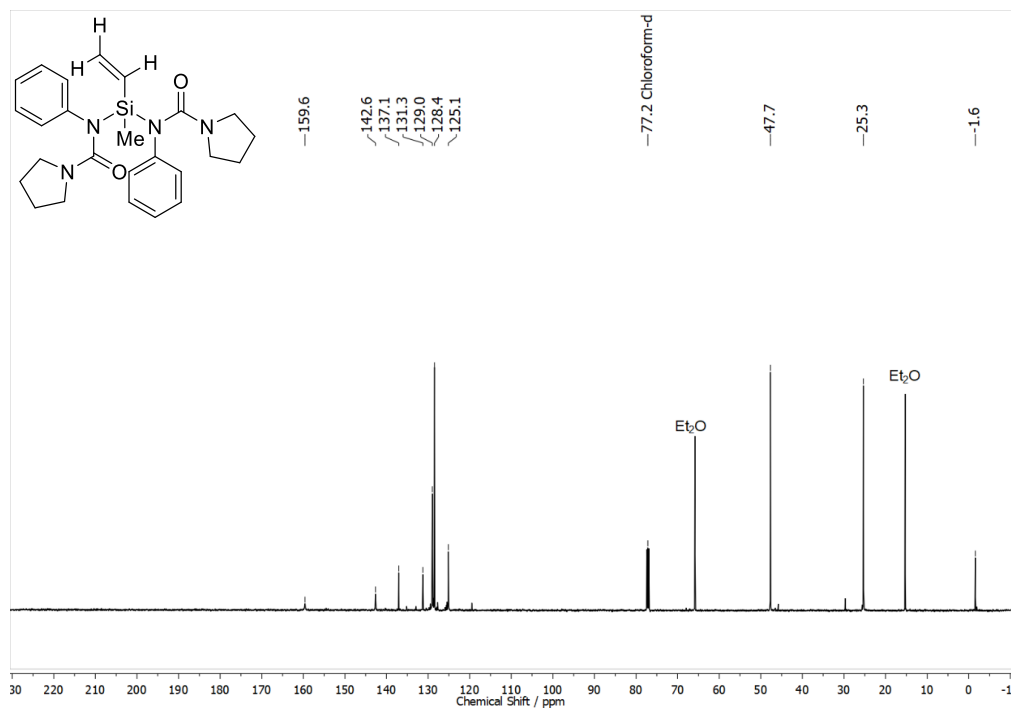
^1H , $^{13}\text{C}\{^1\text{H}\}$ and $^{29}\text{Si}\{^1\text{H}\}$ Spectra of Bis(pyrrolidinyl)methylvinylsilane in Benzene- d_6 



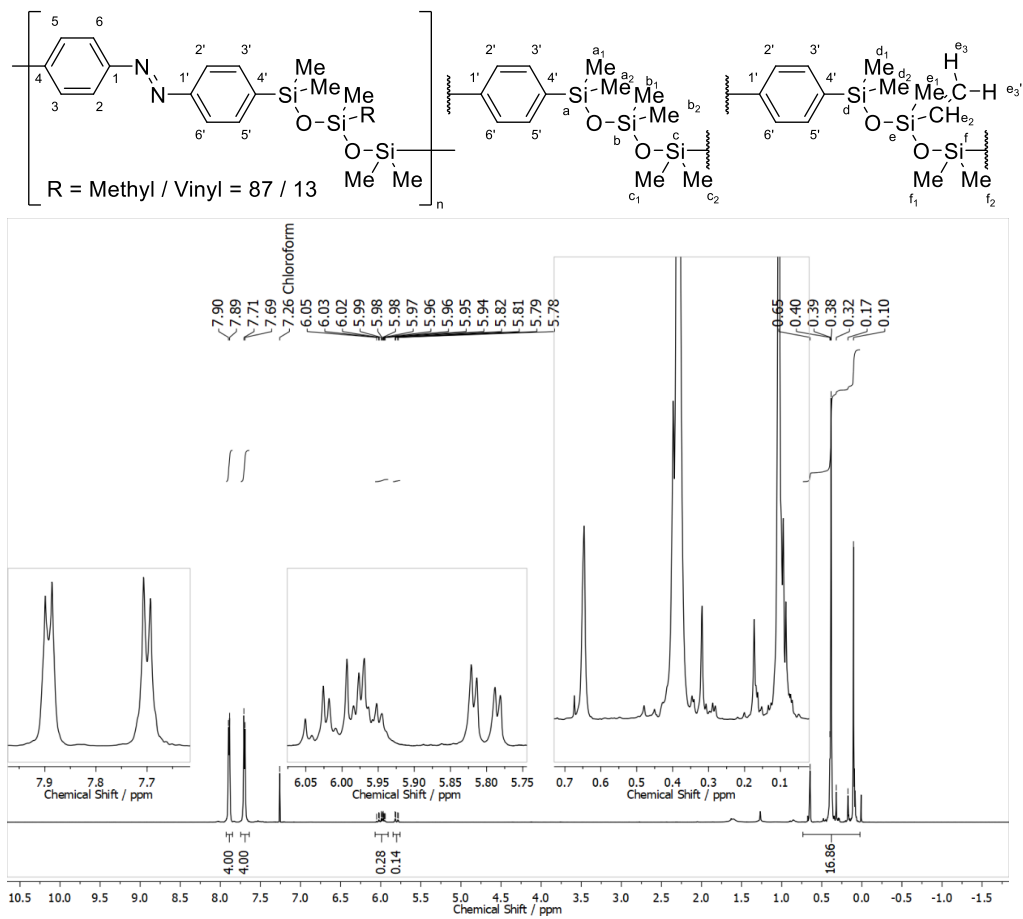
^1H , $^{13}\text{C}\{^1\text{H}\}$ and $^{29}\text{Si}\{^1\text{H}\}$ Spectra of Bis(*N*-phenyl-*N*-pyrrolidinecarbonylamino)methylvinylsilane in Chloroform-*d*

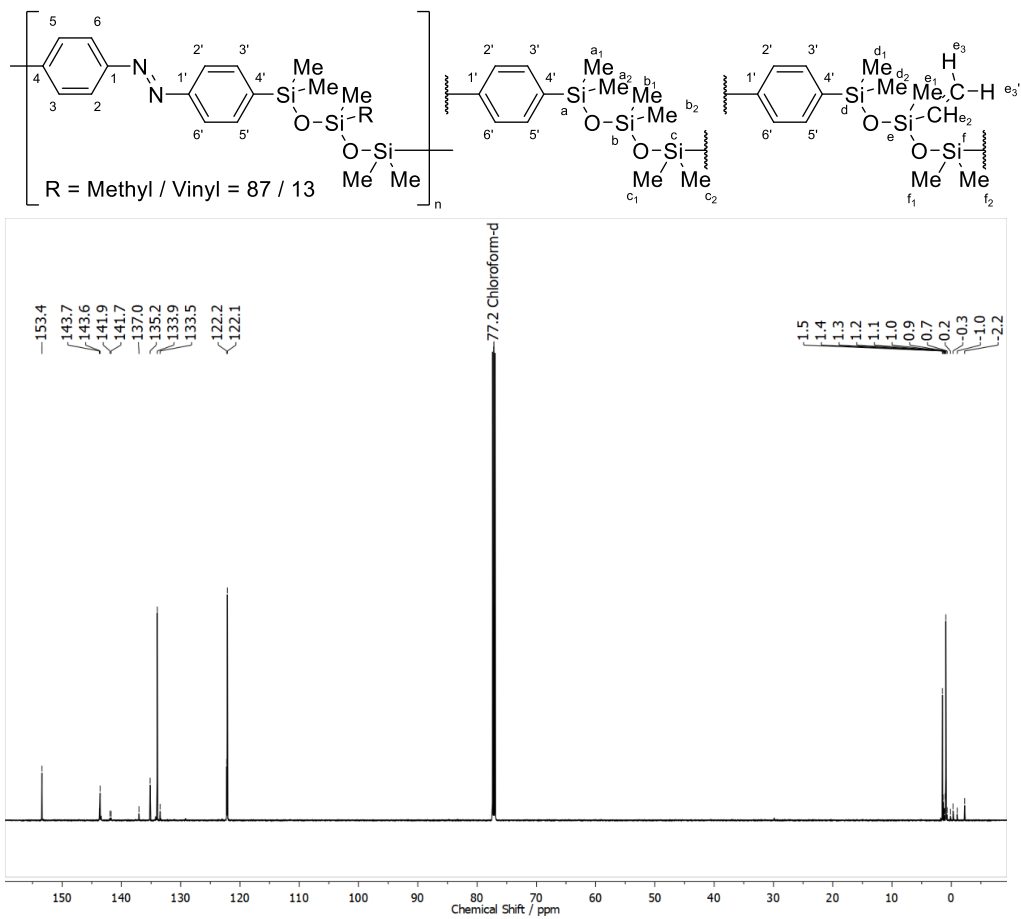


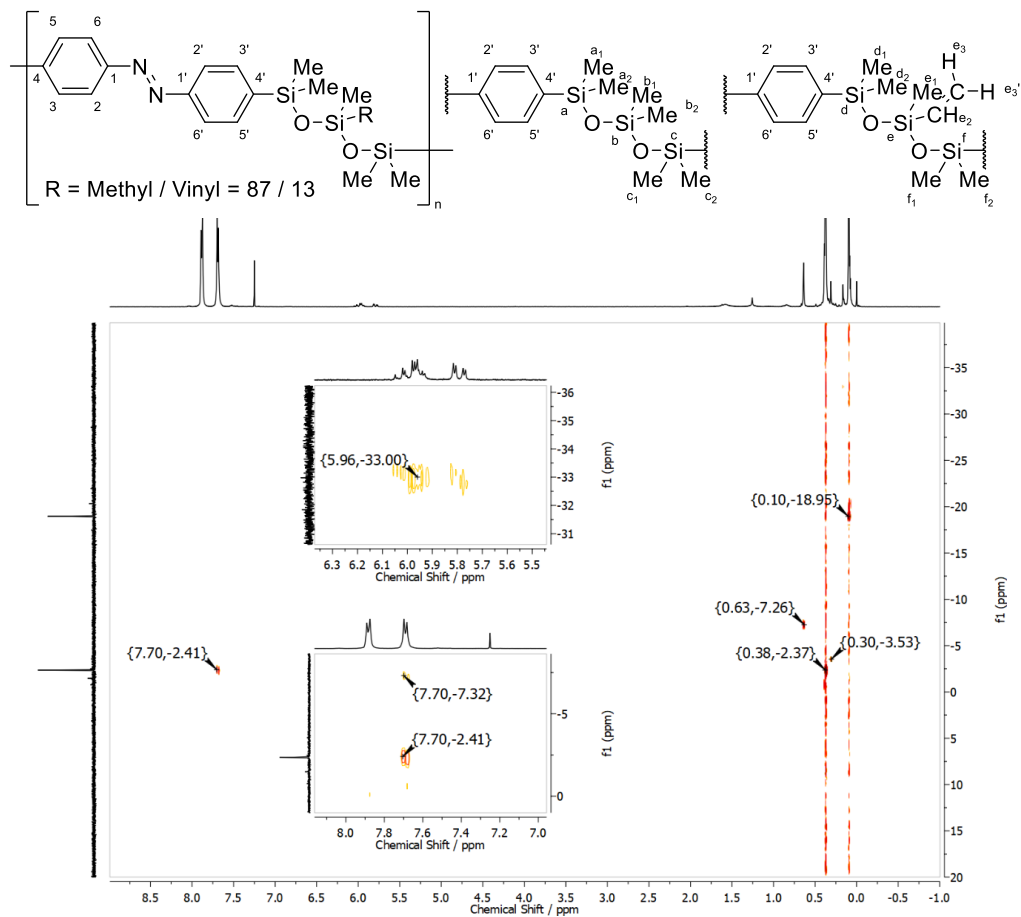
SI-24



^1H , $^{13}\text{C}\{^1\text{H}\}$ and $^{29}\text{Si}\{^1\text{H}\}$ HMBC Spectra of Poly(4,4'-azobenzene-*alt*-(hexamethyl-trisiloxane)-*stat*-(1,1,3,5,5-pentamethyl-3-vinyl-trisiloxane)) (3) in Chloroform-*d*



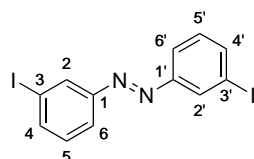




7. A Macrocyclic Azobenzene

7.1. Syntheses

7.1.1. Synthesis of 3,3'-Diiodoazobenzene (65)



Copper(I) bromide (7.24 g, 45.7 mmol) was dissolved in pyridine (90 mL) and stirred at 24 °C for 30 min. After filtration, the filtrate was diluted with pyridine (20 mL) and 3-iodoaniline (14.3 g, 65.3 mmol) was added. The reaction mixture was stirred at 24 °C for 20 h, while air was purged through a syringe (0.2 bar, 250 L h⁻¹, diameter: 1 mm). To separate the phases, diethyl ether (300 mL), DCM (200 mL) and hydrochloric acid (2 mmol L⁻¹, 200 mL) were added. The solvents of the organic phases were removed, before the precipitate was recrystallized from ethanol (300 mL) to give the product **65** as orange solid (9.58 g, 22.1 mmol, 68%, Lit.: 43%,^[114] 82%^[301]).

Mp: T = 152 °C (Lit.:^[302] T = 153 °C to 154 °C).

¹H NMR (600 MHz, C₆D₆): δ = 8.27 (at, ⁴J = 1.8 Hz, 1H, H-2,2'), 7.68 (ddd, ³J = 7.9 Hz, ⁴J = 1.8 Hz, ⁴J = 1.1 Hz, 1H, H-4,4') 7.40 (ddd, ³J = 7.9 Hz, ⁴J = 1.7 Hz, ⁴J = 1.1 Hz, 1H, H-6,6') 6.62 (at, ³J = 7.9 Hz, 1H, H-5,5').

¹³C{¹H} NMR (151 MHz, C₆D₆): δ = 153.4 (C-1,1'), 140.2 (C-6,6'), 131.2 (C-2,2'), 130.7 (C-5,5'), 123.9 (C-4,4'), 94.9 (C3,3') ppm.

IR (ATR): $\tilde{\nu}$ = 3056 (w), 1576 (m), 1557 (m), 1454 (m), 1404 (m), 1191 (m), 1147 (m), 1051 (m), 992 (m), 910 (m), 882 (s), 853 (s), 846 (s), 791 (vs), 682 (vs), 653 (vs), 532 (s), 522 (s) cm⁻¹.

HRMS (EI-TOF): $m/z = [M]^+$ (%) calcd for [C₁₂H₈¹²⁷I₂N₂]⁺ 433.87768, found 433.87963 (100).

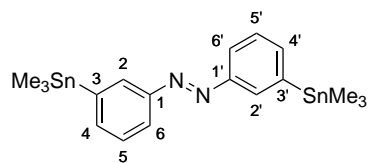
7.1.2. Synthesis of 3,3'-Bis(trimethylstannyl)azobenzene (63)

In a nitrogen filled glovebox, seven identical reaction vials were prepared as follows:^{II}

3,3'-Diiodoazobenzene (**65**, 1.3 g, 3.00 mmol), hexamethyldistannane (2.29 g, 7.00 mmol)

^IIn this reference, the product was obtained via a reductive azo-coupling using 3-iodonitrobenzene as starting material.

^{II}The capacity of the microwave reaction vessels was limited to 20 mL. Therefore, multiple reaction mixtures had to be prepared and were combined for workup.



and Pd(PPh₃)₄ (139 mg, 120 μmol) were dissolved in toluene (18.0 mL) and THF (2.0 mL). The vial was closed with a crimp cap and transferred out of the glovebox. The reaction mixtures were heated by MW heating to 170 °C for 30 min. After cooling to 25 °C, the reaction mixtures were combined and the solvent was removed under reduced pressure. The residue was purified by flash chromatography (*n*-hexane). To remove remaining tin impurities, the crude product was redissolved in ethyl acetate (150 mL) and washed with brine (2 × 150 mL). Drying over magnesium sulfate and removal of solvent yielded the product **63** as orange solid (9.08 g, 17.9 mmol, 85%, Lit.:^[114] 70%).

TLC (UV, *n*-hexane): R_f = 0.65.

Mp: T = 60 °C (Lit.:^[114] T = 61 °C).

¹H NMR (500 MHz, CDCl₃): δ = 8.04 (dd, ⁴J = 2.1 Hz ⁵J = 0.5 Hz, 1H, H-2,2'), 7.84 (ddd, ³J = 7.9 Hz, ⁴J = 2.1 Hz, ⁴J = 1.3 Hz, 1H, H-6,6'), 7.60 (ddd, ³J = 7.1 Hz, ⁴J = 1.3 Hz, ⁴J = 1.3 Hz, 1H, H-4,4'), 7.49 (ddd, ³J = 7.9 Hz, ³J = 7.1 Hz, ⁵J = 0.5 Hz, 1H, H-5,5'), 0.36 (Sn(CH₃)₃) ppm.

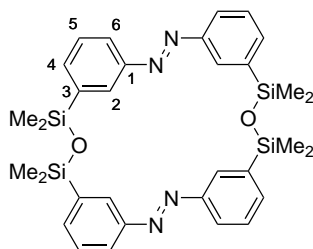
¹³C{¹H} NMR (500 MHz, CDCl₃): δ = 152.3 (C-1,1'), 143.7 (C-3,3'), 138.6 (C-4,4'), 130.6 (C-2,2'), 128.8 (C-5,5'), 121.1 (C-6,6'), -9.2 (Sn(CH₃)₃) ppm.

¹²⁹Sn{¹H} NMR (187 MHz, CDCl₃): δ = -23.97 ppm.

IR (ATR): $\tilde{\nu}$ = 2978 (w), 2915 (w), 1723(w), 1578 (w), 1559 (w), 1398 (s), 1264 (m), 1193 (m), 1157 (s), 1102 (m), 1056 (m), 925 (s), 803 (vs), 762 (vs), 752 (vs), 713 (s), 695 (vs), 529 (vs), 514 (vs) cm⁻¹.

HRMS (EI-TOF): m/z = [M]⁺ (%) calcd for [C₁₈H₂₆N₂¹¹⁸Sn¹¹⁸Sn]⁺ 508.01340, found 508.01534 (30), 492.94 (100) [M-CH₃].

7.1.3. Synthesis of (1(*E*),5(*E*))-2,2,4,4,6,6,8,8-Octamethyl-1,5-(3,3')-diazobenzene-3,7-dioxa-2,4,6,8-tetrasilacyclooctaphane (**64**)



This reaction was carried out under an argon atmosphere.

3,3'-Bis(trimethylstannyl)-azobenzene (3.00 g, 5.91 mmol) was dissolved in dry, degassed THF (70 mL). After cooling to -78 °C, a solution of methyl lithium in 2-methyltetrahydro-

furan and cumene (10 mL, 1.6 mol/L, 16 mmol) was added within 30 s. The solution was stirred at this temperature for 15 min, before dichlorodimethylsilane (24.0 mL, 25.7 g, 199 mmol) was added in one portion to quench the reaction and the mixture was allowed to warm up to 25 °C by removing the cooling bath. The solvent and excess of dichlorodimethylsilane were evaporated under reduced pressure. The residual orange solid was dissolved in THF (40 mL) and added to a solution of sodium methoxide in methanol (13.5 mL of a 4.5 mol/L solution that was diluted with 20 mL methanol; corresponding to 60.8 mmol sodium methoxide in 23.5 mL methanol) with a dropping speed of 1 mL/min.

After this step, the workup continued under ambient conditions. To the resulting mixture, a solution of sodium hydroxide in methanol and water (24 mL, 5 mol/L, 120 mmol; methanol/water: 10/1) was added and the resulting mixture was stirred for 2 h at 30 °C, before it was poured into a vigorously stirred solution of monopotassium phosphate in water (150 mL, 1 mol/L). The layers were separated and the aqueous phase was extracted with chloroform (4 × 50 mL). After drying the combined organic phases over magnesium sulfate and removing the solvent, the crude product was purified by crystallization. Therefore, the crude product was dissolved in chloroform (2 mL), overlaid with *n*-hexane (2 mL) and allowed to crystallize for 16 h at –32 °C. The solvent of the filtrate was removed and the procedure repeated with 1 mL of each, chloroform and *n*-hexane. Combining the crystals gave the product as orange solid (270 mg, 415 μmol, 14%).

The crystals were characterized by single crystal X-ray diffraction and consisted solely of (*E*)/(*E*)-isomers. When dissolved under ambient light, NMR experiments proved the presence of (*E*)/(*E*)-isomers in solutions in CDCl₃. Upon irradiation with UV light (340 nm), a PSS containing 90% (*Z*),(*Z*)-isomer, 6% (*E*),(*Z*)-isomer and 4% (*E*),(*E*)-isomer was reached.

Mp: T = 205 °C.

¹H NMR (500 MHz, CDCl₃): δ = 7.69 – 7.66 (m, 8H, H-2, H-6), 7.54 – 7.50 (m, 4H, H-4), 7.42 – 7.37 (m, 4H, H-5), 0.42 (s, 24H, Si-CH₃) ppm.

¹³C{¹H} NMR (126 MHz, CDCl₃): δ = 151.7 (C-3), 140.3 (C-1), 135.4 (C-4), 128.4 (C-5), 128.0 (C-2), 123.8 (C-6), 0.4 (Si-CH₃) ppm.

²⁹Si{¹H} NMR (99 MHz, CDCl₃): δ = -0.49 ppm.

IR (ATR): $\tilde{\nu}$ = 2961 (w), 1399 (w), 1249 (m), 1160 (m), 1158 (w), 1112 (m), 1050 (s), 928 (w), 899 (m), 819 (m), 793 (s), 778 (s), 694 (s), 665 (s), 646 (w), 533 (m), 522 (m) cm⁻¹.

HRMS (EI-TOF): $m/z = [M]^+$ (%) calcd for [C₃₂H₄₀N₄O₂Si₄]⁺ 624.22283, found 624.22283 (100).

UV (*n*-hexane): λ = 319 nm (ππ*), 445 nm (nπ*).

7.2. X-ray Diffraction Crystal Structure of the (1(*E*),5(*E*)) -Isomer **64a**

Crystals of **64a** were obtained by dissolving **64** in chloroform, while *n*-pentane vapors were allowed to diffuse into the solution over the course of 3 d. The X-ray diffractometry measurements and structure refinement were carried out by Prof. Christian Näther, University of Kiel. The following results were assigned.

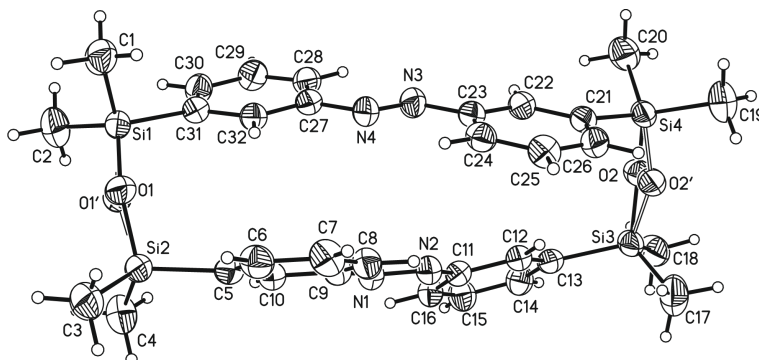


Table 1. Crystal data and structure refinement for staubitz14 (MS8A).

Identification code	staubitz14	
Empirical formula	$C_{32}H_{40}N_4O_2Si_4$	
Formula weight	625.04	
Temperature	170(2) K	
Wavelength	0.71073 Å	
Crystal system	Monoclinic	
Space group	P2 ₁ /c	
Unit cell dimensions	a = 12.1713(4) Å	$\alpha = 90^\circ$.
	b = 13.0106(2) Å	$\beta = 95.225(2)^\circ$.
	c = 21.4590(6) Å	$\gamma = 90^\circ$.
Volume	3384.04(16) Å ³	
Z	4	
Density (calculated)	1.227 Mg/m ³	
Absorption coefficient	0.210 mm ⁻¹	
F(000)	1328	
Crystal size	? x ? x ? mm ³	
Theta range for data collection	1.680 to 26.004°.	
Index ranges	-15 ≤ h ≤ 15, -16 ≤ k ≤ 15, -26 ≤ l ≤ 26	
Reflections collected	24956	
Independent reflections	6580 [R(int) = 0.0296]	
Completeness to theta = 25.242°	98.9 %	
Refinement method	Full-matrix least-squares on F ²	
Data / restraints / parameters	6580 / 4 / 405	
Goodness-of-fit on F ²	1.049	
Final R indices [I > 2σ(I)]	R1 = 0.0393, wR2 = 0.1036	
R indices (all data)	R1 = 0.0488, wR2 = 0.1089	
Extinction coefficient	n/a	
Largest diff. peak and hole	0.271 and -0.271 e.Å ⁻³	

Comments:

All non-hydrogen atoms were refined anisotropically. The C-H H atoms were positioned with idealized geometry (methyl H atoms allowed to rotate but not to tip) and refined isotropically with $U_{iso}(H) = 1.2 U_{eq}(C)$ (1.5 for methyl H atoms). Both O atoms are disordered in two positions and were refined using a split model with sof 70:30 using restraints for the Si-O distances.

Table 2. Atomic coordinates ($\times 10^4$) and equivalent isotropic displacement parameters ($\text{\AA}^2 \times 10^3$). U(eq) is defined as one third of the trace of the orthogonalized U^{ij} tensor.

	x	y	z	U(eq)
Si(1)	755(1)	3180(1)	8744(1)	39(1)
C(1)	-323(2)	4059(2)	8399(1)	52(1)
C(2)	109(2)	2077(2)	9114(1)	64(1)
O(1)	1513(6)	3896(4)	9245(4)	47(1)
O(1')	1599(13)	3579(9)	9309(8)	55(3)
Si(2)	2638(1)	4104(1)	9714(1)	41(1)
C(3)	2263(2)	5108(2)	10267(1)	59(1)
C(4)	3175(2)	2960(2)	10150(1)	60(1)
C(5)	3681(1)	4589(1)	9198(1)	39(1)
C(6)	3706(2)	5614(1)	9007(1)	46(1)
C(7)	4422(2)	5948(1)	8579(1)	50(1)
C(8)	5134(1)	5267(1)	8332(1)	43(1)
C(9)	5120(1)	4239(1)	8512(1)	37(1)
C(10)	4410(1)	3915(1)	8941(1)	38(1)
N(1)	5782(1)	3456(1)	8270(1)	41(1)
N(2)	6400(1)	3765(1)	7874(1)	40(1)
C(11)	7065(1)	2982(1)	7636(1)	37(1)
C(12)	7614(1)	3248(1)	7121(1)	38(1)
C(13)	8318(1)	2558(1)	6851(1)	39(1)
C(14)	8449(1)	1591(1)	7130(1)	46(1)
C(15)	7908(2)	1321(1)	7651(1)	49(1)
C(16)	7213(1)	2007(1)	7905(1)	43(1)
Si(3)	9088(1)	2955(1)	6175(1)	41(1)
C(17)	9980(2)	4052(2)	6426(1)	69(1)
C(18)	9926(2)	1876(2)	5917(1)	58(1)
O(2)	8174(3)	3180(3)	5583(2)	46(1)
O(2')	8359(8)	3555(7)	5617(5)	52(2)
Si(4)	7242(1)	3902(1)	5193(1)	39(1)
C(19)	7834(2)	4905(2)	4713(1)	63(1)
C(20)	6451(2)	2965(2)	4688(1)	57(1)
C(21)	6327(1)	4483(1)	5754(1)	37(1)
C(22)	5499(1)	3888(1)	5984(1)	39(1)
C(23)	4871(1)	4249(1)	6445(1)	37(1)
C(24)	5035(1)	5243(1)	6680(1)	41(1)
C(25)	5843(2)	5848(1)	6455(1)	45(1)
C(26)	6480(1)	5471(1)	6000(1)	42(1)
N(3)	4122(1)	3522(1)	6666(1)	42(1)
N(4)	3568(1)	3848(1)	7087(1)	40(1)
C(27)	2854(1)	3098(1)	7319(1)	37(1)
C(28)	2710(1)	2109(1)	7071(1)	42(1)
C(29)	2010(1)	1438(1)	7336(1)	46(1)
C(30)	1451(1)	1743(1)	7843(1)	44(1)
C(31)	1577(1)	2729(1)	8100(1)	38(1)
C(32)	2298(1)	3395(1)	7825(1)	37(1)

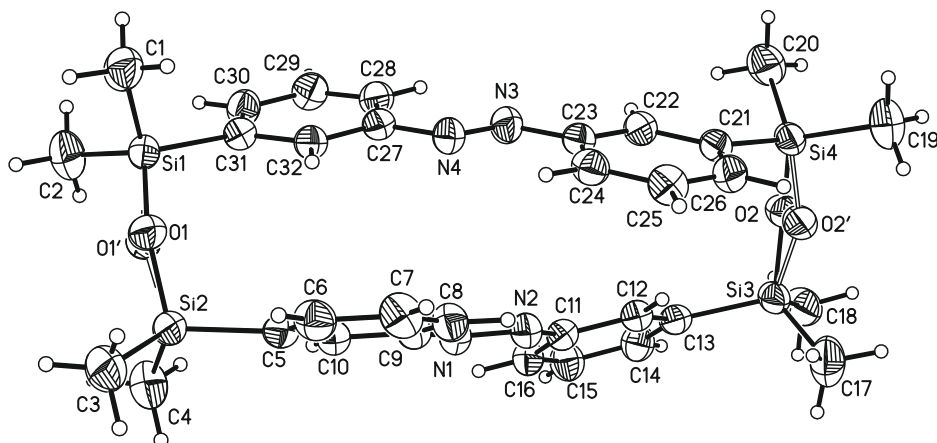


Table 3. Bond lengths [Å] and angles [°].

Si(1)-O(1')	1.602(10)	C(15)-C(16)	1.377(2)
Si(1)-O(1)	1.640(5)	Si(3)-O(2')	1.625(8)
Si(1)-C(1)	1.8438(19)	Si(3)-O(2)	1.638(4)
Si(1)-C(2)	1.849(2)	Si(3)-C(17)	1.843(2)
Si(1)-C(31)	1.8747(17)	Si(3)-C(18)	1.850(2)
O(1)-Si(2)	1.646(4)	O(2)-Si(4)	1.643(4)
O(1')-Si(2)	1.619(10)	O(2')-Si(4)	1.630(8)
Si(2)-C(4)	1.846(2)	Si(4)-C(20)	1.843(2)
Si(2)-C(3)	1.850(2)	Si(4)-C(19)	1.848(2)
Si(2)-C(5)	1.8682(17)	Si(4)-C(21)	1.8724(17)
C(5)-C(10)	1.396(2)	C(21)-C(26)	1.395(2)
C(5)-C(6)	1.397(2)	C(21)-C(22)	1.396(2)
C(6)-C(7)	1.391(3)	C(22)-C(23)	1.385(2)
C(7)-C(8)	1.379(3)	C(23)-C(24)	1.396(2)
C(8)-C(9)	1.392(2)	C(23)-N(3)	1.426(2)
C(9)-C(10)	1.385(2)	C(24)-C(25)	1.380(2)
C(9)-N(1)	1.426(2)	C(25)-C(26)	1.390(2)
N(1)-N(2)	1.2516(19)	N(3)-N(4)	1.2492(19)
N(2)-C(11)	1.424(2)	N(4)-C(27)	1.426(2)
C(11)-C(12)	1.387(2)	C(27)-C(32)	1.386(2)
C(11)-C(16)	1.398(2)	C(27)-C(28)	1.399(2)
C(12)-C(13)	1.402(2)	C(28)-C(29)	1.379(2)
C(13)-C(14)	1.397(2)	C(29)-C(30)	1.393(2)
C(13)-Si(3)	1.8697(17)	C(30)-C(31)	1.400(2)
C(14)-C(15)	1.393(3)	C(31)-C(32)	1.400(2)

Table 3. Bond lengths [Å] and angles [°].

O(1')-Si(1)-C(1)	119.2(5)	O(2')-Si(3)-C(17)	96.4(3)
O(1)-Si(1)-C(1)	104.4(2)	O(2)-Si(3)-C(17)	115.43(14)
O(1')-Si(1)-C(2)	101.3(6)	O(2')-Si(3)-C(18)	115.0(4)
O(1)-Si(1)-C(2)	113.3(3)	O(2)-Si(3)-C(18)	104.86(18)
C(1)-Si(1)-C(2)	109.83(10)	C(17)-Si(3)-C(18)	110.43(11)
O(1')-Si(1)-C(31)	108.1(8)	O(2')-Si(3)-C(13)	115.2(4)
O(1)-Si(1)-C(31)	110.8(3)	O(2)-Si(3)-C(13)	107.33(19)
C(1)-Si(1)-C(31)	107.78(8)	C(17)-Si(3)-C(13)	108.10(9)
C(2)-Si(1)-C(31)	110.49(9)	C(18)-Si(3)-C(13)	110.62(9)
Si(1)-O(1)-Si(2)	151.7(4)	Si(3)-O(2)-Si(4)	152.4(3)
Si(1)-O(1')-Si(2)	163.4(15)	Si(3)-O(2')-Si(4)	156.4(7)
O(1')-Si(2)-C(4)	98.9(5)	O(2')-Si(4)-C(20)	120.6(3)
O(1)-Si(2)-C(4)	114.4(2)	O(2)-Si(4)-C(20)	102.75(14)
O(1')-Si(2)-C(3)	114.5(7)	O(2')-Si(4)-C(19)	99.1(4)
O(1)-Si(2)-C(3)	105.5(3)	O(2)-Si(4)-C(19)	113.66(17)
C(4)-Si(2)-C(3)	109.90(10)	C(20)-Si(4)-C(19)	110.44(10)
O(1')-Si(2)-C(5)	111.4(8)	O(2')-Si(4)-C(21)	105.5(5)
O(1)-Si(2)-C(5)	105.5(3)	O(2)-Si(4)-C(21)	109.1(2)
C(4)-Si(2)-C(5)	110.19(9)	C(20)-Si(4)-C(21)	109.66(8)
C(3)-Si(2)-C(5)	111.21(9)	C(19)-Si(4)-C(21)	110.96(9)
C(10)-C(5)-C(6)	116.90(15)	C(26)-C(21)-C(22)	116.87(15)
C(10)-C(5)-Si(2)	120.77(13)	C(26)-C(21)-Si(4)	123.30(13)
C(6)-C(5)-Si(2)	122.08(13)	C(22)-C(21)-Si(4)	119.63(12)
C(7)-C(6)-C(5)	121.58(16)	C(23)-C(22)-C(21)	121.87(15)
C(8)-C(7)-C(6)	120.37(17)	C(22)-C(23)-C(24)	120.09(15)
C(7)-C(8)-C(9)	119.17(16)	C(22)-C(23)-N(3)	115.11(14)
C(10)-C(9)-C(8)	120.03(15)	C(24)-C(23)-N(3)	124.72(14)
C(10)-C(9)-N(1)	115.65(14)	C(25)-C(24)-C(23)	118.98(15)
C(8)-C(9)-N(1)	124.30(15)	C(24)-C(25)-C(26)	120.38(16)
C(9)-C(10)-C(5)	121.93(15)	C(25)-C(26)-C(21)	121.80(16)
N(2)-N(1)-C(9)	114.36(14)	N(4)-N(3)-C(23)	114.75(14)
N(1)-N(2)-C(11)	114.16(14)	N(3)-N(4)-C(27)	113.93(14)
C(12)-C(11)-C(16)	120.15(15)	C(32)-C(27)-C(28)	120.14(15)
C(12)-C(11)-N(2)	115.93(14)	C(32)-C(27)-N(4)	116.10(14)
C(16)-C(11)-N(2)	123.89(15)	C(28)-C(27)-N(4)	123.75(14)
C(11)-C(12)-C(13)	121.77(15)	C(29)-C(28)-C(27)	119.05(16)
C(14)-C(13)-C(12)	116.75(15)	C(28)-C(29)-C(30)	120.49(16)
C(14)-C(13)-Si(3)	122.35(13)	C(29)-C(30)-C(31)	121.59(16)
C(12)-C(13)-Si(3)	120.82(13)	C(30)-C(31)-C(32)	116.94(15)
C(15)-C(14)-C(13)	121.82(16)	C(30)-C(31)-Si(1)	122.00(13)
C(16)-C(15)-C(14)	120.45(16)	C(32)-C(31)-Si(1)	120.94(12)
C(15)-C(16)-C(11)	119.06(16)	C(27)-C(32)-C(31)	121.80(15)

Table 4. Anisotropic displacement parameters ($\text{\AA}^2 \times 10^3$). The anisotropic displacement factor exponent takes the form: $-2\pi^2 [h^2 a^{*2} U^{11} + \dots + 2 h k a^* b^* U^{12}]$

	U^{11}	U^{22}	U^{33}	U^{23}	U^{13}	U^{12}
Si(1)	33(1)	51(1)	33(1)	-3(1)	6(1)	-6(1)
C(1)	46(1)	60(1)	52(1)	-10(1)	11(1)	4(1)
C(2)	70(1)	69(1)	55(1)	8(1)	24(1)	-8(1)
O(1)	37(1)	61(2)	41(2)	-9(2)	1(1)	-3(2)
O(1')	40(4)	91(9)	35(3)	-6(6)	4(3)	-13(6)
Si(2)	33(1)	56(1)	34(1)	-9(1)	5(1)	-3(1)
C(3)	58(1)	73(1)	48(1)	-15(1)	13(1)	-3(1)
C(4)	64(1)	64(1)	56(1)	6(1)	19(1)	-1(1)
C(5)	34(1)	49(1)	33(1)	-4(1)	1(1)	-1(1)
C(6)	48(1)	47(1)	43(1)	-6(1)	4(1)	6(1)
C(7)	60(1)	41(1)	48(1)	1(1)	8(1)	0(1)
C(8)	45(1)	47(1)	38(1)	2(1)	6(1)	-6(1)
C(9)	33(1)	45(1)	34(1)	-2(1)	2(1)	-1(1)
C(10)	36(1)	43(1)	36(1)	2(1)	4(1)	1(1)
N(1)	37(1)	48(1)	39(1)	2(1)	9(1)	0(1)
N(2)	37(1)	49(1)	36(1)	2(1)	7(1)	0(1)
C(11)	32(1)	43(1)	36(1)	-1(1)	2(1)	-2(1)
C(12)	33(1)	46(1)	34(1)	1(1)	2(1)	-2(1)
C(13)	32(1)	49(1)	36(1)	-3(1)	1(1)	-1(1)
C(14)	43(1)	47(1)	49(1)	-2(1)	10(1)	3(1)
C(15)	53(1)	44(1)	50(1)	5(1)	9(1)	2(1)
C(16)	42(1)	47(1)	40(1)	3(1)	7(1)	-6(1)
Si(3)	35(1)	56(1)	33(1)	3(1)	6(1)	7(1)
C(17)	78(2)	67(1)	67(1)	1(1)	27(1)	-20(1)
C(18)	51(1)	76(1)	48(1)	2(1)	11(1)	18(1)
O(2)	41(2)	61(2)	36(1)	3(2)	4(1)	11(1)
O(2')	36(3)	80(6)	41(3)	12(5)	5(2)	9(4)
Si(4)	36(1)	50(1)	32(1)	6(1)	6(1)	5(1)
C(19)	69(1)	65(1)	58(1)	4(1)	27(1)	-4(1)
C(20)	66(1)	60(1)	45(1)	-5(1)	11(1)	0(1)
C(21)	35(1)	44(1)	32(1)	4(1)	3(1)	3(1)
C(22)	38(1)	43(1)	36(1)	-2(1)	5(1)	0(1)
C(23)	34(1)	44(1)	33(1)	2(1)	2(1)	2(1)
C(24)	41(1)	45(1)	36(1)	-1(1)	4(1)	7(1)
C(25)	51(1)	39(1)	44(1)	0(1)	5(1)	1(1)
C(26)	41(1)	44(1)	42(1)	7(1)	5(1)	-2(1)
N(3)	39(1)	49(1)	38(1)	-3(1)	10(1)	-1(1)
N(4)	37(1)	47(1)	38(1)	0(1)	9(1)	1(1)
C(27)	32(1)	44(1)	34(1)	1(1)	2(1)	2(1)
C(28)	38(1)	48(1)	40(1)	-6(1)	5(1)	4(1)
C(29)	45(1)	44(1)	50(1)	-7(1)	6(1)	-3(1)
C(30)	40(1)	45(1)	47(1)	1(1)	8(1)	-5(1)
C(31)	33(1)	45(1)	35(1)	1(1)	3(1)	0(1)
C(32)	35(1)	42(1)	35(1)	-1(1)	4(1)	2(1)

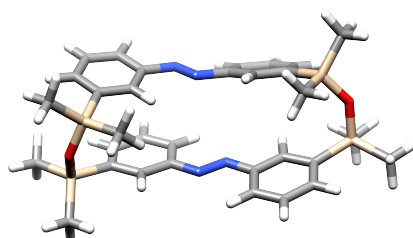
Table 5. Hydrogen coordinates ($\times 10^4$) and isotropic displacement parameters ($\text{\AA}^2 \times 10^{-3}$).

	x	y	z	U(eq)
H(1A)	-761	4312	8728	78
H(1B)	-804	3691	8083	78
H(1C)	24	4641	8203	78
H(2A)	685	1607	9291	96
H(2B)	-379	1713	8799	96
H(2C)	-321	2326	9448	96
H(3A)	1979	5712	10032	89
H(3B)	2917	5301	10542	89
H(3C)	1694	4842	10519	89
H(4A)	2604	2686	10399	91
H(4B)	3825	3152	10429	91
H(4C)	3380	2434	9855	91
H(6)	3222	6095	9172	55
H(7)	4421	6650	8457	59
H(8)	5627	5495	8043	52
H(10)	4419	3214	9065	46
H(12)	7510	3916	6947	45
H(14)	8921	1104	6960	55
H(15)	8020	659	7832	58
H(16)	6839	1821	8258	51
H(17A)	10405	4263	6082	104
H(17B)	10486	3848	6787	104
H(17C)	9522	4627	6545	104
H(18A)	9446	1285	5809	87
H(18B)	10483	1685	6255	87
H(18C)	10292	2086	5549	87
H(19A)	8320	5350	4984	94
H(19B)	7237	5317	4502	94
H(19C)	8258	4580	4400	94
H(20A)	6943	2627	4414	85
H(20B)	5861	3321	4432	85
H(20C)	6128	2448	4949	85
H(22)	5363	3217	5821	46
H(24)	4598	5500	6990	49
H(25)	5964	6525	6612	54
H(26)	7034	5897	5853	51
H(28)	3090	1902	6724	50
H(29)	1909	763	7172	55
H(30)	972	1269	8020	52
H(32)	2409	4068	7991	45

7.3. DFT Calculations of all Switching States

Using Gaussian 09,^[297] the geometry and IR-frequencies of the molecules were optimized. To take intramolecular dispersive interactions between the two neighboring azobenzenes into account, the D3 version of Grimme's empirical dispersion correction was used.^[298] The absence of negative frequencies indicated true minima. The calculations were fully converged. For comparison, the electronic energies (E) and the zero-point energy corrected energies (E_{ZPE}) are given in Hartree accompanied by the point group. Visualization of the optimized structures was performed using UCSF Chimera.^[299]

7.3.1. (*E*),(*E*)-Isomer 64a



Optimized at the B3LYP/6-311G* level of theory.

E -2771.727016 Hartree
 E_{ZPE} -2771.076538 Hartree
 Point Group C_1

Table V.29. Atom Coordinates of **64a** after DFT Optimization.

Coordinates				
Atom Count	Symbol	X	Y	Z
1	C	3.0164946	-3.6253427	1.0329211
2	C	4.2535252	-3.0489758	0.7281418
3	C	4.3545736	-1.9609414	-0.1509238
4	C	3.1689316	-1.4781566	-0.7238694
5	C	1.9273014	-2.0370420	-0.4133437
6	C	1.8517769	-3.1214530	0.4739578
7	N	0.8106628	-1.4358794	-1.0461381
8	N	-0.3058212	-1.8494230	-0.6555400
9	C	-1.4255329	-1.2536415	-1.2842989
10	C	-2.6703197	-1.6774238	-0.8147482
11	C	-3.8667820	-1.1442187	-1.3128654
12	C	-3.7707066	-0.1768544	-2.3216614
13	C	-2.5291567	0.2430483	-2.8098053

Continued on next page

Continued from previous page

Atom Count	Symbol	X	Y	Z
14	C	-1.3552963	-0.2834578	-2.2955418
15	Si	-5.5031374	-1.6317987	-0.5117242
16	O	-5.4520883	-1.1443771	1.0789656
17	Si	5.9850158	-1.0546610	-0.4348579
18	O	5.9748462	0.3079473	0.5221244
19	Si	4.9207610	1.2711388	1.3785243
20	Si	-4.7263103	-0.0309820	2.0825431
21	C	-4.1006599	1.3859902	1.0034206
22	C	3.5706669	1.8308963	0.1846259
23	C	-2.7473279	1.5093141	0.6846716
24	C	-2.3074275	2.4720208	-0.2334892
25	C	-3.2299727	3.3251481	-0.8440266
26	C	-4.5799613	3.2324512	-0.5215891
27	C	-5.0083242	2.2714519	0.3909597
28	C	3.9135822	2.3290877	-1.0825802
29	C	2.9343157	2.7115711	-2.0025351
30	C	1.5894994	2.6246047	-1.6702488
31	C	1.2235071	2.1406978	-0.4072141
32	C	2.2095060	1.7323782	0.4953844
33	N	-0.9616494	2.6276959	-0.6478317
34	N	-0.1151282	2.0095685	0.0386545
35	C	-6.9289538	-0.7671977	-1.3714405
36	C	-5.7129317	-3.4928594	-0.5218851
37	C	7.4394817	-2.1145692	0.0874635
38	C	6.1311897	-0.5326293	-2.2298284
39	C	-6.0269442	0.5792230	3.2860512
40	C	-3.2962354	-0.8506470	2.9759574
41	C	4.1558450	0.2982275	2.7878551
42	C	5.9049095	2.7398552	1.9966015
43	H	2.9665730	-4.4692107	1.7142640
44	H	5.1475546	-3.4566307	1.1910600
45	H	3.1729485	-0.6352099	-1.4069143
46	H	0.8826064	-3.5459155	0.7033068
47	H	-2.6712890	-2.4269632	-0.0284652
48	H	-4.6698221	0.2782620	-2.7254623
49	H	-2.4837621	1.0055368	-3.5808041
50	H	-0.3844868	0.0453221	-2.6435629

Continued on next page

Continued from previous page

Atom Count	Symbol	X	Y	Z
51	H	-2.0058394	0.8472227	1.1134449
52	H	-2.8656721	4.0507497	-1.5631764
53	H	-5.2966912	3.9020022	-0.9865510
54	H	-6.0689078	2.2021305	0.6183601
55	H	4.9592911	2.4044115	-1.3682678
56	H	3.2258766	3.0787083	-2.9819038
57	H	0.8133861	2.9246361	-2.3631122
58	H	1.8755777	1.3321250	1.4472063
59	H	-7.0167669	-1.0627257	-2.4213722
60	H	-7.8755278	-1.0100575	-0.8800254
61	H	-6.8106110	0.3196972	-1.3379547
62	H	-6.6289637	-3.7896410	-0.0028527
63	H	-5.7621463	-3.8828629	-1.5429138
64	H	-4.8757208	-3.9865134	-0.0201360
65	H	8.3786511	-1.5781779	-0.0759598
66	H	7.4874532	-3.0482469	-0.4810199
67	H	7.3944838	-2.3698230	1.1499644
68	H	6.1866870	-1.4001754	-2.8941964
69	H	5.2737642	0.0690247	-2.5427165
70	H	7.0314007	0.0686691	-2.3887740
71	H	-5.6129020	1.3175647	3.9792127
72	H	-6.4294742	-0.2478566	3.8781189
73	H	-6.8678347	1.0477493	2.7666628
74	H	-3.6520950	-1.7062019	3.5574545
75	H	-2.5386110	-1.2207419	2.2798515
76	H	-2.8016669	-0.1620566	3.6677180
77	H	3.4839207	0.9134651	3.3939929
78	H	4.9331254	-0.0883924	3.4537717
79	H	3.5858425	-0.5569119	2.4148143
80	H	6.7247962	2.4197178	2.6463473
81	H	6.3410114	3.2986669	1.1636617
82	H	5.2752766	3.4312632	2.5647026

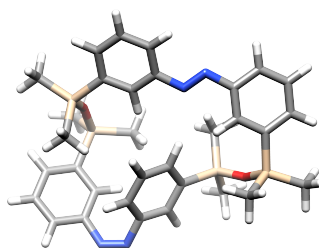
Table V.30. Atomic coordinates ($\times 10^4$) and equivalent isotropic displacement parameters ($\text{\AA}^2 \times 10^3$). $U(\text{eq})$ is defined as one third of the trace of the orthogonalized U^{ij} tensor ??

	X	Y	Z	U(eq)
Si(1)	755(1)	3180(1)	8744(1)	39(1)
C(1)	-323(2)	4059(2)	8399(1)	52(1)
C(2)	109(2)	2077(2)	9114(1)	64(1)
O(1)	1513(6)	3896(4)	9245(4)	47(1)
O(1')	1599(13)	3579(9)	9309(8)	55(3)
Si(2)	2638(1)	4104(1)	9714(1)	41(1)
C(3)	2263(2)	5108(2)	10267(1)	59(1)
C(4)	3175(2)	2960(2)	10150(1)	60(1)
C(5)	3681(1)	4589(1)	9198(1)	39(1)
C(6)	3706(2)	5614(1)	9007(1)	46(1)
C(7)	4422(2)	5948(1)	8579(1)	50(1)
C(8)	5134(1)	5267(1)	8332(1)	43(1)
C(9)	5120(1)	4239(1)	8512(1)	37(1)
C(10)	4410(1)	3915(1)	8941(1)	38(1)
N(1)	5782(1)	3456(1)	8270(1)	41(1)
N(2)	6400(1)	3765(1)	7874(1)	40(1)
C(11)	7065(1)	2982(1)	7636(1)	37(1)
C(12)	7614(1)	3248(1)	7121(1)	38(1)
C(13)	8318(1)	2558(1)	6851(1)	39(1)
C(14)	8449(1)	1591(1)	7130(1)	46(1)
C(15)	7908(2)	1321(1)	7651(1)	49(1)
C(16)	7213(1)	2007(1)	7905(1)	43(1)
Si(3)	9088(1)	2955(1)	6175(1)	41(1)
C(17)	9980(2)	4052(2)	6426(1)	69(1)
C(18)	9926(2)	1876(2)	5917(1)	58(1)
O(2)	8174(3)	3180(3)	5583(2)	46(1)
O(2')	8359(8)	3555(7)	5617(5)	52(2)
Si(4)	7242(1)	3902(1)	5193(1)	39(1)
C(19)	7834(2)	4905(2)	4713(1)	63(1)
C(20)	6451(2)	2965(2)	4688(1)	57(1)
C(21)	6327(1)	4483(1)	5754(1)	37(1)
C(22)	5499(1)	3888(1)	5984(1)	39(1)
C(23)	4871(1)	4249(1)	6445(1)	37(1)
C(24)	5035(1)	5243(1)	6680(1)	41(1)
C(25)	5843(2)	5848(1)	6455(1)	45(1)
C(26)	6480(1)	5471(1)	6000(1)	42(1)

Continued on next page

Continued from previous page

	X	Y	Z	U(eq)
N(3)	4122(1)	3522(1)	6666(1)	42(1)
N(4)	3568(1)	3848(1)	7087(1)	40(1)
C(27)	2854(1)	3098(1)	7319(1)	37(1)
C(28)	2710(1)	2109(1)	7071(1)	42(1)
C(29)	2010(1)	1438(1)	7336(1)	46(1)
C(30)	1451(1)	1743(1)	7843(1)	44(1)
C(31)	1577(1)	2729(1)	8100(1)	38(1)
C(32)	2298(1)	3395(1)	7825(1)	37(1)

7.3.2. (*E*),(*Z*)-Isomer 64b

Optimized at the B3LYP/6-311G* level of theory.

E -2771.702930 Hartree
 E_{ZPE} -2771.052325 Hartree
 Point Group C₁

Table V.31. Atom Coordinates of **64b** after DFT Optimization.

Coordinates				
Atom Count	Symbol	X	Y	Z
1	C	-6.2871593	0.9724397	0.2916140
2	C	-5.1376853	0.3249586	-0.1930182
3	C	-3.9953809	1.0984287	-0.4032401
4	C	-3.9689903	2.4649520	-0.1049094
5	C	-5.1335410	3.0940018	0.3465347
6	C	-6.2893584	2.3450469	0.5436486
7	C	-0.5532161	4.7994607	-0.6359619
8	C	-0.5604354	3.4139217	-0.4112006
9	C	0.6474436	2.7156458	-0.3221014
10	C	1.8820128	3.3682592	-0.4495137

Continued on next page

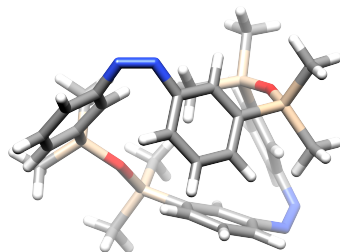
Continued from previous page

Atom Count	Symbol	X	Y	Z
11	C	1.8626765	4.7526956	-0.6692082
12	C	0.6585727	5.4594529	-0.7618781
13	N	-2.8113556	3.2729087	-0.2203495
14	N	-1.7341057	2.6319409	-0.2744712
15	Si	-4.9900948	-1.5371103	-0.4687240
16	O	-3.7561618	-2.0755119	0.4950924
17	Si	-2.2723530	-1.9871045	1.2274242
18	C	-6.5696119	-2.4061302	0.0408146
19	C	-4.5429026	-1.8870968	-2.2552178
20	Si	3.4910046	2.3873840	-0.3695325
21	C	4.9583348	3.5543049	-0.3012677
22	O	3.4696245	1.4868982	1.0184529
23	C	3.6077275	1.2514448	-1.8601660
24	Si	3.4947466	0.0571764	1.8554971
25	C	4.1351655	-1.2685866	0.6726132
26	C	1.7508252	-0.3536704	2.4071218
27	C	4.6542475	0.2667235	3.3122899
28	C	3.3009091	-2.3028597	0.2415717
29	C	3.7075641	-3.1959806	-0.7597197
30	C	4.9958331	-3.0960055	-1.2895399
31	C	5.8414144	-2.0721122	-0.8716852
32	C	5.4121795	-1.1645917	0.0933210
33	N	2.9397552	-4.3223065	-1.2202409
34	N	1.7048726	-4.3030785	-1.3820050
35	C	0.9205889	-3.1086211	-1.2416686
36	C	1.1373286	-1.9805801	-2.0356207
37	C	0.3368480	-0.8585972	-1.8478112
38	C	-0.6500877	-0.8525743	-0.8632689
39	C	-0.9159224	-1.9973930	-0.0914422
40	C	-0.1329889	-3.1345302	-0.3251168
41	C	-2.1024821	-3.4942247	2.3287398
42	C	-2.1360830	-0.4028135	2.2226339
43	H	-7.1939945	0.4026195	0.4732667
44	H	-3.0937344	0.6518441	-0.8002033
45	H	-5.1037717	4.1577422	0.5558386
46	H	-7.1906964	2.8294143	0.9054837
47	H	-1.4969067	5.3253084	-0.7072288

Continued on next page

Continued from previous page

Atom Count	Symbol	X	Y	Z
48	H	0.5982979	1.6468456	-0.1387467
49	H	2.7959719	5.2990240	-0.7702393
50	H	0.6734869	6.5311411	-0.9349453
51	H	-6.4590950	-3.4896663	-0.0582937
52	H	-7.4186385	-2.1040408	-0.5803221
53	H	-6.8247615	-2.1970960	1.0836137
54	H	-5.3110917	-1.5229468	-2.9439291
55	H	-3.5985748	-1.4051899	-2.5249596
56	H	-4.4185876	-2.9606521	-2.4254254
57	H	5.8876688	2.9853697	-0.2019443
58	H	5.0457609	4.1626223	-1.2067045
59	H	4.8955720	4.2315841	0.5549851
60	H	3.4921709	1.8127386	-2.7924282
61	H	4.5667065	0.7283274	-1.8944937
62	H	2.8283412	0.485957	-1.8307827
63	H	1.0761700	-0.4937468	1.5584980
64	H	1.7152198	-1.2638154	3.0140323
65	H	1.3471919	0.4632451	3.0119287
66	H	5.6707164	0.5001996	2.9819305
67	H	4.3245262	1.0826908	3.9619904
68	H	4.7054972	-0.6441328	3.9163497
69	H	2.3186477	-2.4167602	0.6788849
70	H	5.3127861	-3.8260354	-2.0264048
71	H	6.8370826	-1.9884609	-1.2956274
72	H	6.0834158	-0.3661705	0.3994480
73	H	1.9392944	-1.9786021	-2.7653564
74	H	0.4991685	0.0278231	-2.4525416
75	H	-1.2016057	0.0653678	-0.6945490
76	H	-0.2919646	-4.0508578	0.2348787
77	H	-1.1249277	-3.5324015	2.8187816
78	H	-2.8649566	-3.4770548	3.1127984
79	H	-2.2342607	-4.4239527	1.7682799
80	H	-2.0912117	0.4861501	1.5885188
81	H	-2.9950581	-0.2866626	2.8901171
82	H	-1.2309279	-0.4121646	2.8372168

7.3.3. (*Z*),(*Z*)-Isomer **64c**

Optimized at the B3LYP/6-311G* level of theory.

E -2771.683431 Hartree
 E_{ZPE} -2771.033784 Hartree
 Point Group C₁

Table V.32. Atom Coordinates of **64c** after DFT Optimization.

Coordinates				
Atom Count	Symbol	X	Y	Z
1	C	-0.9656305	-0.3065168	-3.2973854
2	C	-0.2141032	-1.1013977	-2.4341314
3	C	-0.8439917	-2.0049217	-1.5624031
4	C	-2.2407440	-2.0408549	-1.5401539
5	C	-2.9992705	-1.1890069	-2.3503624
6	C	-2.3565003	-0.3594472	-3.2713507
7	N	-4.4358792	-1.1791892	-2.3750643
8	N	-5.1371681	-1.2130825	-1.3448571
9	C	-4.5860737	-1.1314236	-0.0200245
10	C	-3.6939387	-0.1283772	0.3698932
11	C	-3.1879467	-0.0789352	1.6714109
12	C	-3.6213720	-1.0528625	2.5868916
13	C	-4.5545877	-2.0204259	2.2181038
14	C	-5.0533612	-2.0524482	0.9189613
15	Si	-1.8628586	1.1907746	2.1005681
16	O	-2.0574252	2.4607091	1.0636627
17	Si	0.1335029	-3.1367777	-0.4240680
18	O	1.5395195	-2.3383851	-0.0514627
19	Si	2.9586235	-2.4270636	0.8063615
20	Si	-1.6908674	3.4724767	-0.1934113
21	C	0.0733237	3.1083034	-0.7526726
22	C	4.0870012	-1.0146882	0.2815385

Continued on next page

Continued from previous page

Atom Count	Symbol	X	Y	Z
23	C	1.1491925	3.3130690	0.1201918
24	C	2.4568547	2.9914759	-0.2471004
25	C	2.7214891	2.5183478	-1.5395936
26	C	1.6706803	2.3529095	-2.4315722
27	C	0.3609288	2.6293274	-2.0385067
28	C	5.2772145	-1.2517397	-0.4236703
29	C	6.1691400	-0.2153813	-0.7016496
30	C	5.8940741	1.0762295	-0.2700322
31	C	4.6865999	1.3424136	0.3807496
32	C	3.7954084	0.3031556	0.6600917
33	N	3.4788369	3.3478449	0.6954464
34	N	4.4952813	2.6635973	0.9070951
35	C	-2.0732796	1.7930191	3.8630648
36	C	-0.1648459	0.4248893	1.8591368
37	C	0.5495343	-4.7468587	-1.2989460
38	C	-0.8605857	-3.4779093	1.1328852
39	C	-2.8880135	3.1558956	-1.6021405
40	C	-1.8217867	5.2345787	0.4296225
41	C	3.7879842	-4.0791325	0.4653453
42	C	2.5852807	-2.2594031	2.6386300
43	H	-0.4664243	0.3573501	-3.9951711
44	H	0.8681483	-1.0189044	-2.4346646
45	H	-2.7581333	-2.7150880	-0.8680835
46	H	-2.9593827	0.2479769	-3.9377924
47	H	-3.3846693	0.6099624	-0.3594253
48	H	-3.2443210	-1.0500220	3.6059393
49	H	-4.8987467	-2.7496051	2.9447239
50	H	-5.7847995	-2.7925421	0.6123450
51	H	0.9967322	3.7278318	1.1128607
52	H	3.7377976	2.3039853	-1.8445913
53	H	1.8737383	2.0020746	-3.4387992
54	H	-0.4429882	2.4781478	-2.7495422
55	H	5.5292596	-2.2586806	-0.7412647
56	H	7.0930814	-0.4205378	-1.2331371
57	H	6.5958146	1.8874840	-0.4327015
58	H	2.8806312	0.5336621	1.1970859
59	H	-1.3251640	2.5529944	4.1077045

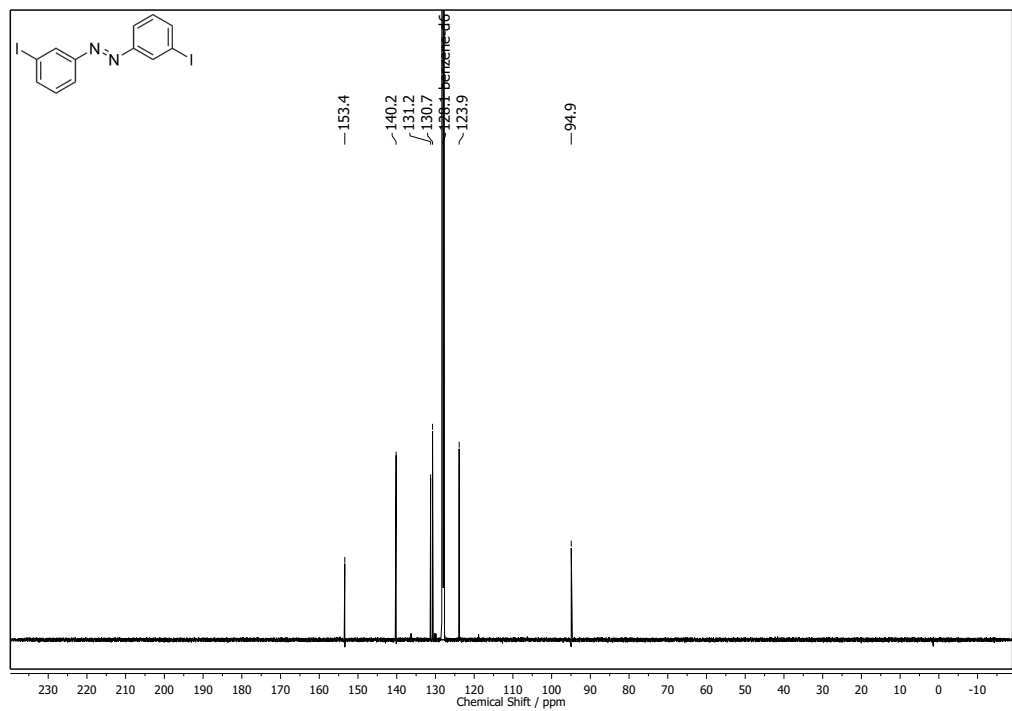
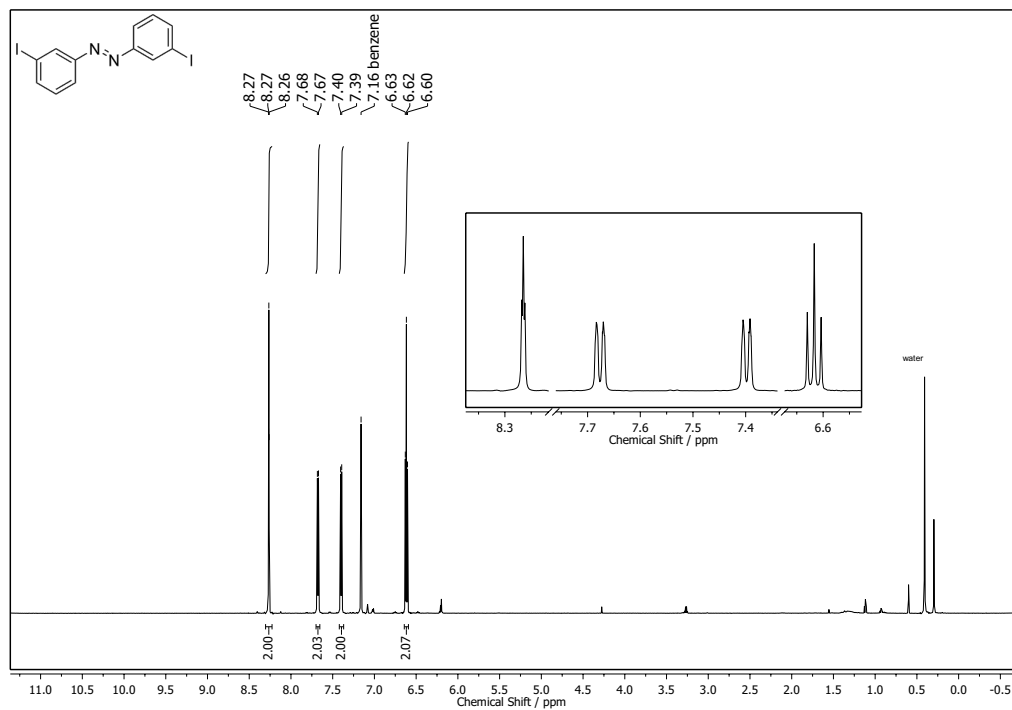
Continued on next page

Continued from previous page

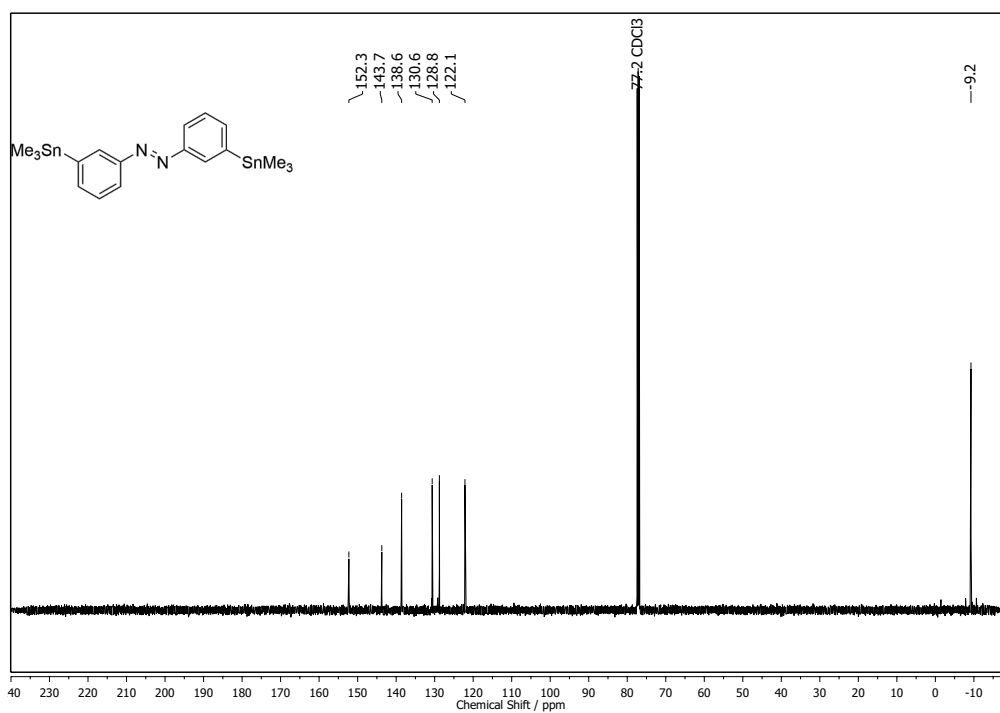
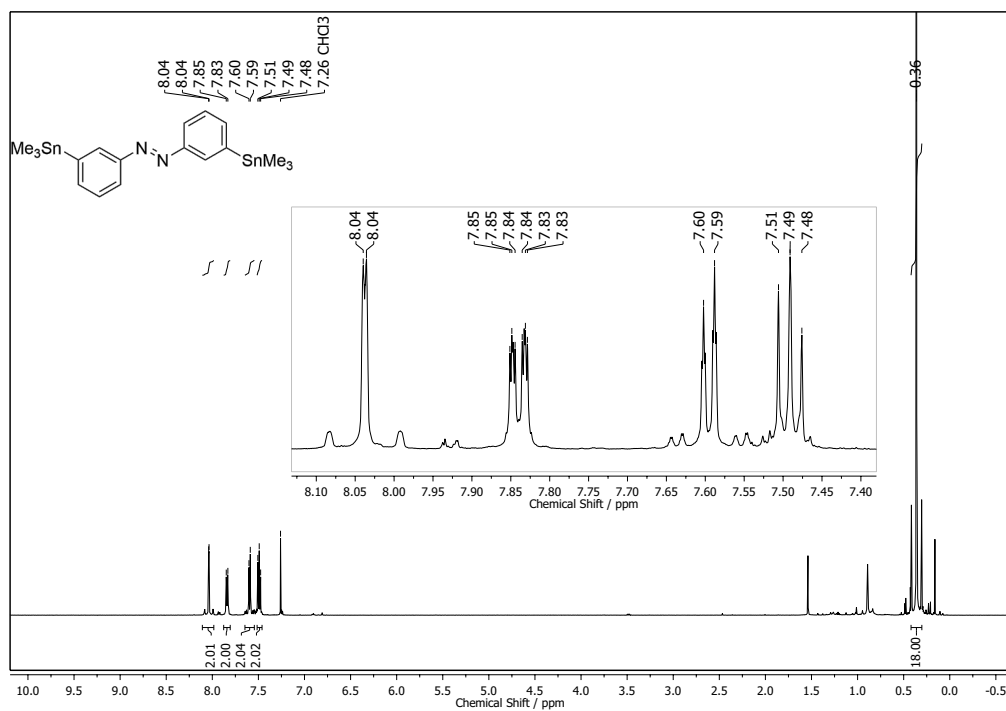
Atom Count	Symbol	X	Y	Z
60	H	-1.9604073	0.9802194	4.5874643
61	H	-3.0611090	2.2367656	4.0128534
62	H	-0.0036837	0.1102255	0.8249592
63	H	0.6246408	1.1376440	2.1148353
64	H	-0.0398520	-0.4558756	2.4951204
65	H	1.0936182	-5.4352889	-0.6452882
66	H	-0.3570368	-5.2578183	-1.6374863
67	H	1.1712431	-4.5643489	-2.1801609
68	H	-1.7395692	-4.0958982	0.9266825
69	H	-0.2586077	-4.0153104	1.8721330
70	H	-1.2170729	-2.5540599	1.5943506
71	H	-3.9203247	3.2396329	-1.2508073
72	H	-2.7663129	2.1566097	-2.0290564
73	H	-2.7574162	3.8792686	-2.4128676
74	H	-2.8287072	5.4432651	0.8029735
75	H	-1.1218128	5.4234651	1.2487446
76	H	-1.6013570	5.9555360	-0.3632527
77	H	4.7588338	-4.1536167	0.9639648
78	H	3.1695285	-4.9026454	0.8348195
79	H	3.9459225	-4.2483971	-0.6034735
80	H	3.4972525	-2.3594152	3.2347462
81	H	2.1469103	-1.2860191	2.8705644
82	H	1.8808405	-3.0258552	2.9755194

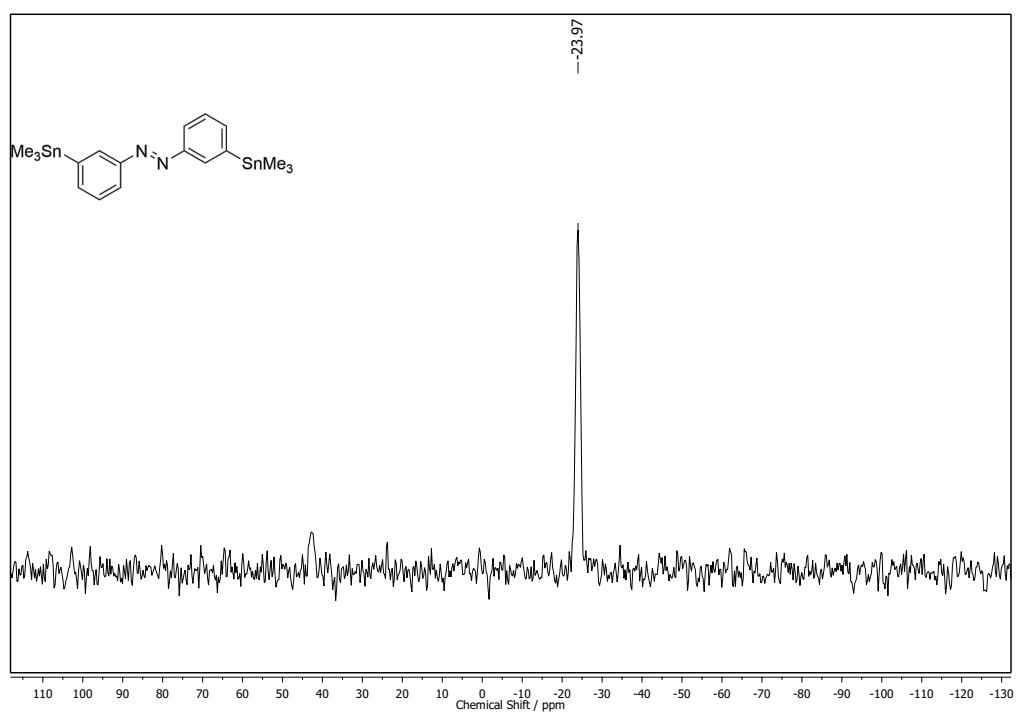
7.4. NMR Spectra

7.4.1. ^1H and $^{13}\text{C}\{^1\text{H}\}$ NMR Spectra of 3,3'-Diiodoazobenzene (65) in Benzene- d_6



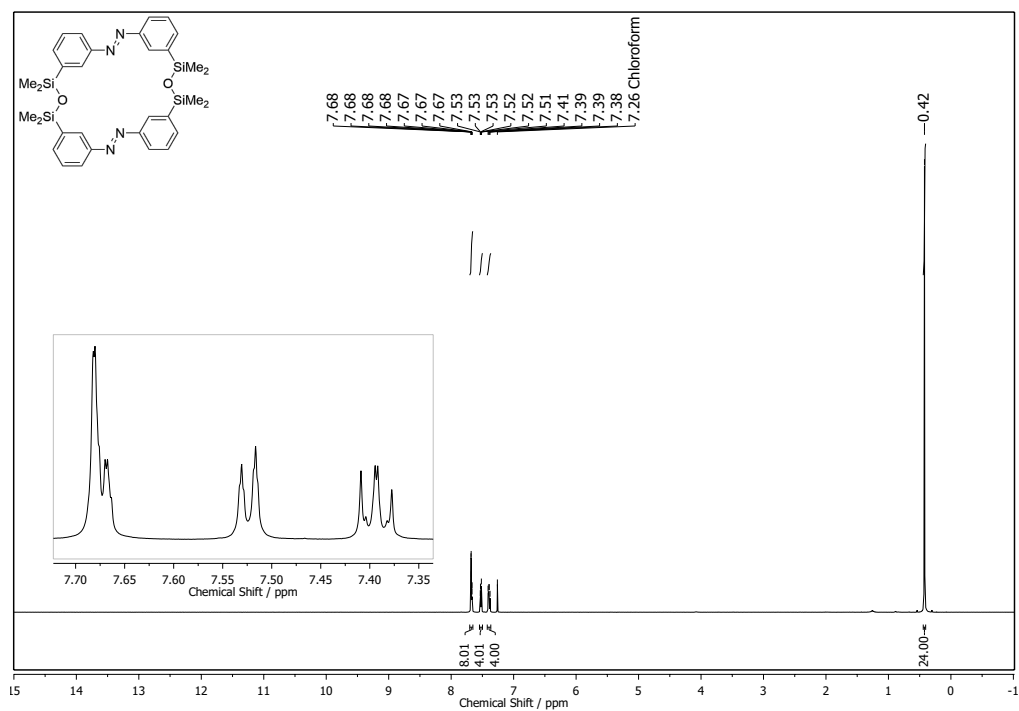
7.4.2. ^1H , $^{13}\text{C}\{^1\text{H}\}$ and $^{119}\text{Sn}\{^1\text{H}\}$ NMR Spectra of
3,3'-Bis(trimethylstannyl)azobenzene (63) in CDCl_3

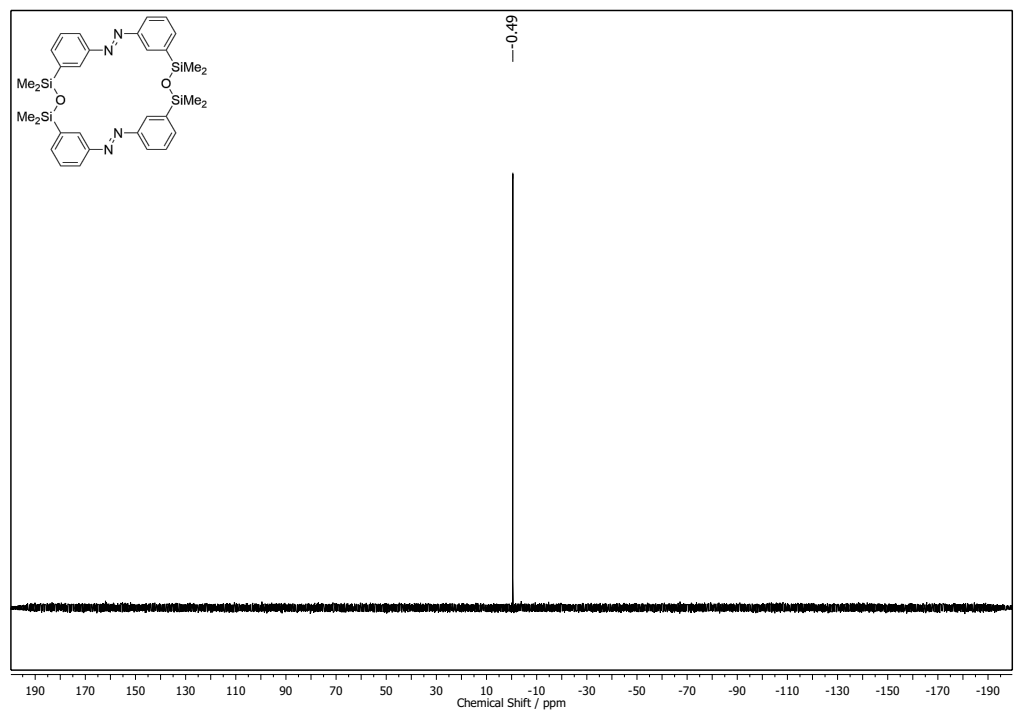
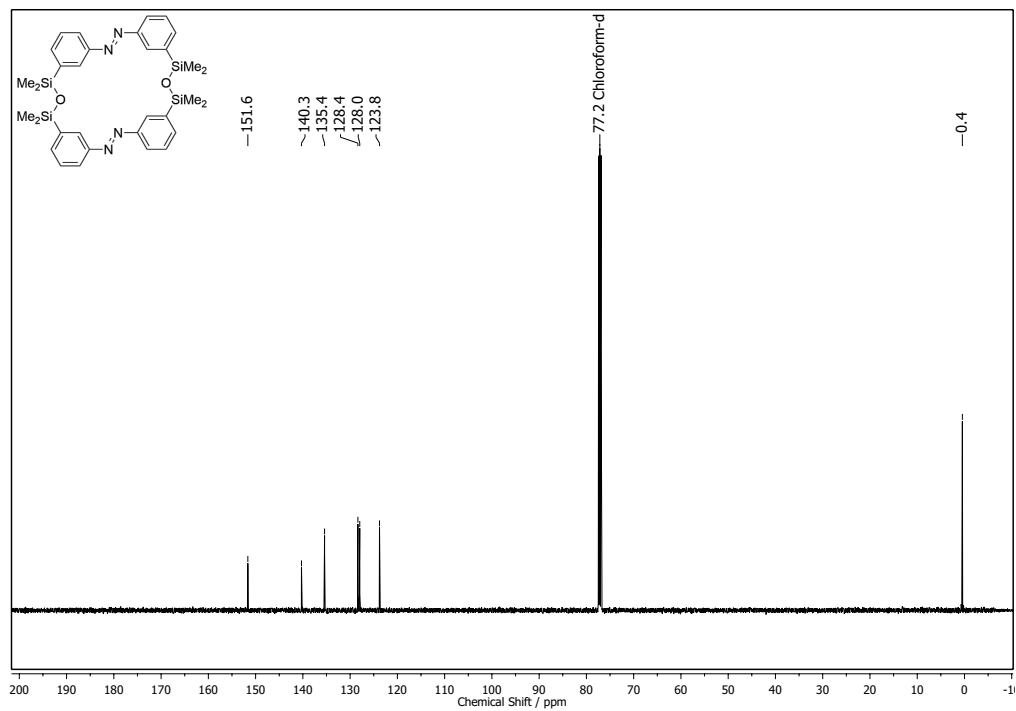




7.4.3. NMR Spectra of
 (1(*E*),5(*E*))-2,2,4,4,6,6,8,8-Octamethyl-1,5-(3,3')-diazobenzena-
 3,7-dioxa-2,4,6,8-tetrasilacyclooctaphane (64)

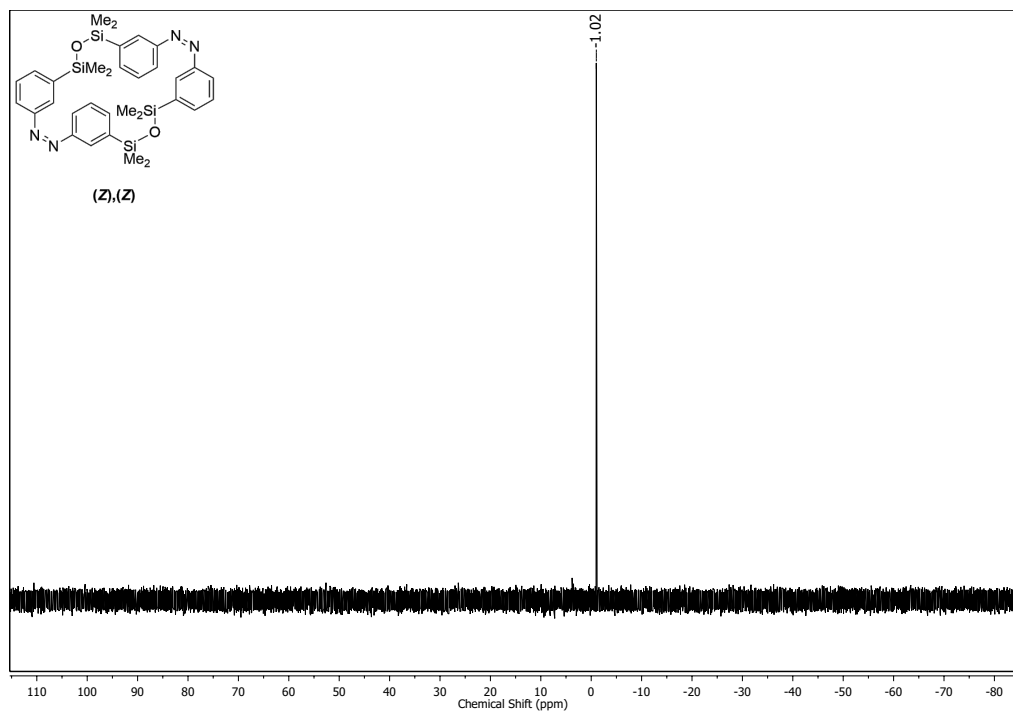
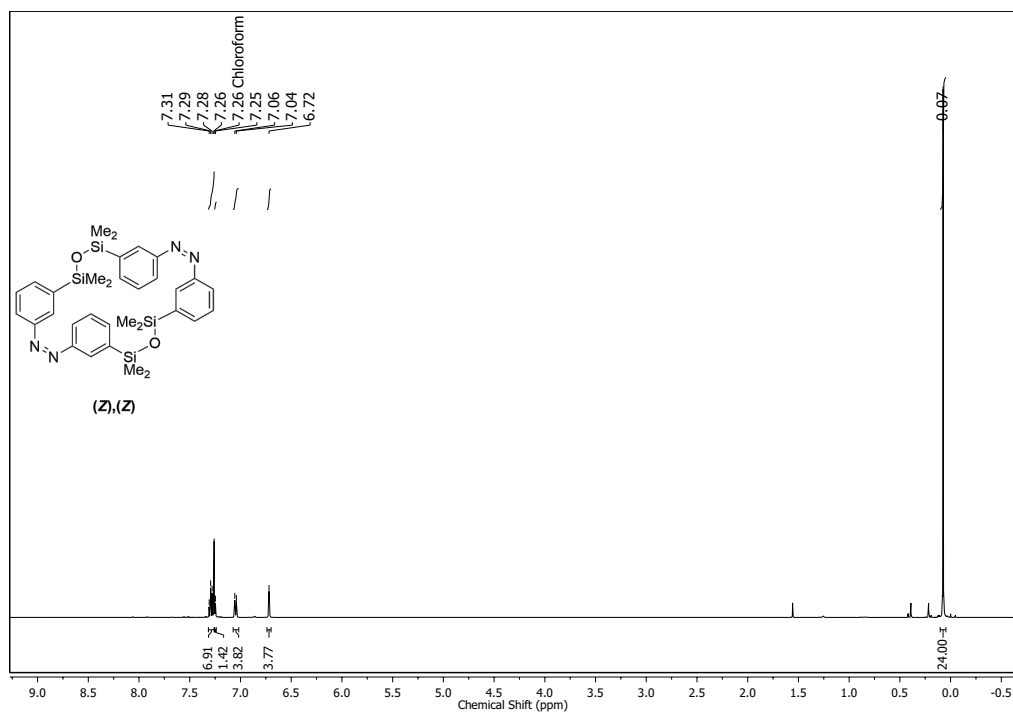
^1H , $^{13}\text{C}\{^1\text{H}\}$ and $^{29}\text{Si}\{^1\text{H}\}$ NMR Spectra of the (*E*),(*E*)-Isomer 64a in CDCl_3





^1H and $^{29}\text{Si}\{^1\text{H}\}$ NMR Spectra of the Photostationary State after Irradiation with UV light (340 nm) in CDCl_3

The following two spectra were recorded by Melanie Walther in the context of her MSc thesis, which she prepared under my supervision.



^1H NMR Spectrum of the Photostationary State of 64 after Irradiation with UV light (340 nm) in $\text{THF-}d_8$

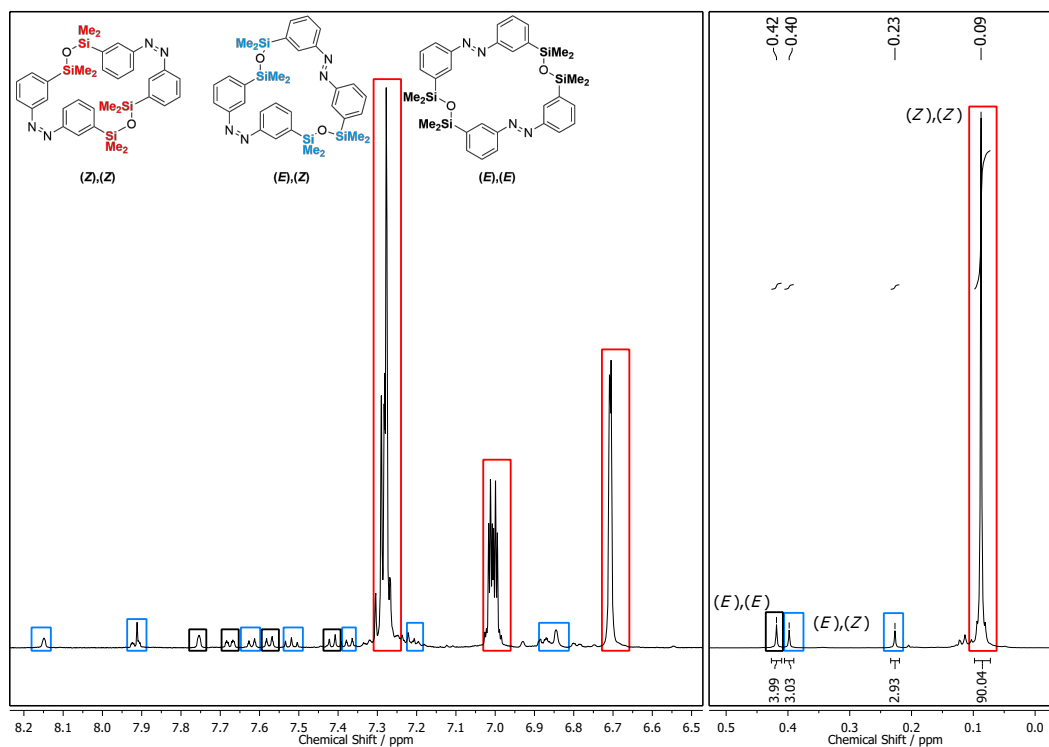


Figure V.6. ^1H NMR of the PSS-340 of azobenzene macrocycle in $\text{THF-}d_8$ that represented the starting point for tracing the thermal decay $(Z),(Z) \rightarrow (E),(Z) \rightarrow (E),(E)$. Left: aromatic region of the ^1H NMR spectrum. Right: signals corresponding to the Si-Me_2 groups of the $(Z),(Z)$ (red boxes, 90%), $(E),(Z)$ (blue boxes, 6%) and $(E),(E)$ (black boxes, 4%).

Bibliography of Part V

- [64] T. P. Kaloni, G. Schreckenbach, M. S. Freund, *J. Phys. Chem. C* **2015**, *119*, 3979–3989.
- [114] J. Strueben, PhD thesis, Christian-Albrechts-Universität, Kiel, **2015**.
- [174] M. Schulz-Senft, P. J. Gates, F. D. Sönnichsen, A. Staubitz, *Dyes Pigm.* **2017**, *136*, 292–301.
- [294] R. K. Harris, E. D. Becker, S. M. Cabral de Menezes, P. Granger, R. E. Hoffman, K. W. Zilm, *Pure Appl. Chem.* **2008**, *80*, 59–84.
- [295] T. Mutai, J.-D. Cheon, S. Arita, K. Araki, *J. Chem. Soc. Perkin Trans. 2* **2001**, 1045–1050.
- [296] R. M. Brady, E. Hatzis, T. Connor, I. P. Street, J. B. Baell, G. Lessene, *Org. Biomol. Chem.* **2012**, *10*, 5230–5237.
- [297] M. J. Frisch, G. W. Trucks, H. B. Schlegel, G. E. Scuseria, M. A. Robb, J. R. Cheeseman, G. Scalmani, V. Barone, G. A. Petersson, H. Nakatsuji, X. Li, M. Caricato, A. Marenich, J. Bloino, B. G. Janesko, R. Gomberts, B. Menucci, H. P. Hratchian, J. V. Ortiz, A. F. Izmaylov, J. L. Sonnenberg, D. Williams-Young, F. Ding, F. Lipparini, F. Egidi, J. Goings, B. Peng, A. Petrone, T. Henderson, D. Ranasinghe, V. G. Zakrzewski, J. Gao, N. Rega, G. Zheng, W. Liang, M. Hada, M. Ehara, K. Toyota, R. Fukuda, J. Hasegawa, M. Ishida, T. Nakajima, Y. Honda, O. Kitao, H. Nakai, T. Vreven, K. Throssell, J. A. Montgomery, Jr., J. E. Peralta, F. Ogliaro, M. Bearpark, J. J. Heyd, E. Brothers, K. N. Kudin, V. N. Staroverov, T. Keith, R. Kobayashi, J. Normand, K. Raghavachari, A. Rendell, J. C. Burant, S. S. Iyengar, J. Tomasi, M. Cossi, J. M. Millam, M. Klene, C. Adamo, J. W. Ochterski, R. L. Martin, K. Morokuma, O. Farkas, J. B. Foresman, D. J. Fox, *Gaussian 09*, Wallingford, CT, **2009**.
- [298] S. Grimme, J. Antony, S. Ehrlich, H. Krieg, *J. Chem. Phys.* **2010**, *132*, 154104.
- [299] E. F. Pettersen, T. D. Goddard, C. C. Huang, G. S. Couch, D. M. Greenblatt, E. C. Meng, T. E. Ferrin, *J. Comput. Chem.* **2004**, *25*, 1605–1612.
- [300] R. Dennington, T. A. Keith, J. M. Millam, *GaussView, Version 6.0.16*, Shawnee Mission, KS, **2016**.
- [301] E. Hedaya, J. H. Kawakami, P. W. Kopf, G. T. Kwiatkowski, D. W. McNeil, D. A. Owen, E. N. Peters, R. W. Tulis, *J. Polym. Sci. Polym. Chem. Ed.* **1977**, *15*, 2229–2238.

- [302] H. Takahashi, T. Ishioka, Y. Koiso, M. Sodeoka, Y. Hashimoto, *Biol. Pharm. Bull.* **2000**, 23, 1387–1390.

Appendix

Miscellaneous Publication:

Nucleophile-Selective Cross-Coupling Reactions

Lu-Ying He was able to establish a route to selectively react vinyl and alkynyl bromides with dinucleophilic aromatic substrates. This work was published in the European Journal of Organic Chemistry in 2015. Reprinted with permission (See page 445) from: Lu-Ying He, Mathias Schulz-Senft, Birk Thiedemann, Julian Linshoef, Paul J. Gates, and Anne Staubitz, Nucleophile-Selective Cross-Coupling Reactions with Vinyl and Alkynyl Bromides on a Dinucleophilic Aromatic Substrate, *Eur. J. Org. Chem.* **2015**, 2498-2502. Copyright 2015 Wiley-VCH Verlag GmbH & Co. KGaA, Weinheim.

DOI: 10.1002/ejoc.201500138

Below, the complete paper and the relevant pages from the supporting information are shown.

Abstract

A nucleophile-selective cross-coupling reaction on an aromatic compound bearing two metal groups, Bpin and SnMe₃, has been developed. Previously, only aryl bromides and iodides could be used as electrophilic components, but in this work, the scope could be extended to vinyl and alkynyl bromides as electrophiles. This means that the roles typical in Sonogashira couplings or Heck reactions of the aromatic ring as the dielectrophile coupling to vinyl and alkynyl metal species are reversed, which presents a new tool for organic synthesis. The first nucleophilic site to react is the stannyl group, and subsequently, a Suzuki–Miyaura cross-coupling reaction can take place on the same molecule.

Scientific Contribution to this Paper

For this publication, I synthesized the molecules **6c** and **6d**.

Nucleophile-Selective Cross-Coupling Reactions with Vinyl and Alkynyl Bromides on a Dinucleophilic Aromatic Substrate

Lu-Ying He,^[a] Mathias Schulz-Senft,^[a] Birk Thiedemann,^[a] Julian Linshoef,^[a]
Paul J. Gates,^[b] and Anne Staubitz*^[a]

Keywords: Cross-coupling / Palladium / C–C coupling / Chemoselectivity / Sulfur heterocycles

A nucleophile-selective cross-coupling reaction on an aromatic compound bearing two metal groups, Bpin and SnMe₃, has been developed. Previously, only aryl bromides and iodides could be used as electrophilic components, but in this work, the scope could be extended to vinyl and alkynyl bromides as electrophiles. This means that the roles typical

in Sonogashira couplings or Heck reactions of the aromatic ring as the dielectrophile coupling to vinyl and alkynyl metal species are reversed, which presents a new tool for organic synthesis. The first nucleophilic site to react is the stannyl group, and subsequently, a Suzuki–Miyaura cross-coupling reaction can take place on the same molecule.

Introduction

Cross-coupling reactions (CCRs) of organometallic compounds R–M with organic compounds R–X have evolved into powerful and general methodologies for carbon–carbon bond formation.^[1] CCRs pervade all areas of organic synthesis^[2] from the construction of polymers,^[3] pharmaceuticals^[4] to natural products. In many cases, functional group tolerance is high, but to build up complex organic scaffolds, highly selective CCRs are essential. Research on electrophile-selective CCRs [differentiating between R–X¹ and R–X² (X = I, Br, Cl, OTf, etc.)] has been intensively pursued.^[5] For Stille reactions, the order of reactivity of halides is I > Br > Cl.^[6] However, nucleophile-selective CCRs with dimetallic (hetero)-aromatic substrates have been very rarely examined.^[7]

In our group, a nucleophile-selective one pot reaction was developed recently on a new thiophene building block that contains both a stannyl group and a boronic ester functional group.^[7c] Furthermore, this reaction was extended to both nucleophile- and electrophile-selective CCRs with aromatic rings based on a thiophene building block.^[7d] For both reactions, excellent chemoselectivity was observed in Stille CCRs with mono-halogenated or di-halogenated electrophiles in high yields.

However, the two reactions could be carried out only with aromatic electrophiles. As double and triple bonds are also very important functional groups that can be intro-

duced by cross-coupling methods, we now focussed on establishing nucleophile-selective CCRs with halogenated vinyl or alkynyl compounds.

Results and Discussion

As a test reaction, dinucleophilic thiophene **1** was cross-coupled with the commercially available β -bromostyrene (**2a/2a'** = 8:1) in toluene at 80 °C under microwave conditions with [Pd(PPh₃)₄] as the catalyst. After 1 h, the starting material was completely consumed, and the products **3a** and **3a'** were isolated in a combined yield of 36%. Although the reaction was highly selective for the nucleophile and no Suzuki–Miyaura cross-coupling occurred, two major homocoupling byproducts, the biaryl **4** in a yield of 17%, and 1,4-diphenylbutadiene **5** in yield of 10% were isolated. Oxidative homocoupling reactions leading to byproducts such as **4** may occur when oxygen is not rigorously excluded,^[8] but the reactions were performed under nitrogen with rigorous exclusion of air and a repeat experiment yielded similar results. Ozawa and co-workers have recently performed a thorough investigation into a similar reaction.^[9] When (*E*)- β -bromostyrene reacted with phenylboronic acid under Suzuki cross-coupling conditions, they also found substantial amounts of byproduct **5** as an *E/Z* mixture and biphenyl. Their detailed mechanistic studies suggested that oxidative addition of the (*E*)- β -bromostyrene to the Pd-centre was followed by a metathesis reaction with (*E*)- β -bromostyrene leading to the homocoupled styryl–styryl species **5** and [Pd(L)₂Br₂]. The latter may be reduced by the aryl–metal species present, giving rise to biaryl compounds such as **4**. This reactivity was not observed for (*Z*)- β -bromostyrene, because of the higher stability of its oxidative insertion product, (*Z*)-styryl–Pd(L)₂Br, towards reac-

[a] Otto Diels-Institute for Organic Chemistry, University of Kiel, Otto-Hahn-Platz 4, 24098 Kiel, Germany
E-mail: astaubitz@oc.uni-kiel.de
<http://www.otto-diels-institut.de/staubitz/>

[b] School of Chemistry, University of Bristol, Cantock's Close, Bristol BS8 1TS, UK

Supporting information for this article is available on the WWW under <http://dx.doi.org/10.1002/ejoc.201500138>.

tion with another equivalent of (*Z*)- β -bromostyrene. As the relative kinetic stabilities of the intermediates in a catalytic cycle are highly dependent on the reaction conditions, it seemed plausible that this reaction could be optimized to improve the yield of the product and minimize the amount of byproducts. Over 40 different reaction conditions were screened (solvents, catalysts, temperature, catalyst loading, reaction time, concentration; for details see the Supporting Information Table S1), all reactions were monitored and quantified by gas chromatography (GC).

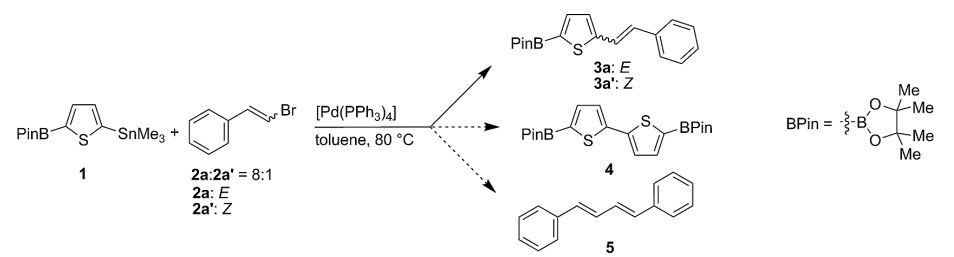
Conversion and yield were highly dependent on the catalysts, solvents and temperature. It emerged that for bidentate and/or very bulky ligands, in the catalysts [Pd(dppe)Cl₂], [Pd(OAc)₂/SPhos], [Pd(dppf)Cl₂] and [Pd(P*t*Bu₃)₂], the yields were low (25, 30, 46 and 39% respectively, Table S1, entries 13–16) because considerable amounts of homocoupled byproducts **4** and **5** formed alongside other non-identified byproducts. Presumably, the intermediate styryl-Pd(L)₂Br species, which forms by oxidative addition, is very reactive towards vinyl bromides in the case of catalysts with bulky ligands. This might be because in the products of the homocoupling reaction, i.e., the complex [PdL₂Br₂] and the byproducts **4** and **5**, steric strain can be released. Therefore, [Pd(PPh₃)₄] as the least hindered catalyst (up to three ligands dissociate)^[10] proved the most suitable catalyst for this reaction (Table 1). Solvent screening of dioxane, toluene, THF, pyridine, acetonitrile and DMF (Table 1, entries 1–6) showed that DMF was the most suitable solvent, giving a combined yield of **3a** + **3a'** of 95% at 60 °C (Table 1, entry 6). However, polarity of the solvent cannot be the only parameter influencing the reaction, because the much less polar toluene, for example, also

gave a good combined yield of **3a** and **3a'** of 66% (Table 1, entry 2). The catalyst loading could be lowered to 1 mol-%, and the product was obtained in 97% yield (**3a** + **3a'**, Table 1, entry 7). The reaction was also efficient at a lower temperature of 40 °C (Table 1, entry 8); whereas 20 °C led to very long reaction times (Table 1, entries 9 and 10). Moreover, at 40 °C, fewer homocoupled byproducts were observed than at 60 °C.

Based on these results, the best reaction conditions for the nucleophile-selective CCR were a catalyst loading of [Pd(PPh₃)₄] as low as 1 mol-% in DMF as the solvent, either at 40 °C or 60 °C. The next aim was to establish whether these conditions would be suitable for a variety of vinyl (Table 2) and alkynyl bromides (Table 3) as electrophiles.

Vinyl bromides were synthesized from corresponding α , β -unsaturated carboxylic acids^[11] or carboxaldehyde^[12] in good yields (see Supporting Information for details). The alkynyl bromides were also easily available in high yields from the corresponding terminal alkynes.^[11] For both types of electrophiles, all reactions were entirely nucleophile-selective (as detectable by GC-MS and NMR spectroscopy) and generally very tolerant towards the electrophiles used. In the case of vinyl bromides, especially for electron-rich compounds, good to excellent yields of the corresponding products were obtained at 40 °C (74–77%; Table 2, **3b**, **3c** and **3e**). However, the amine **3d** could be isolated in only 43% yield because despite the higher temperature of 60 °C and a significantly longer reaction time of 168 h, the conversion to the product was low. Even longer reaction times did not improve the result, which may be caused by the binding of the amine to the Pd centre.^[13] With electron-neutral electro-

Table 1. Optimization of reaction conditions.^[a]



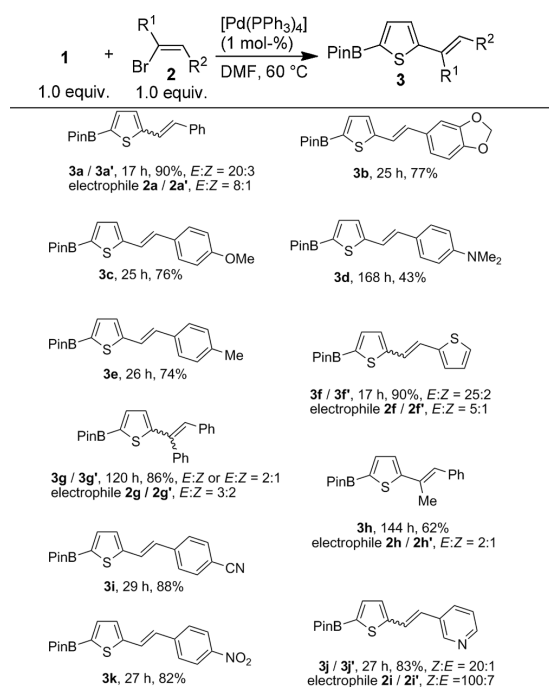
Entry	Solvent	Concentration [mmol/mL]	Cat. loading [mol-%]	<i>T</i> [°C]	<i>t</i> [h]	Conv. ^[b] [%]	Yield [%] ^[c]			
							3a	3a'	4	5
1	Dioxane	0.25	5	60	17	83	51	5	3	0
2	Toluene	0.25	5	60	17	91	59	7	9	6
3	THF	0.25	5	60	17	94	73	8	6	3
4	Pyridine	0.25	5	60	17	93	37	3	16	14
5	MeCN	0.25	5	60	17	100	43	10	22	14
6	DMF	0.25	5	60	17	100	83	12	2	0
7	DMF	0.25	1	60	17	100	86	11	2	0
8	DMF	0.5	1	40	17	96	86	4	1	0
9	DMF	0.5	5	20	17	40	12	0	1	0
10	DMF	0.5	5	20	65	93	70	1	4	0

[a] **1** (1.1 equiv.), **2** (1.0 equiv.). [b] Conversion is based on **2**. [c] Determined by GC with triisopropylbenzene as the internal calibration standard.

FULL PAPER

A. Staubitz et al.

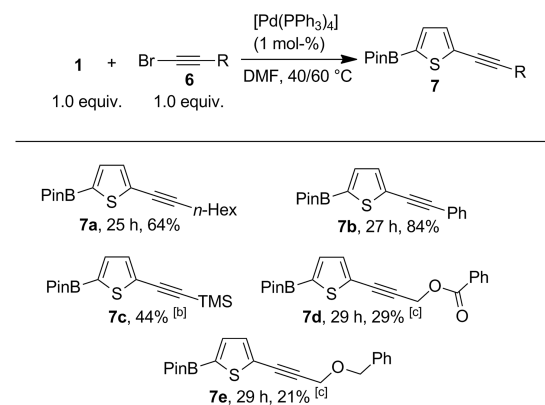
philes, β -bromostyrene **3a** and 2-(2-bromovinyl)-thiophene **3f** also gave good yields of 90%, albeit at 60 °C, i.e., 20 °C higher than for electron-rich vinyl bromides. However, the reaction to form **3g** required about seven times as long as **3e**, which can be attributed to the much greater steric hindrance due to the additional phenyl group geminal to the reacting centre. If the steric hindrance was instead provided by a methyl group (product **3h**), a longer reaction time of 144 h was required. Electron-deficient vinyl bromides gave excellent yields of the products **3i**, **3j** and **3k** in relatively short reaction times of about 30 h (88, 83 and 82%, respectively).

Table 2. Nucleophile-selective CCRs with various vinyl bromides.^[a]

[a] The reactions to obtain **3a**, **3b**, and **3d** were performed at 40 °C.

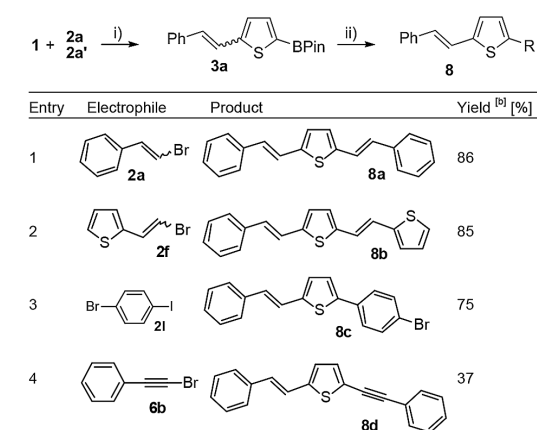
The reaction was further analysed with respect to alkynyl bromides as electrophilic coupling partners (Table 3). For alkynyl bromides with a simple *n*-hexyl (**6a**) or phenyl substituent (**6b**), the reaction gave good yields of 64 and 84%, respectively at 40 °C. However, the reaction with **6c** (R = TMS), only afforded **7c** in a yield of 44% (and could only be isolated as a 1:1 mixture with starting material **1**, even at a temperature of 60 °C and a significantly longer reaction time of 168 h). Although no byproduct formation was observed, the reactivity of the electrophilic component was exceedingly low. For **6d** and **6e**, both reactions were complete in 29 h at 60 °C, but the isolated yield was relatively low. In these cases, the issue was not conversion, but purification. Both products decomposed on a silica column, and it was also not possible to purify them by Kugelrohr distillation. This was a general observation for all products of

type **7** (see Supporting Information for details): If Kugelrohr distillation was not possible, then no pure products could be obtained due to over-absorption onto silica gel, possibly due to interactions of the vacant orbital on boron with nucleophilic moieties in silica gel.^[14]

Table 3. Stille CCRs of alkynyl bromides.^[a]

[a] The reactions to obtain **7a** and **7b** were performed at 40 °C, and those for **7c–7e** were performed at 60 °C. [b] As a 1:1 mixture with the starting material **1**. [c] Contains impurities, for details see the Supporting Information.

After the chemoselective Stille CCR, the products still contain a boronic ester functional group, which can be further coupled with a second electrophile by a Suzuki–Miyaura CCR. By merely adding K_2CO_3 as a base, water and a second electrophile to the reaction mixture after completion of the Stille CCR, this could be accomplished. All of these subsequent reactions were stirred at 100 °C for 6 h (Table 4). This allowed the synthesis of **8a** and **8b** in yields of 86 and 85%, respectively. The synthesis of **8b** demon-

Table 4. Chemoselective one-pot CCRs of thiophene **1**.^[a]

[a] i) **1** (1.0 equiv.), **2a + 2a'** (1.0 equiv.), $[\text{Pd}(\text{PPh}_3)_4]$ (1 mol-%), DMF, 60 °C, 17 h. ii) Electrophiles (1.0 equiv.), K_2CO_3 (2.0 equiv.), H_2O , 100 °C, 6 h. [b] Yields of isolated products.

strates that the strategy of using a nucleophile-selective cross-coupling reaction allows very easy access to non-symmetric di-stilbene-like materials. Aryl iodides can also be used as the second electrophile and in the case of **2l**, the reaction is also highly electrophile selective as shown by the high yield of 75%. In addition, no unselectively cross-coupled byproduct could be detected by GC-MS or NMR spectroscopy. The second Suzuki-Miyaura coupling was also performed with an alkynyl bromide, **6b**, but the yield was lower in this case, reflecting the lower efficiency of such substrates in cross-coupling reactions, as described above (Table 4).

Conclusions

In conclusion, reaction conditions for a nucleophile-selective CCR between vinyl and alkynyl bromides with a dinucleophilic thiophene substrate were established. Although homocoupling of the nucleophile and electrophile, respectively, are potential competing reactions, careful optimisation of the reaction conditions led to a process in which these side reactions could be largely suppressed in all cases. These reactions are general with respect to a wide variety of electrophiles. For vinyl bromides, all products were obtained in good to excellent yields, although time and temperature needed to be adjusted from case to case. Alkynyl bromides proved more difficult electrophilic components, mainly due to purification issues, which are apparently intrinsic for these types of boronic ester containing thiophene alkynyl groups. In both cases, the resulting products are extremely versatile building blocks: they still contain a boronic ester that can be further coupled with a second electrophile by a Suzuki-Miyaura cross-coupling in one-pot reactions. Furthermore, the reactions with the alkynyl bromides provide access to aromatic alkynyl compounds, with a reversal of the roles of nucleophile and electrophile compared with Sonogashira CCRs. This makes this reaction a valuable alternative for volatile aromatic alkynyl compounds, in cases where Sonogashira couplings fail or are unselective. The main advantage of a nucleophile-selective cross-coupling reaction is that a further organometallic site remains for subsequent functionalisation reactions. This was also demonstrated: by merely adding water and a base, a Suzuki-Miyaura reaction could be added to the reaction sequence. Aryl bromides and iodides as well as vinyl bromides and alkynyl bromides react under these conditions.

Experimental Section

General Procedure for Nucleophile-selective CCRs with Various Vinyl Bromides: A solution of **1** (373 mg, 1.00 mmol), the vinyl bromide (1.00 mmol), and [Pd(PPh₃)₄] (11.6 mg, 10.0 μmol, 1 mol-%) in DMF (4 mL) was heated to 40 or 60 °C for a specific time (for details with respect to specific electrophiles see the Supporting Information). The mixture was filtered through a short plug of celite with *n*-hexane (500 mL) as the solvent. The solvent was removed in vacuo and the crude product was purified by Kugelrohr

distillation or column chromatography (for details with respect to specific electrophiles see the Supporting Information).

General Procedure for Nucleophile-selective CCRs with Various Alkynyl Bromides: A solution of **1** (373 mg, 1.00 mmol), the alkynyl bromide (1.00 mmol), and [Pd(PPh₃)₄] (11.6 mg, 10.0 μmol, 1 mol-%) in DMF (4 mL) was heated to 40 or 60 °C for a specific time (for details with respect to specific electrophiles see the Supporting Information). The mixture was filtered through a short plug of celite with *n*-hexane (500 mL) or diethyl ether (50 mL) as the solvent. The solvent was removed in vacuo and the crude product was purified by Kugelrohr distillation or column chromatography (for details with respect to specific electrophiles see the Supporting Information).

General Procedure for Chemo-selective One-pot CCR of Thiophene **1:** A solution of **1** (186 mg, 500 μmol), β-bromostyrene (*E/Z* = 8:1; 91.0 mg, 500 μmol), and [Pd(PPh₃)₄] (5.78 mg, 5.00 μmol, 1 mol-%) in DMF (4 mL) was heated to 60 °C for 17 h. Then the second electrophile (500 μmol) in DMF (4 mL) was added to the solution in one portion in addition to K₂CO₃ (138 mg, 1.00 mmol) in degassed water (1 mL). The solution was heated to 100 °C for 6 h. After the solution cooled down to 20 °C, the solution was diluted with CH₂Cl₂ (8 mL) and filtered through a short plug of silica with CH₂Cl₂ (250 mL). After removing the volatile components in vacuo, the crude product was purified by column chromatography (for details with respect to specific electrophiles see the Supporting Information).

Acknowledgments

L. Y. H. thanks the China Scholarship Council (CSC) for a Ph. D. scholarship and Prof. Zheng-Guo Zhang's and Prof. Xiao-Ming Fang's support for her work.

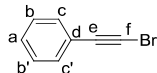
- [1] a) A. Suzuki, *Chem. Commun.* **2005**, 4759–4763; b) C. L. Sun, B. J. Li, Z. J. Shi, *Chem. Commun.* **2010**, 46, 677–685.
- [2] U. Kazmaier, M. Pohlman, *Metal-Catalyzed Cross-Coupling Reactions, Vol. 1*, 2nd ed., Wiley-VCH, Weinheim, **2004**.
- [3] a) A. D. Schlueter, *J. Polym. Sci., Part A* **2001**, 39, 1533–1556; b) T. Yamamoto, *Bull. Chem. Soc. Jpn.* **2010**, 83, 431–455.
- [4] a) C. Torborg, M. Beller, *Adv. Synth. Catal.* **2009**, 351, 3027–3043; b) J. Magano, J. R. Dunetz, *Chem. Rev.* **2011**, 111, 2177–2250; c) M. L. Crawley, B. M. Trost, *Applications of Transition Metal Catalysis in Drug Discovery and Development: An Industrial Perspective*, John Wiley & Sons, Hoboken, **2012**.
- [5] a) G. Y. Cho, P. Remy, J. Jansson, C. Moessner, C. Bolm, *Org. Lett.* **2004**, 6, 3293–3296; b) S. H. Lee, B. B. Jang, Z. H. Kafafi, *J. Am. Chem. Soc.* **2005**, 127, 9071–9078; c) S. Shekhar, J. F. Hartwig, *Organometallics* **2007**, 26, 340–351; d) M. Mosrin, P. Knochel, *Chem. Eur. J.* **2009**, 15, 1468–1477; e) J. J. Peterson, Y. C. Simon, E. B. Coughlin, K. R. Carter, *Chem. Commun.* **2009**, 4950–4952; f) M. Kienle, A. Unsinn, P. Knochel, *Angew. Chem. Int. Ed.* **2010**, 49, 4751–4754; *Angew. Chem.* **2010**, 122, 4860; g) A. Martins, D. A. Candito, M. Lautens, *Org. Lett.* **2010**, 12, 5186–5188.
- [6] N. Miyaura, A. Suzuki, *Chem. Rev.* **1995**, 95, 2457–2483.
- [7] Nucleophile-selective reactions on aromatic compounds: a) E. J. Roskamp, P. S. Dragovich, J. B. Hartung, S. F. Pedersen, *J. Org. Chem.* **1989**, 54, 4736–4737; b) D. R. Williams, A. A. Shah, *Chem. Commun.* **2010**, 46, 4297–4299; c) J. Linschoeft, A. C. J. Heinrich, S. A. W. Segler, P. J. Gates, A. Staubitz, *Org. Lett.* **2012**, 14, 5644–5647; d) A. C. J. Heinrich, B. Thiedemann, P. J. Gates, A. Staubitz, *Org. Lett.* **2013**, 15, 4666–4669; nucleophile-selective reactions on other tin/boron reagents: e) F. Lhermitte, B. Carboni, *Synlett* **1996**, 377–379; f) R. S. Coleman, M. C. Walczak, *Org. Lett.* **2005**, 7, 2289–2291; g) R. S.

FULL PAPER

A. Staubitz et al.

- Coleman, X. L. Lu, I. Modolo, *J. Am. Chem. Soc.* **2007**, *129*, 3826–3827; h) M. Altendorfer, D. Menche, *Chem. Commun.* **2012**, *48*, 8267–8269; nucleophile-selective reactions on other boron/boron reagents: i) S. J. Lee, K. C. Gray, J. S. Paek, M. D. Burke, *J. Am. Chem. Soc.* **2008**, *130*, 466–468; j) G. A. Molander, D. L. Sandrock, *J. Am. Chem. Soc.* **2008**, *130*, 15792–15793; k) H. Noguchi, T. Shioda, C. M. Chou, M. Sugimoto, *Org. Lett.* **2008**, *10*, 377–380; l) M. Tobisu, N. Chatani, *Angew. Chem. Int. Ed.* **2009**, *48*, 3565–3568; *Angew. Chem.* **2009**, *121*, 3617; m) N. Iwamoto, M. Sugimoto, *J. Am. Chem. Soc.* **2010**, *132*, 2548–2549; n) R. R. Singidi, T. V. Rajan-Babu, *Org. Lett.* **2010**, *12*, 2622–2625; o) E. M. Woerly, A. H. Cherney, E. K. Davis, M. D. Burke, *J. Am. Chem. Soc.* **2010**, *132*, 6941–6943; p) S. Fujii, S. Y. Chang, M. D. Burke, *Angew. Chem. Int. Ed.* **2011**, *50*, 7862–7864; *Angew. Chem.* **2011**, *123*, 8008; q) J. C. H. Lee, R. McDonald, D. G. Hall, *Nature Chem.* **2011**, *3*, 894–899; r) K. C. Gray, D. S. Palacios, I. Dailey, M. M. Endo, B. E. Uno, B. C. Wilcock, M. D. Burke, *Proc. Natl. Acad. Sci. USA* **2012**, *109*, 2234–2239; s) L. Xu, S. Y. Ding, P. F. Li, *Angew. Chem. Int. Ed.* **2014**, *53*, 1822–1826; t) L. Xu, P. F. Li, *Synlett* **2014**, *25*, 1799–1802; nucleophile-selective reactions on other boron/zinc reagents: u) Y. Nagashima, R. Takita, K. Yoshida, K. Hirano, M. Uchiyama, *J. Am. Chem. Soc.* **2013**, *135*, 18730–18733; nucleophile-selective reactions on other silicon/boron reagents: v) M. G. McLaughlin, C. A. McAdam, M. J. Cook, *Org. Lett.* **2015**, *17*, 10–13.
- [8] C. Adamo, C. Amatore, I. Ciofini, A. Jutand, H. Lakmini, *J. Am. Chem. Soc.* **2006**, *128*, 6829–6836.
- [9] M. Wakioka, M. Nagao, F. Ozawa, *Organometallics* **2008**, *27*, 602–608.
- [10] a) M. Ahlquist, P. Fristrup, D. Tanner, P. O. Norrby, *Organometallics* **2006**, *25*, 2066–2073; b) Z. Li, Y. Fu, Q. X. Guo, L. Liu, *Organometallics* **2008**, *27*, 4043–4049.
- [11] a) J. P. Das, S. Roy, *J. Org. Chem.* **2002**, *67*, 7861–7864; b) R. A. Fursule, P. O. Patil, B. D. Shewale, S. B. Kosalge, P. K. Deshmukh, D. A. Patil, *Chem. Pharm. Bull.* **2009**, *57*, 1243–1245.
- [12] A. Hayford, J. Kaloko, S. El-Kazaz, G. Bass, C. Harrison, T. Corprew, *Org. Lett.* **2005**, *7*, 2671–2673.
- [13] a) Y. Li, M. A. El-Sayed, *J. Phys. Chem. B* **2001**, *105*, 8938–8943; b) J. H. Li, W. J. Liu, *Org. Lett.* **2004**, *6*, 2809–2811.
- [14] S. Hitosugi, D. Tanimoto, W. Nakanishi, H. Isobe, *Chem. Lett.* **2012**, *41*, 972–973.

Received: January 28, 2015
Published Online: February 27, 2015

(Bromoethynyl)benzene (6b)^[8]

This compound was prepared by a literature method.^[8]

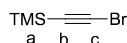
To a stirred solution of ethynylbenzene (1.02 g, 10.0 mmol) in acetone (50 mL), in a flask which was shielded rigorously from light, solid AgNO₃ (84.0 mg, 500 μmol) and *N*-bromosuccinimide (2.53 g, 14.0 mmol) were added in one portion under an air atmosphere. After stirring for 6 h at 22 °C, the solvent was removed *in vacuo* and the crude product was purified by column chromatography over silica gel (*n*hexane, R_f = 0.53) to afford the product (1.70 g, 90%; Lit.: [8]) as yellow oil.

¹H NMR (600 MHz, CDCl₃): δ = 7.47–7.43 (m, 2 H, H-c, c'), 7.36–7.29 (m, 2 H, H-a, b, b') ppm.

¹³C NMR (151 MHz, CDCl₃): δ = 132.0 (C-c, c'), 128.7 (C-a), 128.3 (C-b, b'), 122.7 (C-d), 80.0 (C-e), 49.7 (C-f) ppm.

HRMS (ESI-FTMS) *m/z*: [M]⁺ Calcd for [C₈H₅Br]⁺ 179.9575; Found 179.9574.

IR (ATR): ν̄ = 3062 (w), 2818 (w), 2199 (m), 1595 (m), 1485 (s), 1442 (m), 1070 (m), 1026 (m), 915 (m), 751 (vs), 687 (vs), 611 (s), 519 (vs) cm⁻¹.

(Bromoethynyl)trimethylsilane (6c)

This compound was prepared by a literature method.^[9]

n-BuMgCl (9.49 mL, 15.0 mmol) was added dropwise over the period of 10 min to the stirred solution of ethynyltrimethylsilane (1.47 g, 15.0 mmol) in THF (45 mL) at 20 °C. The solution stirred for 18 h at 20 °C. Then the solution was cooled to -78 °C and stirred for 1 h before bromine (770 μL, 15.0 mmol) was added dropwise over the period of 10 min. Then the solution warmed up to 20 °C. The reaction mixture was quenched slowly with 2 M of Na₂S₂O₃ aqueous solution (15 mL). The yellow solution became colorless and was stirred for additional 5 min. The organic layer was washed with brine (3 x 50 mL) and dried over MgSO₄. The solvent was removed *in vacuo* and the crude product was purified Kugelrohr distillation (60–80 °C, 100 mbar) to afford (1.41 g, 69%, Lit.^[9]: 56%) of colorless oil.

¹H NMR (500 MHz, CDCl₃): δ = 0.18 (s, 9 H, H-a) ppm.

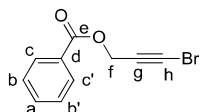
¹³C NMR (125 MHz, CDCl₃): δ = 87.1 (C-b), 61.6 (C-c), 0.1 (C-a) ppm.

²⁹Si NMR (99 MHz, CDCl₃): δ = (-15.50 – -15.85) ppm.¹²

²⁹Si [¹H] DEPT NMR (99 MHz, CDCl₃): δ = 15.67 (s, Si-(CH₃)₃) ppm.

HRMS (EI-sector) *m/z*: [M]⁺ Calcd for [C₅H₉BrSi]⁺ 177.9636; Found 177.9637.

IR (ATR): ν̄ = 2962 (m), 2125 (s), 1251 (s) cm⁻¹.¹³

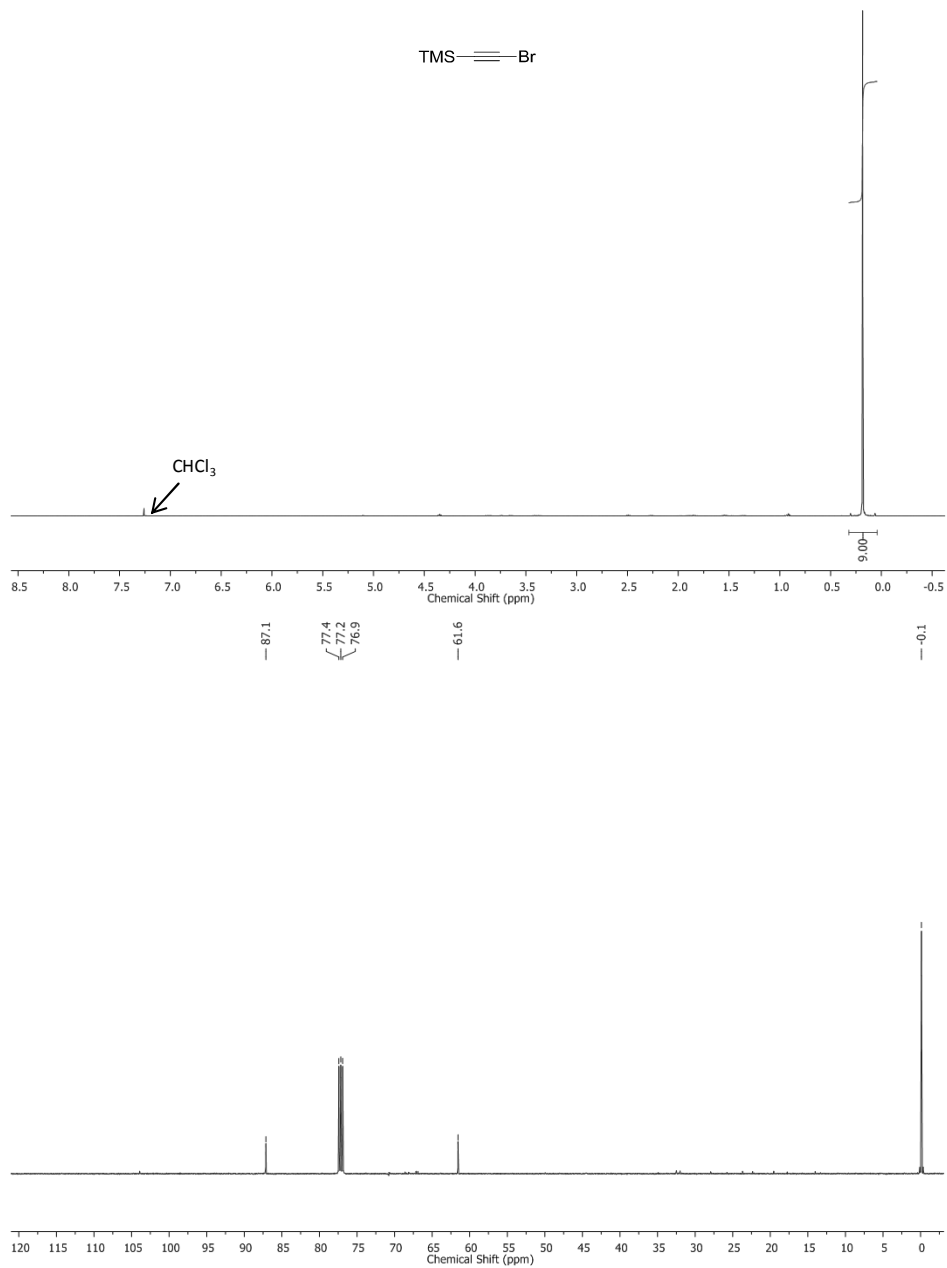
3-Bromoprop-2-yn-1-yl benzoate (6d)

To the mixture of propargyl benzoate (2.40 g, 15.0 mmol) and *N*-bromosuccinimide (3.26 g, 12.0 mmol) in 10 mL of acetone, AgNO₃ (127 mg, 750 μmol) was added in one portion and the mixture was stirred at 20 °C for 3 h. After

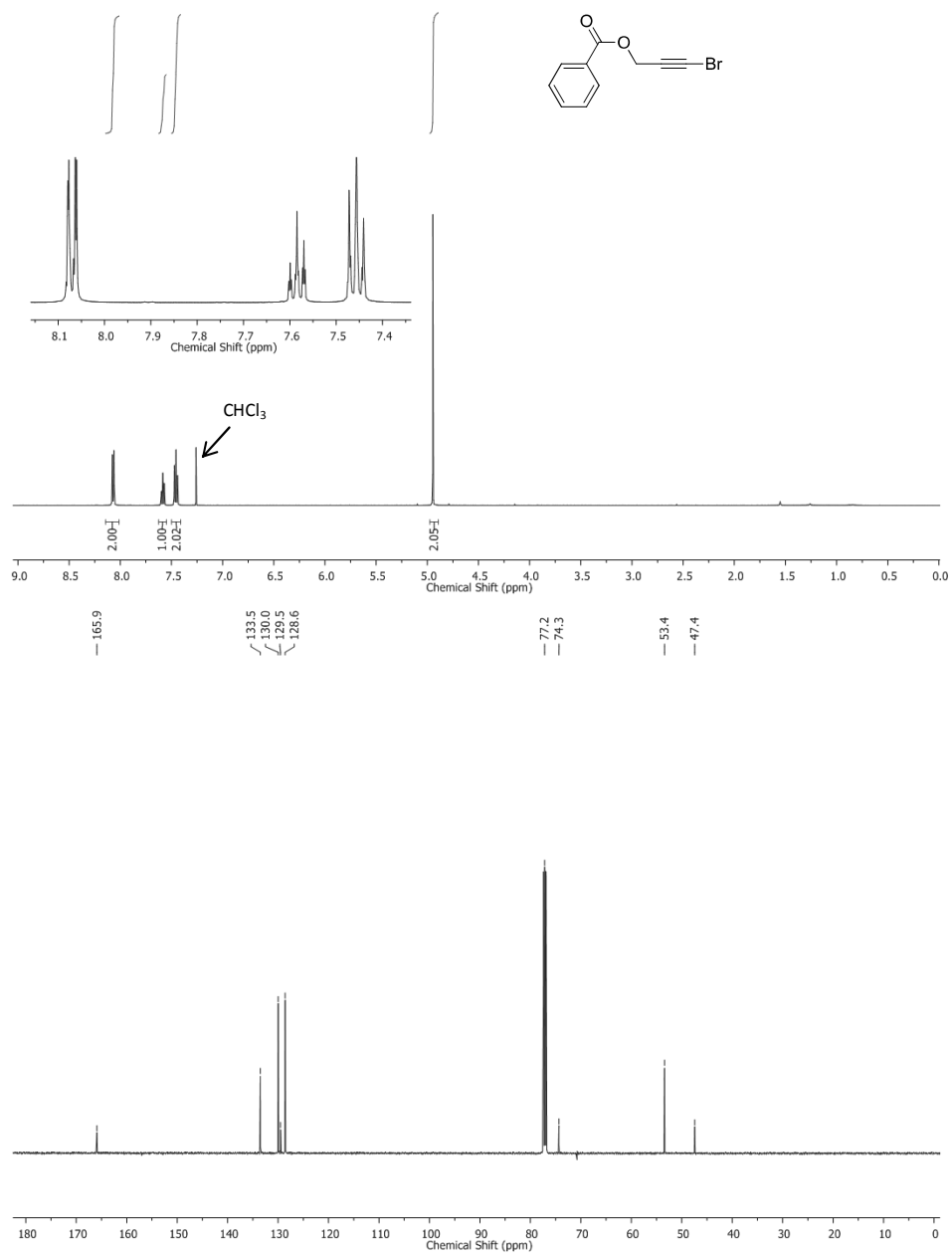
¹² The expected ²J Si-H coupling constant with 6.6 Hz was observed, but the signal/noise ratio is too low to see the complete multiplet.

¹³ No peak at about 3300 cm⁻¹, corresponding to CC-H valence vibration.

(Bromoethynyl)trimethylsilane (6c)



3-Bromoprop-2-yn-1-yl benzoate (6d)



Permissions to Reprint

Figure I.7 was adapted with permission from T. P. Kaloni, G. Schreckenbach, M. S. Freund, *J. Phys. Chem. C* **2015**, *119*, 3979-3989.^[64]

Results of this thesis were published in six articles in peer-review journals. The following articles were reprinted with permission in this thesis:

(1) M. Schulz-Senft, M. Lipfert, A. Staubitz, Mechanopolymerchemie: Molekulare Wirkung durch Kraft, *Chem. Unserer Zeit* **2014**, *48*, 200-214. DOI: 10.1002/ciuz.201400640

(2) S. Shree, M. Schulz-Senft, N. H. Alsleben, Y. K. Mishra, A. Staubitz, R. Adelung, Light, Force, and Heat: A Multi-Stimuli Composite that Reveals its Violent Past, *ACS Appl. Mater. Interfaces* **2017**, *9*, 38000-38007. DOI: 10.1021/acsami.7b09598

(3) S. Shree, M. Dowds, A. Kuntze, S. Li, Y. K. Mishra, A. Staubitz, R. Adelung, Self-reporting mechanochromic coating: a glassfiber reinforced polymer composite that predicts impact induced damage, *Mater. Horiz.* **2019**.

DOI: 10.1039/C9MH01400D

(4) M. Schulz-Senft, P. J. Gates, F. D. Sönnichsen, A. Staubitz, Diversely halogenated spiropyran - Useful synthetic building blocks for a versatile class of molecular switches, *Dyes Pigm.* **2017**, *136*, 292-301. DOI: 10.1016/j.dyepig.2016.08.039

(5) M. Dowds, D. Bank, J. Strüben, D. Presa Soto, F. D. Sönnichsen, F. Renth, F. Temps, A. Staubitz, Efficient reversible photoisomerisation with large solvodynamic size-switching of a main chain poly(azobenzene-*alt*-trisiloxane), *J. Mater. Chem. C* **2020**.

DOI: 10.1039/C9TC05193G

(6) L.-Y. He, M. Schulz-Senft, B. Thiedemann, J. Linshoef, P. J. Gates, A. Staubitz, Nucleophile-Selective Cross-Coupling Reactions with Vinyl and Alkynyl Bromides on a Dinucleophilic Aromatic Substrate *Eur. J. Org. Chem.* **2015**, 2498-2502.

DOI: 10.1002/ejoc.201500138

The permissions to reprint were obtained from the publishers and are attached hereafter.

T. P. Kaloni, et al., *The Journal of Physical Chemistry C* 2015, 119, 3979-3989.

9/20/2019

Rightslink® by Copyright Clearance Center



RightsLink®

Home

Account
Info

Help

ACS Publications
Most Trusted. Most Cited. Most Read.

Title: Structural and Electronic
Properties of Pristine and Doped
Polythiophene: Periodic versus
Molecular Calculations

Logged in as:
Mathias Schulz
Account #:
3000599298

Author: Thaneshwor P. Kaloni, Georg
Schreckenbach, Michael S.
Freund

LOGOUT

Publication: The Journal of Physical
Chemistry C

Publisher: American Chemical Society

Date: Feb 1, 2015

Copyright © 2015, American Chemical Society

PERMISSION/LICENSE IS GRANTED FOR YOUR ORDER AT NO CHARGE

This type of permission/license, instead of the standard Terms & Conditions, is sent to you because no fee is being charged for your order. Please note the following:

- Permission is granted for your request in both print and electronic formats, and translations.
- If figures and/or tables were requested, they may be adapted or used in part.
- Please print this page for your records and send a copy of it to your publisher/graduate school.
- Appropriate credit for the requested material should be given as follows: "Reprinted (adapted) with permission from (COMPLETE REFERENCE CITATION). Copyright (YEAR) American Chemical Society." Insert appropriate information in place of the capitalized words.
- One-time permission is granted only for the use specified in your request. No additional uses are granted (such as derivative works or other editions). For any other uses, please submit a new request.

If credit is given to another source for the material you requested, permission must be obtained from that source.

BACK

CLOSE WINDOW

Copyright © 2019 Copyright Clearance Center, Inc. All Rights Reserved. [Privacy statement](#). [Terms and Conditions](#).
Comments? We would like to hear from you. E-mail us at customercare@copyright.com

M. Schulz-Senft et al., *Chemie in Unserer Zeit* 2014, 48,
200-214.

1/6/2019

RightsLink Printable License

**JOHN WILEY AND SONS LICENSE
TERMS AND CONDITIONS**

Jan 06, 2019

This Agreement between Mathias Schulz ("You") and John Wiley and Sons ("John Wiley and Sons") consists of your license details and the terms and conditions provided by John Wiley and Sons and Copyright Clearance Center.

License Number	4503110292375
License date	Jan 06, 2019
Licensed Content Publisher	John Wiley and Sons
Licensed Content Publication	Chemie in unserer Zeit
Licensed Content Title	Mechanopolymerchemie
Licensed Content Author	Mathias Schulz-Senft, Matthias Lipfert, Anne Staubitz
Licensed Content Date	Apr 1, 2014
Licensed Content Volume	48
Licensed Content Issue	3
Licensed Content Pages	15
Type of use	Dissertation/Thesis
Requestor type	Author of this Wiley article
Format	Print and electronic
Portion	Full article
Will you be translating?	Yes, including English rights
Number of languages	1
Languages	German, English
Title of your thesis / dissertation	Synthesis of Light Responsible Polymer Materials
Expected completion date	Mar 2019
Expected size (number of pages)	300
Requestor Location	Mathias Schulz Otto-Hahn-Platz 4 Kiel, 24098 Germany Attn: Mathias Schulz
Publisher Tax ID	EU826007151
Total	0.00 EUR
Terms and Conditions	

TERMS AND CONDITIONS

This copyrighted material is owned by or exclusively licensed to John Wiley & Sons, Inc. or one of its group companies (each a "Wiley Company") or handled on behalf of a society with which a Wiley Company has exclusive publishing rights in relation to a particular work (collectively "WILEY"). By clicking "accept" in connection with completing this licensing transaction, you agree that the following terms and conditions apply to this transaction (along with the billing and payment terms and conditions established by the Copyright Clearance Center Inc., ("CCC's Billing and Payment terms and conditions"), at the time that

<https://s100.copyright.com/AppDispatchServlet>

1/4

1/6/2019

RightsLink Printable License

you opened your RightsLink account (these are available at any time at <http://myaccount.copyright.com>).

Terms and Conditions

- The materials you have requested permission to reproduce or reuse (the "Wiley Materials") are protected by copyright.
- You are hereby granted a personal, non-exclusive, non-sub licensable (on a stand-alone basis), non-transferable, worldwide, limited license to reproduce the Wiley Materials for the purpose specified in the licensing process. This license, **and any CONTENT (PDF or image file) purchased as part of your order**, is for a one-time use only and limited to any maximum distribution number specified in the license. The first instance of republication or reuse granted by this license must be completed within two years of the date of the grant of this license (although copies prepared before the end date may be distributed thereafter). The Wiley Materials shall not be used in any other manner or for any other purpose, beyond what is granted in the license. Permission is granted subject to an appropriate acknowledgement given to the author, title of the material/book/journal and the publisher. You shall also duplicate the copyright notice that appears in the Wiley publication in your use of the Wiley Material. Permission is also granted on the understanding that nowhere in the text is a previously published source acknowledged for all or part of this Wiley Material. Any third party content is expressly excluded from this permission.
- With respect to the Wiley Materials, all rights are reserved. Except as expressly granted by the terms of the license, no part of the Wiley Materials may be copied, modified, adapted (except for minor reformatting required by the new Publication), translated, reproduced, transferred or distributed, in any form or by any means, and no derivative works may be made based on the Wiley Materials without the prior permission of the respective copyright owner. **For STM Signatory Publishers clearing permission under the terms of the STM Permissions Guidelines only, the terms of the license are extended to include subsequent editions and for editions in other languages, provided such editions are for the work as a whole in situ and does not involve the separate exploitation of the permitted figures or extracts**. You may not alter, remove or suppress in any manner any copyright, trademark or other notices displayed by the Wiley Materials. You may not license, rent, sell, loan, lease, pledge, offer as security, transfer or assign the Wiley Materials on a stand-alone basis, or any of the rights granted to you hereunder to any other person.
- The Wiley Materials and all of the intellectual property rights therein shall at all times remain the exclusive property of John Wiley & Sons Inc, the Wiley Companies, or their respective licensors, and your interest therein is only that of having possession of and the right to reproduce the Wiley Materials pursuant to Section 2 herein during the continuance of this Agreement. You agree that you own no right, title or interest in or to the Wiley Materials or any of the intellectual property rights therein. You shall have no rights hereunder other than the license as provided for above in Section 2. No right, license or interest to any trademark, trade name, service mark or other branding ("Marks") of WILEY or its licensors is granted hereunder, and you agree that you shall not assert any such right, license or interest with respect thereto
- NEITHER WILEY NOR ITS LICENSORS MAKES ANY WARRANTY OR REPRESENTATION OF ANY KIND TO YOU OR ANY THIRD PARTY, EXPRESS, IMPLIED OR STATUTORY, WITH RESPECT TO THE MATERIALS OR THE ACCURACY OF ANY INFORMATION CONTAINED IN THE MATERIALS, INCLUDING, WITHOUT LIMITATION, ANY IMPLIED WARRANTY OF MERCHANTABILITY, ACCURACY, SATISFACTORY QUALITY, FITNESS FOR A PARTICULAR PURPOSE, USABILITY, INTEGRATION OR NON-INFRINGEMENT AND ALL SUCH WARRANTIES

<https://s100.copyright.com/AppDispatchServlet>

2/4

1/6/2019

RightsLink Printable License

ARE HEREBY EXCLUDED BY WILEY AND ITS LICENSORS AND WAIVED BY YOU.

- WILEY shall have the right to terminate this Agreement immediately upon breach of this Agreement by you.
- You shall indemnify, defend and hold harmless WILEY, its Licensors and their respective directors, officers, agents and employees, from and against any actual or threatened claims, demands, causes of action or proceedings arising from any breach of this Agreement by you.
- IN NO EVENT SHALL WILEY OR ITS LICENSORS BE LIABLE TO YOU OR ANY OTHER PARTY OR ANY OTHER PERSON OR ENTITY FOR ANY SPECIAL, CONSEQUENTIAL, INCIDENTAL, INDIRECT, EXEMPLARY OR PUNITIVE DAMAGES, HOWEVER CAUSED, ARISING OUT OF OR IN CONNECTION WITH THE DOWNLOADING, PROVISIONING, VIEWING OR USE OF THE MATERIALS REGARDLESS OF THE FORM OF ACTION, WHETHER FOR BREACH OF CONTRACT, BREACH OF WARRANTY, TORT, NEGLIGENCE, INFRINGEMENT OR OTHERWISE (INCLUDING, WITHOUT LIMITATION, DAMAGES BASED ON LOSS OF PROFITS, DATA, FILES, USE, BUSINESS OPPORTUNITY OR CLAIMS OF THIRD PARTIES), AND WHETHER OR NOT THE PARTY HAS BEEN ADVISED OF THE POSSIBILITY OF SUCH DAMAGES. THIS LIMITATION SHALL APPLY NOTWITHSTANDING ANY FAILURE OF ESSENTIAL PURPOSE OF ANY LIMITED REMEDY PROVIDED HEREIN.
- Should any provision of this Agreement be held by a court of competent jurisdiction to be illegal, invalid, or unenforceable, that provision shall be deemed amended to achieve as nearly as possible the same economic effect as the original provision, and the legality, validity and enforceability of the remaining provisions of this Agreement shall not be affected or impaired thereby.
- The failure of either party to enforce any term or condition of this Agreement shall not constitute a waiver of either party's right to enforce each and every term and condition of this Agreement. No breach under this agreement shall be deemed waived or excused by either party unless such waiver or consent is in writing signed by the party granting such waiver or consent. The waiver by or consent of a party to a breach of any provision of this Agreement shall not operate or be construed as a waiver of or consent to any other or subsequent breach by such other party.
- This Agreement may not be assigned (including by operation of law or otherwise) by you without WILEY's prior written consent.
- Any fee required for this permission shall be non-refundable after thirty (30) days from receipt by the CCC.
- These terms and conditions together with CCC's Billing and Payment terms and conditions (which are incorporated herein) form the entire agreement between you and WILEY concerning this licensing transaction and (in the absence of fraud) supersedes all prior agreements and representations of the parties, oral or written. This Agreement may not be amended except in writing signed by both parties. This Agreement shall be binding upon and inure to the benefit of the parties' successors, legal representatives, and authorized assigns.
- In the event of any conflict between your obligations established by these terms and conditions and those established by CCC's Billing and Payment terms and conditions, these terms and conditions shall prevail.

<https://s100.copyright.com/AppDispatchServlet>

3/4

1/6/2019

RightsLink Printable License

- WILEY expressly reserves all rights not specifically granted in the combination of (i) the license details provided by you and accepted in the course of this licensing transaction, (ii) these terms and conditions and (iii) CCC's Billing and Payment terms and conditions.
- This Agreement will be void if the Type of Use, Format, Circulation, or Requestor Type was misrepresented during the licensing process.
- This Agreement shall be governed by and construed in accordance with the laws of the State of New York, USA, without regards to such state's conflict of law rules. Any legal action, suit or proceeding arising out of or relating to these Terms and Conditions or the breach thereof shall be instituted in a court of competent jurisdiction in New York County in the State of New York in the United States of America and each party hereby consents and submits to the personal jurisdiction of such court, waives any objection to venue in such court and consents to service of process by registered or certified mail, return receipt requested, at the last known address of such party.

WILEY OPEN ACCESS TERMS AND CONDITIONS

Wiley Publishes Open Access Articles in fully Open Access Journals and in Subscription journals offering Online Open. Although most of the fully Open Access journals publish open access articles under the terms of the Creative Commons Attribution (CC BY) License only, the subscription journals and a few of the Open Access Journals offer a choice of Creative Commons Licenses. The license type is clearly identified on the article.

The Creative Commons Attribution License

The [Creative Commons Attribution License \(CC-BY\)](#) allows users to copy, distribute and transmit an article, adapt the article and make commercial use of the article. The CC-BY license permits commercial and non-

Creative Commons Attribution Non-Commercial License

The [Creative Commons Attribution Non-Commercial \(CC-BY-NC\) License](#) permits use, distribution and reproduction in any medium, provided the original work is properly cited and is not used for commercial purposes.(see below)

Creative Commons Attribution-Non-Commercial-NoDerivs License

The [Creative Commons Attribution Non-Commercial-NoDerivs License \(CC-BY-NC-ND\)](#) permits use, distribution and reproduction in any medium, provided the original work is properly cited, is not used for commercial purposes and no modifications or adaptations are made. (see below)

Use by commercial "for-profit" organizations

Use of Wiley Open Access articles for commercial, promotional, or marketing purposes requires further explicit permission from Wiley and will be subject to a fee.

Further details can be found on Wiley Online Library
<http://olabout.wiley.com/WileyCDA/Section/id-410895.html>

Other Terms and Conditions:

v1.10 Last updated September 2015

Questions? customercare@copyright.com or +1-855-239-3415 (toll free in the US) or +1-978-646-2777.

S. Shree et al., *ACS Applied Materials & Interfaces* 2017, 9, 38000-38007.

7/1/2019

Rightslink® by Copyright Clearance Center



RightsLink®

Home

Account Info

Help

ACS Publications
Most Trusted. Most Cited. Most Read.

Title: Light, Force, and Heat: A Multi-Stimuli Composite that Reveals its Violent Past

Author: Sindu Shree, Mathias Schulz-Senft, Nils H. Alsleben, et al

Publication: Applied Materials

Publisher: American Chemical Society

Date: Nov 1, 2017

Copyright © 2017, American Chemical Society

Logged in as:

Mathias Schulz

Account #:

3000599298

LOGOUT

Quick Price Estimate

Permission for this particular request is granted for print and electronic formats, and translations, at no charge. Figures and tables may be modified. Appropriate credit should be given. Please print this page for your records and provide a copy to your publisher. Requests for up to 4 figures require only this record. Five or more figures will generate a printout of additional terms and conditions. Appropriate credit should read: "Reprinted with permission from {COMPLETE REFERENCE CITATION}. Copyright {YEAR} American Chemical Society." Insert appropriate information in place of the capitalized words.

I would like to... ?

reuse in a Thesis/Dissertation

Requestor Type ?

Author (original work)

Portion ?

Full article

Format ?

Print and Electronic

Will you be translating? ?

No

Select your currency

EUR - €

Quick Price

Click Quick Price

This service provides permission for reuse only. If you do not have a copy of the article you are using, you may copy and paste the content and reuse according to the terms of your agreement. Please be advised that obtaining the content you license is a separate transaction not involving Rightslink.

QUICK PRICE

CONTINUE

To request permission for a type of use not listed, please contact [the publisher](#) directly.

Copyright © 2019 Copyright Clearance Center, Inc. All Rights Reserved. [Privacy statement](#). [Terms and Conditions](#). Comments? We would like to hear from you. E-mail us at customercare@copyright.com

7/1/2019

Rightslink® by Copyright Clearance Center



RightsLink®

Home

Account
Info

Help

ACS Publications
Most Trusted. Most Cited. Most Read.**Title:** Light, Force, and Heat: A Multi-Stimuli Composite that Reveals its Violent Past**Author:** Sindu Shree, Mathias Schulz-Senft, Nils H. Alsleben, et al**Publication:** Applied Materials**Publisher:** American Chemical Society**Date:** Nov 1, 2017

Copyright © 2017, American Chemical Society

Logged in as:
Mathias Schulz
Account #:
3000599298

LOGOUT

PERMISSION/LICENSE IS GRANTED FOR YOUR ORDER AT NO CHARGE

This type of permission/license, instead of the standard Terms & Conditions, is sent to you because no fee is being charged for your order. Please note the following:

- Permission is granted for your request in both print and electronic formats, and translations.
- If figures and/or tables were requested, they may be adapted or used in part.
- Please print this page for your records and send a copy of it to your publisher/graduate school.
- Appropriate credit for the requested material should be given as follows: "Reprinted (adapted) with permission from (COMPLETE REFERENCE CITATION). Copyright (YEAR) American Chemical Society." Insert appropriate information in place of the capitalized words.
- One-time permission is granted only for the use specified in your request. No additional uses are granted (such as derivative works or other editions). For any other uses, please submit a new request.

BACK

CLOSE WINDOW

Copyright © 2019 Copyright Clearance Center, Inc. All Rights Reserved. [Privacy statement](#). [Terms and Conditions](#).
Comments? We would like to hear from you. E-mail us at customercare@copyright.com

<https://s100.copyright.com/AppDispatchServlet>

1/1

M. Schulz-Senft et al., *Dyes and Pigments* 2017, 136, 292-301.

S. Shree et al., *Materials Horizons* 2019, DOI: 10.1039/c9mh01400d and M. Dowds et al., *Journal of Materials Chemistry C* 2020, DOI: 10.1039.C9TC05193G

12/15/2019

Licences copyright and permissions



ROYAL SOCIETY
OF CHEMISTRY

[Members' area \(http://www.rsc.org/Membership/Memberzone/index.asp\)](http://www.rsc.org/Membership/Memberzone/index.asp) | [Support us \(/support-us/\)](#)

(/)



Journals, books & databases

Licences, copyright & permissions

Information about copyright, our licence to publish and your deposition and sharing rights

When you publish in a Royal Society of Chemistry journal, you keep the copyright of the manuscript. On this page you can learn more about our Licence to Publish and the rights you retain as an author. We also explain where you can deposit and share your article, and how to request permission to re-use other people's work.

The following details apply only to authors accepting the standard Licence to Publish. Authors who are interested in publishing open access should visit our open access pages for more information about our [open access licences \(/journals-books-databases/open-access/open-access-info/#choose\)](#) and deposition rights.

On this page

[About our licence to publish](#)

[\(/journals-books-databases/journal-authors-reviewers/licences-copyright-permissions/#about-licence\)Rights retained by authors](#)

[\(/journals-books-databases/journal-authors-reviewers/licences-copyright-permissions/#author-rights\)Deposition & sharing rights](#)

[\(/journals-books-databases/journal-authors-reviewers/licences-copyright-permissions/#deposition-sharing\)Re-use permission](#)

[requests \(/journals-books-databases/journal-authors-reviewers/licences-copyright-permissions/#reuse-permission-requests\)](#)

About our licence to publish

In order to publish material the Royal Society of Chemistry must acquire the necessary legal rights from the author(s) of that material. In general, we must obtain from the original author(s) the right to publish the material in all formats, in all media (including specifically print and electronic), with the right to sublicense those rights.

For all articles published in our journals, we require the author to accept a 'licence to publish'. This licence is normally requested after their article is accepted for publication. By signing this licence the author (who is either the copyright owner or who is authorised to sign on behalf of the copyright owner, for example his/her employer) grants to the Royal Society of Chemistry "the exclusive right and licence throughout the world to edit, adapt, translate, reproduce and publish the manuscript in all formats, in all media and by all means (whether now existing or in future devised)".

<https://www.rsc.org/journals-books-databases/journal-authors-reviewers/licences-copyright-permissions/#deposition-sharing>

1/7

12/15/2019

Licences copyright and permissions

The Royal Society of Chemistry thus acquires an exclusive licence to publish and all practical rights to the manuscript, except the copyright. The copyright of the manuscript remains with the copyright owner. The copyright owner also retains certain rights regarding the [sharing and deposition](https://www.rsc.org/journals-books-databases/journal-authors-reviewers/licences-copyright-permissions/#deposition-sharing) ([/journals-books-databases/journal-authors-reviewers/licences-copyright-permissions/#deposition-sharing](https://www.rsc.org/journals-books-databases/journal-authors-reviewers/licences-copyright-permissions/#deposition-sharing)), of their article and [the re-use of the published material](https://www.rsc.org/journals-books-databases/journal-authors-reviewers/licences-copyright-permissions/#reuse-permission-requests) ([/journals-books-databases/journal-authors-reviewers/licences-copyright-permissions/#reuse-permission-requests](https://www.rsc.org/journals-books-databases/journal-authors-reviewers/licences-copyright-permissions/#reuse-permission-requests)). For short items in journals (news items, etc) we take a non-exclusive licence in the form of a brief 'terms and conditions for acceptance' document.

What is copyright? +

Assurances

In the licence to publish, the author provides the assurances that we need to publish the material, including assurances that the work is original to the author, that the work has not been published already and that permissions have been obtained if previously published material has been included.

If the manuscript includes material that belongs to someone else (for example, a figure or diagram), we require the author to obtain all permissions that may be needed from third parties. If you wish to reuse material that was not published originally by the Royal Society of Chemistry please see [Re-use permission requests](https://www.rsc.org/journals-books-databases/journal-authors-reviewers/licences-copyright-permissions/#reuse-permission-requests) ([/journals-books-databases/journal-authors-reviewers/licences-copyright-permissions/#reuse-permission-requests](https://www.rsc.org/journals-books-databases/journal-authors-reviewers/licences-copyright-permissions/#reuse-permission-requests)).

Download the [Royal Society of Chemistry licence to publish](https://www.rsc.org/globalassets/05-journals-books-databases/journal-authors-reviewers/licenses-copyright-permissions/royal-society-of-chemistry-licence-to-publish.pdf) ([/globalassets/05-journals-books-databases/journal-authors-reviewers/licenses-copyright-permissions/royal-society-of-chemistry-licence-to-publish.pdf](https://www.rsc.org/globalassets/05-journals-books-databases/journal-authors-reviewers/licenses-copyright-permissions/royal-society-of-chemistry-licence-to-publish.pdf))

Rights retained by authors

When the author accepts the exclusive licence to publish for a journal article, he/she retains certain rights that may be exercised without reference to the Royal Society of Chemistry.

Reproduce/republish portions of the article (including the abstract).

Photocopy the article and distribute such photocopies and distribute copies of the PDF of the article for personal or professional use only (the Royal Society of Chemistry makes this PDF available to the corresponding author of the article upon publication. Any such copies should not be offered for sale. Persons who receive or access the PDF mentioned above must be notified that this may not be made available further or distributed.).

Adapt the article and reproduce adaptations of the article for any purpose other than the commercial exploitation of a work similar to the original.

Reproduce, perform, transmit and otherwise communicate the article to the public in spoken presentations (including those that are accompanied by visual material such as slides, overheads and computer projections).

The author(s) must submit a written request to the Royal Society of Chemistry for any use other than those specified above.

<https://www.rsc.org/journals-books-databases/journal-authors-reviewers/licences-copyright-permissions/#deposition-sharing>

2/7

12/15/2019

Licences copyright and permissions



All cases of republication/reproduction must be accompanied by an **acknowledgement** ([/journals-books-databases/journal-authors-reviewers/licences-copyright-permissions/#reuse-permission-requests](https://journals-books-databases/journal-authors-reviewers/licences-copyright-permissions/#reuse-permission-requests)), of first publication of the work by the Royal Society of Chemistry, the wording of which depends on the journal in which the article was published originally. The acknowledgement should also include a hyperlink to the article on the Royal Society of Chemistry website.

The author also has some rights concerning the deposition of the whole article.

Deposition and sharing rights

The following details apply only to authors accepting the standard licence to publish. Authors who have accepted one of the open access licences to publish, or are thinking of doing so, should refer to the [details for open access deposition rights](https://journals-books-databases/open-access/open-access-info/#choose) ([/journals-books-databases/open-access/open-access-info/#choose](https://journals-books-databases/open-access/open-access-info/#choose)).

When the author accepts the licence to publish for a journal article, he/she retains certain rights concerning the deposition of the whole article. This table summarises how you may distribute the accepted manuscript and version of record of your article.

Sharing rights	Accepted manuscript	Version of record
Share with individuals on request, for personal use	✓	✓
Use for teaching or training materials	✓	✓
Use in submissions of grant applications, or academic requirements such as theses or dissertations	✓	✓
Share with a closed group of research collaborators, for example via an intranet or privately via a scholarly communication network (/journals-books-databases/open-access/green-open-access/#share).	✓	✓
Share publicly via a scholarly communication network that has signed up to STM sharing principles		×
Share publicly via a personal website, institutional repository (/journals-books-databases/open-access/green-open-access/#share) or other not-for-profit repository		×
Share publicly via a scholarly communication network that has not signed up to STM sharing principles	×	×

<https://www.rsc.org/journals-books-databases/journal-authors-reviewers/licences-copyright-permissions/#deposition-sharing>

3/7

⌚ Accepted manuscripts may be distributed via repositories after an embargo period of 12 months

If you are a reader looking for the terms of use for information published by the Royal Society of Chemistry under our standard licence to publish please refer our [terms of use \(journals-books-databases/librarians-information/products-prices/licensing-terms-and-conditions/#non-commercial-terms\)](https://journals-books-databases/librarians-information/products-prices/licensing-terms-and-conditions/#non-commercial-terms).

CHORUS

We are members of the CHORUS initiative, and therefore make the Accepted manuscript version of articles describing research funded by participating funders publicly available on our web site after an embargo period of 12 months. This is effective for research published from 1st March 2018 onwards. Unless otherwise noted on the article the Accepted manuscript is licensed under the terms of our standard license to publish and is subject to our standard [reuse terms \(journals-books-databases/librarians-information/products-prices/licensing-terms-and-conditions/#non-commercial-terms\)](https://journals-books-databases/librarians-information/products-prices/licensing-terms-and-conditions/#non-commercial-terms).

Re-use permission requests

Material published by the Royal Society of Chemistry and other publishers is subject to all applicable copyright, database protection, and other rights. Therefore, for any publication, whether printed or electronic, permission must be obtained to use material for which the author(s) does not already own the copyright. This material may be, for example, a figure, diagram, table, photo or some other image.

Author reusing their own work published by the Royal Society of Chemistry

You do not need to request permission to reuse your own figures, diagrams, etc, that were originally published in a Royal Society of Chemistry publication. However, permission should be requested for use of the whole article or chapter except if reusing it in a thesis. If you are including an article or book chapter published by us in your thesis please ensure that your co-authors are aware of this.

Reuse of material that was published originally by the Royal Society of Chemistry must be accompanied by the appropriate acknowledgement of the publication. The form of the acknowledgement is dependent on the journal in which it was published originally, as detailed in 'Acknowledgements'.

Material published by the Royal Society of Chemistry to be used in another of our publications

Authors contributing to our publications (journal articles, book or book chapters) do not need to formally request permission to reproduce material contained in another Royal Society of Chemistry publication. However, permission should be requested for use of a whole article or chapter. For all cases of reproduction the correct

12/15/2019

Licences copyright and permissions

acknowledgement of the reproduced material should be given. The form of the acknowledgement is dependent on the journal in which it was published originally, as detailed in the 'Acknowledgements' section.

Acknowledgements +

Using third party material in Royal Society of Chemistry publications

We must ensure that the material we publish does not infringe the copyright of others. We require the author(s) to obtain, at the earliest opportunity, the relevant permissions that might be needed from third parties to include material that belongs to someone else.

Please contact the publisher/copyright owner of the third party material to check how they wish to receive permission requests. Please plan to submit your request well ahead of publication of your material.

The most common procedures for permission requests are outlined below.

- A number of publishers have opted out of receiving express permissions as long as they fall under the rules of the [STM Permission Guidelines](http://www.stm-assoc.org/copyright-legal-affairs/permissions/permissions-guidelines) (<http://www.stm-assoc.org/copyright-legal-affairs/permissions/permissions-guidelines>).
- If they do not fall into the category above, the majority of publishers now use RightsLink from the Copyright Clearance Center (CCC) to process their requests.
- Other publishers have their own permission request forms and/or specify what information they need to process any permission request.
- If the publisher/copyright owner does not have a specific procedure please complete and submit the '[permission request form for non-RSC material](#)' ([./globalassets/05-journals-books-databases/journal-authors-reviewers/licences-copyright-permissions/ag-gc-permission-request-form-for-non-rsc-material.pdf](#)) form. Send the form to the permission administrator or editor of the relevant publication.
- If the copyright owner has opted to publish under a Creative Commons licence, licensees are required to obtain permission to do any of the things with a work that the law reserves exclusively to a licensor and that the licence does not expressly allow. Licensees must credit the licensor, keep copyright notices intact on all copies of the work, and link to the license from copies of the work.

In all cases the following rights need to be obtained.

Permission is required to include the specified material in the work described and in all subsequent editions of the work to be published by the Royal Society of Chemistry for distribution throughout the world, in all media including electronic and microfilm and to use the material in conjunction with computer-based electronic and information retrieval systems, to grant permissions for photocopying, reproductions and reprints, to translate the material and to publish the translation, and to authorise document delivery and abstracting and indexing services.

Please note that the Royal Society of Chemistry is also a signatory to the STM Permission Guidelines.

Using material published by the Royal Society of Chemistry in material for another publisher

If you require permission to use material from one of our publications or website in a publication not owned by us, and you are not the author of our publication, the following procedures should be followed.

Before sending in any request you should check that the material you wish to reproduce is not credited to a source other than the Royal Society of Chemistry. The credit for an image will be given in the caption of the image or sometimes in the list of references.

Please plan to submit your request well ahead of publication of your material. Please note that we are unable to supply artwork for the material you may wish to reproduce.

Reproducing material from a Royal Society of Chemistry journal

To request permission to reproduce material from a Royal Society of Chemistry journal please go to the Copyright Clearance Center. Please note that for open access articles published under a CC-BY licence no formal permission is needed as long as the reproduction includes a full acknowledgement to the Royal Society of Chemistry article. For open access articles published under a CC BY-NC article formal permission is needed to reproduce the material commercially, including but not limited to, all publishers.

How to use the Copyright
Clearance Center +

Reproducing material from other Royal Society of Chemistry publications

If you are reproducing material from a Royal Society of Chemistry book, education or science policy publication or a Royal Society of Chemistry website you must [complete and submit the online permission request form](http://www.rsc.org/publishing/Copyright/permissionform.cfm) (<http://www.rsc.org/publishing/Copyright/permissionform.cfm>) (or the [PDF version of the permission request form for Royal Society of Chemistry material](https://globalassets/05-journals-books-databases/journal-authors-reviewers/licences-copyright-permissions/ag-gc-permission-request-form-for-rsc-material.pdf) ([/globalassets/05-journals-books-databases/journal-authors-reviewers/licences-copyright-permissions/ag-gc-permission-request-form-for-rsc-material.pdf](https://globalassets/05-journals-books-databases/journal-authors-reviewers/licences-copyright-permissions/ag-gc-permission-request-form-for-rsc-material.pdf))).

Requests are usually for use of a figure or diagram, but they may also be for use of the entire article or chapter. Requests to use individual figures or diagrams are invariably granted. Permission for another publisher to print an entire Royal Society of Chemistry article or chapter may be granted in special circumstances.

The permission form should only be used to request permission to reproduce material from Royal Society of Chemistry books, *Chemistry World*, *Education in Chemistry*, and other non-journal publications of the Royal Society of Chemistry. For these requests please complete and send the form to our publishing services team.

12/15/2019

Licences copyright and permissions

Contact our Contracts & Copyright Executive

Email: [Send us an email](#)

Customer Services team

For general publishing and open access enquiries.

Office open: 9am - 5pm Mon-Fri

Tel: +44 (0) 1223 432176

Email: [Send us an email](#)

Share

Advertisement

Not a member?

[Apply for membership \(/membership-and-community/join/\)](#)



[f \(/journals-books- /membership-](#)

[Help \(/help-legal/help/\)](#) | [Advertise \(/advertise/\)](#) | [Legal \(/help-legal/legal/\)](#) |

[Privacy \(/help-legal/legal/privacy/\)](#) | [Accessibility \(/help-legal/legal/accessibility/\)](#)

© Royal Society of Chemistry 2019. Registered charity number 207890.

M. Schulz-Senft et al., *Dyes and Pigments* 2017, 136, 292-301.



SEARCH CART MENU





Personal use

Authors can use their articles, in full or in part, for a wide range of scholarly, non-commercial purposes as outlined below:

- Use by an author in the author’s classroom teaching (including distribution of copies, paper or electronic)
- Distribution of copies (including through e-mail) to known research colleagues for their personal use (but not for Commercial Use)
- Inclusion in a thesis or dissertation (provided that this is not to be published commercially)
- Use in a subsequent compilation of the author’s works
- Extending the Article to book-length form
- Preparation of other derivative works (but not for Commercial Use)
- Otherwise using or re-using portions or excerpts in other works

These rights apply for all Elsevier authors who publish their article as either a subscription article or an open access article. In all cases we require that all Elsevier authors always include a full acknowledgement and, if appropriate, a link to the final published version hosted on Science Direct.

Solutions	▼
Solutions	
Researchers	▼
Researchers	
About Elsevier	▼
About Elsevier	
How can we help?	▼
How can we help?	

    [Select location/language](#)

 [Global - English \(/location-selector\)](#)



<https://www.elsevier.com>

ELSEVIER

Copyright © 2019 Elsevier, except certain content provided by third parties

Cookies are used by this site. To decline or learn more, visit our [Cookies \(/legal/use-of-cookies\)](https://www.elsevier.com/legal/use-of-cookies) page.


[Terms and Conditions \(/legal/elsevier-website-terms-and-conditions\)](https://www.elsevier.com/legal/elsevier-website-terms-and-conditions) [Privacy Policy](#)

[\(/legal/privacy-policy\)](https://www.elsevier.com/legal/privacy-policy) [Sitemap \(/sitemap\)](https://www.elsevier.com/sitemap)



<https://www.elsevier.com>  **RELX Group™** (<https://www.relx.com/>)

ELSEVIER

 **RELX Group™** (<https://www.relx.com/>)

L.-Y. He et al., *European Journal of Organic Chemistry*
2015, 2498-2502.

1/6/2019

RightsLink Printable License

**JOHN WILEY AND SONS LICENSE
TERMS AND CONDITIONS**

Jan 06, 2019

This Agreement between Mathias Schulz ("You") and John Wiley and Sons ("John Wiley and Sons") consists of your license details and the terms and conditions provided by John Wiley and Sons and Copyright Clearance Center.

License Number	4503220586031
License date	Jan 06, 2019
Licensed Content Publisher	John Wiley and Sons
Licensed Content Publication	European Journal of Organic Chemistry
Licensed Content Title	Nucleophile-Selective Cross-Coupling Reactions with Vinyl and Alkynyl Bromides on a Dinucleophilic Aromatic Substrate
Licensed Content Author	Lu-Ying He, Mathias Schulz-Senft, Birk Thiedemann, et al
Licensed Content Date	Feb 27, 2015
Licensed Content Volume	2015
Licensed Content Issue	11
Licensed Content Pages	5
Type of use	Dissertation/Thesis
Requestor type	Author of this Wiley article
Format	Print and electronic
Portion	Full article
Will you be translating?	No
Title of your thesis / dissertation	Synthesis of Light Responsible Polymer Materials
Expected completion date	Mar 2019
Expected size (number of pages)	300
Requestor Location	Mathias Schulz Otto-Hahn-Platz 4 Kiel, 24098 Germany Attn: Mathias Schulz
Publisher Tax ID	EU826007151
Total	0.00 EUR

Terms and Conditions

TERMS AND CONDITIONS

This copyrighted material is owned by or exclusively licensed to John Wiley & Sons, Inc. or one of its group companies (each a "Wiley Company") or handled on behalf of a society with which a Wiley Company has exclusive publishing rights in relation to a particular work (collectively "WILEY"). By clicking "accept" in connection with completing this licensing transaction, you agree that the following terms and conditions apply to this transaction (along with the billing and payment terms and conditions established by the Copyright Clearance Center Inc., ("CCC's Billing and Payment terms and conditions"), at the time that you opened your RightsLink account (these are available at any time at <http://myaccount.copyright.com>).

<https://s100.copyright.com/AppDispatchServlet>

1/4

Terms and Conditions

- The materials you have requested permission to reproduce or reuse (the "Wiley Materials") are protected by copyright.
- You are hereby granted a personal, non-exclusive, non-sub licensable (on a stand-alone basis), non-transferable, worldwide, limited license to reproduce the Wiley Materials for the purpose specified in the licensing process. This license, **and any CONTENT (PDF or image file) purchased as part of your order**, is for a one-time use only and limited to any maximum distribution number specified in the license. The first instance of republication or reuse granted by this license must be completed within two years of the date of the grant of this license (although copies prepared before the end date may be distributed thereafter). The Wiley Materials shall not be used in any other manner or for any other purpose, beyond what is granted in the license. Permission is granted subject to an appropriate acknowledgement given to the author, title of the material/book/journal and the publisher. You shall also duplicate the copyright notice that appears in the Wiley publication in your use of the Wiley Material. Permission is also granted on the understanding that nowhere in the text is a previously published source acknowledged for all or part of this Wiley Material. Any third party content is expressly excluded from this permission.
- With respect to the Wiley Materials, all rights are reserved. Except as expressly granted by the terms of the license, no part of the Wiley Materials may be copied, modified, adapted (except for minor reformatting required by the new Publication), translated, reproduced, transferred or distributed, in any form or by any means, and no derivative works may be made based on the Wiley Materials without the prior permission of the respective copyright owner. **For STM Signatory Publishers clearing permission under the terms of the STM Permissions Guidelines only, the terms of the license are extended to include subsequent editions and for editions in other languages, provided such editions are for the work as a whole in situ and does not involve the separate exploitation of the permitted figures or extracts**, You may not alter, remove or suppress in any manner any copyright, trademark or other notices displayed by the Wiley Materials. You may not license, rent, sell, loan, lease, pledge, offer as security, transfer or assign the Wiley Materials on a stand-alone basis, or any of the rights granted to you hereunder to any other person.
- The Wiley Materials and all of the intellectual property rights therein shall at all times remain the exclusive property of John Wiley & Sons Inc, the Wiley Companies, or their respective licensors, and your interest therein is only that of having possession of and the right to reproduce the Wiley Materials pursuant to Section 2 herein during the continuance of this Agreement. You agree that you own no right, title or interest in or to the Wiley Materials or any of the intellectual property rights therein. You shall have no rights hereunder other than the license as provided for above in Section 2. No right, license or interest to any trademark, trade name, service mark or other branding ("Marks") of WILEY or its licensors is granted hereunder, and you agree that you shall not assert any such right, license or interest with respect thereto
- NEITHER WILEY NOR ITS LICENSORS MAKES ANY WARRANTY OR REPRESENTATION OF ANY KIND TO YOU OR ANY THIRD PARTY, EXPRESS, IMPLIED OR STATUTORY, WITH RESPECT TO THE MATERIALS OR THE ACCURACY OF ANY INFORMATION CONTAINED IN THE MATERIALS, INCLUDING, WITHOUT LIMITATION, ANY IMPLIED WARRANTY OF MERCHANTABILITY, ACCURACY, SATISFACTORY QUALITY, FITNESS FOR A PARTICULAR PURPOSE, USABILITY, INTEGRATION OR NON-INFRINGEMENT AND ALL SUCH WARRANTIES ARE HEREBY EXCLUDED BY WILEY AND ITS LICENSORS AND WAIVED

1/6/2019

RightsLink Printable License

BY YOU.

- WILEY shall have the right to terminate this Agreement immediately upon breach of this Agreement by you.
- You shall indemnify, defend and hold harmless WILEY, its Licensors and their respective directors, officers, agents and employees, from and against any actual or threatened claims, demands, causes of action or proceedings arising from any breach of this Agreement by you.
- IN NO EVENT SHALL WILEY OR ITS LICENSORS BE LIABLE TO YOU OR ANY OTHER PARTY OR ANY OTHER PERSON OR ENTITY FOR ANY SPECIAL, CONSEQUENTIAL, INCIDENTAL, INDIRECT, EXEMPLARY OR PUNITIVE DAMAGES, HOWEVER CAUSED, ARISING OUT OF OR IN CONNECTION WITH THE DOWNLOADING, PROVISIONING, VIEWING OR USE OF THE MATERIALS REGARDLESS OF THE FORM OF ACTION, WHETHER FOR BREACH OF CONTRACT, BREACH OF WARRANTY, TORT, NEGLIGENCE, INFRINGEMENT OR OTHERWISE (INCLUDING, WITHOUT LIMITATION, DAMAGES BASED ON LOSS OF PROFITS, DATA, FILES, USE, BUSINESS OPPORTUNITY OR CLAIMS OF THIRD PARTIES), AND WHETHER OR NOT THE PARTY HAS BEEN ADVISED OF THE POSSIBILITY OF SUCH DAMAGES. THIS LIMITATION SHALL APPLY NOTWITHSTANDING ANY FAILURE OF ESSENTIAL PURPOSE OF ANY LIMITED REMEDY PROVIDED HEREIN.
- Should any provision of this Agreement be held by a court of competent jurisdiction to be illegal, invalid, or unenforceable, that provision shall be deemed amended to achieve as nearly as possible the same economic effect as the original provision, and the legality, validity and enforceability of the remaining provisions of this Agreement shall not be affected or impaired thereby.
- The failure of either party to enforce any term or condition of this Agreement shall not constitute a waiver of either party's right to enforce each and every term and condition of this Agreement. No breach under this agreement shall be deemed waived or excused by either party unless such waiver or consent is in writing signed by the party granting such waiver or consent. The waiver by or consent of a party to a breach of any provision of this Agreement shall not operate or be construed as a waiver of or consent to any other or subsequent breach by such other party.
- This Agreement may not be assigned (including by operation of law or otherwise) by you without WILEY's prior written consent.
- Any fee required for this permission shall be non-refundable after thirty (30) days from receipt by the CCC.
- These terms and conditions together with CCC's Billing and Payment terms and conditions (which are incorporated herein) form the entire agreement between you and WILEY concerning this licensing transaction and (in the absence of fraud) supersedes all prior agreements and representations of the parties, oral or written. This Agreement may not be amended except in writing signed by both parties. This Agreement shall be binding upon and inure to the benefit of the parties' successors, legal representatives, and authorized assigns.
- In the event of any conflict between your obligations established by these terms and conditions and those established by CCC's Billing and Payment terms and conditions, these terms and conditions shall prevail.

<https://s100.copyright.com/AppDispatchServlet>

3/4

1/6/2019

RightsLink Printable License

- WILEY expressly reserves all rights not specifically granted in the combination of (i) the license details provided by you and accepted in the course of this licensing transaction, (ii) these terms and conditions and (iii) CCC's Billing and Payment terms and conditions.
- This Agreement will be void if the Type of Use, Format, Circulation, or Requestor Type was misrepresented during the licensing process.
- This Agreement shall be governed by and construed in accordance with the laws of the State of New York, USA, without regards to such state's conflict of law rules. Any legal action, suit or proceeding arising out of or relating to these Terms and Conditions or the breach thereof shall be instituted in a court of competent jurisdiction in New York County in the State of New York in the United States of America and each party hereby consents and submits to the personal jurisdiction of such court, waives any objection to venue in such court and consents to service of process by registered or certified mail, return receipt requested, at the last known address of such party.

WILEY OPEN ACCESS TERMS AND CONDITIONS

Wiley Publishes Open Access Articles in fully Open Access Journals and in Subscription journals offering Online Open. Although most of the fully Open Access journals publish open access articles under the terms of the Creative Commons Attribution (CC BY) License only, the subscription journals and a few of the Open Access Journals offer a choice of Creative Commons Licenses. The license type is clearly identified on the article.

The Creative Commons Attribution License

The [Creative Commons Attribution License \(CC-BY\)](#) allows users to copy, distribute and transmit an article, adapt the article and make commercial use of the article. The CC-BY license permits commercial and non-

Creative Commons Attribution Non-Commercial License

The [Creative Commons Attribution Non-Commercial \(CC-BY-NC\) License](#) permits use, distribution and reproduction in any medium, provided the original work is properly cited and is not used for commercial purposes.(see below)

Creative Commons Attribution-Non-Commercial-NoDerivs License

The [Creative Commons Attribution Non-Commercial-NoDerivs License \(CC-BY-NC-ND\)](#) permits use, distribution and reproduction in any medium, provided the original work is properly cited, is not used for commercial purposes and no modifications or adaptations are made. (see below)

Use by commercial "for-profit" organizations

Use of Wiley Open Access articles for commercial, promotional, or marketing purposes requires further explicit permission from Wiley and will be subject to a fee.

Further details can be found on Wiley Online Library
<http://olabout.wiley.com/WileyCDA/Section/id-410895.html>

Other Terms and Conditions:

v1.10 Last updated September 2015

Questions? customercare@copyright.com or +1-855-239-3415 (toll free in the US) or +1-978-646-2777.

Bibliography

- [1] M. P. Johnson, *Essays Biochem.* **2016**, *60*, 255–273.
- [2] K.-W. Yau, R. C. Hardie, *Cell* **2009**, *139*, 246–264.
- [3] *Molecular Switches*, 2nd, (Eds.: B. L. Feringa, W. R. Browne), Wiley-VCH, Weinheim, Germany, **2011**.
- [4] J.-P. Launay, C. Coudret, C. Joachim in *Dekker Encyclopedia of Nanoscience and Nanotechnology, Third Edition*, CRC Press, **2014**, pp. 2723–2735.
- [5] B. L. Feringa, *Angew. Chem. Int. Ed.* **2018**, *56*, 11060–11078.
- [6] O. P. Ernst, D. T. Lodowski, M. Elstner, P. Hegemann, L. S. Brown, H. Kandori, *Chem. Rev.* **2014**, *114*, 126–163.
- [7] P. S.-H. Park in *Advances in Pharmacology, Vol. 70*, Elsevier, Oxford, **2014**, pp. 1–36.
- [8] Z. L. Pianowski, *Chem. - Eur. J.* **2019**, *25*, 5128–5144.
- [9] L. Dong, Y. Feng, L. Wang, W. Feng, *Chem. Soc. Rev.* **2018**, *47*, 7339–7368.
- [10] E. Merino, *Chem. Soc. Rev.* **2011**, *40*, 3835–3853.
- [11] H. M. D. Bandara, S. C. Burdette, *Chem. Soc. Rev.* **2012**, *41*, 1809–1825.
- [12] R. Klajn, *Chem. Soc. Rev.* **2014**, *43*, 148–184.
- [13] *Photomechanical Materials, Composites, and Systems*, (Ed.: T. J. White), John Wiley & Sons, Inc., Hoboken, **2017**.
- [14] M. Li, Q. Zhang, Y.-N. Zhou, S. Zhu, *Prog. Polym. Sci.* **2018**, *79*, 26–39.
- [15] H. Staudinger, *Ber. Dtsch. Chem. Ges. B* **1926**, *59*, 3019–3043.
- [16] S. Koltzenburg, M. Maskos, O. Nuyken, *Polymer Chemistry*, Springer-Verlag, Berlin Heidelberg, **2017**.
- [17] G. Odian, *Principles of Polymerization*, 4th ed., John Wiley & Sons, Inc., Hoboken, **2004**.
- [18] K. Matyjaszewski, T. P. Davis, *Handbook of Radical Polymerization*, John Wiley & Sons, Inc., Hoboken, **2002**.
- [19] F. Ciardelli, G. Ruggeri, A. Pucci, *Chem. Soc. Rev.* **2013**, *42*, 857.
- [20] P. Weis, W. Tian, S. Wu, *Chem. - Eur. J.* **2018**, *24*, 6494–6505.
- [21] M. M. Caruso, D. A. Davis, Q. Shen, S. A. Odom, N. R. Sottos, S. R. White, J. S. Moore, *Chem. Rev.* **2009**, *109*, 5755–5798.

- [22] P. Dopieralski, P. Anjukandi, M. Rückert, M. Shiga, J. Ribas–Arino, D. Marx, *J. Mater. Chem.* **2011**, *21*, 8309.
- [23] J. N. Brantley, K. M. Wiggins, C. W. Bielawski, *Polym. Int.* **2013**, *62*, 2–12.
- [24] Y. Li, H. Zhang, C. Qi, X. Guo, *J. Mater. Chem.* **2012**, *22*, 4261.
- [25] Y. Yu, M. Nakano, T. Ikeda, *Nature* **2003**, *425*, 145–145.
- [26] P. Karageorgiev, D. Neher, B. Schulz, B. Stiller, U. Pietsch, M. Giersig, L. Brehmer, *Nat Mater* **2005**, *4*, 699–703.
- [27] D. Habault, H. Zhang, Y. Zhao, *Chem. Soc. Rev.* **2013**, *42*, 7244–7256.
- [28] S. L. Potisek, D. A. Davis, N. R. Sottos, S. R. White, J. S. Moore, *J. Am. Chem. Soc.* **2007**, *129*, 13808–13809.
- [29] D. A. Davis, A. Hamilton, J. Yang, L. D. Cremer, D. Van Gough, S. L. Potisek, M. T. Ong, P. V. Braun, T. J. Martínez, S. R. White, J. S. Moore, N. R. Sottos, *Nature* **2009**, *459*, 68–72.
- [30] W. Qiu, P. A. Gurr, G. G. Qiao, *ACS Appl. Mater. Interfaces* **2019**, *11*, 29268–29275.
- [31] M. Schulz-Senft, M. Lipfert, A. Staubitz, *Chem. Unserer Zeit* **2014**, *48*, 200–214.
- [32] V. Vasiliev, E. Morozov, *Mechanics and Analysis of Composite Materials*, Elsevier, Oxford, **2001**.
- [33] T. Sathishkumar, S. Satheeshkumar, J. Naveen, *J. Reinf. Plast. Compos.* **2014**, *33*, 1258–1275.
- [34] L. Tong, A. P. Mouritz, M. K. Bannister, *3D Fibre Reinforced Polymer Composites*, Elsevier, Oxford, **2002**.
- [35] R. P. L. Nijssen, *Composite Materials*, VKCN, Marknesse, **2015**.
- [36] J. N. Coleman, U. Khan, W. J. Blau, Y. K. Gun'ko, *Carbon* **2006**, *44*, 1624–1652.
- [37] *Dental Composite Materials for Direct Restorations*, (Ed.: V. Miletic), Springer Nature, Cham, Switzerland, **2018**.
- [38] *Polymer Composites: Macro- and Microcomposites, Vol. 1*, (Eds.: S. Thomas, J. Kuruvilla, S. K. Malhotra, K. Goda, M. S. Sreekala), Wiley-VCH, Weinheim, **2012**.
- [39] *Polymer Composites: Nanocomposites, Vol. 2*, (Eds.: S. Thomas, J. Kuruvilla, S. K. Malhotra, K. Goda, M. S. Sreekala), Wiley-VCH, Weinheim, **2012**.
- [40] *Polymer Composites: Biocomposites, Vol. 3*, (Eds.: S. Thomas, J. Kuruvilla, S. K. Malhotra, K. Goda, M. S. Sreekala), Wiley-VCH, Weinheim, **2014**.
- [41] F. Ahmad, H. S. Choi, M. K. Park, *Macromol. Mater. Eng.* **2015**, *300*, 10–24.
- [42] K.-t. Lau, P.-y. Hung, M.-H. Zhu, D. Hui, *Composites Part B* **2018**, *136*, 222–233.
- [43] *Sustainable Polymer Composites and Nanocomposites*, (Eds.: Inamuddin, S. Thomas, R. Kumar Mishra, A. M. Asiri), Springer Nature, Cham, Switzerland, **2019**.

- [44] H. Shirakawa, E. J. Louis, A. G. MacDiarmid, A. J. Heeger, *J. Chem. Soc. Chem. Commun.* **1977**, 578–580.
- [45] H. Shirakawa, *Angew. Chem. Int. Ed.* **2001**, *40*, 2574–2580.
- [46] A. G. MacDiarmid, *Angew. Chem. Int. Ed.* **2001**, *40*, 2581–2590.
- [47] A. J. Heeger, *Angew. Chem. Int. Ed.* **2001**, *40*, 2591–2611.
- [48] A. Köhler, H. Bässler, *Electronic Processes in Organic Semiconductors: An Introduction*, Wiley-VCH, Weinheim, **2015**.
- [49] H. Bässler, A. Köhler in *Unimolecular and Supramolecular Electronics I, Vol. 312*, (Ed.: R. M. Metzger), Springer Berlin Heidelberg, Berlin, Heidelberg, **2011**, pp. 1–65.
- [50] S. Holliday, J. E. Donaghey, I. McCulloch, *Chem. Mater.* **2014**, *26*, 647–663.
- [51] *Conjugated Polymers*, (Eds.: K. Müllen, J. R. Reynolds, T. Masuda), Royal Society of Chemistry, Cambridge, **2014**.
- [52] C. Castiglioni, G. Zerbi, M. Gussoni, *Solid State Commun.* **1985**, *56*, 863–866.
- [53] J. C. S. Costa, R. J. S. Taveira, C. F. R. A. C. Lima, A. Mendes, L. M. N. B. F. Santos, *Opt. Mater.* **2016**, *58*, 51–60.
- [54] F. Yang, Y. Zhang, Y. Hao, Y. Cui, W. Wang, T. Ji, F. Shi, B. Wei, *Appl. Opt.* **2015**, *54*, 10232.
- [55] S. Berny, N. Blouin, A. Distler, H.-J. Egelhaaf, M. Krompiec, A. Lohr, O. R. Lozman, G. E. Morse, L. Nanson, A. Pron, T. Sauermann, N. Seidler, S. Tierney, P. Tiwana, M. Wagner, H. Wilson, *Adv. Sci.* **2016**, *3*, 1500342.
- [56] D. Li, W.-Y. Lai, Y.-Z. Zhang, W. Huang, *Adv. Mater.* **2018**, *30*, 1704738.
- [57] L. Torsi, M. Magliulo, K. Manoli, G. Palazzo, *Chem. Soc. Rev.* **2013**, *42*, 8612.
- [58] *Organic Electronics: Structural and Electronic Properties of OFETs*, (Ed.: C. Wöll), Wiley-VCH, Weinheim, **2009**.
- [59] T. P. Kaloni, P. K. Giesbrecht, G. Schreckenbach, M. S. Freund, *Chem. Mater.* **2017**, *29*, 10248–10283.
- [60] E. Zeglio, O. Inganäs, *Adv. Mater.* **2018**, *30*, 1800941.
- [61] H. Li, W. Shi, J. Song, H.-J. Jang, J. Dailey, J. Yu, H. E. Katz, *Chem. Rev.* **2019**, *119*, 3–35.
- [62] C. Zhao, Y. Guo, Y. Zhang, N. Yan, S. You, W. Li, *J. Mater. Chem. A* **2019**, *7*, 10174–10199.
- [63] L. Zhang, N. S. Colella, B. P. Cherniawski, S. C. B. Mannsfeld, A. L. Briseno, *ACS Appl. Mater. Interfaces* **2014**, *6*, 5327–5343.
- [64] T. P. Kaloni, G. Schreckenbach, M. S. Freund, *J. Phys. Chem. C* **2015**, *119*, 3979–3989.

- [65] S. S. Zade, M. Bendikov, *Chem. - Eur. J.* **2007**, *13*, 3688–3700.
- [66] G. Horowitz, B. Bachet, A. Yassar, P. Lang, F. Demanze, J.-L. Fave, F. Garnier, *Chem. Mater.* **1995**, *7*, 1337–1341.
- [67] A. Marrocchi, D. Lanari, A. Facchetti, L. Vaccaro, *Energy Environ. Sci.* **2012**, *5*, 8457–8474.
- [68] K. Tremel, S. Ludwigs, *Adv. Polym. Sci.* **2014**, *265*, 39–82.
- [69] T. V. Richter, C. H. Braun, S. Link, M. Scheuble, E. J. W. Crossland, F. Stelzl, U. Würfel, S. Ludwigs, *Macromolecules* **2012**, *45*, 5782–5788.
- [70] *P3HT Revisited - from Molecular Scale to Solar Cell Devices*, (Ed.: S. Ludwigs), Springer-Verlag, Berlin Heidelberg, **2014**.
- [71] K. Wagner, M. Zanoni, A. B. S. Elliott, P. Wagner, R. Byrne, L. E. Florea, D. Diamond, K. C. Gordon, G. G. Wallace, D. L. Officer, *J. Mater. Chem. C* **2013**, *1*, 3913.
- [72] A. Yokoyama, R. Miyakoshi, T. Yokozawa, *Macromolecules* **2004**, *37*, 1169–1171.
- [73] E. E. Sheina, J. Liu, M. C. Iovu, D. W. Laird, R. D. McCullough, *Macromolecules* **2004**, *37*, 3526–3528.
- [74] A. Iraqi, G. W. Barker, *J. Mater. Chem.* **1998**, *8*, 25–29.
- [75] I. A. Liversedge, S. J. Higgins, M. Giles, M. Heaney, I. McCulloch, *Tetrahedron Letters* **2006**, *47*, 5143–5146.
- [76] D. Haynes, R. McCulloch in *Conjugated Polymers*, (Eds.: K. Müllen, J. R. Reynolds, T. Masuda), RSC Polymer Chemistry 9, Royal Society of Chemistry, Cambridge, **2014**, pp. 180–200.
- [77] R. Miyakoshi, A. Yokoyama, T. Yokozawa, *J. Am. Chem. Soc.* **2005**, *127*, 17542–17547.
- [78] R. H. Lohwasser, M. Thelakkat, *Macromolecules* **2010**, *43*, 7611–7616.
- [79] R. H. Lohwasser, M. Thelakkat, *Macromolecules* **2011**, *44*, 3388–3397.
- [80] K.-H. Kaesler in *High-Performance Organic Coatings*, (Ed.: A. S. Khanna), Woodhead Publishing Series in Metals and Surface Engineering, Woodhead Publishing, **2008**, pp. 225–246.
- [81] G. Barroso, Q. Li, R. K. Bordia, G. Motz, *J. Mater. Chem. A* **2019**, *7*, 1936–1963.
- [82] J. K. Fink, *Liquid Silicone Rubber*, John Wiley & Sons, Inc., Hoboken, **2019**.
- [83] R. M. Minas'yan, *Polym. Sci. Ser. D* **2011**, *4*, 206–208.
- [84] C. Appiah, C. Arndt, K. Siemsen, A. Heitmann, A. Staubitz, C. Selhuber-Unkel, *Adv. Mater.* **2019**, *0*, 1807747.
- [85] J. Brandrup, E. H. Immergut, E. A. Grulke, *Polymer Handbook*, 4., John Wiley & Sons, New York, **1999**.

- [86] M. Rehahn, W. L. Mattice, U. W. Suter, *Rotational Isomeric State Models in Macromolecular Systems*, Springer Berlin Heidelberg, **1997**.
- [87] L. Goodman, V. Pophristic, *Chem. Phys. Lett.* **1996**, *259*, 287–295.
- [88] B. C. Cope, D. E. Packham, G. Leggett, J. C. Beech, G. B. Lowe, D. Briggs, D. M. Brewis, A. D. Crocombe, D. G. Dixon, W. J. Van Ooij, B. Parbhoo, C. M. Warwick, J. Pritchard, S. Millington, C. Chatfield, J. Comyn, D. A. Dillard, B. Kneafsey, M. E. R. Shanahan, A. V. Pocius in *Handbook of Adhesion*, (Ed.: D. E. Packham), John Wiley & Sons, Ltd, Chichester, **2005**, pp. 439–525.
- [89] W. Noll, *Chemistry and Technology of Silicones*, Academic Press, New York, **1968**.
- [90] R. Schliebs, J. Ackermann, *Chem. Unserer Zeit* **1987**, *21*, 121–127.
- [91] J. Ackermann, V. Damrath, *Chem. Unserer Zeit* **1989**, *23*, 86–99.
- [92] R. Zhang, J. E. Mark, A. R. Pinhas, *Macromolecules* **2000**, *33*, 3508–3510.
- [93] M. Cypryk, Y. Apeloig, *Organometallics* **2002**, *21*, 2165–2175.
- [94] M. Jeon, J. Han, J. Park, *ACS Catal.* **2012**, *2*, 1539–1549.
- [95] Q. Wang, H. Zhang, G. K. S. Prakash, T. E. Hogen-Esch, G. A. Olah, *Macromolecules* **1996**, *29*, 6691–6694.
- [96] B. Yactine, A. Ratsimihety, F. Ganachaud, *Polym. Adv. Technol.* **2010**, *21*, 139–149.
- [97] P. R. Dvornic in *Silicon-Containing Polymers: The Science and Technology of Their Synthesis and Applications*, (Eds.: R. G. Jones, W. Ando, J. Chojnowski), Springer Netherlands, Dordrecht, **2000**, pp. 185–212.
- [98] C. U. Pittman, W. J. Patterson, S. P. McManus, *J. Polym. Sci. Polym. Chem. Ed.* **1976**, *14*, 1715–1734.
- [99] M. J. Owen, P. R. Dvornic in *Polymer Data Handbook*, (Ed.: J. E. Mark), Oxford University Press, Oxford, **1999**, pp. 821–825.
- [100] *Polymer Data Handbook*, (Ed.: J. E. Mark), Oxford University Press, Oxford, **1999**.
- [101] M. A. Gauthier, M. I. Gibson, H.-A. Klok, *Angew. Chem. Int. Ed.* **2009**, *48*, 48–58.
- [102] S. J. Dünki, E. Cuervo-Reyes, D. M. Opris, *Polym. Chem.* **2017**, *8*, 715–724.
- [103] G. Agrawal, J. Wang, B. Brüster, X. Zhu, M. Möller, A. Pich, *Soft Matter* **2013**, *9*, 5380.
- [104] L. Yang, K. Cao, Y. Huang, G. Chang, F. Zhu, J. Yang, *High Perform. Polym.* **2014**, *26*, 463–469.
- [105] M. Bowkett, K. Thanapalan, *Syst. Sci. Control Eng.* **2017**, *5*, 168–177.
- [106] M. Bowkett, K. Thanapalan in *Failure Analysis and Prevention*, (Ed.: A. Ali), InTech, **2017**.
- [107] C. J. Brown, *Acta Crystallogr.* **1966**, *21*, 146–152.

- [108] A. Mostad, C. Rømming, *Acta Chem. Scand.* **1971**, *25*, 3561–3568.
- [109] R. Turanský, M. Konôpka, N. L. Doltsinis, I. Štich, D. Marx, *ChemPhysChem* **2010**, *11*, 345–348.
- [110] R. Turanský, M. Konôpka, N. L. Doltsinis, I. Štich, D. Marx, *Phys. Chem. Chem. Phys.* **2010**, *12*, 13922.
- [111] S. K. Surampudi, H. R. Patel, G. Nagarjuna, D. Venkataraman, *Chem. Commun.* **2013**, *49*, 7519–7521.
- [112] S. Venkataramani, U. Jana, M. Dommaschk, F. D. Sönnichsen, F. Tuczek, R. Herges, *Science* **2011**, *331*, 445–448.
- [113] E. Kizilkan, J. Strueben, A. Staubitz, S. N. Gorb, *Sci. Robot.* **2017**, *2*, eaak9454.
- [114] J. Strueben, PhD thesis, Christian-Albrechts-Universität, Kiel, **2015**.
- [115] J. Strüben, J. Hoffmann, D. Presa-Soto, C. Näther, A. Staubitz, *Acta Crystallogr. Sect. E: Crystallogr. Commun.* **2016**, *72*, 1590–1594.
- [116] R. Reuter, H. A. Wegner, *Chem. Commun.* **2011**, *47*, 12267–12276.
- [117] V. I. Minkin, *Chem. Rev.* **2004**, *104*, 2751–2776.
- [118] B. S. Lukyanov, M. B. Lukyanova, *Chem. Heterocycl. Compd.* **2005**, 281–311.
- [119] L. Kortekaas, W. R. Browne, *Chem. Soc. Rev.* **2019**, *48*, 3406–3424.
- [120] S.-R. Keum, S.-M. Ahn, S.-J. Roh, S.-J. Park, S.-H. Kim, K. Koh, *Magn. Reson. Chem.* **2006**, *44*, 90–94.
- [121] S.-R. Keum, B.-S. Ku, M.-H. Lee, G.-Y. Chi, S.-S. Lim, *Dyes Pigm.* **2009**, *80*, 26–29.
- [122] G. P. Moss, *Pure Appl. Chem.* **1998**, *70*, 143–216.
- [123] M. Levitus, G. Glasser, D. Neher, P. F. Aramendía, *Chem. Phys. Lett.* **1997**, *277*, 118–124.
- [124] M. Bletz, U. Pfeifer-Fukumura, U. Kolb, W. Baumann, *J. Phys. Chem. A* **2002**, *106*, 2232–2236.
- [125] Q. Shen, L. Wang, S. Liu, Y. Cao, L. Gan, X. Guo, M. L. Steigerwald, Z. Shuai, Z. Liu, C. Nuckolls, *Adv. Mater.* **2010**, *22*, 3282–3287.
- [126] I. Panaiotov, S. Taneva, A. Bois, F. Rondelez, *Macromolecules* **1991**, *24*, 4250–4254.
- [127] J. Chen, F. Zeng, S. Wu, *ChemPhysChem* **2010**, *11*, 1036–1043.
- [128] P. Howlader, B. Mondal, P. C. Purba, E. Zangrando, P. S. Mukherjee, *J. Am. Chem. Soc.* **2018**, *140*, 7952–7960.
- [129] M. E. Genovese, E. Colusso, M. Colombo, A. Martucci, A. Athanassiou, D. Fragouli, *J. Mater. Chem. A* **2017**, *5*, 339–348.
- [130] C. Lenoble, R. S. Becker, *J. Phys. Chem.* **1986**, *90*, 62–65.
- [131] N. P. Ernstring, T. Arthen-Engeland, *J. Phys. Chem.* **1991**, *95*, 5502–5509.

- [132] H. Görner, *Phys. Chem. Chem. Phys.* **2001**, *3*, 416–423.
- [133] A. K. Chibisov, H. Görner, *Phys. Chem. Chem. Phys.* **2001**, *3*, 424–431.
- [134] J. Hobley, M. J. Lear, H. Fukumura in *Photochemistry of Organic Molecules in Isotropic and Anisotropic Media*, (Eds.: V. Ramamurthy, K. S. Schanze), Molecular and Supramolecular Photochemistry, Marcel Dekker, Basel, **2003**, pp. 353–367.
- [135] J. Buback, M. Kullmann, F. Langhojer, P. Nuernberger, R. Schmidt, F. Würthner, T. Brixner, *J. Am. Chem. Soc.* **2010**, *132*, 16510–16519.
- [136] J. Hobley, V. Malatesta, R. Millini, L. Montanari, W. O Neil Parker, Jr, *Phys. Chem. Chem. Phys.* **1999**, *1*, 3259–3267.
- [137] R. D. Amos, R. Kobayashi, *Mol. Phys.* **2015**, *113*, 1674–1681.
- [138] N. P. Ernsting, *Chem. Phys. Lett.* **1989**, *159*, 526–531.
- [139] S. A. Krysanov, M. V. Alfimov, **1982**, *91*, 4.
- [140] S. Swansburg, E. Buncel, R. P. Lemieux, *J. Am. Chem. Soc.* **2000**, *122*, 6594–6600.
- [141] C. J. Wohl, D. Kuciauskas, *J. Phys. Chem. B* **2005**, *109*, 22186–22191.
- [142] G. Balasubramanian, J. Schulte, F. Müller-Plathe, M. C. Böhm, *Chem. Phys. Lett.* **2012**, *554*, 60–66.
- [143] J. Hobley, V. Malatesta, *Phys. Chem. Chem. Phys.* **2000**, *2*, 57–59.
- [144] J. Hobley, U. Pfeifer-Fukumura, M. Bletz, T. Asahi, H. Masuhara, H. Fukumura, *J. Phys. Chem. A* **2002**, *106*, 2265–2270.
- [145] D. Kim, Z. Zhang, K. Xu, *J. Am. Chem. Soc.* **2017**, *139*, 9447–9450.
- [146] N. A. Murugan, S. Chakrabarti, H. Ågren, *J. Phys. Chem. B* **2011**, *115*, 4025–4032.
- [147] J. Buback, P. Nuernberger, M. Kullmann, F. Langhojer, R. Schmidt, F. Würthner, T. Brixner, *J. Phys. Chem. A* **2011**, *115*, 3924–3935.
- [148] S. Ruetzel, M. Diekmann, P. Nuernberger, C. Walter, B. Engels, T. Brixner, *J. Chem. Phys.* **2014**, *140*, 224310.
- [149] J. Whelan, D. Abdallah, J. Wojtyk, E. Buncel, *J. Mater. Chem.* **2010**, *20*, 5727–5735.
- [150] J. Harada, Y. Kawazoe, K. Ogawa, *Chem. Commun.* **2010**, *46*, 2593.
- [151] C. Menet, H. Serier-Brault, O. Oms, A. Dolbecq, J. Marrot, A. Saad, P. Mialane, S. Jobic, P. Deniard, R. Dessapt, *RSC Adv.* **2015**, *5*, 79635–79643.
- [152] D. E. Williams, C. R. Martin, E. A. Dolgoplova, A. Swifton, D. C. Godfrey, O. A. Ejegbavwo, P. J. Pellechia, M. D. Smith, N. B. Shustova, *J. Am. Chem. Soc.* **2018**, *140*, 7611–7622.
- [153] D. Samanta, D. Galaktionova, J. Gemen, L. J. W. Shimon, Y. Diskin-Posner, L. Avram, P. Král, R. Klajn, *Nat. Commun.* **2018**, *9*, 641.
- [154] J. T. C. Wojtyk, P. M. Kazmaier, E. Buncel, *Chem. Mater.* **2001**, *13*, 2547–2551.

- [155] S. V. Paramonov, V. Lokshin, O. A. Fedorova, *J. Photochem. Photobiol. C* **2011**, *12*, 209–236.
- [156] K. Kinashi, Y. Harada, Y. Ueda, *Thin Solid Films* **2008**, *516*, 2532–2536.
- [157] K. Kinashi, S. Nakamura, M. Imamura, K. Ishida, Y. Ueda, *J. Phys. Org. Chem.* **2012**, *25*, 462–466.
- [158] L. Kortekaas, J. Chen, D. Jacquemin, W. R. Browne, *J. Phys. Chem. B* **2018**, *122*, 6423–6430.
- [159] T. El-Sayed, A. Aboelnaga, M. A. El-Atawy, M. Hagar, *Molecules* **2018**, *23*, 1348.
- [160] J. L. Howard, Q. Cao, D. L. Browne, *Chem. Sci.* **2018**, *9*, 3080–3094.
- [161] C. Bolm, J. G. Hernández, *Angew. Chem. Int. Ed.* **2019**, *58*, 3285–3299.
- [162] T. G. McKenzie, F. Karimi, M. Ashokkumar, G. G. Qiao, *Chem. - Eur. J.* **2019**, *25*, 5372–5388.
- [163] P. A. May, N. F. Munaretto, M. B. Hamoy, M. J. Robb, J. S. Moore, *ACS Macro Lett.* **2016**, *5*, 177–180.
- [164] M. Schaefer, B. Icli, C. Weder, M. Lattuada, A. F. M. Kilbinger, Y. C. Simon, *Macromolecules* **2016**, *49*, 1630–1636.
- [165] L. Florea, D. Diamond, F. Benito-Lopez, *Macromol. Mater. Eng.* **2012**, *297*, 1148–1159.
- [166] M. Larkowska, M. Wuebbenhorst, S. Kucharski, *Int. J. Polym. Sci.* **2011**, *2011*, 1–6.
- [167] S. Shree, M. Schulz-Senft, N. H. Alsleben, Y. K. Mishra, A. Staubitz, R. Adelung, *ACS Appl. Mater. Interfaces* **2017**, *9*, 38000–38007.
- [168] S. Shree, M. Dowds, A. Kuntze, Y. K. Mishra, A. Staubitz, R. Adelung, *Mater. Horiz.* **2020**, 10.1039.C9MH01400D.
- [169] M. Sommer, H. Komber, *Macromol. Rapid Commun.* **2013**, *34*, 57–62.
- [170] H. Komber, S. Müllers, F. Lombeck, A. Held, M. Walter, M. Sommer, *Polym. Chem.* **2014**, *5*, 443.
- [171] L. Metzler, T. Reichenbach, O. Brüchner, H. Komber, F. Lombeck, S. Müllers, R. Hanselmann, H. Hillebrecht, M. Walter, M. Sommer, *Polym. Chem.* **2015**, *6*, 3694–3707.
- [172] S. B. Schmidt, F. Kempe, O. Brüchner, M. Walter, M. Sommer, *Polymer Chemistry* **2017**, *8*, 5407–5414.
- [173] P. Bauer, M. Sommer, J. Thurn, M. Pärs, J. Köhler, M. Thelakkat, *Chem. Commun.* **2013**, *49*, 4637–4639.
- [174] M. Schulz-Senft, P. J. Gates, F. D. Sönnichsen, A. Staubitz, *Dyes Pigm.* **2017**, *136*, 292–301.
- [175] M. Schulz, Diploma Thesis, Christian-Albrechts-Universität, Kiel, **2012**.

- [176] G. Espino, A. Kurbangalieva, J. M. Brown, *Chem. Commun.* **2007**, 1742.
- [177] C. Cordovilla, C. Bartolomé, J. M. Martínez-Ilarduya, P. Espinet, *ACS Catal.* **2015**, *5*, 3040–3053.
- [178] M. Yurtsever, B. Ustamehmetoglu, A. S. Sarac, A. Mannschreck, *Int. J. Quantum Chem.* **1999**, *75*, 111–117.
- [179] V. Farina, V. Krishnamurthy, W. J. Scott in *Organic Reactions, Vol. 50*, John Wiley & Sons, Inc., **2004**, pp. 1–93.
- [180] S. M. Aldoshin, L. O. Atovmyan, O. A. D'yachenko, M. A. Gal'bershtam, *Izv. Akad. Nauk SSSR Ser. Khim.* **1981**, 2720–2729.
- [181] G. Pareras, M. Palusiak, M. Duran, M. Solà, S. Simon, *J. Phys. Chem. A* **2018**, *122*, 2279–2287.
- [182] T. Yamamoto, Z.-h. Zhou, T. Kanbara, M. Shimura, K. Kizu, T. Maruyama, Y. Nakamura, T. Fukuda, B.-L. Lee, N. Ooba, S. Tomaru, T. Kurihara, T. Kaino, K. Kubota, S. Sasaki, *J. Am. Chem. Soc.* **1996**, *118*, 10389–10399.
- [183] S. Prager, I. Burghardt, A. Dreuw, *J. Phys. Chem. A* **2014**, *118*, 1339–1349.
- [184] T. Chen, L. Zheng, J. Yuan, Z. An, R. Chen, Y. Tao, H. Li, X. Xie, W. Huang, *Sci. Rep.* **2015**, *5*, 10923.
- [185] *Industrial Dyes: Chemistry, Properties, Applications*, (Ed.: K. Hunger), Wiley-VCH, Weinheim, **2003**.
- [186] G. S. Hartley, *Nature* **1937**, *140*, 281.
- [187] J. Henzl, M. Mehlhorn, H. Gawronski, K.-H. Rieder, K. Morgenstern, *Angew. Chem. Int. Ed.* **2006**, *45*, 603–606.
- [188] K. Scheil, T. G. Gopakumar, J. Bahrenburg, F. Temps, R. J. Maurer, K. Reuter, R. Berndt, *J. Phys. Chem. Lett.* **2016**, *7*, 2080–2084.
- [189] T. Kumpulainen, B. Lang, A. Rosspeintner, E. Vauthey, *Chem. Rev.* **2017**, *117*, 10826–10939.
- [190] J. Harada, K. Ogawa, S. Tomoda, *Acta Crystallogr. Sect. B: Struct. Sci.* **1997**, *53*, 662–672.
- [191] G. S. Hartley, R. J. W. L. Fèvre, *J. Chem. Soc.* **1939**, *0*, 531–535.
- [192] M. Quick, A. L. Dobryakov, M. Gerecke, C. Richter, F. Berndt, I. N. Ioffe, A. A. Granovsky, R. Mahrwald, N. P. Ernsting, S. A. Kovalenko, *J. Phys. Chem. B* **2014**, *118*, 8756–8771.
- [193] H. Rau, E. Lüddecke, *J. Am. Chem. Soc.* **1982**, *104*, 1616–1620.
- [194] H. Rau, S. Yu-Quan, *J. Photochem. Photobiol. A* **1988**, *42*, 321–327.
- [195] Y.-C. Lu, E. W.-G. Diau, H. Rau, *J. Phys. Chem. A* **2005**, *109*, 2090–2099.

- [196] T. Pancur, F. Renth, F. Temps, B. Harbaum, A. Krüger, R. Herges, C. Näther, *Phys. Chem. Chem. Phys.* **2005**, *7*, 1985–1989.
- [197] R. Siewertsen, J. B. Schönborn, B. Hartke, F. Renth, F. Temps, *Phys. Chem. Chem. Phys.* **2011**, *13*, 1054–1063.
- [198] T. A. Singleton, K. S. Ramsay, M. M. Barsan, I. S. Butler, C. J. Barrett, *J. Phys. Chem. B* **2012**, *116*, 9860–9865.
- [199] R. S. H. Liu, G. S. Hammond, *Proc. Natl. Acad. Sci. U. S. A.* **2000**, *97*, 11153–11158.
- [200] C.-W. Jiang, R.-H. Xie, F.-L. Li, R. E. Allen, *The Journal of Physical Chemistry A* **2011**, *115*, 244–249.
- [201] M. Böckmann, N. L. Doltsinis, D. Marx, *The Journal of Chemical Physics* **2012**, *137*, 22A505.
- [202] B. Ortiz, P. Villanueva, F. Walls, *J. Org. Chem.* **1972**, *37*, 2748–2750.
- [203] H. Firouzabadi, B. Vessal, M. Naderi, *Tetrahedron Lett.* **1982**, *23*, 1847–1850.
- [204] R. Thorwirth, F. Bernhardt, A. Stolle, B. Ondruschka, J. Asghari, *Chem. Eur. J.* **2010**, *16*, 13236–13242.
- [205] H. K. Hombrecher, K. Lüdtkke, *Tetrahedron* **1993**, *49*, 9489–9494.
- [206] J. Hoffmann, T. Kuczmera, E. Lork, A. Staubitz, *Molecules* **2019**, *24*, 303.
- [207] E. Baer, A. L. Tosoni, *J. Am. Chem. Soc.* **1956**, *78*, 2857–2858.
- [208] K. Müller, J. Wadhwa, J. S. Malhi, L. Schöttner, A. Welle, H. Schwartz, D. Hermann, U. Ruschewitz, L. Heinke, *Chem. Commun.* **2017**, *53*, 8070–8073.
- [209] K. H. Pausacker, *J. Chem. Soc.* **1953**, 1989–1990.
- [210] K. Monir, M. Ghosh, S. Mishra, A. Majee, A. Hajra, *Eur. J. Org. Chem.* **2014**, 1096–1102.
- [211] K. Kinoshita, *Bull. Chem. Soc. Jpn.* **1959**, *32*, 783–787.
- [212] J. Strueben, P. J. Gates, A. Staubitz, *J. Org. Chem.* **2014**, *79*, 1719–1728.
- [213] J. Strueben, M. Lipfert, J.-O. Springer, C. A. Gould, P. J. Gates, F. D. Sönnichsen, A. Staubitz, *Chem. - Eur. J.* **2015**, *21*, 11165–11173.
- [214] S. Hiroto, *Chem. - Asian J.* **2019**, 10.1002/asia.201900213.
- [215] R. F. Nystrom, W. G. Brown, *J. Am. Chem. Soc.* **1948**, *70*, 3738–3740.
- [216] M. L. Di Gioia, A. Leggio, I. F. Guarino, V. Leotta, E. Romio, A. Liguori, *Tetrahedron Lett.* **2015**, *56*, 5341–5344.
- [217] R. O. Hutchins, D. W. Lamson, L. Rua, C. Milewski, B. Maryanoff, *J. Org. Chem.* **1971**, *36*, 803–806.
- [218] K. Pothula, L. Tang, Z. Zha, Z. Wang, *RSC Adv.* **2015**, *5*, 83144–83148.
- [219] W.-h. Wei, T. Tomohiro, M. Kodaka, H. Okuno, *J. Org. Chem.* **2000**, *65*, 8979–8987.

- [220] L. Wang, H. Neumann, M. Beller, *Angew. Chem. Int. Ed.* **2019**, *58*, 5417–5421.
- [221] A. Khan, S. Hecht, *Chem. - Eur. J.* **2006**, *12*, 4764–4774.
- [222] W. Moormann, D. Langbehn, R. Herges, *Synthesis* **2017**, *49*, 3471–3475.
- [223] X. Chi, W. Cen, J. A. Queenan, L. Long, V. M. Lynch, N. M. Khashab, J. L. Sessler, *J. Am. Chem. Soc.* **2019**, *141*, 6468–6472.
- [224] D. Formenti, F. Ferretti, F. K. Scharnagl, M. Beller, *Chem. Rev.* **2019**, *119*, 2611–2680.
- [225] I. Szele, H. Zollinger in *Preparative Organic Chemistry*, Topics in Current Chemistry, Springer, Berlin Heidelberg, **1983**, pp. 1–66.
- [226] A. Tsuge, T. Moriguchi, S. Mataka, M. Tashiro, *J. Chem. Soc. Perkin Trans. 1* **1993**, 2211–2215.
- [227] J. Y. Kim, G. Kim, C. R. Kim, S. H. Lee, J. H. Lee, J. S. Kim, *J. Org. Chem.* **2003**, *68*, 1933–1937.
- [228] C. A. Hunter, L. D. Sarson, *Tetrahedron Lett.* **1996**, *37*, 699–702.
- [229] C. Schütt, G. Heitmann, T. Wendler, B. Krahwinkel, R. Herges, *J. Org. Chem.* **2016**, *81*, 1206–1215.
- [230] G. Heitmann, C. Schütt, R. Herges, *Eur. J. Org. Chem.* **2016**, *2016*, 3817–3823.
- [231] M. H. Davey, V. Y. Lee, R. D. Miller, T. J. Marks, *J. Org. Chem.* **1999**, *64*, 4976–4979.
- [232] I. D. Entwistle, T. Gilkerson, R. A. Johnstone, R. P. Telford, *Tetrahedron* **1978**, *34*, 213–215.
- [233] D. A. Fletcher, B. G. Gowenlock, K. G. Orrell, *J. Chem. Soc. Perkin Trans. 2* **1997**, 2201–2206.
- [234] M. Dommaschk, M. Peters, F. Gutzeit, C. Schütt, C. Näther, F. D. Sönnichsen, S. Tiwari, C. Riedel, S. Boretius, R. Herges, *J. Am. Chem. Soc.* **2015**, *137*, 7552–7555.
- [235] H. Caro, *Angew. Chem.* **1898**, *11*, 845–846.
- [236] K. M. Ibne-Rasa, C. G. Lauro, J. O. Edwards, *J. Am. Chem. Soc.* **1963**, *85*, 1165–1167.
- [237] B. G. Gowenlock, G. B. Richter-Addo, *Chem. Rev.* **2004**, *104*, 3315–3340.
- [238] S. Spyroudis, A. Varvoglis, *Synthesis* **1975**, *1975*, 445–447.
- [239] P. Groves, *Polym. Chem.* **2017**, *8*, 6700–6708.
- [240] M. Dowds, D. Bank, J. Strueben, D. P. Soto, F. D. Sönnichsen, F. Renth, F. Temps, A. Staubitz, *J. Mater. Chem. C* **2020**, 10.1039.C9TC05193G.
- [241] Y. Norikane, *J. Photopolym. Sci. Technol.* **2012**, *25*, 153–158.

- [242] E. Wagner-Wysiecka, N. Łukasik, J. F. Biernat, E. Luboch, *J. Inclusion Phenom. Macrocyclic Chem.* **2018**, *90*, 189–257.
- [243] S. Shinkai, T. Kouno, Y. Kusano, O. Manabe, *J. Chem. Soc. Perkin Trans. 1* **1982**, 2471–2477.
- [244] S. Shinkai, T. Nakaji, Y. Nishida, T. Ogawa, O. Manabe, *J. Am. Chem. Soc.* **1980**, *102*, 5860–5865.
- [245] S. Shinkai, Y. Honda, K. Ueda, O. Manabe, *Bull. Chem. Soc. Jpn.* **1984**, *57*, 2144–2149.
- [246] S. Shinkai, Y. Honda, K. Ueda, O. Manabe, *Isr. J. Chem.* **1984**, *24*, 302–306.
- [247] S. Shinkai, T. Minami, Y. Kusano, O. Manabe, *J. Am. Chem. Soc.* **1983**, *105*, 1851–1856.
- [248] S. Shinkai, Y. Honda, T. Minami, K. Ueda, O. Manabe, M. Tashiro, *Bull. Chem. Soc. Jpn.* **1983**, *56*, 1700–1704.
- [249] S. Shinkai, K. Miyazaki, O. Manabe, *J. Chem. Soc. Perkin Trans. 1* **1987**, 449–456.
- [250] A. Lyapunov, T. Kirichenko, C. Kulygina, R. Zubatyuk, M. Fonari, A. Kyrychenko, A. Doroshenko, *J. Inclusion Phenom. Macrocyclic Chem.* **2015**, *81*, 499–508.
- [251] M. Tlustý, P. Slavík, H. Dvořáková, V. Eigner, P. Lhoták, *Tetrahedron* **2017**, *73*, 1230–1237.
- [252] H. Galán, G. Henrich, J. de Mendoza, P. Prados, *Eur. J. Org. Chem.* **2010**, *2010*, 1249–1257.
- [253] X.-P. Qiu, E. V. Korchagina, J. Rolland, F. M. Winnik, *Polym. Chem.* **2014**, *5*, 3656–3665.
- [254] G. Despras, J. Hain, S. O. Jaeschke, *Chem. - Eur. J.* **2017**, *23*, 10838–10847.
- [255] D. G. Flint, J. R. Kumita, O. S. Smart, G. A. Woolley, *Chem. Biol.* **2002**, *9*, 391–397.
- [256] S. Bellotto, S. Chen, I. Rentero Rebollo, H. A. Wegner, C. Heinis, *J. Am. Chem. Soc.* **2014**, *136*, 5880–5883.
- [257] A. A. Beharry, G. A. Woolley, *Chem. Soc. Rev.* **2011**, *40*, 4422–4437.
- [258] X. Zhang, X. Ma, K. Wang, S. Lin, S. Zhu, Y. Dai, F. Xia, *Macromol. Rapid Commun.* **2018**, *39*, 1800142.
- [259] N. Tamaoki, K. Koseki, T. Yamaoka, *Angew. Chem. Int. Ed. Engl.* **1990**, *29*, 105–106.
- [260] A. Heindl, L. Schweighauser, C. Logemann, H. Wegner, *Synthesis* **2017**, *49*, 2632–2639.
- [261] C. Slavov, C. Yang, A. H. Heindl, T. Stauch, H. A. Wegner, A. Dreuw, J. Wachtveitl, *J. Phys. Chem. Lett.* **2018**, *9*, 4776–4781.
- [262] Y. Norikane, K. Kitamoto, N. Tamaoki, *Org. Lett.* **2002**, *4*, 3907–3910.

- [263] Y. Norikane, R. Katoh, N. Tamaoki, *Chem. Commun.* **2008**, 1898.
- [264] R. Reuter, N. Hostettler, M. Neuburger, H. A. Wegner, *Eur. J. Org. Chem.* **2009**, *2009*, 5647–5652.
- [265] R. Reuter, N. Hostettler, M. Neuburger, H. A. Wegner, *Chimia* **2010**, *64*, 180–183.
- [266] H.-W. Losensky, H. Spelthann, A. Ehlen, F. Vögtle, J. Bargon, *Angew. Chem. Int. Ed. Engl.* **1988**, *27*, 1189–1191.
- [267] Y. Norikane, K. Kitamoto, N. Tamaoki, *J. Org. Chem.* **2003**, *68*, 8291–8304.
- [268] Y. Norikane, Y. Hirai, M. Yoshida, *Chem. Commun.* **2011**, *47*, 1770–1772.
- [269] R. Reuter, H. A. Wegner, *Chem. - Eur. J.* **2011**, *17*, 2987–2995.
- [270] R. Reuter, H. A. Wegner, *Org. Lett.* **2011**, *13*, 5908–5911.
- [271] N. Tamaoki, K. Ogata, K. Koseki, T. Yamaoka, *Tetrahedron* **1990**, *46*, 5931–5942.
- [272] N. Tamaoki, T. Yamaoka, *J. Chem. Soc. Perkin Trans. 2* **1991**, 873–878.
- [273] N. Tamaoki, S. Yoshimura, T. Yamaoka, *Thin Solid Films* **1992**, *221*, 132–139.
- [274] A. H. Heindl, J. Becker, H. A. Wegner, *Chem. Sci.* **2019**, 10.1039.C9SC02347J.
- [275] K. Takaishi, A. Muranaka, M. Kawamoto, M. Uchiyama, *Org. Lett.* **2012**, *14*, 276–279.
- [276] G. Ritter, G. Haefelinger, E. Lueddecke, H. Rau, *J. Am. Chem. Soc.* **1989**, *111*, 4627–4635.
- [277] D. Röttger, H. Rau, *J. Photochem. Photobiol. A* **1996**, *101*, 205–214.
- [278] L. Schweighauser, H. A. Wegner, *Chem. Commun.* **2013**, *49*, 4397–4399.
- [279] L. Schweighauser, D. Häussinger, M. Neuburger, H. A. Wegner, *Org. Biomol. Chem.* **2014**, *12*, 3371.
- [280] A. Vlasceanu, M. Koerstz, A. B. Skov, K. V. Mikkelsen, M. B. Nielsen, *Angew. Chem. Int. Ed.* **2018**, *57*, 6069–6072.
- [281] *Silicon-containing polymers: the science and technology of their synthesis and applications*, (Eds.: R. G. Jones, A. Waturo, J. Chojnowski), Springer Science+Business, Dordrecht; Boston; London, **2000**.
- [282] R. Lehnert, A. Porzel, K. Rühlmann, *Z. Chem.* **1988**, *28*, 190–192.
- [283] J. A. Cella, J. C. Carpenter, *J. Organomet. Chem.* **1994**, *480*, 23–26.
- [284] H. Matsumoto, K. Shono, Y. Nagai, *Org. Prep. Proced. Int.* **1981**, *13*, 118–123.
- [285] M. Walther, Master Thesis, Christian-Albrechts-Universität, Kiel, **2018**.
- [286] K. G. Yager, C. J. Barrett, *J. Photochem. Photobiol. A* **2006**, *182*, 250–261.
- [287] D. J. Fisher, *Mechanochromism*, Materials Research Forum LLC, Millersville, **2019**.
- [288] A. Kim, M. Schulz, A. Staubitz in, 249th ACS National Meeting & Exposition, American Chemical Society, Denver, **2015**.

- [289] L. Zhang, K. Hashimoto, K. Tajima, *Polym. J.* **2012**, *44*, 1145–1148.
- [290] J. Linshoef, A. C. J. Heinrich, S. A. W. Segler, P. J. Gates, A. Staubitz, *Org. Lett.* **2012**, *14*, 5644–5647.
- [291] A. C. J. Heinrich, B. Thiedemann, P. J. Gates, A. Staubitz, *Org. Lett.* **2013**, *15*, 4666–4669.
- [292] P. R. Dvornic, R. W. Lenz, *J. Polym. Sci. Polym. Chem. Ed.* **1982**, *20*, 951–966.
- [293] L. Rossa, F. Vögtle in *Cyclophanes I*, (Ed.: F. Vögtle), Topics in Current Chemistry, Springer, Berlin, Heidelberg, **1983**, pp. 1–86.
- [294] R. K. Harris, E. D. Becker, S. M. Cabral de Menezes, P. Granger, R. E. Hoffman, K. W. Zilm, *Pure Appl. Chem.* **2008**, *80*, 59–84.
- [295] T. Mutai, J.-D. Cheon, S. Arita, K. Araki, *J. Chem. Soc. Perkin Trans. 2* **2001**, 1045–1050.
- [296] R. M. Brady, E. Hatzis, T. Connor, I. P. Street, J. B. Baell, G. Lessene, *Org. Biomol. Chem.* **2012**, *10*, 5230–5237.
- [297] M. J. Frisch, G. W. Trucks, H. B. Schlegel, G. E. Scuseria, M. A. Robb, J. R. Cheeseman, G. Scalmani, V. Barone, G. A. Petersson, H. Nakatsuji, X. Li, M. Caricato, A. Marenich, J. Bloino, B. G. Janesko, R. Gomberts, B. Mennucci, H. P. Hratchian, J. V. Ortiz, A. F. Izmaylov, J. L. Sonnenberg, D. Williams-Young, F. Ding, F. Lipparini, F. Egidi, J. Goings, B. Peng, A. Petrone, T. Henderson, D. Ranasinghe, V. G. Zakrzewski, J. Gao, N. Rega, G. Zheng, W. Liang, M. Hada, M. Ehara, K. Toyota, R. Fukuda, J. Hasegawa, M. Ishida, T. Nakajima, Y. Honda, O. Kitao, H. Nakai, T. Vreven, K. Throssell, J. A. Montgomery, Jr., J. E. Peralta, F. Ogliaro, M. Bearpark, J. J. Heyd, E. Brothers, K. N. Kudin, V. N. Staroverov, T. Keith, R. Kobayashi, J. Normand, K. Raghavachari, A. Rendell, J. C. Burant, S. S. Iyengar, J. Tomasi, M. Cossi, J. M. Millam, M. Klene, C. Adamo, J. W. Ochterski, R. L. Martin, K. Morokuma, O. Farkas, J. B. Foresman, D. J. Fox, *Gaussian 09*, Wallingford, CT, **2009**.
- [298] S. Grimme, J. Antony, S. Ehrlich, H. Krieg, *J. Chem. Phys.* **2010**, *132*, 154104.
- [299] E. F. Pettersen, T. D. Goddard, C. C. Huang, G. S. Couch, D. M. Greenblatt, E. C. Meng, T. E. Ferrin, *J. Comput. Chem.* **2004**, *25*, 1605–1612.
- [300] R. Dennington, T. A. Keith, J. M. Millam, *GaussView, Version 6.0.16*, Shawnee Mission, KS, **2016**.
- [301] E. Hedaya, J. H. Kawakami, P. W. Kopf, G. T. Kwiatkowski, D. W. McNeil, D. A. Owen, E. N. Peters, R. W. Tulis, *J. Polym. Sci. Polym. Chem. Ed.* **1977**, *15*, 2229–2238.
- [302] H. Takahashi, T. Ishioka, Y. Koiso, M. Sodeoka, Y. Hashimoto, *Biol. Pharm. Bull.* **2000**, *23*, 1387–1390.

List of Figures

I.1.	Effects of sunlight.	3
I.2.	Step growth and chain growth polymerization mechanisms.	7
I.3.	Possibilities to classify photochromic polymer systems.	8
I.4.	Schematic structure of fiber reinforced polymer composites.	25
I.5.	Development of the band structure of polyacetylene and principles of doping.	26
I.6.	Solar trees constructed with OPV modules at the EXPO 2015, Milan.	27
I.7.	Structure and frontier orbitals of oligothiophenes.	28
I.8.	Detection of mechanical stress in composites.	35
I.9.	Spiropyran connected to polythiophenes.	36
I.10.	Switching poly(azobenzene-siloxanes).	37
I.11.	Azobenzophanes were to be synthesized to test the flexibility of siloxane linkers in the constrained environment of macrocycles. Rigid cycles were expected to drastically influence the azobenzene's switching properties.	38
II.1.	Fully assigned ^1H NMR spectrum of the Stille reaction of 9a	87
II.2.	Crystal structure of 8-bromo-spiropyran. ^[180]	88
II.3.	Photographs of dithiophene-spiropyran 19	90
II.4.	UV vis and fluorescence of the dithiophene-spiropyran 19	96
III.1.	Examples of azobenzophane dimers with short linkers.	137
III.2.	Switching of the azobenzene cyclophane 64	140
III.3.	Evolution of the SiMe_2 signals in the ^1H NMR spectra of the azobenzene macrocycle 64	141
III.4.	DFT optimized structures of the switching states (<i>E</i>),(<i>E</i>) (left), (<i>E</i>),(<i>Z</i>) (left), and (<i>Z</i>),(<i>Z</i>) (right) of the azobenzene cyclophane 64	142
IV.1.	Photoswitching of a spiropyran with thiophene substituents.	153
IV.2.	Switchable OFETs	155
IV.3.	Structure of the azobenzene-siloxane macrocycle 64	157
V.1.	Overview of the identified substances by ^1H NMR spectroscopy after Stille coupling. The reaction mixtures contained either 9 or a mixture of 9 and 18	268
V.2.	Energies of frontier orbitals of 40a , 40b and 40c as Obtained by DFT Optimization.	281
V.3.	Frontier orbitals of 40a	282

V.4. Frontier orbitals of **40b**. 285
V.5. Frontier orbitals of **40c**. 288
V.6. ¹H NMR of the PSS-340 of azobenzene macrocycle in THF-*d*₈ 407

List of Schemes

I.1. Examples of photoswitchable molecules with (<i>E</i>),(<i>Z</i>)-isomerization.	4
I.2. Examples of photoswitchable molecules showing ring-opening or cyclization reactions.	5
I.3. Regioselective synthesis of P3HT.	29
I.4. Synthesis of PDMS by step growth polymerizations.	30
I.5. Siloxane degradation catalyzed by hydrochloric acid.	31
I.6. Ring-opening polymerization of cyclic siloxanes.	31
I.7. Variation of backbone and side chains of poly(siloxanes).	32
I.8. Cross-linking of PDMS.	32
I.9. Electrophile selective cross-coupling of spiropyrans	36
II.1. Typical synthesis of the spiropyran 1	47
II.2. Switching of the spiropyran 1	48
II.3. Degradation reaction of the spiropyran 1 with the epoxy-additive 5	61
II.4. Schematic of the use of spiropyran as conductivity switch in P3HT.	71
II.5. Retrosynthetic disconnection of spiropyran connected with P3HT.	72
II.6. Schematic of the selective functionalization of spiropyrans with aryl groups.	73
II.7. Optimized synthetic route of 9b	74
II.8. Synthesis of the thiophene-functionalized spiropyran 19	89
III.1. Possible isomerization mechanisms of azobenzene (41).	107
III.2. Common synthetical routes towards azobenzenes 43	108
III.3. Synthesis of the siloxane functionalized azobenzene 48 and the disiloxane functionalized azobenzene 51	111
III.4. Polymerization of the polymers 54 and 55 by polycondensation.	112
III.5. Synthetic route to yield the cyclophane dimer 64	139
IV.1. Spiropyran degradation during epoxy curing.	151
IV.2. Spiropyrans with bromide, iodide, hydroxy and OTf substituents.	152
IV.3. Metallation of poly(thiophenes).	154
IV.4. Overview of azobenzene-siloxane compounds.	156

List of Tables

II.1. Investigation of the reactivity of the spiropyrans 9a–c in Stille reactions with trimethylphenylstannane (16).	86
II.2. Geometrical properties of phenol derivatives and reaction energy of the deprotonation with phosphate as base.	91
II.3. Geometrical properties of anisole derivatives and reaction energy of the cleavage of the methoxy group with phosphate as base.	92
II.4. DFT optimized structures of 40a , 40b , and 40c and selected geometrical parameters and physical properties of the three isomers of 40 obtained by DFT optimization.	97
V.1. List of Chemicals and Reagents.	165
V.2. List of Solvents.	166
V.3. Weighed portions of the solid substances used in the Stille coupling reactions.	268
V.4. Reaction conditions of the Stille coupling of 9b	269
V.5. Reaction conditions of the Stille coupling of 9c	270
V.6. Energies of Frontier Orbitals of 40a , 40b and 40c as Obtained by DFT Optimization.	281
V.7. Atom Coordinates of 40a after DFT Optimization.	282
V.8. Atom Coordinates of 40b after DFT Optimization.	285
V.9. Atom Coordinates of 40c after DFT Optimization.	288
V.10. Calculated energies of starting materials and products of the deprotonation of phenols and the demethylation of anisoles with phosphate and derived reaction energy differences.	292
V.11. Atom Coordinates of 33a after DFT Optimization.	293
V.12. Atom Coordinates of 33b after DFT Optimization.	293
V.13. Atom Coordinates of 33c after DFT Optimization.	294
V.14. Atom Coordinates of 29a after DFT Optimization.	295
V.15. Atom Coordinates of 29b after DFT Optimization.	296
V.16. Atom Coordinates of 29c after DFT Optimization.	297
V.17. Atom Coordinates of 30a after DFT Optimization.	297
V.18. Atom Coordinates of 30b after DFT Optimization.	298
V.19. Atom Coordinates of 30c after DFT Optimization.	299
V.20. Atom Coordinates of 3a after DFT Optimization.	300
V.21. Atom Coordinates of 3b after DFT Optimization.	301

V.22	Atom Coordinates of 3c after DFT Optimization.	302
V.23	Atom Coordinates of 31a after DFT Optimization.	303
V.24	Atom Coordinates of 31b after DFT Optimization.	304
V.25	Atom Coordinates of 31c after DFT Optimization.	306
V.26	Atom Coordinates of 32a after DFT Optimization.	307
V.27	Atom Coordinates of 32b after DFT Optimization.	308
V.28	Atom Coordinates of 32c after DFT Optimization.	309
V.29	Atom Coordinates of 64a after DFT Optimization.	391
V.30	Atomic coordinates ($\times 10^4$) and equivalent isotropic displacement parameters ($\text{\AA}^2 \times 10^3$). $U(\text{eq})$ is defined as one third of the trace of the orthogonalized U^{ij} tensor ??	394
V.31	Atom Coordinates of 64b after DFT Optimization.	395
V.32	Atom Coordinates of 64c after DFT Optimization.	398

Abbreviations

AFM atomic force microscopy	MEMS microelectromechanical system
at apparent triplet	Mp melting point
ATR attenuated total reflection	MW microwave
calcd calculated	NB norbornadiene
d doublet	NMR nuclear magnetic resonance (spectroscopy)
dba dibenzylideneacetone	OFET organic field effect transistor
DCM dichloromethane	OLED organic light emitting diode
dd doublet of doublets	OPV organic photovoltaic
ddd doublet of doublet of doublets	OTf trifluoromethanesulfonyl
DFT density functional theory	P3HT poly(3-hexylthiophene)
DHA dihydroazulene	PDMS poly(dimethylsiloxane)
DMF <i>N,N</i> -dimethylformamide	PNIPAM poly(<i>N</i> -isopropylacrylamide)
DOSY diffusion-ordered spectroscopy	POM poly(oxymethylene)
dppf 1,1'-bis(diphenylphosphino)ferrocene	PSS photostationary state
DTE dithienylethene	PTU poly(thiourethane)
E_{ZPE} zero-point energy corrected energy	QC quadricyclane
EDG electron donating group	ROP ring-opening polymerization
EI electron ionization	s singlet
ESI electrospray ionization	SP spiropyran
EWG electron withdrawing group	SPhos 2-dicyclohexylphosphino-2',6'-dimethoxybiphenyl
FTAS femtosecond transient absorption spectroscopy	t triplet
GPC gel permeation chromatography	T_g glass-transition temperature
HOMO highest occupied molecular orbital	TEA triethylamine
HRMS high-resolution mass spectrometry	TLC thin layer chromatography
IR infrared spectroscopy	TMS tetramethyl silane
IUPAC International Union of Pure and Applied Chemistry	TOF time-of-flight
LUMO lowest unoccupied molecular orbital	tt triplet of triplets
m multiplet	UV ultraviolet
MC merocyanine	VHF vinylheptafulvene

Danksagung

An dieser Stelle möchte ich allen danken, die zur Fertigstellung dieser Arbeit beigetragen haben.

Zuvorderst gilt mein Dank meiner Doktormutter, Prof. Dr. Anne Staubitz. Sie hat mir nicht nur dieses faszinierende und ergiebige Thema anvertraut, sondern auch die richtige Mischung aus Anleitung und Freilauf gefunden. Über all die Jahre hat sie stets meinen Forscherdrang ermutigt, kreative Ideen unterstützt und auch Besuche der ein- oder anderen Tagung ermöglicht.

Die meisten Ideen und Lösungen wären ohne die enge und rundum angenehme Zusammenarbeit mit meinen Kooperationspartnern undenkbar gewesen. Dr. Sindu Shree und Prof. Dr. Rainer Adeling haben über die Lange Zeit immer wieder meinen Blick über den chemischen Tellerrand gelenkt und es war stets eine Freude, an der TF zu Gast zu sein. Ohne Dennis Bank, Dr. Falk Renth und Prof. Dr. Friedrich Temps wüsste ich jetzt vermutlich nur die Hälfte über Azobenzole.

Prof. Dr. Thisbe Lindhorst hat neben den üblichen Verdächtigen (SFB 677, ODI, Uni Bremen) meine Stelle für einen längeren Zeitraum finanziert. Ich bin Ihnen äußerst dankbar dafür!

Vielen Dank auch an Prof. Dr. Ulrich Lüning und Prof. Dr. Anna McConnell, die sich für die Übernahme des Zweitgutachtens bereiterklärt haben.

Die Ratschläge von Prof. Dr. Frank Sönnichsen haben die Untersuchung von Azobenzolen und Spiropyranen erst richtig ermöglicht. Prof. Dr. Näther danke ich für die Anfertigung der Kristallstruktur and many thanks to Dr. Paul Gates for measuring the high resolution mass spectra during the beginning of my work.

Holger Franzen, Marion Höftmann und Gitta Kohlmeyer-Yilmaz haben nicht nur unzählige Spektren gemessen, sondern mir auch bei nicht wenigen Sonderwünschen, Extramessungen und unerwarteten Problemen stets mit Rat und Tat zur Seite gestanden. Dirk Meyer, Silke Rühl und Rolf Schmied danke ich für die vielen gemessenen Massenspektren.

Im Laufe der Jahre haben auch eine ganze Reihe HiWis, Praktikanten, PostDocs und andere Mitarbeiter der Staubitzgruppe entweder direkt am Projekt oder an Seitenprojekten mitgearbeitet. Annika, Christin, Imke, Jan, Jonas, Jörn, Melanie, Miriam, Nils, Ruchira, Sarah, Sebastian, Yannik: Danke für die Unterstützung. Es war mir eine Freude. I also had the pleasure to work with international interns, who helped me improve my English skills (speaking of it: thank you, Gary Owston, too. I hope you won't judge me for writing in American English.) and worked hard. Thank you, Ashley, Brittany, Clara, David and Patrick! Die Abzüge habe ich mit Jan, JOle, Lu und Shuo geteilt. Sie waren zwar sehr unterschiedlich, aber allesamt angenehme Labor- und Büropartner. Allen anderen „Staubitzen“ danke ich

für die schöne Zeit und rundum gute Zusammenarbeit. Die ganze Zeit ist auch Dr. Jan Strüben zu verdanken, der mir damals in einem F3 Projekt erst den Arbeitskreis schmackhaft gemacht hat. Sein Kaffee war allerdings nicht immer so gut wie seine Forschung...

Die besten Diskussionen kamen jedoch in der Frühstücksrunde auf. Die letzten Mohikaner – JOle, Katrin und Nils – haben den ein oder anderen Mittwoch zu einem Highlight gemacht.

Ohne Dr. Matze wären die letzten Jahre vor allem eins gewesen: fad. Aber so hatte ich Abwechslung während der Arbeitszeit und einen Korrekturleser. Nach Feierabend sogar einen Spießgesellen.

Natürlich möchte ich auch meinen Freunden danken. Die Volleyballer und die Montagsrunde haben mir während schwieriger Phasen dringend nötige Ablenkung geboten.

Danke auch an meine Familie, die mich stets unterstützt hat und auch Verständnis während stressiger Zeiten hatte.

Marie. Danke. Für alles. Ohne Dich wäre alles nichts.